# ATTACHMENT 9.4

## DOCUMENT 19

DEPARTMENT OF PLANNING, INDUSTRY & ENVIRONMENT

# Climate change impacts in the NSW and ACT Alpine region

**Projected changes in snowmaking conditions**

environment.nsw.gov.au

Cover photo: Winter landscape in Kosciuszko National Park. John Spencer/DPIE

This report should be cited as:

Fei Ji 2019, *Climate change impacts in the NSW and ACT Alpine region: Projected changes in snowmaking conditions*, NSW Department of Planning, Industry and Environment, Sydney, Australia.

Published by:

Environment, Energy and Science
Department of Planning, Industry and Environment
59 Goulburn Street, Sydney NSW 2000
PO Box A290, Sydney South NSW 1232
Phone: +61 2 9995 5000 (switchboard)
Phone: 1300 361 967 (Environment, Energy and Science enquiries)
TTY users: phone 133 677, then ask for 1300 361 967
Speak and listen users: phone 1300 555 727, then ask for 1300 361 967
Email: info@environment.nsw.gov.au
Website: www.environment.nsw.gov.au

Report pollution and environmental incidents
Environment Line: 131 555 (NSW only) or info@environment.nsw.gov.au
See also www.environment.nsw.gov.au

ISBN 978 1 922318 16 9
EES 2020/0021
January 2020

**Find out more about your environment at:**

**www.environment.nsw.gov.au**

# Contents



# List of tables



# List of figures

# List of shortened forms

| | |
|---|---|
| ACE CRC | Antarctic Climate & Ecosystems Cooperative Research Centre |
| ACT | Australian Capital Territory |
| CMIP | Coupled Model Intercomparison Project |
| CSIRO | Commonwealth Scientific and Industrial Research Organisation |
| DPIE | Department of Planning, Industry and Environment |
| ECL | East Coast Low |
| GCM | Global Climate Model |
| MCAS-S | Multi-Criteria Analysis Shell for Spatial Decision Support |
| MM | Murray-Murrumbidgee state planning region |
| NARCliM | NSW/ACT Regional Climate Modelling project |
| NetCDF | Network Common Data Form |
| NSW | New South Wales |
| OEH | Office of Environment and Heritage |
| RCM | Regional Climate Model |
| RH | relative humidity |
| SET | South East and Tablelands |
| SRES | Special Report on Emissions Scenarios |
| UNSW | The University of New South Wales |
| WRF | Weather Research and Forecasting |

# Summary of findings

## Projected changes in snowmaking conditions in the NSW and ACT Alpine region

1. Recent observations and projections indicate that natural snow depth has declined and will continue to decline in the future, meaning that more snow will need to be made artificially to achieve the required snow depth to sustain the ski industry. However, projections indicate that the number of hours suitable for snowmaking will decline substantially over the NSW and ACT Alpine region.
2. Larger absolute decreases in snowmaking conditions are projected for higher elevation areas while larger relative decreases occur at lower elevations. Lower elevation locations might not be suitable for making snow in the future. Specifically, a more than 20% reduction of suitable snowmaking conditions is projected for 2020 to 2039 relative to 1990 to 2009. A more than 60% decrease is projected for 2060 to 2079 relative to 1990 to 2009.
3. If snow is made at warmer temperatures, opportunities for snowmaking may be able to be maintained at current levels (–2°C wet bulb temperature) until 2020 to 2039 (–1°C wet bulb temperature), or until 2060 to 2079 if snow can be made at a 0.5°C wet bulb temperature. However, making snow at warmer temperatures may be associated with trade-offs in cost and quality of snow.
4. The relative changes in future snowmaking conditions are projected to decrease similarly when using different wet bulb temperature thresholds. Regardless of the threshold used, approximately 20% and 50% reductions are projected for the near and far future periods, respectively.

# 1. Introduction

## 1.1 Background

The New South Wales (NSW) and Australian Capital Territory (ACT) Alpine region is located in the south-eastern corner of mainland Australia and is the highest mountain range in Australia. Though it comprises only about 0.16% of Australia in size, it is an important region for ecosystems, biodiversity, energy generation and winter tourism. It forms the southern end of the Great Dividing Range, covering a total area of 1.64 million hectares that extend over 500 kilometres. The highest peak, Mount Kosciuszko, rises to an altitude of 2228 metres.

This report is part of a larger project delivered by the NSW Department of Planning, Industry and Environment (DPIE) on the various impacts from climate change on the NSW and ACT Alpine region, hereafter referred to as the Alpine region. The full study region covers the Murray-Murrumbidgee region (MM), South East and Tablelands (SET) and the ACT, bordering the Victorian border in the south (Figure 1).

Australia's most popular snow holiday destination and some of the largest ski resorts in the southern hemisphere are in the Alpine region. The existence of the alpine resorts provides significant benefits to regional areas adjoining them. Many of the alpine shires have high levels of structural unemployment so the alpine industry is important in improving employment outcomes for residents of these regions (NIEIR 2006). In addition, The Snowy Hydroelectric Scheme collects and diverts water from rainfall and snowmelt into the MM rivers, providing irrigation resources for the Murray–Darling Basin, the largest agricultural region in Australia.

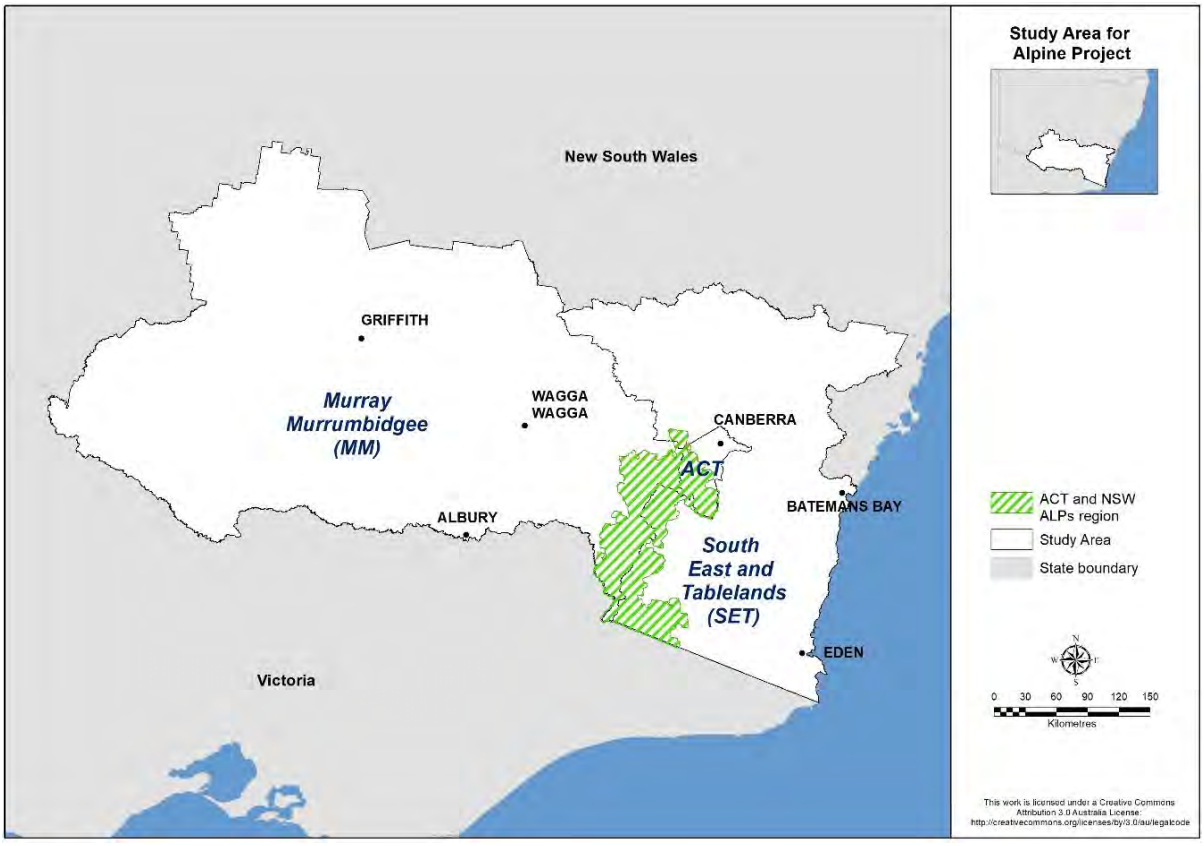


**Figure 1** **The study area for the Alpine project, including the NSW and ACT Alpine region, Murray-Murrumbidgee region and South East and Tablelands**

Seasonal snow cover in the Alpine region is critical to some species and winter sports. Several studies have examined long-term snow depth observations from a limited number of sites in the Australia Alpine Region (Ruddell et al. 1990; Nicholls 2005; Hennessy et al. 2008; Davis 2013; Fiddes et al. 2015). These observations begin in the 1950s and 1960s and generally show some consistent decreases in snow depth, although usually statistically insignificant (Figure 2).

A more recent report focusing on Victoria alone demonstrated that since about 1985, maximum snow depths have declined and the snow season has finished earlier as temperatures have increased across Australia (Bhend et al. 2012). Studies have investigated the future climate impact on snow in the Alpine region (Whetton et al. 1996; Hennessy et al. 2008; Fiddes et al. 2015). These studies all use future projections simulated by Global Climate Models (GCMs) to estimate climate change for the Alpine region, despite the GCM resolution being too coarse to capture mountains. These studies project large decreases in snow cover into the future, which will have significant impacts on alpine ecosystems (Pickering 2007; Slatyer 2010). Estimates of future climate change from both GCMs and a statistical downscaling method over Victoria found that statistical downscaling often predicts a larger decline in precipitation than the GCMs (Timbal et al. 2016). This suggests that the use of GCMs to estimate future change may not be appropriate for the Alpine region.

Recently, Di Luca et al. (2018) used 10 kilometre resolution simulations from the NSW/ACT Regional Climate Modelling (NARCliM) project (Evans et al. 2014) to evaluate simulated snow cover and snow depth and undertake future climate projections. Their results show that snow cover extent and snow depths decrease by approximately 15–60% for 2020 to 2039 and 2060 to 2079, relative to 1990 to 2009 (Figure 3). The large decrease in snow cover extent and snow depths will substantially impact the winter ski business.

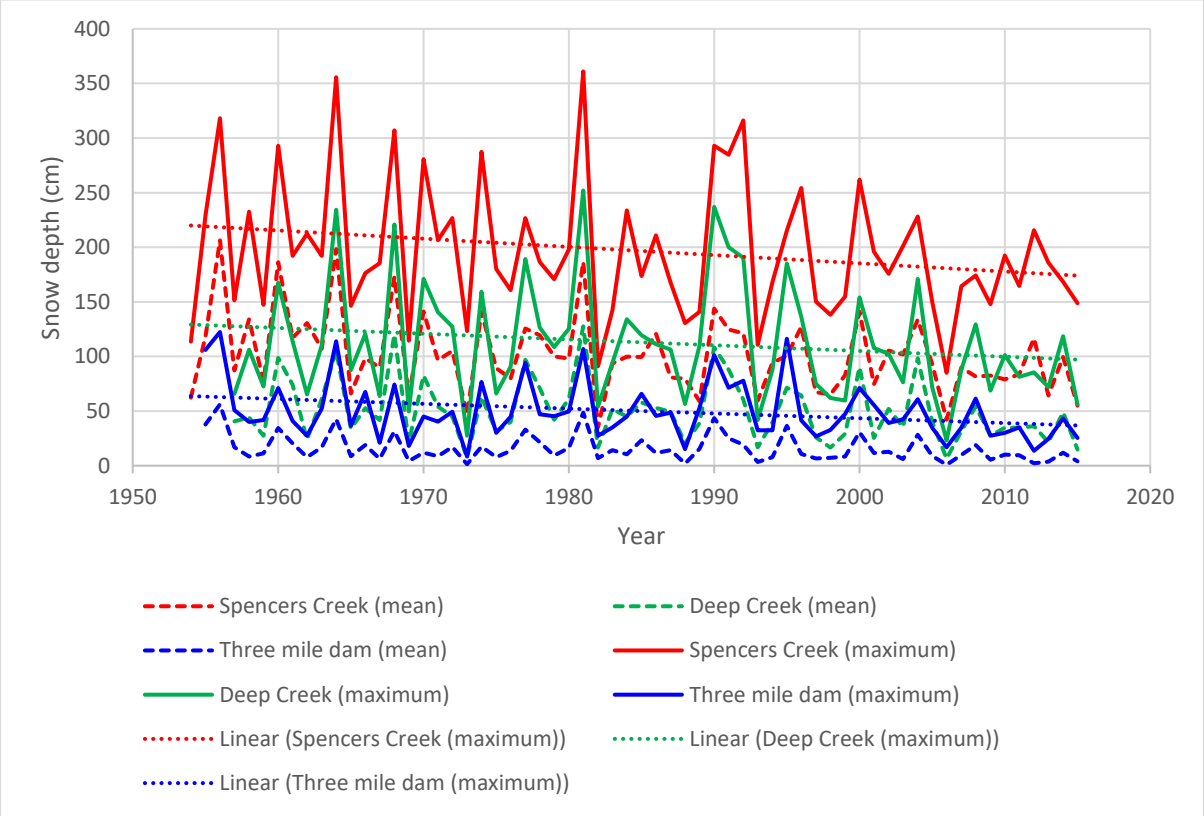


**Figure 2** **Observed mean and maximum snow depth (cm) for three snow monitoring sites within NSW, where the solid line = maximum snow depth, dash lines = mean snow depth, dotted line = linear trends in maximum snow depth**

Regional climate modelling outputs project changes to occur in variables important for snowmaking (e.g. temperature, precipitation and snow cover) at six Victorian alpine resorts by the end of century (2070 to 2099) compared to a baseline period of1961 to 2010 (Harris et al. 2016).

Snowmaking was first conducted in Australia as a demonstration exercise at Perisher in 1967, with systematic snowmaking being introduced to Australian ski resort slopes a couple of years later. Most Australian resorts installed significant snowmaking systems during the 1980s and 1990s. Snowmaking is now a common practice and is increasingly used within Australian ski resorts to:

- ensure seasonal length and viability
- improve and maintain the quality of the slopes during the season by topping up natural snow in areas that have poor cover, either because of intensive use by skiers and snowboarders or because of inadequate natural snowpack
- overcome restrictions on skier and snowboarder circulation caused by inadequate levels of natural snow.

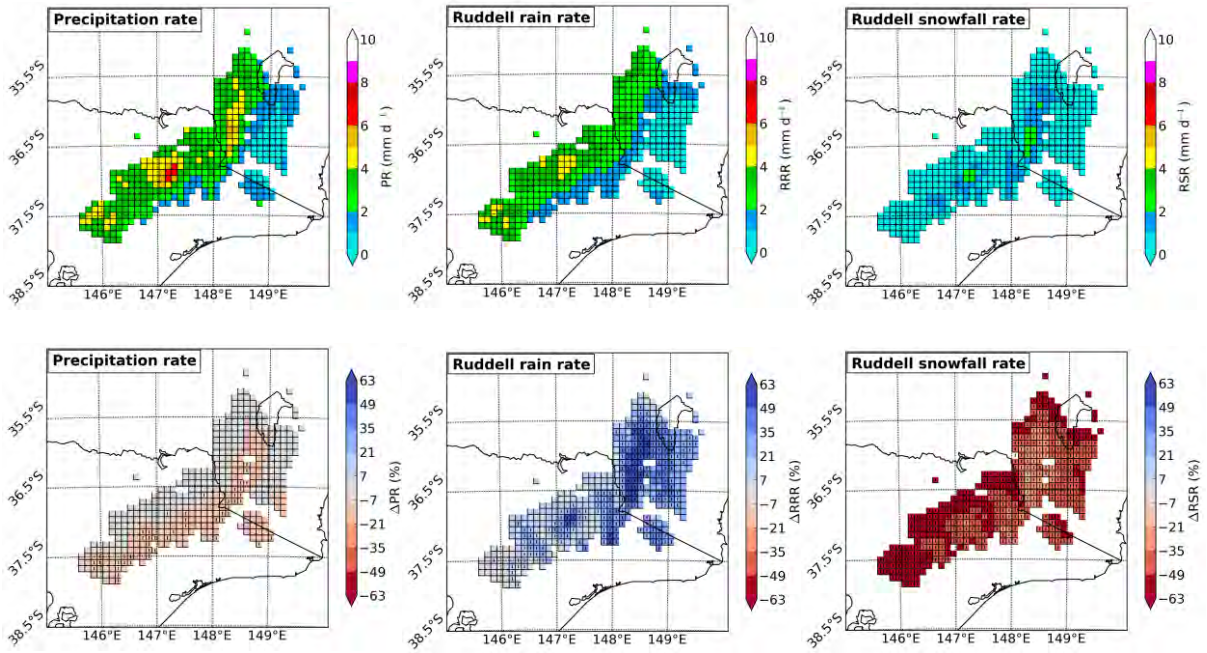


**Figure 3** **Simulated precipitation, rainfall and snow for 1990 to 2009 (top row) and their future changes for 2060 to 2079 relative to the 1990 to 2009 baseline period (bottom row) (from Di Luca et al. 2016)**

The proposed snowmaking coverage for the resorts has been determined primarily by identifying the best opportunities for skiing that could be supplied with man-made snow early in the season, and linking these with suitable trails for skier and snowboarder circulation. Environmental conditions are generally also an important consideration influencing the preferred skiing areas, the staging of their development and the location of snowmaking mains. Water supply and maintaining environmental flows in resort creeks is a major planning consideration.

With increases in temperature projected for the future, snowmaking is becoming an increasingly important function at Australian ski resorts to meet the requirements of winter ski sports. Weather conditions are undoubtedly critical to make snow even if snow can currently be made at any temperature. Traditionally, wet bulb temperatures below –2°C were considered suitable for snowmaking. In this study, we use 10 kilometre resolution NARCliM simulations to assess how suitable snowmaking conditions in the Alpine region will change under future climate.

## 1.2 Objectives

Observations have shown a clear increase in maximum and minimum temperatures and a decrease in precipitation and snow depth for the Alpine region (Di Luca et al. 2016, 2018). Available future snow projections also demonstrate decreases in snow cover, snow depth and snow season length in the future (Di Luca et al. 2016, 2018). To adapt to snow depth declines, snowmaking is playing an increasing role to sustain the ski industry.

The viability of conventional snowmaking is determined by the frequency at which wet bulb temperatures are below some specific thresholds suitable for making snow. In this study, we used outputs of 12 baseline and future Regional Climate Model (RCM) simulations (each with three time periods: 1990 to 2009, 2020 to 2039, and 2060 to 2079) from the NARCliM project to investigate changes in frequency of suitable snowmaking conditions for the Alpine region. The number of hours suitable for snowmaking (based on threshold temperatures, such as –2°C) was calculated for a baseline period (1990 to 2009) and two future periods (2020 to 2039 and 2060 to 2079) for each of the 12 simulations. These time periods were compared to investigate if the frequency of suitable snowmaking will change in the future.

## 1.3 Outputs

| Output | Details | Key users |
|---|---|---|
| Report | Projected changes in snowmaking conditions | Researchers |
| Data (surface layer) | Daily wet bulb temperature for all three epochs<br>Suitable snowmaking conditions for three wet bulb temperature thresholds (–2, –1 and 0.5°C) (60 years)<br>Seasonal and annual suitable snowmaking hours and relative change (%) in the near future and far future | NSW National Parks & Wildlife Service |
| Maps | Map layouts of the above data (NetCDF) | Councils, ski resorts, etc. |

# 2. Methods

## 2.1 Source of data

NARCliM simulations from four CMIP3 GCMs were used to drive three RCMs to form a 12-member GCM/RCM ensemble (Evans et al. 2014). The four selected GCMs are MIROC3.2, ECHAM5, CCCMA3.1, and CSIRO-MK3.0 (hereafter referred to in short-hand as MIROC, ECHAM, CCCMA and CSIRO). For the future projections the Special Report on Emissions Scenarios (SRES) business-as-usual A2 scenario was used (IPCC 2000). The three selected RCMs are three physics scheme combinations of the Weather Research and Forecasting (WRF) model. Each simulation consists of three 20-year runs (1990 to 2009, 2020 to 2039 and 2060 to 2079). The four GCMs were chosen based on a number of criteria: i) adequate performance when simulating historic climate; ii) most independent; iii) cover the largest range of plausible future precipitation and temperature changes for Australia. The three RCMs correspond to three different physics scheme combinations of the WRF V3.3 model (Skamarock et al. 2008), which were also chosen for adequate skill and error independence, following a comprehensive analysis of 36 different combinations of physics parameterisations over eight significant East Coast Lows (ECLs) (Evans et al. 2012; Ji et al. 2014). For the selected three RCMs, the WRF Double Moment 5-class (WDM5) microphysics scheme and NOAH land surface scheme are used in all cases. Refer to Evans et al. (2014) for more details on each physics scheme.

We acknowledge that the results are model dependent (as all model studies are) but through the use of this carefully selected ensemble we have attempted to minimize this dependence. By using this model selection process, we have shown that it is possible to create relatively small ensembles that are able to reproduce the ensemble mean and variance from the large parent ensemble (i.e. the many GCMs) as well as minimize the overall error (Evans et al., 2013a).

Some initial evaluation of NARCliM simulations shows that they have strong skill in simulating the precipitation and temperature of Australia, with a small cold bias and overestimation of precipitation on the Great Dividing Range (Evans et al. 2013b, Ji et al. 2016). The differing responses of the different RCMs confirm the utility of considering model independence when choosing the RCMs. The RCM response to large-scale modes of variability also agrees well with observations (Fita et al. 2016). Through these evaluations we found that while there is a spread in model predictions, all models perform adequately with no single model performing the best for all variables and metrics. The use of the full ensemble provides a measure of robustness such that any result that is common through all models in the ensemble is considered to have higher confidence.

For ease of reference in this report, the simulations driven by the same GCM were referred to as ‘same GCM driven simulations’. The simulations using the same RCM were referred to as ‘same RCM used simulations’. In total, there were four same GCM driven simulations (average of three members) and three same RCM used simulations (average of four members). The outputs from NARCliM are used to calculate the wet bulb temperature.

## 2.2 Analysis

For each grid point within the NARCliM domain, 3-hourly wet bulb temperature was calculated using simulated temperature, pressure and relative humidity for 12 simulations, each across three time periods (1990 to 2009, 2020 to 2039 and 2060 to 2079).

Wet bulb temperatures below –2°C were considered suitable for snowmaking, as this corresponds to peak efficiency in snowmaking (snow can be made at much warmer temperatures at increasing cost). The total number of hours for suitable snowmaking is then accumulated for each month and each year and used to analyse long-term mean monthly distribution and the inter-annual variability.

The changes in the number of hours suitable for snowmaking, hereafter suitable snowmaking hours, are expressed as differences and relative changes between the future periods (2020 to 2039 and 2060 to 2079) and the baseline period (1990 to 2009). The results for each ensemble member were averaged to get the ensemble mean.

There are four ski resorts within New South Wales, with different elevations. We analyse differences in snowmaking conditions for each of them. The four sites are located at relatively high elevations throughout the Alpine region (Table 1).

The critical temperature for traditional snowmaking is a wet bulb temperature of approximately –2°C, but recent advances in snowmaking approaches enable snow to be made at higher temperatures. For this reason, we present results for the number of hours below thresholds of –2°C, –1°C and 0.5°C wet bulb temperature.

**Table 1 Location and elevation for four ski resorts in the NSW and ACT Alpine region**

| Sites | Latitude | Longitude | Elevation (m) |
|---|---|---|---|
| Charlotte Pass | –36.423 | 148.329 | 1,832 |
| Perisher | –36.404 | 148.414 | 1,881 |
| Selwyn | –35.908 | 148.452 | 1,855 |
| Thredbo | –36.500 | 148.300 | 1,780 |

### Wet bulb temperature

The wet bulb temperature is the temperature that a parcel of air would have if it were cooled to saturation (100% relative humidity) by the evaporation of water into it, with the latent heat being supplied by the parcel. The wet bulb temperature is the lowest temperature that can be reached under current ambient conditions by the evaporation of water only. Wet bulb temperature is largely determined by both actual air temperature (dry-bulb temperature) and the amount of moisture in the air (humidity). At 100% relative humidity, the wet bulb temperature equals the dry-bulb temperature.

Wet bulb temperature incorporates relative humidity, which determines the temperature at which snow can be made. The calculation of wet bulb temperature, although relatively common, has historically been done by hand using specialised charts, for one or two values. An iterative function was developed in the R language to calculate wet bulb temperature from climate model outputs.

### Wet bulb temperature calculations

Wet bulb temperature was calculated using model output for 2-metre air temperature, relative humidity (RH) and atmospheric pressure, using the standard equations used by the National Oceanographic and Atmospheric Administration:

1. Saturation vapour pressure (es):

   es = 6.112 * 10^((7.5 * T) / (T + 237.3)), where T = dry bulb temperature (°C)

2. Actual vapour pressure, hPa (e):

   e = (es * RH) / 100

3. Initial conditions for the iteration:

   Saturation vapour pressure at each increment:

   Ewg = 6.112 * 10^((7.5 * Tw)/(Tw + 237.3))

   Actual vapour pressure at each increment:

   eg = Ewg - ((P * (T – Tw)) * 0.00066 * (1 + (0.00115*Tw)))

   where P = station pressure, Tw = wet bulb temperature at each increment

4. Vapour pressure difference (Ed):

   Ed = e – eg

These equations were solved iteratively, with wet bulb temperature being increased in increments of 10°, and the increment being divided by 10 when the consecutive vapour pressure difference (Ed) changed sign. The iteration was stopped when the vapour pressure difference was equal to zero or the absolute value of Ed was less than 0.005.

Final wet bulb temperature = wet bulb at final increment + (increment*previous sign).

## 2.3 Quality control

The input data used in the study (temperature, relative humidity and surface pressure) have been quality controlled and released for public use. The analysis method is similar to what was used in the study for Victoria's ski resorts (Harris et al. 2016), which was externally reviewed by experts at the Commonwealth Scientific and Industrial Research Organisation (CSIRO).

The method has been reviewed by Dr Tom Remenyi at ACE CRC's Climate Futures who was working on the Victoria project (Harris et at. 2016). The report was reviewed both internally and externally, and followed the procedures as set out in DPIE's Scientific Rigour Position Statement (OEH 2013).

## 2.4 Data storage and access

All output data were converted to raster format (ArcGIS ESRI grid) and supplied to the MCAS-S (Multi-Criteria Analysis Shell for Spatial Decision Support) datapacks for distribution and storage. All input data to the model and by-products are stored on hard disk drives. All data are in the NARCliM coordinate system. The extent of the datasets includes the MM region, ACT and SET with the boundary at top: –32.671254, left: 143.317445, right: 150.745676, and bottom: –37.505077.

# 3. Results

In this section, we will first present suitable snowmaking hours over the Alpine region using wet bulb temperature below a –2°C threshold, then show how snowmaking changes in the future, including seasonal variation. This will be followed by an analysis of the four individual NSW ski resorts. We then proceed to test wet bulb temperature thresholds below –1°C and 0.5°C to compare with the snowmaking results presented for the –2°C threshold.

## 3.1 Snowmaking below –2°C

### Annual mean suitable snowmaking time

Annual mean suitable snowmaking hours for the baseline and two future periods are calculated for each of the 12 ensemble members. The ensemble mean is presented in Figure 4.

In the baseline projections (Figure 4), there are more than 600 suitable snowmaking hours a year for high elevation areas (above 1700 m) and fewer than 100 suitable snowmaking hours a year for lower elevation areas (below 1500 m). The gradient of suitable snowmaking condition within the Alpine region is quite large, indicating that snowmaking condition is sensitive to elevation. There are essentially zero snowmaking hours below 500 metres.

Large decreases in suitable snowmaking hours are projected for 2020 to 2039 and 2060 to 2079 relative to 1990 to 2009 (Figure 4). Lower elevation sites are projected to become unsuitable for making snow, and higher elevation sites are projected to have about 300 fewer suitable snowmaking hours for 2060 to 2079. The largest relative changes are projected for lower elevation areas, with up to 80% fewer suitable snowmaking hours in the far future (figure not shown).

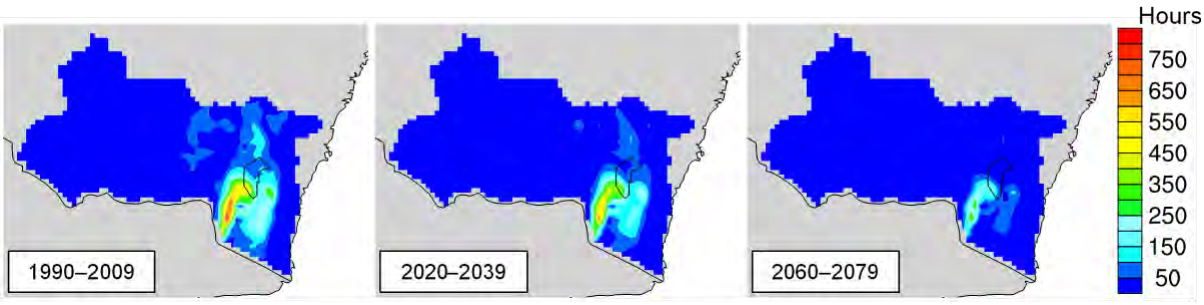


**Figure 4** **Suitable snowmaking conditions (in hours) for 1990 to 2009, 2020 to 2039 and 2060 to 2079 for the –2°C threshold**

## Monthly variation in time suitable for snowmaking

Accumulated monthly suitable snowmaking hours is presented in Figure 5. The three solid lines are averages of the 12 NARCliM ensemble members for the baseline and future periods. The three dashed lines show the best-case scenario (largest value in the 12-member ensemble), and dotted lines show the worst-case scenario (smallest value in the 12-member ensemble).

Across the Alpine region, compared to the baseline period, there is a clear decrease in the absolute number of suitable snowmaking hours into the future. The seasonal distribution is relatively unchanged, with the peak occurring in winter (June, July, August – JJA); however, there is a significant contraction of the entire season, with much fewer suitable snowmaking hours in the shoulder seasons (April, May and September, October). The largest absolute decreases are projected to occur in winter.

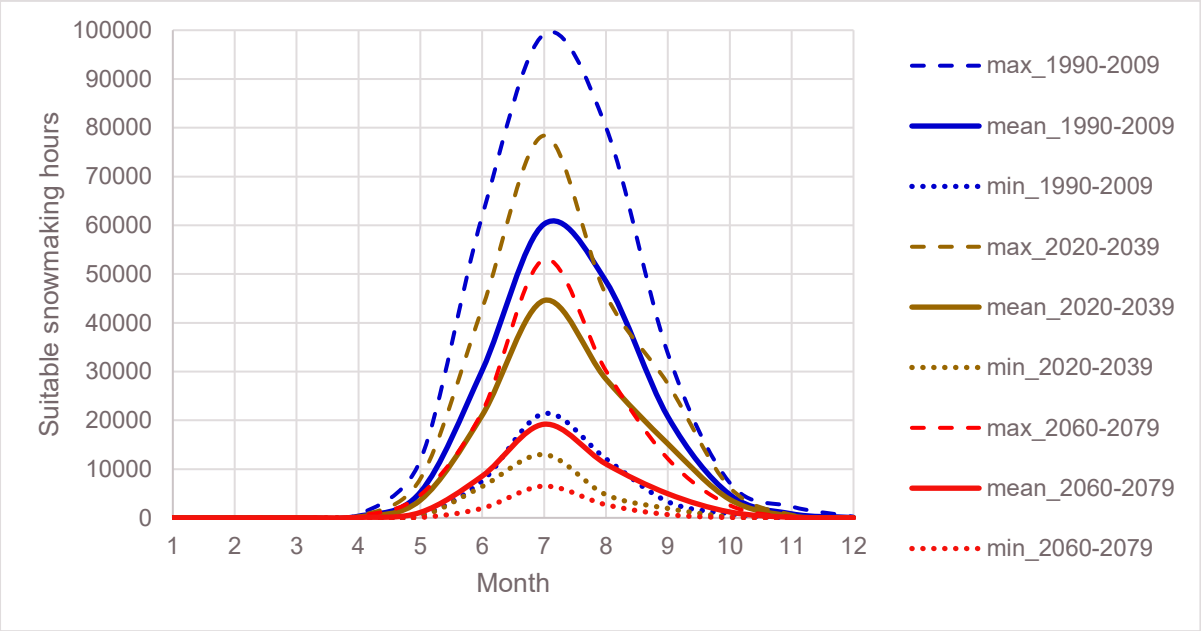


**Figure 5** **Simulated monthly distribution of suitable snowmaking conditions for the Alpine region for best (dashed lines), mean (solid lines) and worst-case (dotted lines) scenarios in the 12-member NARCliM ensemble for the –2°C threshold**

The differences between the best-case and worst-case scenarios are very large (up to 400% for the best-case scenario relative to the worst-case scenario in July), especially for the winter season. This implies there is large uncertainty within the ensemble. This is understandable as GCMs selected in the NARCliM project were chosen based on a number of criteria that include spanning the range of future changes in the GCM ensemble (Evans et al. 2014).

## Differences between GCM/RCM simulations

Changes in suitable snowmaking hours for 2060 to 2079 relative to 1990 to 2009 are large for the Alpine region. Differences in projections across GCM simulations are large, although they all project larger decreases in lower elevation areas than in higher elevation areas (Figure 6). Simulations based on the CCCMA model project the largest decreases in suitable snowmaking hours for lower elevation (> 90%) and higher elevation areas (> 70%). Simulations driven by MIROC project similar decreases for lower elevation areas, but smaller decreases for higher elevation areas (60–70%). Both the ECHAM and CSIRO driven simulations project less severe changes, about half those of CCCMA and MIROC.

The three RCM simulations generally project similar decreases in suitable snowmaking hours for the Alpine region with 60–70% decreases for higher elevation areas and 80–90% decreases for lower elevation areas. For areas outside the Alpine region boundary, there are some differences between the three RCM simulations since the R3 simulations projected slightly larger increases in temperature.

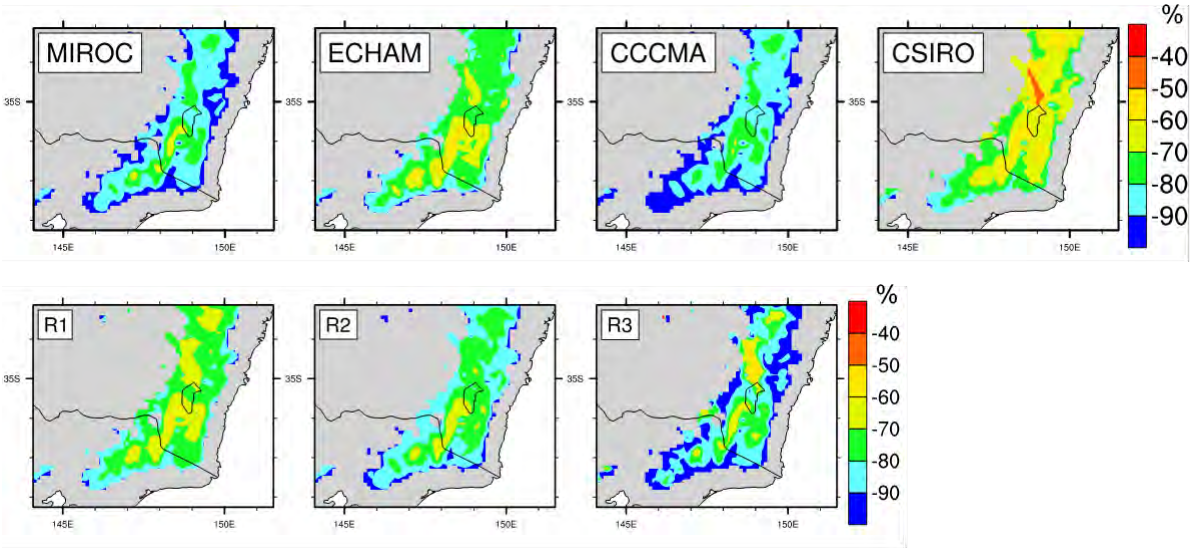


**Figure 6** **Relative changes in snowmaking conditions (%) for 2060 to 2079 relative to the 1990 to 2009 baseline period for four GCM and three RCM simulations for the –2°C threshold**

## Inter-annual variability for ski resorts

Suitable snowmaking hours have clear inter-annual variability (Figure 7), which is related to the inter-annual variation in temperature. Here we show results for four ski resorts. Correlation of suitable snowmaking hours across different sites is related to elevation, with those sites at similar elevations correlating the best (> 0.9). Generally, snowmaking conditions show similar inter-annual variability for these four ski resorts.

Although there is little difference in peak elevation (< 100 m across all four resorts), the differences in suitable snowmaking conditions are large. For example, Thredbo is 101 metres lower than Perisher. The difference in suitable snowmaking conditions is about 150 hours a year, about 25% of the annual suitable snowmaking time of Perisher. This indicates that snowmaking conditions are very sensitive to elevation.

A decreasing trend in snowmaking conditions can be observed for each ski resort for each of the 20-year projection periods. Changes in suitable snowmaking conditions are projected to decrease 20–30% for 2020 to 2039 relative to 1990 to 2009, and 60–70% for 2060 to 2079 relative to 1990 to 2009, for all ski resorts.

## Monthly variation for ski resorts

Within the model, July is the best time for making snow in all locations. Suitable snowmaking hours across the year are longer for higher elevation locations, which start earlier and finish later. The opposite is true for lower elevation locations, where shorter snowmaking hours are projected across the year that start later and finish earlier.

Larger decreases in suitable snowmaking hours are projected for all locations, especially in the peak month, July, for higher elevation locations (Figure 8). Under a future climate, the period of suitable snowmaking hours will get shorter (that is, start later and finish earlier) at all locations. Differences in suitable snowmaking conditions between different ski resorts are larger in JJA than the shoulder seasons, with the largest difference in July.

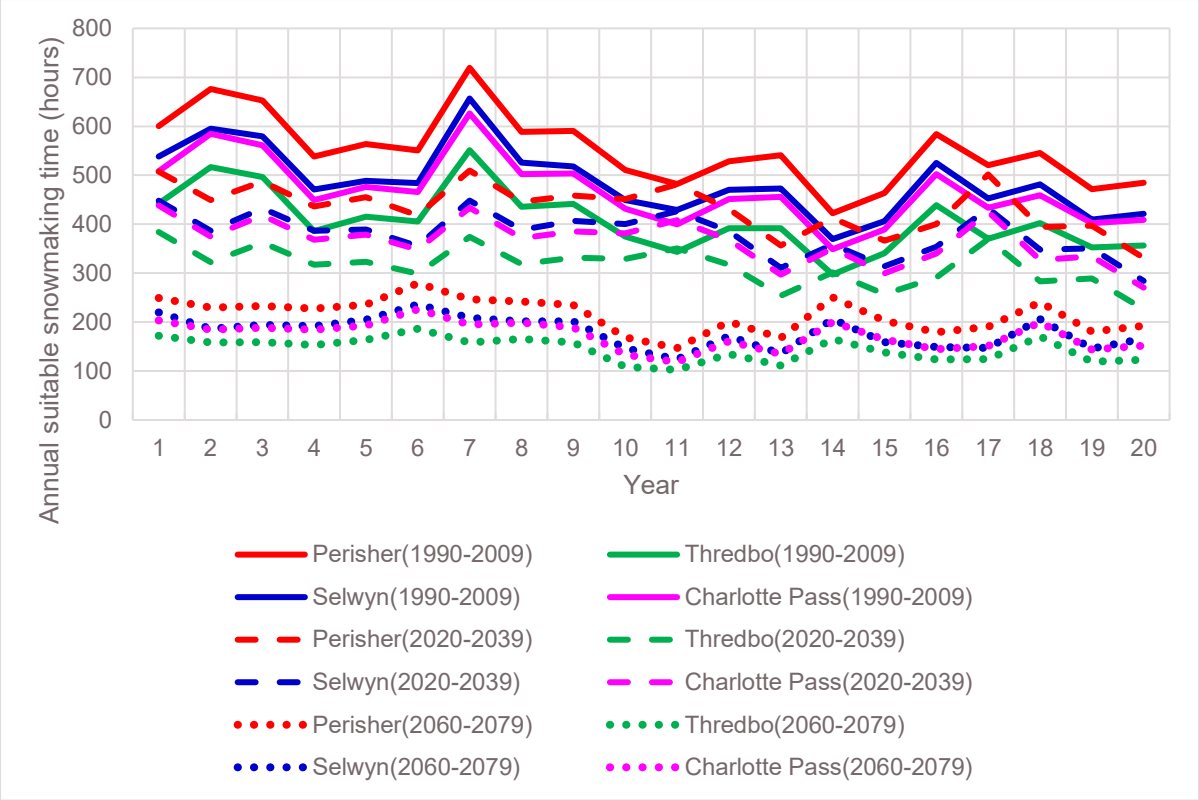


**Figure 7** **Inter-annual variability of suitable snowmaking time for four ski resorts for 1990 to 2009, 2020 to 2039 and 2060 to 2079 for the –2°C threshold**

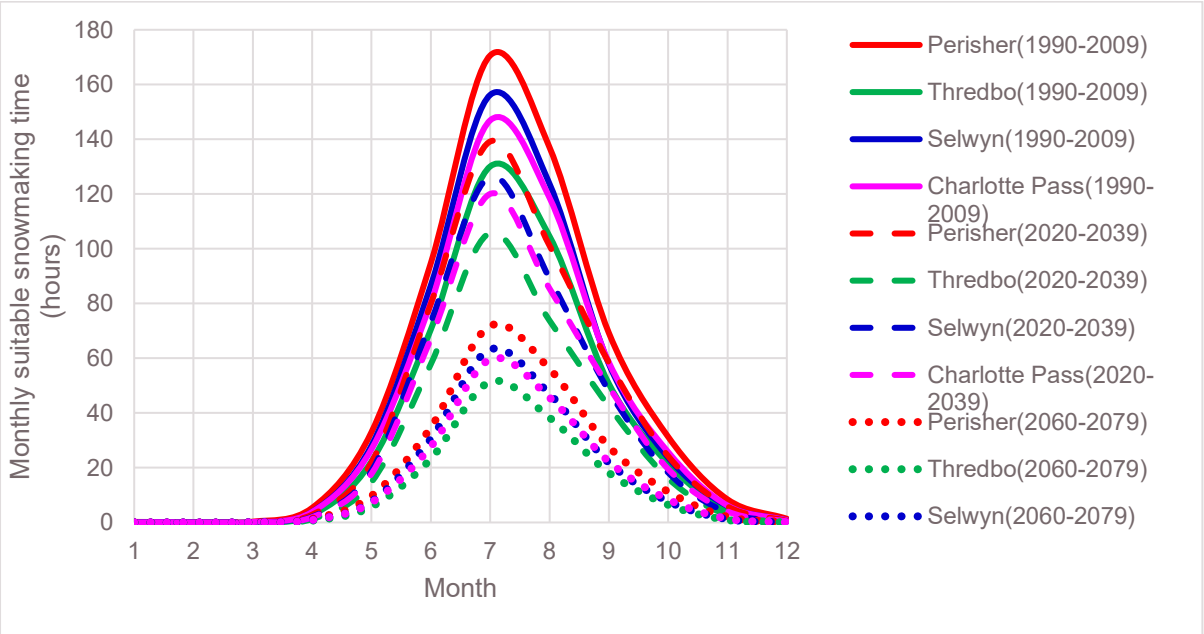


**Figure 8** **Monthly suitable snowmaking time for four ski resorts for 1990 to 2009, 2020 to 2039 and 2060 to 2079 for the –2°C threshold**

## Relative changes in annual suitable snowmaking conditions

Changes in annual suitable snowmaking hours for 2020 to 2039 relative to 1990 to 2009 are relatively small (Figure 9). The major decreases are observed in the Alpine region and along high elevation areas within SET, where decreases of more than 20% are projected. Relatively smaller decreases, however, are projected for the mountain peaks in the Alpine region. Small decreases are projected for elsewhere. This indicates that future climate change mostly impacts on snowmaking conditions for high topography areas.

Future changes in snowmaking conditions are much larger for the far future compared to the near future (Figure 9 & Figure 10). A greater than 50% decrease in annual suitable snowmaking hours is projected for the Alpine region in the far future, with much smaller decreases elsewhere (Figure 10).

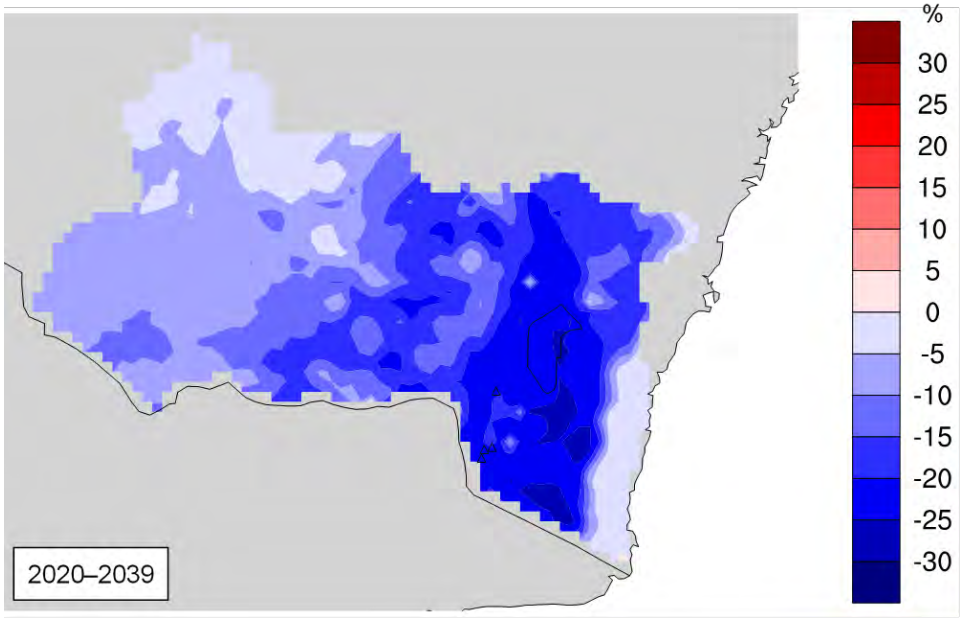


**Figure 9** **Changes in suitable snowmaking conditions (%) for 2020 to 2039 relative to the 1990 to 2009 baseline period for the –2°C threshold**

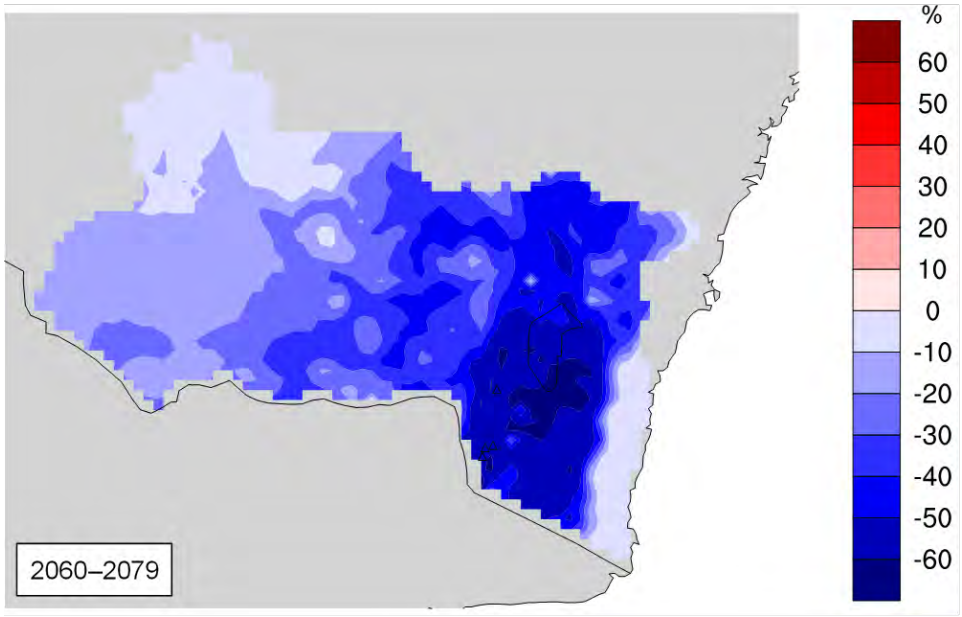


**Figure 10** **Changes in suitable snowmaking conditions (%) for 2060 to 2079 relative to the 1990 to 2009 baseline period for the –2°C threshold**

## 3.2 Snowmaking below –1°C

### Annual mean suitable snowmaking time

The annual mean suitable snowmaking hours for the baseline and two future periods are presented in Figure 11. When compared with Figure 4, there is about 50% more suitable snowmaking time for the Alpine region and high elevation areas in the SET region. When snow can be made at a higher wet bulb temperature (–1°C threshold), the lower elevation areas surrounding the Alpine region have 100–200 hours a year suitable for making snow for 1990 to 2009.

A 200–300 hour a year decrease in suitable snowmaking conditions is projected for the Alpine region for 2020 to 2039 relative to 1990 to 2009. The greatest decrease is observed at the highest elevations. There are 600–800 hours a year still suitable for making snow for 2020 to 2039, which is at a similar range of suitable snowmaking conditions for 1990 to 2009 using –2°C as threshold.

Similar to Figure 4, changes for 2060 to 2079 for the –1.5°C threshold are much larger than those for 2020 to 2039 (Figure 11). The greatest decreases are observed at the highest elevations. At the lower elevations, there is almost no time suitable for snowmaking.

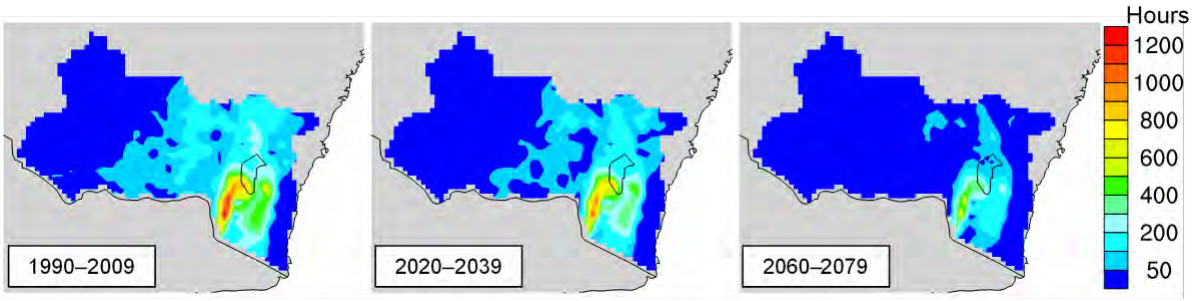


**Figure 11** **Suitable snowmaking conditions (in hours) for 1990 to 2009, 2020 to 2039 and 2060 to 2079 for the –1°C threshold**

### Inter-annual variability for ski resorts

Suitable snowmaking hours for a –1°C threshold have similar inter-annual variability to those using –2°C as a threshold (shown in Figure 7); however, the magnitude of variability is larger (Figure 12). A decreasing trend is found for each ski resort for both future projection periods. Differences between 2020 to 2039 and 1990 to 2009 are relatively small for each ski resort (approximately 20%); however, those for 2060 to 2079 relative to 1990 to 2009 are between 50 and 60%.

### Monthly variations for ski resorts

Monthly variations in suitable snowmaking hours using a –1°C threshold (Figure 13) are similar to those using a –2°C threshold (Figure 8), for each ski resort and each time period, but many more suitable snowmaking hours are available when using a –1°C threshold. Most of the additional available snowmaking hours are found in JJA, and the remainder in the shoulder seasons.

The absolute changes in suitable snowmaking hours for future periods relative to the historical period are also large when using a –1°C threshold; however, the relative changes in suitable snowmaking hours are similar (or even a little smaller). Again, relative changes in suitable snowmaking hours are small for 2020 to 2039 (about 20%) and large for 2060 to 2079 (50%), relative to 1990 to 2009.

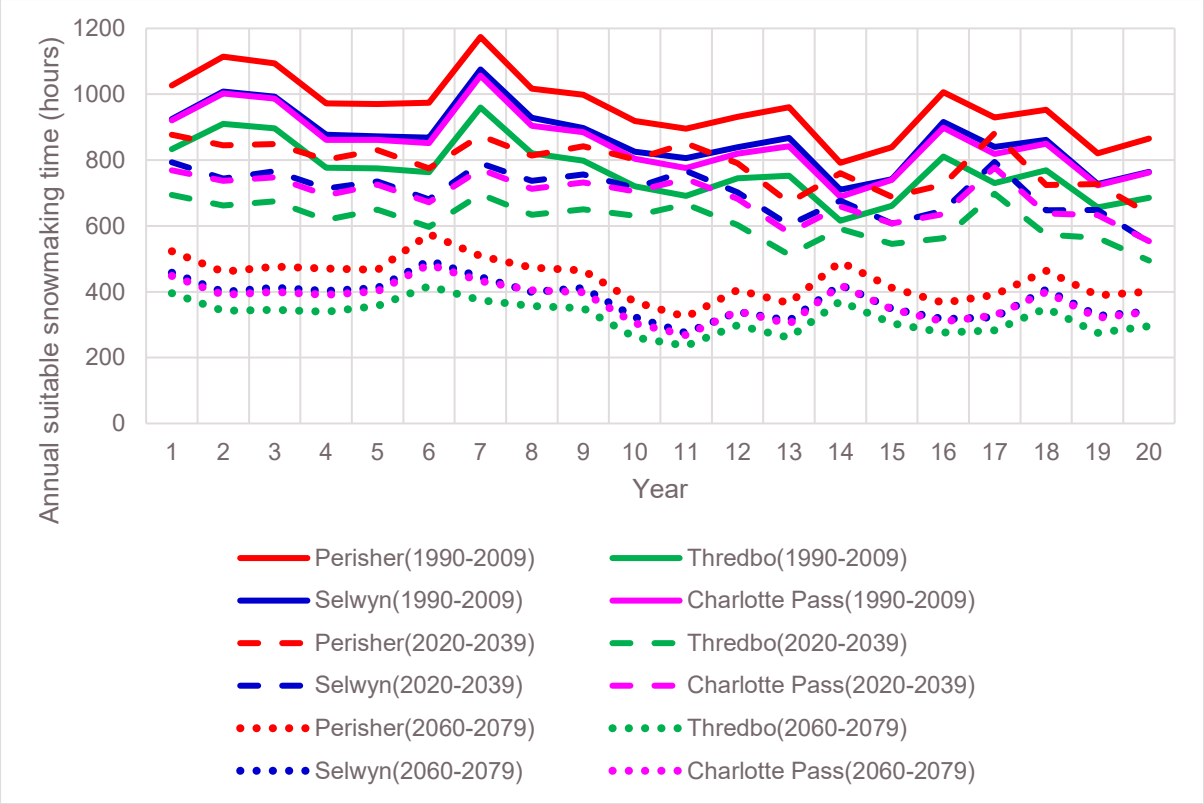


**Figure 12** **Inter-annual variability of suitable snowmaking time for four ski resorts for 1990 to 2009, 2020 to 2039 and 2060 to 2079 for the –1°C threshold**

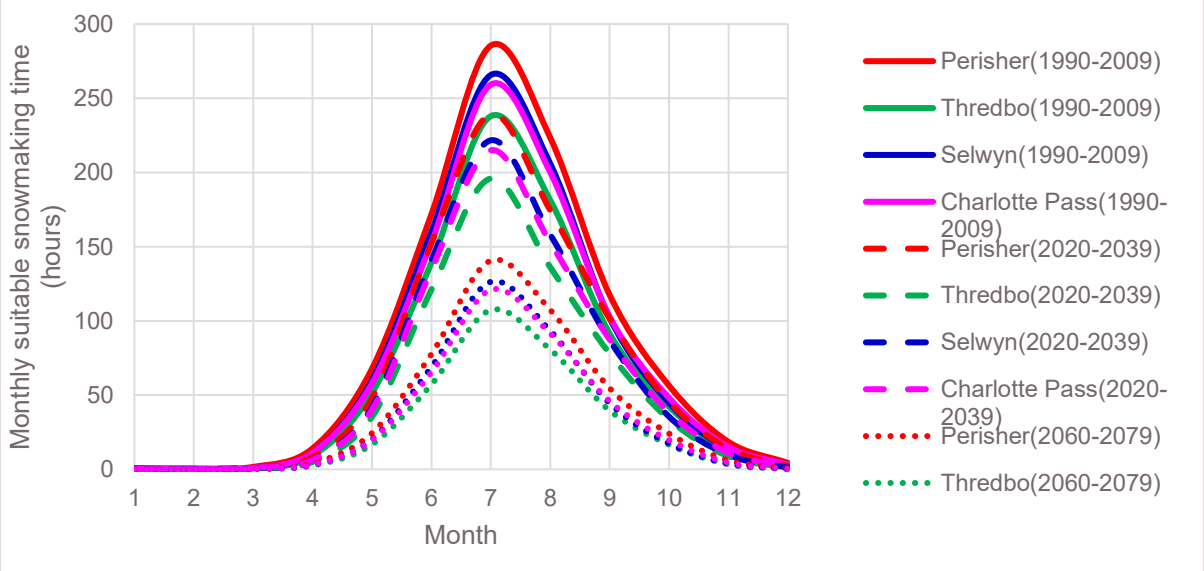


**Figure 13** **Monthly suitable snowmaking time for four ski resorts for 1990 to 2009, 2020 to 2039 and 2060 to 2079 for the –1°C threshold**

## Relative changes in annual suitable snowmaking conditions

The changes for 2020 to 2039 relative to 1990 to 2009 (Figure 14) span a similar range to those shown in Figure 9. The large decreases are observed in the Alpine region and along high topography areas within SET, where 20–25% decreases are projected; however a smaller decrease (15–20%) is found for the mountain peaks in the Alpine region. A small decrease is projected for other regions. This indicates that future climate change mostly impacts on snowmaking conditions for high topography areas.

Future changes in snowmaking conditions are much larger for the far future projections than the near future projections (Figure 15). A more than 50% decrease in snowmaking conditions is projected for the Alpine region and much smaller elsewhere, which is similar to what is shown in Figure 10.

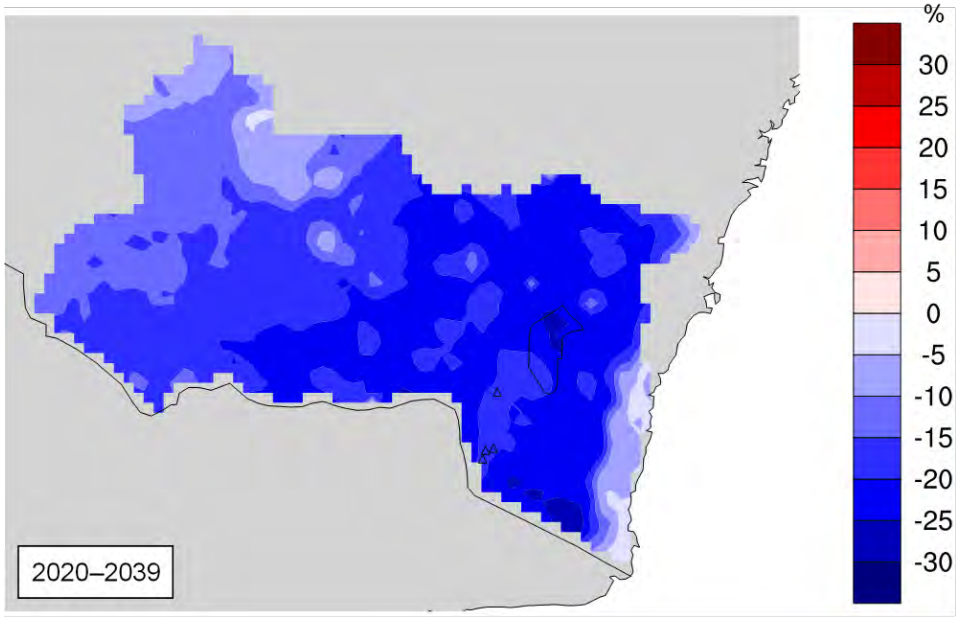


**Figure 14** **Changes in suitable snowmaking conditions (%) for 2020 to 2039 relative to the 1990 to 2009 baseline period for the –1°C threshold**

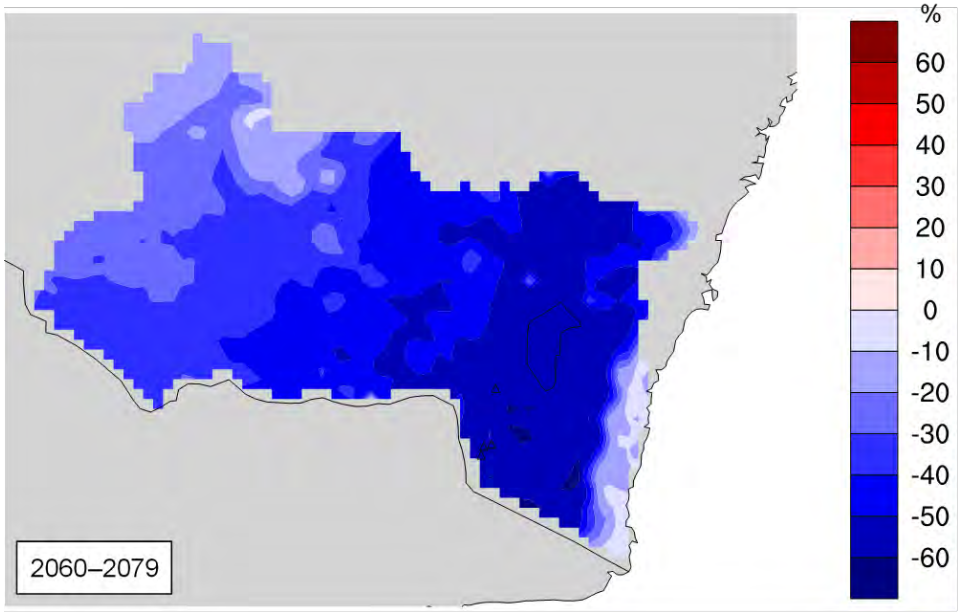


**Figure 15** **Changes in suitable snowmaking conditions (%) for 2060 to 2079 relative to the 1990 to 2009 baseline period for the –1°C threshold**

## 3.3 Snowmaking below 0.5°C

### Annual mean suitable snowmaking time

The annual mean suitable snowmaking hours for the baseline period and two future projection periods are presented in Figure 16. When compared with Figure 4, there is approximately 120% more suitable snowmaking time for the alpine and high elevation areas in the SET region. When snow can be made at an even higher wet bulb temperature (0.5°C), lower elevation areas surrounding the Alpine region have 200–400 hours a year suitable for making snow in the 1990 to 2009 baseline period.

There is a 400–600 hour a year decrease in suitable snowmaking condition projected for the Alpine region for 2020 to 2039 relative to 1990 to 2009. The greatest decrease is at the highest elevations. There are 800–1000 hours a year suitable for making snow for 2060 to 2079. This is within similar range of suitable snowmaking condition for 1990 to 2009 using –2°C as the threshold.

Similar to Figure 4, changes for 2060 to 2079 are much larger than that for 2020 to 2039. The largest decreases are observed at the highest elevations, and there are fewer hours for suitable snowmaking for lower elevation areas.

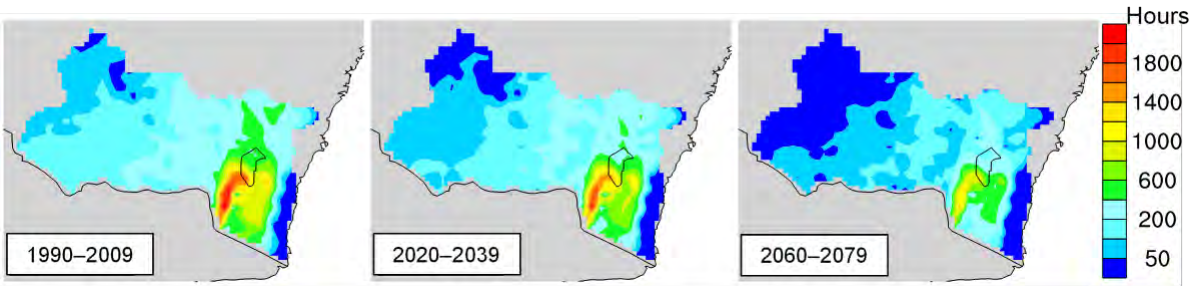


**Figure 16** **Suitable snowmaking conditions (in hours) for 1990 to 2009, 2020 to 2039 and 2060 to 2079 for the 0.5°C threshold**

### Inter-annual variability for ski resorts

When using a 0.5°C threshold, suitable snowmaking hours have similar inter-annual variability to those using a –2°C threshold (Figure 7); however, the magnitude of variability is much larger (Figure 17). Again, a decreasing trend can be observed for each ski resort for all three time periods. Differences between 2020 to 2039 and 1990 to 2009 are relatively small for each ski resort (~20%); however, those for 2060 to 2079 relative to 1990 to 2009 are about 50%.

### Monthly variation for ski resorts

Monthly variations of suitable snowmaking hours when using a 0.5°C threshold (Figure 18) are similar to that for using a –2°C threshold (Figure 8), for each ski resort and each time period; however, much more suitable snowmaking hours are available when using a 0.5°C threshold. Most of the extra available snowmaking hours are between June and August and the rest of the change is in the shoulder seasons.

The actual changes between different time periods are also large when using a 0.5°C threshold; however, the relative change is smaller when compared with using a –2°C and –1°C threshold. Again, the relative change is small for 2020 to 2039 (15–20%), and large for 2060 to 2079 (40–50%).

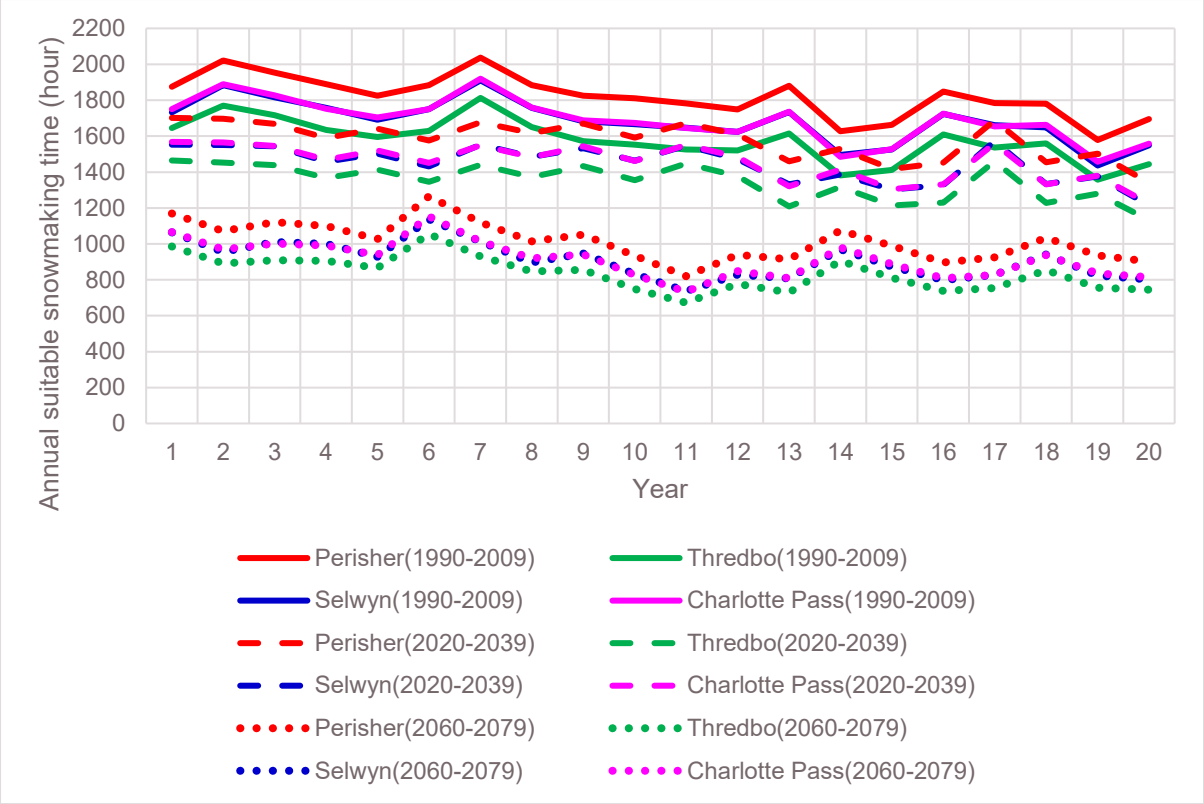


**Figure 17** **Inter-annual variability of suitable snowmaking time for four ski resorts for 1990 to 2009, 2020 to 2039 and 2060 to 2079 for the 0.5°C threshold**

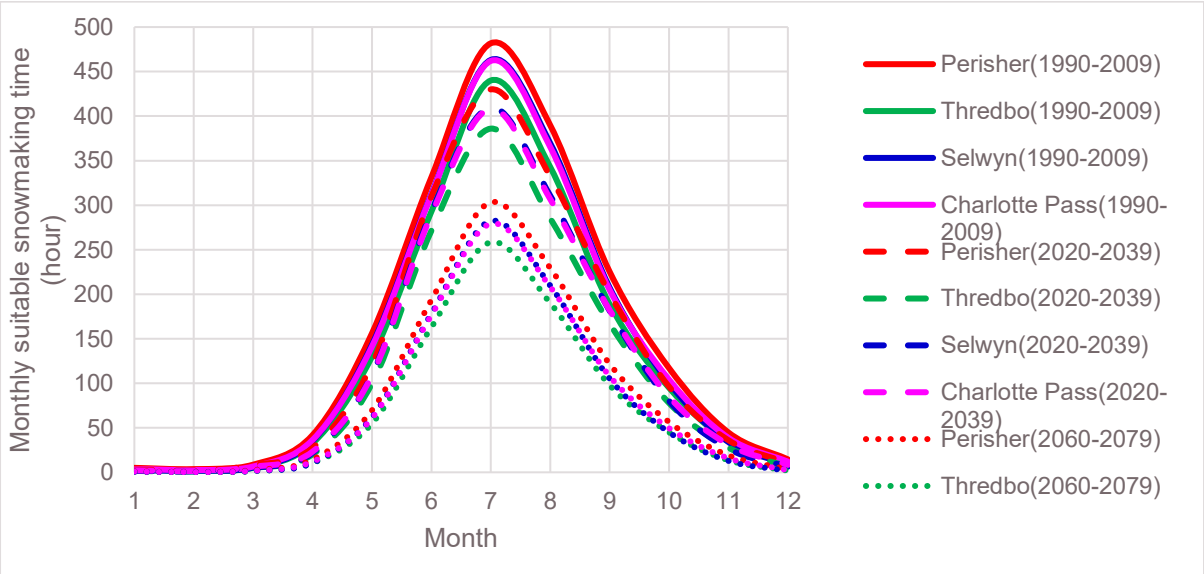


**Figure 18** **Monthly suitable snowmaking time for four ski resorts for 1990 to 2009, 2020 to 2039 and 2060 to 2079 for the 0.5°C threshold**

## Relative changes in annual suitable snowmaking conditions

The changes for 2020 to 2039 relative to 1990 to 2009 (Figure 19) are at similar ranges to those shown in Figure 9. The major changes are observed in the Alpine region and along high topography areas within SET, where 15–20% decreases are projected; however relatively smaller decrease (10–15%) for the mountain peaks in the Alpine region. Larger decreases (20–25%) are projected elsewhere, which is very different from those using a –2°C and –1°C threshold (see Figure 9 and Figure 14). This indicates that future climate change mostly impacts on snowmaking conditions not only for high topography areas but also for lower elevation areas.

Future changes in snowmaking conditions are much larger for the far future than near future. A 40–50% decrease is projected for the Alpine region, with 50–60% decreases projected in surrounding lower elevation areas and 40–50% for the MM region (Figure 20).

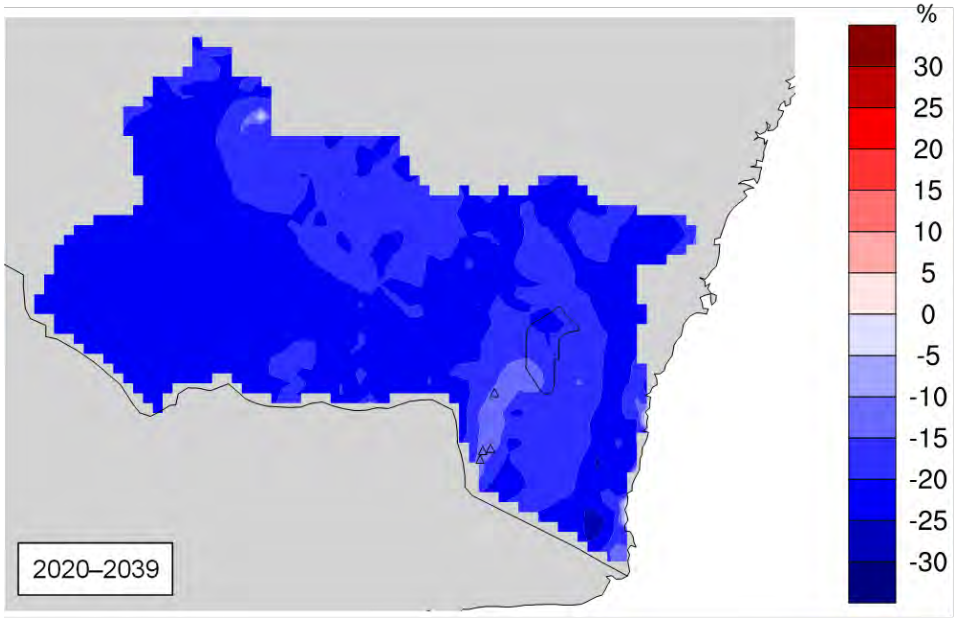


**Figure 19** **Changes in suitable snowmaking conditions (%) for 2020 to 2039 relative to the 1990 to 2009 baseline period for the 0.5°C threshold**

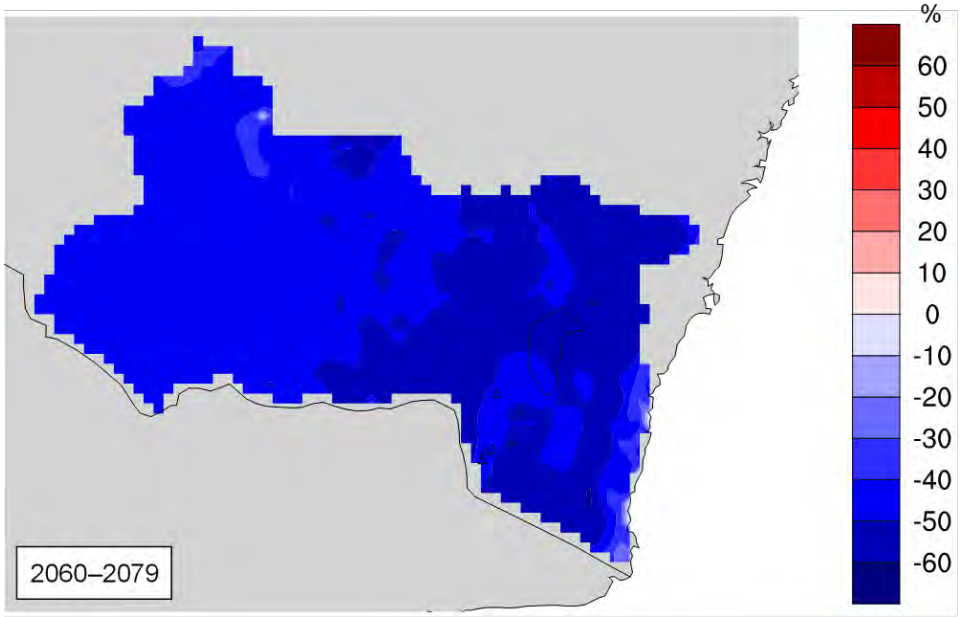


**Figure 20** **Changes in suitable snowmaking conditions (%) for 2060 to 2079 relative to the 1990 to 2009 baseline period for the 0.5°C threshold**

# 4. Discussion

## 4.1 Key findings

Suitable snowmaking conditions are sensitive to two key parameters: wet bulb temperature threshold and elevation. When snow can be made in a higher temperature environment (–1°C or 0.5°C), there is far more time suitable for snowmaking (note that cost of snowmaking and snow quality are not considered). The higher elevation ski resort generally has more time suitable for snowmaking. In addition, we find the following:

- There is a clear monthly variation in snowmaking conditions with peak values in July. Inter-annual variations in snowmaking conditions are correlated with mean temperature.
- There is an approximately 20% decrease in snowmaking conditions projected for 2020 to 2039 relative to 1990 to 2009, and a 50–60% decrease for 2060 to 2079 relative to 1990 to 2009.
- Larger absolute decreases in snowmaking conditions are projected for higher elevation areas, but larger relative decreases for lower elevation areas. Lower elevation locations might not be suitable for making snow in the future.
- Regardless of the threshold used, the future changes in suitable snowmaking hours are similar (around 20% and around 50% reduction for near and far futures).

## 4.2 Limitations and further research

The following factors influence the accuracy of the findings in Section 4.1.

Daily time-step NARCliM GCM/RCM projections (temperature, humidity, etc.) are at a spatial resolution of approximately 10 kilometres. This is considered rather coarse for the Alpine region where elevation might change a few hundred metres between neighbouring cells. As the suitable snowmaking conditions are very sensitive to the elevation, the inter-annual and monthly results are only for the specific locations of the four ski resorts. Some ski resorts might span a few hundred metres in elevation, and higher topography areas generally have more hours suitable for making snow.

In addition, there are large uncertainties between the 12 NARCliM ensemble members (Figure 6). This is understandable as GCMs selected in the NARCliM project were chosen based on criteria that include spanning the range of future changes in the GCM ensemble (Evans et al. 2014). For Australia, MIROC projects a slightly warmer and much wetter future, CCCMA projects an extremely warmer and slightly wetter future, CSIRO slightly warmer and drier, and ECHAM projects an extremely warmer and slightly drier future. The differences in temperature and humidity projected by the four GCMs result in diverse change in magnitude of suitable snowmaking conditions for four ‘same GCM used simulations’ shown in Figure 6. This is consistent with the findings from previous uncertainty studies, which suggest that the largest uncertainty in future projections is sourced from the GCMs (Chen et al. 2011; Vaze et al. 2011; Teng et al. 2012).

# 5. Conclusion

The NARCliM outputs are used in the study for calculating wet bulb temperature. Three wet bulb temperature thresholds (–2°C, –1°C and 0.5°C) were used to quantify suitable snowmaking hours for 1990 to 2009 (baseline), 2020 to 2039 (near future) and 2060 to 2079 (far future). Results for the multi-model mean, instead of each ensemble member, are presented in this study. The results show that:

- A more than 20% reduction of snowmaking conditions is projected for the near future, and a more than 60% reduction is projected for the far future.
- Larger absolute decreases in snowmaking conditions are projected for higher elevation areas but larger relative decreases are projected for lower elevation areas. In the future, lower elevation areas may not be suitable for snowmaking.
- If snow is made at warmer temperatures, opportunities for snowmaking may be maintained at current levels (–2°C wet bulb temperature) until 2020 to 2039 (–1°C wet bulb temperature), or until 2060 to 2079 if snow can be made at a 0.5°C wet bulb temperature. However, making snow at warmer temperatures may be associated with trade-offs in cost and quality of snow.
- The relative changes in snowmaking conditions are at a similar range for future periods when using different wet bulb temperature thresholds. Regardless of the threshold used, approximately 20% and 50% reductions are projected for the near and far future periods, respectively.

# 6. References

Bhend J, Bathols J and Hennessy K 2012, *Climate change impacts on snow in Victoria*, CSIRO report for the Victorian Department of Sustainability and Environment, publications.csiro.au/rpr/pub?list=SEA&pid=csiro:EP117309&sb=RECENT&expert=false&n=12&rpp=25&page=1&tr=425&q=Hennessy&dr=all.

Chen J, Brissette FP, Poulin A and Leconte R 2011, Overall uncertainty study of the hydrological impacts of climate change for a Canadian watershed, *Water Resources Research*, vol.47 W12509.

Davis CJ 2013, Towards the development of long-term winter records for the snowy mountains, *Australian Meteorological and Oceanographic Journal*, vol.63, no.2, pp.303–314.

Di Luca AJ, Evans P and Ji F 2016, *Australian Snowpack: NARCliM ensemble valuation, statistical correction and future projections*, NARCliM Technical Note 7, NARCliM Consortium, Sydney, Australia, 88pp.

Di Luca AJ, Evans P and Ji F 2018, Australian snowpack in the NARCliM ensemble: evaluation, bias correction and future projections, *Climate Dynamics*, vol.51, no.1–2, pp.639–666.

Evans JP, Ekstrom M and Ji F 2012, Evaluating the performance of a WRF physics ensemble over South-East Australia, *Climate Dynamics*, vol.39, no.6, pp.1241–1258.

Evans JP, Ji F, Abramowitz G, Ekstrom M 2013a, Optimally choosing small ensemble members to produce robust climate simulations, *Environmental Research Letters*, vol.8.

Evans JP, Fita L, Argüeso D and Liu Y 2013b, Initial NARCliM evaluation, in Piantadosi J, Anderssen RS and Boland J (eds), *MODSIM2013, 20th International Congress on Modelling and Simulation*, Modelling and Simulation Society of Australia and New Zealand, December 2013, pp.2765–2771.

Evans J, Ji F, Lee C, Smith P, Argüeso D and Fita L 2014, Design of a regional climate modelling projection ensemble experiment–NARCliM, *Geoscientific Model Development,* vol.7, pp.621–629.

Fiddes SL, Pezza AB and Barras V 2015, A new perspective on Australian snow, *Atmospheric Science Letters*, vol.16, no.3, pp.246–252.

Fita L, Evans JP, Argüeso D, King AD and Liu Y 2016, Evaluation of the regional climate response to large-scale modes in the historical NARCliM simulations, *Climate Dynamics*, pp.1–15, doi: 10.1007/s00382-016-3484-x.

Harris RMB, Remenyi T and Bindoff NL 2016, *The potential impacts of climate change on Victoria Alpine Resorts*, a report for the Alpine Resorts Co-ordinating Council, Antarctic Climate and Ecosystems Cooperative Research Centre, Hobart TAS.

Hennessy KJ, Whetton PH, Walsh K, Smith IN, Bathols JM, Hutchinson M and Sharples J 2008, Climate change effects on snow conditions in mainland Australia and adaptation at ski resorts through snowmaking, *Climate Research*, vol.35, no.3, pp.255–270.

IPCC 2000, *Special Report on Emissions Scenarios: A Special Report of Working Group III of the Intergovernmental Panel on Climate Change*, published for the Intergovernmental Panel on Climate Change by Cambridge University Press, Cambridge, UK.

Ji F, Ekstrom M, Evans JP and Teng J 2014, Evaluating rainfall patterns using physics scheme ensembles from a regional atmospheric model, *Theoretical and Applied Climatology*, vol.115, pp.297–304.

Ji F, Evans JP, Teng J, Scorgie Y, Argüeso D and Di Luca A 2016, Evaluation of long-term precipitation and temperature WRF simulations for southeast Australia, *Climate Research*, vol.67, pp.99–115, DOI 10.3354/cr01366.

Nicholls N 2005, Climate variability, climate change and the Australian snow season, *Australian Meteorological Magazine*, vol.54, no.3, pp 177–185.

NIEIR (National Institute of Economic and Industry Research) 2006, *The economic significance of the Australian alpine resorts – summary report*, Alpine Resorts Co-ordinating Council.

OEH 2013, *Scientific Rigour Position Statement*, NSW Office of Environment and Heritage, www.environment.nsw.gov.au/-/media/OEH/Corporate-Site/Documents/Research/Our-science-and-research/oeh-scientific-rigour-position-statement-2013.pdf.

Pickering C 2007, 'Climate change and other threats in the Australian Alps', in M Taylor and P Figgis (eds): *Protected Areas: buffering nature against climate change*, WWF-Australia, Sydney, pp.28–34.

Ruddell AR, Budd WF, Smith IN, Keage PL and Jones R 1990, *The south east Australian alpine climate study*, a report by the Meteorology Department, University of Melbourne for the Alpine Resorts Commission.

Skamarock WC, Klemp JB, Dudhia J, Gill DO, Barker DM, Duda MG, Huang XY, Wang W and Powers JG 2008, *A description of the advanced research WRF Version 3,* NCAR Technical Note, National Center for Atmospheric Research, Boulder Colorado, USA.

Slatyer R 2010, Climate change impacts on Australia's alpine ecosystems, *The ANU Undergraduate Research Journal*, vol.2.

Teng J, Vaze J, Chiew FHS, Wang B, Perraud J-M 2012, Estimating the relative uncertainties sourced from GCMs and hydrological models in modeling climate change impact on runoff, *Journal of Hydrometeorology*, vol.13, no.1, pp.122–139.

Timbal B, Ekstrom M, Fiddes SL, Grose M, Kirono DGC, Lim E, Lucas C and Wilson L 2016, *Climate change science and Victoria*, Bureau Research Report No. 14, 92pp.

Vaze J, Teng J and Chiew FHS 2011, Assessment of GCM simulations of annual and seasonal rainfall and daily rainfall distribution across south-east Australia, *Hydrological Processes*, vol.25, no.9, pp.1486–1497.

Whetton PH, Haylock MR and Galloway R 1996, Climate change and snow-cover duration in the Australian Alps, *Climatic Change*, vol.32, no.4, pp.447–479.

DOCUMENT 20

DEPARTMENT OF PLANNING, INDUSTRY & ENVIRONMENT

# Climate change impacts in the NSW and ACT Alpine region

## Impacts of extreme rainfall on soil erosivity and hillslope erosion

environment.nsw.gov.au

Cover photo: Winter landscape in Kosciuszko National Park. John Spencer/DPIE

This report should be cited as:

Zhu EQ and Yang X 2019, *Climate change impacts in the NSW and ACT Alpine region: Impacts of extreme rainfall on soil erosivity and hillslope erosion*, NSW Department of Planning, Industry and Environment, Sydney, Australia.

Published by:

Environment, Energy and Science
Department of Planning, Industry and Environment
59 Goulburn Street, Sydney NSW 2000
PO Box A290, Sydney South NSW 1232
Phone: +61 2 9995 5000 (switchboard)
Phone: 1300 361 967 (Environment, Energy and Science enquiries)
TTY users: phone 133 677, then ask for 1300 361 967
Speak and listen users: phone 1300 555 727, then ask for 1300 361 967
Email: info@environment.nsw.gov.au
Website: www.environment.nsw.gov.au

Report pollution and environmental incidents
Environment Line: 131 555 (NSW only) or info@environment.nsw.gov.au
See also www.environment.nsw.gov.au

ISBN 978 1 922318 16 9
EES 2020/0021
January 2020

**Find out more about your environment at:**

**www.environment.nsw.gov.au**

# Contents



# List of tables

# List of figures

# List of shortened forms

| | |
|---|---|
| ACT | Australian Capital Territory |
| BoM | Australian Bureau of Meteorology |
| CSIRO | Commonwealth Scientific and Industrial Research Organisation |
| DEM | Digital Elevation Model |
| DJF | December January February |
| DPIE | Department of Planning, Industry and Environment |
| ERIs | extreme rainfall indices |
| GCM | Global Climate Model |
| GIS | geographic information system |
| JJA | June July August |
| LS | slope-steepness factor |
| MAM | March April May |
| MCAS-S | Multi-Criteria Analysis Shell for Spatial Decision Support |
| MLR | multiple linear regression |
| MM | Murray-Murrumbidgee state planning region |
| NARCliM | NSW/ACT Regional Climate Modelling project |
| NSW | New South Wales |
| OEH | Office of Environment and Heritage |
| RCM | Regional Climate Model |
| RR | daily precipitation on a specified day |
| RUSLE | revised universal soil loss equation |
| SET | Southeast and Tablelands state planning region |
| SON | September October November |
| SRTM | Shuttle Radar Topography Mission |

# Summary of findings

## Impacts of extreme rainfall on soil erosivity and hillslope erosion

1. Extreme rainfall impacts erosivity and hillslope erosion.
2. Extreme rainfall indices can be used to predict potential high-risk areas of rainfall erosivity and hillslope erosion. There is a good linear relationship between the 5-day maximum precipitation index (Rx5Day) and rainfall erosivity ($R^2 > 0.81$).
3. A snowmelt adjusted erosivity model and snow cover data have been applied in the Alpine region.
4. Rainfall erosivity and hillslope erosion in the NSW Alpine region are projected to increase by 2–8% in the near future (2020 to 2039), and 8–18% in the far future (2060 to 2079), even if the groundcover is maintained at the current level.
5. The change in rainfall erosivity and erosion risk is highly uneven in both location and season. Summer is projected to have the highest erosion risk with an increase of about 25% in the next 20 to 50 years.
6. The highest erosion risk area within the study area is projected to be in the South East and Tablelands (SET, maximum rate: 19.95 t $ha^{-1}$ $yr^{-1}$), but on average, the ACT has the highest erosion rate, which is above 1.3 tonnes per hectare per year in all periods. The maximum rainfall erosivity in the region is projected to be in SET with 1233.87 megajoule millimetres per hectare per hour per year in the far future.
7. The impact of snowmelt on rainfall erosivity and erosion needs to be considered in the Alpine region in both the baseline and near future periods. The snowmelt in spring can increase the erosivity by about 13–24% in the Alpine area; however, with the projected temperature rise and projected decreases in snow cover, the snowmelt impact on erosivity and erosion can largely be ignored in the far future.

# 1. Introduction

## 1.1 Background

The New South Wales (NSW) and Australian Capital Territory (ACT) Alpine region is located in the south-eastern corner of mainland Australia and is the highest mountain range in Australia. Though it comprises only about 0.16% of Australia in size, it is an important region for ecosystems, biodiversity, energy generation and winter tourism. It forms the southern end of the Great Dividing Range, covering a total area of 1.64 million hectares that extend over 500 kilometres. The highest peak, Mount Kosciuszko, rises to an altitude of 2228 metres.

This report is part of a larger project delivered by the NSW Department of Planning, Industry and Environment on the various impacts from climate change on the NSW and ACT Alpine region, hereafter referred to as the Alpine region. The full study region covers the Murray-Murrumbidgee region (MM), South East and Tablelands (SET) and the ACT, bordering the Victorian border in the south (Figure 1).

The Alpine region is vulnerable to climate change. Observations have shown substantial changes in precipitation and temperature for this area (Di Luca et al. 2018), which have already impacted biodiversity and ecosystems (Hughes 2011). In 2014, the NSW/ACT Regional Climate Modelling (NARCliM) project was delivered. Climate snapshots for each of the 11 NSW planning regions and the ACT were developed to demonstrate observed and projected climate change; however, the snapshots only show changes for some variables and focus on each planning region.

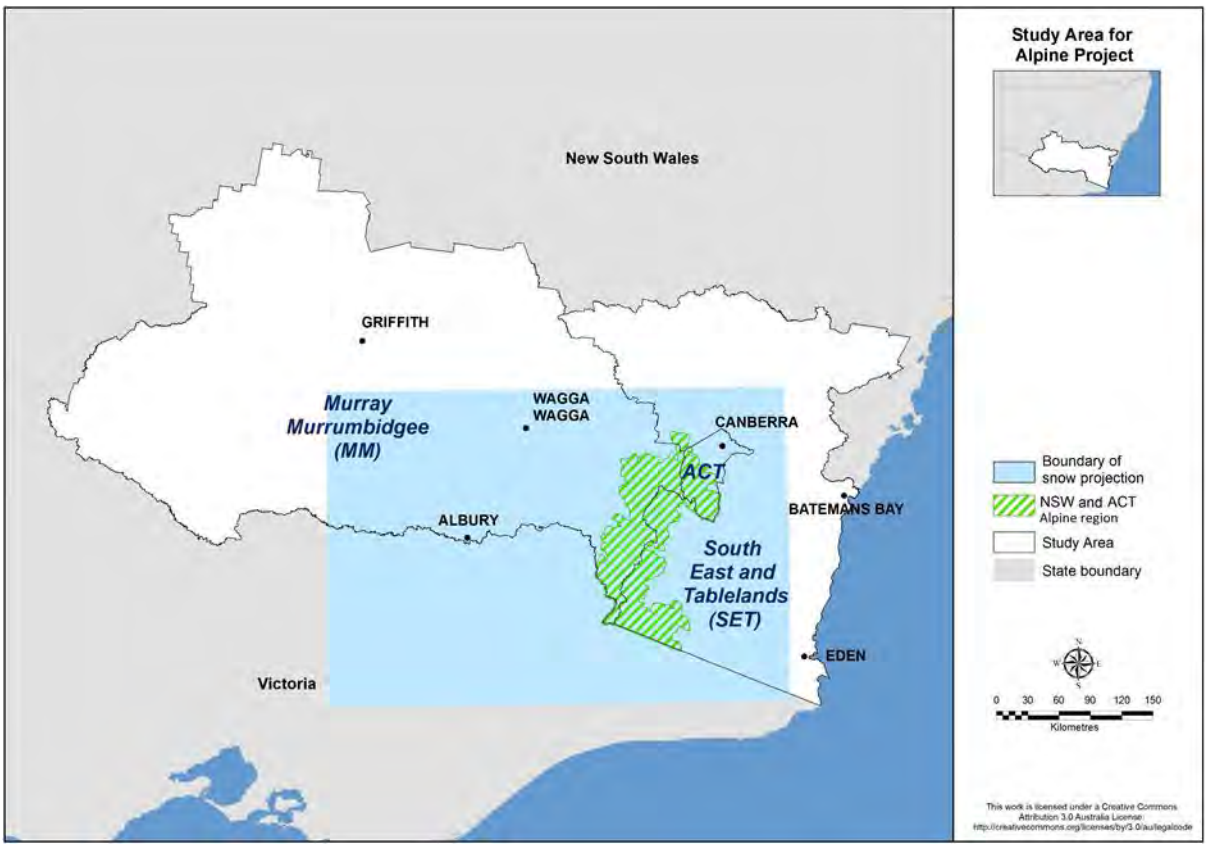


**Figure 1** **The domain of the snow projections, the NSW and ACT Alpine region and the boundaries of the state planning regions within the study area in NSW**

## 1.2 Objectives

Climate extremes have attracted global attention in recent decades because they are often more important to natural and human systems than the mean values of climate variables (Cruse et al. 2006). Research on rainfall extremes reports significant changes in percentiles and frequency of extreme events, and the magnitude and sign of the changes varies with season and region (Alexander et al. 2007; CSIRO & BoM 2015). Hillslope erosion rates may be expected to change in response to changes in climate; for example, change in the erosive power of rainfall (e.g. Nearing et al. 2004). Hillslope erosion occurs mostly during severe storms or extreme events. Large and erosive storms are more variable than annual rainfall totals. Trends and changes in erosive storms or rainfall extremes are therefore much more important but also difficult to detect, when compared with rainfall totals.

The downscaled 10 kilometre rainfall projections from NARCliM (Evans et al. 2014a) have become available for this project for a baseline period (1990 to 2009), near future period (2020 to 2039) and far future period (2060 to 2079). The NARCliM projected rainfall and snow in these three periods and 12 ensembles (four Global Climate Models (GCMs) and three Regional Climate Models (RCMs)) (Evans et al. 2014a) were used to calculate extreme rainfall indices (ERIs). The indices in the baseline period (1990 to 2009) were compared to those calculated from rainfall data from the Bureau of Meteorology (BoM).

The objectives of this study were to: i) model and predict the changes in rainfall extremes and the impacts on hillslope erosion risk across the Alpine region based on the NARCliM projections; and ii) predict locations and times with high erosion risk across the study area. Outcomes from this study include: i) maps of six ERIs; ii) time-series hillslope erosion risk maps; iii) impact assessment of extreme rainfall on hillslope erosion; iv) reports; and v) spatial data layers in a geographic information system (GIS). These outcomes will assist long-term climate change adaptation and regional planning in the Alpine region.

In this study, we examined the relationship between ERI and rainfall erosivity across the study area. This relationship was used as an approximation of rainfall erosivity and compared with estimates from the previous studies (Yang & Yu 2015; Yang et al. 2016). The projected rainfall erosivity was used to estimate hillslope erosion based on the revised universal soil loss equation (RUSLE) along with the slope-steepness factor and the soil erodibility factor (Renard et al. 1997). Rainfall erosivity was calibrated using the snowmelt runoff in spring (September, October and November – SON). Time-series (monthly and annual) rainfall extremes and erosion risk for the study area for each of the 20-year periods have been produced and spatially interpolated to a high spatial resolution of 100 metres in GIS using a spline interpolation method.

Statistical tests were used to quantify the spatial and temporal changes in rainfall extremes and the impacts on hillslope erosion across the study area and its subregions. The time-series maps for each of the 20-year periods were used to identify the high erosion risk seasons and areas. Automated GIS scripts were developed to calculate the time-series rainfall erosivity and hillslope erosion so the processes of large quantity NARCliM data are realistic, repeatable and portable.

## 1.3 Outputs

| Output | Details | Key user |
|---|---|---|
| Report | Impact assessment of extreme rainfall on hillslope erosion | Researchers |
| Data (GIS layers) | Extreme rainfall indices (six)<br>Monthly and annual rainfall erosivity and hillslope erosion risk maps for all three periods (60 years)<br>Seasonal and annual rainfall erosivity and erosion change (%) in the near future and far future | NSW National Parks & Wildlife Service |
| Maps | Map layouts of the above data (in JPEG and GeoTiff) | Councils, etc. |

# 2. Method

## 2.1 Source of data

NARCliM simulations from four Coupled Model Intercomparison Project phase 3 (CMIP3) Global Climate Models (GCMs) were used to drive three Regional Climate Models (RCMs) to form a 12-member GCM/RCM ensemble (Evans et al. 2014a). The four selected GCMs are MIROC3.2, ECHAM5, CCCMA3.1 and CSIRO-MK3.0. For future projections, the Special Report on Emissions Scenarios (SRES) business-as-usual A2 scenario was used (IPCC 2000). The three selected RCMs are three physics scheme combinations of the Weather Research and Forecasting (WRF) model. Each simulation consists of three 20-year runs (1990 to 2009, 2020 to 2039, and 2060 to 2079). The four GCMs were chosen based on a number of criteria: i) adequate performance when simulating historic climate; ii) most independent; iii) cover the largest range of plausible future precipitation and temperature changes for Australia. The three RCMs correspond to three different physics scheme combinations of the WRF V3.3 model (Skamarock et al. 2008), which were also chosen for adequate skill and error independence, following a comprehensive analysis of 36 different combinations of physics parameterisations over eight significant East Coast Lows (ECLs) (Evans et al. 2012; Ji et al. 2014). For the selected three RCMs, the WRF Double Moment 5-class (WDM5) microphysics scheme and NOAH land surface scheme are used in all cases. Refer to Evans et al. (2014a) for more details on each physics scheme.

We acknowledge that the results are model dependent (as all model studies are) but through the use of this carefully selected ensemble we have attempted to minimise this dependence. By using this model selection process, we have shown that it is possible to create relatively small ensembles that are able to reproduce the ensemble mean and variance from the large parent ensemble (i.e. the many GCMs) as well as minimise the overall error (Evans et al. 2013a).

Some initial evaluation of NARCliM simulations shows that they have strong skill in simulating the precipitation and temperature of Australia, with a small cold bias and overestimation of precipitation on the Great Dividing Range (Evans et al. 2013b; Ji et al. 2016). The differing responses of the different RCMs confirm the utility of considering model independence when choosing the RCMs. The RCM response to large-scale modes of variability also agrees well with observations (Fita et al. 2016). Through these evaluations we found that while there is a spread in model projections, all models perform adequately with no single model performing the best for all variables and metrics. The use of the full ensemble provides a measure of robustness such that any result that is common through all models in the ensemble is considered to have higher confidence.

This study uses the bias-corrected rainfall extremes projections with a spatial resolution of 10 kilometres (Evans et al. 2017) from NARCliM to estimate the future rainfall erosivity in the Alpine region. Snow projection and daily mean temperature products from NARCliM were obtained from the Department of Planning, Industry and Environment (DPIE) and University of New South Wales (UNSW) at a 10 kilometre spatial resolution. Snow depth and density simulation for the 60 years were extracted from the snow projections and used to estimate and adjust the snowmelt runoff (Bormann et al. 2014) and rainfall erosivity during the melting season (i.e. spring). For adjustment of erosivity in spring we only used the projections from MIROC3.2_R2, as it is regarded as the best model ensemble for capturing daily precipitation compared to R1 and R3 (Ji et al. 2016).

Soil property projections for New South Wales (soil organic carbon) were obtained from DPIE (Gray & Bishop 2017) and used to calculate soil erodibility based on Yang et al. (2017). Other input data include soil texture from the Soil and Landscape Grid of Australia (Grundy et al. 2015) at a spatial resolution of 3 arc seconds (about 90 m), the 30 metre

Digital Elevation Model (DEM) (Shuttle Radar Topography Mission, SRTM), and the latest satellite-derived fractional vegetation cover (Version 3.0.2) at a spatial resolution of 500 metres and on a monthly basis since 2000 (Guerschman et al. 2009).

## The extreme rainfall indices (ERIs)

Various ERIs were calculated from the NARCliM projections (Evans et al. 2014b) (Table 1). These ERIs represent annual accumulated precipitation (e.g. R95p and R99p), count days with extreme rainfall depth (e.g. R20mm and Rnnmm), and illustrate monthly rainfall variation (e.g. Rx1day and Rx5day).

Six ERIs (R20mm, Rnnmm, R95p, R99p, Rx1day and Rx5day) were selected to compare and assess their relationships with rainfall erosivity for each ensemble and period. These six indices were chosen because they are common and representative in time-steps. Note that only Rx1day and Rx5day are defined on a monthly basis, while all the other indices are defined on an annual basis; therefore, only Rx1day and Rx5day were applied to examine the seasonal rainfall extremes and their relationships with the rainfall erosivity and erosion rates.

**Table 1 The selected six extreme rainfall indices and their definitions**

| ERI | Description | Unit |
|---|---|---|
| R20mm | Annual counts of days with rainfall above 20 mm. Count the days where: $RR_{ij} \geq 20$ mm | days |
| Rnnmm | Annual counts of days with rainfall above 25 mm. Count the days where: $RR_{ij} \geq 25$ mm | days |
| Rx1day (monthly) | Daily maximum 1-day precipitation. $Rx1day_j = \max(RR_{ij})$ | mm |
| Rx5day (monthly)<br>Rx5day_y (annually) | Maximum 5-day accumulated precipitation (annual and monthly). Let $RR_{kj}$ be the precipitation amount for the 5-day interval ending $_k$ period $_j$. $Rx5day_j = \max(RR_{kj})$ | mm |
| R95p | Accumulated precipitation from events above the 95th percentile. Let $RR_{wj}$ be the daily precipitation amount on a wet day w (RR ≥ 1.0 mm) in period I and let $RR_{wn}95$ be the 95th percentile of precipitation on wet days in the period. If W represents the number of wet days in the period, then: $R95p_j = \sum_{w=1}^{w} RR_{wj}$ where $RR_{wj} > RR_{wn}95$ | mm |
| R99p | Accumulated precipitation from events above the 99th percentile. Let $RR_{wj}$ be the daily precipitation amount on a wet day w (RR ≥ 1.0 mm) in period I and let $RR_{wn}99$ be the 99th percentile of precipitation on wet days in the period. If W represents the number of wet days in the period, then: $R99p_j = \sum_{w=1}^{w} RR_{wj}$ where $RR_{wj} > RR_{wn}99$ | mm |

Note: Let $RR_{ij}$ be the daily precipitation amount on day i in period j

## Rainfall erosivity

The rainfall erosivity model (equation (1), based on Yang et al. 2016):

$$\hat{E}_j = \alpha[1 + \eta\cos(2\pi fj - \omega)]\sum_{d=1}^{N} R_d^{\beta} \quad (1)$$

where the rainfall erosivity (E) for month j is estimated from the daily rainfall amount $R_d$ (mm day$^{-1}$); N represents the number of rain days in the month; $\alpha, \beta, \eta$ and $\omega$ are the model parameters. More information about the parameters and model is presented in Yang et al. (2016).

Snowfall in the Alpine region is common; however, it was neglected in previous studies (Yang & Yu 2015; Yang et al. 2016). It is believed that the exclusion of snowmelt in erosion modelling would result in underestimation of rainfall erosivity and erosion, particularly in the Alpine region and its surrounding areas. Studies of the impact of snowmelt on erosion have been conducted in other parts of the world; for example, Switzerland (Meusburger et al. 2014), Canada (Hayhoe et al. 1995) and Germany (Ollesch et al. 2006), but such research has not yet been done in Australia.

In this study, snowmelt was considered in simulating and calibrating the rainfall erosivity across the Alpine region in spring. The daily snowmelt was estimated from the models described in Bormann et al. (2014) and Rango and Martinec (1995):

$$Mp = k \cdot \frac{\rho_s}{\rho_w} \cdot (T_{mean} - T_{ref}) \quad (2)$$

where $Mp$ is potential snowmelt (mm day$^{-1}$), $\rho_s$ is snow density (g cm$^{-3}$) simulated based on multiple linear regression (MLR) and climate variables, $\rho_w$ is water density (assumed to be 1 g cm$^{-3}$), $T_{mean}$ refers to the daily mean temperature and $T_{ref}$ is set to 0°C. The calculation of rainfall erosivity was adjusted by adding the snowmelt to the rainfall density using the daily rainfall erosivity model as presented in Yang et al. (2016) and equation (1) is rewritten as:

$$\hat{E}_j = \alpha[1 + \eta \cos(2\pi \mathrm{fj} - \omega)] \sum_{d=1}^{N} (R_d + Mp)^{\beta} \quad (3)$$

The daily rainfall amount $R_d$ was calculated from the bias-corrected daily rainfall projections of all the 12 NARCliM ensembles; however, the snowmelt was only derived from the MIROC3.2_R2 as this model ensemble is more trustworthy in reproducing precipitation compare to R1 and R3 in terms of daily scale (Ji et al. 2016), while the performance of the four GCMs are similar.

Once the rainfall erosivity is estimated, the hillslope erosion can be calculated using RUSLE along with other factors, the slope-steepness factor (LS), groundcover (C) and the soil erodibility (K) (Renard et al. 1997):

$$A = R \acute{} K \acute{} LS \acute{} C \acute{} P \quad (4)$$

where A is the predicted soil loss (t ha$^{-1}$ yr$^{-1}$), R is rainfall erosivity (MJ mm ha$^{-1}$ hr$^{-1}$ yr$^{-1}$) as described above, K is the soil erodibility factor (t ha hr ha$^{-1}$ MJ$^{-1}$ mm$^{-1}$), LS represents the slope and steepness factor (unitless) estimated from DEM, and C is the cover and management (C) factor (unitless). The erosion control (P) factor (unitless) is not considered in this work.

The K factor was estimated based on Yang et al. (2017) using the recent digital soil maps and soil property projections including soil texture and organic matter (Grundy et al. 2015; Gray et al. 2016). The LS-factor was calculated from the 30 metre DEM (SRTM) based on a comprehensive method as described in Yang (2015). The C factor was estimated on a monthly basis and updated from the latest satellite-derived fractional vegetation cover (Version 3.0.2) (Guerschman et al. 2009) based on methods described in Yang (2014). The C factor was adjusted with snow cover in winter months (June, July, August – JJA) based on a snow mask prepared from the snow depth projection, and a specific value (0.0044) was assigned to the areas covered by snow.

Adequate random points (> 5000 for the entire study area and 1550 for the Alpine region) were used to sample ERI, rainfall erosivity and hillslope erosion rates for the baseline (1990 to 2009), near future (2020 to 2039) and far future (2060 to 2079) periods. These randomly sampled data were used for statistical analyses and identification of the relationship between rainfall extremes, erosivity and erosion.

Model performance is measured by the coefficient of efficiency, $E_c$ (Nash & Sutcliffe 1970) as it is commonly used to assess model performance in hydrology and soil sciences (Loague & Freeze 1985; Risse et al. 1993):

$$E_c = 1 - \sum_{i=1}^{M}(y_i - \hat{y})^2 / \sum_{i=1}^{M}(y_i - \bar{y})^2 \quad (5)$$

where $y_i$ are observed values while $\hat{y}$ are modelled values; $\bar{y}$ is the average of observed values, and M represented the sample size. Essentially, $E_c$ is an indicator of how close the scatters of predicted versus actual values are to the 1:1 line (Yang & Yu 2015).

## 2.2 Quality control

We used RUSLE to estimate rainfall erosivity and hillslope erosion. All RUSLE factors were estimated based on the well-established and published methods as described in Section 2.1. All input data sets are published and come with a quality indicator.

The report was reviewed by internal and external reviewers, and followed the procedures as set out in DPIE's Scientific Rigour Position Statement (OEH 2013).

## 2.3 Data storage and access

All output data (time-series rainfall erosivity and erosion) were converted to raster format (ArcGIS ESRI grid) and supplied to the MCAS-S (Multi-Criteria Analysis Shell for Spatial Decision Support) datapacks for distribution and storage. All input data to the model and by-products are stored on hard disk drives. All data are in a coordinate system of GCS WGS84 at 0.001 degree (about 100 m). The extent of the datasets includes the MM region, ACT and SET with the boundary at top: –32.671254, left: 143.317445, right: 150.745676, and bottom: –37.505077.

To meet the naming limitation of ArcGIS we used a simple and short naming approach; for example, 'ero_2038' represents the projected mean hillslope erosion in 2038 from all model ensembles; and 'r_2038' represents the projected mean erosivity in 2038 from all model ensembles. Rather than use long file names with many repeating or redundant characters (such as previously used in the NARCliM project), we prefer short file names under well-structured folders (e.g. Alpine\erosion\2020_39\annual\ero_2038).

# 3. Results

## 3.1 Correlation between extreme rainfall indices and rainfall erosivity

Six ERI maps have been prepared for the study area, for the baseline (1990 to 2009), near future (2020 to 2039) and far future (2060 to 2079) periods. The impacts of ERIs on rainfall erosivity and erosion were assessed and compared using 5000 random points within the region. The relationship between the ERIs and the corresponding rainfall erosivity for each period is shown in Figure 2. Six ERIs at the annual step were compared to examine their correlation with rainfall erosivity (Figure 2a). Rx5day (annual step) is the most effective index; it has stronger correlation with rainfall erosivity for the baseline ($R^2$=0.841), near future ($R^2$=0.842) and far future ($R^2$=0.827) periods.

The impact of the corresponding ERIs on hillslope erosion (correlation < 0.3) is much less compared to that of rainfall erosivity (Figure 2b), since hillslope erosion is related to factors such as groundcover, soil property, slope steepness and length, but rainfall erosivity is predominately related to rainfall duration and intensity.

Both ERIs (Rx1day, Rx5day) have higher correlations with rainfall erosivity in summer (DJF) compared with other seasons (Table 2), possibly due to greater rainfall and higher intensity in summer. The projection in winter (JJA) and autumn (March, April, May – MAM) is less accurate ($R^2$ and $E_c$ around 0.7). Rx5day has a slightly higher seasonal correlation with erosivity (and therefore erosion) than Rx1day in all periods (Table 2). On an annual basis,

the correlation between the mean annual erosivity (from all 12 ensembles) and Rx5day is stronger ($R^2$ = 0.813) and higher than any other ERI (Figure 3). Thus, Rx5day was selected to predict the erosivity and seasonal variation in this study.

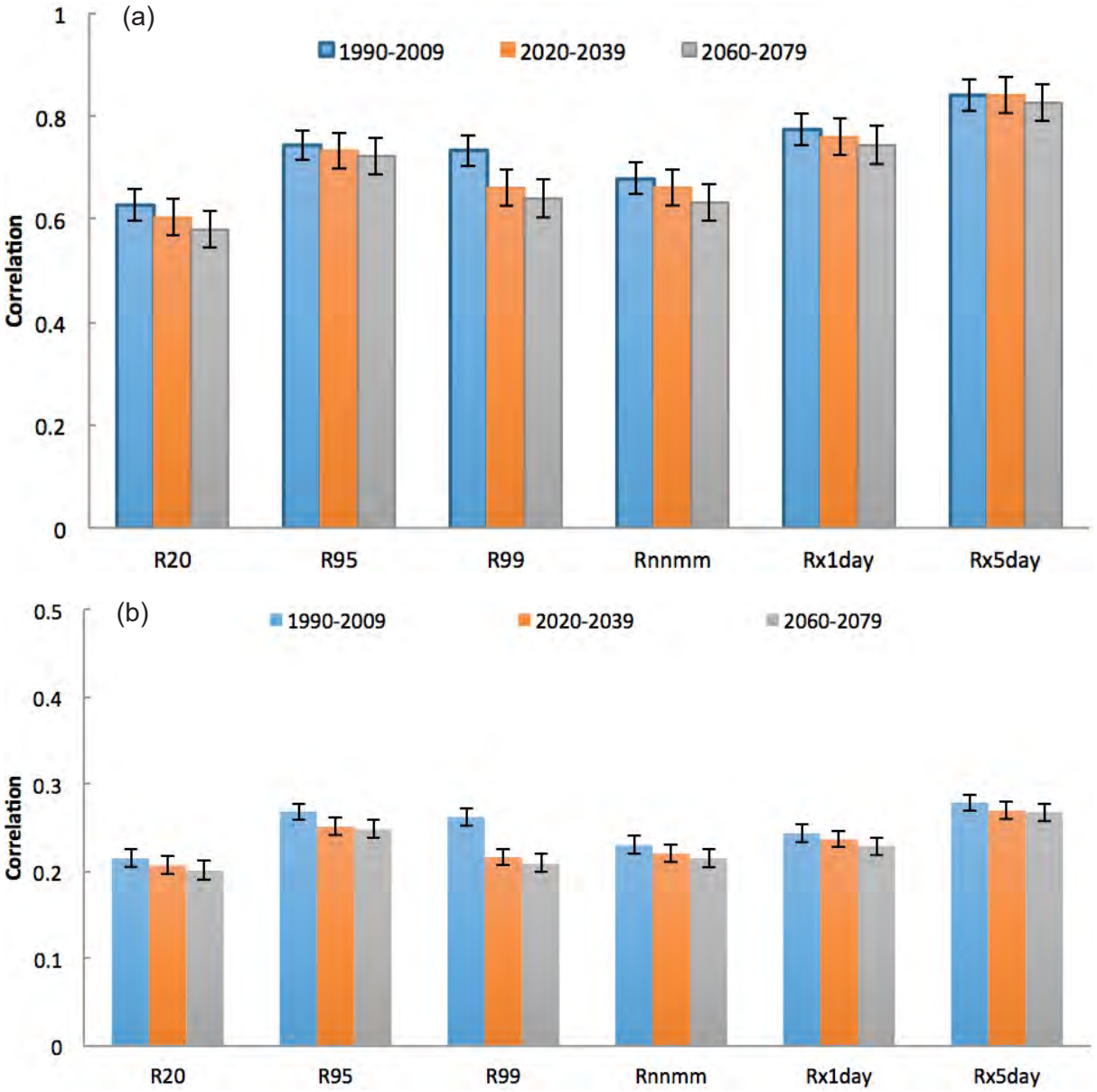


**Figure 2** **Correlation coefficients between different extreme rainfall indices (refer to Table 1) and rainfall erosivity (a) and erosion (b) for the baseline period (1990 to 2009), near future (2020 to 2039) and far future (2060 to 2079)**

**Table 2** **Seasonal comparison between extreme rainfall indices, Rx1day and Rx5day, and their correlation with rainfall erosivity**

| Correlation between ERI and erosivity | Baseline (1990 to 2009) | | Near future (2020 to 2039) | | Far future (2060 to 2079) | |
|---|---|---|---|---|---|---|
| | Rx1day | Rx5day | Rx1day | Rx5day | Rx1day | Rx5day |
| DJF (summer) | 0.790 | 0.819 | 0.779 | 0.798 | 0.789 | 0.803 |
| MAM (autumn) | 0.725 | 0.766 | 0.701 | 0.750 | 0.672 | 0.715 |
| JJA (winter) | 0.790 | 0.802 | 0.783 | 0.801 | 0.758 | 0.778 |
| SON (spring) | 0.793 | 0.794 | 0.778 | 0.767 | 0.757 | 0.764 |

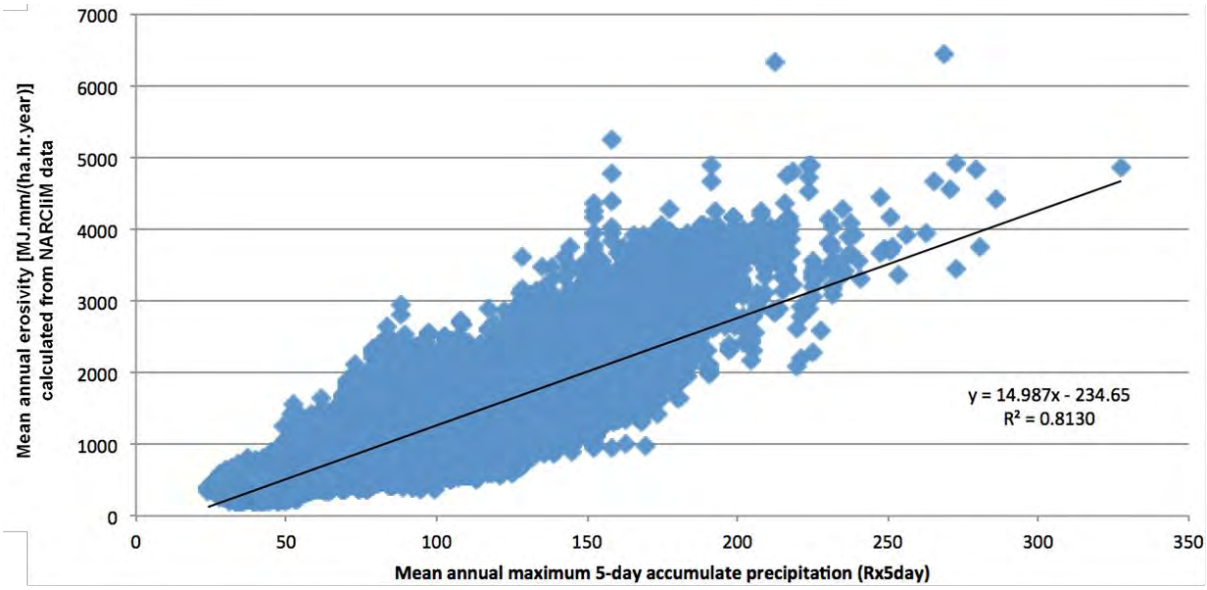


**Figure 3** **Relationship between mean annual erosivity and Rx5day index**

## 3.2 Annual and seasonal rainfall erosivity

There is large spatial and seasonal variation in rainfall erosivity in the two projection periods across the Alpine region (Table 3, Figure 4). The SET region is projected to have higher rainfall erosivity in both near future and far futures (1121 and 1234 MJ mm $ha^{-1}$ $hr^{-1}$ $yr^{-1}$ respectively) though ACT has a slightly higher mean annual rainfall erosivity in the baseline period (1133 MJ mm $ha^{-1}$ $hr^{-1}$ $yr^{-1}$). SET is estimated to be at a higher risk in summer and autumn in the future. The ACT is projected to have higher rainfall erosivity in winter and spring, although still less than that from the Alpine region (Table 3). Like the Rx5day projected erosivity, summer is believed to be the season with highest rainfall erosivity, while winter always has the least across the study area in all three time periods. Moreover, the risk of rainfall erosivity generally tends to increase in both mean annual value and seasonal estimation across the study area.

**Table 3** **Annual and seasonal mean values of rainfall erosivity in the baseline, near future and far future periods across the study area**

| | Baseline (1990 to 2009) | | | | | Near Future (2020 to 2039) | | | | | Far Future (2060 to 2079) | | | | |
|---|---|---|---|---|---|---|---|---|---|---|---|---|---|---|---|
| Rainfall erosivity | MM | SET | ACT | Study area | Alpine | MM | SET | ACT | Study area | Alpine | MM | SET | ACT | Study area | Alpine |
| DJF | 249 | 504 | 503 | 334 | 326 | 308 | 554 | 515 | 389 | 376 | 289 | 593 | 477 | 389 | 382 |
| MAM | 134 | 274 | 250 | 180 | 206 | 126 | 287 | 208 | 178 | 179 | 212 | 333 | 312 | 252 | 272 |
| JJA | 61 | 83 | 110 | 69 | 171 | 55 | 59 | 100 | 57 | 164 | 75 | 68 | 124 | 73 | 172 |
| SON | 143 | 222 | 263 | 170 | 295 | 165 | 223 | 280 | 185 | 296 | 168 | 241 | 256 | 192 | 243 |
| ANN | 587 | 1082 | 1133 | 752 | 998 | 654 | 1121 | 1108 | 809 | 1015 | 743 | 1234 | 1175 | 905 | 1071 |

Note: DJF = summer, MAM = autumn, JJA = winter, SON = spring, ANN = annual

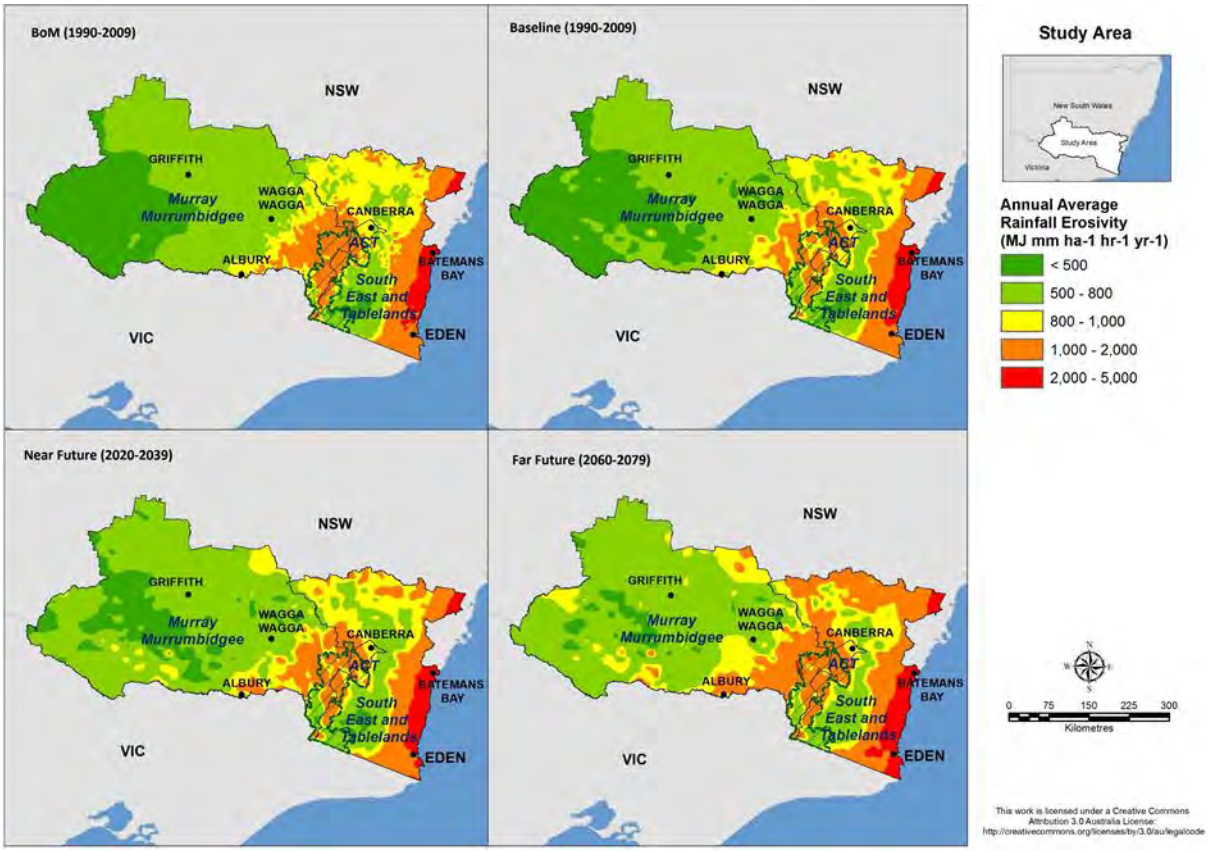


**Figure 4** **Mean annual rainfall erosivity in the baseline (1990 to 2009), near future (2020 to 2039) and far future (2060 to 2079) periods, compared with that calculated from BoM gridded rainfall in the 1990 to 2009 baseline period**

## 3.3 Future change in rainfall erosivity

The future change in mean annual rainfall erosivity across the study area is shown in Figures 5 and 6. The changes for both projection periods are spatially heterogenous, ranging from around 50–60% in the near future in the western MM region to negative changes in the SET (Figure 5). Spatially similar but greater magnitude annual changes are apparent for the far future (Figure 6). The relative seasonal changes in rainfall erosivity range from an around 29% decrease in winter in SET in the near future (Figure 7) to an about 64% increase in autumn in the MM region in the far future (Figure 8), when compared to the baseline period.

Table 4 lists the details of the rainfall erosivity changes from the baseline period (1990 to 2009) to the near future (2020 to 2039) and far future (2060 to 2079). Green cells represent decreases in rainfall erosivity while the rest represent increases. Rainfall erosivity risk is projected to decrease over all three regions (MM, SET and ACT) in autumn and winter in the near future (Figure 7), but expected to increase in the far future (Figure 8).

In terms of the mean annual change, the rainfall erosivity is estimated to increase (9.7% on average) in the study area, except for some areas in the ACT (–2.15%). The rainfall erosivity in the Alpine region has a 2.22% increase in the near future and a further 8.31% increase in the far future. For seasonal changes, as much as a 20.79% increase occurs in summer, while about a 17% decrease across the study area is projected in winter in the near future. The largest change occurs in autumn (+51.73%) rather than summer (+17.89%) in the far future period. The SET area has greater seasonal variation in the near future (+10.57% in summer and ‑28.89% in winter) but the MM region is projected to have much more deviation in the far future (+64.27% in autumn and +19.44% in spring).

**Table 4** **Changes in mean annual and seasonal rainfall erosivity (%) in the near future (2020 to 2039) and far future (2060 to 2079)**

Green cells indicate decreases in rainfall erosivity.

| Rainfall erosivity change | Change (%) in near future | | | | | Change (%) in far future | | | | |
|---|---|---|---|---|---|---|---|---|---|---|
| | MM | SET | ACT | Study area | Alpine | MM | SET | ACT | Study area | Alpine |
| **DJF** | 26.04 | 10.57 | 2.45 | 20.79 | 18.43 | 18.22 | 18.16 | –4.90 | 17.89 | 21.47 |
| **MAM** | –3.35 | –2.39 | –16.82 | –3.23 | –12.65 | 64.27 | 26.63 | 23.99 | 51.73 | 32.71 |
| **JJA** | –11.37 | –28.89 | –9.12 | –16.91 | –6.27 | 30.23 | –13.78 | 14.67 | 16.01 | –0.07 |
| **SON** | 16.72 | 3.55 | 6.05 | 12.38 | 1.53 | 19.44 | 10.39 | –1.72 | 16.26 | –15.27 |
| **ANN** | 13.00 | 3.22 | –2.15 | 9.68 | **2.22** | 28.63 | 15.83 | 3.73 | 24.21 | **8.31** |

Note: DJF = summer, MAM = autumn, JJA = winter, SON = autumn, ANN = annual

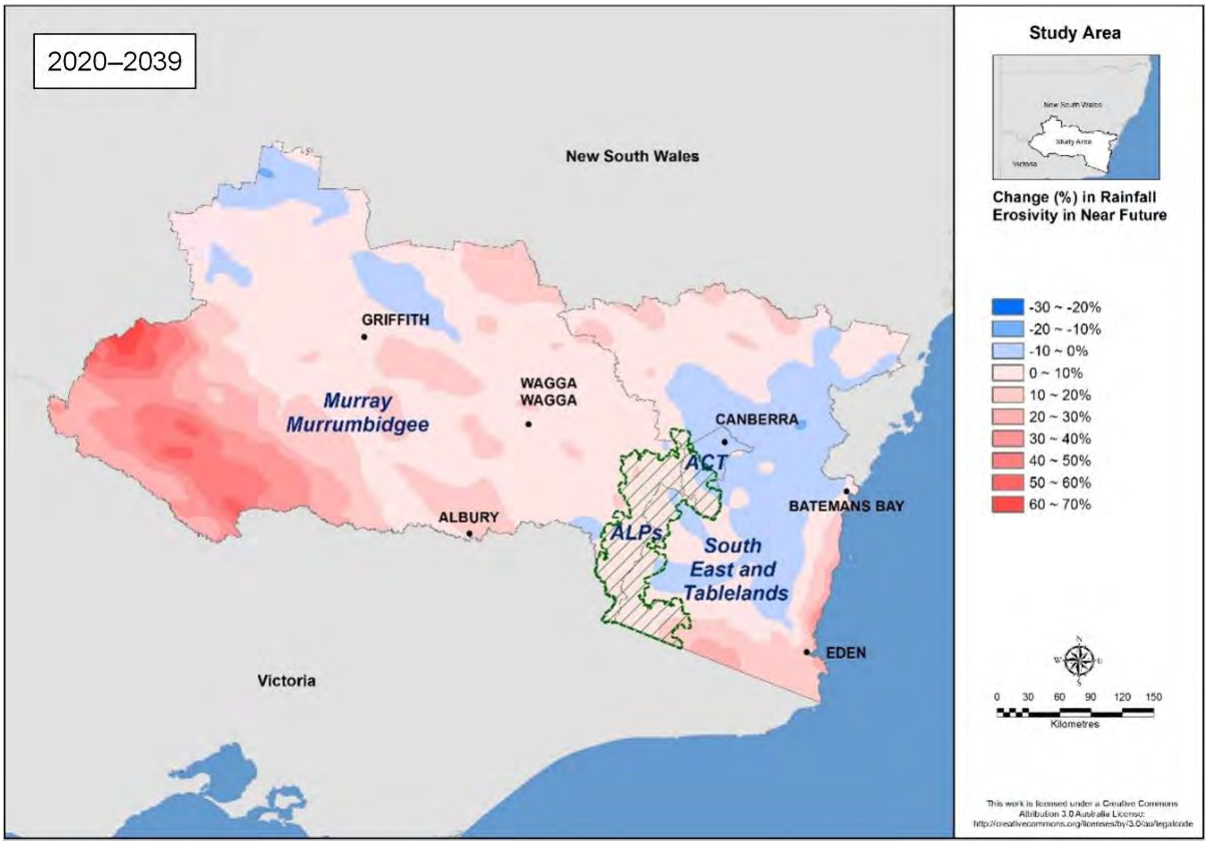


**Figure 5** **Changes in mean annual rainfall erosivity (%) in the near future (2020 to 2039) relative to the 1990 to 2009 baseline period**

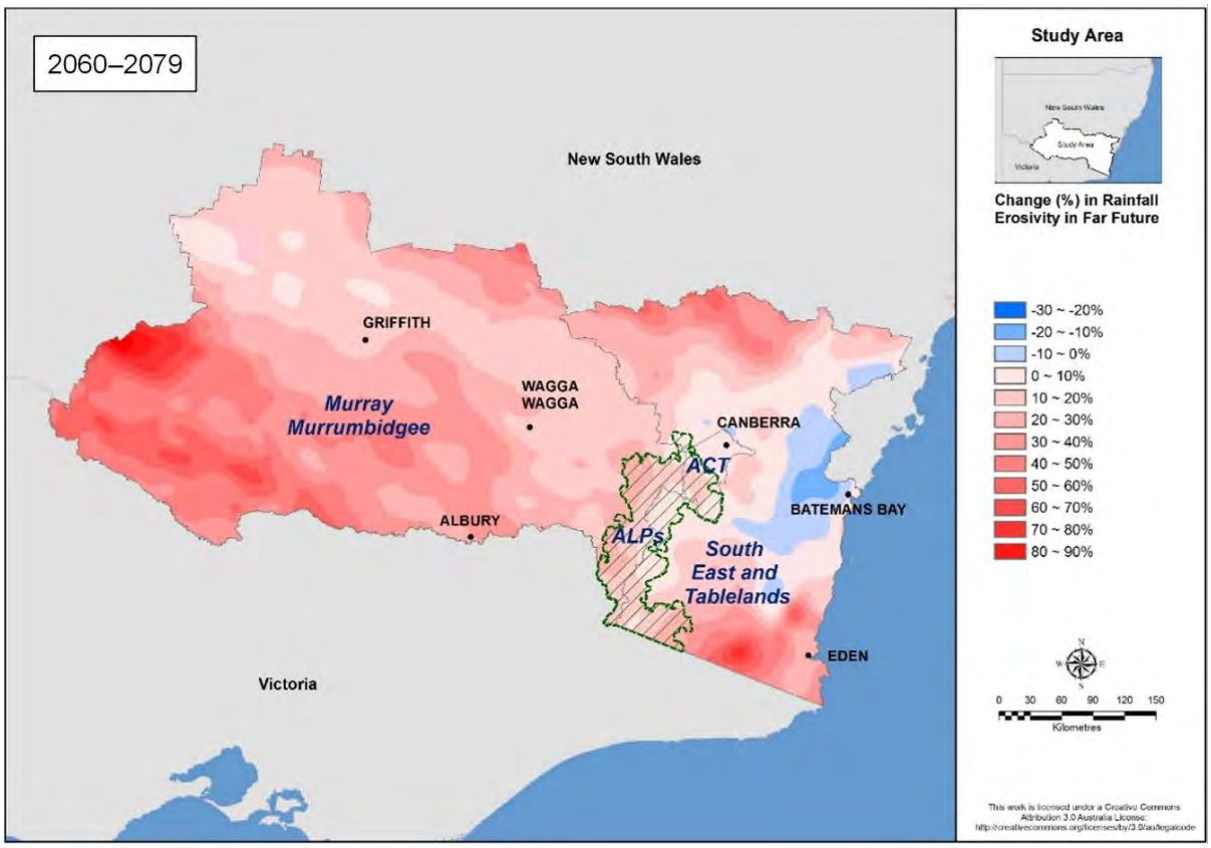


**Figure 6** **Changes in mean annual rainfall erosivity (%) in the far future (2060 to 2079) relative to the 1990 to 2009 baseline period**

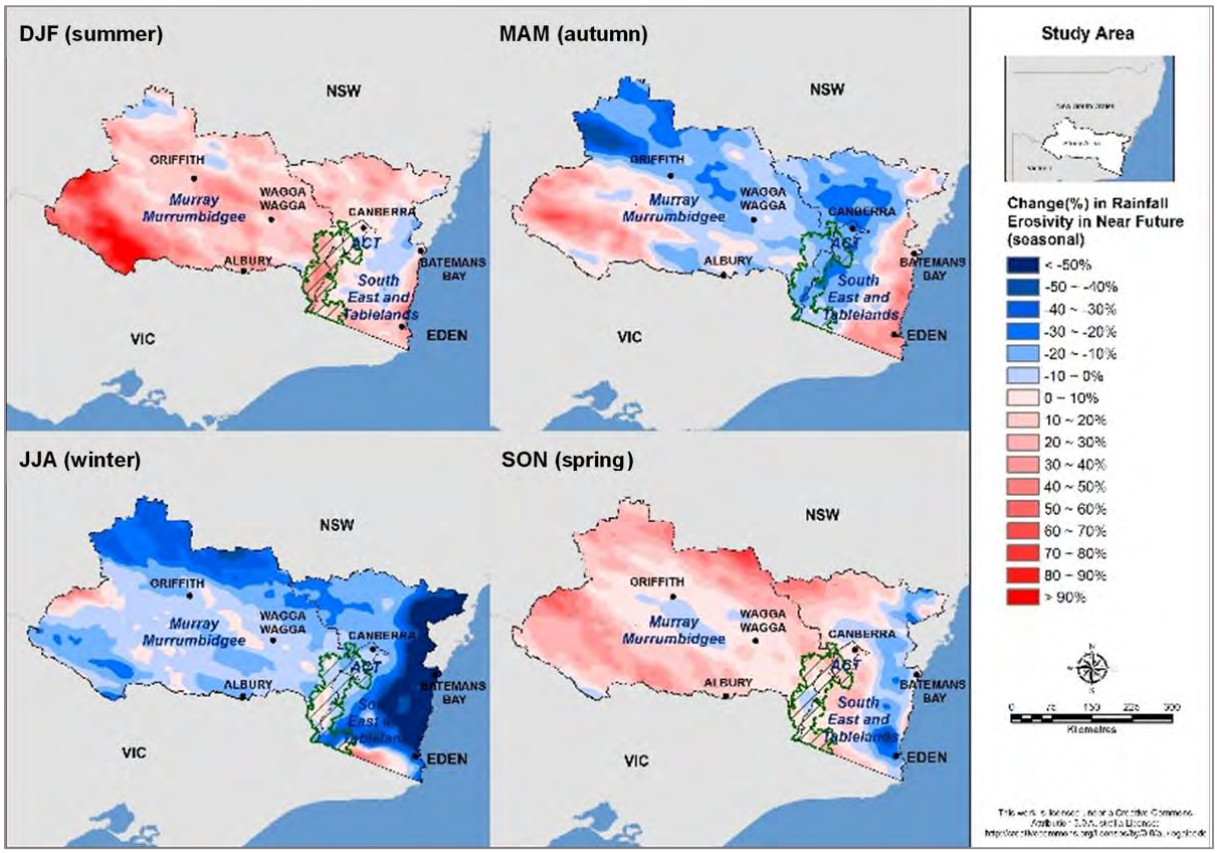


**Figure 7** **Changes in mean seasonal rainfall erosivity (%) in the near future (2020 to 2039) relative to the 1990 to 2009 baseline period**

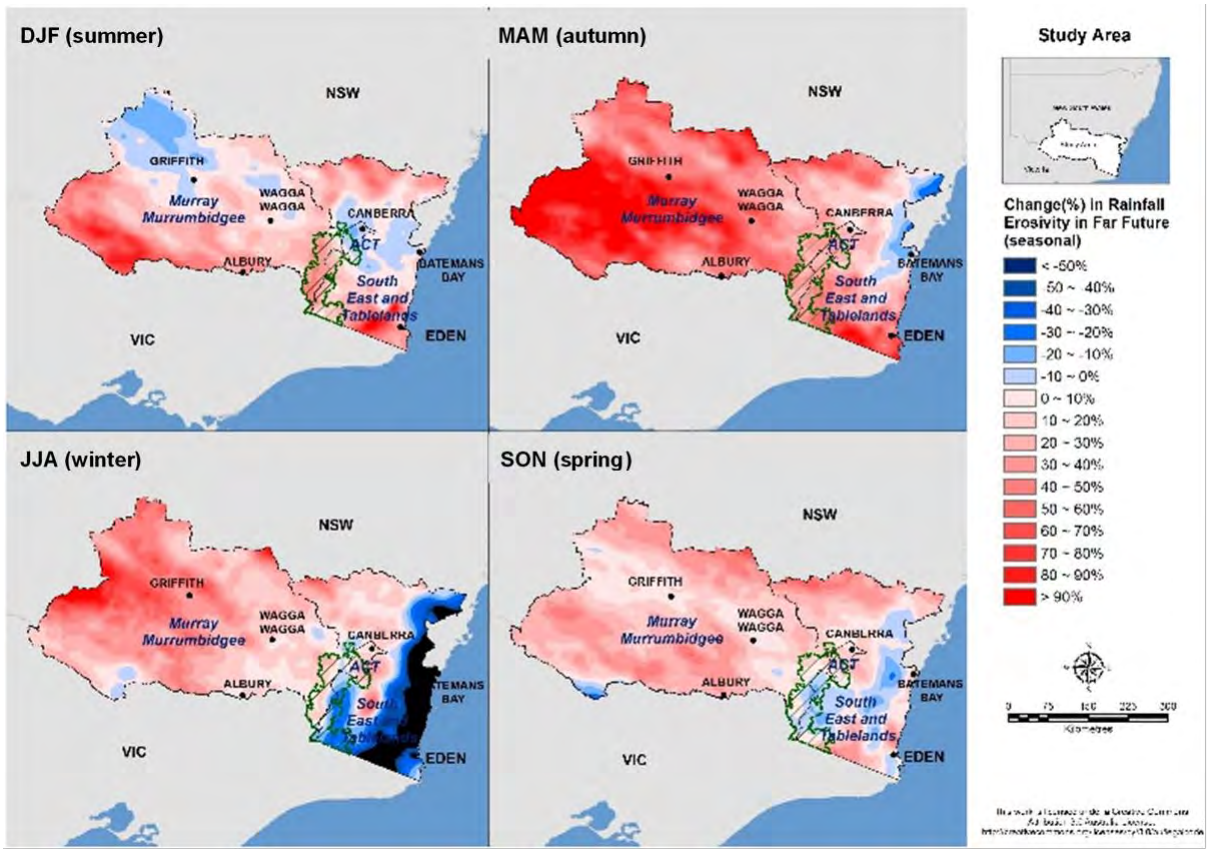


**Figure 8** **Changes in mean seasonal rainfall erosivity (%) in the far future (2060 to 2079) relative to the 1990 to 2009 baseline period**

## 3.4 Impact of snowmelt on erosivity

Adding the snowmelt (mm day$^{-1}$) as additional rainfall (Loague & Freeze 1985; Risse et al. 1993) to the daily rainfall erosivity model (Yang & Yu 2015) resulted in greater variation in rainfall erosivity estimates in the Alpine region, especially in spring and October. To examine the snowmelt impact, rainfall erosivity estimates adjusted by snowmelt and rainfall (Equations (2)–(3)) from the 12 NARCliM ensembles were compared to those calculated from NARCliM rainfall projections without snowmelt (Yang et al. 2016). Figure 9 shows the per cent change in rainfall erosivity calculated with and without the snowmelt component for the three periods across the Alpine region. The snowmelt in spring increases the rainfall erosivity in the Alpine region by about 12% in the baseline period, 19% in the near future period, but there is almost nil (< 1%) impact in the far future owing to the projected temperature rise. On an annual basis, the snowmelt impact on mean annual rainfall erosivity is not obvious, with change being less than 3% in the baseline and near future periods, and nil (or negative) impact in the far future, as snowmelt mostly occurs in spring and has little impact on rainfall erosivity in other seasons.

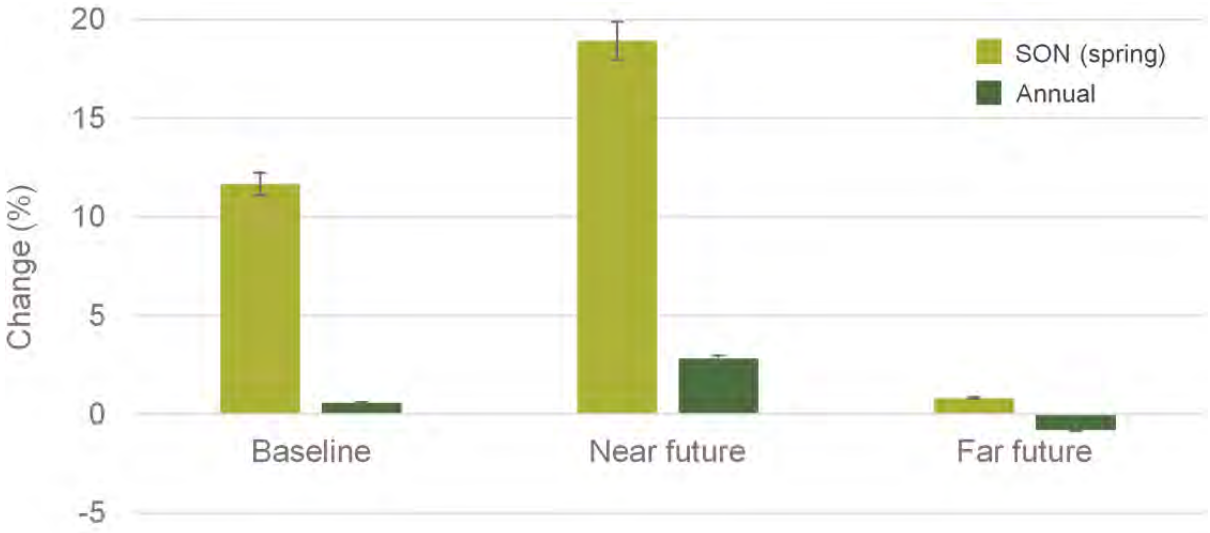


**Figure 9** **Projected change (%) in rainfall erosivity with and without snowmelt for the baseline (1990 to 2009), near future (2020 to 2039) and far future (2060 to 2079) periods**

## 3.5 Hillslope erosion projection and changes

In general, hillslope erosion is projected to increase in the future with great variation in season and location. The high erosion risk area is projected to be in the ACT and SET in all periods. This includes some reserved areas such as Wadbilliga National Park, Monga National Park close to Batemans Bay and wildness areas near Goobarragandra (Figure 10 to Figure 12).

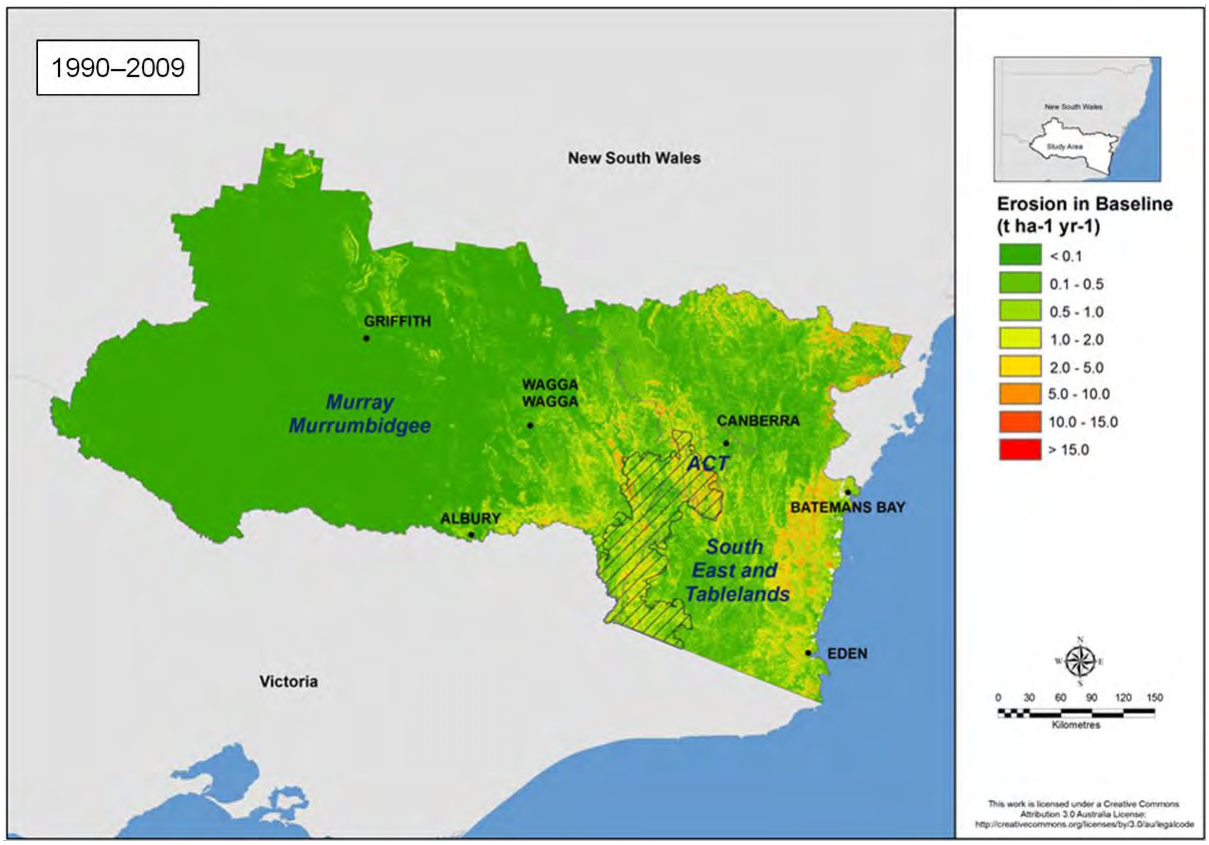


**Figure 10** **Projected hillslope erosion risk (t ha$^{-1}$ yr$^{-1}$) for the 1990 to 2009 baseline period**

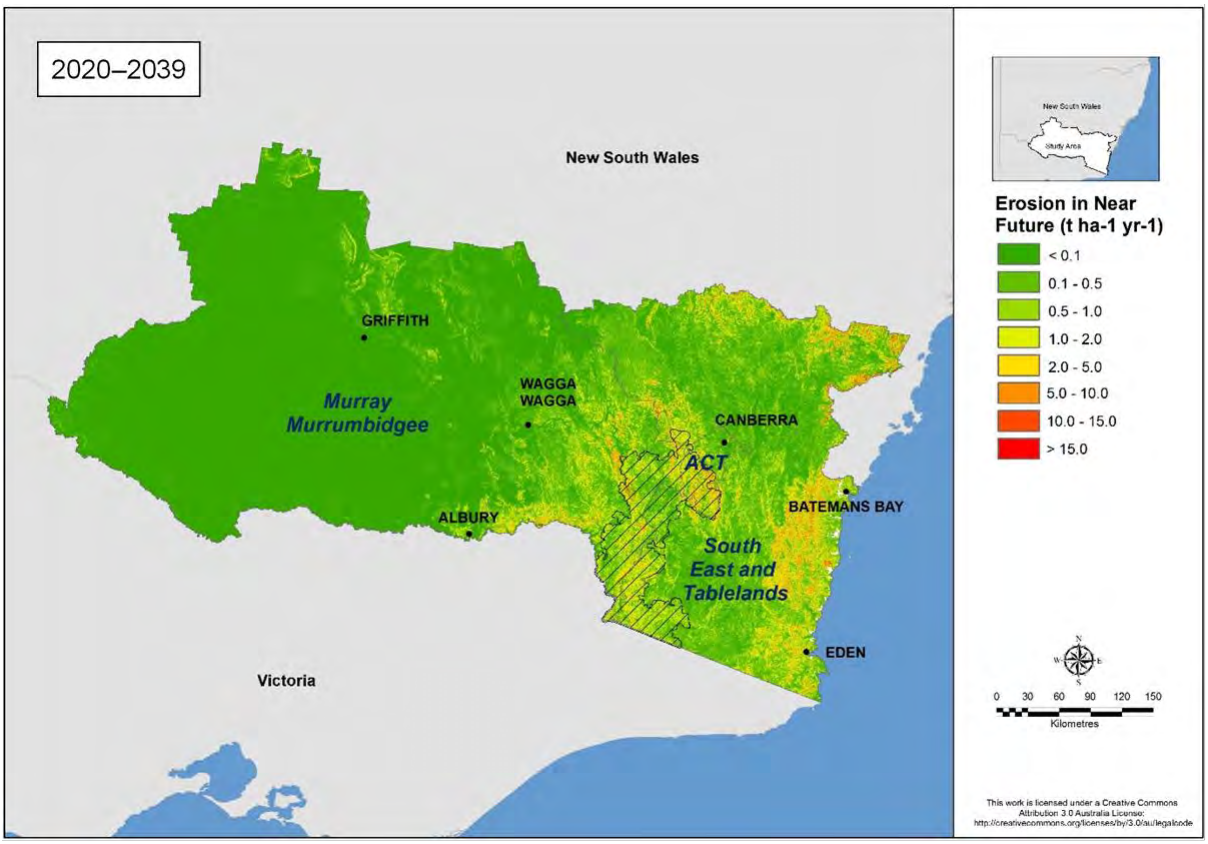


**Figure 11** **Projected hillslope erosion risk (t ha$^{-1}$ yr$^{-1}$) for the near future (2020 to 2039)**

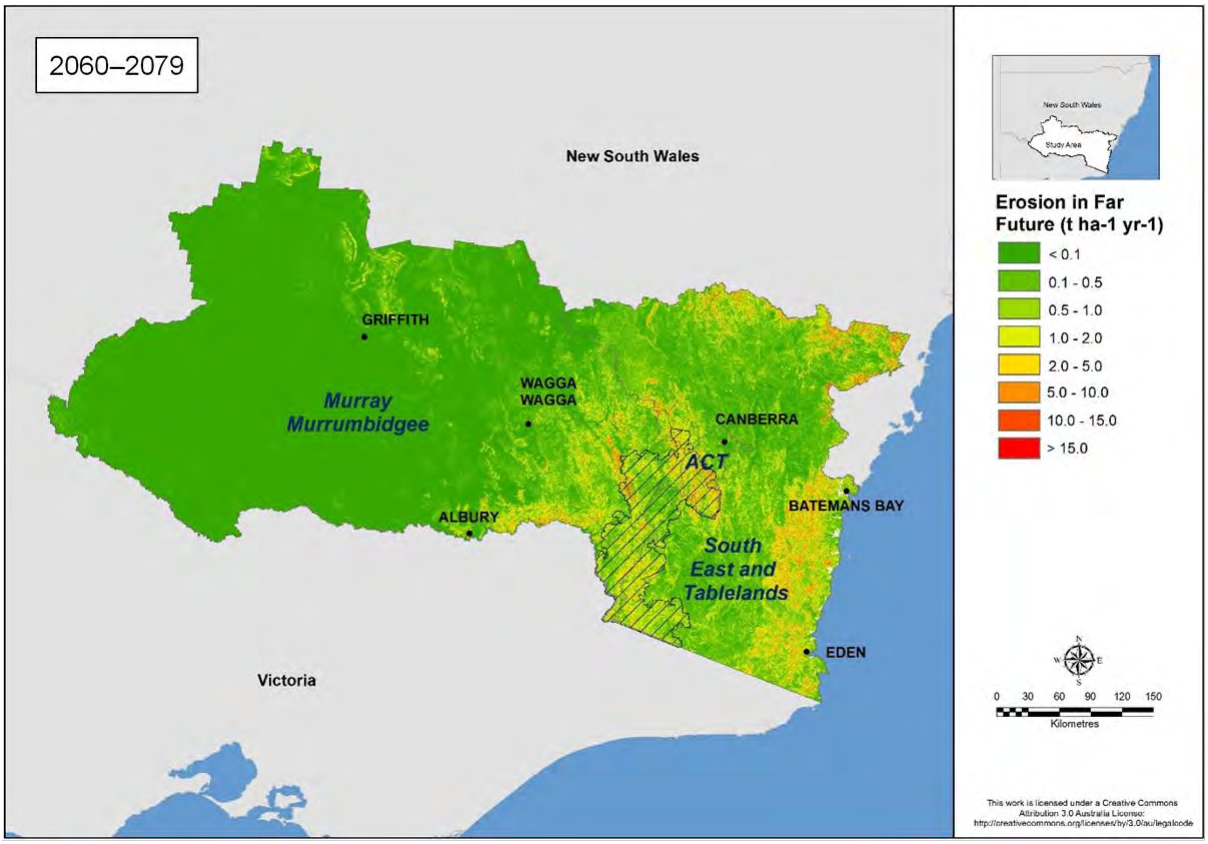


**Figure 12** **Projected hillslope erosion risk (t ha$^{-1}$ yr$^{-1}$) for the far future (2060 to 2079)**

Table 5 shows the statistics of the annual erosion rates across the region in the baseline and future periods. From the estimated maximum values, the highest risk areas are located in SET, where erosion reaches 19.95 tonnes per hectare per year in the baseline period and slightly decreases in the near future (17.33 t $ha^{-1}$ $yr^{-1}$) and far future (19.85 t $ha^{-1}$ $yr^{-1}$). However, if the mean values are compared, the ACT (followed by the Alpine region) is likely to experience higher annual erosion than any other areas across the study area, where the mean annual erosion is 1.36 tonnes per hectare per year in the baseline period. There is little change projected in the near future (1.40 t $ha^{-1}$ $yr^{-1}$) and increases to 1.54 tonnes per hectare per year projected for the far future.

**Table 5** **Mean and maximum annual erosion values (t $ha^{-1}$ $yr^{-1}$) across the study area in the baseline (1990 to 2009), near future (2020 to 2039) and far future (2060 to 2079) periods**

| Erosion (t $ha^{-1}$ $yr^{-1}$) | Baseline (1990 to 2009) | | Near future (2020 to 2039) | | Far future (2060 to 2079) | |
|---|---|---|---|---|---|---|
| | MAX | MEAN | MAX | MEAN | MAX | MEAN |
| **MM** | 14.16 | 0.16 | 14.81 | 0.17 | 17.08 | 0.19 |
| **SET** | 19.95 | 0.79 | 17.33 | 0.83 | 19.85 | 0.92 |
| **ACT** | 10.54 | 1.36 | 10.32 | 1.40 | 11.56 | 1.54 |
| **Study area** | 19.95 | 0.37 | 17.33 | 0.40 | 19.85 | 0.44 |
| **Alpine** | 12.30 | 1.14 | 12.89 | 1.20 | 13.99 | 1.30 |

Table 6 presents the change (%) in mean annual erosion from the baseline to future periods in the study area. SET is likely to experience greater variation in erosion change in the near future, where mean change is +18.76% in summer and the minimum change is –23.69% in winter. In the far future, more variation in erosion change is projected for the MM region (+69.11% in autumn and +21.70% in spring). Summer is the most vulnerable season with the highest change to the future periods compared to the other seasons.

**Table 6** **Changes (%) in mean annual and seasonal erosion values across the study area in the near future (2020 to 2039) and far future (2060 to 2079)**

| Erosion change | Change in near future (%) | | | | | Change in far future (%) | | | | |
|---|---|---|---|---|---|---|---|---|---|---|
| | MM | SET | ACT | Study area | Alpine | MM | SET | ACT | Study area | Alpine |
| **DJF** | 27.72 | 18.76 | 9.24 | 24.62 | 24.79 | 21.01 | 30.47 | 5.93 | 23.81 | 33.28 |
| **MAM** | –3.30 | 4.66 | –11.73 | –0.89 | –7.81 | 69.11 | 40.43 | 39.57 | 59.60 | 48.13 |
| **JJA** | –9.45 | –23.69 | –3.60 | –13.89 | –2.10 | 35.43 | –4.99 | 26.85 | 22.48 | 7.18 |
| **SON** | 19.53 | 11.00 | 13.68 | 16.74 | 7.39 | 21.70 | 21.48 | 11.12 | 21.48 | –6.34 |
| **ANN** | 15.74 | 10.95 | 4.55 | 14.07 | **7.91** | 31.31 | 27.87 | 15.56 | 30.00 | **18.16** |

Note: DJF = summer, MAM = autumn, JJA = winter, SON = spring, ANN = annual

As estimated from the RUSLE model, the ACT has the highest risk of hillslope erosion rather than the Alpine region (Figure 13). Though the Alpine region (a mountainous region) has the highest LS-factor, the K-factor and C-factor are relatively low compared to those from the other parts of study area (MM and SET) (Figure 14). It is projected that the ACT has higher values in the K-factor, C-factor and LS-factor. These factors, along with the adjusted rainfall erosivity factor, result in the highest erosion in the ACT. Despite higher K and C values in the MM region, the corresponding hillslope erosion is projected to be very low since the area is flat and the LS values are very low.

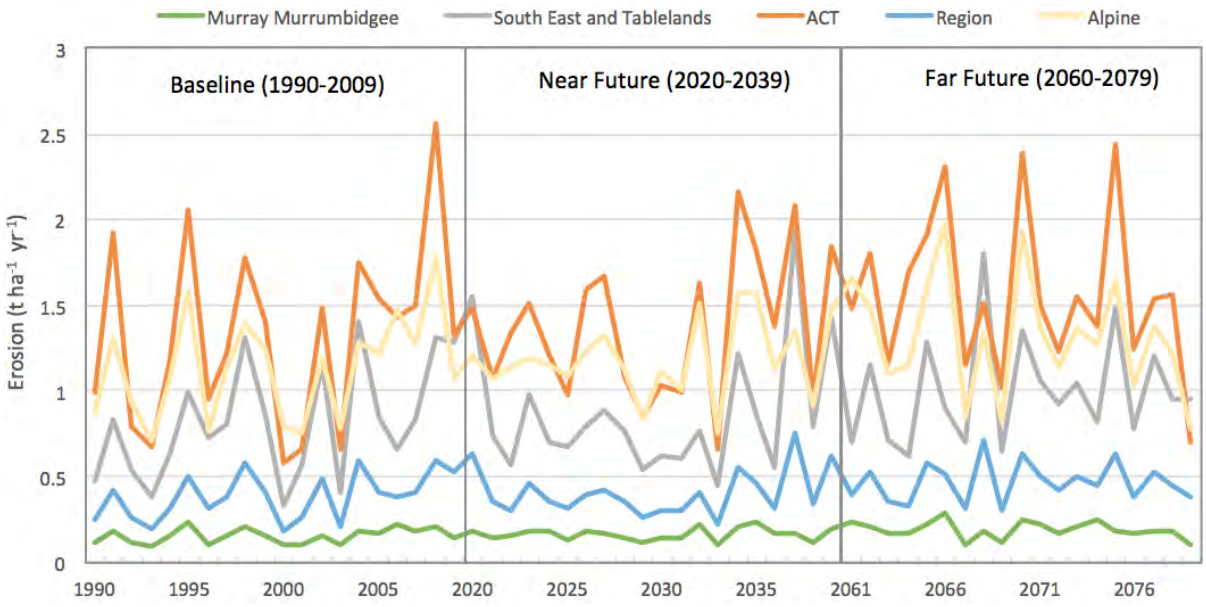


**Figure 13** **Projected hillslope erosion risk across the study area for the baseline (1990 to 2009), the near future (2020 to 2039) and the far future (2069 to 2079) periods**

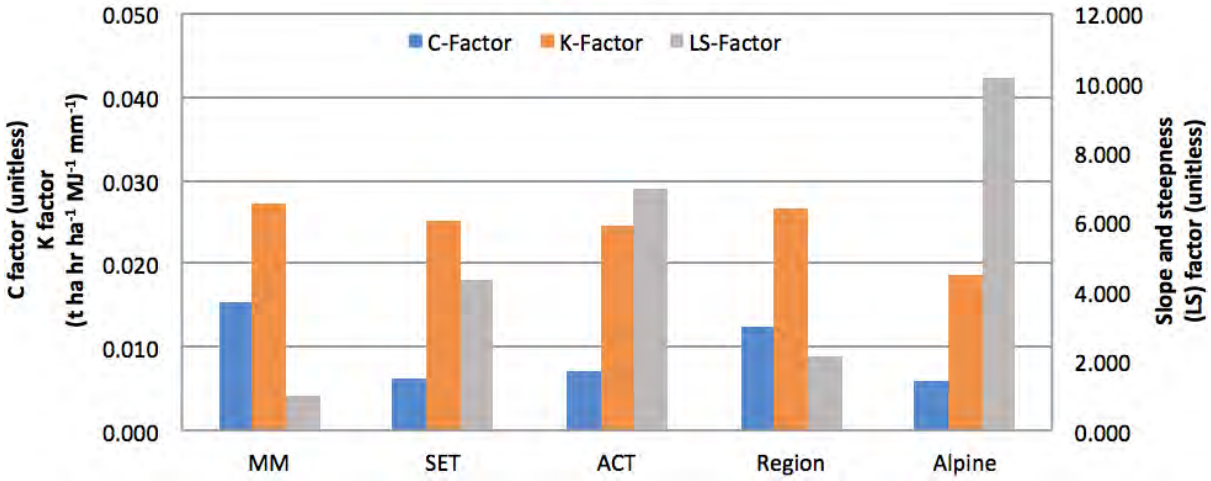


**Figure 14** **The C, K and LS factors of RUSLE across the study area**

# 4. Discussion

## 4.1 Extra rainfall erosivity in spring

The impact of snowmelt on rainfall erosivity and erosion needs to be considered in the Alpine region in the baseline and near future periods. The snowmelt in spring can increase erosivity by 24% in the Alpine region; however, with the projected temperature rise and snow cover decreasing, the snowmelt impact on erosivity and erosion can largely be ignored in the far future.

## 4.2 High risk areas

The highest erosion risk area is projected to be in the ACT, followed by SET. The high erosion risk in these areas is due to the combined effects of steep lands and intense rainfall, as well as snowmelt. This highlights the importance of groundcover maintenance and soil management in these regions.

## 4.3 Limitations and further research

The following factors influence the accuracy of these outcomes:

- Daily NARCliM GCM/RCM projections (rainfall, snow, temperature) are at a spatial resolution of approximately 10 kilometres. This is considered a relatively coarse resolution and is a limiting factor in local ecosystem (erosion) modelling.
- Only one model ensemble was used to consider snowmelt impact on erosivity. This model might be biased, though it has been shown to be the most suitable model for this region.
- Further investigation into snow impacts on groundcover and erosivity is required. More model ensembles need to be used to remove biases and increase robustness.

# 5. Conclusion

Extreme rainfall has a significant impact on erosivity and erosion. Extreme rainfall indices can be used as indicators for potential hillslope erosion risk and to predict erosivity; however, the relationships vary among seasons and locations. Predictions in summer are likely to be more reliable than other seasons due to higher correlations and coefficients of efficiency.

The impact of snowmelt on rainfall erosivity and erosion needs to be considered in the Alpine region for both the baseline and near future periods. The snowmelt in spring can increase the erosivity by about 13–24% in the Alpine region; however, with the projected temperature rise and projected decreases in snow cover, the snowmelt impact on erosivity and erosion can largely be ignored in the far future.

The high erosion risk area is projected to be in the ACT, followed by the Alpine region if the mean erosion rates are considered. The high erosion risk is due to the combined effects of steep lands and intense rainfall, as well as snowmelt. This highlights the importance of groundcover maintenance and soil management in these regions. Rainfall erosivity and hillslope erosion in the study area are projected to increase by around 10% and 14%, respectively, in the near future (2020 to 2039), increasing by a further 24% and 30%, respectively, in the far future (2060 to 2079). These increases are expected to occur even if the groundcover is maintained at the current level.

This research was the first attempt to use snow data and projections to adjust erosivity in models to factor in hillslope erosion modelling. The methodology has been developed and applied in the Alpine region, with potential to be used globally.

# 6. References

Alexander LV, Hope P, Collins D, Trewin B, Lynch A and Nicholls N 2007, Trends in Australia's climate means and extremes: a global context, *Australian Meteorological Magazine*, vol.56, pp.1–18.

Bormann KJ, Evans JP and McCabe MF 2014, Constraining snowmelt in a temperature-index model using simulated snow densities, *Journal of Hydrology*, vol.517, pp.652–667.

Cruse R, Flanagan D, Frankenberger J, Gelder B, Herzmann D, James D, Krajewski W, Kraszewski M, Laflen J, Opsomer J and Todey D 2006, Daily estimates of rainfall, water runoff, and hillslope erosion in Iowa, *Journal of soil and water conservation*, vol.61, pp.191–199.

CSIRO and BoM 2015, *Climate Change in Australia Information for Australia's Natural Resource Management Regions: Technical Report*, CSIRO and Bureau of Meteorology, Australia.

Di Luca AJ, Evans P and Ji F 2018, Australian snowpack in the NARCliM ensemble: evaluation, bias correction and future projections, *Climate Dynamics*, vol.51, no.1–2, pp.639–666.

Evans JP, Ekstrom M and Ji F 2012, Evaluating the performance of a WRF physics ensemble over South-East Australia, *Climate Dynamics*, vol.39, no.6, pp.1241–1258.

Evans JP, Ji F, Abramowitz G, Ekstrom M 2013a, Optimally choosing small ensemble members to produce robust climate simulations, *Environmental Research Letters*, vol.8.

Evans JP, Fita L, Argüeso D and Liu Y 2013b, Initial NARCliM evaluation, in Piantadosi J, Anderssen RS and Boland J (eds), *MODSIM2013, 20th International Congress on Modelling and Simulation*, Modelling and Simulation Society of Australia and New Zealand, December 2013, pp.2765–2771.

Evans J, Ji F, Lee C, Smith P, Argüeso D and Fita L 2014a, Design of a regional climate modelling projection ensemble experiment–NARCliM, *Geoscientific Model Development,* vol.7, pp.621–629.

Evans JP, Argüeso D, Olson R and Di Luca A 2014b, 'NARCliM extreme precipitation indices report', NARCliM technical note 6, report to the NSW Office of Environment and Heritage, Sydney Australia, pp.109.

Evans JP, Argüeso D, Olson R and Di Luca A 2017, Bias-corrected regional climate projections of extreme rainfall in south-east Australia, *Theoretical and Applied Climatology,* vol.130, nos3–4, pp.1085–1098.

Fita L, Evans JP, Argüeso D, King AD and Liu Y 2016, Evaluation of the regional climate response to large-scale modes in the historical NARCliM simulations, *Climate Dynamics*, pp.1–15, doi: 10.1007/s00382-016-3484-x.

Gray JM and Bishop TFA 2017, *Climate change impacts on three key soil properties in NSW*, Technical Report, NSW Office of Environment and Heritage, Sydney.

Gray JM, Thomas FA, Bishop TFA and Wilford JR 2016, Lithology and soil relationships for soil modelling and mapping, *Catena*, vol.147, pp.429–440.

Grundy MJ, Viscarra RA, Searle RA, Searle RD, Wilson PL, Chen C and Gregory LJ 2015, Soil and Landscape Grid of Australia, *Soil Research*, vol.53, no.8, pp.835–844.

Guerschman JP, Hill MJ, Renzullo LJ, Barrett DJ, Marks AS and Botha EJ 2009, Estimating fractional cover of photosynthetic vegetation, nonphotosynthetic vegetation and bare soil in the Australian tropical savanna region upscaling the EO-1 Hyperion and MODIS sensors, *Remote Sensing of Environment*, vol.113, pp.928–945.

Hayhoe H, Pelletier R and Coote D 1995, Estimating snowmelt runoff erosion indices for Canada, *Journal of Soil and Water Conservation*, vol.50, pp.174–179.

Hughes L 2011, Climate change and Australia: key vulnerable regions, *Regional Environmental Change*, vol.11, no.1, pp.189–195.

IPCC 2000, Special Report on Emissions Scenarios: A Special Report of Working Group III of the Intergovernmental Panel on Climate Change, published for the Intergovernmental Panel on Climate Change by Cambridge University Press, Cambridge, UK.

Ji F, Ekstrom M, Evans JP and Teng J 2014, Evaluating rainfall patterns using physics scheme ensembles from a regional atmospheric model, *Theoretical and Applied Climatology*, vol.115, pp.297–304.

Ji F, Evans JP, Teng J, Scorgie Y, Argüeso D and Di Luca A 2016, Evaluation of long-term precipitation and temperature WRF simulations for southeast Australia, *Climate Research*, vol.67, pp.99–115, DOI 10.3354/cr01366.

Loague KM and Freeze RA 1985, A comparison of rainfall-runoff modeling techniques on small upland catchments, *Water Resources Research*, vol.21, pp.229–248.

Meusburger K, Leitinger G, Mabit L, Mueller M, Walter A and Alewell C 2014, Hillslope erosion by snow gliding–a first quantification attempt in a subalpine area in Switzerland, *Hydrology and Earth System Sciences*, vol.18, pp.3763–3775.

Nash JE and Sutcliffe JV 1970, River flow forecasting through conceptual models part I—A discussion of principles, *Journal of Hydrology*, vol.10, pp.282–290.

Nearing MA, Pruski FF and O'ne MR 2004, Expected climate change impacts on hillslope erosion rates: A review, *Journal of Soil and Water Conservation*, vol.59, no.1, pp.43–50.

OEH 2013, *Scientific Rigour Position Statement*, NSW Office of Environment and Heritage, www.environment.nsw.gov.au/-/media/OEH/Corporate-Site/Documents/Research/Our-science-and-research/oeh-scientific-rigour-position-statement-2013.pdf.

Ollesch G, Kistner I, Meissner R and Lindenschmidt KE 2006, Modelling of snowmelt erosion and sediment yield in a small low-mountain catchment in Germany, *Catena*, vol.68, pp.161–176.

Rango A and Martinec J 1995, Revisiting the degree-day method for snowmelt computations, *Journal of the American Water Resources Association*, vol.31, pp.657–669.

Renard KG, Foster GR, Weesies G, McCool D and Yoder D 1997, *Predicting hillslope erosion by water: a guide to conservation planning with the Revised Universal Soil Loss Equation (RUSLE)*, US Government Printing Office Washington, DC.

Risse L, Nearing M, Laflen J and Nicks A 1993, Error assessment in the universal soil loss equation, *Soil Science Society of America Journal*, vol.57, pp.825–833.

Skamarock WC, Klemp JB, Dudhia J, Gill DO, Barker DM, Duda MG, Huang XY, Wang W and Powers JG 2008, *A description of the advanced research WRF Version 3,* NCAR Technical Note, National Center for Atmospheric Research, Boulder Colorado, USA.

Yang X 2014, Deriving RUSLE cover factor from time-series fractional vegetation cover for hillslope erosion modelling in New South Wales, *Soil Research*, vol.52, pp.253–261.

Yang X 2015, Digital mapping of RUSLE slope length and steepness factor across New South Wales, Australia, *Soil Research*, vol.53, pp.216–225.

Yang X and Yu B 2015, Modelling and mapping rainfall erosivity in New South Wales, *Soil Research*, vol.53, pp.178–189.

Yang X, Yu B, Zhu Q and Liu D 2016, Predicting Changes of Rainfall Erosivity and Hillslope Erosion across New South Wales, Australia, *Journal of Earth Science Climate Change*, vol.7, no.3, p.2.

Yang X, Gray J, Chapman C, Zhu Q, Tulau M and McInnes-Clarke S 2017, Digital mapping of soil erodibility for water erosion in New South Wales, Australia, *Soil Research*, vol.56, no.2, pp.158–170.

**DOCUMENT 21**

**DEPARTMENT OF PLANNING, INDUSTRY & ENVIRONMENT**

# Climate change impacts in the NSW and ACT Alpine region

## Impacts on water availability

**environment.nsw.gov.au**

Cover photo: Winter landscape in Kosciuszko National Park. John Spencer/DPIE

This report should be cited as:

Young J and Littleboy M 2019, *Climate change impacts in the NSW and ACT Alpine region: Impacts on water availability*, NSW Department of Planning, Industry and Environment, Sydney, Australia.

Published by:

Environment, Energy and Science
Department of Planning, Industry and Environment
59 Goulburn Street, Sydney NSW 2000
PO Box A290, Sydney South NSW 1232
Phone: +61 2 9995 5000 (switchboard)
Phone: 1300 361 967 (Environment, Energy and Science enquiries)
TTY users: phone 133 677, then ask for 1300 361 967
Speak and listen users: phone 1300 555 727, then ask for 1300 361 967
Email: info@environment.nsw.gov.au
Website: www.environment.nsw.gov.au

Report pollution and environmental incidents
Environment Line: 131 555 (NSW only) or info@environment.nsw.gov.au
See also www.environment.nsw.gov.au

ISBN 978 1 922318 16 9
EES 2020/0021
January 2020

**Find out more about your environment at:**

**www.environment.nsw.gov.au**

# Contents

# List of tables



# List of figures

# List of shortened forms

| | |
|---|---|
| ACT | Australian Capital Territory |
| ALUM | Australian Land Use and Management Classification |
| ANN | Annual |
| AWAP | Australian Water Availability Project |
| CAP | Catchment Action Plan |
| CMIP | Coupled Model Intercomparison Project |
| DJF | December January February |
| DPIE | NSW Department of Planning, Industry and Environment |
| ET | evapotranspiration |
| FPC | foliage projective cover |
| GCM | Global Climate Model |
| GSG | Great Soil Groups classification |
| HGL | hydrogeological landscape (HGL) |
| JJA | June July August |
| MAM | March April May |
| MCAS-S | Multi-Criteria Analysis Shell for Spatial Decision Support |
| mm | millimetre |
| MM | Murray-Murrumbidgee state planning region |
| NARCliM | NSW/ACT Regional Climate Modelling project |
| NetCDF | Network Common Data Form |
| NSW | New South Wales |
| NVAT | Native Vegetation Assessment Tool |
| OEH | Office of Environment and Heritage |
| RCM | Regional Climate Model |
| SET | South East and Tablelands |
| SON | September October November |
| SRES | Special Report on Emissions Scenarios |
| SRTM | Shuttle Radar Topography Mission |
| WRF | Weather Research and Forecasting |
| WDM5 | WRF Double Moment 5-class |

# Summary of findings

## Impacts on water availability in the NSW and ACT Alpine region

1. Impacts of climate change on water availability affect water quality, salinity and aquatic biodiversity. Climate change is projected to affect water availability through changes in surface runoff and recharge to groundwater.
2. In the near future (2020 to 2039), most of the study area is likely to have less surface runoff, while areas from Balranald to Deniliquin, Griffith and northern parts from West Wyalong to Goulburn are likely to experience increased surface runoff. In the far future (2060 to 2079), reductions in surface runoff of more than 40 millimetres/year are projected for higher alpine areas, generally bounded by the NSW and ACT Alpine region, from Tumut to Canberra to the Victorian border in the south.
3. Changes in recharge to groundwater in near future projections are slightly less than changes in the far future projections. Both scenarios project reduced recharge. For both near future and far future projections, areas bounded by the NSW and ACT alpine park reserves are significantly impacted, with a substantial reduction in recharge.
4. In the near future, most of the study area is likely to have less recharge, except for some areas west of Deniliquin and Griffith that show a slight increase. Far future projections predict less recharge in summer, winter and autumn, with the largest decreases during in spring.
5. For the near future, most Catchment Action Plan (CAP) regions currently designated as low salinity hazard show no change in hazard. There is potential for less dilution flow from low hazard CAP regions in alpine areas, which could increase downstream catchment-scale salinity. Most CAP regions with moderate, high or very high salinity hazard show either no change in hazard or lower salinity hazard in the near future. The only exceptions are CAP regions west of Deniliquin that show an increase in salinity hazard.
6. For the far future, most CAP regions currently designated as low salinity hazard show no change in hazard. Some low hazard areas north of Griffith show the potential for higher dilution flows that could be beneficial for catchment-scale salinity. CAP regions that are currently moderate, high or very high salinity hazard show either no change in hazard or higher salinity hazard in the far future. CAP regions west of Narrandera consistently show an increase in salinity hazard.
7. All CAP regions with high irrigation land use (e.g. Griffith, Leeton) have a potential for high salinity hazard.

# 1. Introduction

## 1.1 Background

The New South Wales (NSW) and Australian Capital Territory (ACT) Alpine region is located in the south-eastern corner of mainland Australia and is the highest mountain range in Australia. Though it comprises only about 0.16% of Australia in size, it is an important region for ecosystems, biodiversity, energy generation and winter tourism. It forms the southern end of the Great Dividing Range, covering a total area of 1.64 million hectares that extend over 500 kilometres. The highest peak, Mount Kosciuszko, rises to an altitude of 2228 metres.

This report is part of a larger project delivered by the NSW Department of Planning, Industry and Environment on the various impacts from climate change on the NSW and ACT Alpine region, hereafter referred to as the Alpine region. The full study region covers the Murray-Murrumbidgee region (MM), South East and Tablelands (SET) and the ACT, bordering the Victorian border in the south (Figure 1).

The Alpine region is vulnerable to climate change. Observations have shown substantial changes in precipitation and temperature for this area (Di Luca et al. 2018), which have already impacted biodiversity and ecosystems (Hughes 2011). In 2014, the NSW/ACT Regional Climate Modelling (NARCliM) project was delivered. Climate snapshots for each of the 11 NSW planning regions and the ACT were developed to demonstrate observed and projected climate change; however, the snapshots only show changes for some variables and focus on each planning region.

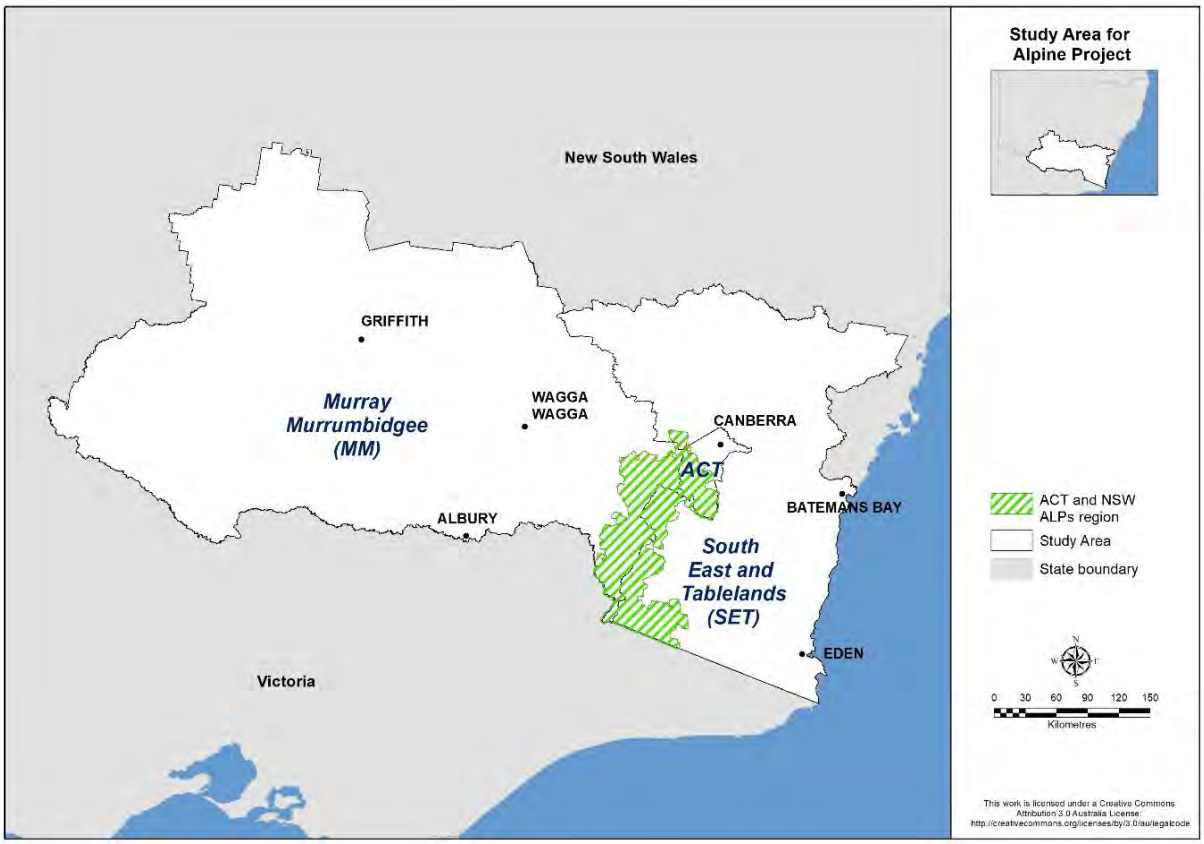


**Figure 1** **The study area for the Alpine project, including the NSW and ACT Alpine region, Murray-Murrumbidgee region and South East and Tablelands**

## 1.2 Objectives

This study provides projections for potential impacts of climate change on the surface runoff and recharge to groundwater within the MM region, ACT and SET areas of New South Wales. Surface flow and groundwater recharge projections can assist decisions on adaptation options for managing water resources, water quality and waterway health that affect the ecosystem services our waterways provide. Combining surface runoff and recharge projections allows us to explore changes in landscape water movement and its impact on salinity hazard and dilution flows within sub-catchments.

We used the NARCliM ensemble of climate projections for south-east Australia. This ensemble is designed to provide robust projections that span the range of likely future changes to climate (Evans et al. 2014). NARCliM projections over three climate time periods were used as inputs to a water balance model, PERFECT (Littleboy et al. 1992). The three time periods consisted of a baseline (1990 to 2009), near future (2020 to 2039) and far future (2060 to 2079).

Unlike the hydrological assessment for New South Wales in 2010 (Vaze et al. 2010), which used a conceptually lumped rainfall–runoff model (Chiew et al. 2002), this impact assessment applies a daily time-step, one-dimensional model to each grid cell. Using rainfall and areal potential evapotranspiration (Morton 1983; Ji et al. 2015) as inputs, the model partitions non-transpired water into surface flows and groundwater recharge. This partitioning is driven by soil properties, land use and topography. The major benefit of this type of modelling is that results are not constrained to catchment boundaries and impacts on surface flows and recharge can be obtained for individual parts of the landscape. However, a change in surface runoff does not directly correlate to a similar change in streamflow at the catchment outlet. Not all surface runoff will flow into the river itself, flowing instead into farm dams, wetlands and other waterbodies.

Changes in surface runoff and recharge to groundwater can also be used to explore hydrological changes at a landscape scale. Salinity and landscape water movement are inextricably linked. Salinity is the accumulation of salt in the landscape. It can be mobilised by surface runoff, subsurface flow, groundwater recharge or groundwater discharge.

Salinity is an important variable in landscape systems and is often a determining factor in the capacity of the landscape to absorb change (Smithson et al. 2004). It has a three-pronged impact on landscapes namely land salinisation, in-stream salt load and in-stream salt concentration. Any of these impacts can themselves or together affect landscape resilience.

In New South Wales, Salinity Hazard for Catchment Action Plans (CAP) provides a framework to better understand how salinity influences landscape resilience. Catchment Action Plan products are appropriate for planning at a catchment scale. This existing mapping provides a consistent salinity mapping product that covers the entire study area.

## 1.3 Outputs

Raster format spatial data, maps and graphs from this modelling form part of this climate impact profile to assess projected biophysical changes across the study area. Maps show central estimates or arithmetic means of near and far future projections. Bar graphs are used to present projections as ranges of plausible change, illustrating the projections from the 12 individual simulations as well as the central estimate.

| Output | Details | Key users |
|---|---|---|
| Report | This report | Researchers |
| Maps | .jpg | Councils, etc. |
| Data | geoTIFF format rasters, .csv | Spatial analysts |

## 1.4 Focus region

The study area covers an area of more than 171,000 square kilometres and extends across the SET, ACT and MM catchments, bordering the Victorian border in the south. It spans three distinct physiographic provinces (Pain et al. 2011):

- Kosciuszkan Uplands Province 107, (mountains and plateaus ranging from the highest point in Australia to the coast) covering most of the catchment
- a small coverage of Macquarie Uplands Province 106, (dissected plateaus on sub-horizontal resistant sandstones, mainly of the Sydney Basin) to the north of Goulburn, and Cootamundra
- Murray Lowlands Province 203 (more-or-less coincident with the Murray sedimentary basin, consisting of flat alluvium with aeolian cover in places) to the western third of the catchment from Corowa in the south to Leeton in the north.

The area falls completely within the temperate climatic zone (BoM 2006) and mean annual temperatures of –0.4°C to 21.1°C and annual rainfall averages of 313–1828 millimetres span this climatic zone.

# 2. Method

## 2.1 Source of data

NARCliM simulations from four Coupled Model Intercomparison Project phase 3 (CMIP3) Global Climate Models (GCMs) were used to drive three Regional Climate Models (RCMs) to form a 12-member GCM/RCM ensemble (Evans et al. 2014). The four selected GCMs are MIROC3.2, ECHAM5, CCCMA3.1 and CSIRO-MK3.0. For future projections, the Special Report on Emissions Scenarios (SRES) business-as-usual A2 scenario was used (IPCC 2000). The three selected RCMs are three physics scheme combinations of the Weather Research and Forecasting (WRF) model. Each simulation consists of three 20-year runs (1990 to 2009, 2020 to 2039, and 2060 to 2079). The four GCMs were chosen based on a number of criteria: i) adequate performance when simulating historic climate; ii) most independent; iii) cover the largest range of plausible future precipitation and temperature changes for Australia. The three RCMs correspond to three different physics scheme combinations of the WRF V3.3 model (Skamarock et al. 2008), which were also chosen for adequate skill and error independence, following a comprehensive analysis of 36 different combinations of physics parameterisations over eight significant East Coast Lows (ECLs) (Evans et al. 2012; Ji et al. 2014). For the selected three RCMs, the WRF Double Moment 5-class (WDM5) microphysics scheme and NOAH land surface scheme are used in all cases. Refer to Evans et al. (2014) for more details on each physics scheme.

We acknowledge that the results are model dependent (as all model studies are) but through the use of this carefully selected ensemble we have attempted to minimise this dependence. By using this model selection process, we have shown that it is possible to create relatively small ensembles that are able to reproduce the ensemble mean and variance from the large parent ensemble (i.e. the many GCMs) as well as minimise the overall error (Evans et al. 2013a).

Some initial evaluation of NARCliM simulations shows that they have strong skill in simulating the precipitation and temperature of Australia, with a small cold bias and overestimation of precipitation on the Great Dividing Range (Evans et al. 2013b, Ji et al. 2016). The differing responses of the different RCMs confirm the utility of considering model independence when choosing the RCMs. The RCM response to large-scale modes of variability also agrees well with observations (Fita et al. 2016). Through these evaluations we found that while there is a spread in model predictions, all models perform adequately

with no single model performing the best for all variables and metrics. The use of the full ensemble provides a measure of robustness such that any result that is common through all models in the ensemble is considered to have higher confidence.

In total, there were four same GCM driven simulations (average of three members) and three same RCM used simulations (average of four members). The analyses in this study are based on the ensemble mean of these simulations.

## 2.2 Climate projections

While the climate models produce a range of variables, only daily maximum temperature, daily minimum temperature, precipitation and evapotranspiration (ET) are required to drive the water balance model. Bias-corrected precipitation was considered, but due to incomplete spatial coverage was not used. Cell resolution of the NARCliM domain is at 10 kilometres, data is WGS84 regular grid.

## 2.3 Water balance model

This work has been undertaken using the application of the water balance model PERFECT (Littleboy et al. 1992) using spatially specific key input drivers of land use, foliage projective cover, soils, and the NARCliM ensemble of climate projections for south-east Australia (Evans et al. 2014). Outputs are presented for the near future (2020 to 2039) and far future (2060 to 2079), of annual and seasonal surface runoff and recharge in comparison to a baseline period (1999 to 2009) for a high emissions scenario – the A2 scenario from the Special Report on Emissions Scenarios (SRES) (IPCC 2000). Changes under lower emissions are likely to be similar in nature but weaker in magnitude than these projections; also, changes outside those contained in the NARCliM projections are also possible.

The water balance model used daily time-series of NARCliM non-bias-corrected rainfall and areal potential evapotranspiration (Morton 1983; Ji et al. 2015) modelled by each GCM/RCM as inputs. Actual ET was calculated daily using areal potential ET and seasonal crop factors. Crop factors varied by land-use category and foliage projective cover (FPC). Using FPC to disaggregate land-use categories to account for different levels of tree cover was crucial to account for spatial variability within a single land-use polygon.

Partitioning between surface flow and recharge is driven by soil properties and topography for each ~90 metre (3 arc-second) cell within a NARCliM 10 kilometre cell. Volumes of surface flow are governed by model parameters and variables describing potential infiltration, antecedent soil water, surface and vegetative cover and slope. Volumes of recharge are controlled by parameters and variables quantifying drainage rates through the soil profile, soil depth and slope.

PERFECT is a one-dimensional, daily time-step water balance model which predicts the water balance in a single column of soil. It does not predict lateral subsurface movement of water. Any excess soil water is assumed to move vertically as deep drainage to groundwater. Therefore, estimates of drainage from PERFECT are a combination of subsurface lateral flow and vertical drainage. To partition excess soil water moving laterally and vertically, the HYDRUS 2D model (Simunek et al. 1999) was applied to develop a generic model of lateral water movement (Rassam & Littleboy 2003).

## 2.4 Salinity analysis

The salinity assessment is based on existing salinity hazard mapping undertaken in NSW Catchment Action Plans (CAPs). These maps were designed to be appropriate for planning at a catchment scale as they show the broad salinity hazard distribution across the study

area. They are fully documented and represent the only consistent salinity dataset currently available across the entire study area. The maps depict the potential severity of salinity underpinned by a practical understanding of the factors that cause salinity at the time.

Each salinity hazard map defines spatial units based on relevant biophysical datasets including groundwater flow systems mapping, depth to water table maps, soil mapping and terrain. Each spatial unit has been assigned a salinity hazard ranking – Very High, High, Moderate, Low and Very Low. Hazard ratings were derived from other statewide and catchment data sets that influence salinity. In addition, consideration was given to the presence or absence of known dryland salinity outbreaks, influence of local or regional groundwater systems, climatic impacts and any other relevant modifiers impacting on the hazard area. Existing hydrogeological landscape (HGL) hazard information was integrated in areas where it was available.

Salt mobilisation occurs when movement of water within a landscape intercepts a salt store, producing saline discharge. Changes to the volume of water added to the natural system intensify the processes that cause salinity as the water cycle tries to find a new balance. As such, any increases in landscape water movement inputs due to climate change may intensify salinity impacts. Conversely, less movement of water within landscapes may reduce the impacts of salinity.

Volumes of surface runoff and recharge to groundwater can be used to quantify the surplus water movement in a landscape that could potentially mobilise salt. In this study, changes in runoff and recharge were combined to calculate the change in surplus water.

These changes were split into three categories, namely: greater than 10% drier, greater than 10% wetter or no change (Table 1). The impacts of changes in surplus water on salinity vary depending on the likely salt stores.

For areas with low salinity hazard, changes in surplus water will mainly affect freshwater flows or dilution flows within the catchment. Dilution flows from non-saline areas are crucial for catchment salt export because they dilute salt water from saline areas. More dilution flow is usually seen as beneficial because it provides more fresh water into the catchment. Less dilution flow can cause higher stream salinity concentrations at the end of the catchment.

For areas with moderate to high salinity hazard, it is more likely that salt stores are currently being intercepted by water moving through the landscape. If the climate change analysis is forecasting less water movement, then salinity hazard will be reduced. Conversely, more water movement through higher salinity hazard areas is likely to mobilise additional salt and hence increase salinity hazard.

**Table 1** **Categories of potential salinity hazard/dilution flow change**

Blue and red colours denote low and high CAP hazard, respectively.

| Change in surplus water (runoff + recharge) | | CAP hazard | | | | |
|---|---|---|---|---|---|---|
| | | Very Low | Low | Moderate | High | Very High |
| Drier | < –10% | Potential for lower dilution flows | | Lower salinity hazard | | |
| No change | –10% to +10% | No change to salinity hazard | | | | |
| Wetter | > +10% | Potential for higher dilution flows | | Higher salinity hazard | | |

## 2.5 Spatial datasets

PERFECT requires spatial data for land use, soil and slope. Land use, soil type and slope vary significantly and spatially over the study area and are assumed to be static through time. Other inputs (NARCliM projections) do vary over time and space. In this study, the spatial resolution is 3 arc-seconds for land use, soil, slope, predRH (Rassam & Littleboy 2003), and ~10 kilometres for NARCliM grid.

### Land use and foliage projective cover

Land use, land management and foliage cover have major effects on the water balance, with impacts on water infiltration, evapotranspiration, soil water-holding capacity, nutrients, plants and animals. Detailed land-use mapping shown in Figure 2 was derived from the NSW Land use v1 and ACT ACLUMP. The combined attributes, derived from Australian Land Use and Management Classification (ALUM), were allocated to nine simplified categories (Conservation, Forest, Grazing, Cropping, Horticulture, Tree Horticulture, Cleared, Urban, Irrigation and Water; water areas were excluded from this modelling). These categories were selected to better reflect hydrological response across different land-use types.

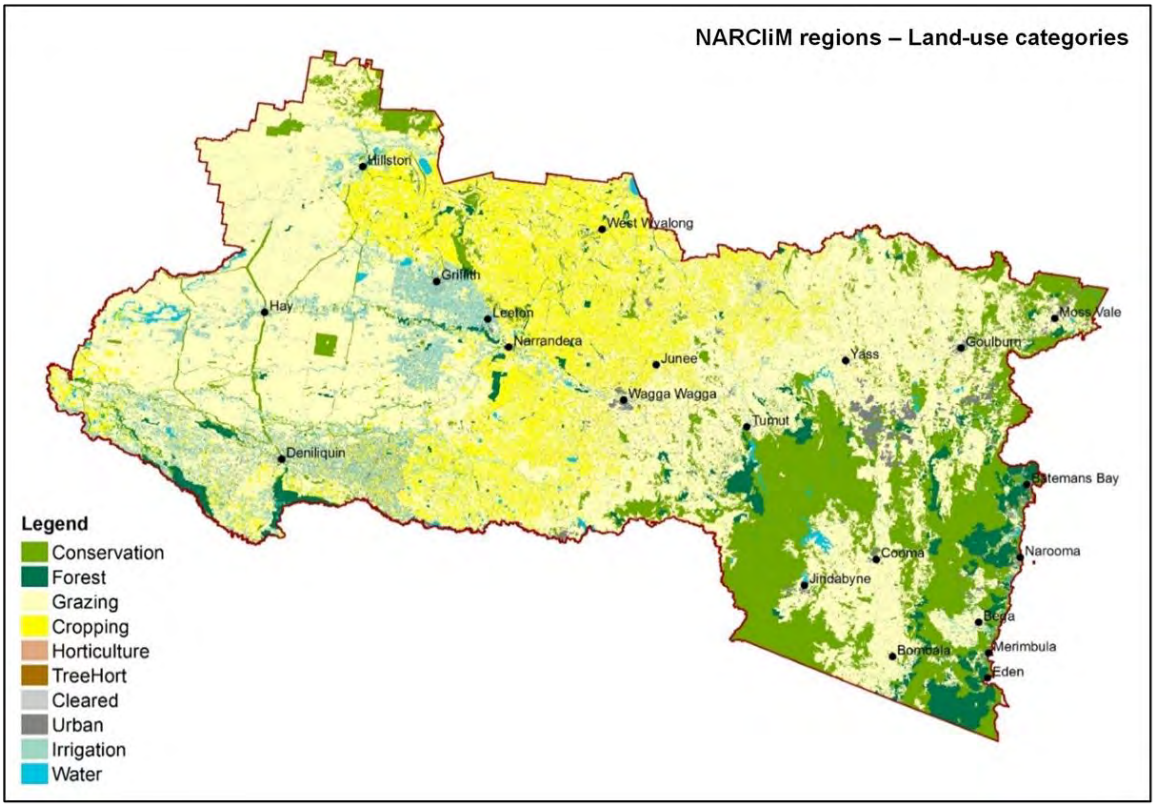


**Figure 2** **Detailed land-use categories derived from the DPIE NSW Land use v1 and Sydney 1:100k mapping**

To better model hydrology within the land-use categories, foliage projective cover (FPC) shown in Figure 3 was derived from the NSW woody vegetation and FPC 2011 statewide dataset and categorised to four classes (0–20%, 20–40%, 40–65%, ≥65%). The categorised FPC layer was intersected with the land-use layer to create hydrological response units. Using FPC was crucial for land-use categories such as grazing because it allowed us to separate grazing areas into open grasslands, open woodlands and closed woodlands. In that way, we captured the varying hydrological responses that are inherent within a single and generic land-use category.

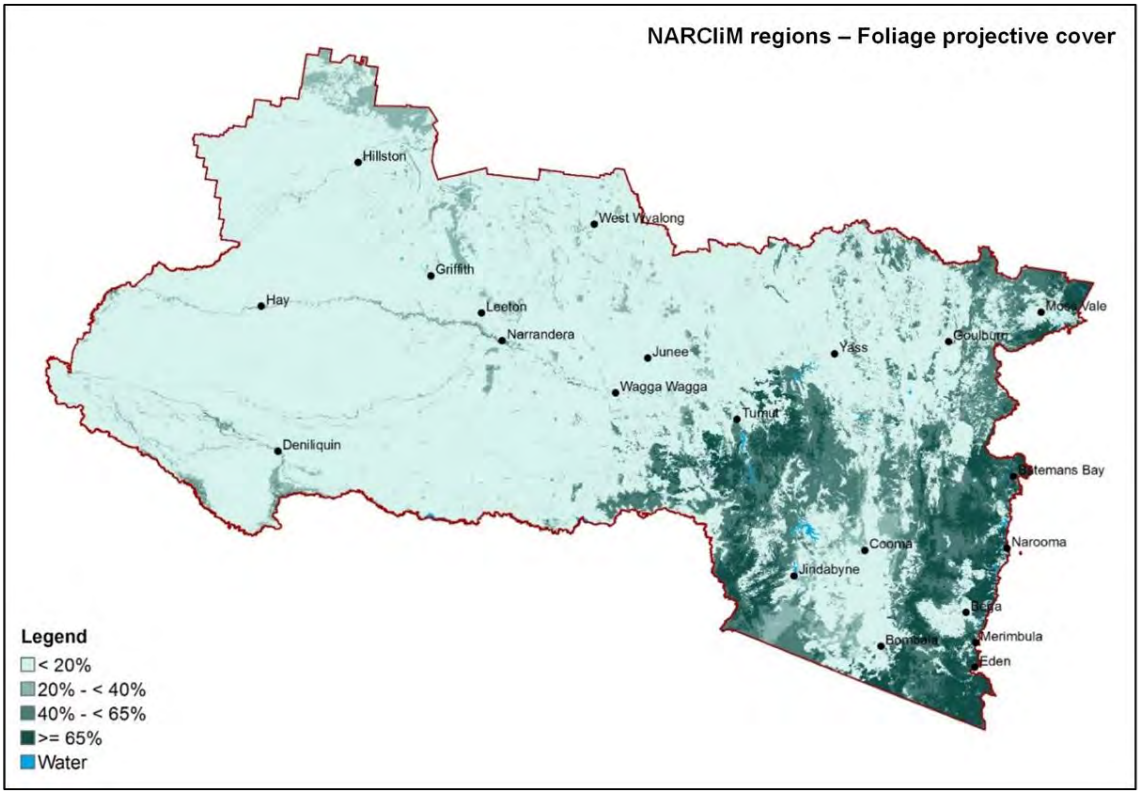


**Figure 3** **Percentage of foliage projective cover derived from the DPIE NSW woody vegetation and FPC 2011 statewide dataset**

## Soil types (Great Soil Groups of NSW)

The nature and conditions of the underlying soils (depth, type, texture, chemical composition, physical properties, available moisture content, hydraulic conductivity, and bulk density) all affect the water balance within a catchment.

Soil types across the region are shown in Figure 4 and have been classified using a modified version of the Great Soil Groups (GSG) classification. It uses the best available soils and natural resource mapping coverage provided by the NSW Government.

The dominant soil type for each ~90 metre cell within the study area was determined. Soil hydraulic properties (water content, wilting point, field capacity, saturation, and hydraulic conductivity) for each GSG as compiled by (Littleboy et al. 2003, 2009) were used to define soil hydraulic parameters. These parameters are input files to the PERFECT model.

## Lateral flow partitioning coefficient (Rh)

Mean slope for each ~90 metre (3 arc-second) cell and values for lateral flow partitioning coefficient (Rassam & Littleboy, 2003) were calculated from the Shuttle Radar Topography Mission (SRTM) 30 metre resolution Digital Elevation Model.

## Modelling environment (Python 2.7)

Modelling was performed using a Python-based system, backed by the core PERFECT water balance model, implemented in FORTRAN and compiled to executable (exe) format. The Python software managed the various spatial and temporal data inputs and pre-processed this data for input to the point-based PERFECT model, before assembling the outputs into spatial and aggregate output files as ESRI raster format. At its core, the system manages unique ‘scenarios’, which describe a set of PERFECT model runs based on three

key information sources for the area of interest: climate, soil and land-use/foliage cover inputs. The intersection of these three information sources identifies a unique spatial area and determines the corresponding PERFECT model inputs and parameters required for the unit to be modelled. To minimise run times, only unique combinations of land use and soil within a single 10 kilometre NARCliM cell were processed.

For the simulations presented in this report, the multi-step system was configured to:

- read the post-processed NARCliM netCDFs containing daily data for rainfall and evapotranspiration, convert to PERFECT model input file type
- index 10 kilometre NARCliM cell and determine the number of unique combinations of 100 metre drivers (land use, soil) and execute PERFECT for each unique driver combination
- compile modelled outputs as ESRI raster format for input to ArcGIS
- provide post-processing of drainage partitioning. For each GCM/RCM scenario (annual and monthly), combine lateral flow and recharge to define total drainage and using lateral flow partitioning coefficient (Rassam & Littleboy 2003), partition to groundwater recharge and surface runoff
- generate seasonal grids by combining each GCM/RCM scenario. Summer is December, January, February (DJF), autumn is March, April, May (MAM), winter is June, July, August (JJA), and spring is September, October, November (SON)
- extract annual and seasonal means for each period (1990 to 2009, 2020 to 2039 and 2060 to 2079) as input .csv for R scripts. The R scripts produce the relevant graph-based outputs of absolute change.

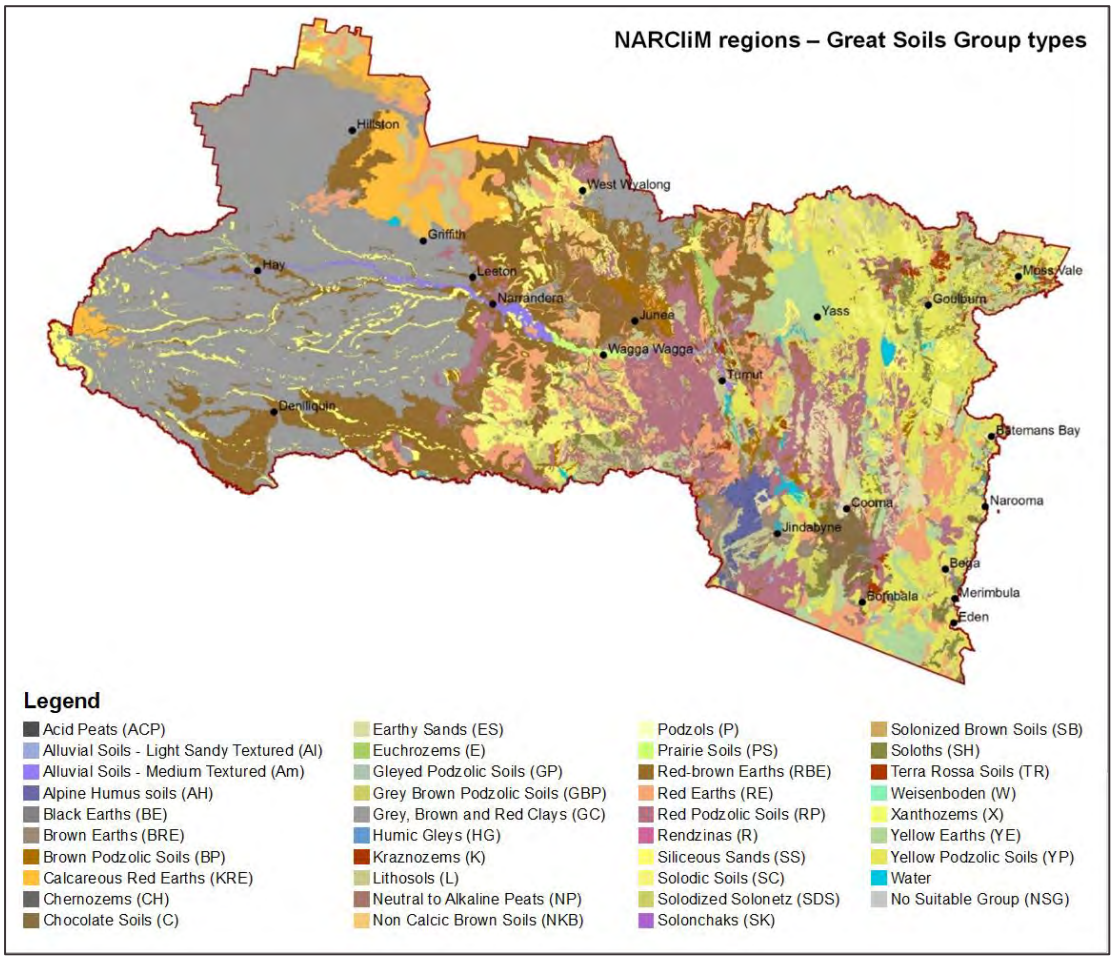


**Figure 4** **Dominant soil type distribution derived from the DPIE NSW Great Soil Groups statewide dataset**

## 2.6 Quality control

### Datasets

Using the Department of Planning, Industry and Environment (DPIE) corporate licensed spatial software (ArcGIS 10.x), spatial datasets as inputs to the modelling are a by-product of existing corporate and external sources. The quality of the by-product datasets is at least as good as the source data. All data has been converted to raster format, projected to WGS 84 at a resolution of 3 arc-seconds (approx. 90 m) and aligned to SRTM DEM. Stored data is in ESRI TIFF, GCS WGS84, 3 arc-second format and is available as individual files or zipped. Dataset completeness is study area; MM, ACT, South East and Tablelands as a single coverage, extent boundary top: –32.671254 dd, left: 143.317445 dd, right: 150.745676 dd, bot: –37.505077dd.

Output files (.tif, .csv, .jpg) are named using the standard NARCliM convention:

{Version}_{Domain}_{Model}_{Measure}_{Actual/Change}_
{time period_{Variable}_{Unit}_{Annual/Season}_{region prefix}_{region}.{ext}

i.e. v001_20170907_d02_multimodel_mean_chg_2060_2079_Recharge_mm_SON_ALPINE_0.jpg

where:

- {Ver} is used for version control (version: vxxx + date: yyyymmdd)
- {Domain} is d02 and indicates the 10 kilometre resolution NARCliM domain
- {Model} is the combination of GCMs (reanalysis, MIROC3.2, ECHAM5, CCCMA3.1, CSIRO-MK3.0) and RCMs (R1, R2, R3). Multi-model represents the mean of all model combinations
- {Measure} is the representation of the method of combining data from multiple models (i.e. mean, median, mode)
- {Actual/Change} represents whether it is the actual value for the time period or the difference between the 1990 to 2009 baseline period and 2020 to 2039 or 2060 to 2079 near and far future time periods (i.e. the change)
- {Epoch} is one of the three temporal periods: 1990 to 2009, 2020 to 2039 and 2060 to 2079
- {Variable} is the name of the output modelled variable – Recharge, Surface Flow
- {Unit} is the unit of measure for the variable
- {Annual/Season} can be ANN, DJF, MAM, JJA, SON; for annual and seasonal time periods
- {region prefix} ALPINE = Alpine Project
- {region} is 0 = ALPINE (MM, ACT and SET).

### Water balance model PERFECT 3.0

The water balance model used in this study is the PERFECT model (Littleboy et. al. 1992). It was developed as a cropping systems model to predict the water balance (runoff, infiltration, soil evaporation, transpiration and recharge) for crop/fallow sequences. It has been previously applied to estimate water balance for a range of perennial pasture systems and tree water use in eastern Australia. A major strength of PERFECT is that it contains robust and well-tested algorithms, often based on proven water balance models developed by the United States Department of Agriculture. Many examples of previous model validation in Eastern Australia are documented (e.g. Abbs & Littleboy 1998).

The modelling used in this study is consistent with other modelling activities across New South Wales including:

- coastal estuarine monitoring, evaluation and reporting modelling (Littleboy et al. 2009; Roper et al. 2011)
- future salinity-trend modelling for the 2009 Salinity Audit (DECC 2009)
- salinity tools used in the Native Vegetation Assessment Tool or NVAT (DECCW 2011) and enhancements proposed under the Environmental Outcomes Assessment Methodology (OEH 2012)
- previous statewide assessments for the impacts of climate change on hydrology (Littleboy et al. 1992, 2003, 2009).

### Salinity hazard

A meeting was held on Thursday 31 August 2017 at the NSW Office of Environment and Heritage (now DPIE) Cowra office to expertly review the potential impact of change to salinity hazard under future climate projections. Present at the meeting to discuss the outputs were Allan Nicholson (NSW Department of Primary Industries (DPI), Principal Salinity Officer), Andrew Wooldridge (NSW DPI, Salinity Officer), Rob Muller (NSW OEH, Senior Scientist) and John Young (NSW OEH, Scientist) who presented the results based on modelling criteria (Wooldridge et al. 2012).

Expert knowledge of salinity hazard across the area comes from previous and continued work in hydrogeological landscapes in: Central West, ACT, Yass, Jugiong, Tumut, Bega, Cooma and Wagga, and work completed for the Salinity Hazard for Catchment Action Plans (CAP) program.

With an understanding that CAP mapping is the only dataset currently available for entire coverage of the study area and is a broad-scale salinity hazard spatial coverage, findings from modelling of potential change in salinity hazard were positive:

- Based on geological parameters, the interpretation of the hazards using the +/–10% was deemed reasonable.
- Salinity hazard mapping was not consistent across the whole study area. There is greater confidence in areas where more information was available, and where HGL mapping was able to be incorporated.
- The main limitation stems from how irrigation areas are attributed. In the CAP hazard mapping, any polygon that has significant irrigation automatically becomes high hazard for the whole polygon. Key examples can be seen around Griffith and Leeton. Irrigation was not specifically modelled as a land-use category.

## 2.7 Data storage and access

All output data were converted to raster format (ArcGIS ESRI grid) and supplied to the MCAS-S (Multi-Criteria Analysis Shell for Spatial Decision Support) datapacks for distribution and storage. All input data to the model and by-products are stored on hard disk drives. All data are in the NARCliM coordinate system. The extent of the datasets includes the MM region, ACT and SET with the boundary at top: –32.671254, left: 143.317445, right: 150.745676, and bottom: –37.505077.

# 3. Results

## 3.1 Surface runoff

### Changes in surface runoff – entire study area

Over most of the study area, surface runoff is likely to decrease (drying) in the near future (Figure 5). An increase in surface runoff (wetting) is evident in the far future (Figure 6) based on the multi-model mean of simulations. There is a large variation in likely changes across the 12 different GCM/RCM model simulations however; some combinations suggest more runoff while others suggest less runoff. Largest increases (wetting) are projected in areas from Balranald to Deniliquin, and around West Wyalong and south of Griffith. In the far future, reductions in surface runoff of more than 40 millimetres/year are projected for higher alpine areas, generally bounded by the Alpine region, from Tumut to Canberra to the Victorian border in the south.

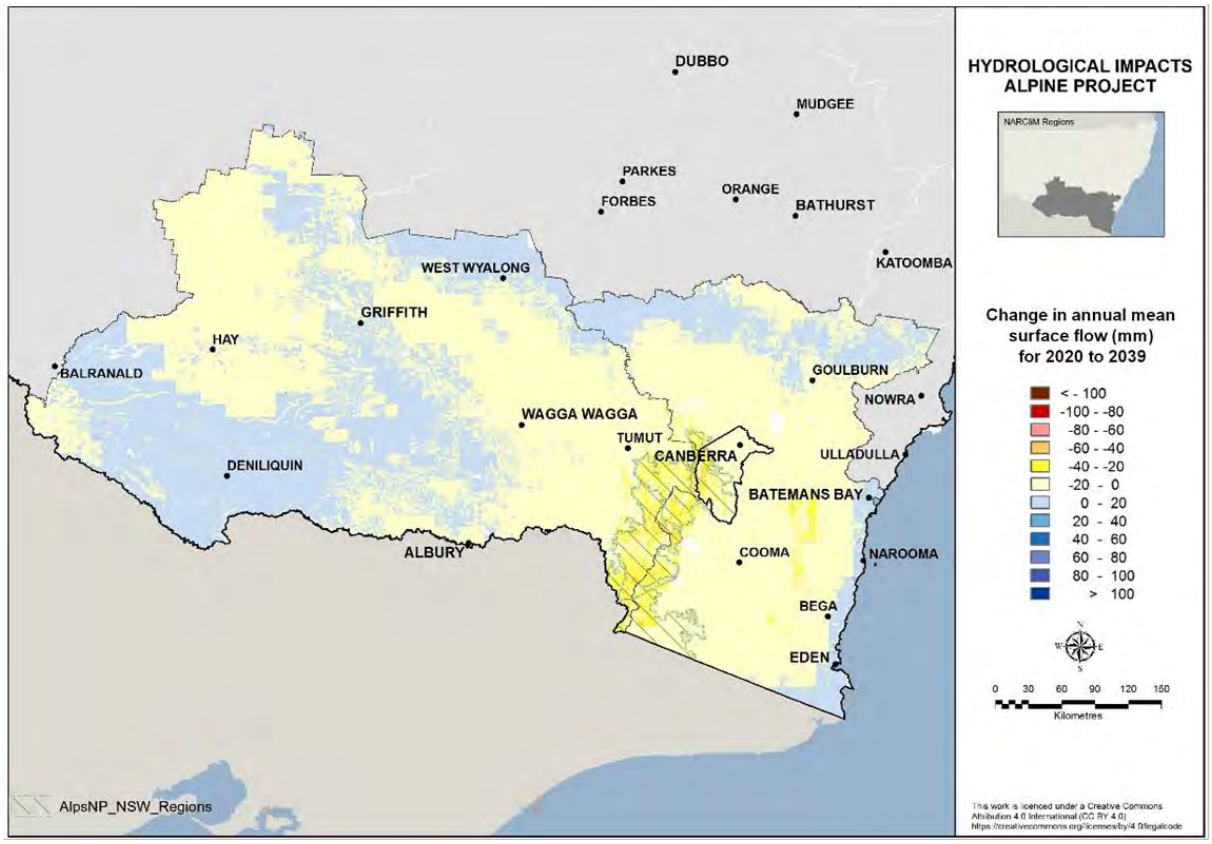


**Figure 5** **Changes in mean annual surface runoff (mm) across the study area for 2020 to 2039 relative to the 1990 to 2009 baseline period**

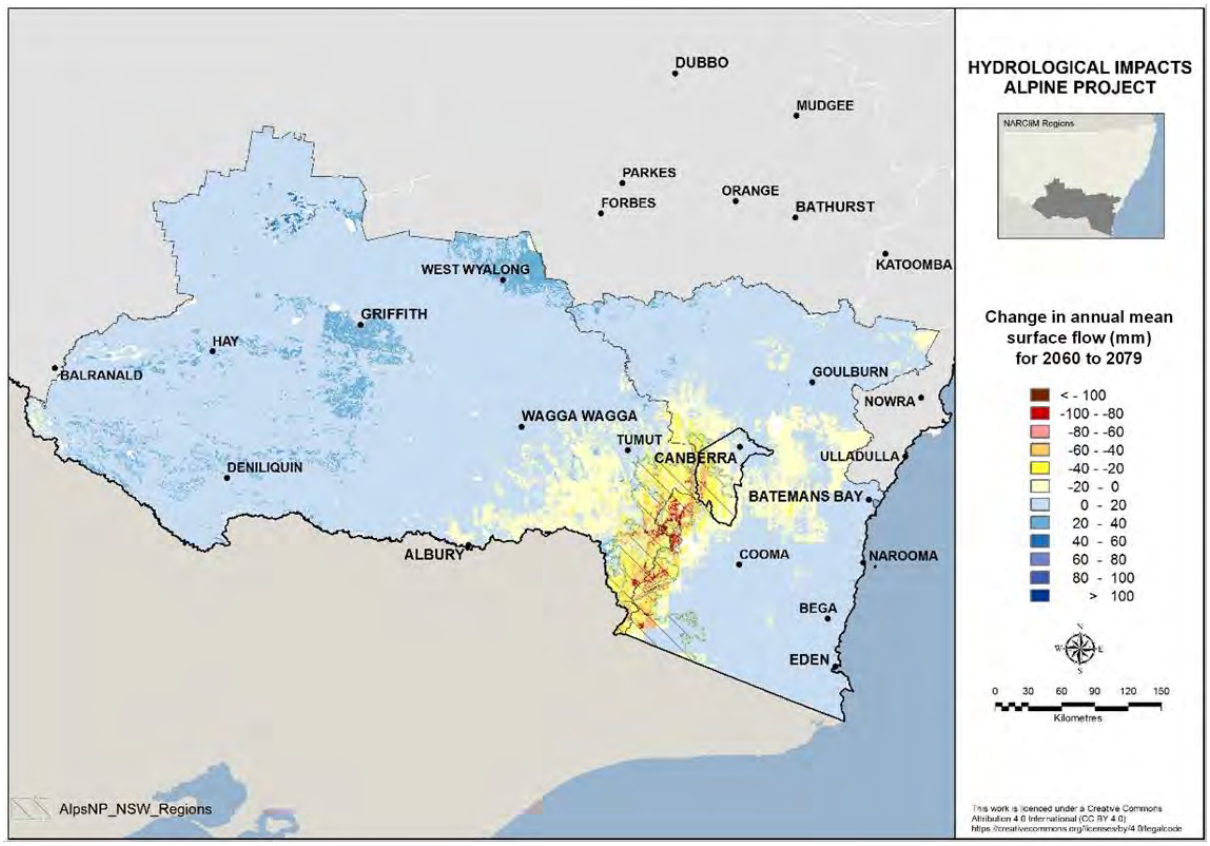


**Figure 6** **Changes in mean annual surface runoff (mm) across the study area for 2060 to 2079 relative to the 1990 to 2009 baseline period**

As noted above, there are a range of projections for mean annual surface runoff ranging from a decrease of 13.0 millimetres (drying) to an increase of 10.8 millimetres (wetting) for the near future, and drying of 5.4 millimetres to wetting of 15.9 millimetres for the far future (Figure 7).

Near future scenario projections show surface runoff in summer ranging from –11.2 to +4.3 millimetres, autumn ranging from –5.3 to +8.5 millimetres, winter ranging from –2.1 to +1.9 millimetres, and spring ranging from –3.6 to +0.6 millimetres. For the far future scenario, summer surface runoff ranges from –2.5 to +14.2 millimetres, autumn –2.2 to +8.1 millimetres, winter –3.7 to +4.0 millimetres, and spring –7.4 to +2.2 millimetres (Figure 7).

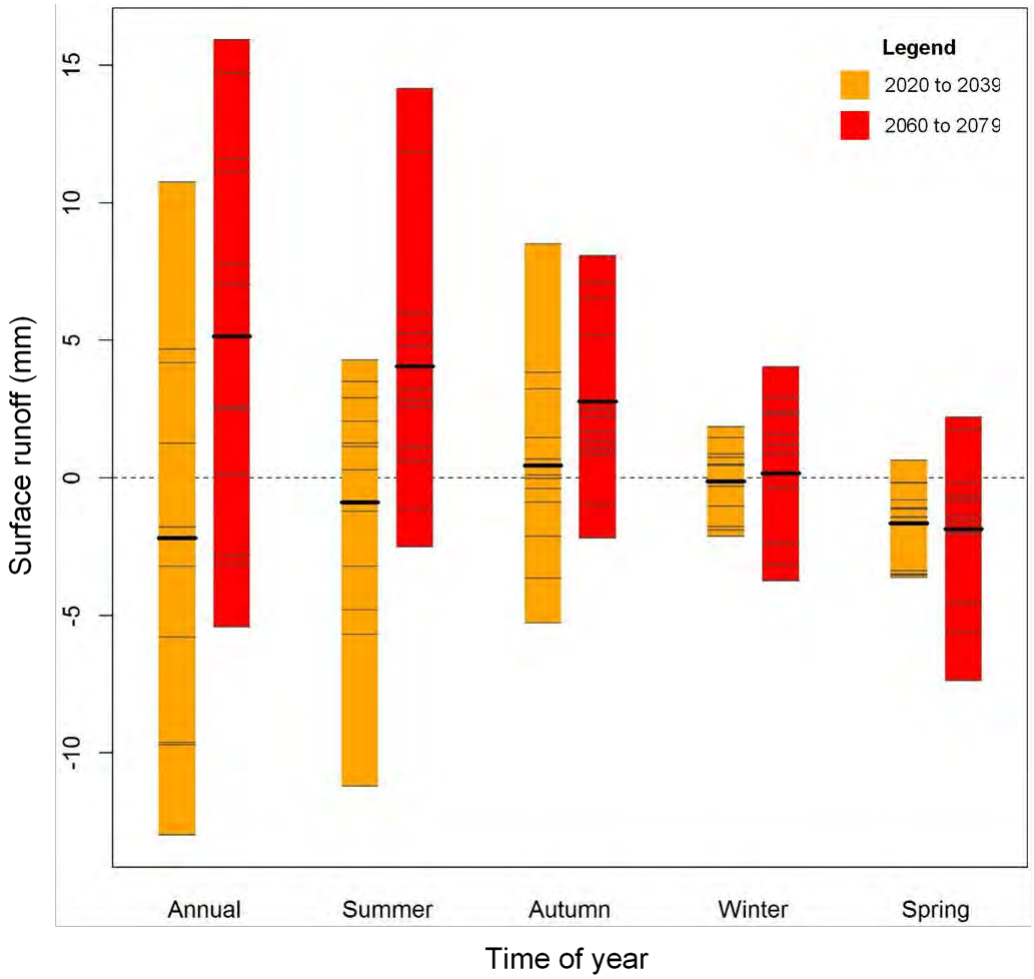


**Figure 7** **Absolute change in seasonal and annual surface runoff (mm) across the study area**

Colours denote the near future (2020 to 2039) and far future (2060 to 2079) NARCliM projection periods.

For the near future, the NARCliM simulations using CCCMA3.1 and MIROC3.2_R3 as hosts forecast a slight increase in surface runoff (wetting), whereas those using CSIRO-MK3.0, ECHAM5 and MIROC3.2_R1/R2 project less surface runoff (drying). For the far future, nine of the 12 NARCliM simulations project higher surface runoff, and those using CSIRO-MK3.0 project less surface runoff. The largest variability across GCM/RCM combinations on a seasonal basis occurs for summer and autumn periods in both the near future and far future (Table 2).

Table 2 presents mean annual and seasonal surface runoff predictions and Table 3 provides changes in annual and seasonal surface runoff for each GCM/RCM combination across the entire region. Change is calculated from the climate baseline (1990 to 2009) to the near future (2020 to 2039) and far future (2060 to 2079).

**Table 2** **Mean annual and seasonal surface runoff (mm) across the study area for each GCM/RCM combination**

Pink and green colours denote maximum and minimum changes in surface runoff, respectively. ANN = annual, DJF = summer, MAM = autumn, JJA = winter and SON = spring.

| | Baseline 1990 to 2009 | | | | | Near future 2020 to 2039 | | | | | Far future 2060 to 2079 | | | | |
|---|---|---|---|---|---|---|---|---|---|---|---|---|---|---|---|
| GCM/RCM model | ANN | DJF | MAM | JJA | SON | ANN | DJF | MAM | JJA | SON | ANN | DJF | MAM | JJA | SON |
| MIROC3.2_R1 | 72.9 | 21.9 | 14.7 | 17.7 | 18.7 | 71.1 | 23.1 | 14.8 | 18.2 | 15.1 | 87.6 | 36.0 | 15.7 | 21.7 | 14.2 |
| MIROC3.2_R2 | 64.7 | 16.0 | 11.3 | 19.9 | 17.5 | 62.9 | 18.9 | 10.5 | 19.6 | 14.0 | 64.8 | 13.5 | 18.4 | 22.8 | 10.1 |
| MIROC3.2_R3 | 72.8 | 16.8 | 15.4 | 20.1 | 20.5 | 74.1 | 21.1 | 15.0 | 20.9 | 17.0 | 88.7 | 28.7 | 23.5 | 21.7 | 14.9 |
| ECHAM5_R1 | 53.6 | 23.3 | 7.5 | 17.2 | 5.6 | 40.6 | 12.1 | 9.0 | 15.1 | 4.5 | 64.7 | 29.3 | 10.0 | 18.1 | 7.4 |
| ECHAM5_R2 | 38.2 | 9.9 | 7.8 | 15.3 | 5.2 | 36.0 | 10.2 | 5.6 | 15.2 | 5.0 | 45.2 | 12.5 | 10.0 | 17.8 | 5.0 |
| ECHAM5_R3 | 53.1 | 18.0 | 10.0 | 17.5 | 7.6 | 47.3 | 16.7 | 10.7 | 15.6 | 4.2 | 64.7 | 23.2 | 16.6 | 15.1 | 9.8 |
| CSIRO-MK3.0_R1 | 55.5 | 21.2 | 12.5 | 14.2 | 7.6 | 45.9 | 16.4 | 7.2 | 16.1 | 6.2 | 52.4 | 26.0 | 10.4 | 10.5 | 5.5 |
| CSIRO-MK3.0_R2 | 35.0 | 9.8 | 4.7 | 14.5 | 6.0 | 31.8 | 6.6 | 4.7 | 16.0 | 4.6 | 29.6 | 8.6 | 5.5 | 10.8 | 4.6 |
| CSIRO-MK3.0_R3 | 48.8 | 20.5 | 9.9 | 11.7 | 6.8 | 39.1 | 14.8 | 6.2 | 12.4 | 5.7 | 46.0 | 23.7 | 8.9 | 8.6 | 4.8 |
| CCCMA3.1_R1 | 19.8 | 4.8 | 2.9 | 7.7 | 4.2 | 30.5 | 6.0 | 11.5 | 8.2 | 4.9 | 27.5 | 6.0 | 8.1 | 10.0 | 3.4 |
| CCCMA3.1_R2 | 17.4 | 1.6 | 1.9 | 9.3 | 4.6 | 22.1 | 3.6 | 5.7 | 8.3 | 4.4 | 19.8 | 2.2 | 3.2 | 10.5 | 3.9 |
| CCCMA3.1_R3 | 20.1 | 2.4 | 4.8 | 8.1 | 4.7 | 24.3 | 5.9 | 8.0 | 6.4 | 3.9 | 22.6 | 5.2 | 6.4 | 7.8 | 3.2 |
| | | | | | | | | | | | | | | | |
| Maximum: | 72.9 | 23.3 | 15.4 | 20.1 | 20.5 | 74.1 | 23.1 | 15.0 | 20.9 | 17.0 | 88.7 | 36.0 | 23.5 | 22.8 | 14.9 |
| Minimum: | 17.4 | 1.6 | 1.9 | 7.7 | 4.2 | 22.1 | 3.6 | 4.7 | 6.4 | 3.9 | 19.8 | 2.2 | 3.2 | 7.8 | 3.2 |
| Range: | 55.5 | 21.7 | 13.5 | 12.3 | 16.3 | 52.0 | 19.5 | 10.4 | 14.5 | 13.1 | 68.9 | 33.8 | 20.3 | 15.0 | 11.7 |

**Table 3** **Changes in mean annual and seasonal surface runoff (mm) across the study area for each GCM/RCM combination**

Grey and blue colours denote maximum and minimum changes in surface runoff, respectively. ANN = annual, DJF = summer, MAM = autumn, JJA = winter and SON = spring.

| | Near future (2020 to 2039) | | | | | Far future (2060 to 2079) | | | | |
|---|---|---|---|---|---|---|---|---|---|---|
| GCM/RCM model | ANN | DJF | MAM | JJA | SON | ANN | DJF | MAM | JJA | SON |
| MIROC3.2_R1 | –1.8 | 1.3 | 0.1 | 0.5 | –3.6 | 14.7 | 14.2 | 1.1 | 4.0 | –4.5 |
| MIROC3.2_R2 | –1.8 | 2.9 | –0.9 | –0.3 | –3.5 | 0.1 | –2.5 | 7.1 | 2.9 | –7.4 |
| MIROC3.2_R3 | 1.3 | 4.3 | –0.4 | 0.9 | –3.5 | 15.9 | 11.9 | 8.1 | 1.6 | –5.6 |
| ECHAM5_R1 | –13.0 | –11.2 | 1.5 | –2.1 | –1.1 | 11.1 | 6.0 | 2.5 | 0.9 | 1.8 |
| ECHAM5_R2 | –2.2 | 0.3 | –2.1 | –0.2 | –0.2 | 7.0 | 2.6 | 2.2 | 2.4 | –0.2 |
| ECHAM5_R3 | –5.8 | –1.2 | 0.7 | –1.9 | –3.4 | 11.6 | 5.3 | 6.5 | –2.4 | 2.2 |
| CSIRO-MK3.0_R1 | –9.6 | –4.8 | –5.3 | 1.9 | –1.4 | –3.1 | 4.8 | –2.2 | –3.7 | –2.0 |
| CSIRO-MK3.0_R2 | –3.2 | –3.2 | 0.0 | 1.5 | –1.4 | –5.4 | –1.1 | 0.8 | –3.7 | –1.4 |
| CSIRO-MK3.0_R3 | –9.7 | –5.7 | –3.6 | 0.7 | –1.1 | –2.8 | 3.2 | –0.9 | –3.2 | –1.9 |
| CCCMA3.1_R1 | 10.8 | 1.1 | 8.5 | 0.5 | 0.6 | 7.8 | 1.1 | 5.2 | 2.3 | –0.8 |
| CCCMA3.1_R2 | 4.7 | 2.1 | 3.8 | –1.0 | –0.2 | 2.5 | 0.6 | 1.3 | 1.2 | –0.7 |
| CCCMA3.1_R3 | 4.2 | 3.5 | 3.2 | –1.8 | –0.8 | 2.6 | 2.8 | 1.7 | –0.4 | –1.6 |
| | | | | | | | | | | |
| Maximum: | 10.8 | 4.3 | 8.5 | 1.9 | 0.6 | 15.9 | 14.2 | 8.1 | 4.0 | 2.2 |
| Minimum: | –13.0 | –11.2 | –5.3 | –2.1 | –3.6 | –5.4 | –2.5 | –2.2 | –3.7 | –7.4 |
| Scenarios > 0: | 4 | 7 | 6 | 6 | 1 | 9 | 10 | 10 | 7 | 2 |
| Scenarios ≤ 0: | 8 | 5 | 6 | 6 | 11 | 3 | 2 | 2 | 5 | 10 |
| Range: | 23.7 | 15.5 | 13.8 | 4.0 | 4.3 | 21.3 | 16.7 | 10.3 | 7.8 | 9.6 |

## Changes in surface runoff – NSW and ACT Alpine region

Surface runoff is projected to decrease (drying) in the near future (2020 to 2039) across much of the NSW and ACT Alpine region based on the multi-model mean of the 12 GCM/RCM simulations (Figure 8). In the far future (2060 to 2079), surface runoff is also projected to decrease for most areas in the region except for a slight increase in runoff projected for a small area east of Thredbo (Figure 9). This increase is relatively small and less than 20 millimetres/year.

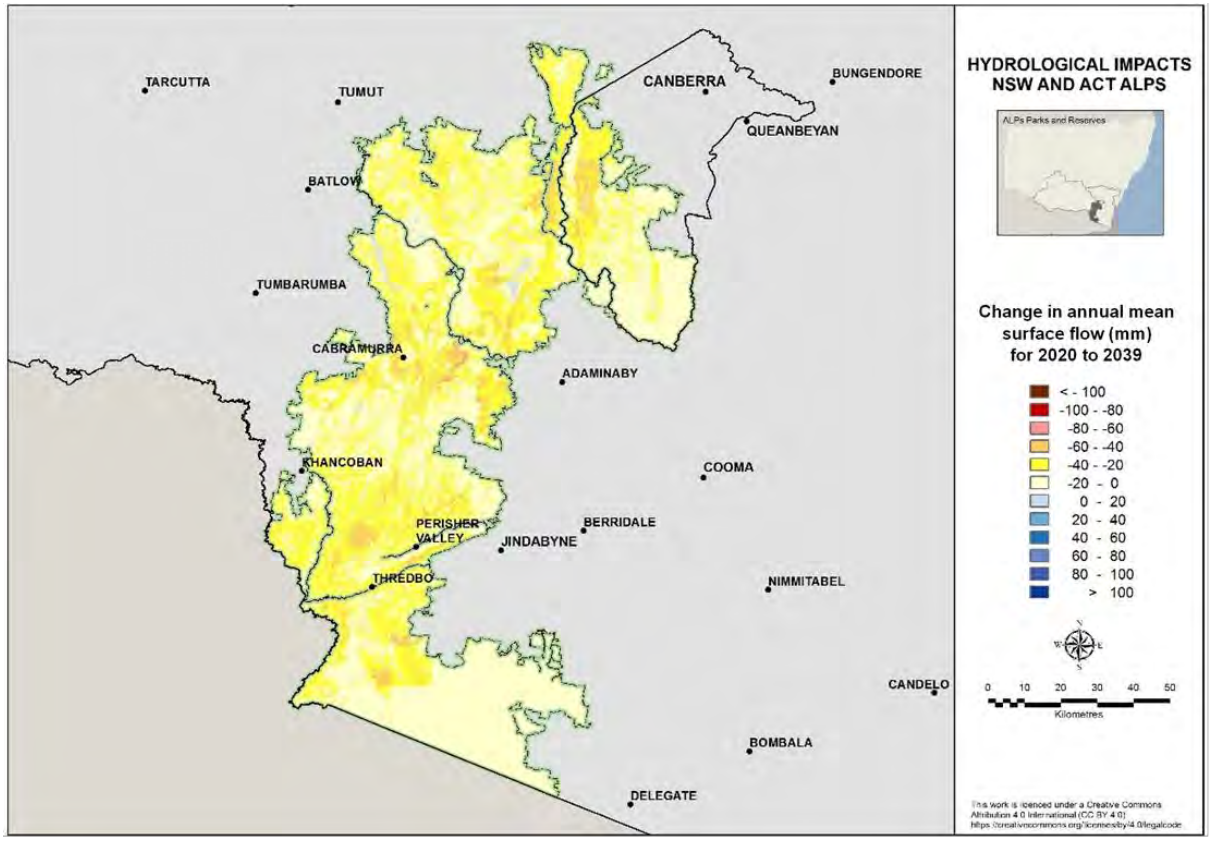


**Figure 8** **Changes in mean annual surface runoff (mm) in the NSW and ACT Alpine region for 2020 to 2039 relative to the 1990 to 2009 baseline period**

The multi-model mean is the average of a range of different model forecasts. Near future projections for changes in mean annual runoff range from a decrease (drying) of –51.7 millimetres to an increase (wetting) of +22.5 millimetres (Figure 10). For the far future, forecasts also span both drying and wetting scenarios (–72.0 mm to +16.6 mm) (Figure 10).

Figure 10 and Table 4 show seasonal changes in surface runoff for the near future that include both increases and decreases in summer (–18.5 to +9.3 mm), autumn (–11.3 to +13.7 mm), winter (–17.3 to +18.9 mm) and spring (–28.9 to +7.7 mm). For the far future, the changes in surface runoff in summer range from –14.8 to +22.5 millimetres, in autumn –4.5 to +10.9 millimetres, winter –35.8 to +39.6 millimetres, while projected surface runoff in spring shows a decrease only, ranging from –65.8 to –4.6 millimetres.

Based on mean annual runoff for the near future, simulations excluding CCCMA3.1_R1 tend to project less recharge (drying). For the far future, nine of the 12 NARCliM ensembles forecast a decrease in surface runoff and three show more surface runoff. Most variability across the GCM/RCM combinations is evident during the winter and spring periods for the near future, and winter for the far future (Table 5).

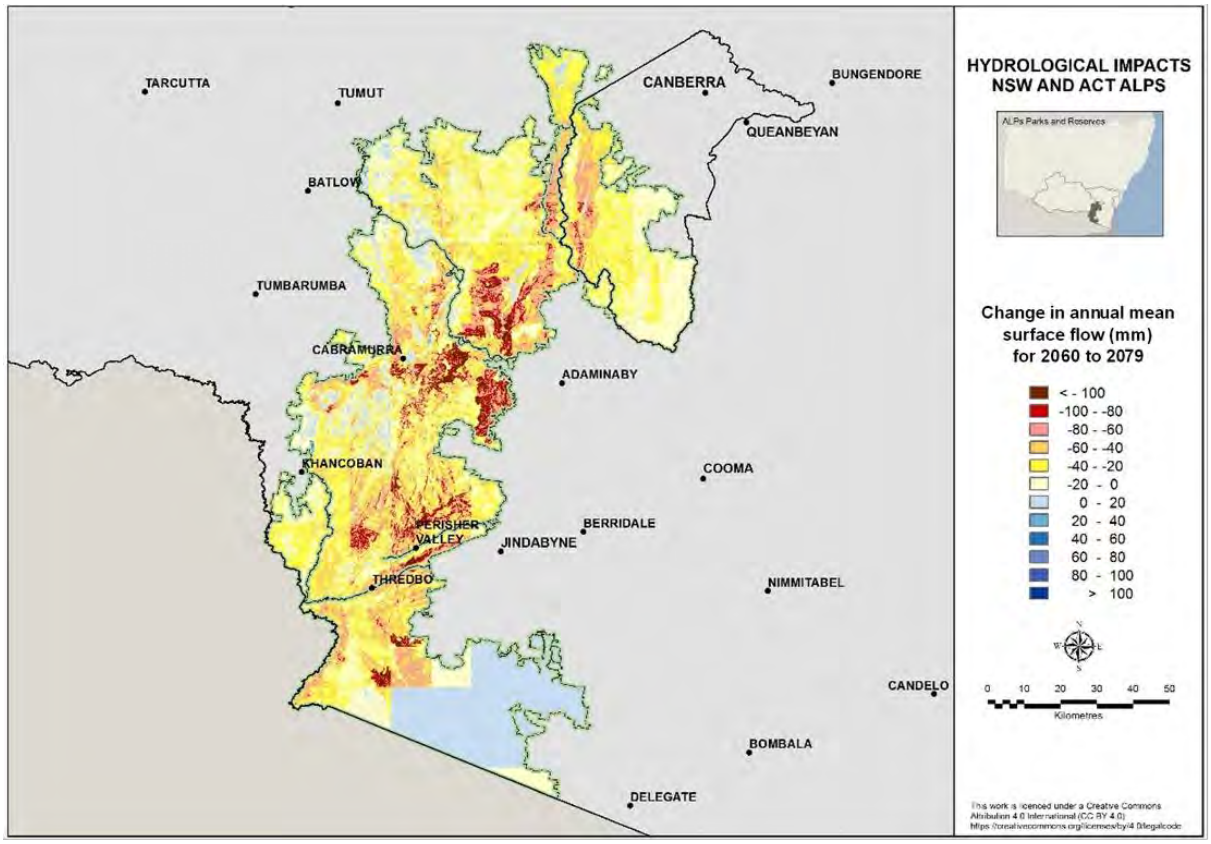


**Figure 9** **Changes in mean annual surface runoff (mm) in the NSW and ACT Alpine region for 2060 to 2079 relative to the 1990 to 2009 baseline period**

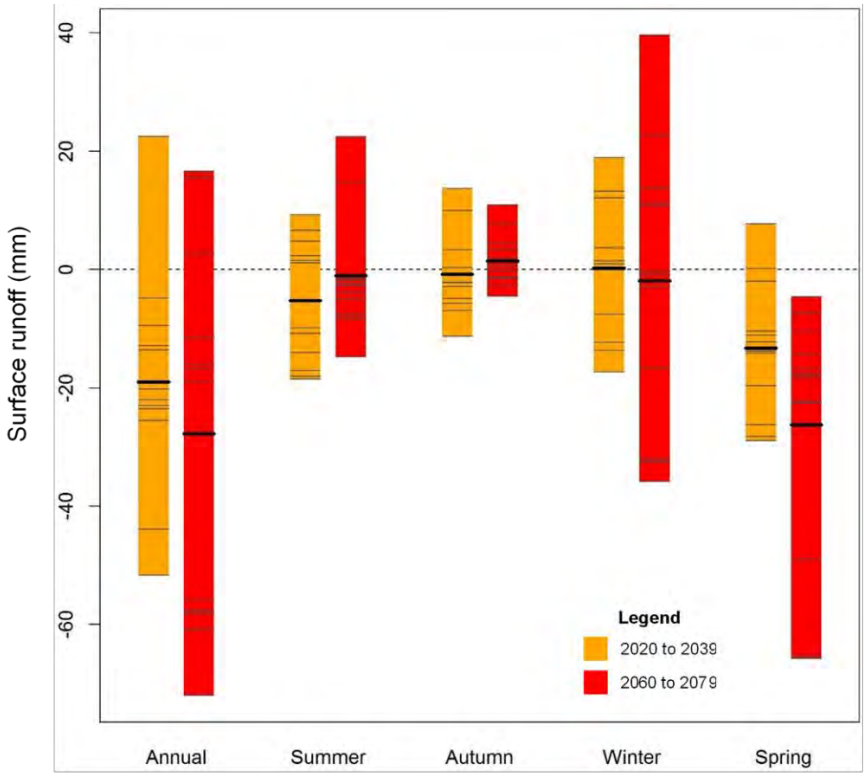


**Figure 10** **Absolute change in seasonal and annual surface runoff (mm) in the NSW and ACT Alpine region**

Colours denote the near future (2020 to 2039) and far future (2060 to 2079) NARCliM projection periods.

**Table 4** **Mean annual and seasonal surface runoff (mm) in the NSW and ACT Alpine region for each GCM/RCM combination**

Pink and green colours denote maximum and minimum changes in surface runoff, respectively. ANN = annual, DJF = summer, MAM = autumn, JJA = winter and SON = spring.

| | Baseline 1990 to 2009 | | | | | Near future 2020 to 2039 | | | | | Far future 2060 to 2079 | | | | |
|---|---|---|---|---|---|---|---|---|---|---|---|---|---|---|---|
| GCM/RCM model | ANN | DJF | MAM | JJA | SON | ANN | DJF | MAM | JJA | SON | ANN | DJF | MAM | JJA | SON |
| MIROC3.2_R1 | 454.2 | 56.2 | 76.3 | 175.5 | 146.3 | 432.2 | 60.9 | 74.0 | 179.2 | 118.0 | 437.4 | 78.6 | 75.0 | 186.6 | 97.2 |
| MIROC3.2_R2 | 462.4 | 47.2 | 69.0 | 195.9 | 150.3 | 439.5 | 56.4 | 62.1 | 196.8 | 124.1 | 401.6 | 44.7 | 76.8 | 195.6 | 84.6 |
| MIROC3.2_R3 | 474.1 | 49.5 | 75.4 | 193.3 | 155.8 | 450.5 | 56.1 | 70.5 | 197.0 | 126.9 | 402.0 | 64.1 | 70.9 | 176.7 | 90.3 |
| ECHAM5_R1 | 298.5 | 41.2 | 32.8 | 161.5 | 62.9 | 246.8 | 23.2 | 27.1 | 147.7 | 48.8 | 301.2 | 38.5 | 33.4 | 184.1 | 45.2 |
| ECHAM5_R2 | 277.8 | 27.8 | 29.9 | 156.6 | 63.5 | 257.7 | 18.0 | 29.3 | 158.0 | 52.4 | 294.4 | 23.9 | 33.3 | 196.2 | 41.0 |
| ECHAM5_R3 | 284.2 | 42.6 | 27.3 | 148.0 | 66.4 | 240.3 | 25.5 | 27.6 | 140.5 | 46.8 | 265.3 | 27.8 | 31.7 | 161.7 | 44.0 |
| CSIRO-MK3.0_R1 | 351.7 | 63.4 | 48.0 | 167.7 | 72.7 | 338.7 | 44.9 | 45.1 | 186.5 | 62.3 | 293.8 | 55.0 | 47.8 | 135.1 | 55.9 |
| CSIRO-MK3.0_R2 | 303.2 | 27.6 | 33.7 | 177.9 | 64.1 | 289.6 | 16.8 | 31.5 | 191.1 | 50.2 | 247.4 | 20.1 | 35.6 | 142.0 | 49.7 |
| CSIRO-MK3.0_R3 | 288.0 | 43.8 | 38.4 | 144.0 | 61.8 | 262.5 | 29.7 | 27.1 | 156.1 | 49.5 | 229.9 | 38.7 | 35.7 | 111.8 | 43.5 |
| CCCMA3.1_R1 | 163.8 | 11.8 | 12.3 | 95.6 | 44.1 | 186.3 | 13.0 | 26.0 | 95.5 | 51.8 | 179.3 | 10.2 | 23.2 | 106.4 | 39.5 |
| CCCMA3.1_R2 | 188.2 | 6.0 | 11.8 | 119.0 | 51.3 | 183.4 | 8.4 | 21.8 | 101.7 | 51.5 | 176.7 | 4.1 | 10.5 | 118.2 | 43.9 |
| CCCMA3.1_R3 | 156.6 | 7.9 | 13.7 | 90.4 | 44.6 | 147.1 | 9.4 | 17.1 | 78.0 | 42.6 | 140.5 | 6.8 | 12.2 | 87.4 | 34.1 |
| | | | | | | | | | | | | | | | |
| Maximum: | 474.1 | 63.4 | 76.3 | 195.9 | 155.8 | 450.5 | 60.9 | 74.0 | 197.0 | 126.9 | 437.4 | 78.6 | 76.8 | 196.2 | 97.2 |
| Minimum: | 156.6 | 6.0 | 11.8 | 90.4 | 44.1 | 147.1 | 8.4 | 17.1 | 78.0 | 42.6 | 140.5 | 4.1 | 10.5 | 87.4 | 34.1 |
| Range: | 317.5 | 57.3 | 64.5 | 105.5 | 111.7 | 303.5 | 52.6 | 57.0 | 119.0 | 84.3 | 296.9 | 74.5 | 66.3 | 108.8 | 63.1 |

**Table 5** **Changes in mean annual and seasonal surface runoff (mm) in the NSW and ACT Alpine region for each GCM/RCM combination**

Grey and blue colours denote maximum and minimum changes in surface runoff, respectively. ANN = annual, DJF = summer, MAM = autumn, JJA = winter and SON = spring.

| | Near future 2020 to 2039 | | | | | Far future 2060 to 2079 | | | | |
|---|---|---|---|---|---|---|---|---|---|---|
| GCM/RCM model | ANN | DJF | MAM | JJA | SON | ANN | DJF | MAM | JJA | SON |
| MIROC3.2_R1 | –22.0 | 4.8 | –2.3 | 3.7 | –28.3 | –16.8 | 22.5 | –1.3 | 11.1 | –49.1 |
| MIROC3.2_R2 | –23.0 | 9.3 | –6.9 | 0.9 | –26.3 | –60.9 | –2.5 | 7.7 | –0.3 | –65.8 |
| MIROC3.2_R3 | –23.5 | 6.6 | –4.9 | 3.7 | –28.9 | –72.0 | 14.6 | –4.5 | –16.6 | –65.4 |
| ECHAM5_R1 | –51.7 | –18.1 | –5.8 | –13.7 | –14.2 | 2.7 | –2.7 | 0.5 | 22.7 | –17.8 |
| ECHAM5_R2 | –20.2 | –9.8 | –0.6 | 1.4 | –11.1 | 16.6 | –3.9 | 3.4 | 39.6 | –22.5 |
| ECHAM5_R3 | –43.9 | –17.1 | 0.4 | –7.5 | –19.6 | –19.0 | –14.8 | 4.4 | 13.7 | –22.4 |
| CSIRO-MK3.0_R1 | –12.9 | –18.5 | –2.9 | 18.9 | –10.4 | –57.8 | –8.3 | –0.2 | –32.5 | –16.8 |
| CSIRO-MK3.0_R2 | –13.6 | –10.8 | –2.2 | 13.2 | –13.8 | –55.8 | –7.5 | 1.9 | –35.8 | –14.3 |
| CSIRO-MK3.0_R3 | –25.5 | –14.1 | –11.3 | 12.1 | –12.3 | –58.1 | –5.0 | –2.7 | –32.2 | –18.2 |
| CCCMA3.1_R1 | 22.5 | 1.2 | 13.7 | –0.1 | 7.7 | 15.5 | –1.6 | 10.9 | 10.8 | –4.6 |
| CCCMA3.1_R2 | –4.9 | 2.3 | 9.9 | –17.3 | 0.1 | –11.6 | –1.9 | –1.4 | –0.8 | –7.4 |
| CCCMA3.1_R3 | –9.5 | 1.5 | 3.3 | –12.4 | –2.0 | –16.0 | –1.1 | –1.5 | –2.9 | –10.5 |
| | | | | | | | | | | |
| Maximum: | 22.5 | 9.3 | 13.7 | 18.9 | 7.7 | 16.6 | 22.5 | 10.9 | 39.6 | –4.6 |
| Minimum: | –51.7 | –18.5 | –11.3 | –17.3 | –28.9 | –72.0 | –14.8 | –4.5 | –35.8 | –65.8 |
| Scenarios > 0: | 1 | 6 | 4 | 7 | 2 | 3 | 2 | 6 | 5 | 0 |
| Scenarios ≤ 0: | 11 | 6 | 8 | 5 | 10 | 9 | 10 | 6 | 7 | 12 |
| Range: | 74.2 | 27.8 | 25.0 | 36.2 | 36.6 | 88.6 | 37.2 | 15.4 | 75.4 | 61.1 |

## 3.2 Recharge to groundwater

### Changes in recharge to groundwater – entire study area

Recharge is a vital component of the total water balance of a catchment and changes in recharge can influence the availability and vulnerability of groundwater resources and the volumes of base flow in streams. Secondary impacts such as salinity and water quality with subsequent impacts on aquatic biodiversity can also occur.

For the near future, less recharge (drying) is projected across much of the study area based on the multi-model mean of the 12 GCM/RCM simulations. Areas bounded by the Alpine region and areas of higher elevation near Batemans Bay to the south-east show reductions of more than 40 millimetres/year (Figure 11). For some areas along the western part of the study area, west of Griffith, higher recharge is projected, but these increases are relatively small.

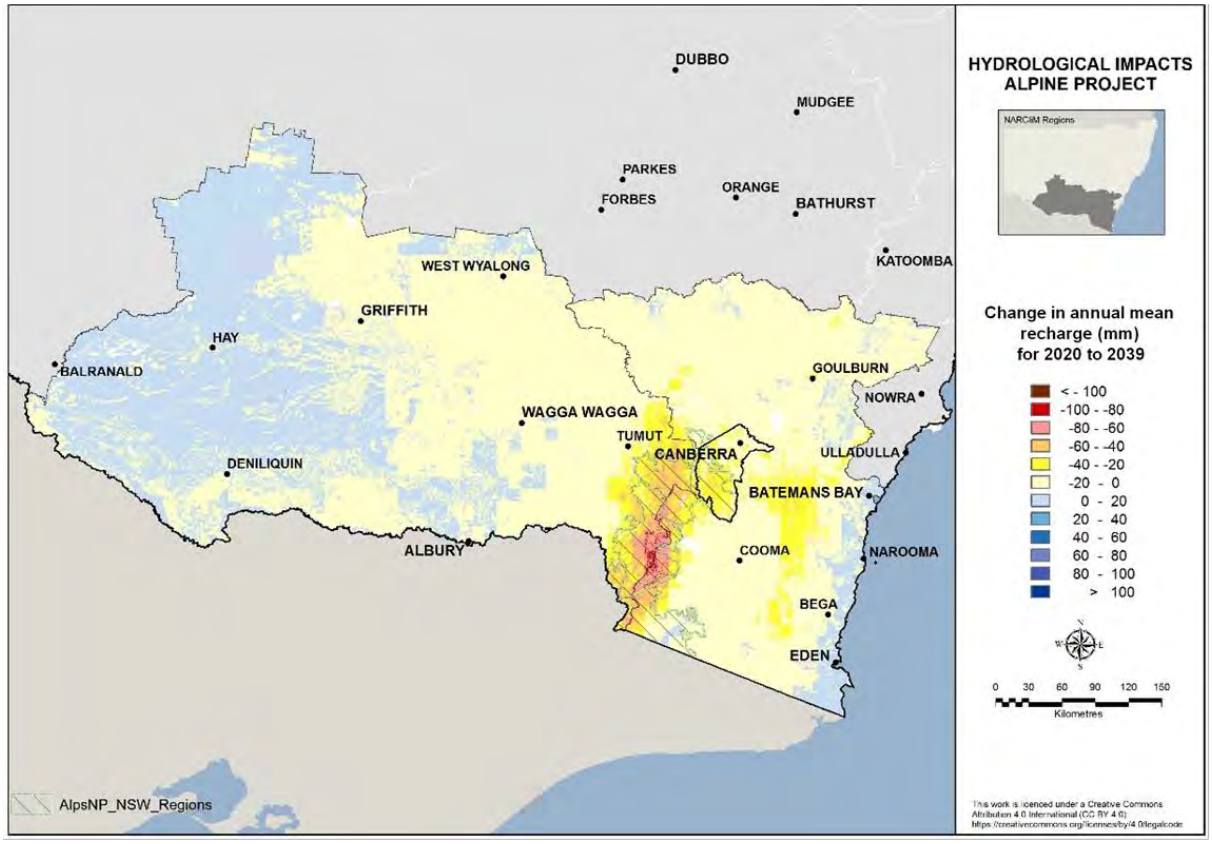


**Figure 11** **Changes in mean annual recharge (mm) across the study area for 2020 to 2039 relative to the 1990 to 2009 baseline period**

In the far future, recharge is projected to decrease across many parts of the study area (Figure 12), with highest the reductions within the ACT and Alpine region. A slight increase in recharge is projected in areas west of Wagga Wagga, north of Griffith, and between Balranald and Deniliquin. Areas along the eastern boundary of the region and Cooma to the south show an increase in recharge.

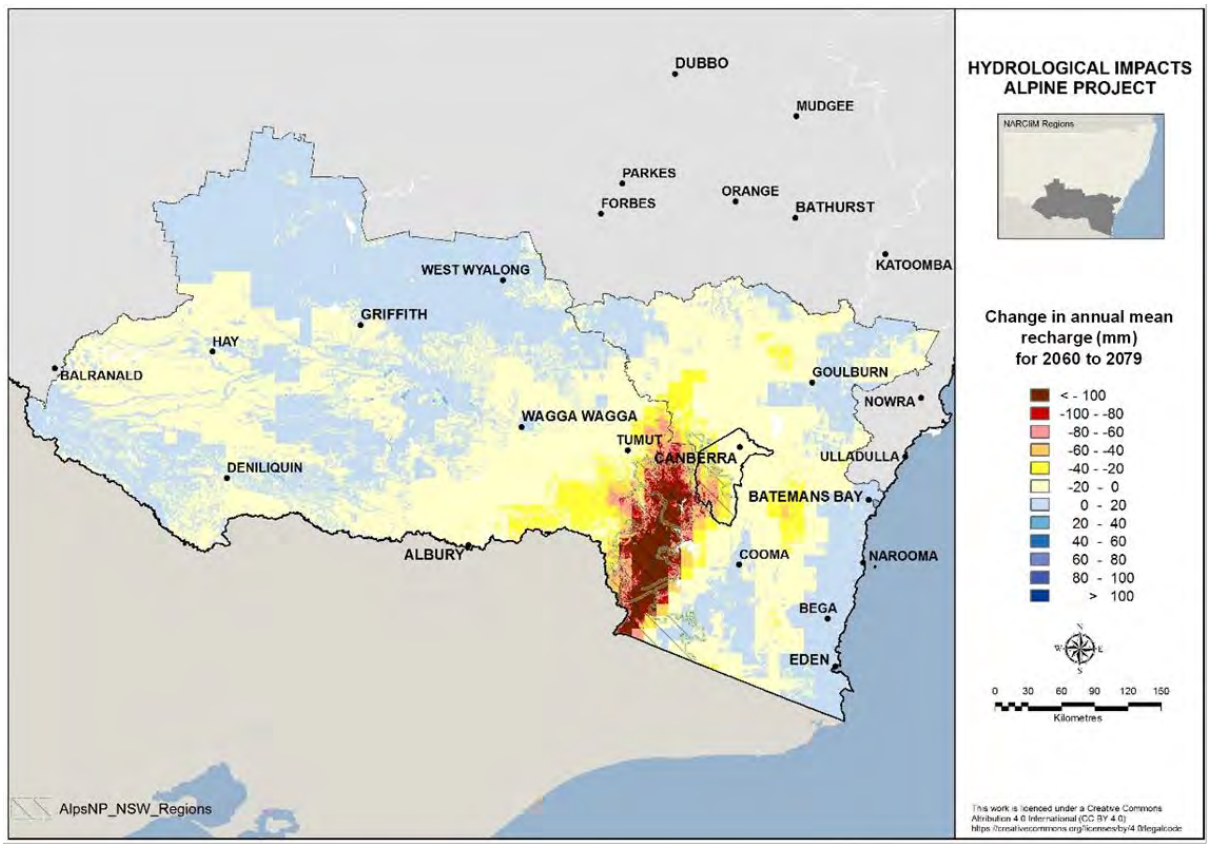


**Figure 12** **Changes in mean annual recharge (mm) across the study area for 2060 to 2079 relative to the 1990 to 2009 baseline period**

As for surface runoff, the multi-model mean is the average of a large range of model forecasts. Changes in mean annual recharge range from a decrease (drying) of –14.6 millimetres to an increase (wetting) of +5.5 millimetres for the near future (Figure 13, Table 6), and still span both drying and wetting scenarios (–20.9 to +3.9 mm) for the far future (Figure 13, Table 6).

Mean seasonal projections for the near future include both increases and decreases in recharge during summer (–7.2 to +2.7 mm), autumn (–5.1 to +3.6 mm), winter (–2.5 to +3.4 mm), and spring (–7.7 to +1.2 mm). For the far future, the projections for recharge in summer range from –4.6 to +4.4 millimetres, autumn –2.9 to +4.9 millimetres, winter –10.8 to +5.4 millimetres, and spring –17.5 to –0.3 millimetres.

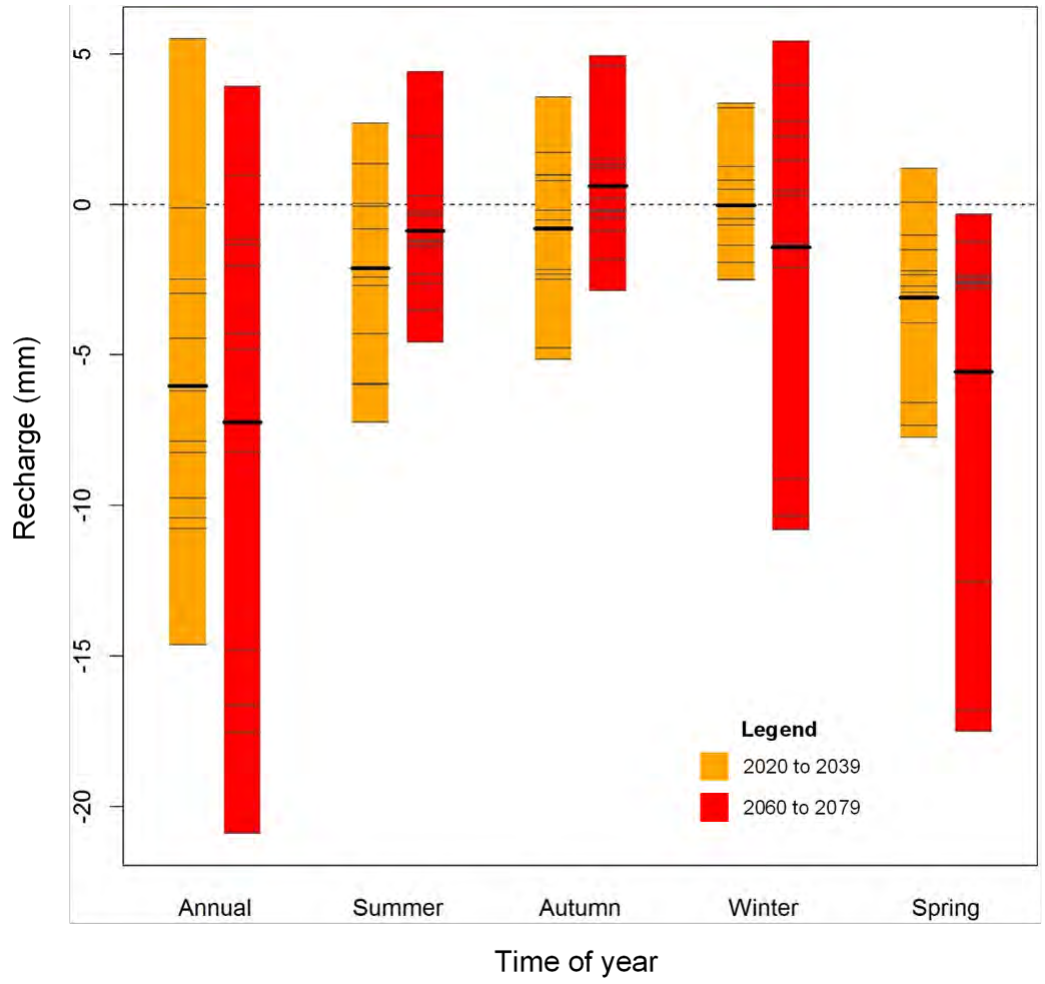


**Figure 13** **Absolute change in seasonal and annual recharge (mm) across the study area**
Colours denote the near future (2020 to 2039) and far future (2060 to 2079) NARCliM projection periods.

Table 7 presents annual mean recharge for the near future, simulations using MIROC3.2, ECHAM5, CSIRO-MK3.0 and CCCMA3.1_R2/R3, which all tend to forecast less recharge (drying). In contrast, the simulation using CCCMA3.1_R1 tends to project more recharge (wetting). For the far future, 10 of the 12 NARCliM ensembles forecast a decrease in recharge and two project an increase in recharge. Most variability across the 12 GCM/RCM combinations is evident during summer for the near future, and spring for the far future.

**Table 6** **Mean annual and seasonal recharge (mm) across the study area for each GCM/RCM combination**

Pink and green colours denote maximum and minimum changes in recharge, respectively. ANN = annual, DJF = summer, MAM = autumn, JJA = winter and SON = spring.

| | Baseline 1990 to 2009 | | | | | Near future 2020 to 2039 | | | | | Far future 2060 to 2079 | | | | |
|---|---|---|---|---|---|---|---|---|---|---|---|---|---|---|---|
| GCM/RCM model | ANN | DJF | MAM | JJA | SON | ANN | DJF | MAM | JJA | SON | ANN | DJF | MAM | JJA | SON |
| MIROC3.2_R1 | 105.4 | 14.2 | 15.8 | 43.3 | 32.0 | 97.1 | 13.4 | 16.6 | 42.8 | 24.3 | 100.6 | 16.5 | 17.4 | 47.2 | 19.5 |
| MIROC3.2_R2 | 102.9 | 10.3 | 13.6 | 47.3 | 31.7 | 95.1 | 11.7 | 13.1 | 46.0 | 24.4 | 85.4 | 6.8 | 14.9 | 48.8 | 14.9 |
| MIROC3.2_R3 | 110.7 | 10.5 | 16.6 | 48.8 | 34.8 | 107.8 | 13.2 | 17.5 | 48.8 | 28.2 | 102.5 | 15.0 | 21.2 | 49.1 | 17.3 |
| ECHAM5_R1 | 63.3 | 11.2 | 7.3 | 34.4 | 10.5 | 48.7 | 4.0 | 5.1 | 31.9 | 7.8 | 61.3 | 9.8 | 6.8 | 36.6 | 8.1 |
| ECHAM5_R2 | 54.5 | 5.4 | 7.3 | 32.2 | 9.5 | 48.3 | 2.7 | 4.8 | 32.7 | 8.0 | 55.4 | 3.1 | 7.5 | 37.7 | 7.1 |
| ECHAM5_R3 | 62.8 | 11.2 | 7.2 | 33.1 | 11.3 | 52.0 | 5.2 | 7.0 | 32.4 | 7.4 | 61.7 | 10.0 | 12.1 | 31.0 | 8.5 |
| CSIRO-MK3.0_R1 | 79.7 | 17.9 | 14.1 | 34.4 | 13.3 | 69.9 | 11.9 | 9.3 | 37.8 | 10.9 | 58.8 | 13.3 | 11.2 | 23.6 | 10.6 |
| CSIRO-MK3.0_R2 | 58.8 | 6.3 | 7.1 | 34.3 | 11.2 | 54.4 | 3.9 | 4.8 | 37.5 | 8.3 | 42.2 | 3.7 | 6.2 | 23.9 | 8.4 |
| CSIRO-MK3.0_R3 | 66.7 | 15.1 | 12.1 | 28.0 | 11.5 | 56.3 | 10.8 | 6.9 | 29.3 | 9.3 | 51.9 | 13.8 | 10.2 | 18.9 | 8.9 |
| CCCMA3.1_R1 | 26.4 | 1.5 | 1.7 | 16.2 | 7.0 | 31.9 | 1.4 | 5.3 | 17.0 | 8.2 | 30.3 | 1.8 | 2.9 | 19.0 | 6.7 |
| CCCMA3.1_R2 | 30.7 | 0.7 | 1.5 | 20.0 | 8.4 | 30.5 | 0.7 | 3.3 | 18.1 | 8.5 | 29.3 | 0.3 | 1.3 | 20.5 | 7.2 |
| CCCMA3.1_R3 | 27.3 | 1.2 | 2.6 | 15.6 | 8.0 | 24.8 | 1.2 | 3.5 | 13.1 | 7.0 | 23.0 | 0.9 | 2.3 | 14.3 | 5.4 |
| | | | | | | | | | | | | | | | |
| Maximum: | 110.7 | 17.9 | 16.6 | 48.8 | 34.8 | 107.8 | 13.4 | 17.5 | 48.8 | 28.2 | 102.5 | 16.5 | 21.2 | 49.1 | 19.5 |
| Minimum: | 26.4 | 0.7 | 1.5 | 15.6 | 7.0 | 24.8 | 0.7 | 3.3 | 13.1 | 7.0 | 23.0 | 0.3 | 1.3 | 14.3 | 5.4 |
| Range: | 84.3 | 17.2 | 15.0 | 33.2 | 27.8 | 83.0 | 12.7 | 14.3 | 35.7 | 21.2 | 79.5 | 16.2 | 19.8 | 34.8 | 14.0 |

**Table 7** **Changes in mean annual and seasonal recharge (mm) across the study area for each GCM/RCM combination**

Grey and blue colours denote maximum and minimum changes in surface runoff, respectively. ANN = annual, DJF = summer, MAM = autumn, JJA = winter and SON = spring.

| | Near future 2020 to 2039 | | | | | Far future 2060 to 2079 | | | | |
|---|---|---|---|---|---|---|---|---|---|---|
| GCM/RCM model | ANN | DJF | MAM | JJA | SON | ANN | DJF | MAM | JJA | SON |
| MIROC3.2_R1 | –8.3 | –0.8 | 0.8 | –0.5 | –7.7 | –4.8 | 2.3 | 1.5 | 4.0 | –12.5 |
| MIROC3.2_R2 | –7.9 | 1.3 | –0.5 | –1.4 | –7.3 | –17.5 | –3.5 | 1.3 | 1.5 | –16.8 |
| MIROC3.2_R3 | –3.0 | 2.7 | 1.0 | 0.0 | –6.6 | –8.2 | 4.4 | 4.6 | 0.3 | –17.5 |
| ECHAM5_R1 | –14.6 | –7.2 | –2.2 | –2.5 | –2.7 | –2.0 | –1.4 | –0.5 | 2.3 | –2.4 |
| ECHAM5_R2 | –6.2 | –2.7 | –2.5 | 0.5 | –1.5 | 0.9 | –2.3 | 0.2 | 5.4 | –2.4 |
| ECHAM5_R3 | –10.8 | –6.0 | –0.2 | –0.7 | –3.9 | –1.2 | –1.2 | 4.9 | –2.1 | –2.8 |
| CSIRO-MK3.0_R1 | –9.8 | –6.0 | –4.8 | 3.4 | –2.3 | –20.9 | –4.6 | –2.9 | –10.8 | –2.7 |
| CSIRO-MK3.0_R2 | –4.4 | –2.4 | –2.3 | 3.2 | –2.9 | –16.6 | –2.6 | –0.9 | –10.4 | –2.8 |
| CSIRO-MK3.0_R3 | –10.4 | –4.3 | –5.1 | 1.2 | –2.2 | –14.8 | –1.3 | –1.8 | –9.1 | –2.6 |
| CCCMA3.1_R1 | 5.5 | –0.1 | 3.6 | 0.8 | 1.2 | 3.9 | 0.3 | 1.2 | 2.8 | –0.3 |
| CCCMA3.1_R2 | –0.1 | 0.0 | 1.7 | –1.9 | 0.1 | –1.3 | –0.4 | –0.2 | 0.5 | –1.2 |
| CCCMA3.1_R3 | –2.5 | 0.0 | 1.0 | –2.5 | –1.0 | –4.3 | –0.2 | –0.2 | –1.3 | –2.5 |
| | | | | | | | | | | |
| Maximum: | 5.5 | 2.7 | 3.6 | 3.4 | 1.2 | 3.9 | 4.4 | 4.9 | 5.4 | –0.3 |
| Minimum: | –14.6 | –7.2 | –5.1 | –2.5 | –7.7 | –20.9 | –4.6 | –2.9 | –10.8 | –17.5 |
| Scenarios > 0: | 1 | 4 | 5 | 5 | 2 | 2 | 3 | 6 | 7 | 0 |
| Scenarios ≤ 0: | 11 | 8 | 7 | 7 | 10 | 10 | 9 | 6 | 5 | 12 |
| Range: | 20.1 | 9.9 | 8.7 | 5.9 | 8.9 | 24.8 | 9.0 | 7.8 | 16.2 | 17.2 |

## Changes in recharge to groundwater – NSW and ACT Alpine region

Less recharge to groundwater (drying) is likely in the near future across the Alpine region, based on the multi-model mean of the 12 GCM/RCM simulations (Figure 14). For the far future, the recharge is predicted to decrease further (up to –100 mm/year) (Figure 15).

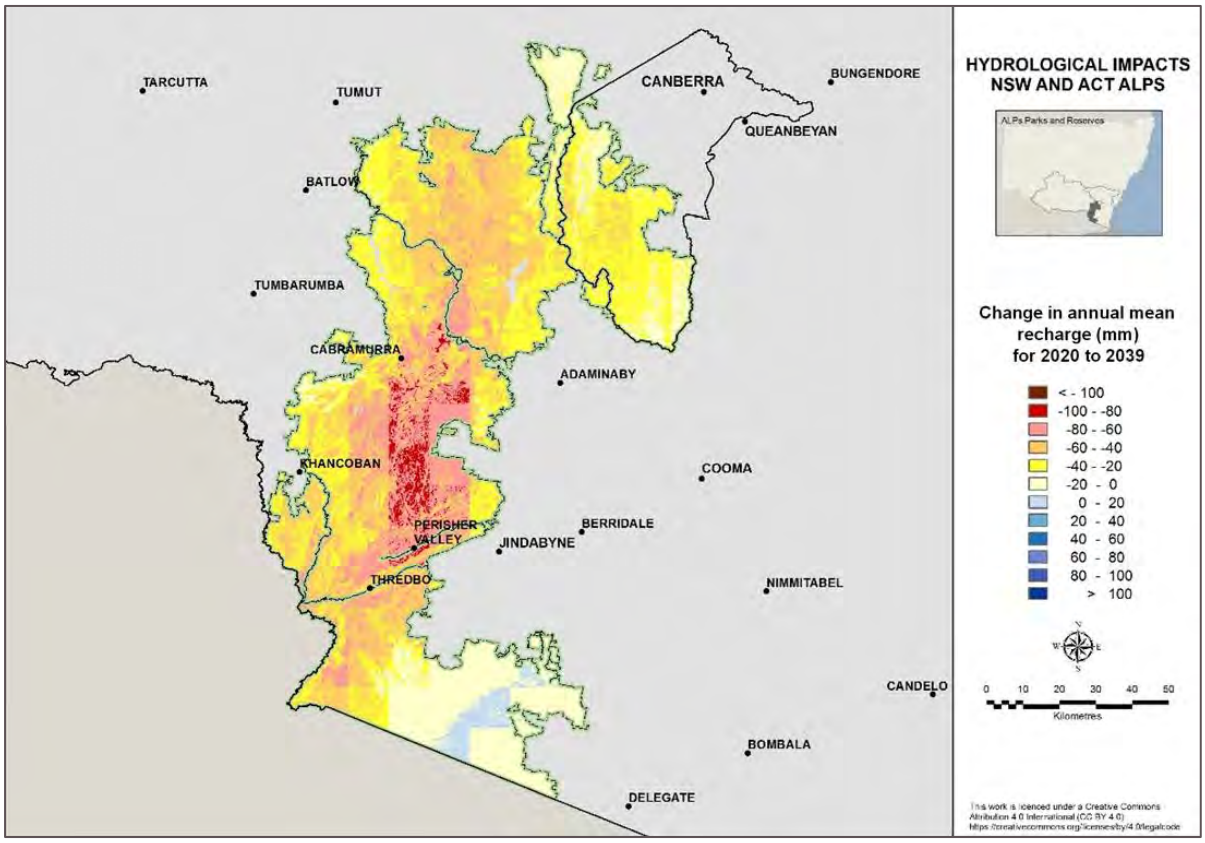


**Figure 14** **Changes in mean annual recharge (mm) in the NSW and ACT Alpine region for 2020 to 2039 relative to the 1990 to 2009 baseline period**

In both the near future and far future projections, the variability across the individual models is large (Figure 16, Table 8 and Table 9). For the near future, the annual means range from drying of –67.7 millimetres/year to an increase (wetting) of 17.5 millimetres/year, with 11 of the 12 models predicting less recharge. For the far future, all 12 models predict less recharge ranging from –170.3 millimetres/year to –0.6 millimetres/year.

For the near future, most models show less recharge for summer, autumn and spring. In winter, the predicted changes in mean annual recharge range from –33.5 to +33.9 millimetres. For the far future projections, most models forecast less recharge in summer, autumn and winter. For spring, all 12 models predict less mean annual recharge (–118.8 to –11.4 mm) (Table 9).

Based on annual mean recharge for the near future (Table 8, Table 9), NARCliM simulations using MIROC3.2, ECHAM5, CSIRO-MK3.0 and CCCMA3.1_R2/R3 as hosts all tend to project less recharge (drying), while simulations using CCCMA3.1_R1 as host tend to project more recharge (wetting). For the far future, all 12 NARCliM ensembles project a decrease in recharge.

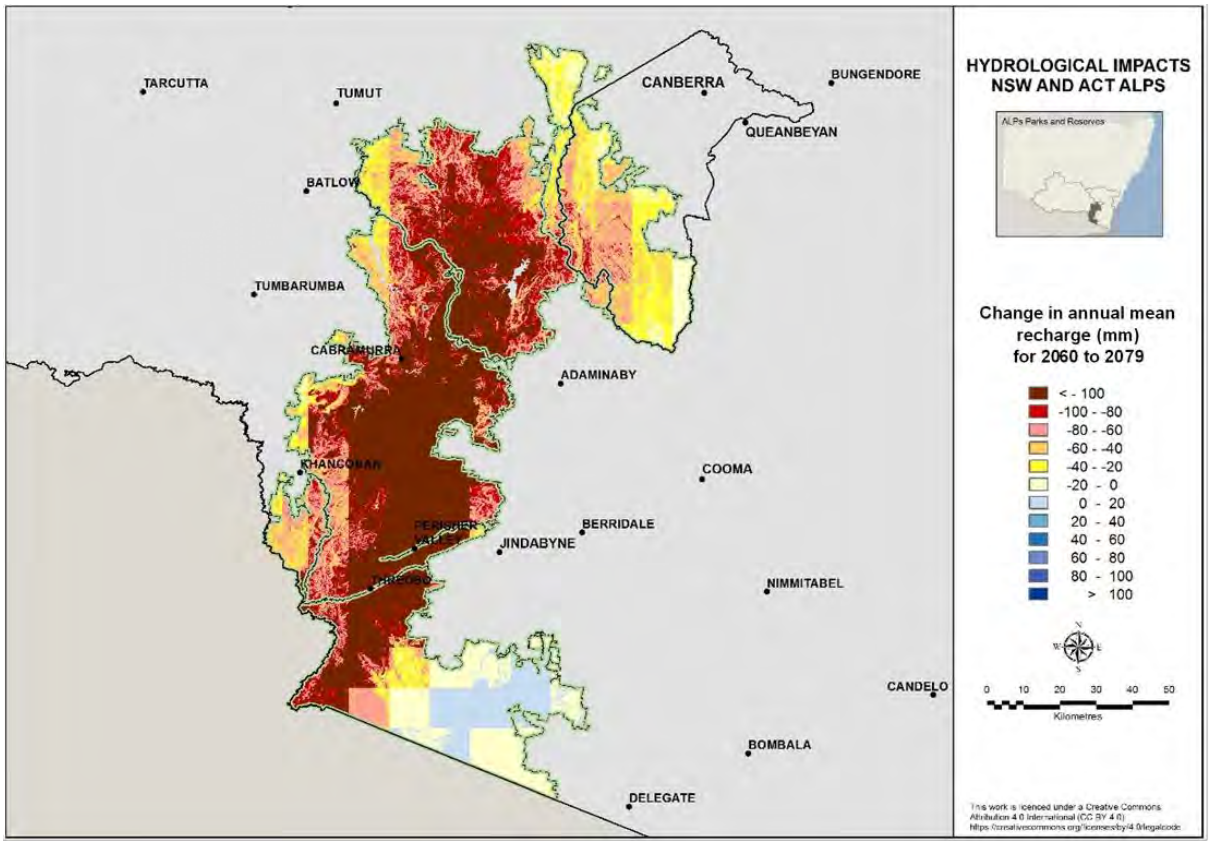


**Figure 15** **Changes in mean annual recharge (mm) in the NSW and ACT Alpine region for 2060 to 2079 relative to the 1990 to 2009 baseline period**

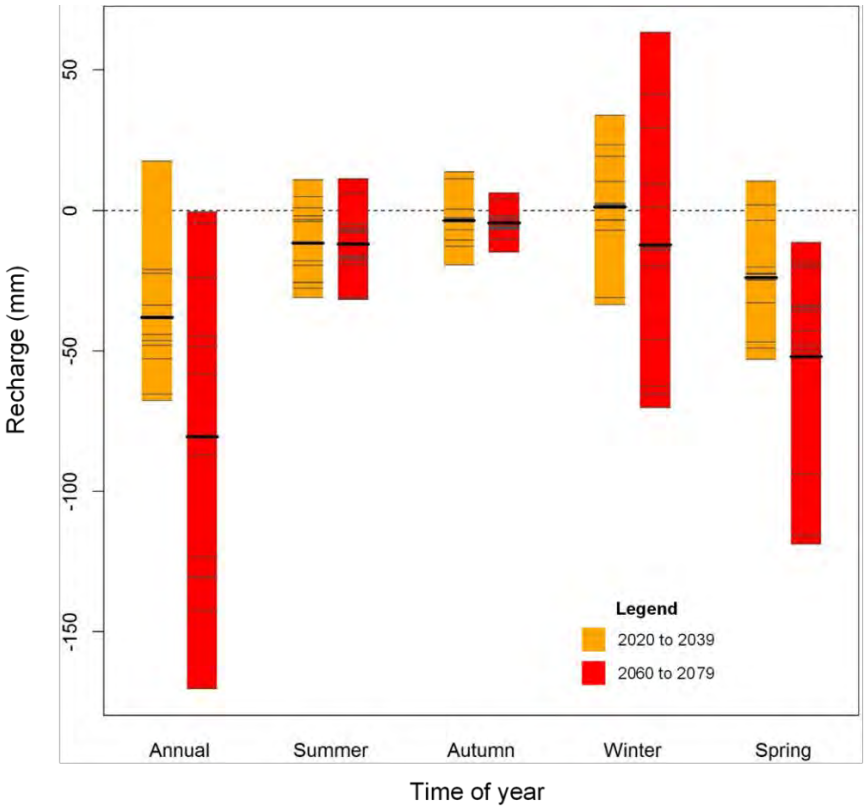


**Figure 16** **Absolute change in seasonal and annual recharge (mm) in the NSW and ACT Alpine region**

Colours denote the near future (2020 to 2039) and far future (2060 to 2079) NARCliM projection periods.

**Table 8** **Mean annual and seasonal recharge (mm) in the NSW and ACT Alpine region for each GCM/RCM combination**

Pink and green colours denote maximum and minimum changes in recharge, respectively. ANN = annual, DJF = summer, MAM = autumn, JJA = winter and SON = spring.

| | Baseline 1990 to 2009 | | | | | Near future 2020 to 2039 | | | | | Far future 2060 to 2079 | | | | |
|---|---|---|---|---|---|---|---|---|---|---|---|---|---|---|---|
| GCM/RCM model | ANN | DJF | MAM | JJA | SON | ANN | DJF | MAM | JJA | SON | ANN | DJF | MAM | JJA | SON |
| MIROC3.2_R1 | 816.0 | 82.7 | 131.7 | 336.9 | 264.6 | 763.2 | 87.7 | 124.9 | 339.0 | 211.6 | 728.8 | 94.0 | 125.8 | 338.1 | 170.9 |
| MIROC3.2_R2 | 844.2 | 74.6 | 119.1 | 373.4 | 277.1 | 800.0 | 85.4 | 116.6 | 369.8 | 228.2 | 701.8 | 66.7 | 123.1 | 353.7 | 158.3 |
| MIROC3.2_R3 | 845.6 | 77.1 | 125.4 | 364.7 | 278.3 | 799.3 | 78.1 | 122.3 | 367.4 | 231.5 | 675.2 | 83.2 | 110.5 | 318.8 | 162.7 |
| ECHAM5_R1 | 526.2 | 53.9 | 51.4 | 297.8 | 123.1 | 458.5 | 28.2 | 40.8 | 290.8 | 98.7 | 502.1 | 37.2 | 45.7 | 339.0 | 80.2 |
| ECHAM5_R2 | 514.9 | 40.1 | 50.2 | 299.4 | 125.2 | 481.3 | 22.3 | 46.9 | 309.6 | 102.4 | 510.4 | 23.9 | 46.8 | 362.7 | 77.1 |
| ECHAM5_R3 | 496.5 | 57.1 | 43.5 | 270.5 | 125.4 | 431.1 | 26.0 | 40.1 | 272.5 | 92.5 | 438.4 | 25.5 | 37.6 | 300.0 | 75.3 |
| CSIRO-MK3.0_R1 | 653.6 | 91.3 | 88.8 | 329.9 | 143.7 | 632.6 | 63.5 | 81.8 | 363.7 | 123.6 | 523.0 | 60.1 | 86.1 | 267.3 | 109.4 |
| CSIRO-MK3.0_R2 | 594.3 | 44.1 | 70.1 | 349.5 | 130.7 | 560.6 | 24.6 | 57.3 | 372.9 | 105.9 | 470.7 | 26.4 | 68.2 | 279.3 | 96.8 |
| CSIRO-MK3.0_R3 | 543.5 | 64.3 | 68.7 | 287.9 | 122.6 | 495.5 | 38.8 | 49.3 | 307.2 | 100.2 | 412.7 | 45.0 | 58.3 | 222.6 | 86.8 |
| CCCMA3.1_R1 | 321.1 | 16.0 | 17.6 | 195.9 | 91.6 | 338.6 | 12.8 | 31.3 | 192.5 | 102.0 | 320.5 | 11.2 | 23.8 | 205.3 | 80.2 |
| CCCMA3.1_R2 | 377.7 | 10.4 | 18.4 | 240.6 | 108.2 | 355.3 | 8.5 | 29.6 | 207.1 | 110.1 | 332.8 | 4.0 | 12.0 | 227.2 | 89.5 |
| CCCMA3.1_R3 | 306.1 | 11.8 | 19.2 | 184.5 | 90.6 | 268.1 | 7.9 | 19.5 | 153.5 | 87.1 | 257.5 | 4.3 | 12.4 | 170.3 | 70.5 |
| | | | | | | | | | | | | | | | |
| Maximum: | 845.6 | 91.3 | 131.7 | 373.4 | 278.3 | 800.0 | 87.7 | 124.9 | 372.9 | 231.5 | 728.8 | 94.0 | 125.8 | 362.7 | 170.9 |
| Minimum: | 306.1 | 10.4 | 17.6 | 184.5 | 90.6 | 268.1 | 7.9 | 19.5 | 153.5 | 87.1 | 257.5 | 4.0 | 12.0 | 170.3 | 70.5 |
| Range: | 539.5 | 80.8 | 114.1 | 188.9 | 187.7 | 531.9 | 79.8 | 105.3 | 219.4 | 144.4 | 471.3 | 90.1 | 113.7 | 192.4 | 100.3 |

**Table 9** **Changes in mean annual and seasonal recharge (mm) in the NSW and ACT Alpine region for each GCM/RCM combination**

Grey and blue colours denote maximum and minimum changes in surface runoff, respectively. ANN = annual, DJF = summer, MAM = autumn, JJA = winter and SON = spring.

| | Near future 2020 to 2039 | | | | | Far future 2060 to 2079 | | | | |
|---|---|---|---|---|---|---|---|---|---|---|
| GCM/RCM model | ANN | DJF | MAM | JJA | SON | ANN | DJF | MAM | JJA | SON |
| MIROC3.2_R1 | –52.8 | 5.0 | –6.9 | 2.1 | –53.1 | –87.2 | 11.3 | –6.0 | 1.2 | –93.8 |
| MIROC3.2_R2 | –44.2 | 10.9 | –2.5 | –3.6 | –48.9 | –142.4 | –7.9 | 4.0 | –19.8 | –118.8 |
| MIROC3.2_R3 | –46.3 | 0.9 | –3.1 | 2.7 | –46.8 | –170.3 | 6.1 | –14.9 | –45.9 | –115.7 |
| ECHAM5_R1 | –67.7 | –25.7 | –10.5 | –7.0 | –24.4 | –24.1 | –16.8 | –5.7 | 41.2 | –42.8 |
| ECHAM5_R2 | –33.7 | –17.8 | –3.3 | 10.2 | –22.8 | –4.5 | –16.3 | –3.5 | 63.3 | –48.1 |
| ECHAM5_R3 | –65.4 | –31.1 | –3.4 | 1.9 | –32.9 | –58.2 | –31.7 | –5.9 | 29.5 | –50.1 |
| CSIRO-MK3.0_R1 | –21.0 | –27.8 | –6.9 | 33.9 | –20.2 | –130.6 | –31.1 | –2.6 | –62.5 | –34.3 |
| CSIRO-MK3.0_R2 | –33.7 | –19.5 | –12.8 | 23.4 | –24.8 | –123.5 | –17.7 | –1.8 | –70.2 | –33.9 |
| CSIRO-MK3.0_R3 | –48.0 | –25.5 | –19.3 | 19.3 | –22.4 | –130.8 | –19.3 | –10.4 | –65.4 | –35.8 |
| CCCMA3.1_R1 | 17.5 | –3.2 | 13.7 | –3.4 | 10.4 | –0.6 | –4.8 | 6.2 | 9.4 | –11.4 |
| CCCMA3.1_R2 | –22.3 | –1.9 | 11.2 | –33.5 | 1.9 | –44.9 | –6.4 | –6.3 | –13.4 | –18.7 |
| CCCMA3.1_R3 | –38.0 | –3.8 | 0.4 | –31.0 | –3.6 | –48.6 | –7.5 | –6.8 | –14.3 | –20.1 |
| | | | | | | | | | | |
| Maximum: | 17.5 | 10.9 | 13.7 | 33.9 | 10.4 | –0.6 | 11.3 | 6.2 | 63.3 | –11.4 |
| Minimum: | –67.7 | –31.1 | –19.3 | –33.5 | –53.1 | –170.3 | –31.7 | –14.9 | –70.2 | –118.8 |
| Scenarios > 0: | 1 | 3 | 3 | 7 | 2 | 0 | 2 | 2 | 5 | 0 |
| Scenarios ≤ 0: | 11 | 9 | 9 | 5 | 10 | 12 | 10 | 10 | 7 | 12 |
| Range: | 85.2 | 41.9 | 33.1 | 67.4 | 63.5 | 169.7 | 43.0 | 21.1 | 133.5 | 107.4 |

## 3.3 Impact on salinity hazard potential

For the near future, changes in salinity hazard are shown in Figure 17. Areas that are currently described as low salinity hazard are shown in blue. Less dilution flow is likely from some low salinity hazard areas, especially in the higher elevation Alpine region. Less dilution flow from alpine areas could increase catchment-scale salinity further downstream.

Most CAP regions with moderate, high or very high salinity hazard (yellow, pink and red) show no change in salinity hazard or a lowering of salinity hazard. Of interest are areas around Cootamundra, Yass and Young which contain some of the highest dryland salinity in the state. However, some high hazard areas west of Deniliquin do show an increase in salinity hazard.

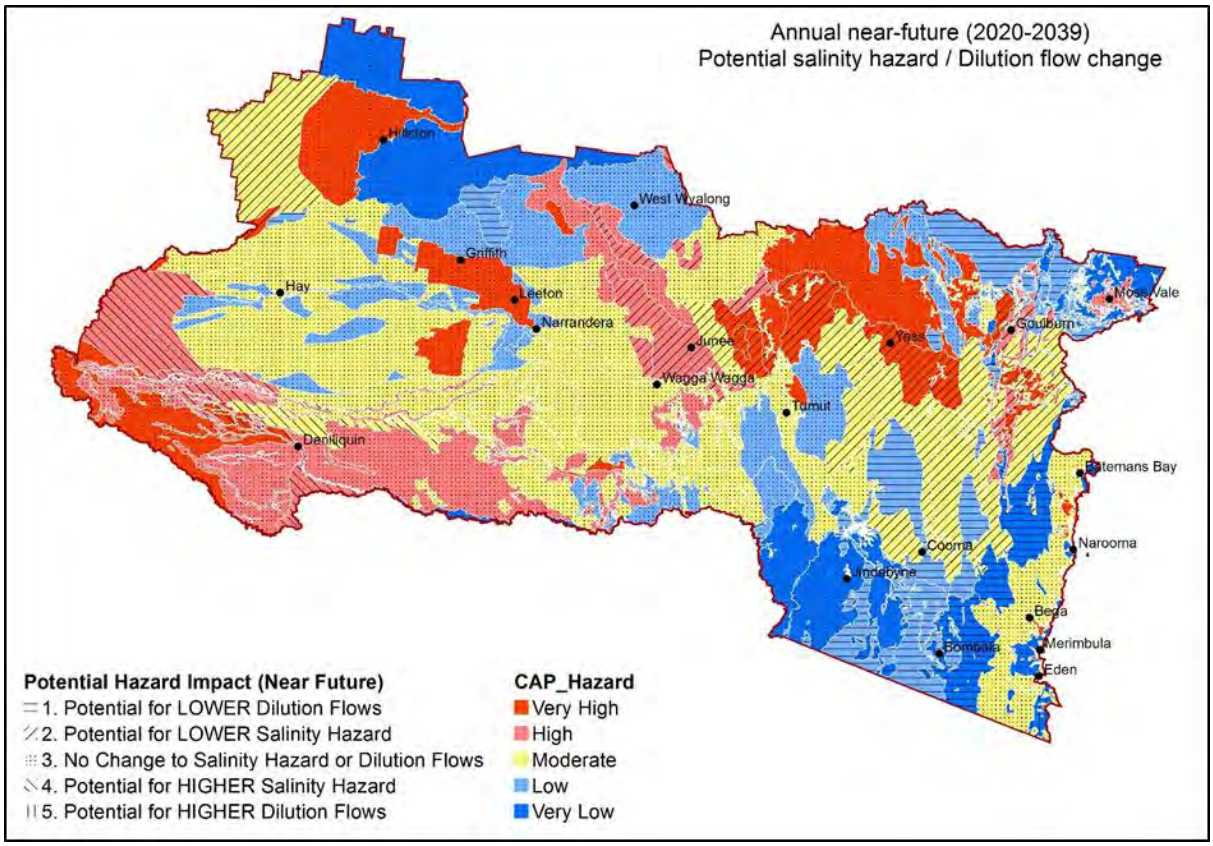


**Figure 17** **Potential impact on salinity hazard and dilution flow in the near future (2020 to 2039)**

For the far future, changes are shown in Figure 18. Many areas that are currently low salinity hazard (blue), show no change in hazard. Some low hazard areas north of Griffith and along the Murrumbidgee River as it crosses the Riverina show the potential for higher dilution flows that could be beneficial for catchment scale salinity.

CAP regions that are currently moderate, high or very high salinity hazard (yellow, pink and red) show either no change in hazard or higher salinity hazard. CAP regions west of Corowa to Balranald consistently show an increase in salinity hazard, as do areas around Griffith and Leeton. Of interest, are the areas around Cootamundra, Yass and Young, which contain some of the highest dryland salinity in the state. Salinity hazard is not forecast to get worse in the near or far future in these catchments (Yass River, Jugiong Creek and Muttama Creek).

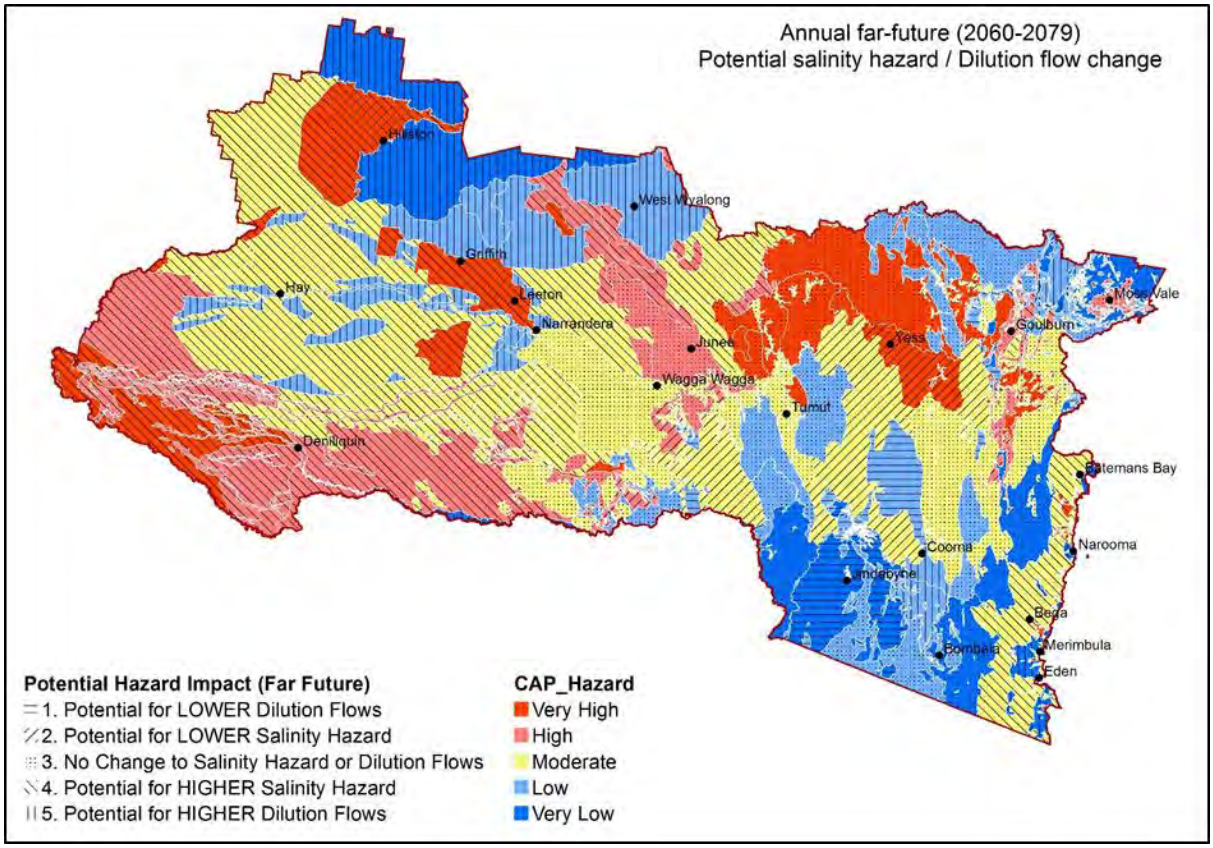


**Figure 18** **Potential impact on salinity hazard and dilution flow in the far future (2060 to 2079)**

# 4. Discussion

## 4.1 Key findings

Decreases in surface runoff can impact high mountain wetlands that are highly dependent on the surface hydrology. In the near future most of the study area is likely to have less surface runoff while in the far future, reductions in surface runoff of more than 40 millimetres/year are projected for higher alpine areas.

The biggest hydrological impact of these decreases in surface runoff is the reduction in recharge in alpine areas, especially in the far future. Most of the study area is likely to have less recharge in the near future, while far future projections predict less recharge in summer, winter and autumn, with the largest decreases during in spring.

While salinity hazard potential is sensitive to changes in climate, at a whole-of-catchment scale, decreases in hazard (e.g. around Cootamundra) may be offset by increased hazard in other areas.

## 4.2 Limitations and further research

The following factors influence the interpretation of these results:

- The daily time-step NARCliM projections are only available at a 10 kilometre spatial resolution. Local variations due to topography that can occur at a finer resolution cannot be captured.
- The bias-corrected rainfall could not be used due to missing data along eastern parts of the study area.
- Snow formation and snow melt were not considered within water balance modelling. Similarly, hydrological effects of frozen soil preventing infiltration was not modelled.
- Salinity hazard products were catchment-specific and used data sources available for that catchment. Data sources vary and discrepancies in ratings may occur on some boundaries.

Further investigation into snow conditions and their effects on surface runoff and recharge would be beneficial.

A finer-scale assessment of salinity impacts would require new hydrogeological landscape mapping. Improved salinity modelling using this new mapping could be integrated with river flow and management models to quantify salinity impacts at mid-valley and end-of-valley salinity target sites.

# 5. Conclusion

Previous impact analyses on the AdaptNSW webpage are at a statewide scale and showed the impacts of climate change on surface runoff and groundwater recharge at a 10 kilometre resolution. This study overcame this limitation by using finer-scale information for soil type, topography and land use (100 m resolution) and producing maps showing changes in surface runoff and recharge to groundwater at a landscape scale rather than a lumped 10 kilometre pixel resolution. These new datasets can identify those landscapes most affected by climate change.

This study produced the first salinity impact assessment based on the NARCliM projections by combining projected changes in surface runoff and recharge with catchment-scale salinity data.

# 6. References

Abbs K and Littleboy M 1998, Recharge estimation for the Liverpool Plains, *Australian Journal of Soil Research*, vol.36, pp.335–357.

BoM 2006, *Gridded Köppen classification metadata*, Australian Bureau of Meteorology, accessed July 2017, www.bom.gov.au/climate/averages/climatology/gridded-data-info/metadata/md_koppen_classification.shtml.

Chiew FHS, Peel MC and Western AW 2002, 'Application and testing of the simple rainfall-runoff model SIMHYD', in VP Singh and DK Frevert (eds), *Mathematical models of small watershed hydrology and applications*, Water Resources Publication, Littleton, Colorado, USA, pp.335–367.

DECC 2009, *Salinity Audit: Upland catchments of the New South Wales Murray–Darling Basin*, NSW Department of Environment and Climate Change, Sydney NSW.

DECCW 2011, *Operational Manual for* BioMetric 3.1*: A tool for assessing clearing and ecological thinning proposals on terrestrial biodiversity under the* Native Vegetation Act 2003, NSW Department of Environment, Climate Change and Water, Sydney NSW.

Di Luca AJ, Evans P and Ji F 2018, Australian snowpack in the NARCliM ensemble: evaluation, bias correction and future projections, *Climate Dynamics*, vol.51, no.1–2, pp.639–666.

Evans JP, Ekstrom M and Ji F 2012, Evaluating the performance of a WRF physics ensemble over South-East Australia, *Climate Dynamics*, vol.39, no.6, pp.1241–1258.

Evans JP, Ji F, Abramowitz G, Ekstrom M 2013a, Optimally choosing small ensemble members to produce robust climate simulations, *Environmental Research Letters*, vol.8.

Evans JP, Fita L, Argüeso D and Liu Y 2013b, Initial NARCliM evaluation, in Piantadosi J, Anderssen RS and Boland J (eds), *MODSIM2013, 20th International Congress on Modelling and Simulation*, Modelling and Simulation Society of Australia and New Zealand, December 2013, pp.2765–2771.

Evans J, Ji F, Lee C, Smith P, Argüeso D and Fita L 2014, Design of a regional climate modelling projection ensemble experiment–NARCliM, *Geoscientific Model Development,* vol.7, pp.621–629.

Fita L, Evans JP, Argüeso D, King AD and Liu Y 2016, Evaluation of the regional climate response to large-scale modes in the historical NARCliM simulations, *Climate Dynamics*, pp.1–15, doi: 10.1007/s00382-016-3484-x.

Hughes L 2011, Climate change and Australia: key vulnerable regions, *Regional Environmental Change*, vol.11, no.1, pp.189–195.

IPCC 2000, *Special Report on Emissions Scenarios (SRES): A Special Report of Working Group III of the Intergovernmental Panel on Climate Change*, published for the Intergovernmental Panel on Climate Change by Cambridge University Press, Cambridge, UK.

Ji F, Ekstrom M, Evans JP and Teng J 2014, Evaluating rainfall patterns using physics scheme ensembles from a regional atmospheric model, *Theoretical and Applied Climatology*, vol.115, pp.297–304.

Ji F, Littleboy M, Rahman J and Young J 2015, 'Morton's Areal Evapotranspiration Study Design and Methods' (in draft), NSW Office of Environment and Heritage internal document.

Ji F, Evans JP, Teng J, Scorgie Y, Argüeso D and Di Luca A 2016, Evaluation of long-term precipitation and temperature WRF simulations for southeast Australia, *Climate Research*, vol.67, pp.99–115, DOI 10.3354/cr01366.

Littleboy M, Silburn DM, Freebairn DM, Woodruff DR, Hammer GL and Leslie JK 1992, Impact of soil erosion on production in cropping systems, Development and validation of a simulation model, *Australian Journal of Soil Research*, vol.30, no.5, pp.757–774.

Littleboy M, Herron N and Barnett P 2003, 'Applying unsaturated zone modelling to develop recharge maps for the Murray-Darling Basin in New South Wales, Australia', in *Proceedings International Congress on Modelling and Simulation*, Modelling and Simulation Society of Australia and New Zealand, Townsville, 14–17 July 2003.

Littleboy M, Sayers J and Dela-Cruz J 2009, 'Hydrological modelling of coastal catchments in New South Wales', in *Proceedings International Congress on Modelling and Simulation*, Modelling and Simulation Society of Australia and New Zealand, Cairns, July 2009.

Morton FI 1983, Operational estimates of areal evapotranspiration and their significance to the science and practice of hydrology, *Journal of Hydrology*, vol.66, pp.1–76.

OEH 2012, *Native Vegetation Regulation 2012: Environmental Outcomes Assessment Methodology*, Draft for public consultation, 2012/0178, Office of Environment and Heritage, Sydney NSW.

Pain C, Gregory L, Wilson P and McKenzie N 2011, *The physiographic regions of Australia – Explanatory notes 2011*, Australian Collaborative Land Evaluation Program and National Committee on Soil and Terrain, www.clw.csiro.au/aclep/documents/PhysiographicRegions_2011.pdf

Rassam D and Littleboy M 2003, 'Identifying the Lateral Component of Drainage Flux in Hill Slopes', in *Proceedings International Congress on Modelling and Simulation*, Modelling and Simulation Society of Australia and New Zealand, Townsville, 14–17 July 2003.

Roper T, Creese B, Scanes P, Stephens K, William R, Dela-Cruz J, Coade G, Coates B and Fraser M 2011, *Assessing the condition of estuaries and coastal lake ecosystems in NSW*, Monitoring, evaluation and reporting program, Technical report series, Office of Environment and Heritage, Sydney.

Simunek J, Sejna M and van Genuchten MTh 1999, *The HYDRUS-2D software package for simulating two-dimensional movement of water, heat, and multiple solutes in variably saturated media*, Version 2.0, IGWMC – TPS – 53, International Ground Water Modelling Centre, Colorado School of Mines, Golden, Colorado USA.

Skamarock WC, Klemp JB, Dudhia J, Gill DO, Barker DM, Duda MG, Huang XY, Wang W and Powers JG 2008, *A description of the advanced research WRF Version 3,* NCAR Technical Note, National Center for Atmospheric Research, Boulder Colorado, USA.

Smithson A, Muller R, Nicholson A and Wooldridge A 2004, *Groundwater Flow Systems in the Central West Region, NSW (Stage 1), A Technical Framework for Salinity Management*, NSW Department of Infrastructure, Planning and Natural Resources, Orange, NSW, ISBN 7347 5525 2.

Vaze J, Chiew FHS, Perraud J-M, Viney N, Post D, Teng J, Wang B, Lerat J and Goswami M 2010, Rainfall-Runoff Modelling Across Southeast Australia: Datasets, Models and Results, *Australian Journal of Water Resources*, vol.14, pp.101–116.

Wooldridge A, Cook W, Jenkins B, Muller R, Nicholson A and Winkler M 2012, *Salinity hazard report for Catchment Action Plan upgrade – Lachlan CMA*, NSW Department of Primary Industries, Sydney.

DOCUMENT 22

# Summary for Policymakers

SPM

# Summary for Policymakers

**Drafting Authors:**
Myles Allen (UK), Mustafa Babiker (Sudan), Yang Chen (China), Heleen de Coninck (Netherlands/EU), Sarah Connors (UK), Renée van Diemen (Netherlands), Opha Pauline Dube (Botswana), Kristie L. Ebi (USA), Francois Engelbrecht (South Africa), Marion Ferrat (UK/France), James Ford (UK/Canada), Piers Forster (UK), Sabine Fuss (Germany), Tania Guillén Bolaños (Germany/Nicaragua), Jordan Harold (UK), Ove Hoegh-Guldberg (Australia), Jean-Charles Hourcade (France), Daniel Huppmann (Austria), Daniela Jacob (Germany), Kejun Jiang (China), Tom Gabriel Johansen (Norway), Mikiko Kainuma (Japan), Kiane de Kleijne (Netherlands/EU), Elmar Kriegler (Germany), Debora Ley (Guatemala/Mexico), Diana Liverman (USA), Natalie Mahowald (USA), Valérie Masson-Delmotte (France), J. B. Robin Matthews (UK), Richard Millar (UK), Katja Mintenbeck (Germany), Angela Morelli (Norway/Italy), Wilfran Moufouma-Okia (France/Congo), Luis Mundaca (Sweden/Chile), Maike Nicolai (Germany), Chukwumerije Okereke (UK/Nigeria), Minal Pathak (India), Antony Payne (UK), Roz Pidcock (UK), Anna Pirani (Italy), Elvira Poloczanska (UK/Australia), Hans-Otto Pörtner (Germany), Aromar Revi (India), Keywan Riahi (Austria), Debra C. Roberts (South Africa), Joeri Rogelj (Austria/Belgium), Joyashree Roy (India), Sonia I. Seneviratne (Switzerland), Priyadarshi R. Shukla (India), James Skea (UK), Raphael Slade (UK), Drew Shindell (USA), Chandni Singh (India), William Solecki (USA), Linda Steg (Netherlands), Michael Taylor (Jamaica), Petra Tschakert (Australia/Austria), Henri Waisman (France), Rachel Warren (UK), Panmao Zhai (China), Kirsten Zickfeld (Canada).

**This Summary for Policymakers should be cited as:**
IPCC, 2018: Summary for Policymakers. In: *Global Warming of 1.5°C. An IPCC Special Report on the impacts of global warming of 1.5°C above pre-industrial levels and related global greenhouse gas emission pathways, in the context of strengthening the global response to the threat of climate change, sustainable development, and efforts to eradicate poverty* [Masson-Delmotte, V., P. Zhai, H.-O. Pörtner, D. Roberts, J. Skea, P.R. Shukla, A. Pirani, W. Moufouma-Okia, C. Péan, R. Pidcock, S. Connors, J.B.R. Matthews, Y. Chen, X. Zhou, M.I. Gomis, E. Lonnoy, T. Maycock, M. Tignor, and T. Waterfield (eds.)]. In Press.

# Introduction

This Report responds to the invitation for IPCC '... to provide a Special Report in 2018 on the impacts of global warming of 1.5°C above pre-industrial levels and related global greenhouse gas emission pathways' contained in the Decision of the 21st Conference of Parties of the United Nations Framework Convention on Climate Change to adopt the Paris Agreement.[1]

The IPCC accepted the invitation in April 2016, deciding to prepare this Special Report on the impacts of global warming of 1.5°C above pre-industrial levels and related global greenhouse gas emission pathways, in the context of strengthening the global response to the threat of climate change, sustainable development, and efforts to eradicate poverty.

This Summary for Policymakers (SPM) presents the key findings of the Special Report, based on the assessment of the available scientific, technical and socio-economic literature[2] relevant to global warming of 1.5°C and for the comparison between global warming of 1.5°C and 2°C above pre-industrial levels. The level of confidence associated with each key finding is reported using the IPCC calibrated language.[3] The underlying scientific basis of each key finding is indicated by references provided to chapter elements. In the SPM, knowledge gaps are identified associated with the underlying chapters of the Report.

# A. Understanding Global Warming of 1.5°C[4]

## A.1 Human activities are estimated to have caused approximately 1.0°C of global warming[5] above pre-industrial levels, with a *likely* range of 0.8°C to 1.2°C. Global warming is *likely* to reach 1.5°C between 2030 and 2052 if it continues to increase at the current rate. (*high confidence*) (Figure SPM.1) {1.2}

A.1.1 Reflecting the long-term warming trend since pre-industrial times, observed global mean surface temperature (GMST) for the decade 2006–2015 was 0.87°C (*likely* between 0.75°C and 0.99°C)[6] higher than the average over the 1850–1900 period (*very high confidence*). Estimated anthropogenic global warming matches the level of observed warming to within ±20% (*likely range*). Estimated anthropogenic global warming is currently increasing at 0.2°C (*likely* between 0.1°C and 0.3°C) per decade due to past and ongoing emissions (*high confidence*). {1.2.1, Table 1.1, 1.2.4}

A.1.2 Warming greater than the global annual average is being experienced in many land regions and seasons, including two to three times higher in the Arctic. Warming is generally higher over land than over the ocean. (*high confidence*) {1.2.1, 1.2.2, Figure 1.1, Figure 1.3, 3.3.1, 3.3.2}

A.1.3 Trends in intensity and frequency of some climate and weather extremes have been detected over time spans during which about 0.5°C of global warming occurred (*medium confidence*). This assessment is based on several lines of evidence, including attribution studies for changes in extremes since 1950. {3.3.1, 3.3.2, 3.3.3}

---

1 Decision 1/CP.21, paragraph 21.

2 The assessment covers literature accepted for publication by 15 May 2018.

3 Each finding is grounded in an evaluation of underlying evidence and agreement. A level of confidence is expressed using five qualifiers: very low, low, medium, high and very high, and typeset in italics, for example, *medium confidence*. The following terms have been used to indicate the assessed likelihood of an outcome or a result: virtually certain 99–100% probability, very likely 90–100%, likely 66–100%, about as likely as not 33–66%, unlikely 0–33%, very unlikely 0–10%, exceptionally unlikely 0–1%. Additional terms (extremely likely 95–100%, more likely than not >50–100%, more unlikely than likely 0–<50%, extremely unlikely 0–5%) may also be used when appropriate. Assessed likelihood is typeset in italics, for example, *very likely*. This is consistent with AR5.

4 See also Box SPM.1: Core Concepts Central to this Special Report.

5 Present level of global warming is defined as the average of a 30-year period centred on 2017 assuming the recent rate of warming continues.

6 This range spans the four available peer-reviewed estimates of the observed GMST change and also accounts for additional uncertainty due to possible short-term natural variability. {1.2.1, Table 1.1}

## A.2 Warming from anthropogenic emissions from the pre-industrial period to the present will persist for centuries to millennia and will continue to cause further long-term changes in the climate system, such as sea level rise, with associated impacts (*high confidence*), but these emissions alone are *unlikely* to cause global warming of 1.5°C (*medium confidence*). (Figure SPM.1) {1.2, 3.3, Figure 1.5}

A.2.1 Anthropogenic emissions (including greenhouse gases, aerosols and their precursors) up to the present are *unlikely* to cause further warming of more than 0.5°C over the next two to three decades (*high confidence*) or on a century time scale (*medium confidence*). {1.2.4, Figure 1.5}

A.2.2 Reaching and sustaining net zero global anthropogenic $CO_2$ emissions and declining net non-$CO_2$ radiative forcing would halt anthropogenic global warming on multi-decadal time scales (*high confidence*). The maximum temperature reached is then determined by cumulative net global anthropogenic $CO_2$ emissions up to the time of net zero $CO_2$ emissions (*high confidence*) and the level of non-$CO_2$ radiative forcing in the decades prior to the time that maximum temperatures are reached (*medium confidence*). On longer time scales, sustained net negative global anthropogenic $CO_2$ emissions and/or further reductions in non-$CO_2$ radiative forcing may still be required to prevent further warming due to Earth system feedbacks and to reverse ocean acidification (*medium confidence*) and will be required to minimize sea level rise (*high confidence*). {Cross-Chapter Box 2 in Chapter 1, 1.2.3, 1.2.4, Figure 1.4, 2.2.1, 2.2.2, 3.4.4.8, 3.4.5.1, 3.6.3.2}

## A.3 Climate-related risks for natural and human systems are higher for global warming of 1.5°C than at present, but lower than at 2°C (*high confidence*). These risks depend on the magnitude and rate of warming, geographic location, levels of development and vulnerability, and on the choices and implementation of adaptation and mitigation options (*high confidence*). (Figure SPM.2) {1.3, 3.3, 3.4, 5.6}

A.3.1 Impacts on natural and human systems from global warming have already been observed (*high confidence*). Many land and ocean ecosystems and some of the services they provide have already changed due to global warming (*high confidence*). (Figure SPM.2) {1.4, 3.4, 3.5}

A.3.2 Future climate-related risks depend on the rate, peak and duration of warming. In the aggregate, they are larger if global warming exceeds 1.5°C before returning to that level by 2100 than if global warming gradually stabilizes at 1.5°C, especially if the peak temperature is high (e.g., about 2°C) (*high confidence*). Some impacts may be long-lasting or irreversible, such as the loss of some ecosystems (*high confidence*). {3.2, 3.4.4, 3.6.3, Cross-Chapter Box 8 in Chapter 3}

A.3.3 Adaptation and mitigation are already occurring (*high confidence*). Future climate-related risks would be reduced by the upscaling and acceleration of far-reaching, multilevel and cross-sectoral climate mitigation and by both incremental and transformational adaptation (*high confidence*). {1.2, 1.3, Table 3.5, 4.2.2, Cross-Chapter Box 9 in Chapter 4, Box 4.2, Box 4.3, Box 4.6, 4.3.1, 4.3.2, 4.3.3, 4.3.4, 4.3.5, 4.4.1, 4.4.4, 4.4.5, 4.5.3}

# Cumulative emissions of $CO_2$ and future non-$CO_2$ radiative forcing determine the probability of limiting warming to 1.5°C

## a) Observed global temperature change and modeled responses to stylized anthropogenic emission and forcing pathways

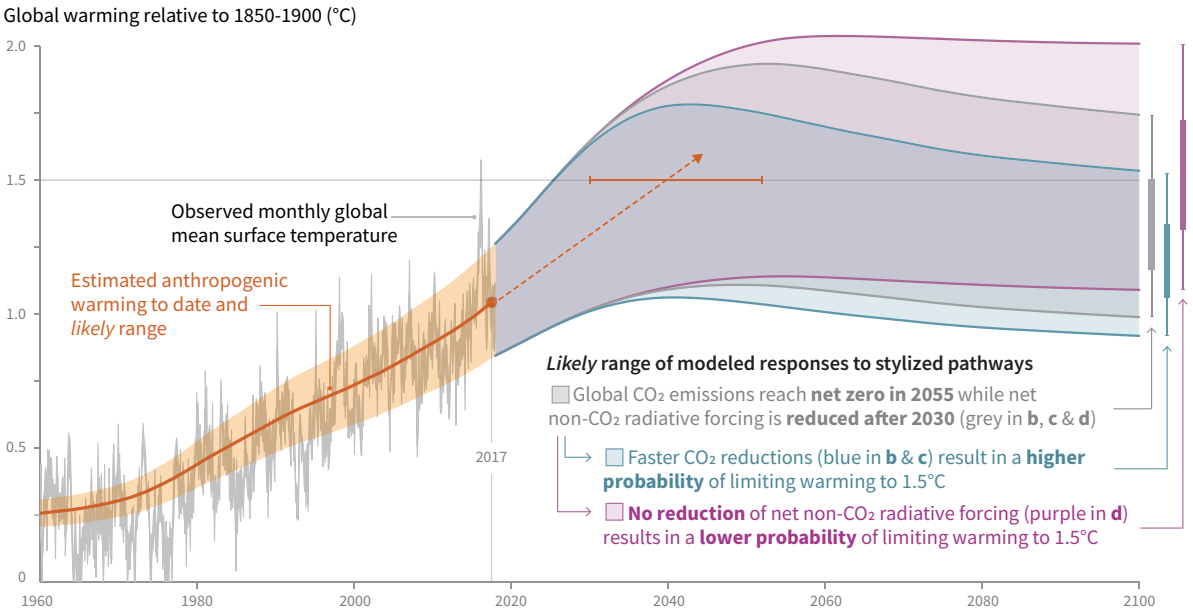


**b) Stylized net global $CO_2$ emission pathways**
Billion tonnes $CO_2$ per year ($GtCO_2$/yr)

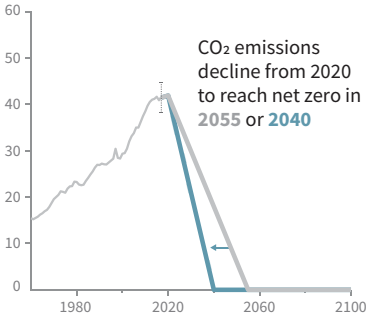


Faster immediate $CO_2$ emission reductions limit cumulative $CO_2$ emissions shown in panel **(c)**.

**c) Cumulative net $CO_2$ emissions**
Billion tonnes $CO_2$ ($GtCO_2$)

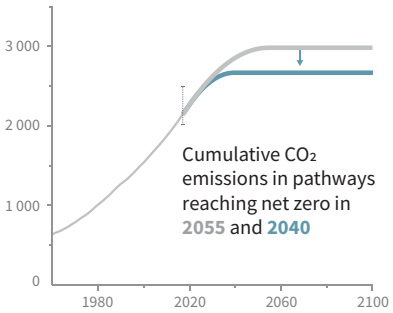


**d) Non-$CO_2$ radiative forcing pathways**
Watts per square metre ($W/m^2$)

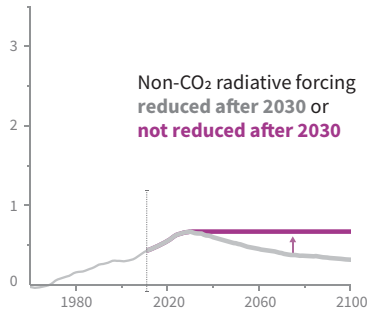


Maximum temperature rise is determined by cumulative net $CO_2$ emissions and net non-$CO_2$ radiative forcing due to methane, nitrous oxide, aerosols and other anthropogenic forcing agents.

**Figure SPM.1 |** Panel a: Observed monthly global mean surface temperature (GMST, grey line up to 2017, from the HadCRUT4, GISTEMP, Cowtan–Way, and NOAA datasets) change and estimated anthropogenic global warming (solid orange line up to 2017, with orange shading indicating assessed *likely* range). Orange dashed arrow and horizontal orange error bar show respectively the central estimate and *likely* range of the time at which 1.5°C is reached if the current rate of warming continues. The grey plume on the right of panel a shows the *likely* range of warming responses, computed with a simple climate model, to a stylized pathway (hypothetical future) in which net $CO_2$ emissions (grey line in panels b and c) decline in a straight line from 2020 to reach net zero in 2055 and net non-$CO_2$ radiative forcing (grey line in panel d) increases to 2030 and then declines. The blue plume in panel a) shows the response to faster $CO_2$ emissions reductions (blue line in panel b), reaching net zero in 2040, reducing cumulative $CO_2$ emissions (panel c). The purple plume shows the response to net $CO_2$ emissions declining to zero in 2055, with net non-$CO_2$ forcing remaining constant after 2030. The vertical error bars on right of panel a) show the *likely* ranges (thin lines) and central terciles (33rd – 66th percentiles, thick lines) of the estimated distribution of warming in 2100 under these three stylized pathways. Vertical dotted error bars in panels b, c and d show the *likely* range of historical annual and cumulative global net $CO_2$ emissions in 2017 (data from the Global Carbon Project) and of net non-$CO_2$ radiative forcing in 2011 from AR5, respectively. Vertical axes in panels c and d are scaled to represent approximately equal effects on GMST. {1.2.1, 1.2.3, 1.2.4, 2.3, Figure 1.2 and Chapter 1 Supplementary Material, Cross-Chapter Box 2 in Chapter 1}

# B. Projected Climate Change, Potential Impacts and Associated Risks

**B.1 Climate models project robust[7] differences in regional climate characteristics between present-day and global warming of 1.5°C,[8] and between 1.5°C and 2°C.[8] These differences include increases in: mean temperature in most land and ocean regions (*high confidence*), hot extremes in most inhabited regions (*high confidence*), heavy precipitation in several regions (*medium confidence*), and the probability of drought and precipitation deficits in some regions (*medium confidence*). {3.3}**

B.1.1 Evidence from attributed changes in some climate and weather extremes for a global warming of about 0.5°C supports the assessment that an additional 0.5°C of warming compared to present is associated with further detectable changes in these extremes (*medium confidence*). Several regional changes in climate are assessed to occur with global warming up to 1.5°C compared to pre-industrial levels, including warming of extreme temperatures in many regions (*high confidence*), increases in frequency, intensity, and/or amount of heavy precipitation in several regions (*high confidence*), and an increase in intensity or frequency of droughts in some regions (*medium confidence*). {3.2, 3.3.1, 3.3.2, 3.3.3, 3.3.4, Table 3.2}

B.1.2 Temperature extremes on land are projected to warm more than GMST (*high confidence*): extreme hot days in mid-latitudes warm by up to about 3°C at global warming of 1.5°C and about 4°C at 2°C, and extreme cold nights in high latitudes warm by up to about 4.5°C at 1.5°C and about 6°C at 2°C (*high confidence*). The number of hot days is projected to increase in most land regions, with highest increases in the tropics (*high confidence*). {3.3.1, 3.3.2, Cross-Chapter Box 8 in Chapter 3}

B.1.3 Risks from droughts and precipitation deficits are projected to be higher at 2°C compared to 1.5°C of global warming in some regions (*medium confidence*). Risks from heavy precipitation events are projected to be higher at 2°C compared to 1.5°C of global warming in several northern hemisphere high-latitude and/or high-elevation regions, eastern Asia and eastern North America (*medium confidence)*. Heavy precipitation associated with tropical cyclones is projected to be higher at 2°C compared to 1.5°C global warming (*medium confidence*). There is generally *low confidence* in projected changes in heavy precipitation at 2°C compared to 1.5°C in other regions. Heavy precipitation when aggregated at global scale is projected to be higher at 2°C than at 1.5°C of global warming (*medium confidence*). As a consequence of heavy precipitation, the fraction of the global land area affected by flood hazards is projected to be larger at 2°C compared to 1.5°C of global warming (*medium confidence*). {3.3.1, 3.3.3, 3.3.4, 3.3.5, 3.3.6}

**B.2 By 2100, global mean sea level rise is projected to be around 0.1 metre lower with global warming of 1.5°C compared to 2°C (*medium confidence*). Sea level will continue to rise well beyond 2100 (*high confidence*), and the magnitude and rate of this rise depend on future emission pathways. A slower rate of sea level rise enables greater opportunities for adaptation in the human and ecological systems of small islands, low-lying coastal areas and deltas (*medium confidence*). {3.3, 3.4, 3.6}**

B.2.1 Model-based projections of global mean sea level rise (relative to 1986–2005) suggest an indicative range of 0.26 to 0.77 m by 2100 for 1.5°C of global warming, 0.1 m (0.04–0.16 m) less than for a global warming of 2°C (*medium confidence*). A reduction of 0.1 m in global sea level rise implies that up to 10 million fewer people would be exposed to related risks, based on population in the year 2010 and assuming no adaptation (*medium confidence*). {3.4.4, 3.4.5, 4.3.2}

B.2.2 Sea level rise will continue beyond 2100 even if global warming is limited to 1.5°C in the 21st century (*high confidence*). Marine ice sheet instability in Antarctica and/or irreversible loss of the Greenland ice sheet could result in multi-metre rise in sea level over hundreds to thousands of years. These instabilities could be triggered at around 1.5°C to 2°C of global warming (*medium confidence*). (Figure SPM.2) {3.3.9, 3.4.5, 3.5.2, 3.6.3, Box 3.3}

---

7 Robust is here used to mean that at least two thirds of climate models show the same sign of changes at the grid point scale, and that differences in large regions are statistically significant.

8 Projected changes in impacts between different levels of global warming are determined with respect to changes in global mean surface air temperature.

B.2.3 Increasing warming amplifies the exposure of small islands, low-lying coastal areas and deltas to the risks associated with sea level rise for many human and ecological systems, including increased saltwater intrusion, flooding and damage to infrastructure (*high confidence*). Risks associated with sea level rise are higher at 2°C compared to 1.5°C. The slower rate of sea level rise at global warming of 1.5°C reduces these risks, enabling greater opportunities for adaptation including managing and restoring natural coastal ecosystems and infrastructure reinforcement (*medium confidence*). (Figure SPM.2) {3.4.5, Box 3.5}

### B.3 On land, impacts on biodiversity and ecosystems, including species loss and extinction, are projected to be lower at 1.5°C of global warming compared to 2°C. Limiting global warming to 1.5°C compared to 2°C is projected to lower the impacts on terrestrial, freshwater and coastal ecosystems and to retain more of their services to humans (*high confidence*). (Figure SPM.2) {3.4, 3.5, Box 3.4, Box 4.2, Cross-Chapter Box 8 in Chapter 3}

B.3.1 Of 105,000 species studied,[9] 6% of insects, 8% of plants and 4% of vertebrates are projected to lose over half of their climatically determined geographic range for global warming of 1.5°C, compared with 18% of insects, 16% of plants and 8% of vertebrates for global warming of 2°C (*medium confidence*). Impacts associated with other biodiversity-related risks such as forest fires and the spread of invasive species are lower at 1.5°C compared to 2°C of global warming (*high confidence*). {3.4.3, 3.5.2}

B.3.2 Approximately 4% (interquartile range 2–7%) of the global terrestrial land area is projected to undergo a transformation of ecosystems from one type to another at 1°C of global warming, compared with 13% (interquartile range 8–20%) at 2°C (*medium confidence*). This indicates that the area at risk is projected to be approximately 50% lower at 1.5°C compared to 2°C (*medium confidence*). {3.4.3.1, 3.4.3.5}

B.3.3 High-latitude tundra and boreal forests are particularly at risk of climate change-induced degradation and loss, with woody shrubs already encroaching into the tundra (*high confidence*) and this will proceed with further warming. Limiting global warming to 1.5°C rather than 2°C is projected to prevent the thawing over centuries of a permafrost area in the range of 1.5 to 2.5 million km$^2$ (*medium confidence*). {3.3.2, 3.4.3, 3.5.5}

### B.4 Limiting global warming to 1.5°C compared to 2°C is projected to reduce increases in ocean temperature as well as associated increases in ocean acidity and decreases in ocean oxygen levels (*high confidence*). Consequently, limiting global warming to 1.5°C is projected to reduce risks to marine biodiversity, fisheries, and ecosystems, and their functions and services to humans, as illustrated by recent changes to Arctic sea ice and warm-water coral reef ecosystems (*high confidence*). {3.3, 3.4, 3.5, Box 3.4, Box 3.5}

B.4.1 There is *high confidence* that the probability of a sea ice-free Arctic Ocean during summer is substantially lower at global warming of 1.5°C when compared to 2°C. With 1.5°C of global warming, one sea ice-free Arctic summer is projected per century. This likelihood is increased to at least one per decade with 2°C global warming. Effects of a temporary overshoot are reversible for Arctic sea ice cover on decadal time scales (*high confidence*). {3.3.8, 3.4.4.7}

B.4.2 Global warming of 1.5°C is projected to shift the ranges of many marine species to higher latitudes as well as increase the amount of damage to many ecosystems. It is also expected to drive the loss of coastal resources and reduce the productivity of fisheries and aquaculture (especially at low latitudes). The risks of climate-induced impacts are projected to be higher at 2°C than those at global warming of 1.5°C (*high confidence*). Coral reefs, for example, are projected to decline by a further 70–90% at 1.5°C (*high confidence*) with larger losses (>99%) at 2°C (*very high confidence*). The risk of irreversible loss of many marine and coastal ecosystems increases with global warming, especially at 2°C or more (*high confidence*). {3.4.4, Box 3.4}

9 Consistent with earlier studies, illustrative numbers were adopted from one recent meta-study.

B.4.3 The level of ocean acidification due to increasing $CO_2$ concentrations associated with global warming of 1.5°C is projected to amplify the adverse effects of warming, and even further at 2°C, impacting the growth, development, calcification, survival, and thus abundance of a broad range of species, for example, from algae to fish (*high confidence*). {3.3.10, 3.4.4}

B.4.4 Impacts of climate change in the ocean are increasing risks to fisheries and aquaculture via impacts on the physiology, survivorship, habitat, reproduction, disease incidence, and risk of invasive species (*medium confidence*) but are projected to be less at 1.5°C of global warming than at 2°C. One global fishery model, for example, projected a decrease in global annual catch for marine fisheries of about 1.5 million tonnes for 1.5°C of global warming compared to a loss of more than 3 million tonnes for 2°C of global warming (*medium confidence*). {3.4.4, Box 3.4}

## B.5 Climate-related risks to health, livelihoods, food security, water supply, human security, and economic growth are projected to increase with global warming of 1.5°C and increase further with 2°C. (Figure SPM.2) {3.4, 3.5, 5.2, Box 3.2, Box 3.3, Box 3.5, Box 3.6, Cross-Chapter Box 6 in Chapter 3, Cross-Chapter Box 9 in Chapter 4, Cross-Chapter Box 12 in Chapter 5, 5.2}

B.5.1 Populations at disproportionately higher risk of adverse consequences with global warming of 1.5°C and beyond include disadvantaged and vulnerable populations, some indigenous peoples, and local communities dependent on agricultural or coastal livelihoods (*high confidence*). Regions at disproportionately higher risk include Arctic ecosystems, dryland regions, small island developing states, and Least Developed Countries (*high confidence*). Poverty and disadvantage are expected to increase in some populations as global warming increases; limiting global warming to 1.5°C, compared with 2°C, could reduce the number of people both exposed to climate-related risks and susceptible to poverty by up to several hundred million by 2050 (*medium confidence*). {3.4.10, 3.4.11, Box 3.5, Cross-Chapter Box 6 in Chapter 3, Cross-Chapter Box 9 in Chapter 4, Cross-Chapter Box 12 in Chapter 5, 4.2.2.2, 5.2.1, 5.2.2, 5.2.3, 5.6.3}

B.5.2 Any increase in global warming is projected to affect human health, with primarily negative consequences (*high confidence*). Lower risks are projected at 1.5°C than at 2°C for heat-related morbidity and mortality (*very high confidence*) and for ozone-related mortality if emissions needed for ozone formation remain high (*high confidence*). Urban heat islands often amplify the impacts of heatwaves in cities (*high confidence*). Risks from some vector-borne diseases, such as malaria and dengue fever, are projected to increase with warming from 1.5°C to 2°C, including potential shifts in their geographic range (*high confidence*). {3.4.7, 3.4.8, 3.5.5.8}

B.5.3 Limiting warming to 1.5°C compared with 2°C is projected to result in smaller net reductions in yields of maize, rice, wheat, and potentially other cereal crops, particularly in sub-Saharan Africa, Southeast Asia, and Central and South America, and in the $CO_2$-dependent nutritional quality of rice and wheat (*high confidence*). Reductions in projected food availability are larger at 2°C than at 1.5°C of global warming in the Sahel, southern Africa, the Mediterranean, central Europe, and the Amazon (*medium confidence*). Livestock are projected to be adversely affected with rising temperatures, depending on the extent of changes in feed quality, spread of diseases, and water resource availability (*high confidence*). {3.4.6, 3.5.4, 3.5.5, Box 3.1, Cross-Chapter Box 6 in Chapter 3, Cross-Chapter Box 9 in Chapter 4}

B.5.4 Depending on future socio-economic conditions, limiting global warming to 1.5°C compared to 2°C may reduce the proportion of the world population exposed to a climate change-induced increase in water stress by up to 50%, although there is considerable variability between regions (*medium confidence*). Many small island developing states could experience lower water stress as a result of projected changes in aridity when global warming is limited to 1.5°C, as compared to 2°C (*medium confidence*). {3.3.5, 3.4.2, 3.4.8, 3.5.5, Box 3.2, Box 3.5, Cross-Chapter Box 9 in Chapter 4}

B.5.5 Risks to global aggregated economic growth due to climate change impacts are projected to be lower at 1.5°C than at 2°C by the end of this century[10] (*medium confidence*). This excludes the costs of mitigation, adaptation investments and the benefits of adaptation. Countries in the tropics and Southern Hemisphere subtropics are projected to experience the largest impacts on economic growth due to climate change should global warming increase from 1.5°C to 2°C (*medium confidence*). {3.5.2, 3.5.3}

10 Here, impacts on economic growth refer to changes in gross domestic product (GDP). Many impacts, such as loss of human lives, cultural heritage and ecosystem services, are difficult to value and monetize.

B.5.6 Exposure to multiple and compound climate-related risks increases between 1.5°C and 2°C of global warming, with greater proportions of people both so exposed and susceptible to poverty in Africa and Asia (*high confidence*). For global warming from 1.5°C to 2°C, risks across energy, food, and water sectors could overlap spatially and temporally, creating new and exacerbating current hazards, exposures, and vulnerabilities that could affect increasing numbers of people and regions (*medium confidence*). {Box 3.5, 3.3.1, 3.4.5.3, 3.4.5.6, 3.4.11, 3.5.4.9}

B.5.7 There are multiple lines of evidence that since AR5 the assessed levels of risk increased for four of the five Reasons for Concern (RFCs) for global warming to 2°C (*high confidence*). The risk transitions by degrees of global warming are now: from high to very high risk between 1.5°C and 2°C for RFC1 (Unique and threatened systems) (*high confidence*); from moderate to high risk between 1°C and 1.5°C for RFC2 (Extreme weather events) (*medium confidence*); from moderate to high risk between 1.5°C and 2°C for RFC3 (Distribution of impacts) (*high confidence*); from moderate to high risk between 1.5°C and 2.5°C for RFC4 (Global aggregate impacts) (*medium confidence*); and from moderate to high risk between 1°C and 2.5°C for RFC5 (Large-scale singular events) (*medium confidence*). (Figure SPM.2) {3.4.13; 3.5, 3.5.2}

**B.6 Most adaptation needs will be lower for global warming of 1.5°C compared to 2°C (*high confidence*). There are a wide range of adaptation options that can reduce the risks of climate change (*high confidence*). There are limits to adaptation and adaptive capacity for some human and natural systems at global warming of 1.5°C, with associated losses (*medium confidence*). The number and availability of adaptation options vary by sector (*medium confidence*). {Table 3.5, 4.3, 4.5, Cross-Chapter Box 9 in Chapter 4, Cross-Chapter Box 12 in Chapter 5}**

B.6.1 A wide range of adaptation options are available to reduce the risks to natural and managed ecosystems (e.g., ecosystem-based adaptation, ecosystem restoration and avoided degradation and deforestation, biodiversity management, sustainable aquaculture, and local knowledge and indigenous knowledge), the risks of sea level rise (e.g., coastal defence and hardening), and the risks to health, livelihoods, food, water, and economic growth, especially in rural landscapes (e.g., efficient irrigation, social safety nets, disaster risk management, risk spreading and sharing, and community-based adaptation) and urban areas (e.g., green infrastructure, sustainable land use and planning, and sustainable water management) (*medium confidence*). {4.3.1, 4.3.2, 4.3.3, 4.3.5, 4.5.3, 4.5.4, 5.3.2, Box 4.2, Box 4.3, Box 4.6, Cross-Chapter Box 9 in Chapter 4}.

B.6.2 Adaptation is expected to be more challenging for ecosystems, food and health systems at 2°C of global warming than for 1.5°C (*medium confidence*). Some vulnerable regions, including small islands and Least Developed Countries, are projected to experience high multiple interrelated climate risks even at global warming of 1.5°C (*high confidence*). {3.3.1, 3.4.5, Box 3.5, Table 3.5, Cross-Chapter Box 9 in Chapter 4, 5.6, Cross-Chapter Box 12 in Chapter 5, Box 5.3}

B.6.3 Limits to adaptive capacity exist at 1.5°C of global warming, become more pronounced at higher levels of warming and vary by sector, with site-specific implications for vulnerable regions, ecosystems and human health (*medium confidence*). {Cross-Chapter Box 12 in Chapter 5, Box 3.5, Table 3.5}

# How the level of global warming affects impacts and/or risks associated with the Reasons for Concern (RFCs) and selected natural, managed and human systems

Five Reasons For Concern (RFCs) illustrate the impacts and risks of different levels of global warming for people, economies and ecosystems across sectors and regions.

## Impacts and risks associated with the Reasons for Concern (RFCs)

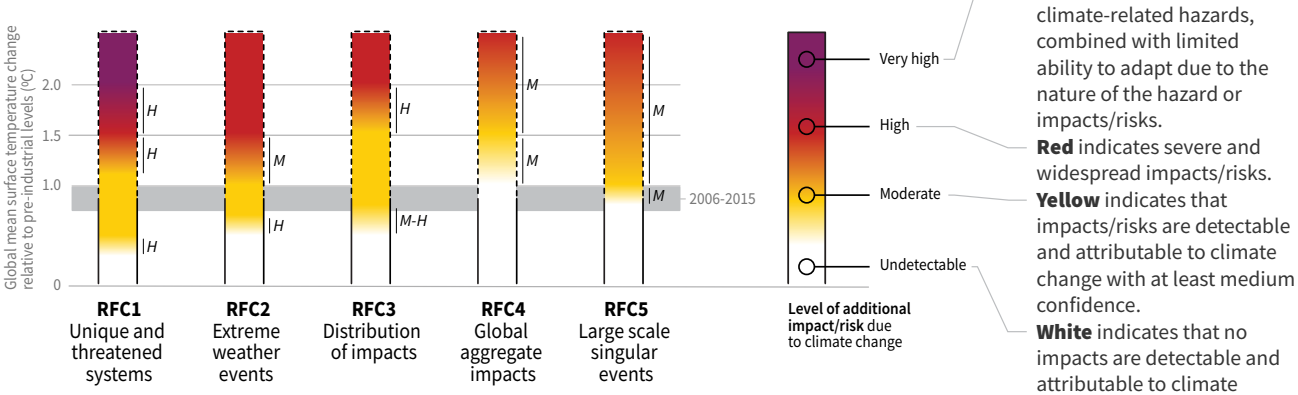


**Purple** indicates very high risks of severe impacts/risks and the presence of significant irreversibility or the persistence of climate-related hazards, combined with limited ability to adapt due to the nature of the hazard or impacts/risks.
**Red** indicates severe and widespread impacts/risks.
**Yellow** indicates that impacts/risks are detectable and attributable to climate change with at least medium confidence.
**White** indicates that no impacts are detectable and attributable to climate change.

## Impacts and risks for selected natural, managed and human systems

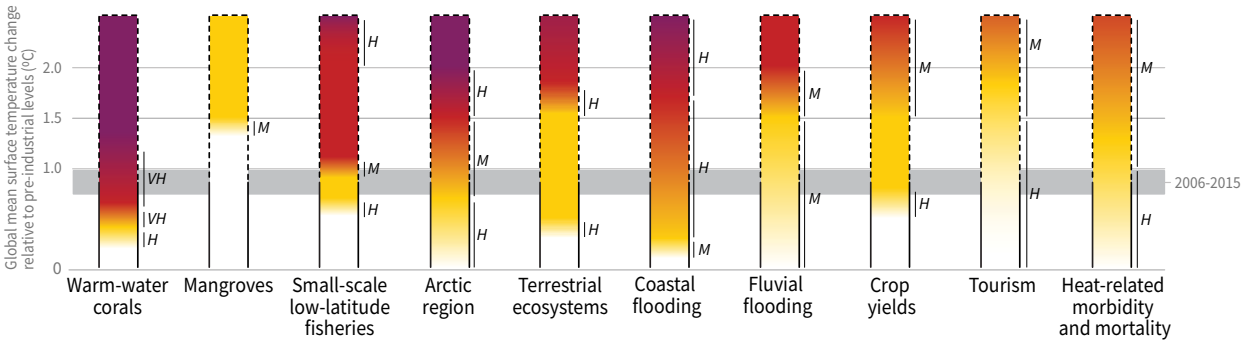


**Confidence level for transition:** *L*=Low, *M*=Medium, *H*=High and *VH*=Very high

**Figure SPM.2 |** Five integrative reasons for concern (RFCs) provide a framework for summarizing key impacts and risks across sectors and regions, and were introduced in the IPCC Third Assessment Report. RFCs illustrate the implications of global warming for people, economies and ecosystems. Impacts and/or risks for each RFC are based on assessment of the new literature that has appeared. As in AR5, this literature was used to make expert judgments to assess the levels of global warming at which levels of impact and/or risk are undetectable, moderate, high or very high. The selection of impacts and risks to natural, managed and human systems in the lower panel is illustrative and is not intended to be fully comprehensive. {3.4, 3.5, 3.5.2.1, 3.5.2.2, 3.5.2.3, 3.5.2.4, 3.5.2.5, 5.4.1, 5.5.3, 5.6.1, Box 3.4}

**RFC1 Unique and threatened systems:** ecological and human systems that have restricted geographic ranges constrained by climate-related conditions and have high endemism or other distinctive properties. Examples include coral reefs, the Arctic and its indigenous people, mountain glaciers and biodiversity hotspots.
**RFC2 Extreme weather events:** risks/impacts to human health, livelihoods, assets and ecosystems from extreme weather events such as heat waves, heavy rain, drought and associated wildfires, and coastal flooding.
**RFC3 Distribution of impacts:** risks/impacts that disproportionately affect particular groups due to uneven distribution of physical climate change hazards, exposure or vulnerability.
**RFC4 Global aggregate impacts:** global monetary damage, global-scale degradation and loss of ecosystems and biodiversity.
**RFC5 Large-scale singular events:** are relatively large, abrupt and sometimes irreversible changes in systems that are caused by global warming. Examples include disintegration of the Greenland and Antarctic ice sheets.

# C. Emission Pathways and System Transitions Consistent with 1.5°C Global Warming

**C.1 In model pathways with no or limited overshoot of 1.5°C, global net anthropogenic $CO_2$ emissions decline by about 45% from 2010 levels by 2030 (40–60% interquartile range), reaching net zero around 2050 (2045–2055 interquartile range). For limiting global warming to below 2°C[11] $CO_2$ emissions are projected to decline by about 25% by 2030 in most pathways (10–30% interquartile range) and reach net zero around 2070 (2065–2080 interquartile range). Non-$CO_2$ emissions in pathways that limit global warming to 1.5°C show deep reductions that are similar to those in pathways limiting warming to 2°C. (*high confidence*) (Figure SPM.3a) {2.1, 2.3, Table 2.4}**

C.1.1 $CO_2$ emissions reductions that limit global warming to 1.5°C with no or limited overshoot can involve different portfolios of mitigation measures, striking different balances between lowering energy and resource intensity, rate of decarbonization, and the reliance on carbon dioxide removal. Different portfolios face different implementation challenges and potential synergies and trade-offs with sustainable development. (*high confidence*) (Figure SPM.3b) {2.3.2, 2.3.4, 2.4, 2.5.3}

C.1.2 Modelled pathways that limit global warming to 1.5°C with no or limited overshoot involve deep reductions in emissions of methane and black carbon (35% or more of both by 2050 relative to 2010). These pathways also reduce most of the cooling aerosols, which partially offsets mitigation effects for two to three decades. Non-$CO_2$ emissions[12] can be reduced as a result of broad mitigation measures in the energy sector. In addition, targeted non-$CO_2$ mitigation measures can reduce nitrous oxide and methane from agriculture, methane from the waste sector, some sources of black carbon, and hydrofluorocarbons. High bioenergy demand can increase emissions of nitrous oxide in some 1.5°C pathways, highlighting the importance of appropriate management approaches. Improved air quality resulting from projected reductions in many non-$CO_2$ emissions provide direct and immediate population health benefits in all 1.5°C model pathways. (*high confidence*) (Figure SPM.3a) {2.2.1, 2.3.3, 2.4.4, 2.5.3, 4.3.6, 5.4.2}

C.1.3 Limiting global warming requires limiting the total cumulative global anthropogenic emissions of $CO_2$ since the pre-industrial period, that is, staying within a total carbon budget (*high confidence*).[13] By the end of 2017, anthropogenic $CO_2$ emissions since the pre-industrial period are estimated to have reduced the total carbon budget for 1.5°C by approximately 2200 ± 320 $GtCO_2$ (*medium confidence*). The associated remaining budget is being depleted by current emissions of 42 ± 3 $GtCO_2$ per year (*high confidence*). The choice of the measure of global temperature affects the estimated remaining carbon budget. Using global mean surface air temperature, as in AR5, gives an estimate of the remaining carbon budget of 580 $GtCO_2$ for a 50% probability of limiting warming to 1.5°C, and 420 $GtCO_2$ for a 66% probability (*medium confidence*).[14] Alternatively, using GMST gives estimates of 770 and 570 $GtCO_2$, for 50% and 66% probabilities,[15] respectively (*medium confidence*). Uncertainties in the size of these estimated remaining carbon budgets are substantial and depend on several factors. Uncertainties in the climate response to $CO_2$ and non-$CO_2$ emissions contribute ±400 $GtCO_2$ and the level of historic warming contributes ±250 $GtCO_2$ (*medium confidence*). Potential additional carbon release from future permafrost thawing and methane release from wetlands would reduce budgets by up to 100 $GtCO_2$ over the course of this century and more thereafter (*medium confidence*). In addition, the level of non-$CO_2$ mitigation in the future could alter the remaining carbon budget by 250 $GtCO_2$ in either direction (*medium confidence*). {1.2.4, 2.2.2, 2.6.1, Table 2.2, Chapter 2 Supplementary Material}

C.1.4 Solar radiation modification (SRM) measures are not included in any of the available assessed pathways. Although some SRM measures may be theoretically effective in reducing an overshoot, they face large uncertainties and knowledge gaps

11 References to pathways limiting global warming to 2°C are based on a 66% probability of staying below 2°C.

12 Non-$CO_2$ emissions included in this Report are all anthropogenic emissions other than $CO_2$ that result in radiative forcing. These include short-lived climate forcers, such as methane, some fluorinated gases, ozone precursors, aerosols or aerosol precursors, such as black carbon and sulphur dioxide, respectively, as well as long-lived greenhouse gases, such as nitrous oxide or some fluorinated gases. The radiative forcing associated with non-$CO_2$ emissions and changes in surface albedo is referred to as non-$CO_2$ radiative forcing. {2.2.1}

13 There is a clear scientific basis for a total carbon budget consistent with limiting global warming to 1.5°C. However, neither this total carbon budget nor the fraction of this budget taken up by past emissions were assessed in this Report.

14 Irrespective of the measure of global temperature used, updated understanding and further advances in methods have led to an increase in the estimated remaining carbon budget of about 300 $GtCO_2$ compared to AR5. (*medium confidence*) {2.2.2}

15 These estimates use observed GMST to 2006–2015 and estimate future temperature changes using near surface air temperatures.

as well as substantial risks and institutional and social constraints to deployment related to governance, ethics, and impacts on sustainable development. They also do not mitigate ocean acidification. (*medium confidence*) {4.3.8, Cross-Chapter Box 10 in Chapter 4}

## Global emissions pathway characteristics

General characteristics of the evolution of anthropogenic net emissions of $CO_2$, and total emissions of methane, black carbon, and nitrous oxide in model pathways that limit global warming to 1.5°C with no or limited overshoot. Net emissions are defined as anthropogenic emissions reduced by anthropogenic removals. Reductions in net emissions can be achieved through different portfolios of mitigation measures illustrated in Figure SPM.3b.

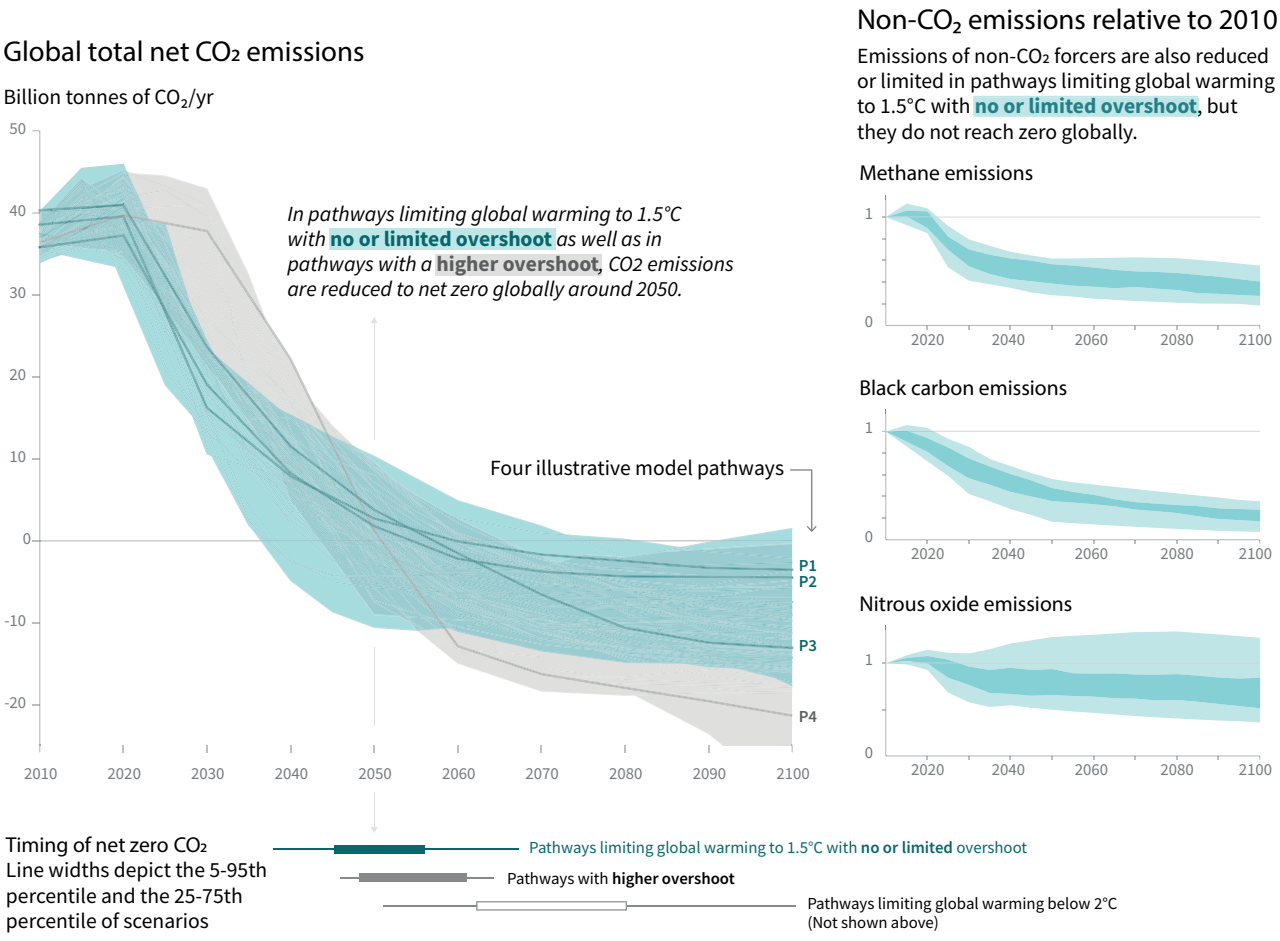


**Figure SPM.3a |** Global emissions pathway characteristics. The main panel shows global net anthropogenic $CO_2$ emissions in pathways limiting global warming to 1.5°C with no or limited (less than 0.1°C) overshoot and pathways with higher overshoot. The shaded area shows the full range for pathways analysed in this Report. The panels on the right show non-$CO_2$ emissions ranges for three compounds with large historical forcing and a substantial portion of emissions coming from sources distinct from those central to $CO_2$ mitigation. Shaded areas in these panels show the 5–95% (light shading) and interquartile (dark shading) ranges of pathways limiting global warming to 1.5°C with no or limited overshoot. Box and whiskers at the bottom of the figure show the timing of pathways reaching global net zero $CO_2$ emission levels, and a comparison with pathways limiting global warming to 2°C with at least 66% probability. Four illustrative model pathways are highlighted in the main panel and are labelled P1, P2, P3 and P4, corresponding to the LED, S1, S2, and S5 pathways assessed in Chapter 2. Descriptions and characteristics of these pathways are available in Figure SPM.3b. {2.1, 2.2, 2.3, Figure 2.5, Figure 2.10, Figure 2.11}

# Characteristics of four illustrative model pathways

Different mitigation strategies can achieve the net emissions reductions that would be required to follow a pathway that limits global warming to 1.5°C with no or limited overshoot. All pathways use Carbon Dioxide Removal (CDR), but the amount varies across pathways, as do the relative contributions of Bioenergy with Carbon Capture and Storage (BECCS) and removals in the Agriculture, Forestry and Other Land Use (AFOLU) sector. This has implications for emissions and several other pathway characteristics.

## Breakdown of contributions to global net $CO_2$ emissions in four illustrative model pathways

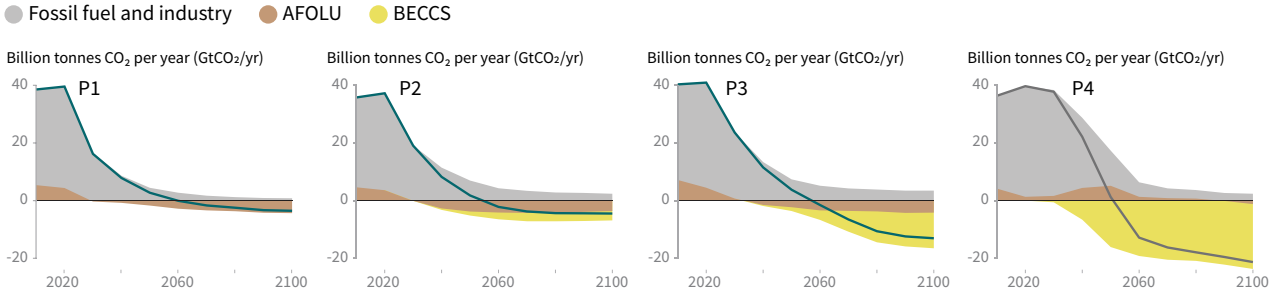


**P1:** A scenario in which social, business and technological innovations result in lower energy demand up to 2050 while living standards rise, especially in the global South. A downsized energy system enables rapid decarbonization of energy supply. Afforestation is the only CDR option considered; neither fossil fuels with CCS nor BECCS are used.

**P2:** A scenario with a broad focus on sustainability including energy intensity, human development, economic convergence and international cooperation, as well as shifts towards sustainable and healthy consumption patterns, low-carbon technology innovation, and well-managed land systems with limited societal acceptability for BECCS.

**P3:** A middle-of-the-road scenario in which societal as well as technological development follows historical patterns. Emissions reductions are mainly achieved by changing the way in which energy and products are produced, and to a lesser degree by reductions in demand.

**P4:** A resource- and energy-intensive scenario in which economic growth and globalization lead to widespread adoption of greenhouse-gas-intensive lifestyles, including high demand for transportation fuels and livestock products. Emissions reductions are mainly achieved through technological means, making strong use of CDR through the deployment of BECCS.

| **Global indicators** | P1 | P2 | P3 | P4 | **Interquartile range** |
|---|---|---|---|---|---|
| *Pathway classification* | No or limited overshoot | No or limited overshoot | No or limited overshoot | Higher overshoot | No or limited overshoot |
| *$CO_2$ emission change in 2030 (% rel to 2010)* | -58 | -47 | -41 | 4 | (-58,-40) |
| *↳ in 2050 (% rel to 2010)* | -93 | -95 | -91 | -97 | (-107,-94) |
| *Kyoto-GHG emissions* in 2030 (% rel to 2010)* | -50 | -49 | -35 | -2 | (-51,-39) |
| *↳ in 2050 (% rel to 2010)* | -82 | -89 | -78 | -80 | (-93,-81) |
| *Final energy demand** in 2030 (% rel to 2010)* | -15 | -5 | 17 | 39 | (-12,7) |
| *↳ in 2050 (% rel to 2010)* | -32 | 2 | 21 | 44 | (-11,22) |
| *Renewable share in electricity in 2030 (%)* | 60 | 58 | 48 | 25 | (47,65) |
| *↳ in 2050 (%)* | 77 | 81 | 63 | 70 | (69,86) |
| *Primary energy from coal in 2030 (% rel to 2010)* | -78 | -61 | -75 | -59 | (-78, -59) |
| *↳ in 2050 (% rel to 2010)* | -97 | -77 | -73 | -97 | (-95, -74) |
| *from oil in 2030 (% rel to 2010)* | -37 | -13 | -3 | 86 | (-34,3) |
| *↳ in 2050 (% rel to 2010)* | -87 | -50 | -81 | -32 | (-78,-31) |
| *from gas in 2030 (% rel to 2010)* | -25 | -20 | 33 | 37 | (-26,21) |
| *↳ in 2050 (% rel to 2010)* | -74 | -53 | 21 | -48 | (-56,6) |
| *from nuclear in 2030 (% rel to 2010)* | 59 | 83 | 98 | 106 | (44,102) |
| *↳ in 2050 (% rel to 2010)* | 150 | 98 | 501 | 468 | (91,190) |
| *from biomass in 2030 (% rel to 2010)* | -11 | 0 | 36 | -1 | (29,80) |
| *↳ in 2050 (% rel to 2010)* | -16 | 49 | 121 | 418 | (123,261) |
| *from non-biomass renewables in 2030 (% rel to 2010)* | 430 | 470 | 315 | 110 | (245,436) |
| *↳ in 2050 (% rel to 2010)* | 833 | 1327 | 878 | 1137 | (576,1299) |
| *Cumulative CCS until 2100 ($GtCO_2$)* | 0 | 348 | 687 | 1218 | (550,1017) |
| *↳ of which BECCS ($GtCO_2$)* | 0 | 151 | 414 | 1191 | (364,662) |
| *Land area of bioenergy crops in 2050 (million $km^2$)* | 0.2 | 0.9 | 2.8 | 7.2 | (1.5,3.2) |
| *Agricultural $CH_4$ emissions in 2030 (% rel to 2010)* | -24 | -48 | 1 | 14 | (-30,-11) |
| *in 2050 (% rel to 2010)* | -33 | -69 | -23 | 2 | (-47,-24) |
| *Agricultural $N_2O$ emissions in 2030 (% rel to 2010)* | 5 | -26 | 15 | 3 | (-21,3) |
| *in 2050 (% rel to 2010)* | 6 | -26 | 0 | 39 | (-26,1) |

*NOTE: Indicators have been selected to show global trends identified by the Chapter 2 assessment. National and sectoral characteristics can differ substantially from the global trends shown above.*

** Kyoto-gas emissions are based on IPCC Second Assessment Report GWP-100*
*** Changes in energy demand are associated with improvements in energy efficiency and behaviour change*

**Figure SPM.3b |** Characteristics of four illustrative model pathways in relation to global warming of 1.5°C introduced in Figure SPM.3a. These pathways were selected to show a range of potential mitigation approaches and vary widely in their projected energy and land use, as well as their assumptions about future socio-economic developments, including economic and population growth, equity and sustainability. A breakdown of the global net anthropogenic $CO_2$ emissions into the contributions in terms of $CO_2$ emissions from fossil fuel and industry; agriculture, forestry and other land use (AFOLU); and bioenergy with carbon capture and storage (BECCS) is shown. AFOLU estimates reported here are not necessarily comparable with countries' estimates. Further characteristics for each of these pathways are listed below each pathway. These pathways illustrate relative global differences in mitigation strategies, but do not represent central estimates, national strategies, and do not indicate requirements. For comparison, the right-most column shows the interquartile ranges across pathways with no or limited overshoot of 1.5°C. Pathways P1, P2, P3 and P4 correspond to the LED, S1, S2 and S5 pathways assessed in Chapter 2 (Figure SPM.3a). {2.2.1, 2.3.1, 2.3.2, 2.3.3, 2.3.4, 2.4.1, 2.4.2, 2.4.4, 2.5.3, Figure 2.5, Figure 2.6, Figure 2.9, Figure 2.10, Figure 2.11, Figure 2.14, Figure 2.15, Figure 2.16, Figure 2.17, Figure 2.24, Figure 2.25, Table 2.4, Table 2.6, Table 2.7, Table 2.9, Table 4.1}

## C.2 Pathways limiting global warming to 1.5°C with no or limited overshoot would require rapid and far-reaching transitions in energy, land, urban and infrastructure (including transport and buildings), and industrial systems (*high confidence*). These systems transitions are unprecedented in terms of scale, but not necessarily in terms of speed, and imply deep emissions reductions in all sectors, a wide portfolio of mitigation options and a significant upscaling of investments in those options (*medium confidence*). {2.3, 2.4, 2.5, 4.2, 4.3, 4.4, 4.5}

C.2.1 Pathways that limit global warming to 1.5°C with no or limited overshoot show system changes that are more rapid and pronounced over the next two decades than in 2°C pathways (*high confidence*). The rates of system changes associated with limiting global warming to 1.5°C with no or limited overshoot have occurred in the past within specific sectors, technologies and spatial contexts, but there is no documented historic precedent for their scale (*medium confidence*). {2.3.3, 2.3.4, 2.4, 2.5, 4.2.1, 4.2.2, Cross-Chapter Box 11 in Chapter 4}

C.2.2 In energy systems, modelled global pathways (considered in the literature) limiting global warming to 1.5°C with no or limited overshoot (for more details see Figure SPM.3b) generally meet energy service demand with lower energy use, including through enhanced energy efficiency, and show faster electrification of energy end use compared to 2°C (*high confidence*). In 1.5°C pathways with no or limited overshoot, low-emission energy sources are projected to have a higher share, compared with 2°C pathways, particularly before 2050 (*high confidence*). In 1.5°C pathways with no or limited overshoot, renewables are projected to supply 70–85% (interquartile range) of electricity in 2050 (*high confidence*). In electricity generation, shares of nuclear and fossil fuels with carbon dioxide capture and storage (CCS) are modelled to increase in most 1.5°C pathways with no or limited overshoot. In modelled 1.5°C pathways with limited or no overshoot, the use of CCS would allow the electricity generation share of gas to be approximately 8% (3–11% interquartile range) of global electricity in 2050, while the use of coal shows a steep reduction in all pathways and would be reduced to close to 0% (0–2% interquartile range) of electricity (*high confidence*). While acknowledging the challenges, and differences between the options and national circumstances, political, economic, social and technical feasibility of solar energy, wind energy and electricity storage technologies have substantially improved over the past few years (*high confidence*). These improvements signal a potential system transition in electricity generation. (Figure SPM.3b) {2.4.1, 2.4.2, Figure 2.1, Table 2.6, Table 2.7, Cross-Chapter Box 6 in Chapter 3, 4.2.1, 4.3.1, 4.3.3, 4.5.2}

C.2.3 $CO_2$ emissions from industry in pathways limiting global warming to 1.5°C with no or limited overshoot are projected to be about 65–90% (interquartile range) lower in 2050 relative to 2010, as compared to 50–80% for global warming of 2°C (*medium confidence*). Such reductions can be achieved through combinations of new and existing technologies and practices, including electrification, hydrogen, sustainable bio-based feedstocks, product substitution, and carbon capture, utilization and storage (CCUS). These options are technically proven at various scales but their large-scale deployment may be limited by economic, financial, human capacity and institutional constraints in specific contexts, and specific characteristics of large-scale industrial installations. In industry, emissions reductions by energy and process efficiency by themselves are insufficient for limiting warming to 1.5°C with no or limited overshoot (*high confidence*). {2.4.3, 4.2.1, Table 4.1, Table 4.3, 4.3.3, 4.3.4, 4.5.2}

C.2.4 The urban and infrastructure system transition consistent with limiting global warming to 1.5°C with no or limited overshoot would imply, for example, changes in land and urban planning practices, as well as deeper emissions reductions in transport and buildings compared to pathways that limit global warming below 2°C (*medium confidence*). Technical measures

and practices enabling deep emissions reductions include various energy efficiency options. In pathways limiting global warming to 1.5°C with no or limited overshoot, the electricity share of energy demand in buildings would be about 55–75% in 2050 compared to 50–70% in 2050 for 2°C global warming (*medium confidence*). In the transport sector, the share of low-emission final energy would rise from less than 5% in 2020 to about 35–65% in 2050 compared to 25–45% for 2°C of global warming (*medium confidence*). Economic, institutional and socio-cultural barriers may inhibit these urban and infrastructure system transitions, depending on national, regional and local circumstances, capabilities and the availability of capital (*high confidence*). {2.3.4, 2.4.3, 4.2.1, Table 4.1, 4.3.3, 4.5.2}

C.2.5 Transitions in global and regional land use are found in all pathways limiting global warming to 1.5°C with no or limited overshoot, but their scale depends on the pursued mitigation portfolio. Model pathways that limit global warming to 1.5°C with no or limited overshoot project a 4 million $km^2$ reduction to a 2.5 million $km^2$ increase of non-pasture agricultural land for food and feed crops and a 0.5–11 million $km^2$ reduction of pasture land, to be converted into a 0–6 million $km^2$ increase of agricultural land for energy crops and a 2 million $km^2$ reduction to 9.5 million $km^2$ increase in forests by 2050 relative to 2010 (*medium confidence*).[16] Land-use transitions of similar magnitude can be observed in modelled 2°C pathways (*medium confidence*). Such large transitions pose profound challenges for sustainable management of the various demands on land for human settlements, food, livestock feed, fibre, bioenergy, carbon storage, biodiversity and other ecosystem services (*high confidence*). Mitigation options limiting the demand for land include sustainable intensification of land-use practices, ecosystem restoration and changes towards less resource-intensive diets (*high confidence*). The implementation of land-based mitigation options would require overcoming socio-economic, institutional, technological, financing and environmental barriers that differ across regions (*high confidence*). {2.4.4, Figure 2.24, 4.3.2, 4.3.7, 4.5.2, Cross-Chapter Box 7 in Chapter 3}

C.2.6 Additional annual average energy-related investments for the period 2016 to 2050 in pathways limiting warming to 1.5°C compared to pathways without new climate policies beyond those in place today are estimated to be around 830 billion USD2010 (range of 150 billion to 1700 billion USD2010 across six models[17]). This compares to total annual average energy supply investments in 1.5°C pathways of 1460 to 3510 billion USD2010 and total annual average energy demand investments of 640 to 910 billion USD2010 for the period 2016 to 2050. Total energy-related investments increase by about 12% (range of 3% to 24%) in 1.5°C pathways relative to 2°C pathways. Annual investments in low-carbon energy technologies and energy efficiency are upscaled by roughly a factor of six (range of factor of 4 to 10) by 2050 compared to 2015 (*medium confidence*). {2.5.2, Box 4.8, Figure 2.27}

C.2.7 Modelled pathways limiting global warming to 1.5°C with no or limited overshoot project a wide range of global average discounted marginal abatement costs over the 21st century. They are roughly 3-4 times higher than in pathways limiting global warming to below 2°C (*high confidence*). The economic literature distinguishes marginal abatement costs from total mitigation costs in the economy. The literature on total mitigation costs of 1.5°C mitigation pathways is limited and was not assessed in this Report. Knowledge gaps remain in the integrated assessment of the economy-wide costs and benefits of mitigation in line with pathways limiting warming to 1.5°C. {2.5.2; 2.6; Figure 2.26}

16 The projected land-use changes presented are not deployed to their upper limits simultaneously in a single pathway.

17 Including two pathways limiting warming to 1.5°C with no or limited overshoot and four pathways with higher overshoot.

**C.3 All pathways that limit global warming to 1.5°C with limited or no overshoot project the use of carbon dioxide removal (CDR) on the order of 100–1000 $GtCO_2$ over the 21st century. CDR would be used to compensate for residual emissions and, in most cases, achieve net negative emissions to return global warming to 1.5°C following a peak (*high confidence*). CDR deployment of several hundreds of $GtCO_2$ is subject to multiple feasibility and sustainability constraints (*high confidence*). Significant near-term emissions reductions and measures to lower energy and land demand can limit CDR deployment to a few hundred $GtCO_2$ without reliance on bioenergy with carbon capture and storage (BECCS) (*high confidence*). {2.3, 2.4, 3.6.2, 4.3, 5.4}**

C.3.1 Existing and potential CDR measures include afforestation and reforestation, land restoration and soil carbon sequestration, BECCS, direct air carbon capture and storage (DACCS), enhanced weathering and ocean alkalinization. These differ widely in terms of maturity, potentials, costs, risks, co-benefits and trade-offs (*high confidence*). To date, only a few published pathways include CDR measures other than afforestation and BECCS. {2.3.4, 3.6.2, 4.3.2, 4.3.7}

C.3.2 In pathways limiting global warming to 1.5°C with limited or no overshoot, BECCS deployment is projected to range from 0–1, 0–8, and 0–16 $GtCO_2\ yr^{-1}$ in 2030, 2050, and 2100, respectively, while agriculture, forestry and land-use (AFOLU) related CDR measures are projected to remove 0–5, 1–11, and 1–5 $GtCO_2\ yr^{-1}$ in these years (*medium confidence*). The upper end of these deployment ranges by mid-century exceeds the BECCS potential of up to 5 $GtCO_2\ yr^{-1}$ and afforestation potential of up to 3.6 $GtCO_2\ yr^{-1}$ assessed based on recent literature (*medium confidence*). Some pathways avoid BECCS deployment completely through demand-side measures and greater reliance on AFOLU-related CDR measures (*medium confidence*). The use of bioenergy can be as high or even higher when BECCS is excluded compared to when it is included due to its potential for replacing fossil fuels across sectors (*high confidence*). (Figure SPM.3b) {2.3.3, 2.3.4, 2.4.2, 3.6.2, 4.3.1, 4.2.3, 4.3.2, 4.3.7, 4.4.3, Table 2.4}

C.3.3 Pathways that overshoot 1.5°C of global warming rely on CDR exceeding residual $CO_2$ emissions later in the century to return to below 1.5°C by 2100, with larger overshoots requiring greater amounts of CDR (Figure SPM.3b) (*high confidence*). Limitations on the speed, scale, and societal acceptability of CDR deployment hence determine the ability to return global warming to below 1.5°C following an overshoot. Carbon cycle and climate system understanding is still limited about the effectiveness of net negative emissions to reduce temperatures after they peak (*high confidence*). {2.2, 2.3.4, 2.3.5, 2.6, 4.3.7, 4.5.2, Table 4.11}

C.3.4 Most current and potential CDR measures could have significant impacts on land, energy, water or nutrients if deployed at large scale (*high confidence*). Afforestation and bioenergy may compete with other land uses and may have significant impacts on agricultural and food systems, biodiversity, and other ecosystem functions and services (*high confidence*). Effective governance is needed to limit such trade-offs and ensure permanence of carbon removal in terrestrial, geological and ocean reservoirs (*high confidence*). Feasibility and sustainability of CDR use could be enhanced by a portfolio of options deployed at substantial, but lesser scales, rather than a single option at very large scale (*high confidence*). (Figure SPM.3b) {2.3.4, 2.4.4, 2.5.3, 2.6, 3.6.2, 4.3.2, 4.3.7, 4.5.2, 5.4.1, 5.4.2; Cross-Chapter Boxes 7 and 8 in Chapter 3, Table 4.11, Table 5.3, Figure 5.3}

C.3.5 Some AFOLU-related CDR measures such as restoration of natural ecosystems and soil carbon sequestration could provide co-benefits such as improved biodiversity, soil quality, and local food security. If deployed at large scale, they would require governance systems enabling sustainable land management to conserve and protect land carbon stocks and other ecosystem functions and services (*medium confidence*). (Figure SPM.4) {2.3.3, 2.3.4, 2.4.2, 2.4.4, 3.6.2, 5.4.1, Cross-Chapter Boxes 3 in Chapter 1 and 7 in Chapter 3, 4.3.2, 4.3.7, 4.4.1, 4.5.2, Table 2.4}

# D. Strengthening the Global Response in the Context of Sustainable Development and Efforts to Eradicate Poverty

**D.1 Estimates of the global emissions outcome of current nationally stated mitigation ambitions as submitted under the Paris Agreement would lead to global greenhouse gas emissions[18] in 2030 of 52–58 $GtCO_2eq\ yr^{-1}$ (*medium confidence*). Pathways reflecting these ambitions would not limit global warming to 1.5°C, even if supplemented by very challenging increases in the scale and ambition of emissions reductions after 2030 (*high confidence*). Avoiding overshoot and reliance on future large-scale deployment of carbon dioxide removal (CDR) can only be achieved if global $CO_2$ emissions start to decline well before 2030 (*high confidence*). {1.2, 2.3, 3.3, 3.4, 4.2, 4.4, Cross-Chapter Box 11 in Chapter 4}**

D.1.1 Pathways that limit global warming to 1.5°C with no or limited overshoot show clear emission reductions by 2030 (*high confidence*). All but one show a decline in global greenhouse gas emissions to below 35 $GtCO_2eq\ yr^{-1}$ in 2030, and half of available pathways fall within the 25–30 $GtCO_2eq\ yr^{-1}$ range (interquartile range), a 40–50% reduction from 2010 levels (*high confidence*). Pathways reflecting current nationally stated mitigation ambition until 2030 are broadly consistent with cost-effective pathways that result in a global warming of about 3°C by 2100, with warming continuing afterwards (*medium confidence*). {2.3.3, 2.3.5, Cross-Chapter Box 11 in Chapter 4, 5.5.3.2}

D.1.2 Overshoot trajectories result in higher impacts and associated challenges compared to pathways that limit global warming to 1.5°C with no or limited overshoot (*high confidence*). Reversing warming after an overshoot of 0.2°C or larger during this century would require upscaling and deployment of CDR at rates and volumes that might not be achievable given considerable implementation challenges (*medium confidence*). {1.3.3, 2.3.4, 2.3.5, 2.5.1, 3.3, 4.3.7, Cross-Chapter Box 8 in Chapter 3, Cross-Chapter Box 11 in Chapter 4}

D.1.3 The lower the emissions in 2030, the lower the challenge in limiting global warming to 1.5°C after 2030 with no or limited overshoot (*high confidence*). The challenges from delayed actions to reduce greenhouse gas emissions include the risk of cost escalation, lock-in in carbon-emitting infrastructure, stranded assets, and reduced flexibility in future response options in the medium to long term (*high confidence*). These may increase uneven distributional impacts between countries at different stages of development (*medium confidence*). {2.3.5, 4.4.5, 5.4.2}

**D.2 The avoided climate change impacts on sustainable development, eradication of poverty and reducing inequalities would be greater if global warming were limited to 1.5°C rather than 2°C, if mitigation and adaptation synergies are maximized while trade-offs are minimized (*high confidence*). {1.1, 1.4, 2.5, 3.3, 3.4, 5.2, Table 5.1}**

D.2.1 Climate change impacts and responses are closely linked to sustainable development which balances social well-being, economic prosperity and environmental protection. The United Nations Sustainable Development Goals (SDGs), adopted in 2015, provide an established framework for assessing the links between global warming of 1.5°C or 2°C and development goals that include poverty eradication, reducing inequalities, and climate action. (*high confidence*) {Cross-Chapter Box 4 in Chapter 1, 1.4, 5.1}

D.2.2 The consideration of ethics and equity can help address the uneven distribution of adverse impacts associated with 1.5°C and higher levels of global warming, as well as those from mitigation and adaptation, particularly for poor and disadvantaged populations, in all societies (*high confidence*). {1.1.1, 1.1.2, 1.4.3, 2.5.3, 3.4.10, 5.1, 5.2, 5.3. 5.4, Cross-Chapter Box 4 in Chapter 1, Cross-Chapter Boxes 6 and 8 in Chapter 3, and Cross-Chapter Box 12 in Chapter 5}

D.2.3 Mitigation and adaptation consistent with limiting global warming to 1.5°C are underpinned by enabling conditions, assessed in this Report across the geophysical, environmental-ecological, technological, economic, socio-cultural and institutional

18 GHG emissions have been aggregated with 100-year GWP values as introduced in the IPCC Second Assessment Report.

dimensions of feasibility. Strengthened multilevel governance, institutional capacity, policy instruments, technological innovation and transfer and mobilization of finance, and changes in human behaviour and lifestyles are enabling conditions that enhance the feasibility of mitigation and adaptation options for 1.5°C-consistent systems transitions. (*high confidence*) {1.4, Cross-Chapter Box 3 in Chapter 1, 2.5.1, 4.4, 4.5, 5.6}

## D.3 Adaptation options specific to national contexts, if carefully selected together with enabling conditions, will have benefits for sustainable development and poverty reduction with global warming of 1.5°C, although trade-offs are possible (*high confidence*). {1.4, 4.3, 4.5}

D.3.1 Adaptation options that reduce the vulnerability of human and natural systems have many synergies with sustainable development, if well managed, such as ensuring food and water security, reducing disaster risks, improving health conditions, maintaining ecosystem services and reducing poverty and inequality (*high confidence*). Increasing investment in physical and social infrastructure is a key enabling condition to enhance the resilience and the adaptive capacities of societies. These benefits can occur in most regions with adaptation to 1.5°C of global warming (*high confidence*). {1.4.3, 4.2.2, 4.3.1, 4.3.2, 4.3.3, 4.3.5, 4.4.1, 4.4.3, 4.5.3, 5.3.1, 5.3.2}

D.3.2 Adaptation to 1.5°C global warming can also result in trade-offs or maladaptations with adverse impacts for sustainable development. For example, if poorly designed or implemented, adaptation projects in a range of sectors can increase greenhouse gas emissions and water use, increase gender and social inequality, undermine health conditions, and encroach on natural ecosystems (*high confidence*). These trade-offs can be reduced by adaptations that include attention to poverty and sustainable development (*high confidence*). {4.3.2, 4.3.3, 4.5.4, 5.3.2; Cross-Chapter Boxes 6 and 7 in Chapter 3}

D.3.3 A mix of adaptation and mitigation options to limit global warming to 1.5°C, implemented in a participatory and integrated manner, can enable rapid, systemic transitions in urban and rural areas (*high confidence*). These are most effective when aligned with economic and sustainable development, and when local and regional governments and decision makers are supported by national governments (*medium confidence*). {4.3.2, 4.3.3, 4.4.1, 4.4.2}

D.3.4 Adaptation options that also mitigate emissions can provide synergies and cost savings in most sectors and system transitions, such as when land management reduces emissions and disaster risk, or when low-carbon buildings are also designed for efficient cooling. Trade-offs between mitigation and adaptation, when limiting global warming to 1.5°C, such as when bioenergy crops, reforestation or afforestation encroach on land needed for agricultural adaptation, can undermine food security, livelihoods, ecosystem functions and services and other aspects of sustainable development. (*high confidence*) {3.4.3, 4.3.2, 4.3.4, 4.4.1, 4.5.2, 4.5.3, 4.5.4}

## D.4 Mitigation options consistent with 1.5°C pathways are associated with multiple synergies and trade-offs across the Sustainable Development Goals (SDGs). While the total number of possible synergies exceeds the number of trade-offs, their net effect will depend on the pace and magnitude of changes, the composition of the mitigation portfolio and the management of the transition. (*high confidence*) (Figure SPM.4) {2.5, 4.5, 5.4}

D.4.1 1.5°C pathways have robust synergies particularly for the SDGs 3 (health), 7 (clean energy), 11 (cities and communities), 12 (responsible consumption and production) and 14 (oceans) (*very high confidence*). Some 1.5°C pathways show potential trade-offs with mitigation for SDGs 1 (poverty), 2 (hunger), 6 (water) and 7 (energy access), if not managed carefully (*high confidence*). (Figure SPM.4) {5.4.2; Figure 5.4, Cross-Chapter Boxes 7 and 8 in Chapter 3}

D.4.2 1.5°C pathways that include low energy demand (e.g., see P1 in Figure SPM.3a and SPM.3b), low material consumption, and low GHG-intensive food consumption have the most pronounced synergies and the lowest number of trade-offs with respect to sustainable development and the SDGs (*high confidence*). Such pathways would reduce dependence on CDR. In modelled pathways, sustainable development, eradicating poverty and reducing inequality can support limiting warming to 1.5°C (*high confidence*). (Figure SPM.3b, Figure SPM.4) {2.4.3, 2.5.1, 2.5.3, Figure 2.4, Figure 2.28, 5.4.1, 5.4.2, Figure 5.4}

# Indicative linkages between mitigation options and sustainable development using SDGs (The linkages do not show costs and benefits)

Mitigation options deployed in each sector can be associated with potential positive effects (synergies) or negative effects (trade-offs) with the Sustainable Development Goals (SDGs). The degree to which this potential is realized will depend on the selected portfolio of mitigation options, mitigation policy design, and local circumstances and context. Particularly in the energy-demand sector, the potential for synergies is larger than for trade-offs. The bars group individually assessed options by level of confidence and take into account the relative strength of the assessed mitigation-SDG connections.

**Length shows strength of connection**

The overall **size of the coloured bars** depict **the relative potential** for synergies and trade-offs between the sectoral mitigation options and the SDGs.

**Shades show level of confidence**


The shades depict **the level of confidence** of the assessed potential for **Trade-offs**/**Synergies**.

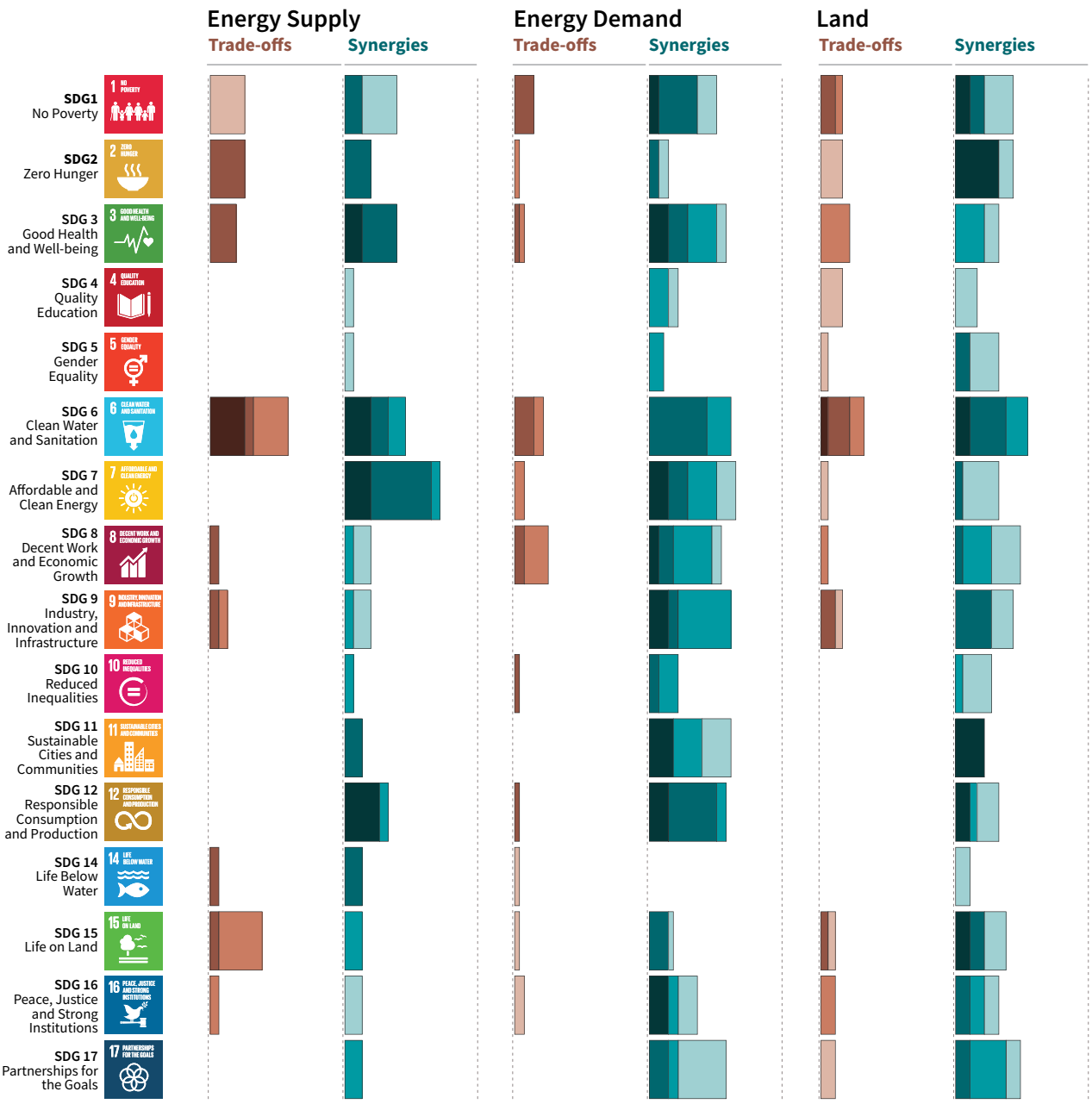

**Figure SPM.4 |** Potential synergies and trade-offs between the sectoral portfolio of climate change mitigation options and the Sustainable Development Goals (SDGs). The SDGs serve as an analytical framework for the assessment of the different sustainable development dimensions, which extend beyond the time frame of the 2030 SDG targets. The assessment is based on literature on mitigation options that are considered relevant for 1.5°C. The assessed strength of the SDG interactions is based on the qualitative and quantitative assessment of individual mitigation options listed in Table 5.2. For each mitigation option, the strength of the SDG-connection as well as the associated confidence of the underlying literature (shades of green and red) was assessed. The strength of positive connections (synergies) and negative connections (trade-offs) across all individual options within a sector (see Table 5.2) are aggregated into sectoral potentials for the whole mitigation portfolio. The (white) areas outside the bars, which indicate no interactions, have *low confidence* due to the uncertainty and limited number of studies exploring indirect effects. The strength of the connection considers only the effect of mitigation and does not include benefits of avoided impacts. SDG 13 (climate action) is not listed because mitigation is being considered in terms of interactions with SDGs and not vice versa. The bars denote the strength of the connection, and do not consider the strength of the impact on the SDGs. The energy demand sector comprises behavioural responses, fuel switching and efficiency options in the transport, industry and building sector as well as carbon capture options in the industry sector. Options assessed in the energy supply sector comprise biomass and non-biomass renewables, nuclear, carbon capture and storage (CCS) with bioenergy, and CCS with fossil fuels. Options in the land sector comprise agricultural and forest options, sustainable diets and reduced food waste, soil sequestration, livestock and manure management, reduced deforestation, afforestation and reforestation, and responsible sourcing. In addition to this figure, options in the ocean sector are discussed in the underlying report. {5.4, Table 5.2, Figure 5.2}

Information about the net impacts of mitigation on sustainable development in 1.5°C pathways is available only for a limited number of SDGs and mitigation options. Only a limited number of studies have assessed the benefits of avoided climate change impacts of 1.5°C pathways for the SDGs, and the co-effects of adaptation for mitigation and the SDGs. The assessment of the indicative mitigation potentials in Figure SPM.4 is a step further from AR5 towards a more comprehensive and integrated assessment in the future.

D.4.3 1.5°C and 2°C modelled pathways often rely on the deployment of large-scale land-related measures like afforestation and bioenergy supply, which, if poorly managed, can compete with food production and hence raise food security concerns (*high confidence*). The impacts of carbon dioxide removal (CDR) options on SDGs depend on the type of options and the scale of deployment (*high confidence*). If poorly implemented, CDR options such as BECCS and AFOLU options would lead to trade-offs. Context-relevant design and implementation requires considering people's needs, biodiversity, and other sustainable development dimensions (*very high confidence*). (Figure SPM.4) {5.4.1.3, Cross-Chapter Box 7 in Chapter 3}

D.4.4 Mitigation consistent with 1.5°C pathways creates risks for sustainable development in regions with high dependency on fossil fuels for revenue and employment generation (*high confidence*). Policies that promote diversification of the economy and the energy sector can address the associated challenges (*high confidence*). {5.4.1.2, Box 5.2}

D.4.5 Redistributive policies across sectors and populations that shield the poor and vulnerable can resolve trade-offs for a range of SDGs, particularly hunger, poverty and energy access. Investment needs for such complementary policies are only a small fraction of the overall mitigation investments in 1.5°C pathways. (*high confidence*) {2.4.3, 5.4.2, Figure 5.5}

## D.5 Limiting the risks from global warming of 1.5°C in the context of sustainable development and poverty eradication implies system transitions that can be enabled by an increase of adaptation and mitigation investments, policy instruments, the acceleration of technological innovation and behaviour changes (*high confidence*). {2.3, 2.4, 2.5, 3.2, 4.2, 4.4, 4.5, 5.2, 5.5, 5.6}

D.5.1 Directing finance towards investment in infrastructure for mitigation and adaptation could provide additional resources. This could involve the mobilization of private funds by institutional investors, asset managers and development or investment banks, as well as the provision of public funds. Government policies that lower the risk of low-emission and adaptation investments can facilitate the mobilization of private funds and enhance the effectiveness of other public policies. Studies indicate a number of challenges, including access to finance and mobilization of funds. (*high confidence*) {2.5.1, 2.5.2, 4.4.5}

D.5.2 Adaptation finance consistent with global warming of 1.5°C is difficult to quantify and compare with 2°C. Knowledge gaps include insufficient data to calculate specific climate resilience-enhancing investments from the provision of currently underinvested basic infrastructure. Estimates of the costs of adaptation might be lower at global warming of 1.5°C than for 2°C. Adaptation needs have typically been supported by public sector sources such as national and subnational government budgets, and in developing countries together with support from development assistance, multilateral development banks, and United Nations Framework Convention on Climate Change channels (*medium confidence*). More recently there is a

growing understanding of the scale and increase in non-governmental organizations and private funding in some regions (*medium confidence*). Barriers include the scale of adaptation financing, limited capacity and access to adaptation finance (*medium confidence*). {4.4.5, 4.6}

D.5.3 Global model pathways limiting global warming to 1.5°C are projected to involve the annual average investment needs in the energy system of around 2.4 trillion USD2010 between 2016 and 2035, representing about 2.5% of the world GDP (*medium confidence*). {4.4.5, Box 4.8}

D.5.4 Policy tools can help mobilize incremental resources, including through shifting global investments and savings and through market and non-market based instruments as well as accompanying measures to secure the equity of the transition, acknowledging the challenges related with implementation, including those of energy costs, depreciation of assets and impacts on international competition, and utilizing the opportunities to maximize co-benefits (*high confidence*). {1.3.3, 2.3.4, 2.3.5, 2.5.1, 2.5.2, Cross-Chapter Box 8 in Chapter 3, Cross-Chapter Box 11 in Chapter 4, 4.4.5, 5.5.2}

D.5.5 The systems transitions consistent with adapting to and limiting global warming to 1.5°C include the widespread adoption of new and possibly disruptive technologies and practices and enhanced climate-driven innovation. These imply enhanced technological innovation capabilities, including in industry and finance. Both national innovation policies and international cooperation can contribute to the development, commercialization and widespread adoption of mitigation and adaptation technologies. Innovation policies may be more effective when they combine public support for research and development with policy mixes that provide incentives for technology diffusion. (*high confidence*) {4.4.4, 4.4.5}.

D.5.6 Education, information, and community approaches, including those that are informed by indigenous knowledge and local knowledge, can accelerate the wide-scale behaviour changes consistent with adapting to and limiting global warming to 1.5°C. These approaches are more effective when combined with other policies and tailored to the motivations, capabilities and resources of specific actors and contexts (*high confidence*). Public acceptability can enable or inhibit the implementation of policies and measures to limit global warming to 1.5°C and to adapt to the consequences. Public acceptability depends on the individual's evaluation of expected policy consequences, the perceived fairness of the distribution of these consequences, and perceived fairness of decision procedures (*high confidence*). {1.1, 1.5, 4.3.5, 4.4.1, 4.4.3, Box 4.3, 5.5.3, 5.6.5}

### D.6 Sustainable development supports, and often enables, the fundamental societal and systems transitions and transformations that help limit global warming to 1.5°C. Such changes facilitate the pursuit of climate-resilient development pathways that achieve ambitious mitigation and adaptation in conjunction with poverty eradication and efforts to reduce inequalities (*high confidence*). {Box 1.1, 1.4.3, Figure 5.1, 5.5.3, Box 5.3}

D.6.1 Social justice and equity are core aspects of climate-resilient development pathways that aim to limit global warming to 1.5°C as they address challenges and inevitable trade-offs, widen opportunities, and ensure that options, visions, and values are deliberated, between and within countries and communities, without making the poor and disadvantaged worse off (*high confidence*). {5.5.2, 5.5.3, Box 5.3, Figure 5.1, Figure 5.6, Cross-Chapter Boxes 12 and 13 in Chapter 5}

D.6.2 The potential for climate-resilient development pathways differs between and within regions and nations, due to different development contexts and systemic vulnerabilities (*very high confidence*). Efforts along such pathways to date have been limited (*medium confidence*) and enhanced efforts would involve strengthened and timely action from all countries and non-state actors (*high confidence*). {5.5.1, 5.5.3, Figure 5.1}

D.6.3 Pathways that are consistent with sustainable development show fewer mitigation and adaptation challenges and are associated with lower mitigation costs. The large majority of modelling studies could not construct pathways characterized by lack of international cooperation, inequality and poverty that were able to limit global warming to 1.5°C. (*high confidence*) {2.3.1, 2.5.1, 2.5.3, 5.5.2}

**D.7 Strengthening the capacities for climate action of national and sub-national authorities, civil society, the private sector, indigenous peoples and local communities can support the implementation of ambitious actions implied by limiting global warming to 1.5°C (*high confidence*). International cooperation can provide an enabling environment for this to be achieved in all countries and for all people, in the context of sustainable development. International cooperation is a critical enabler for developing countries and vulnerable regions (*high confidence*). {1.4, 2.3, 2.5, 4.2, 4.4, 4.5, 5.3, 5.4, 5.5, 5.6, 5, Box 4.1, Box 4.2, Box 4.7, Box 5.3, Cross-Chapter Box 9 in Chapter 4, Cross-Chapter Box 13 in Chapter 5}**

D.7.1 Partnerships involving non-state public and private actors, institutional investors, the banking system, civil society and scientific institutions would facilitate actions and responses consistent with limiting global warming to 1.5°C (*very high confidence*). {1.4, 4.4.1, 4.2.2, 4.4.3, 4.4.5, 4.5.3, 5.4.1, 5.6.2, Box 5.3}.

D.7.2 Cooperation on strengthened accountable multilevel governance that includes non-state actors such as industry, civil society and scientific institutions, coordinated sectoral and cross-sectoral policies at various governance levels, gender-sensitive policies, finance including innovative financing, and cooperation on technology development and transfer can ensure participation, transparency, capacity building and learning among different players (*high confidence*). {2.5.1, 2.5.2, 4.2.2, 4.4.1, 4.4.2, 4.4.3, 4.4.4, 4.4.5, 4.5.3, Cross-Chapter Box 9 in Chapter 4, 5.3.1, 5.5.3, Cross-Chapter Box 13 in Chapter 5, 5.6.1, 5.6.3}

D.7.3 International cooperation is a critical enabler for developing countries and vulnerable regions to strengthen their action for the implementation of 1.5°C-consistent climate responses, including through enhancing access to finance and technology and enhancing domestic capacities, taking into account national and local circumstances and needs (*high confidence*). {2.3.1, 2.5.1, 4.4.1, 4.4.2, 4.4.4, 4.4.5, 5.4.1 5.5.3, 5.6.1, Box 4.1, Box 4.2, Box 4.7}.

D.7.4 Collective efforts at all levels, in ways that reflect different circumstances and capabilities, in the pursuit of limiting global warming to 1.5°C, taking into account equity as well as effectiveness, can facilitate strengthening the global response to climate change, achieving sustainable development and eradicating poverty (*high confidence*). {1.4.2, 2.3.1, 2.5.1, 2.5.2, 2.5.3, 4.2.2, 4.4.1, 4.4.2, 4.4.3, 4.4.4, 4.4.5, 4.5.3, 5.3.1, 5.4.1, 5.5.3, 5.6.1, 5.6.2, 5.6.3}

## Box SPM.1: Core Concepts Central to this Special Report

**Global mean surface temperature (GMST):** Estimated global average of near-surface air temperatures over land and sea ice, and sea surface temperatures over ice-free ocean regions, with changes normally expressed as departures from a value over a specified reference period. When estimating changes in GMST, near-surface air temperature over both land and oceans are also used.[19] {1.2.1.1}

**Pre-industrial:** The multi-century period prior to the onset of large-scale industrial activity around 1750. The reference period 1850–1900 is used to approximate pre-industrial GMST. {1.2.1.2}

**Global warming:** The estimated increase in GMST averaged over a 30-year period, or the 30-year period centred on a particular year or decade, expressed relative to pre-industrial levels unless otherwise specified. For 30-year periods that span past and future years, the current multi-decadal warming trend is assumed to continue. {1.2.1}

**Net zero $CO_2$ emissions:** Net zero carbon dioxide ($CO_2$) emissions are achieved when anthropogenic $CO_2$ emissions are balanced globally by anthropogenic $CO_2$ removals over a specified period.

**Carbon dioxide removal (CDR):** Anthropogenic activities removing $CO_2$ from the atmosphere and durably storing it in geological, terrestrial, or ocean reservoirs, or in products. It includes existing and potential anthropogenic enhancement of biological or geochemical sinks and direct air capture and storage, but excludes natural $CO_2$ uptake not directly caused by human activities.

**Total carbon budget:** Estimated cumulative net global anthropogenic $CO_2$ emissions from the pre-industrial period to the time that anthropogenic $CO_2$ emissions reach net zero that would result, at some probability, in limiting global warming to a given level, accounting for the impact of other anthropogenic emissions. {2.2.2}

**Remaining carbon budget:** Estimated cumulative net global anthropogenic $CO_2$ emissions from a given start date to the time that anthropogenic $CO_2$ emissions reach net zero that would result, at some probability, in limiting global warming to a given level, accounting for the impact of other anthropogenic emissions. {2.2.2}

**Temperature overshoot:** The temporary exceedance of a specified level of global warming.

**Emission pathways:** In this Summary for Policymakers, the modelled trajectories of global anthropogenic emissions over the 21st century are termed emission pathways. Emission pathways are classified by their temperature trajectory over the 21st century: pathways giving at least 50% probability based on current knowledge of limiting global warming to below 1.5°C are classified as 'no overshoot'; those limiting warming to below 1.6°C and returning to 1.5°C by 2100 are classified as '1.5°C limited-overshoot'; while those exceeding 1.6°C but still returning to 1.5°C by 2100 are classified as 'higher-overshoot'.

**Impacts:** Effects of climate change on human and natural systems. Impacts can have beneficial or adverse outcomes for livelihoods, health and well-being, ecosystems and species, services, infrastructure, and economic, social and cultural assets.

**Risk:** The potential for adverse consequences from a climate-related hazard for human and natural systems, resulting from the interactions between the hazard and the vulnerability and exposure of the affected system. Risk integrates the likelihood of exposure to a hazard and the magnitude of its impact. Risk also can describe the potential for adverse consequences of adaptation or mitigation responses to climate change.

**Climate-resilient development pathways (CRDPs):** Trajectories that strengthen sustainable development at multiple scales and efforts to eradicate poverty through equitable societal and systems transitions and transformations while reducing the threat of climate change through ambitious mitigation, adaptation and climate resilience.

19 Past IPCC reports, reflecting the literature, have used a variety of approximately equivalent metrics of GMST change.

PERSPECTIVE

# Trajectories of the Earth System in the Anthropocene

Will Steffen[a,b,1], Johan Rockström[a], Katherine Richardson[c], Timothy M. Lenton[d], Carl Folke[a,e], Diana Liverman[f], Colin P. Summerhayes[g], Anthony D. Barnosky[h], Sarah E. Cornell[a], Michel Crucifix[i,j], Jonathan F. Donges[a,k], Ingo Fetzer[a], Steven J. Lade[a,b], Marten Scheffer[l], Ricarda Winkelmann[k,m], and Hans Joachim Schellnhuber[a,k,m,1]

Edited by William C. Clark, Harvard University, Cambridge, MA, and approved July 6, 2018 (received for review June 19, 2018)

**We explore the risk that self-reinforcing feedbacks could push the Earth System toward a planetary threshold that, if crossed, could prevent stabilization of the climate at intermediate temperature rises and cause continued warming on a "Hothouse Earth" pathway even as human emissions are reduced. Crossing the threshold would lead to a much higher global average temperature than any interglacial in the past 1.2 million years and to sea levels significantly higher than at any time in the Holocene. We examine the evidence that such a threshold might exist and where it might be. If the threshold is crossed, the resulting trajectory would likely cause serious disruptions to ecosystems, society, and economies. Collective human action is required to steer the Earth System away from a potential threshold and stabilize it in a habitable interglacial-like state. Such action entails stewardship of the entire Earth System—biosphere, climate, and societies—and could include decarbonization of the global economy, enhancement of biosphere carbon sinks, behavioral changes, technological innovations, new governance arrangements, and transformed social values.**

Earth System trajectories | climate change | Anthropocene | biosphere feedbacks | tipping elements

The Anthropocene is a proposed new geological epoch (1) based on the observation that human impacts on essential planetary processes have become so profound (2) that they have driven the Earth out of the Holocene epoch in which agriculture, sedentary communities, and eventually, socially and technologically complex human societies developed. The formalization of the Anthropocene as a new geological epoch is being considered by the stratigraphic community (3), but regardless of the outcome of that process, it is becoming apparent that Anthropocene conditions transgress Holocene conditions in several respects (2). The knowledge that human activity now rivals geological forces in influencing the trajectory of the Earth System has important implications for both Earth System science and societal decision making. While recognizing that different societies around the world have contributed differently and unequally to pressures on the Earth System and will have varied capabilities to alter future trajectories (4), the sum total of human impacts on the system needs to be taken into account for analyzing future trajectories of the Earth System.

Here, we explore potential future trajectories of the Earth System by addressing the following questions.

Is there a planetary threshold in the trajectory of the Earth System that, if crossed, could prevent stabilization in a range of intermediate temperature rises?

Given our understanding of geophysical and biosphere feedbacks intrinsic to the Earth System, where might such a threshold be?

[a]Stockholm Resilience Centre, Stockholm University, 10691 Stockholm, Sweden; [b]Fenner School of Environment and Society, The Australian National University, Canberra, ACT 2601, Australia; [c]Center for Macroecology, Evolution, and Climate, University of Copenhagen, Natural History Museum of Denmark, 2100 Copenhagen, Denmark; [d]Earth System Science Group, College of Life and Environmental Sciences, University of Exeter, EX4 4QE Exeter, United Kingdom; [e]The Beijer Institute of Ecological Economics, The Royal Swedish Academy of Science, SE-10405 Stockholm, Sweden; [f]School of Geography and Development, The University of Arizona, Tucson, AZ 85721; [g]Scott Polar Research Institute, Cambridge University, CB2 1ER Cambridge, United Kingdom; [h]Jasper Ridge Biological Preserve, Stanford University, Stanford, CA 94305; [i]Earth and Life Institute, Université catholique de Louvain, 1348 Louvain-la-Neuve, Belgium; [j]Belgian National Fund of Scientific Research, 1000 Brussels, Belgium; [k]Research Domain Earth System Analysis, Potsdam Institute for Climate Impact Research, 14473 Potsdam, Germany; [l]Department of Environmental Sciences, Wageningen University & Research, 6700AA Wageningen, The Netherlands; and [m]Department of Physics and Astronomy, University of Potsdam, 14469 Potsdam, Germany

Author contributions: W.S., J.R., K.R., T.M.L., C.F., D.L., C.P.S., A.D.B., S.E.C., M.C., J.F.D., I.F., S.J.L., M.S., R.W., and H.J.S. wrote the paper.

The authors declare no conflict of interest.

This article is a PNAS Direct Submission.



[1]To whom correspondence may be addressed. Email: will.steffen@anu.edu.au or john@pik-potsdam.de.

This article contains supporting information online at www.pnas.org/lookup/suppl/doi:10.1073/pnas.1810141115/-/DCSupplemental.

Published online August 6, 2018.

If a threshold is crossed, what are the implications, especially for the wellbeing of human societies?

What human actions could create a pathway that would steer the Earth System away from the potential threshold and toward the maintenance of interglacial-like conditions?

Addressing these questions requires a deep integration of knowledge from biogeophysical Earth System science with that from the social sciences and humanities on the development and functioning of human societies (5). Integrating the requisite knowledge can be difficult, especially in light of the formidable range of timescales involved. Increasingly, concepts from complex systems analysis provide a framework that unites the diverse fields of inquiry relevant to the Anthropocene (6). Earth System dynamics can be described, studied, and understood in terms of trajectories between alternate states separated by thresholds that are controlled by nonlinear processes, interactions, and feedbacks. Based on this framework, we argue that social and technological trends and decisions occurring over the next decade or two could significantly influence the trajectory of the Earth System for tens to hundreds of thousands of years and potentially lead to conditions that resemble planetary states that were last seen several millions of years ago, conditions that would be inhospitable to current human societies and to many other contemporary species.

## Risk of a Hothouse Earth Pathway

***Limit Cycles and Planetary Thresholds.*** The trajectory of the Earth System through the Late Quaternary, particularly the Holocene, provides the context for exploring the human-driven changes of the Anthropocene and the future trajectories of the system (*SI Appendix* has more detail). Fig. 1 shows a simplified representation of complex Earth System dynamics, where the physical climate system is subjected to the effects of slow changes in Earth's orbit and inclination. Over the Late Quaternary (past 1.2 million years), the system has remained bounded between glacial and interglacial extremes. Not every glacial–interglacial cycle of the past million years follows precisely the same trajectory (7), but the cycles follow the same overall pathway (a term that we use to refer to a family of broadly similar trajectories). The full glacial and interglacial states and the ca. 100,000-years oscillations between them in the Late Quaternary loosely constitute limit cycles (technically, the asymptotic dynamics of ice ages are best modeled as pullback attractors in a nonautonomous dynamical system). This limit cycle is shown in a schematic fashion in blue in Fig. 1, *Lower Left* using temperature and sea level as the axes. The Holocene is represented by the top of the limit cycle loop near the label A.

The current position of the Earth System in the Anthropocene is shown in Fig. 1, *Upper Right* by the small ball on the pathway that leads away from the glacial–interglacial limit cycle. In Fig. 2, a stability landscape, the current position of the Earth System is represented by the globe at the end of the solid arrow in the deepening Anthropocene basin of attraction.

The Anthropocene represents the beginning of a very rapid human-driven trajectory of the Earth System away from the glacial–interglacial limit cycle toward new, hotter climatic conditions and a profoundly different biosphere (2, 8, 9) (*SI Appendix*). The current position, at over 1 °C above a preindustrial baseline (10), is nearing the upper envelope of interglacial conditions over the past 1.2 million years (*SI Appendix*, Table S1). More importantly, the rapid trajectory of the climate system over the past half-century along with technological lock in and socioeconomic

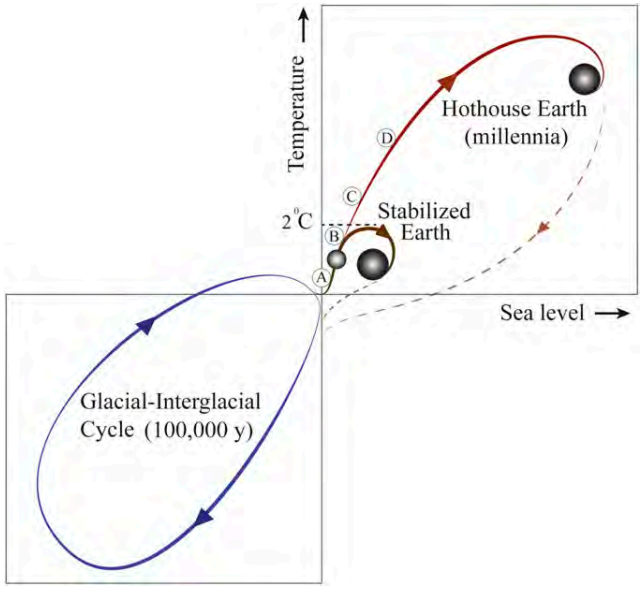


**Fig. 1. A schematic illustration of possible future pathways of the climate against the background of the typical glacial–interglacial cycles (*Lower Left*). The interglacial state of the Earth System is at the top of the glacial–interglacial cycle, while the glacial state is at the bottom. Sea level follows temperature change relatively slowly through thermal expansion and the melting of glaciers and ice caps. The horizontal line in the middle of the figure represents the preindustrial temperature level, and the current position of the Earth System is shown by the small sphere on the red line close to the divergence between the Stabilized Earth and Hothouse Earth pathways. The proposed planetary threshold at ∼2 °C above the preindustrial level is also shown. The letters along the Stabilized Earth/Hothouse Earth pathways represent four time periods in Earth's recent past that may give insights into positions along these pathways (*SI Appendix*): A, Mid-Holocene; B, Eemian; C, Mid-Pliocene; and D, Mid-Miocene. Their positions on the pathway are approximate only. Their temperature ranges relative to preindustrial are given in *SI Appendix*, Table S1.**

inertia in human systems commit the climate system to conditions beyond the envelope of past interglacial conditions. We, therefore, suggest that the Earth System may already have passed one "fork in the road" of potential pathways, a bifurcation (near A in Fig. 1) taking the Earth System out of the next glaciation cycle (11).

In the future, the Earth System could potentially follow many trajectories (12, 13), often represented by the large range of global temperature rises simulated by climate models (14). In most analyses, these trajectories are largely driven by the amount of greenhouse gases that human activities have already emitted and will continue to emit into the atmosphere over the rest of this century and beyond—with a presumed quasilinear relationship between cumulative carbon dioxide emissions and global temperature rise (14). However, here we suggest that biogeophysical feedback processes within the Earth System coupled with direct human degradation of the biosphere may play a more important role than normally assumed, limiting the range of potential future trajectories and potentially eliminating the possibility of the intermediate trajectories. We argue that there is a significant risk that these internal dynamics, especially strong nonlinearities in feedback processes, could become an important or perhaps, even dominant factor in steering the trajectory that the Earth System actually follows over coming centuries.

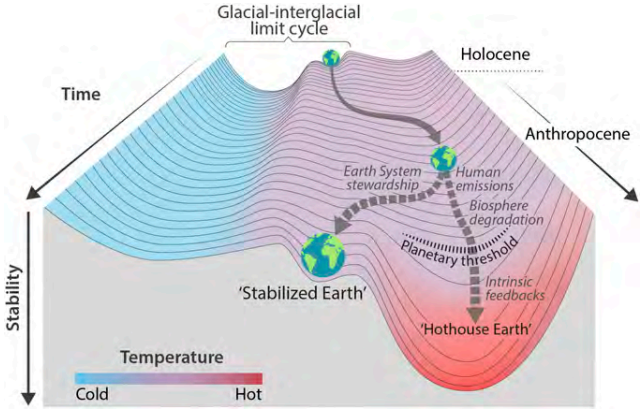


**Fig. 2. Stability landscape showing the pathway of the Earth System out of the Holocene and thus, out of the glacial–interglacial limit cycle to its present position in the hotter Anthropocene. The fork in the road in Fig. 1 is shown here as the two divergent pathways of the Earth System in the future (broken arrows). Currently, the Earth System is on a Hothouse Earth pathway driven by human emissions of greenhouse gases and biosphere degradation toward a planetary threshold at ~2 °C (horizontal broken line at 2 °C in Fig. 1), beyond which the system follows an essentially irreversible pathway driven by intrinsic biogeophysical feedbacks. The other pathway leads to Stabilized Earth, a pathway of Earth System stewardship guided by human-created feedbacks to a quasistable, human-maintained basin of attraction. "Stability" (vertical axis) is defined here as the inverse of the potential energy of the system. Systems in a highly stable state (deep valley) have low potential energy, and considerable energy is required to move them out of this stable state. Systems in an unstable state (top of a hill) have high potential energy, and they require only a little additional energy to push them off the hill and down toward a valley of lower potential energy.**

This risk is represented in Figs. 1 and 2 by a planetary threshold (horizontal broken line in Fig. 1 on the Hothouse Earth pathway around 2 °C above preindustrial temperature). Beyond this threshold, intrinsic biogeophysical feedbacks in the Earth System (*Biogeophysical Feedbacks*) could become the dominant processes controlling the system's trajectory. Precisely where a potential planetary threshold might be is uncertain (15, 16). We suggest 2 °C because of the risk that a 2 °C warming could activate important tipping elements (12, 17), raising the temperature further to activate other tipping elements in a domino-like cascade that could take the Earth System to even higher temperatures (*Tipping Cascades*). Such cascades comprise, in essence, the dynamical process that leads to thresholds in complex systems (section 4.2 in ref. 18).

This analysis implies that, even if the Paris Accord target of a 1.5 °C to 2.0 °C rise in temperature is met, we cannot exclude the risk that a cascade of feedbacks could push the Earth System irreversibly onto a "Hothouse Earth" pathway. The challenge that humanity faces is to create a "Stabilized Earth" pathway that steers the Earth System away from its current trajectory toward the threshold beyond which is Hothouse Earth (Fig. 2). The human-created Stabilized Earth pathway leads to a basin of attraction that is not likely to exist in the Earth System's stability landscape without human stewardship to create and maintain it. Creating such a pathway and basin of attraction requires a fundamental change in the role of humans on the planet. This stewardship role requires deliberate and sustained action to become an integral, adaptive part of Earth System dynamics, creating feedbacks that keep the system on a Stabilized Earth pathway (*Alternative Stabilized Earth Pathway*).

We now explore this critical question in more detail by considering the relevant biogeophysical feedbacks (*Biogeophysical Feedbacks*) and the risk of tipping cascades (*Tipping Cascades*).

***Biogeophysical Feedbacks.*** The trajectory of the Earth System is influenced by biogeophysical feedbacks within the system that can maintain it in a given state (negative feedbacks) and those that can amplify a perturbation and drive a transition to a different state (positive feedbacks). Some of the key negative feedbacks that could maintain the Earth System in Holocene-like conditions—notably, carbon uptake by land and ocean systems—are weakening relative to human forcing (19), increasing the risk that positive feedbacks could play an important role in determining the Earth System's trajectory. Table 1 summarizes carbon cycle feedbacks that could accelerate warming, while *SI Appendix*, Table S2 describes in detail a more complete set of biogeophysical feedbacks that can be triggered by forcing levels likely to be reached within the rest of the century.

Most of the feedbacks can show both continuous responses and tipping point behavior in which the feedback process becomes self-perpetuating after a critical threshold is crossed; subsystems exhibiting this behavior are often called "tipping elements" (17). The type of behavior—continuous response or tipping point/abrupt change—can depend on the magnitude or the rate of forcing, or both. Many feedbacks will show some gradual change before the tipping point is reached.

A few of the changes associated with the feedbacks are reversible on short timeframes of 50–100 years (e.g., change in Arctic sea ice extent with a warming or cooling of the climate; Antarctic sea ice may be less reversible because of heat accumulation in the Southern Ocean), but most changes are largely irreversible on timeframes that matter to contemporary societies (e.g., loss of permafrost carbon). A few of the feedbacks do not have apparent thresholds (e.g., change in the land and ocean physiological carbon sinks, such as increasing carbon uptake due

**Table 1. Carbon cycle feedbacks in the Earth System that could accelerate global warming**

| Feedback | Strength of feedback by 2100,* °C | Refs. (*SI Appendix*, Table S2 has more details) |
|---|---|---|
| Permafrost thawing | 0.09 (0.04–0.16) | 20–23 |
| Relative weakening of land and ocean physiological C sinks | 0.25 (0.13–0.37) | 24 |
| Increased bacterial respiration in the ocean | 0.02 | 25, 26 |
| Amazon forest dieback | 0.05 (0.03–0.11) | 27 |
| Boreal forest dieback | 0.06 (0.02–0.10) | 28 |
| Total | 0.47 (0.24–0.66) | |

The strength of the feedback is estimated at 2100 for an ~2 °C warming.
*The additional temperature rise (degrees Celsius) by 2100 arising from the feedback.

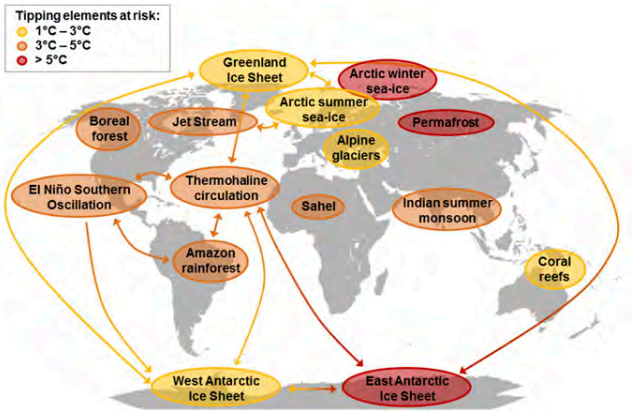


**Fig. 3. Global map of potential tipping cascades. The individual tipping elements are color- coded according to estimated thresholds in global average surface temperature (tipping points) (12, 34). Arrows show the potential interactions among the tipping elements based on expert elicitation that could generate cascades. Note that, although the risk for tipping (loss of) the East Antarctic Ice Sheet is proposed at >5 °C, some marine-based sectors in East Antarctica may be vulnerable at lower temperatures (35–38).**

to the $CO_2$ fertilization effect or decreasing uptake due to a decrease in rainfall). For some of the tipping elements, crossing the tipping point could trigger an abrupt, nonlinear response (e.g., conversion of large areas of the Amazon rainforest to a savanna or seasonally dry forest), while for others, crossing the tipping point would lead to a more gradual but self-perpetuating response (large-scale loss of permafrost). There could also be considerable lags after the crossing of a threshold, particularly for those tipping elements that involve the melting of large masses of ice. However, in some cases, ice loss can be very rapid when occurring as massive iceberg outbreaks (e.g., Heinrich Events).

For some feedback processes, the magnitude—and even the direction—depend on the rate of climate change. If the rate of climate change is small, the shift in biomes can track the change in temperature/moisture, and the biomes may shift gradually, potentially taking up carbon from the atmosphere as the climate warms and atmospheric $CO_2$ concentration increases. However, if the rate of climate change is too large or too fast, a tipping point can be crossed, and a rapid biome shift may occur via extensive disturbances (e.g., wildfires, insect attacks, droughts) that can abruptly remove an existing biome. In some terrestrial cases, such as widespread wildfires, there could be a pulse of carbon to the atmosphere, which if large enough, could influence the trajectory of the Earth System (29).

Varying response rates to a changing climate could lead to complex biosphere dynamics with implications for feedback processes. For example, delays in permafrost thawing would most likely delay the projected northward migration of boreal forests (30), while warming of the southern areas of these forests could result in their conversion to steppe grasslands of significantly lower carbon storage capacity. The overall result would be a positive feedback to the climate system.

The so-called "greening" of the planet, caused by enhanced plant growth due to increasing atmospheric $CO_2$ concentration (31), has increased the land carbon sink in recent decades (32). However, increasing atmospheric $CO_2$ raises temperature, and hotter leaves photosynthesize less well. Other feedbacks are also involved—for instance, warming the soil increases microbial respiration, releasing $CO_2$ back into the atmosphere.

Our analysis focuses on the strength of the feedback between now and 2100. However, several of the feedbacks that show negligible or very small magnitude by 2100 could nevertheless be triggered well before then, and they could eventually generate significant feedback strength over longer timeframes—centuries and even millennia—and thus, influence the long-term trajectory of the Earth System. These feedback processes include permafrost thawing, decomposition of ocean methane hydrates, increased marine bacterial respiration, and loss of polar ice sheets accompanied by a rise in sea levels and potential amplification of temperature rise through changes in ocean circulation (33).

***Tipping Cascades.*** Fig. 3 shows a global map of some potential tipping cascades. The tipping elements fall into three clusters based on their estimated threshold temperature (12, 17, 39). Cascades could be formed when a rise in global temperature reaches the level of the lower-temperature cluster, activating tipping elements, such as loss of the Greenland Ice Sheet or Arctic sea ice. These tipping elements, along with some of the non-tipping element feedbacks (e.g., gradual weakening of land and ocean physiological carbon sinks), could push the global average temperature even higher, inducing tipping in mid- and higher-temperature clusters. For example, tipping (loss) of the Greenland Ice Sheet could trigger a critical transition in the Atlantic Meridional Ocean Circulation (AMOC), which could together, by causing sea-level rise and Southern Ocean heat accumulation, accelerate ice loss from the East Antarctic Ice Sheet (32, 40) on timescales of centuries (41).

Observations of past behavior support an important contribution of changes in ocean circulation to such feedback cascades. During previous glaciations, the climate system flickered between two states that seem to reflect changes in convective activity in the Nordic seas and changes in the activity of the AMOC. These variations caused typical temperature response patterns called the "bipolar seesaw" (42–44). During extremely cold conditions in the north, heat accumulated in the Southern Ocean, and Antarctica warmed. Eventually, the heat made its way north and generated subsurface warming that may have been instrumental in destabilizing the edges of the Northern Hemisphere ice sheets (45).

If Greenland and the West Antarctic Ice Sheet melt in the future, the freshening and cooling of nearby surface waters will have significant effects on the ocean circulation. While the probability of significant circulation changes is difficult to quantify, climate model simulations suggest that freshwater inputs compatible with current rates of Greenland melting are sufficient to have measurable effects on ocean temperature and circulation (46, 47). Sustained warming of the northern high latitudes as a result of this process could accelerate feedbacks or activate tipping elements in that region, such as permafrost degradation, loss of Arctic sea ice, and boreal forest dieback.

While this may seem to be an extreme scenario, it illustrates that a warming into the range of even the lower-temperature cluster (i.e., the Paris targets) could lead to tipping in the mid- and higher-temperature clusters via cascade effects. Based on this analysis of tipping cascades and taking a risk-averse approach, we suggest that a potential planetary threshold could occur at a temperature rise as low as ~2.0 °C above preindustrial (Fig. 1).

## Alternative Stabilized Earth Pathway

If the world's societies want to avoid crossing a potential threshold that locks the Earth System into the Hothouse Earth pathway, then it is critical that they make deliberate decisions to avoid this risk

and maintain the Earth System in Holocene-like conditions. This human-created pathway is represented in Figs. 1 and 2 by what we call Stabilized Earth (small loop at the bottom of Fig. 1, *Upper Right*), in which the Earth System is maintained in a state with a temperature rise no greater than 2 °C above preindustrial (a "super-Holocene" state) (11). Stabilized Earth would require deep cuts in greenhouse gas emissions, protection and enhancement of biosphere carbon sinks, efforts to remove $CO_2$ from the atmosphere, possibly solar radiation management, and adaptation to unavoidable impacts of the warming already occurring (48). The short broken red line beyond Stabilized Earth in Fig. 1, *Upper Right* represents a potential return to interglacial-like conditions in the longer term.

In essence, the Stabilized Earth pathway could be conceptualized as a regime of the Earth System in which humanity plays an active planetary stewardship role in maintaining a state intermediate between the glacial–interglacial limit cycle of the Late Quaternary and a Hothouse Earth (Fig. 2). We emphasize that Stabilized Earth is not an intrinsic state of the Earth System but rather, one in which humanity commits to a pathway of ongoing management of its relationship with the rest of the Earth System.

A critical issue is that, if a planetary threshold is crossed toward the Hothouse Earth pathway, accessing the Stabilized Earth pathway would become very difficult no matter what actions human societies might take. Beyond the threshold, positive (reinforcing) feedbacks within the Earth System—outside of human influence or control—could become the dominant driver of the system's pathway, as individual tipping elements create linked cascades through time and with rising temperature (Fig. 3). In other words, after the Earth System is committed to the Hothouse Earth pathway, the alternative Stabilized Earth pathway would very likely become inaccessible as illustrated in Fig. 2.

***What Is at Stake?*** Hothouse Earth is likely to be uncontrollable and dangerous to many, particularly if we transition into it in only a century or two, and it poses severe risks for health, economies, political stability (12, 39, 49, 50) (especially for the most climate vulnerable), and ultimately, the habitability of the planet for humans.

Insights into the risks posed by the rapid climatic changes emerging in the Anthropocene can be obtained not only from contemporary observations (51–55) but also, from interactions in the past between human societies and regional and seasonal hydroclimate variability. This variability was often much more pronounced than global, longer-term Holocene variability (*SI Appendix*). Agricultural production and water supplies are especially vulnerable to changes in the hydroclimate, leading to hot/dry or cool/wet extremes. Societal declines, collapses, migrations/resettlements, reorganizations, and cultural changes were often associated with severe regional droughts and with the global megadrought at 4.2–3.9 thousand years before present, all occurring within the relative stability of the narrow global Holocene temperature range of approximately ±1 °C (56).

*SI Appendix*, Table S4 summarizes biomes and regional biosphere–physical climate subsystems critical for human wellbeing and the resultant risks if the Earth System follows a Hothouse Earth pathway. While most of these biomes or regional systems may be retained in a Stabilized Earth pathway, most or all of them would likely be substantially changed or degraded in a Hothouse Earth pathway, with serious challenges for the viability of human societies.

For example, agricultural systems are particularly vulnerable, because they are spatially organized around the relatively stable Holocene patterns of terrestrial primary productivity, which depend on a well-established and predictable spatial distribution of temperature and precipitation in relation to the location of fertile soils as well as on a particular atmospheric $CO_2$ concentration. Current understanding suggests that, while a Stabilized Earth pathway could result in an approximate balance between increases and decreases in regional production as human systems adapt, a Hothouse Earth trajectory will likely exceed the limits of adaptation and result in a substantial overall decrease in agricultural production, increased prices, and even more disparity between wealthy and poor countries (57).

The world's coastal zones, especially low-lying deltas and the adjacent coastal seas and ecosystems, are particularly important for human wellbeing. These areas are home to much of the world's population, most of the emerging megacities, and a significant amount of infrastructure vital for both national economies and international trade. A Hothouse Earth trajectory would almost certainly flood deltaic environments, increase the risk of damage from coastal storms, and eliminate coral reefs (and all of the benefits that they provide for societies) by the end of this century or earlier (58).

***Human Feedbacks in the Earth System.*** In the dominant climate change narrative, humans are an external force driving change to the Earth System in a largely linear, deterministic way; the higher the forcing in terms of anthropogenic greenhouse gas emissions, the higher the global average temperature. However, our analysis argues that human societies and our activities need to be recast as an integral, interacting component of a complex, adaptive Earth System. This framing puts the focus not only on human system dynamics that reduce greenhouse gas emissions but also, on those that create or enhance negative feedbacks that reduce the risk that the Earth System will cross a planetary threshold and lock into a Hothouse Earth pathway.

Humanity's challenge then is to influence the dynamical properties of the Earth System in such a way that the emerging unstable conditions in the zone between the Holocene and a very hot state become a de facto stable intermediate state (Stabilized Earth) (Fig. 2). This requires that humans take deliberate, integral, and adaptive steps to reduce dangerous impacts on the Earth System, effectively monitoring and changing behavior to form feedback loops that stabilize this intermediate state.

There is much uncertainty and debate about how this can be done—technically, ethically, equitably, and economically—and there is no doubt that the normative, policy, and institutional aspects are highly challenging. However, societies could take a wide range of actions that constitute negative feedbacks, summarized in *SI Appendix*, Table S5, to steer the Earth System toward Stabilized Earth. Some of these actions are already altering emission trajectories. The negative feedback actions fall into three broad categories: (*i*) reducing greenhouse gas emissions, (*ii*) enhancing or creating carbon sinks (e.g., protecting and enhancing biosphere carbon sinks and creating new types of sinks) (59), and (*iii*) modifying Earth's energy balance (for example, via solar radiation management, although that particular feedback entails very large risks of destabilization or degradation of several key processes in the Earth System) (60, 61). While reducing emissions is a priority, much more could be done to reduce direct human pressures on critical biomes that contribute to the regulation of the state of the Earth System through carbon sinks and moisture feedbacks, such as the Amazon and boreal forests (Table 1), and to build much more effective stewardship of the marine and terrestrial biospheres in general.

The present dominant socioeconomic system, however, is based on high-carbon economic growth and exploitative resource use (9). Attempts to modify this system have met with some

success locally but little success globally in reducing greenhouse gas emissions or building more effective stewardship of the biosphere. Incremental linear changes to the present socioeconomic system are not enough to stabilize the Earth System. Widespread, rapid, and fundamental transformations will likely be required to reduce the risk of crossing the threshold and locking in the Hothouse Earth pathway; these include changes in behavior, technology and innovation, governance, and values (48, 62, 63).

International efforts to reduce human impacts on the Earth System while improving wellbeing include the United Nations Sustainable Development Goals and the commitment in the Paris agreement to keep warming below 2 °C. These international governance initiatives are matched by carbon reduction commitments by countries, cities, businesses, and individuals (64–66) , but as yet, these are not enough to meet the Paris target. Enhanced ambition will need new collectively shared values, principles, and frameworks as well as education to support such changes (67, 68). In essence, effective Earth System stewardship is an essential precondition for the prosperous development of human societies in a Stabilized Earth pathway (69, 70).

In addition to institutional and social innovation at the global governance level, changes in demographics, consumption, behavior, attitudes, education, institutions, and socially embedded technologies are all important to maximize the chances of achieving a Stabilized Earth pathway (71). Many of the needed shifts may take decades to have a globally aggregated impact (*SI Appendix*, Table S5), but there are indications that society may be reaching some important societal tipping points. For example, there has been relatively rapid progress toward slowing or reversing population growth through declining fertility resulting from the empowerment of women, access to birth control technologies, expansion of educational opportunities, and rising income levels (72, 73). These demographic changes must be complemented by sustainable per capita consumption patterns, especially among the higher per capita consumers. Some changes in consumer behavior have been observed (74, 75), and opportunities for consequent major transitions in social norms over broad scales may arise (76). Technological innovation is contributing to more rapid decarbonization and the possibility for removing $CO_2$ from the atmosphere (48).

Ultimately, the transformations necessary to achieve the Stabilized Earth pathway require a fundamental reorientation and restructuring of national and international institutions toward more effective governance at the Earth System level (77), with a much stronger emphasis on planetary concerns in economic governance, global trade, investments and finance, and technological development (78).

***Building Resilience in a Rapidly Changing Earth System.*** Even if a Stabilized Earth pathway is achieved, humanity will face a turbulent road of rapid and profound changes and uncertainties on route to it—politically, socially, and environmentally—that challenge the resilience of human societies (79–82). Stabilized Earth will likely be warmer than any other time over the last 800,000 years at least (83) (that is, warmer than at any other time in which fully modern humans have existed).

In addition, the Stabilized Earth trajectory will almost surely be characterized by the activation of some tipping elements (*Tipping Cascades* and Fig. 3) and by nonlinear dynamics and abrupt shifts at the level of critical biomes that support humanity (*SI Appendix*, Table S4). Current rates of change of important features of the Earth System already match or exceed those of abrupt geophysical events in the past (*SI Appendix*). With these trends likely to continue for the next several decades at least, the contemporary way of guiding development founded on theories, tools, and beliefs of gradual or incremental change, with a focus on economy efficiency, will likely not be adequate to cope with this trajectory. Thus, in addition to adaptation, increasing resilience will become a key strategy for navigating the future.

Generic resilience-building strategies include developing insurance, buffers, redundancy, diversity, and other features of resilience that are critical for transforming human systems in the face of warming and possible surprise associated with tipping points (84). Features of such a strategy include (*i*) maintenance of diversity, modularity, and redundancy; (*ii*) management of connectivity, openness, slow variables, and feedbacks; (*iii*) understanding social–ecological systems as complex adaptive systems, especially at the level of the Earth System as a whole (85); (*iv*) encouraging learning and experimentation; and (*v*) broadening of participation and building of trust to promote polycentric governance systems (86, 87).

## Conclusions

Our systems approach, focusing on feedbacks, tipping points, and nonlinear dynamics, has addressed the four questions posed in the Introduction.

Our analysis suggests that the Earth System may be approaching a planetary threshold that could lock in a continuing rapid pathway toward much hotter conditions—Hothouse Earth. This pathway would be propelled by strong, intrinsic, biogeophysical feedbacks difficult to influence by human actions, a pathway that could not be reversed, steered, or substantially slowed.

Where such a threshold might be is uncertain, but it could be only decades ahead at a temperature rise of ∼2.0 °C above preindustrial, and thus, it could be within the range of the Paris Accord temperature targets.

The impacts of a Hothouse Earth pathway on human societies would likely be massive, sometimes abrupt, and undoubtedly disruptive.

Avoiding this threshold by creating a Stabilized Earth pathway can only be achieved and maintained by a coordinated, deliberate effort by human societies to manage our relationship with the rest of the Earth System, recognizing that humanity is an integral, interacting component of the system. Humanity is now facing the need for critical decisions and actions that could influence our future for centuries, if not millennia (88).

How credible is this analysis? There is significant evidence from a number of sources that the risk of a planetary threshold and thus, the need to create a divergent pathway should be taken seriously:

First, the complex system behavior of the Earth System in the Late Quaternary is well-documented and understood. The two bounding states of the system—glacial and interglacial—are reasonably well-defined, the ca. 100,000-years periodicity of the limit cycle is established, and internal (carbon cycle and ice albedo feedbacks) and external (changes in insolation caused by changes in Earth's orbital parameters) driving processes are generally well-known. Furthermore, we know with high confidence that the progressive disintegration of ice sheets and the transgression of other tipping elements are difficult to reverse after critical levels of warming are reached.

Second, insights from Earth's recent geological past (*SI Appendix*) suggest that conditions consistent with the Hothouse Earth pathway are accessible with levels of atmospheric $CO_2$ concentration and temperature rise either already realized or projected for this century (*SI Appendix*, Table S1).

Third, the tipping elements and feedback processes that operated over Quaternary glacial–interglacial cycles are the same as several of those proposed as critical for the future trajectory of the Earth System (*Biogeophysical Feedbacks*, *Tipping Cascades*, Fig. 3, Table 1, and *SI Appendix*, Table S2).

Fourth, contemporary observations (29, 38) (*SI Appendix*) of tipping element behavior at an observed temperature anomaly of about 1 °C above preindustrial suggest that some of these elements are vulnerable to tipping within just a 1 °C to 3 °C increase in global temperature, with many more of them vulnerable at higher temperatures (*Biogeophysical Feedbacks* and *Tipping Cascades*) (12, 17, 39). This suggests that the risk of tipping cascades could be significant at a 2 °C temperature rise and could increase sharply beyond that point. We argue that a planetary threshold in the Earth System could exist at a temperature rise as low as 2 °C above preindustrial.

The Stabilized Earth trajectory requires deliberate management of humanity's relationship with the rest of the Earth System if the world is to avoid crossing a planetary threshold. We suggest that a deep transformation based on a fundamental reorientation of human values, equity, behavior, institutions, economies, and technologies is required. Even so, the pathway toward Stabilized Earth will involve considerable changes to the structure and functioning of the Earth System, suggesting that resilience-building strategies be given much higher priority than at present in decision making. Some signs are emerging that societies are initiating some of the necessary transformations. However, these transformations are still in initial stages, and the social/political tipping points that definitively move the current trajectory away from Hothouse Earth have not yet been crossed, while the door to the Stabilized Earth pathway may be rapidly closing.

Our initial analysis here needs to be underpinned by more in-depth, quantitative Earth System analysis and modeling studies to address three critical questions. (*i*) Is humanity at risk for pushing the system across a planetary threshold and irreversibly down a Hothouse Earth pathway? (*ii*) What other pathways might be possible in the complex stability landscape of the Earth System, and what risks might they entail? (*iii*) What planetary stewardship strategies are required to maintain the Earth System in a manageable Stabilized Earth state?


## Acknowledgments

We thank the three reviewers for their comments on the first version of the manuscript and two of the reviewers for further comments on a revised version of the manuscript. These comments were very helpful in the revisions. We thank a member of the PNAS editorial board for a comprehensive and very helpful review. W.S. and C.P.S. are members of the Anthropocene Working Group. W.S., J.R., K.R., S.E.C., J.F.D., I.F., S.J.L., R.W. and H.J.S. are members of the Planetary Boundaries Research Network PB.net and the Earth League's EarthDoc Programme supported by the Stordalen Foundation. T.M.L. was supported by a Royal Society Wolfson Research Merit Award and the European Union Framework Programme 7 Project HELIX. C.F. was supported by the Erling–Persson Family Foundation. The participation of D.L. was supported by the Haury Program in Environment and Social Justice and National Science Foundation (USA) Decadal and Regional Climate Prediction using Earth System Models Grant 1243125. S.E.C. was supported in part by Swedish Research Council Formas Grant 2012-742. J.F.D. and R.W. were supported by Leibniz Association Project DOMINOES. S.J.L. receives funding from Formas Grant 2014-589. This paper is a contribution to European Research Council Advanced Grant 2016, Earth Resilience in the Anthropocene Project 743080.



1 Crutzen PJ (2002) Geology of mankind. *Nature* 415:23.
2 Steffen W, Broadgate W, Deutsch L, Gaffney O, Ludwig C (2015) The trajectory of the Anthropocene: The great acceleration. *Anthropocene Rev* 2:81–98.
3 Waters CN, et al. (2016) The Anthropocene is functionally and stratigraphically distinct from the Holocene. *Science* 351:aad2622.
4 Malm A, Hornborg A (2014) The geology of mankind? A critique of the Anthropocene narrative. *Anthropocene Rev* 1:62–69.
5 Donges JF, et al. (2017) Closing the loop: Reconnecting human dynamics to Earth System science. *Anthropocene Rev* 4:151–157.
6 Levin SA (2003) Complex adaptive systems: Exploring the known, the unknown and the unknowable. *Bull Am Math Soc* 40:3–20.
7 Past Interglacial Working Group of PAGES (2016) Interglacials of the last 800,000 years. *Rev Geophys* 54:162–219.
8 Williams M, et al. (2015) The Anthropocene biosphere. *Anthropocene Rev* 2:196–219.
9 McNeill JR, Engelke P (2016) *The Great Acceleration* (Harvard Univ Press, Cambridge, MA).
10 Hawkins E, et al. (2017) Estimating changes in global temperature since the pre-industrial period. *Bull Am Meteorol Soc* 98:1841–1856.
11 Ganopolski A, Winkelmann R, Schellnhuber HJ (2016) Critical insolation-$CO_2$ relation for diagnosing past and future glacial inception. *Nature* 529:200–203.
12 Schellnhuber HJ, Rahmstorf S, Winkelmann R (2016) Why the right climate target was agreed in Paris. *Nat Clim Change* 6:649–653.
13 Schellnhuber HJ (1999) 'Earth system' analysis and the second Copernican revolution. *Nature* 402(Suppl):C19–C23.
14 IPCC (2013) Summary for policymakers. *Climate Change 2013: The Physical Science Basis, Contribution of Working Group I to the Fifth Assessment Report of the Intergovernmental Panel on Climate Change*, eds Stocker TF, et al. (Cambridge Univ Press, Cambridge, UK), pp 3–29.
15 Drijfhout S, et al. (2015) Catalogue of abrupt shifts in Intergovernmental Panel on Climate Change climate models. *Proc Natl Acad Sci USA* 112:E5777–E5786.
16 Stocker TF, et al. (2013) Technical summary. *Climate Change 2013: The Physical Science Basis. Contribution of Working Group I to the Fifth Assessment Report of the Intergovernmental Panel on Climate Change*, eds Stocker TF, et al. (Cambridge Univ Press, Cambridge, UK).
17 Lenton TM, et al. (2008) Tipping elements in the Earth's climate system. *Proc Natl Acad Sci USA* 105:1786–1793.
18 Scheffer M (2009) *Critical Transitions in Nature and Society* (Princeton Univ Press, Princeton).
19 Raupach MR, et al. (2014) The declining uptake rate of atmospheric $CO_2$ by land and ocean sinks. *Biogeosciences* 11:3453–3475.
20 Schaefer K, Lantuit H, Romanovsky VE, Schuur EAG, Witt R (2014) The impact of the permafrost carbon feedback on global climate. *Environ Res Lett* 9:085003.
21 Schneider von Deimling T, et al. (2015) Observation-based modelling of permafrost carbon fluxes with accounting for deep carbon deposits and thermokarst activity. *Biogeosciences* 12:3469–3488.
22 Koven CD, et al. (2015) A simplified, data-constrained approach to estimate the permafrost carbon-climate feedback. *Philos Trans A Math Phys Eng Sci* 373:20140423.
23 Chadburn SE, et al. (2017) An observation-based constraint on permafrost loss as a function of global warming. *Nat Clim Change* 7:340–344.
24 Ciais P, et al. (2013) Carbon and other biogeochemical cycles. *Climate Change 2013: The Physical Science Basis, Contribution of Working Group I to the Fifth Assessment Report of the Intergovernmental Panel on Climate Change*, eds Stocker TF, et al. (Cambridge Univ Press, Cambridge, UK), pp 465–570.
25 Segschneider J, Bendtsen J (2013) Temperature-dependent remineralization in a warming ocean increases surface $pCO_2$ through changes in marine ecosystem composition. *Global Biogeochem Cycles* 27:1214–1225.
26 Bendtsen J, Hilligsøe KM, Hansen J, Richardson K (2015) Analysis of remineralisation, lability, temperature sensitivity and structural composition of organic matter from the upper ocean. *Prog Oceanogr* 130:125–145.
27 Jones C, Lowe J, Liddicoat S, Betts R (2009) Committed terrestrial ecosystem changes due to climate change. *Nat Geosci* 2:484–487.
28 Kurz WA, Apps MJ (1999) A 70-year retrospective analysis of carbon fluxes in the Canadian forest sector. *Ecol Appl* 9:526–547.
29 Lewis SL, Brando PM, Phillips OL, van der Heijden GMF, Nepstad D (2011) The 2010 Amazon drought. *Science* 331:554.
30 Herzschuh U, et al. (2016) Glacial legacies on interglacial vegetation at the Pliocene-Pleistocene transition in NE Asia. *Nature Commun* 7:11967.

31 Mao J, et al. (2016) Human-induced greening of the northern extratropical land surface. *Nat Clim Change* 6:959–963.
32 Keenan TF, et al. (2016) Recent pause in the growth rate of atmospheric $CO_2$ due to enhanced terrestrial carbon uptake. *Nature Commun* 7:13428, and erratum (2017) 8:16137.
33 Hansen J, et al. (2016) Ice melt, sea level rise and superstorms: Evidence from paleoclimatedata, climate modeling, and modern observations that 2 °C global warming could be dangerous. *Atmos Chem Phys* 16:3761–3812.
34 Kriegler E, Hall JW, Held H, Dawson R, Schellnhuber HJ (2009) Imprecise probability assessment of tipping points in the climate system. *Proc Natl Acad Sci USA* 106:5041–5046.
35 Pollard D, DeConto RM (2009) Modelling West Antarctic ice sheet growth and collapse through the past five million years. *Nature* 458:329–332.
36 Pollard D, DeConto RM, Alley RB (2015) Potential Antarctic Ice Sheet retreat driven by hydrofracturing and ice cliff failure. *Earth Planet Sci Lett* 412:112–121.
37 DeConto RM, Pollard D (2016) Contribution of Antarctica to past and future sea-level rise. *Nature* 531:591–597.
38 Rintoul SR, et al. (2016) Ocean heat drives rapid basal melt of the Totten Ice Shelf. *Sci Adv* 2:e1601610.
39 US Department of Defense (2015) National security implications of climate-related risks and a changing climate. Available at archive.defense.gov/pubs/150724-congressional-report-on-national-implications-of-climate-change.pdf?source=govdelivery. Accessed February 7, 2018.
40 Mengel M, Levermann A (2014) Ice plug prevents irreversible discharge from East Antarctica. *Nat Clim Change* 4:451–455.
41 Armour KC, et al. (2016) Southern Ocean warming delayed by circumpolar upwelling and equatorward transport. *Nat Geosci* 9:549–554.
42 Stocker TF, Johnsen SJ (2003) A minimum thermodynamic model for the bipolar seesaw. *Paleoceanography* 18:1087.
43 Rahmstorf S (2002) Ocean circulation and climate during the past 120,000 years. *Nature* 419:207–214.
44 Hemming SR (2004) Heinrich events: Massive late Pleistocene detritus layers of the North Atlantic and their global climate imprint. *Rev Geophys* 42:1–43.
45 Alvarez-Solas J, et al. (2010) Link between ocean temperature and iceberg discharge during Heinrich events. *Nat Geosci* 3:122–126.
46 Stouffer RJ, et al. (2006) Investigating the causes of the response of the thermohaline circulation to past and future climate changes. *J Clim* 19:1365–1387.
47 Swingedow D, et al. (2013) Decadal fingerprints of freshwater discharge around Greenland in a multi-model ensemble. *Clim Dyn* 41:695–720.
48 Rockström J, et al. (2017) A roadmap for rapid decarbonization. *Science* 355:1269–1271.
49 Schleussner C-F, Donges JF, Donner RV, Schellnhuber HJ (2016) Armed-conflict risks enhanced by climate-related disasters in ethnically fractionalized countries. *Proc Natl Acad Sci USA* 113:9216–9221.
50 McMichael AJ, et al., eds (2003) *Climate Change and Human Health: Risks and Responses* (WHO, Geneva).
51 Udmale PD, et al. (2015) How did the 2012 drought affect rural livelihoods in vulnerable areas? Empirical evidence from India. *Int J Disaster Risk Reduct* 13:454–469.
52 Maldonado JK, Shearer C, Bronen R, Peterson K, Lazrus H (2013) The impact of climate change on tribal communities in the US: Displacement, relocation, and human rights. *Clim Change* 120:601–614.
53 Warner K, Afifi T (2014) Where the rain falls: Evidence from 8 countries on how vulnerable households use migration to manage the risk of rainfall variability and food insecurity. *Clim Dev* 6:1–17.
54 Cheung WW, Watson R, Pauly D (2013) Signature of ocean warming in global fisheries catch. *Nature* 497:365–368.
55 Nakano K (2017) Screening of climatic impacts on a country's international supply chains: Japan as a case study. *Mitig Adapt Strategies Glob Change* 22:651–667.
56 Latorre C, Wilmshurst J, von Gunten L, eds (2016) Climate change and cultural evolution. *PAGES (Past Global Changes) Magazine* 24:1–32.
57 IPCC (2014) Summary for policymakers. *Climate Change 2014: Impacts, Adaptation, and Vulnerability. Part A: Global and Sectoral Aspects. Contribution of Working Group II to the Fifth Assessment Report of the Intergovernmental Panel on Climate Change*, eds Field CB, et al. (Cambridge Univ Press, Cambridge, UK), pp 1–32.
58 Schleussner C-F, et al. (2016) Science and policy characteristics of the Paris Agreement temperature goal. *Nat Clim Change* 6:827–835.
59 Griscom BW, et al. (2017) Natural climate solutions. *Proc Natl Acad Sci USA* 114:11645–11650.
60 Barrett S, et al. (2014) Climate engineering reconsidered. *Nat Clim Change* 4:527–529.
61 Mathesius S, Hofmann M, Calderia K, Schellnhuber HJ (2015) Long-term response of oceans to $CO_2$ removal from the atmosphere. *Nat Clim Change* 5:1107–1113.
62 Geels FW, Sovacool BK, Schwanen T, Sorrell S (2017) Sociotechnical transitions for deep decarbonization. *Science* 357:1242–1244.
63 O'Brien K (2018) Is the 1.5 °C target possible? Exploring the three spheres of transformation. *Curr Opin Environ Sustain* 31:153–160.
64 Young OR, et al. (2006) The globalization of socioecological systems: An agenda for scientific research. *Glob Environ Change* 16:304–316.
65 Adger NW, Eakin H, Winkels A (2009) Nested and teleconnected vulnerabilities to environmental change. *Front Ecol Environ* 7:150–157.
66 UN General Assembly (2015) *Transforming Our World: The 2030 Agenda for Sustainable Development*, A/RES/70/1. Available at https://sustainabledevelopment.un.org/content/documents/21252030%20Agenda%20for%20Sustainable%20Development%20web.pdf. Accessed July 18, 2018.
67 Wals AE, Brody M, Dillon J, Stevenson RB (2014) Science education. Convergence between science and environmental education. *Science* 344:583–584.
68 O'Brien K, et al. (2013) You say you want a revolution? Transforming education and capacity building in response to global change. *Environ Sci Policy* 28:48–59.
69 Chapin FS, III, et al. (2011) Earth stewardship: A strategy for social–ecological transformation to reverse planetary degradation. *J Environ Stud Sci* 1:44–53.
70 Folke C, Biggs R, Norström AV, Reyers B, Rockström J (2016) Social-ecological resilience and biosphere-based sustainability science. *Ecol Soc* 21:41.
71 Westley F, et al. (2011) Tipping toward sustainability: Emerging pathways of transformation. *Ambio* 40:762–780.
72 Lutz W, Muttarak R, Striessnig E (2014) Environment and development. Universal education is key to enhanced climate adaptation. *Science* 346:1061–1062.
73 Bongaarts J (2016) Development: Slow down population growth. *Nature* 530:409–412.
74 Defila R, Di Giulio A, Kaufmann-Hayoz R, eds (2012) *The Nature of Sustainable Consumption and How to Achieve It: Results from the Focal Topic "From Knowledge to Action–New Paths Towards Sustainable Consumption"* (Oakum, Munich).
75 Cohen MJ, Szejnwald Brown H, Vergragt P, eds (2013) *Innovations in Sustainable Consumption: New Economics, Socio-Technical Transitions and Social Practices* (Edward Elgar, Cheltenham, UK).
76 Nyborg K, et al. (2016) Social norms as solutions. *Science* 354:42–43.
77 Biermann F, et al. (2012) Science and government. Navigating the anthropocene: Improving Earth system governance. *Science* 335:1306–1307.
78 Galaz V (2014) *Global Environmental Governance, Technology and Politics: The Anthropocene Gap* (Edward Elgar, Cheltenham, UK).
79 Peters DPC, et al. (2004) Cross-scale interactions, nonlinearities, and forecasting catastrophic events. *Proc Natl Acad Sci USA* 101:15130–15135.
80 Walker B, et al. (2009) Environment. Looming global-scale failures and missing institutions. *Science* 325:1345–1346.
81 Hansen J, Sato M, Ruedy R (2012) Perception of climate change. *Proc Natl Acad Sci USA* 109:E2415–E2423.
82 Galaz V, et al. (2017) Global governance dimensions of globally networked risks: The state of the art in social science research. *Risks Hazards Crisis Public Policy* 8:4–27.
83 Augustin L, et al.; EPICA community members (2004) Eight glacial cycles from an Antarctic ice core. *Nature* 429:623–628.
84 Polasky S, Carpenter SR, Folke C, Keeler B (2011) Decision-making under great uncertainty: Environmental management in an era of global change. *Trends Ecol Evol* 26:398–404.
85 Capra F, Luisi PL (2014) *The Systems View of Life; A Unifying Vision* (Cambridge Univ Press, Cambridge, UK).
86 Carpenter SR, et al. (2012) General resilience to cope with extreme events. *Sustainability* 4:3248–3259.
87 Biggs R, et al. (2012) Toward principles for enhancing the resilience of ecosystem services. *Annu Rev Environ Resour* 37:421–448.
88 Figueres C, et al. (2017) Three years to safeguard our climate. *Nature* 546:593–595.

# 10 Detection and Attribution of Climate Change: from Global to Regional

**Coordinating Lead Authors:**
Nathaniel L. Bindoff (Australia), Peter A. Stott (UK)

**Lead Authors:**
Krishna Mirle AchutaRao (India), Myles R. Allen (UK), Nathan Gillett (Canada), David Gutzler (USA), Kabumbwe Hansingo (Zambia), Gabriele Hegerl (UK/Germany), Yongyun Hu (China), Suman Jain (Zambia), Igor I. Mokhov (Russian Federation), James Overland (USA), Judith Perlwitz (USA), Rachid Sebbari (Morocco), Xuebin Zhang (Canada)

**Contributing Authors:**
Magne Aldrin (Norway), Beena Balan Sarojini (UK/India), Jürg Beer (Switzerland), Olivier Boucher (France), Pascale Braconnot (France), Oliver Browne (UK), Ping Chang (USA), Nikolaos Christidis (UK), Tim DelSole (USA), Catia M. Domingues (Australia/Brazil), Paul J. Durack (USA/Australia), Alexey Eliseev (Russian Federation), Kerry Emanuel (USA), Graham Feingold (USA), Chris Forest (USA), Jesus Fidel González Rouco (Spain), Hugues Goosse (Belgium), Lesley Gray (UK), Jonathan Gregory (UK), Isaac Held (USA), Greg Holland (USA), Jara Imbers Quintana (UK), William Ingram (UK), Johann Jungclaus (Germany), Georg Kaser (Austria), Veli-Matti Kerminen (Finland), Thomas Knutson (USA), Reto Knutti (Switzerland), James Kossin (USA), Mike Lockwood (UK), Ulrike Lohmann (Switzerland), Fraser Lott (UK), Jian Lu (USA/Canada), Irina Mahlstein (Switzerland), Valérie Masson-Delmotte (France), Damon Matthews (Canada), Gerald Meehl (USA), Blanca Mendoza (Mexico), Viviane Vasconcellos de Menezes (Australia/Brazil), Seung-Ki Min (Republic of Korea), Daniel Mitchell (UK), Thomas Mölg (Germany/Austria), Simone Morak (UK), Timothy Osborn (UK), Alexander Otto (UK), Friederike Otto (UK), David Pierce (USA), Debbie Polson (UK), Aurélien Ribes (France), Joeri Rogelj (Switzerland/Belgium), Andrew Schurer (UK), Vladimir Semenov (Russian Federation), Drew Shindell (USA), Dmitry Smirnov (Russian Federation), Peter W. Thorne (USA/Norway/UK), Muyin Wang (USA), Martin Wild (Switzerland), Rong Zhang (USA)

**Review Editors:**
Judit Bartholy (Hungary), Robert Vautard (France), Tetsuzo Yasunari (Japan)

**This chapter should be cited as:**
Bindoff, N.L., P.A. Stott, K.M. AchutaRao, M.R. Allen, N. Gillett, D. Gutzler, K. Hansingo, G. Hegerl, Y. Hu, S. Jain, I.I. Mokhov, J. Overland, J. Perlwitz, R. Sebbari and X. Zhang, 2013: Detection and Attribution of Climate Change: from Global to Regional. In: Climate Change 2013: *The Physical Science Basis. Contribution of Working Group I to the Fifth Assessment Report of the Intergovernmental Panel on Climate Change* [Stocker, T.F., D. Qin, G.-K. Plattner, M. Tignor, S.K. Allen, J. Boschung, A. Nauels, Y. Xia, V. Bex and P.M. Midgley (eds.)]. Cambridge University Press, Cambridge, United Kingdom and New York, NY, USA.

# Table of Contents

## Executive Summary

### Atmospheric Temperatures

**More than half of the observed increase in global mean surface temperature (GMST) from 1951 to 2010 is *very likely*[1] due to the observed anthropogenic increase in greenhouse gas (GHG) concentrations.** The consistency of observed and modeled changes across the climate system, including warming of the atmosphere and ocean, sea level rise, ocean acidification and changes in the water cycle, the cryosphere and climate extremes points to a large-scale warming resulting primarily from anthropogenic increases in GHG concentrations. Solar forcing is the only known natural forcing acting to warm the climate over this period but it has increased much less than GHG forcing, and the observed pattern of long-term tropospheric warming and stratospheric cooling is not consistent with the expected response to solar irradiance variations. The Atlantic Multi-decadal Oscillation (AMO) could be a confounding influence but studies that find a significant role for the AMO show that this does not project strongly onto 1951–2010 temperature trends. {10.3.1, Table 10.1}

**It is *extremely likely* that human activities caused more than half of the observed increase in GMST from 1951 to 2010.** This assessment is supported by robust evidence from multiple studies using different methods. Observational uncertainty has been explored much more thoroughly than previously and the assessment now considers observations from the first decade of the 21st century and simulations from a new generation of climate models whose ability to simulate historical climate has improved in many respects relative to the previous generation of models considered in AR4. Uncertainties in forcings and in climate models' temperature responses to individual forcings and difficulty in distinguishing the patterns of temperature response due to GHGs and other anthropogenic forcings prevent a more precise quantification of the temperature changes attributable to GHGs. {9.4.1, 9.5.3, 10.3.1, Figure 10.5, Table 10.1}

**GHGs contributed a global mean surface warming *likely* to be between 0.5°C and 1.3°C over the period 1951–2010, with the contributions from other anthropogenic forcings *likely* to be between –0.6°C and 0.1°C, from natural forcings *likely* to be between –0.1°C and 0.1°C, and from internal variability *likely* to be between –0.1°C and 0.1°C.** Together these assessed contributions are consistent with the observed warming of approximately 0.6°C over this period. {10.3.1, Figure 10.5}

**It is *virtually certain* that internal variability alone cannot account for the observed global warming since 1951.** The observed global-scale warming since 1951 is large compared to climate model estimates of internal variability on 60-year time scales. The Northern Hemisphere (NH) warming over the same period is far outside the range of any similar length trends in residuals from reconstructions of the past millennium. The spatial pattern of observed warming differs from those associated with internal variability. The model-based simulations of internal variability are assessed to be adequate to make this assessment. {9.5.3, 10.3.1, 10.7.5, Table 10.1}

**It is *likely* that anthropogenic forcings, dominated by GHGs, have contributed to the warming of the troposphere since 1961 and *very likely* that anthropogenic forcings, dominated by the depletion of the ozone layer due to ozone-depleting substances, have contributed to the cooling of the lower stratosphere since 1979.** Observational uncertainties in estimates of tropospheric temperatures have now been assessed more thoroughly than at the time of AR4. The structure of stratospheric temperature trends and multi-year to decadal variations are well represented by models and physical understanding is consistent with the observed and modelled evolution of stratospheric temperatures. Uncertainties in radiosonde and satellite records make assessment of causes of observed trends in the upper troposphere less confident than an assessment of the overall atmospheric temperature changes. {2.4.4, 9.4.1, 10.3.1, Table 10.1}

**Further evidence has accumulated of the detection and attribution of anthropogenic influence on temperature change in different parts of the world.** Over every continental region, except Antarctica, it is *likely* that anthropogenic influence has made a substantial contribution to surface temperature increases since the mid-20th century. The robust detection of human influence on continental scales is consistent with the global attribution of widespread warming over land to human influence. It is *likely* that there has been an anthropogenic contribution to the very substantial Arctic warming over the past 50 years. For Antarctica large observational uncertainties result in *low confidence*[2] that anthropogenic influence has contributed to the observed warming averaged over available stations. Anthropogenic influence has *likely* contributed to temperature change in many sub-continental regions. {2.4.1, 10.3.1, Table 10.1}

**Robustness of detection and attribution of global-scale warming is subject to models correctly simulating internal variability.** Although estimates of multi-decadal internal variability of GMST need to be obtained indirectly from the observational record because the observed record contains the effects of external forcings (meaning the combination of natural and anthropogenic forcings), the standard deviation of internal variability would have to be underestimated in climate models by a factor of at least three to account for the observed warming in the absence of anthropogenic influence. Comparison with observations provides no indication of such a large difference between climate models and observations. {9.5.3, Figures 9.33, 10.2, 10.3.1, Table 10.1}

10

[1] In this Report, the following terms have been used to indicate the assessed likelihood of an outcome or a result: Virtually certain 99–100% probability, Very likely 90–100%, Likely 66–100%, About as likely as not 33–66%, Unlikely 0–33%, Very unlikely 0-10%, Exceptionally unlikely 0–1%. Additional terms (Extremely likely: 95–100%, More likely than not >50–100%, and Extremely unlikely 0–5%) may also be used when appropriate. Assessed likelihood is typeset in italics, e.g., *very likely* (see Section 1.4 and Box TS.1 for more details).

[2] In this Report, the following summary terms are used to describe the available evidence: limited, medium, or robust; and for the degree of agreement: low, medium, or high. A level of confidence is expressed using five qualifiers: very low, low, medium, high, and very high, and typeset in italics, e.g., *medium confidence*. For a given evidence and agreement statement, different confidence levels can be assigned, but increasing levels of evidence and degrees of agreement are correlated with increasing confidence (see Section 1.4 and Box TS.1 for more details).

**The observed recent warming hiatus, defined as the reduction in GMST trend during 1998–2012 as compared to the trend during 1951–2012, is attributable in roughly equal measure to a cooling contribution from internal variability and a reduced trend in external forcing (expert judgement, *medium confidence*).** The forcing trend reduction is primarily due to a negative forcing trend from both volcanic eruptions and the downward phase of the solar cycle. However, there is *low confidence* in quantifying the role of forcing trend in causing the hiatus because of uncertainty in the magnitude of the volcanic forcing trends and *low confidence* in the aerosol forcing trend. Many factors, in addition to GHGs, including changes in tropospheric and stratospheric aerosols, stratospheric water vapour, and solar output, as well as internal modes of variability, contribute to the year-to-year and decade- to-decade variability of GMST. {Box 9.2, 10.3.1, Figure 10.6}

### Ocean Temperatures and Sea Level Rise

**It is *very likely* that anthropogenic forcings have made a substantial contribution to upper ocean warming (above 700 m) observed since the 1970s.** This anthropogenic ocean warming has contributed to global sea level rise over this period through thermal expansion. New understanding since AR4 of measurement errors and their correction in the temperature data sets have increased the agreement in estimates of ocean warming. Observations of ocean warming are consistent with climate model simulations that include anthropogenic and volcanic forcings but are inconsistent with simulations that exclude anthropogenic forcings. Simulations that include both anthropogenic and natural forcings have decadal variability that is consistent with observations. These results are a major advance on AR4. {3.2.3, 10.4.1, Table 10.1}

**It is *very likely* that there is a substantial contribution from anthropogenic forcings to the global mean sea level rise since the 1970s.** It is *likely* that sea level rise has an anthropogenic contribution from Greenland melt since 1990 and from glacier mass loss since 1960s. Observations since 1971 indicate with *high confidence* that thermal expansion and glaciers (excluding the glaciers in Antarctica) explain 75% of the observed rise. {10.4.1, 10.4.3, 10.5.2, Table 10.1, 13.3.6}

### Ocean Acidification and Oxygen Change

**It is *very likely* that oceanic uptake of anthropogenic carbon dioxide has resulted in acidification of surface waters which is observed to be between –0.0014 and –0.0024 pH units per year.** There is *medium confidence* that the observed global pattern of decrease in oxygen dissolved in the oceans from the 1960s to the 1990s can be attributed in part to human influences. {3.8.2, Box 3.2, 10.4.4, Table 10.1}

### The Water Cycle

**New evidence is emerging for an anthropogenic influence on global land precipitation changes, on precipitation increases in high northern latitudes, and on increases in atmospheric humidity.** There is *medium confidence* that there is an anthropogenic contribution to observed increases in atmospheric specific humidity since 1973 and to global scale changes in precipitation patterns over land since 1950, including increases in NH mid to high latitudes. Remaining observational and modelling uncertainties, and the large internal variability in precipitation, preclude a more confident assessment at this stage. {2.5.1, 2.5.4, 10.3.2, Table 10.1}

**It is *very likely* that anthropogenic forcings have made a discernible contribution to surface and subsurface oceanic salinity changes since the 1960s.** More than 40 studies of regional and global surface and subsurface salinity show patterns consistent with understanding of anthropogenic changes in the water cycle and ocean circulation. The expected pattern of anthropogenic amplification of climatological salinity patterns derived from climate models is detected in the observations although there remains incomplete understanding of the observed internal variability of the surface and sub-surface salinity fields. {3.3.2, 10.4.2, Table 10.1}

**It is *likely* that human influence has affected the global water cycle since 1960.** This assessment is based on the combined evidence from the atmosphere and oceans of observed systematic changes that are attributed to human influence in terrestrial precipitation, atmospheric humidity and oceanic surface salinity through its connection to precipitation and evaporation. This is a major advance since AR4. {3.3.2, 10.3.2, 10.4.2, Table 10.1}

### Cryosphere

**Anthropogenic forcings are *very likely* to have contributed to Arctic sea ice loss since 1979.** There is a robust set of results from simulations that show the observed decline in sea ice extent is simulated only when models include anthropogenic forcings. There is *low confidence* in the scientific understanding of the observed increase in Antarctic sea ice extent since 1979 owing to the incomplete and competing scientific explanations for the causes of change and *low confidence* in estimates of internal variability. {10.5.1, Table 10.1}

**Ice sheets and glaciers are melting, and anthropogenic influences are *likely* to have contributed to the surface melting of Greenland since 1993 and to the retreat of glaciers since the 1960s.** Since 2007, internal variability is *likely* to have further enhanced the melt over Greenland. For glaciers there is a high level of scientific understanding from robust estimates of observed mass loss, internal variability and glacier response to climatic drivers. Owing to a low level of scientific understanding there is *low confidence* in attributing the causes of the observed loss of mass from the Antarctic ice sheet since 1993. {4.3.3, 10.5.2, Table 10.1}

**It is *likely* that there has been an anthropogenic component to observed reductions in NH snow cover since 1970.** There is high agreement across observations studies and attribution studies find a human influence at both continental and regional scales. {10.5.3, Table 10.1}

### Climate Extremes

**There has been a strengthening of the evidence for human influence on temperature extremes since the AR4 and IPCC Special Report on Managing the Risks of Extreme Events and Disasters to Advance Climate Change Adaptation (SREX) reports.** It is *very likely* that anthropogenic forcing has contributed to the observed changes in the frequency and intensity of daily temperature extremes on the global scale since the mid-20th century. Attribution of changes in temperature extremes to anthropogenic influence is robustly seen in independent analyses using different methods and different data sets. It is *likely* that human influence has substantially increased the probability of occurrence of heatwaves in some locations. {10.6.1, 10.6.2, Table 10.1}

**In land regions where observational coverage is sufficient for assessment, there is *medium confidence* that anthropogenic forcing has contributed to a global-scale intensification of heavy precipitation over the second half of the 20th century.** There is *low confidence* in attributing changes in drought over global land areas since the mid-20th century to human influence owing to observational uncertainties and difficulties in distinguishing decadal-scale variability in drought from long-term trends. {10.6.1, Table 10.1}

**There is *low confidence* in attribution of changes in tropical cyclone activity to human influence owing to insufficient observational evidence, lack of physical understanding of the links between anthropogenic drivers of climate and tropical cyclone activity and the low level of agreement between studies as to the relative importance of internal variability, and anthropogenic and natural forcings.** This assessment is consistent with that of SREX. {10.6.1, Table 10.1}

### Atmospheric Circulation

**It is *likely* that human influence has altered sea level pressure patterns globally.** Detectable anthropogenic influence on changes in sea level pressure patterns is found in several studies. Changes in atmospheric circulation are important for local climate change since they could lead to greater or smaller changes in climate in a particular region than elsewhere. There is *medium confidence* that stratospheric ozone depletion has contributed to the observed poleward shift of the southern Hadley Cell border during austral summer. There are large uncertainties in the magnitude of this poleward shift. It is *likely* that stratospheric ozone depletion has contributed to the positive trend in the Southern Annular Mode seen in austral summer since the mid-20th century which corresponds to sea level pressure reductions over the high latitudes and an increase in the subtropics. There is *medium confidence* that GHGs have also played a role in these trends of the southern Hadley Cell border and the Southern Annular Mode in Austral summer. {10.3.3, Table 10.1}

### A Millennia to Multi-Century Perspective

**Taking a longer term perspective shows the substantial role played by anthropogenic and natural forcings in driving climate variability on hemispheric scales prior to the twentieth century.** It is *very unlikely* that NH temperature variations from 1400 to 1850 can be explained by internal variability alone. There is *medium confidence* that external forcing contributed to NH temperature variability from 850 to 1400 and that external forcing contributed to European temperature variations over the last five centuries. {10.7.2, 10.7.5, Table 10.1}

### Climate System Properties

**The extended record of observed climate change has allowed a better characterization of the basic properties of the climate system that have implications for future warming.** New evidence from 21st century observations and stronger evidence from a wider range of studies have strengthened the constraint on the transient climate response (TCR) which is estimated with *high confidence* to be *likely* between 1°C and 2.5°C and *extremely unlikely* to be greater than 3°C. The Transient Climate Response to Cumulative $CO_2$ Emissions (TCRE) is estimated with *high confidence* to be *likely* between 0.8°C and 2.5°C per 1000 PgC for cumulative $CO_2$ emissions less than about 2000 PgC until the time at which temperatures peak. Estimates of the Equilibrium Climate Sensitivity (ECS) based on multiple and partly independent lines of evidence from observed climate change indicate that there is *high confidence* that ECS is *extremely unlikely* to be less than 1°C and *medium confidence* that the ECS is *likely* to be between 1.5°C and 4.5°C and *very unlikely* greater than 6°C. These assessments are consistent with the overall assessment in Chapter 12, where the inclusion of additional lines of evidence increases confidence in the assessed *likely* range for ECS. {10.8.1, 10.8.2, 10.8.4, Box 12.2}

### Combination of Evidence

**Human influence has been detected in the major assessed components of the climate system. Taken together, the combined evidence increases the level of confidence in the attribution of observed climate change, and reduces the uncertainties associated with assessment based on a single climate variable. From this combined evidence it is *virtually certain* that human influence has warmed the global climate system.** Anthropogenic influence has been identified in changes in temperature near the surface of the Earth, in the atmosphere and in the oceans, as well as changes in the cryosphere, the water cycle and some extremes. There is strong evidence that excludes solar forcing, volcanoes and internal variability as the strongest drivers of warming since 1950. {10.9.2, Table 10.1}

## 10.1 Introduction

This chapter assesses the causes of observed changes assessed in Chapters 2 to 5 and uses understanding of physical processes, climate models and statistical approaches. The chapter adopts the terminology for detection and attribution proposed by the IPCC good practice guidance paper on detection and attribution (Hegerl et al., 2010) and for uncertainty Mastrandrea et al. (2011). Detection and attribution of impacts of climate changes are assessed by Working Group II, where Chapter 18 assesses the extent to which atmospheric and oceanic changes influence ecosystems, infrastructure, human health and activities in economic sectors.

Evidence of a human influence on climate has grown stronger over the period of the four previous assessment reports of the IPCC. There was little observational evidence for a detectable human influence on climate at the time of the First IPCC Assessment Report. By the time of the second report there was sufficient additional evidence for it to conclude that 'the balance of evidence suggests a discernible human influence on global climate'. The Third Assessment Report found that a distinct greenhouse gas (GHG) signal was robustly detected in the observed temperature record and that 'most of the observed warming over the last fifty years is *likely* to have been due to the increase in greenhouse gas concentrations.'

With the additional evidence available by the time of the Fourth Assessment Report, the conclusions were further strengthened. This evidence included a wider range of observational data, a greater variety of more sophisticated climate models including improved representations of forcings and processes and a wider variety of analysis techniques. This enabled the AR4 report to conclude that 'most of the observed increase in global average temperatures since the mid-20th century is *very likely* due to the observed increase in anthropogenic greenhouse gas concentrations'. The AR4 also concluded that 'discernible human influences now extend to other aspects of climate, including ocean warming, continental-average temperatures, temperature extremes and wind patterns.'

A number of uncertainties remained at the time of AR4. For example, the observed variability of ocean temperatures appeared inconsistent with climate models, thereby reducing the confidence with which observed ocean warming could be attributed to human influence. Also, although observed changes in global rainfall patterns and increases in heavy precipitation were assessed to be qualitatively consistent with expectations of the response to anthropogenic forcings, detection and attribution studies had not been carried out. Since the AR4, improvements have been made to observational data sets, taking more complete account of systematic biases and inhomogeneities in observational systems, further developing uncertainty estimates, and correcting detected data problems (Chapters 2 and 3). A new set of simulations from a greater number of AOGCMs have been performed as part of the Coupled Model Intercomparison Project Phase 5 (CMIP5). These new simulations have several advantages over the CMIP3 simulations assessed in the AR4 (Hegerl et al., 2007b). They incorporate some moderate increases in resolution, improved parameterizations, and better representation of aerosols (Chapter 9). Importantly for attribution, in which it is necessary to partition the response of the climate system to different forcings, most CMIP5 models include simulations of the response to natural forcings only, and the response to increases in well mixed GHGs only (Taylor et al., 2012).

The advances enabled by this greater wealth of observational and model data are assessed in this chapter. In this assessment, there is increased focus on the extent to which the climate system as a whole is responding in a coherent way across a suite of climate variables such as surface mean temperature, temperature extremes, ocean heat content, ocean salinity and precipitation change. There is also a global to regional perspective, assessing the extent to which not just global mean changes but also spatial patterns of change across the globe can be attributed to anthropogenic and natural forcings.

## 10.2 Evaluation of Detection and Attribution Methodologies

Detection and attribution methods have been discussed in previous assessment reports (Hegerl et al., 2007b) and the IPCC Good Practice Guidance Paper (Hegerl et al., 2010), to which we refer. This section reiterates key points and discusses new developments and challenges.

### 10.2.1 The Context of Detection and Attribution

In IPCC Assessments, detection and attribution involve quantifying the evidence for a causal link between external drivers of climate change and observed changes in climatic variables. It provides the central, although not the only (see Section 1.2.3) line of evidence that has supported statements such as 'the balance of evidence suggests a discernible human influence on global climate' or 'most of the observed increase in global average temperatures since the mid-20th century is *very likely* due to the observed increase in anthropogenic greenhouse gas concentrations.'

The definition of detection and attribution used here follows the terminology in the IPCC guidance paper (Hegerl et al., 2010). '*Detection* of change is defined as the process of demonstrating that climate or a system affected by climate has changed in some defined statistical sense without providing a reason for that change. An identified change is detected in observations if its likelihood of occurrence by chance due to internal variability alone is determined to be small' (Hegerl et al., 2010). *Attribution* is defined as 'the process of evaluating the relative contributions of multiple causal factors to a change or event with an assignment of statistical confidence'. As this wording implies, attribution is more complex than detection, combining statistical analysis with physical understanding (Allen et al., 2006; Hegerl and Zwiers, 2011). In general, a component of an observed change is attributed to a specific causal factor if the observations can be shown to be consistent with results from a process-based model that includes the causal factor in question, and inconsistent with an alternate, otherwise identical, model that excludes this factor. The evaluation of this consistency in both of these cases takes into account internal chaotic variability and known uncertainties in the observations and responses to external causal factors.

Attribution does not require, and nor does it imply, that every aspect of the response to the causal factor in question is simulated correctly. Suppose, for example, the global cooling following a large volcano matches the cooling simulated by a model, but the model underestimates the magnitude of this cooling: the observed global cooling can still be attributed to that volcano, although the error in magnitude would suggest that details of the model response may be unreliable. Physical understanding is required to assess what constitutes a plausible discrepancy above that expected from internal variability. Even with complete consistency between models and data, attribution statements can never be made with 100% certainty because of the presence of internal variability.

This definition of attribution can be extended to include antecedent conditions and internal variability among the multiple causal factors contributing to an observed change or event. Understanding the relative importance of internal versus external factors is important in the analysis of individual weather events (Section 10.6.2), but the primary focus of this chapter will be on attribution to factors external to the climate system, like rising GHG levels, solar variability and volcanic activity.

There are four core elements to any detection and attribution study:

1. Observations of one or more climate variables, such as surface temperature, that are understood, on physical grounds, to be relevant to the process in question

2. An estimate of how external drivers of climate change have evolved before and during the period under investigation, including both the driver whose influence is being investigated (such as rising GHG levels) and potential confounding influences (such as solar activity)

3. A quantitative physically based understanding, normally encapsulated in a model, of how these external drivers are thought to have affected these observed climate variables

4. An estimate, often but not always derived from a physically based model, of the characteristics of variability expected in these observed climate variables due to random, quasi-periodic and chaotic fluctuations generated in the climate system that are not due to externally driven climate change

A climate model driven with external forcing alone is not expected to replicate the observed evolution of internal variability, because of the chaotic nature of the climate system, but it should be able to capture the statistics of this variability (often referred to as 'noise'). The reliability of forecasts of short-term variability is also a useful test of the representation of relevant processes in the models used for attribution, but forecast skill is not necessary for attribution: attribution focuses on changes in the underlying moments of the 'weather attractor', meaning the expected weather and its variability, while prediction focuses on the actual trajectory of the weather around this attractor.

In proposing that 'the process of attribution requires the detection of a change in the observed variable *or closely associated variables*' (Hegerl et al., 2010), the new guidance recognized that it may be possible, in some instances, to attribute a change in a particular variable to some external factor before that change could actually be detected in the variable itself, provided there is a strong body of knowledge that links a change in that variable to some other variable in which a change can be detected and attributed. For example, it is impossible in principle to detect a trend in the frequency of 1-in-100-year events in a 100-year record, yet if the probability of occurrence of these events is physically related to large-scale temperature changes, and we detect and attribute a large-scale warming, then the new guidance allows attribution of a change in probability of occurrence before such a change can be detected in observations of these events alone. This was introduced to draw on the strength of attribution statements from, for example, time-averaged temperatures, to attribute changes in closely related variables.

Attribution of observed changes is not possible without some kind of model of the relationship between external climate drivers and observable variables. We cannot observe a world in which either anthropogenic or natural forcing is absent, so some kind of model is needed to set up and evaluate quantitative hypotheses: to provide estimates of how we would expect such a world to behave and to respond to anthropogenic and natural forcings (Hegerl and Zwiers, 2011). Models may be very simple, just a set of statistical assumptions, or very complex, complete global climate models: it is not necessary, or possible, for them to be correct in all respects, but they must provide a physically consistent representation of processes and scales relevant to the attribution problem in question.

One of the simplest approaches to detection and attribution is to compare observations with model simulations driven with natural forcings alone, and with simulations driven with all relevant natural and anthropogenic forcings. If observed changes are consistent with simulations that include human influence, and inconsistent with those that do not, this would be sufficient for attribution providing there were no other confounding influences and it is assumed that models are simulating the responses to all external forcings correctly. This is a strong assumption, and most attribution studies avoid relying on it. Instead, they typically assume that models simulate the *shape* of the response to external forcings (meaning the large-scale pattern in space and/or time) correctly, but do not assume that models simulate the *magnitude* of the response correctly. This is justified by our fundamental understanding of the origins of errors in climate modelling. Although there is uncertainty in the size of key forcings and the climate response, the overall shape of the response is better known: it is set in time by the timing of emissions and set in space (in the case of surface temperatures) by the geography of the continents and differential responses of land and ocean (see Section 10.3.1.1.2).

So-called 'fingerprint' detection and attribution studies characterize their results in terms of a best estimate and uncertainty range for 'scaling factors' by which the model-simulated responses to individual forcings can be scaled up or scaled down while still remaining consistent with the observations, accounting for similarities between the patterns of response to different forcings and uncertainty due to internal climate variability. If a scaling factor is significantly larger than zero (at some significance level), then the response to that forcing, as simulated by

that model and given that estimate of internal variability and other potentially confounding responses, is detectable in these observations, whereas if the scaling factor is consistent with unity, then that model-simulated response is consistent with observed changes. Studies do not require scaling factors to be consistent with unity for attribution, but any discrepancy from unity should be understandable in terms of known uncertainties in forcing or response: a scaling factor of 10, for example, might suggest the presence of a confounding factor, calling into question any attribution claim. Scaling factors are estimated by fitting model-simulated responses to observations, so results are unaffected, at least to first order, if the model has a transient climate response, or aerosol forcing, that is too low or high. Conversely, if the spatial or temporal *pattern* of forcing or response is wrong, results can be affected: see Box 10.1 and further discussion in Section 10.3.1.1 and Hegerl and Zwiers (2011) and Hegerl et al. (2011b). Sensitivity of results to the pattern of forcing or response can be assessed by comparing results across multiple models or by representing pattern uncertainty explicitly (Huntingford et al., 2006), but errors that are common to all models (through limited vertical resolution, for example) will not be addressed in this way and are accounted for in this assessment by downgrading overall assessed likelihoods to be generally more conservative than the quantitative likelihoods provided by individual studies.

Attribution studies must compromise between estimating responses to different forcings separately, which allows for the possibility of different errors affecting different responses (errors in aerosol forcing that do not affect the response to GHGs, for example), and estimating responses to combined forcings, which typically gives smaller uncertainties because it avoids the issue of 'degeneracy': if two responses have very similar shapes in space and time, then it may be impossible to estimate the magnitude of both from a single set of observations because amplification of one may be almost exactly compensated for by amplification or diminution of the other (Allen et al., 2006). Many studies find it is possible to estimate the magnitude of the responses to GHG and other anthropogenic forcings separately, particularly when spatial information is included. This is important, because it means the estimated response to GHG increase is not dependent on the uncertain magnitude of forcing and response due to aerosols (Hegerl et al., 2011b).

The simplest way of fitting model-simulated responses to observations is to assume that the responses to different forcings add linearly, so the response to any one forcing can be scaled up or down without affecting any of the others and that internal climate variability is independent of the response to external forcing. Under these conditions, attribution can be expressed as a variant of linear regression (see Box 10.1). The additivity assumption has been tested and found to hold for large-scale temperature changes (Meehl et al., 2003; Gillett et al., 2004) but it might not hold for other variables like precipitation (Hegerl et al., 2007b; Hegerl and Zwiers, 2011; Shiogama et al., 2012), nor for regional temperature changes (Terray, 2012). In principle, additivity is not required for detection and attribution, but to date non-additive approaches have not been widely adopted.

The estimated properties of internal climate variability play a central role in this assessment. These are either estimated empirically from the observations (Section 10.2.2) or from paleoclimate reconstructions (Section 10.7.1) (Esper et al., 2012) or derived from control simulations of coupled models (Section 10.2.3). The majority of studies use modelled variability and routinely check that the residual variability from observations is consistent with modelled internal variability used over time scales shorter than the length of the instrumental record (Allen and Tett, 1999). Assessing the accuracy of model-simulated variability on longer time scales using paleoclimate reconstructions is complicated by the fact that some reconstructions may not capture the full spectrum of variability because of limitations of proxies and reconstruction methods, and by the unknown role of external forcing in the pre-instrumental record. In general, however, paleoclimate reconstructions provide no clear evidence either way whether models are over- or underestimating internal variability on time scales relevant for attribution (Esper et al., 2012; Schurer et al., 2013).

### 10.2.2 Time Series Methods, Causality and Separating Signal from Noise

Some studies attempt to distinguish between externally driven climate change and changes due to internal variability minimizing the use of climate models, for example, by separating signal and noise by time scale (Schneider and Held, 2001), spatial pattern (Thompson et al., 2009) or both. Other studies use model control simulations to identify patterns of maximum predictability and contrast these with the forced component in climate model simulations (DelSole et al., 2011): see Section 10.3.1. Conclusions of most studies are consistent with those based on fingerprint detection and attribution, while using a different set of assumptions (see review in Hegerl and Zwiers, 2011).

A number of studies have applied methods developed in the econometrics literature (Engle and Granger, 1987) to assess the evidence for a causal link between external drivers of climate and observed climate change, using the observations themselves to estimate the expected properties of internal climate variability (e.g., Kaufmann and Stern, 1997). The advantage of these approaches is that they do not depend on the accuracy of any complex global climate model, but they nevertheless have to assume some kind of model, or restricted class of models, of the properties of the variables under investigation. Attribution is impossible without a model: although this model may be implicit in the statistical framework used, it is important to assess its physical consistency (Kaufmann et al., 2013). Many of these time series methods can be cast in the overall framework of co-integration and error correction (Kaufmann et al., 2011), which is an approach to analysing relationships between stationary and non-stationary time series. If there is a consistent causal relationship between two or more possibly non-stationary time series, then it should be possible to find a linear combination such that the residual is stationary (contains no stochastic trend) over time (Kaufmann and Stern, 2002; Kaufmann et al., 2006; Mills, 2009). Co-integration methods are thus similar in overall principle to regression-based approaches (e.g., Douglass et al., 2004; Stone and Allen, 2005; Lean, 2006) to the extent that regression studies take into account the expected time series properties of the data—the example described in Box 10.1 might be characterized as looking for a linear combination of anthropogenic and natural forcings such that the observed residuals were consistent with internal climate variability as simulated by the CMIP5 models. Co-integration and error correction methods, however, generally make more explicit use of time

## Box 10.1 | How Attribution Studies Work

This box presents an idealized demonstration of the concepts underlying most current approaches to detection and attribution of climate change and how these relate to conventional linear regression. The coloured dots in Box 10.1a, Figure 1 show observed annual GMST from 1861 to 2012, with warmer years coloured red and colder years coloured blue. Observations alone indicate, unequivocally, that the Earth has warmed, but to quantify how different external factors have contributed to this warming, studies must compare such observations with the expected responses to these external factors. The orange line shows an estimate of the GMST response to anthropogenic (GHG and aerosol) forcing obtained from the mean of the CMIP3 and CMIP5 ensembles, while the blue line shows the CMIP3/CMIP5 ensemble mean response to natural (solar and volcanic) forcing.

In statistical terms, attribution involves finding the combination of these anthropogenic and natural responses that best fits these observations: this is shown by the black line in panel (a). To show how this fit is obtained in non-technical terms, the data are plotted against model-simulated anthropogenic warming, instead of time, in panel (b). There is a strong correlation between observed temperatures and model-simulated anthropogenic warming, but because of the presence of natural factors and internal climate variability, correlation alone is not enough for attribution.

To quantify how much of the observed warming is attributable to human influence, panel (c) shows observed temperatures plotted against the model-simulated response to anthropogenic forcings in one direction and natural forcings in the other. Observed temperatures increase with both natural and anthropogenic model-simulated warming: the warmest years are in the far corner of the box. A flat surface through these points (here obtained by an ordinary least-squares fit), indicated by the coloured mesh, slopes up away from the viewer.

The orientation of this surface indicates how model-simulated responses to natural and anthropogenic forcing need to be scaled to reproduce the observations. The best-fit gradient in the direction of anthropogenic warming (visible on the rear left face of the box) is 0.9, indicating the CMIP3/CMIP5 ensemble average overestimates the magnitude of the observed response to anthropogenic forcing by about 10%. The best-fit gradient in the direction of natural changes (visible on the rear right face) is 0.7, indicating that the observed response to natural forcing is 70% of the average model-simulated response. The black line shows the points on this flat surface that are directly above or below the observations: each 'pin' corresponds to a different year. When re-plotted against time, indicated by the years on the rear left face of the box, this black line gives the black line previously seen in panel (a). The length of the pins indicates 'residual' temperature fluctuations due to internal variability.

The timing of these residual temperature fluctuations is unpredictable, representing an inescapable source of uncertainty. We can quantify this uncertainty by asking how the gradients of the best-fit surface might vary if El Niño events, for example, had occurred in different years in the observed temperature record. To do this, we repeat the analysis in panel (c), replacing observed temperatures with samples of simulated internal climate variability from control runs of coupled climate models. Grey diamonds in panel (d) show the results: these gradients cluster around zero, because control runs have no anthropogenic or natural forcing, but there is still some scatter. Assuming that internal variability in global temperature simply adds to the response to external forcing, this scatter provides an estimate of uncertainty in the gradients, or scaling factors, required to reproduce the observations, shown by the red cross and ellipse.

The red cross and ellipse are clearly separated from the origin, which means that the slope of the best-fit surface through the observations cannot be accounted for by internal variability: some climate change is detected in these observations. Moreover, it is also separated from both the vertical and horizontal axes, which means that the responses to both anthropogenic and natural factors are individually detectable.

The magnitude of observed temperature change is consistent with the CMIP3/CMIP5 ensemble average response to anthropogenic forcing (uncertainty in this scaling factor spans unity) but is significantly lower than the model-average response to natural forcing (this 5 to 95% confidence interval excludes unity). There are, however, reasons why these models may be underestimating the response to volcanic forcing (e.g., Driscoll et al, 2012), so this discrepancy does not preclude detection and attribution of both anthropogenic and natural influence, as simulated by the CMIP3/CMIP5 ensemble average, in the observed GMST record.

The top axis in panel (d) indicates the attributable anthropogenic warming over 1951–2010, estimated from the anthropogenic warming in the CMIP3/CMIP5 ensemble average, or the gradient of the orange line in panel (a) over this period. Because the model-simulated responses have been scaled to fit the observations, the attributable anthropogenic warming in this example is 0.6°C to 0.9°C and does not depend on the magnitude of the raw model-simulated changes. Hence an attribution statement based on such an analysis,

*(continued on next page)*

*Box 10.1 (continued)*

such as 'most of the warming over the past 50 years is attributable to anthropogenic drivers', depends only on the shape, or time history, not the size, of the model-simulated warming, and hence does not depend on the models' sensitivity to rising GHG levels.

Formal attribution studies like this example provide objective estimates of how much recent warming is attributable to human influence. Attribution is not, however, a purely statistical exercise. It also requires an assessment that there are no confounding factors that could have caused a large part of the 'attributed' change. Statistical tests can be used to check that observed residual temperature fluctuations (the lengths and clustering of the pins in panel (c)) are consistent with internal variability expected from coupled models, but ultimately these tests must complement physical arguments that the combination of responses to anthropogenic and natural forcing is the only available consistent explanation of recent observed temperature change.

This demonstration assumes, for visualization purposes, that there are only two candidate contributors to the observed warming, anthropogenic and natural, and that only GMST is available. More complex attribution problems can be undertaken using the same principles, such as aiming to separate the response to GHGs from other anthropogenic factors by also including spatial information. These require, in effect, an extension of panel (c), with additional dimensions corresponding to additional causal factors, and additional points corresponding to temperatures in different regions.



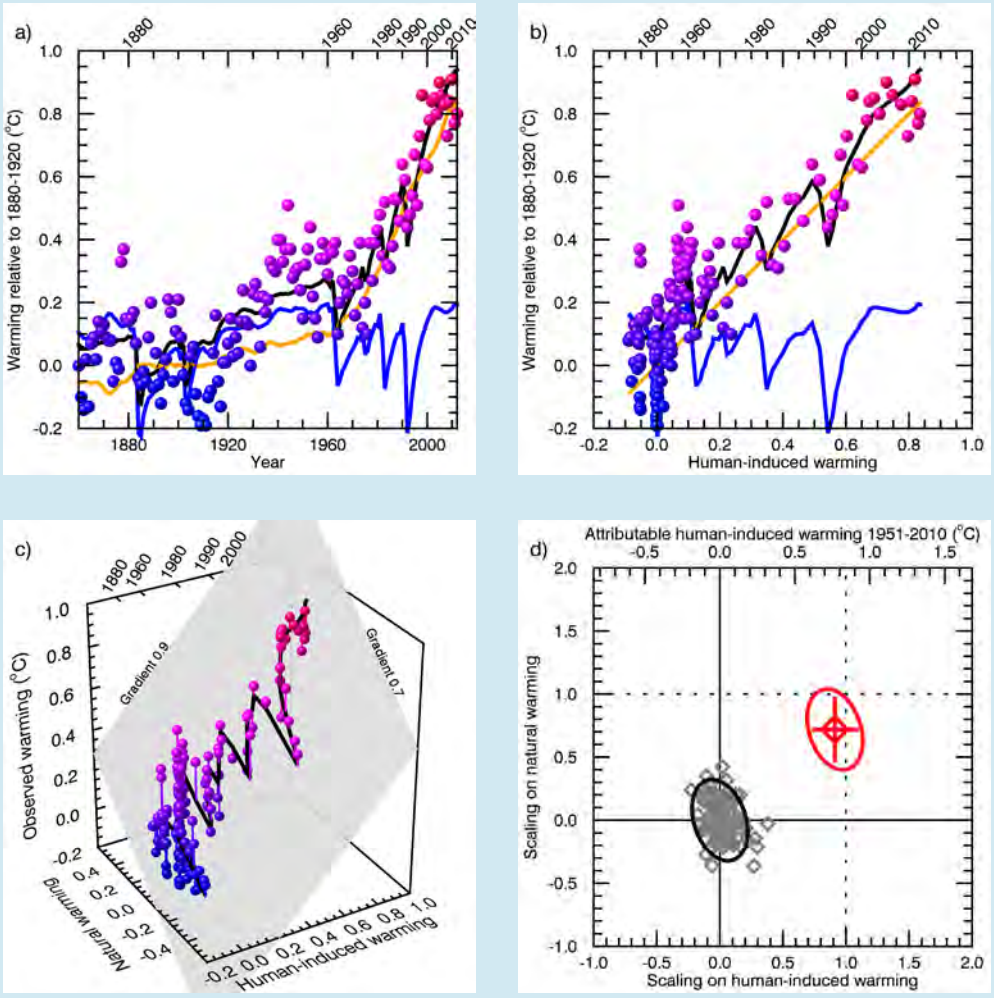


**Box 10.1, Figure 1 |** Example of a simplified detection and attribution study. (a) Observed global annual mean temperatures relative to 1880–1920 (coloured dots) compared with CMIP3/CMIP5 ensemble-mean response to anthropogenic forcing (orange), natural forcing (blue) and best-fit linear combination (black). (b) As (a) but all data plotted against model-simulated anthropogenic warming in place of time. Selected years (increasing nonlinearly) shown on top axis. (c) Observed temperatures versus model-simulated anthropogenic and natural temperature changes, with best-fit plane shown by coloured mesh. (d) Gradient of best-fit plane in (c), or scaling on model-simulated responses required to fit observations (red diamond) with uncertainty estimate (red ellipse and cross) based on CMIP5 control integrations (grey diamonds). Implied attributable anthropogenic warming over the period 1951–2010 is indicated by the top axis. Anthropogenic and natural responses are noise-reduced with 5-point running means, with no smoothing over years with major volcanoes.

series properties (notice how date information is effectively discarded in panel (b) of Box 10.1, Figure 1) and require fewer assumptions about the stationarity of the input series.

All of these approaches are subject to the issue of confounding factors identified by Hegerl and Zwiers (2011). For example, Beenstock et al. (2012) fail to find a consistent co-integrating relationship between atmospheric carbon dioxide ($CO_2$) concentrations and GMST using polynomial cointegration tests, but the fact that $CO_2$ concentrations are derived from different sources in different periods (ice cores prior to the mid-20th-century, atmospheric observations thereafter) makes it difficult to assess the physical significance of their result, particularly in the light of evidence for co-integration between temperature and radiative forcing (RF) reported by Kaufmann et al. (2011) using tests of linear cointegration, and also the results of Gay-Garcia et al. (2009), who find evidence for external forcing of climate using time series properties.

The assumptions of the statistical model employed can also influence results. For example, Schlesinger and Ramankutty (1994) and Zhou and Tung (2013a) show that GMST are consistent with a linear anthropogenic trend, enhanced variability due to an approximately 70-year Atlantic Meridional Oscillation (AMO) and shorter-term variability. If, however, there are physical grounds to expect a nonlinear anthropogenic trend (see Box 10.1 Figure 1a), the assumption of a linear trend can itself enhance the variance assigned to a low-frequency oscillation. The fact that the AMO index is estimated from detrended historical temperature observations further increases the risk that its variance may be overestimated, because regressors and regressands are not independent. Folland et al. (2013), using a physically based estimate of the anthropogenic trend, find a smaller role for the AMO in recent warming.

Time series methods ultimately depend on the structural adequacy of the statistical model employed. Many such studies, for example, use models that assume a single exponential decay time for the response to both external forcing and stochastic fluctuations. This can lead to an overemphasis on short-term fluctuations, and is not consistent with the response of more complex models (Knutti et al., 2008). Smirnov and Mokhov (2009) propose an alternative characterization that allows them to distinguish a 'long-term causality' that focuses on low-frequency changes. Trends that appear significant when tested against an AR(1) model may not be significant when tested against a process that supports this 'long-range dependence' (Franzke, 2010). Although the evidence for long-range dependence in global temperature data remains a topic of debate (Mann, 2011; Rea et al., 2011) , it is generally desirable to explore sensitivity of results to the specification of the statistical model, and also to other methods of estimating the properties of internal variability, such as more complex climate models, discussed next. For example, Imbers et al. (2013) demonstrate that the detection of the influence of increasing GHGs in the global temperature record is robust to the assumption of a Fractional Differencing (FD) model of internal variability, which supports long-range dependence.

### 10.2.3 Methods Based on General Circulation Models and Optimal Fingerprinting

Fingerprinting methods use climate model simulations to provide more complete information about the expected response to different external drivers, including spatial information, and the properties of internal climate variability. This can help to separate patterns of forced change both from each other and from internal variability. The price, however, is that results depend to some degree on the accuracy of the shape of model-simulated responses to external factors (e.g., North and Stevens, 1998), which is assessed by comparing results obtained with expected responses estimated from different climate models. When the signal-to-noise (S/N) ratio is low, as can be the case for some regional indicators and some variables other than temperature, the accuracy of the specification of variability becomes a central factor in the reliability of any detection and attribution study. Many studies of such variables inflate the variability estimate from models to determine if results are sensitive to, for example, doubling of variance in the control (e.g., Zhang et al., 2007), although Imbers et al. (2013) note that errors in the spectral properties of simulated variability may also be important.

A full description of optimal fingerprinting is provided in Appendix 9.A of Hegerl et al. (2007b) and further discussion is to be found in Hasselmann (1997), Allen and Tett (1999), Allen et al. (2006), and Hegerl and Zwiers (2011). Box 10.1 provides a simple example of 'fingerprinting' based on GMST alone. In a typical fingerprint analysis, model-simulated spatio-temporal patterns of response to different combinations of external forcings, including segments of control integrations with no forcing, are 'observed' in a similar manner to the historical record (masking out times and regions where observations are absent). The magnitudes of the model-simulated responses are then estimated in the observations using a variant of linear regression, possibly allowing for signals being contaminated by internal variability (Allen and Stott, 2003) and structural model uncertainty (Huntingford et al., 2006).

In 'optimal' fingerprinting, model-simulated responses and observations are normalized by internal variability to improve the S/N ratio. This requires an estimate of the inverse noise covariance estimated from the sample covariance matrix of a set of unforced (control) simulations (Hasselmann, 1997), or from variations within an initial-condition ensemble. Because these control runs are generally too short to estimate the full covariance matrix, a truncated version is used, retaining only a small number, typically of order 10 to 20, of high-variance principal components. Sensitivity analyses are essential to ensure results are robust to this, relatively arbitrary, choice of truncation (Allen and Tett, 1999; Ribes and Terray, 2013; Jones et al., 2013 ). Ribes et al. (2009) use a regularized estimate of the covariance matrix, meaning a linear combination of the sample covariance matrix and a unit matrix that has been shown (Ledoit and Wolf, 2004) to provide a more accurate estimate of the true covariance, thereby avoiding dependence on truncation. Optimization of S/N ratio is not, however, essential for many attribution results (see, e.g., Box 10.1) and uncertainty analysis in conventional optimal fingerprinting does not require the covariance matrix to be inverted, so although regularization may help in some cases, it is not essential. Ribes et al. (2010) also propose a hybrid of the model-based optimal fingerprinting and time series approaches, referred to as 'temporal optimal detection', under which each signal is assumed to consist of a single spatial pattern modulated by a smoothly varying time series estimated from a climate model (see also Santer et al., 1994).

The final statistical step in an attribution study is to check that the residual variability, after the responses to external drivers have been estimated and removed, is consistent with the expected properties of internal climate variability, to ensure that the variability used for uncertainty analysis is realistic, and that there is no evidence that a potentially confounding factor has been omitted. Many studies use a standard *F*-test of residual consistency for this purpose (Allen and Tett, 1999). Ribes et al. (2013) raise some issues with this test, but key results are not found to be sensitive to different formulations. A more important issue is that the *F*-test is relatively weak (Berliner et al., 2000; Allen et al., 2006; Terray, 2012), so 'passing' this test is not a safeguard against unrealistic variability, which is why estimates of internal variability are discussed in detail in this chapter and in Chapter 9.

A further consistency check often used in optimal fingerprinting is whether the estimated magnitude of the externally driven responses are consistent between model and observations (scaling factors consistent with unity in Box 10.1): if they are not, attribution is still possible provided the discrepancy is explicable in terms of known uncertainties in the magnitude of either forcing or response. As is emphasized in Section 10.2.1 and Box 10.1, attribution is not a purely statistical assessment: physical judgment is required to assess whether the combination of responses considered allows for all major potential confounding factors and whether any remaining discrepancies are consistent with a physically based understanding of the responses to external forcing and internal climate variability.



### 10.2.4 Single-Step and Multi-Step Attribution and the Role of the Null Hypothesis

Attribution studies have traditionally involved explicit simulation of the response to external forcing of an observable variable, such as surface temperature, and comparison with corresponding observations of that variable. This so-called 'single-step attribution' has the advantage of simplicity, but restricts attention to variables for which long and consistent time series of observations are available and that can be simulated explicitly in current models driven solely with external climate forcing.

To address attribution questions for variables for which these conditions are not satisfied, Hegerl et al. (2010) introduced the notation of 'multi-step attribution', formalizing existing practice (e.g., Stott et al., 2004). In a multi-step attribution study, the attributable change in a variable such as large-scale surface temperature is estimated with a single-step procedure, along with its associated uncertainty, and the implications of this change are then explored in a further (physically or statistically based) modelling step. Overall conclusions can only be as robust as the least certain link in the multi-step procedure. As the focus shifts towards more noisy regional changes, it can be difficult to separate the effect of different external forcings. In such cases, it can be useful to detect the response to all external forcings, and then determine the most important factors underlying the attribution results by reference to a closely related variable for which a full attribution analysis is available (e.g., Morak et al., 2011).

Attribution results are typically expressed in terms of conventional 'frequentist' confidence intervals or results of hypothesis tests: when it is reported that the response to anthropogenic GHG increase is *very likely* greater than half the total observed warming, it means that the null hypothesis that the GHG-induced warming is less than half the total can be rejected with the data available at the 10% significance level. Expert judgment is required in frequentist attribution assessments, but its role is limited to the assessment of whether internal variability and potential confounding factors have been adequately accounted for, and to downgrade nominal significance levels to account for remaining uncertainties. Uncertainties may, in some cases, be further reduced if prior expectations regarding attribution results themselves are incorporated, using a Bayesian approach, but this not currently the usual practice.

This traditional emphasis on single-step studies and placing lower bounds on the magnitude of signals under investigation means that, very often, the communication of attribution results tends to be conservative, with attention focussing on whether or not human influence in a particular variable might be zero, rather than the upper end of the confidence interval, which might suggest a possible response much bigger than current model-simulated changes. Consistent with previous Assessments and the majority of the literature, this chapter adopts this conservative emphasis. It should, however, be borne in mind that this means that positive attribution results will tend to be biased towards well-observed, well-modelled variables and regions, which should be taken into account in the compilation of global impact assessments (Allen, 2011; Trenberth, 2011a).

## 10.3 Atmosphere and Surface

This section assesses causes of change in the atmosphere and at the surface over land and ocean.

### 10.3.1 Temperature

Temperature is first assessed near the surface of the Earth in Section 10.3.1.1 and then in the free atmosphere in Section 10.3.1.2.

#### 10.3.1.1 Surface (Air Temperature and Sea Surface Temperature)

##### 10.3.1.1.1 Observations of surface temperature change

GMST warmed strongly over the period 1900–1940, followed by a period with little trend, and strong warming since the mid-1970s (Section 2.4.3, Figure 10.1). Almost all observed locations have warmed since 1901 whereas over the satellite period since 1979 most regions have warmed while a few regions have cooled (Section 2.4.3; Figure 10.2). Although this picture is supported by all available global near-surface temperature data sets, there are some differences in detail between them, but these are much smaller than both interannual variability and the long-term trend (Section 2.4.3). Since 1998 the trend in GMST has been small (see Section 2.4.3, Box 9.2). Urbanization is *unlikely* to have caused more than 10% of the measured centennial trend in land mean surface temperature, though it may have contributed substantially more to regional mean surface temperature trends in rapidly developing regions (Section 2.4.1.3).

10.3.1.1.2 Simulations of surface temperature change

As discussed in Section 10.1, the CMIP5 simulations have several advantages compared to the CMIP3 simulations assessed by (Hegerl et al., 2007b) for the detection and attribution of climate change. Figure 10.1a shows that when the effects of anthropogenic and natural external forcings are included in the CMIP5 simulations the spread of simulated GMST anomalies spans the observational estimates of GMST anomaly in almost every year whereas this is not the case for simulations in which only natural forcings are included (Figure 10.1b) (see also Jones et al., 2013; Knutson et al., 2013). Anomalies are shown relative to 1880–1919 rather than absolute temperatures. Showing anomalies is necessary to prevent changes in observational coverage being reflected in the calculated global mean and is reasonable

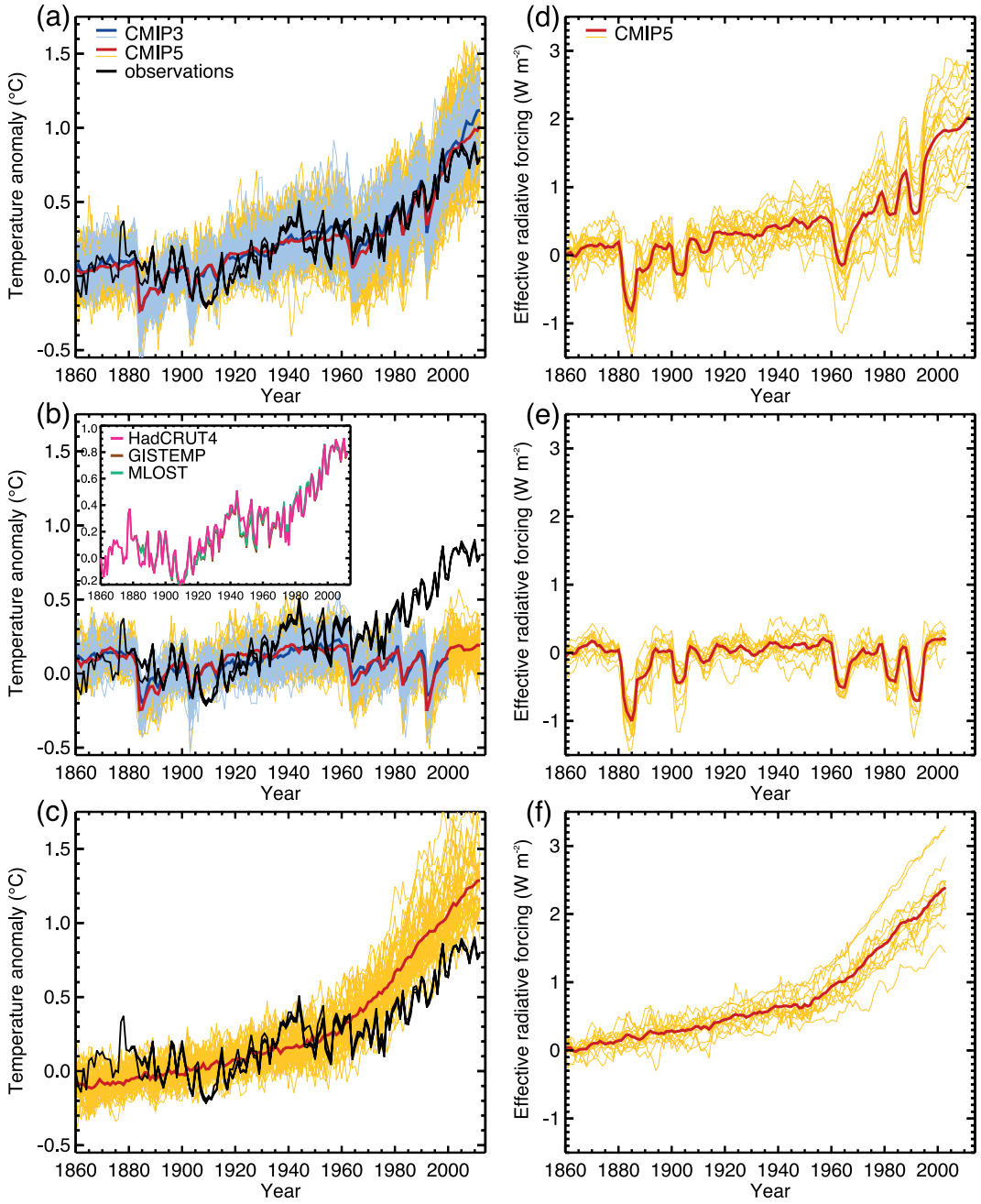


**Figure 10.1 |** (Left-hand column) Three observational estimates of global mean surface temperature (GMST, black lines) from Hadley Centre/Climatic Research Unit gridded surface temperature data set 4 (HadCRUT4), Goddard Institute of Space Studies Surface Temperature Analysis (GISTEMP), and Merged Land–Ocean Surface Temperature Analysis (MLOST), compared to model simulations [CMIP3 models – thin blue lines and CMIP5 models – thin yellow lines] with anthropogenic and natural forcings (a), natural forcings only (b) and greenhouse gas (GHG) forcing only (c). Thick red and blue lines are averages across all available CMIP5 and CMIP3 simulations respectively. CMIP3 simulations were not available for GHG forcing only (c). All simulated and observed data were masked using the HadCRUT4 coverage (as this data set has the most restricted spatial coverage), and global average anomalies are shown with respect to 1880–1919, where all data are first calculated as anomalies relative to 1961–1990 in each grid box. Inset to (b) shows the three observational data sets distinguished by different colours. (Adapted from Jones et al., 2013.) (Right-hand column) Net adjusted forcing in CMIP5 models due to anthropogenic and natural forcings (d), natural forcings only (e) and GHGs only (f). (From Forster et al., 2013.) Individual ensemble members are shown by thin yellow lines, and CMIP5 multi-model means are shown as thick red lines.

because climate sensitivity is not a strong function of the bias in GMST in the CMIP5 models (Section 9.7.1; Figure 9.42). Simulations with GHG changes only, and no changes in aerosols or other forcings, tend to simulate more warming than observed (Figure 10.1c), as expected. Better agreement between models and observations when the models include anthropogenic forcings is also seen in the CMIP3 simulations (Figure 10.1, thin blue lines). RF in the simulations including anthropogenic and natural forcings differs considerably among models (Figure 10.1d), and forcing differences explain much of the differences in temperature response between models over the historical period (Forster et al., 2013 ). Differences between observed GMST based on three observational data sets are small compared to forced changes (Figure 10.1).

As discussed in Section 10.2, detection and attribution assessments are more robust if they consider more than simple consistency arguments. Analyses that allow for the possibility that models might be consistently over- or underestimating the magnitude of the response to climate forcings are assessed in Section 10.3.1.1.3, the conclusions from which are not affected by evidence that model spread in GMST in CMIP3, is smaller than implied by the uncertainty in RF (Schwartz et al., 2007). Although there is evidence that CMIP3 models with a higher climate sensitivity tend to have a smaller increase in RF over the historical period (Kiehl, 2007; Knutti, 2008; Huybers, 2010), no such relationship was found in CMIP5 (Forster et al., 2013 ) which may explain the wider spread of the CMIP5 ensemble compared to the CMIP3 ensemble (Figure 10.1a). Climate model parameters are typically chosen primarily to reproduce features of the mean climate and variability (Box 9.1), and CMIP5 aerosol emissions are standardized across models and based on historical emissions (Lamarque et al., 2010; Section 8.2.2), rather than being chosen by each modelling group independently (Curry and Webster, 2011; Hegerl et al., 2011c).

Figure 10.2a shows the pattern of annual mean surface temperature trends observed over the period 1901–2010, based on Hadley Centre/Climatic Research Unit gridded surface temperature data set 4 (HadCRUT4). Warming has been observed at almost all locations with sufficient observations available since 1901. Rates of warming are generally higher over land areas compared to oceans, as is also apparent over the 1951–2010 period (Figure 10.2c), which simulations indicate is due mainly to differences in local feedbacks and a net anomalous heat transport from oceans to land under GHG forcing, rather than differences in thermal inertia (e.g., Boer, 2011). Figure 10.2e demonstrates that a similar pattern of warming is simulated in the CMIP5 simulations with natural and anthropogenic forcing over the 1901–2010 period. Over most regions, observed trends fall between the 5th and 95th percentiles of simulated trends, and van Oldenborgh et al. (2013) find that over the 1950–2011 period the pattern of observed grid cell trends agrees with CMIP5 simulated trends to within a combination of

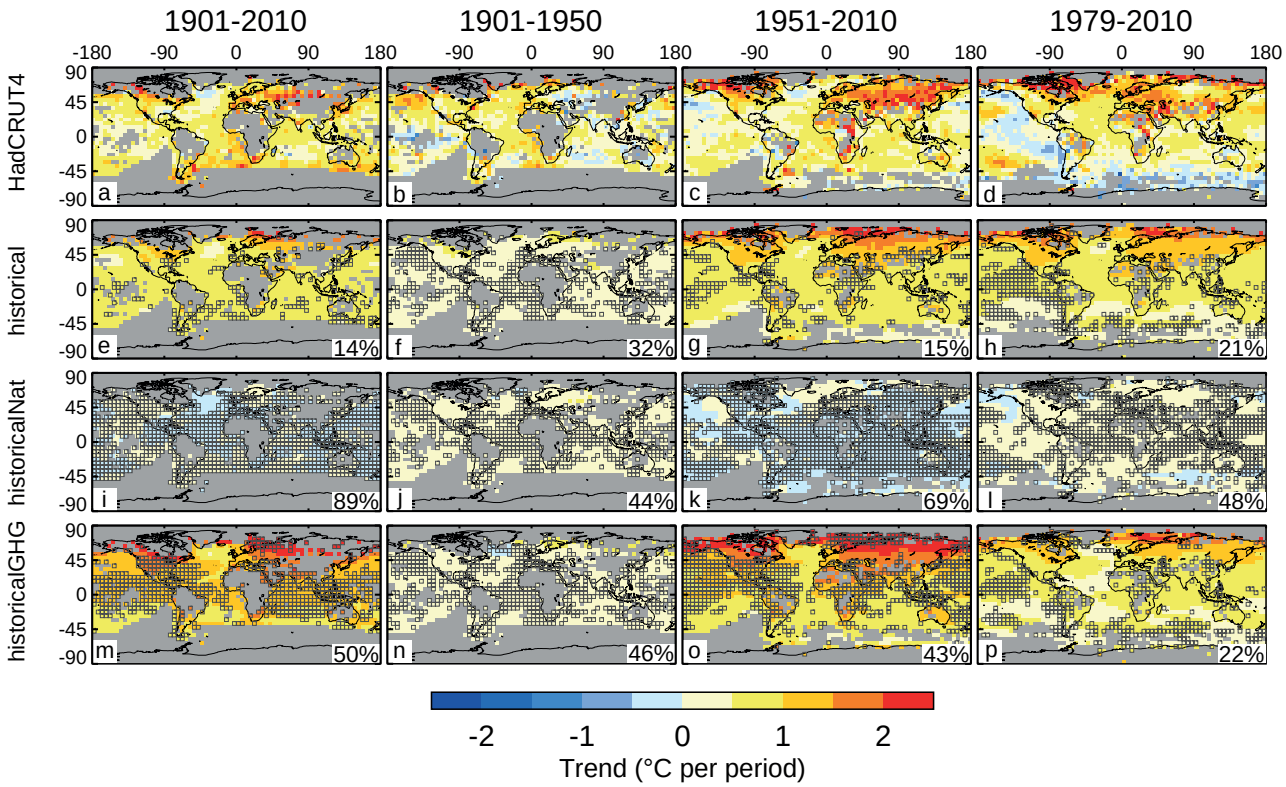


**Figure 10.2 |** Trends in observed and simulated temperatures (K over the period shown) over the 1901–2010 (a, e, i, m), 1901–1950 (b, f, j, n), 1951–2010 (c, g, k, o) and 1979–2010 (d, h, l, p) periods. Trends in observed temperatures from the Hadley Centre/Climatic Research Unit gridded surface temperature data set 4 (HadCRUT4) (a–d), CMIP3 and CMIP5 model simulations including anthropogenic and natural forcings (e–h), CMIP3 and CMIP5 model simulations including natural forcings only (i–l) and CMIP3 and CMIP5 model simulations including greenhouse gas forcing only (m–p). Trends are shown only where sufficient observational data are available in the HadCRUT4 data set, and grid cells with insufficient observations to derive trends are shown in grey. Boxes in (e–p) show where the observed trend lies outside the 5 to 95th percentile range of simulated trends, and the ratio of the number of such grid cells to the total number of grid cells with sufficient data is shown as a percentage in the lower right of each panel. (Adapted from Jones et al., 2013.)

model spread and internal variability. Areas of disagreement over the 1901–2010 period include parts of Asia and the Southern Hemisphere (SH) mid-latitudes, where the simulations warm less than the observations, and parts of the tropical Pacific, where the simulations warm more than the observations (Jones et al., 2013; Knutson et al., 2013). Stronger warming in observations than models over parts of East Asia could in part be explained by uncorrected urbanization influence in the observations (Section 2.4.1.3), or by an overestimate of the response to aerosol increases. Trends simulated in response to natural forcings only are generally close to zero, and inconsistent with observed trends in most locations (Figure 10.2i) (see also Knutson et al., 2013). Trends simulated in response to GHG changes only over the 1901–2010 period are larger than those observed at most locations, and in many cases significantly so (Figure 10.2m). This is expected because these simulations do not include the cooling effects of aerosols. Differences in patterns of simulated and observed seasonal mean temperature trends and possible causes are considered in more detail in Box 11.2.

Over the period 1979–2010 most observed regions exhibited warming (Figure 10.2d), but much of the eastern Pacific and Southern Oceans cooled. These regions of cooling are not seen in the simulated trends over this period in response to anthropogenic and natural forcing (Figure 10.2h), which show significantly more warming in much of these regions (Jones et al., 2013; Knutson et al., 2013). This cooling and reduced warming in observations over the Southern Hemisphere mid-latitudes over the 1979–2010 period can also be seen in the zonal mean trends (Figure 10.3d), which also shows that the models tend to warm too much in this region over this period. However, there is no discrepancy in zonal mean temperature trends over the longer 1901–2010 period in this region (Figure 10.3a), suggesting that the discrepancy over the 1979–2010 period either may be an unusually strong manifestation of internal variability in the observations or relate to regionally important forcings over the past three decades which are not included in most CMIP5 simulations, such as sea salt aerosol increases due to strengthened high latitude winds (Korhonen et al., 2010), or sea ice extent increases driven by freshwater input from ice shelf melting (Bintanja et al., 2013). Except at high latitudes, zonal mean trends over the 1901–2010 period in all three data sets are inconsistent with naturally forced trends, indicating a detectable anthropogenic signal in most zonal means over this period (Figure 10.3a). McKitrick and Tole (2012) find that few CMIP3 models have significant explanatory power when fitting the spatial pattern of 1979–2002 trends in surface temperature over land, by which they mean that these models add little or no skill to a fit including the spatial pattern of tropospheric temperature trends as well as the major atmospheric oscillations. This is to be expected, as temperatures in the troposphere are well correlated in the vertical, and local temperature trends over so short a period are dominated by internal variability.

CMIP5 models generally exhibit realistic variability in GMST on decadal to multi-decadal time scales (Jones et al., 2013; Knutson et al., 2013; Section 9.5.3.1, Figure 9.33), although it is difficult to evaluate internal variability on multi-decadal time scales in observations given the shortness of the observational record and the presence of external forcing. The observed trend in GMST since the 1950s is very large compared to model estimates of internal variability (Stott et al., 2010; Drost et al., 2012; Drost and Karoly, 2012). Knutson et al. (2013) compare observed

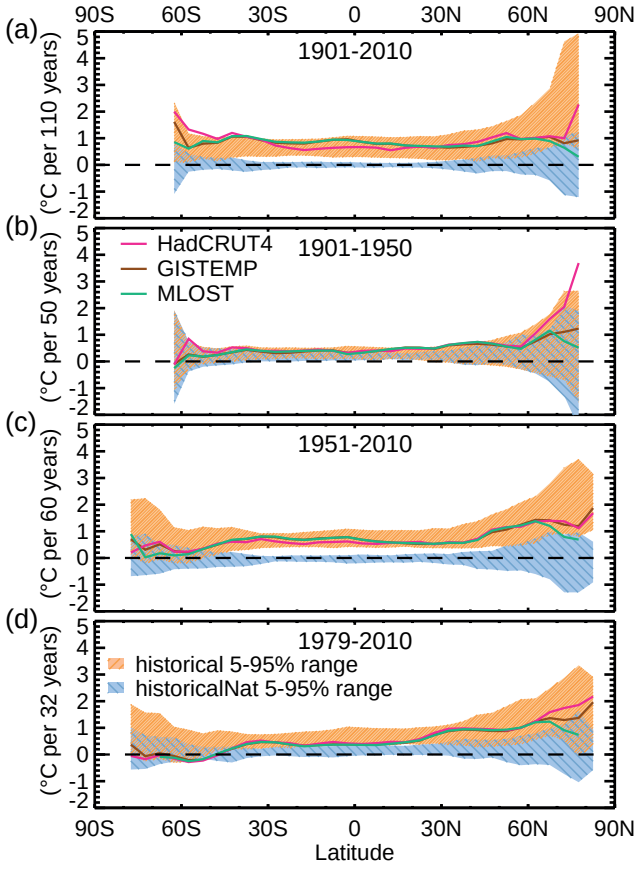


**Figure 10.3 |** Zonal mean temperature trends over the 1901–2010 (a), 1901–1950 (b), 1951–2010 (c) and 1979–2010 (d) periods. Solid lines show Hadley Centre/Climatic Research Unit gridded surface temperature data set 4 (HadCRUT4, red), Goddard Institute of Space Studies Surface Temperature Analysis (GISTEMP, brown) and Merged Land–Ocean Surface Temperature Analysis (MLOST, green) observational data sets, orange hatching represents the 90% central range of CMIP3 and CMIP5 simulations with anthropogenic and natural forcings, and blue hatching represents the 90% central range of CMIP3 and CMIP5 simulations with natural forcings only. All model and observations data are masked to have the same coverage as HadCRUT4. (Adapted from Jones et al., 2013.)

trends in GMST with a combination of simulated internal variability and the response to natural forcings and find that the observed trend would still be detected for trends over this period even if the magnitude of the simulated natural variability (i.e., the standard deviation of trends) were tripled.

#### 10.3.1.1.3 Attribution of observed global-scale temperature changes

**The evolution of temperature since the start of the global instrumental record**

Since the AR4, detection and attribution studies have been carried out using new model simulations with more realistic forcings, and new observational data sets with improved representation of uncertainty (Christidis et al., 2010; Jones et al., 2011, 2013; Gillett et al., 2012, 2013; Stott and Jones, 2012; Knutson et al., 2013; Ribes and Terray, 2013). Although some inconsistencies between the simulated and observed responses to forcings in individual models were identified ( Gillett et al., 2013; Jones et al., 2013; Ribes and Terray, 2013) over-

all these results support the AR4 assessment that GHG increases *very likely* caused most (>50%) of the observed GMST increase since the mid-20th century (Hegerl et al., 2007b).

The results of multiple regression analyses of observed temperature changes onto the simulated responses to GHG, other anthropogenic and natural forcings are shown in Figure 10.4 (Gillett et al., 2013; Jones et al., 2013; Ribes and Terray, 2013). The results, based on HadCRUT4 and a multi-model average, show robustly detected responses to GHG in the observational record whether data from 1861–2010 or only from 1951–2010 are analysed (Figure 10.4b). The advantage of analysing the longer period is that more information on observed and modelled changes is included, while a disadvantage is that it is difficult to validate climate models' estimates of internal variability over such a long period. Individual model results exhibit considerable spread among scaling factors, with estimates of warming attributable to each forcing sensitive to the model used for the analsys (Figure 10.4; Gillett et al., 2013; Jones et al., 2013; Ribes and Terray, 2013), the period over which the analysis is applied (Figure 10.4; Gillett et al., 2013; Jones et al., 2013), and the Empirical Orthogonal Function (EOF) truncation or degree of spatial filtering (Jones et al., 2013; Ribes and Terray, 2013). In some cases the GHG response is not detectable in regressions using individual models (Figure 10.4; Gillett et al., 2013; Jones et al., 2013; Ribes and Terray, 2013), or a residual test is failed (Gillett et al., 2013; Jones et al., 2013; Ribes and Terray, 2013), indicating a poor fit between the simulated response and observed changes. Such cases are probably due largely to errors in the spatio-temporal pattern of responses to forcings simulated in individual models (Ribes and Terray, 2013), although observational error and internal variability errors could also play a role. Nonetheless, analyses in which responses are averaged across multiple models generally show much less sensitivity to period and EOF trucation (Gillett et al., 2013; Jones et al., 2013), and more consistent residuals (Gillett et al., 2013), which may be because model response errors are smaller in a multi-model mean.



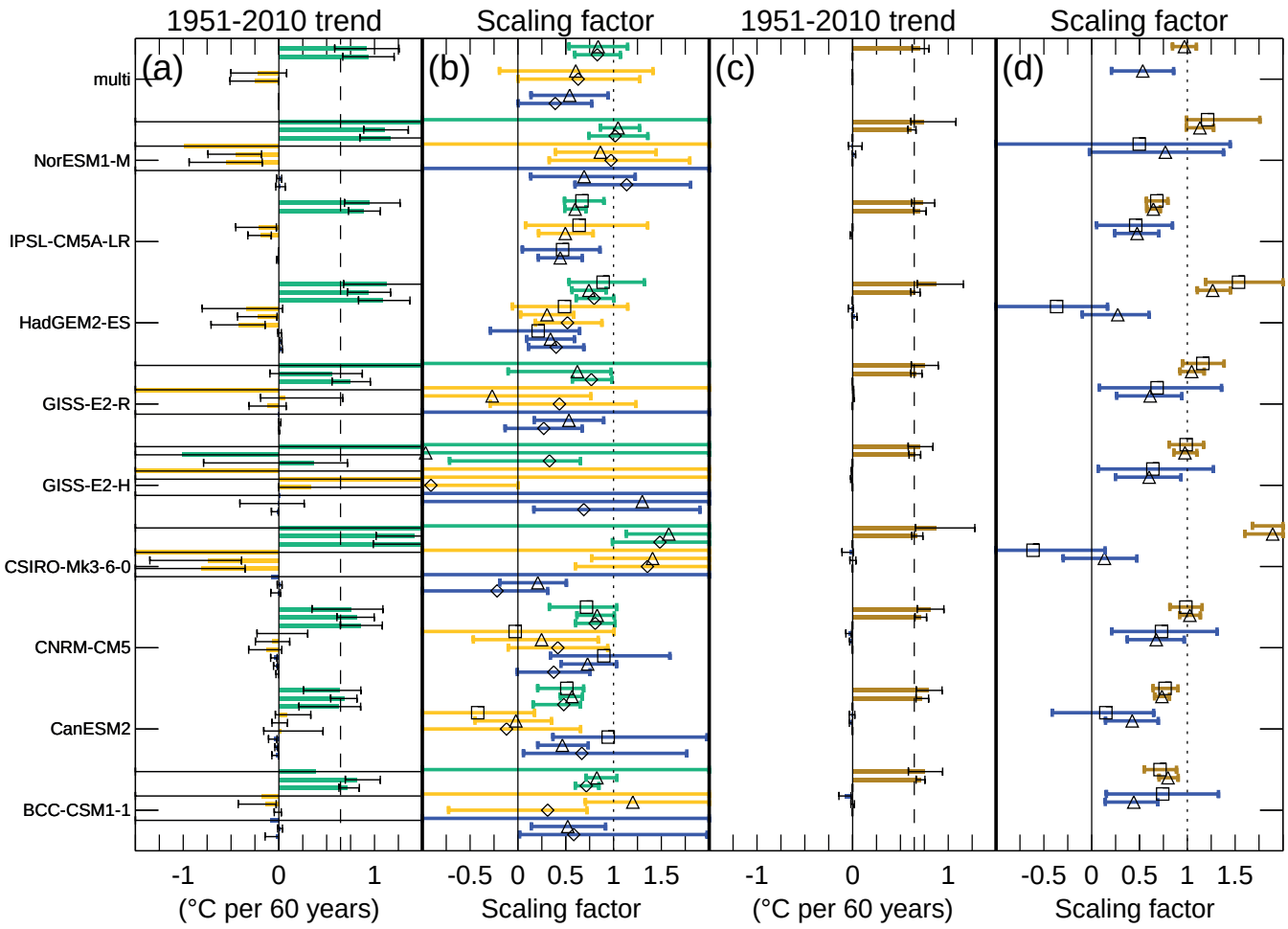


**Figure 10.4 |** (a) Estimated contributions of greenhouse gas (GHG, green), other anthropogenic (yellow) and natural (blue) forcing components to observed global mean surface temperature (GMST) changes over the 1951–2010 period. (b) Corresponding scaling factors by which simulated responses to GHG (green), other anthropogenic (yellow) and natural forcings (blue) must be multiplied to obtain the best fit to Hadley Centre/Climatic Research Unit gridded surface temperature data set 4 (HadCRUT4; Morice et al., 2012) observations based on multiple regressions using response patterns from nine climate models individually and multi-model averages (multi). Results are shown based on an analysis over the 1901–2010 period (squares, Ribes and Terray, 2013), an analysis over the 1861–2010 period (triangles, Gillett et al., 2013) and an analysis over the 1951–2010 period (diamonds, Jones et al., 2013). (c, d) As for (a) and (b) but based on multiple regressions estimating the contributions of total anthropogenic forcings (brown) and natural forcings (blue) based on an analysis over 1901–2010 period (squares, Ribes and Terray, 2013) and an analysis over the 1861–2010 period (triangles, Gillett et al., 2013). Coloured bars show best estimates of the attributable trends (a and c) and 5 to 95% confidence ranges of scaling factors (b and d). Vertical dashed lines in (a) and (c) show the best estimate HadCRUT4 observed trend over the period concerned. Vertical dotted lines in (b) and d) denote a scaling factor of unity.

We derive assessed ranges for the attributable contributions of GHGs, other anthropogenic forcings and natural forcings by taking the smallest ranges with a precision of one decimal place that span the 5 to 95% ranges of attributable trends over the 1951–2010 period from the Jones et al. (2013) weighted multi-model analysis and the Gillett et al. (2013) multi-model analysis considering observational uncertainty (Figure 10.4a). The assessed range for the attributable contribution of combined anthropogenic forcings was derived in the same way from the Gillett et al. (2013) multi-model attributable trend and shown in Figure 10.4c. We moderate our likelihood assessment and report *likely* ranges rather than the *very likely* ranges directly implied by these studies in order to account for residual sources of uncertainty including sensitivity to EOF truncation and analysis period (e.g., Ribes and Terray, 2013). In this context, GHGs means well-mixed greenhouse gases (WMGHGs), other anthropogenic forcings means aerosol changes, and in most models ozone changes and land use changes, and natural forcings means solar irradiance changes and volcanic aerosols. Over the 1951–2010 period, the observed GMST increased by approximately 0.6°C. GHG increases *likely* contributed 0.5°C to 1.3°C, other anthropogenic forcings *likely* contributed –0.6°C to 0.1°C and natural forcings *likely* contributed –0.1°C to 0.1°C to observed GMST trends over this period. Internal variability *likely* contributed –0.1°C to 0.1°C to observed trends over this period (Knutson et al., 2013). This assessment is shown schematically in Figure 10.5. The assessment is supported additionally by a complementary analysis in which the parameters of an Earth System Model of Intermediate Complexity (EMIC) were constrained using observations of near-surface temperature and ocean heat content, as well as prior information on the magnitudes of forcings, and which concluded that GHGs have caused 0.6°C to 1.1°C (5 to 95% uncertainty) warming since the mid-20th century (Huber and Knutti, 2011); an analysis by Wigley and Santer (2013), who used an energy balance model and RF and climate sensitivity estimates from AR4, and they concluded that there was about a 93% chance that GHGs caused a warming greater than observed over the 1950–2005 period; and earlier detection and attribution studies assessed in the AR4 (Hegerl et al., 2007b).

The inclusion of additional data to 2010 (AR4 analyses stopped at 1999; Hegerl et al. (2007b)) helps to better constrain the magnitude of the GHG-attributable warming (Drost et al., 2012; Gillett et al., 2012; Stott and Jones, 2012; Gillett et al., 2013), as does the inclusion of spatial information (Stott et al., 2006; Gillett et al., 2013), though Ribes and Terray (2013) caution that in some cases there are inconsistencies between observed spatial patterns of response and those simulated in indvidual models. While Hegerl et al. (2007b) assessed that a significant cooling of about 0.2 °C was attributable to natural forcings over the 1950–1999 period, the temperature trend attributable to natural forcings over the 1951–2010 period is very small (<0.1°C). This is because, while Mt Pinatubo cooled global temperatures in the early 1990s, there have been no large volcanic eruptions since, resulting in small simulated trends in response to natural forcings over the 1951–2010 period (Figure 10.1b). Regression coefficients for natural forcings tend to be smaller than one, suggesting that the response to natural forcings may be overestimated by the CMIP5 models on average (Figure 10.4; Gillett et al., 2013; Knutson et al., 2013). Attribution of observed changes is robust to observational uncertainty which is comparably important to internal climate variability as a source of uncertainty in GHG-attributable warming and aerosol-attributable cooling (Jones and Stott, 2011; Gillett et al., 2013; Knutson et al., 2013). The response to GHGs was detected using Hadley Centre new Global Environmental Model 2-Earth System (HadGEM2-ES; Stott and Jones, 2012), Canadian Earth System Model 2 (CanESM2; Gillett et al., 2012) and other CMIP5 models except for Goddard Institute for Space Studies-E2-H (GISS-E2-H; Gillett et al., 2013; Jones et al., 2013) (Figure 10.4). However, the influence of other anthropogenic forcings was detected only in some CMIP5 models (Figure 10.4). This lack of detection of other anthropogenic forcings compared to detection of an aerosol response using four CMIP3 models over the period 1900–1999 (Hegerl et al., 2007b) does not only relate to the use of data to 2010 rather than 2000 (Stott and Jones, 2012), although this could play a role (Gillett et al., 2013; Ribes and Terray, 2013). Whether it is associated with a cancellation of aerosol cooling by ozone and black carbon (BC) warming in the CMIP5 simulations, making the signal harder to detect, or by some aspect of the response to other anthropogenic forcings that is less realistic in these models is not clear.

Although closely constraining the GHG and other anthropogenic contributions to observed warming remains challenging owing to their degeneracy and sensitivity to methodological choices (Jones et al., 2013; Ribes and Terray, 2013), a total anthropogenic contribution to warming can be much more robustly constrained by a regression of observed temperature changes onto the simulated responses to all anthropogenic forcings and natural forcings (Figure 10.4; Gillett et al., 2013; Ribes and Terray, 2013). Robust detection of anthropogenic influence is also found if a new optimal detection methodology, the Regularised Optimal Fingerprint approach (see Section 10.2; Ribes et al., 2013), is applied (Ribes and Terray, 2013). A better constrained estimate of the total anthropogenic contribution to warming since the mid-20th century than the GHG contribution is also found by Wigley and Santer (2013). Knutson et al. (2013) demonstrate that observed trends in GMST are inconsistent with the simulated response to natural forcings alone, but consistent with the simulated response to natural and anthropogenic forcings for all periods beginning between 1880 and 1990 and ending in 2010, which they interpret as evidence that warming is in part attributable to anthropogenic influence over these periods. Based on the well-constrained attributable anthropogenic trends shown in Figure 10.4 we assess that anthropogenic forcings *likely* contributed 0.6°C to 0.8°C to the observed warming over the 1951–2010 period (Figure 10.5).

There are some inconsistencies in the simulated and observed magnitudes of responses to forcing for some CMIP5 models (Figure 10.4); for example, CanESM2 has a GHG regression coefficient significantly less than 1 and a regression coefficient for other anthropogenic forcings also significantly less than 1 (Gillett et al., 2012; Gillett et al., 2013; Jones et al., 2013; Ribes and Terray, 2013), indicating that this model overestimates the magnitude of the response to GHGs and to other anthropogenic forcings. Averaged over the ensembles of models considered by Gillett et al. (2013) and Jones et al. (2013), the best-estimate GHG and OA scaling factors are less than 1 (Figure 10.4), indicating that the model mean GHG and OA responses should be scaled down to best match observations. The best-estimate GHG scaling factors are larger than the best-estimate OA scaling factors, although the discrepancy from 1 is not significant in either case and the ranges of the GHG

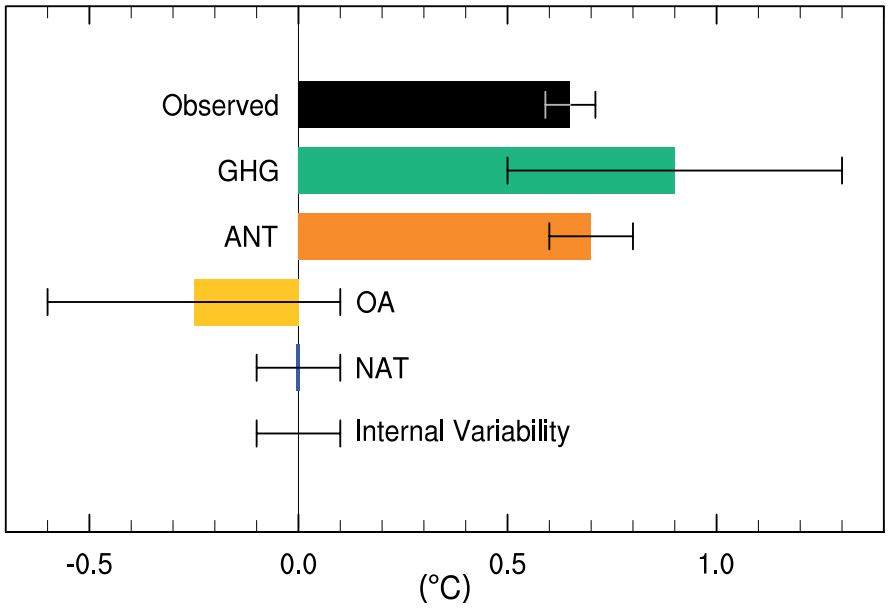


**Figure 10.5 |** Assessed *likely* ranges (whiskers) and their mid-points (bars) for attributable warming trends over the 1951–2010 period due to well-mixed greenhouse gases, other anthropogenic forcings (OA), natural forcings (NAT), combined anthropogenic forcings (ANT) and internal variability. The Hadley Centre/Climatic Research Unit gridded surface temperature data set 4 (HadCRUT4) observations are shown in black with the 5 to 95% uncertainty range due to observational uncertainty in this record (Morice et al., 2012).



and OA scaling factors are overlapping. Overall there is some evidence that some CMIP5 models have a higher transient response to GHGs and a larger response to other anthropogenic forcings (dominated by the effects of aerosols) than the real world (*medium confidence*). Inconsistencies between simulated and observed trends in GMST were also identified in several CMIP3 models by Fyfe et al. (2010) after removing volcanic, El Niño-Southern Oscillation (ENSO), and Cold Ocean/Warm Land pattern (COWL) signals from GMST, although uncertainties may have been underestimated because residuals were modelled by a first-order autoregressive processes. A longer observational record and a better understanding of the temporal changes in forcing should make it easier to identify discrepancies between the magnitude of the observed response to a forcing, and the magnitude of the response simulated in individual models. To the extent that inconsistencies between simulated and observed changes are independent between models, this issue may be addressed by basing our assessment on attribution analyses using the mean response from multiple models, and by accounting for model uncertainty when making such assessments.

In conclusion, although some inconsistencies in the forced responses of individual models and observations have been identified, the detection of the global temperature response to GHG increases using average responses from multiple models is robust to observational uncertainty and methodological choices. It is supported by basic physical arguments. We conclude, consistent with Hegerl et al. (2007b), that more than half of the observed increase in GMST from 1951 to 2010 is *very likely* due to the observed anthropogenic increase in GHG concentrations.

The influence of BC aerosols (from fossil and biofuel sources) has been detected in the recent global temperature record in one analysis, although the warming attributable to BC by Jones et al. (2011) is small compared to that attributable to GHG increases. This warming is simulated mainly over the Northern Hemisphere (NH) with a sufficiently distinct spatio-temporal pattern that it could be separated from the response to other forcings in this study.

Several recent studies have used techniques other than regression-based detection and attribution analyses to address the causes of recent global temperature changes. Drost and Karoly (2012) demonstrated that observed GMST, land–ocean temperature contrast, meridional temperature gradient and annual cycle amplitude exhibited trends over the period 1956–2005 that were outside the 5 to 95% range of simulated internal variability in eight CMIP5 models, based on three different observational data sets. They also found that observed trends in GMST and land–ocean temperature contrast were larger than those simulated in any of 36 CMIP5 simulations with natural forcing only. Drost et al. (2012) found that 1961–2010 trends in GMST and land–ocean temperature contrast were significantly larger than simulated internal variability in eight CMIP3 models. By comparing observed GMST with simple statistical models, Zorita et al. (2008) concluded that there is a very low probability that observed clustering of very warm years in the last decade occurred by chance. Smirnov and Mokhov (2009), adopting an approach that allowed them to distinguish between conventional Granger causality and a 'long-term causality' that focuses on low-frequency changes (see Section 10.2), found that increasing $CO_2$ concentrations are the principal determining factor in the rise of GMST over recent decades. Sedlacek and Knutti (2012) found that the spatial patterns of sea surface temperature (SST) trends from simulations forced with increases in GHGs and other anthropogenic forcings agree well with observations but differ from warming patterns associated with internal variability.

Several studies that have aimed to separate forced surface temperature variations from those associated with internal variability have identified the North Atlantic as a dominant centre of multi-decadal

internal variability, and in particular modes of variability related to the Atlantic Multi-decadal Oscillation (AMO; Section 14.7.6). The AMO index is defined as an area average of North Atlantic SSTs, and it has an apparent period of around 70 years, which is long compared to the length of observational record making it difficult to deduce robust conclusions about the role of the AMO from only two cycles. Nevertheless, several studies claim a role for internal variability associated with the AMO in driving enhanced warming in the 1980s and 1990s as well as the recent slow down in warming (Box 9.2), while attributing long-term warming to anthropogenically forced variations either by analysing time series of GMST, forcings and indices of the AMO (Rohde et al., 2013; Tung and Zhou, 2013; Zhou and Tung, 2013a) or by analysing both spatial and temporal patterns of temperature (Swanson et al., 2009; DelSole et al., 2011; Wu et al., 2011). Studies based on global mean time series could risk falsely attributing variability to the AMO when variations in external forcings, for example, associated with aerosols, could also cause similar variability. In contrast, studies using space–time patterns seek to distinguish the spatial structure of temperature anomalies associated with the AMO from those associated with forced variability. Unforced climate simulations indicate that internal multi-decadal variability in the Atlantic is characterized by surface anomalies of the same sign from the equator to the high latitudes, with maximum amplitudes in subpolar regions (Delworth and Mann, 2000; Latif et al., 2004; Knight et al., 2005; DelSole et al., 2011) while the net response to anthropogenic and natural forcing over the 20th century, such as observed temperature change, is characterized by warming nearly everywhere on the globe, but with minimum warming or even cooling in the subpolar regions of the North Atlantic (Figure 10.2; Ting et al., 2009; DelSole et al., 2011).

Some studies implicate tropospheric aerosols in driving decadal variations in Atlantic SST (Evan et al., 2011; Booth et al., 2012; Terray, 2012), and temperature variations in eastern North America (Leibensperger et al., 2012). Booth et al. (2012) find that most multi-decadal variability in North Atlantic SSTs is simulated in one model mainly in response to aerosol variations, although its simulated changes in North Atlantic ocean heat content and salinity have been shown to be inconsistent with observations (Zhang et al., 2012). To the extent that climate models simulate realistic internal variability in the AMO (Section 9.5.3.3.2), AMO variability is accounted for in uncertainty estimates from regression-based detection and attribution studies (e.g., Figure 10.4).

To summarize, recent studies using spatial features of observed temperature variations to separate AMO variability from externally forced changes find that detection of external influence on global temperatures is not compromised by accounting for AMO-congruent variability (*high confidence*). There remains some uncertainty about how much decadal variability of GMST that is attributed to AMO in some studies is actually related to forcing, notably from aerosols. There is agreement among studies that the contribution of the AMO to global warming since 1951 is very small (considerably less than 0.1°C; see also Figure 10.6) and given that observed warming since 1951 is very large compared to climate model estimates of internal variability (Section 10.3.1.1.2), which are assessed to be adequate at global scale (Section 9.5.3.1), we conclude that it is *virtually certain* that internal variability alone cannot account for the observed global warming since 1951.



## Box 10.2 | The Sun's Influence on the Earth's Climate

A number of studies since AR4 have addressed the possible influences of long-term fluctuations of solar irradiance on past climates, particularly related to the relative warmth of the Medieval Climate Anomaly (MCA) and the relative coolness in the Little Ice Age (LIA). There is *medium confidence* that both external solar and volcanic forcing, and internal variability, contributed substantially to the spatial patterns of surface temperature changes between the MCA and the LIA, but *very low confidence* in quantitative estimates of their relative contributions (Sections 5.3.5.3 and 5.5.1). The combined influence of volcanism, solar forcing and a small drop in greenhouse gases (GHGs) *likely* contributed to Northern Hemisphere cooling during the LIA (Section 10.7.2). Solar radiative forcing (RF) from the Maunder Minimum (1745) to the satellite era (average of 1976–2006) has been estimated to be +0.08 to +0.18 W $m^{-2}$ (*low confidence*, Section 8.4.1.2). This may have contributed to early 20th century warming (*low confidence*, Section 10.3.1).

More recently, it is *extremely unlikely* that the contribution from solar forcing to the observed global warming since 1950 was larger than that from GHGs (Section 10.3.1.1.3). It is *very likely* that there has been a small decrease in solar forcing of –0.04 [–0.08 to 0.00] W $m^{-2}$ over a period with direct satellite measurements of solar output from 1986 to 2008 (Section 8.4.1.1). There is *high confidence* that changes in total solar irradiance have not contributed to global warming during that period.

Since AR4, there has been considerable new research that has connected solar forcing to climate. The effect of solar forcing on GMST trends has been found to be small, with less than 0.1°C warming attributable to combined solar and volcanic forcing over the 1951–2010 period (Section 10.3.1), although the 11-year cycle of solar variability has been found to have some influence on GMST variability over the 20th century. GMST changes between solar maxima and minima are estimated to be of order 0.1°C from some regression studies of GMST and forcing estimates (Figure 10.6), although several studies have suggested these results may be too large owing to issues including degeneracy between forcing and with internal variability, overfitting of forcing indices and underestimated uncertainties in responses (Ingram, 2007; Benestad and Schmidt, 2009; Stott and Jones, 2009). Climate models generally show less than half this variability (Jones et al., 2012). *(continued on next page)*

*Box 10.2 (continued)*

Variability associated with the 11-year solar cycle has also been shown to produce measurable short-term regional and seasonal climate anomalies (Miyazaki and Yasunari, 2008; Gray et al., 2010; Lockwood, 2012; National Research Council, 2012) particularly in the Indo-Pacific, Northern Asia and North Atlantic regions (*medium evidence*). For example, studies have suggested an 11-year solar response in the Indo-Pacific region in which the equatorial eastern Pacific sea surface temperatures (SSTs) tend to be below normal, the sea level pressure (SLP) in the Gulf of Alaska and the South Pacific above normal, and the tropical convergence zones on both hemispheres strengthened and displaced polewards under solar maximum conditions, although it can be difficult to discriminate the solar-forced signal from the El Niño-Southern Oscillation (ENSO) signal (van Loon et al., 2007; van Loon and Meehl, 2008; White and Liu, 2008; Meehl and Arblaster, 2009; Roy and Haigh, 2010, 2012; Tung and Zhou, 2010; Bal et al., 2011; Haam and Tung, 2012; Hood and Soukharev, 2012; Misios and Schmidt, 2012). For northern summer, there is evidence that for peaks in the 11-year solar cycle, the Indian monsoon is intensified (Kodera, 2004; van Loon and Meehl, 2012), with solar variability affecting interannual connections between the Indian and Pacific sectors due to a shift in the location of the descending branch of the Walker Circulation (Kodera et al., 2007). In addition, model sensitivity experiments (Ineson et al., 2011) suggest that the negative phase of the North Atlantic Oscillation (NAO) is more prevalent during solar minima and there is some evidence of this in observations, including an indication of increased frequency of high-pressure 'blocking' events over Europe in winter (Barriopedro et al., 2008; Lockwood et al., 2010; Woollings et al., 2010).

Two mechanisms have been identified in observations and simulated with climate models that could explain these low amplitude regional responses (Gray et al., 2010; *medium evidence*). These mechanisms are additive and may reinforce one another so that the response to an initial small change in solar irradiance is amplified regionally (Meehl et al., 2009). The first mechanism is a top-down mechanism first noted by Haigh (1996) where greater solar ultraviolet radiation (UV) in peak solar years warms the stratosphere directly via increased radiation and indirectly via increased ozone production. This can result in a chain of processes that influences deep tropical convection (Balachandran et al., 1999; Shindell et al., 1999; Kodera and Kuroda, 2002; Haigh et al., 2005; Kodera, 2006; Matthes et al., 2006). In addition, there is less heating than average in the tropical upper stratosphere under solar minimum conditions which weakens the equator-to-pole temperature gradient. This signal can propagate downward to weaken the tropospheric mid-latitude westerlies, thus favoring a negative phase of the Arctic Oscillation (AO) or NAO. This response has been shown in several models (e.g., Shindell et al., 2001; Ineson et al., 2011) though there is no significant AO or NAO response to solar irradiance variations on average in the CMIP5 models (Gillett and Fyfe, 2013).

The second mechanism is a bottom-up mechanism that involves coupled air–sea radiative processes in the tropical and subtropical Pacific that also influence convection in the deep tropics (Meehl et al., 2003, 2008; Rind et al., 2008; Bal et al., 2011; Cai and Tung, 2012; Zhou and Tung, 2013b). Such mechanisms have also been shown to influence regional temperatures over longer time scales (decades to centuries), and can help explain patterns of regional temperature changes seen in paleoclimate data (e.g., Section 10.7.2; Mann et al., 2009; Goosse et al., 2012b) although they have little effect on global or hemispheric mean temperatures at either short or long time scales.

A possible amplifying mechanism linking solar variability and the Earth's climate system via cosmic rays has been postulated. It is proposed that variations in the cosmic ray flux associated with changes in solar magnetic activity affect ion-induced aerosol nucleation and cloud condensation nuclei (CCN) production in the troposphere (Section 7.4.6). A strong solar magnetic field would deflect cosmic rays and lead to fewer CCN and less cloudiness, thereby allowing for more solar energy into the system. Since AR4, there has been further evidence to disprove the importance of this amplifying mechanism. Correlations between cosmic ray flux and observed aerosol or cloud properties are weak and local at best, and do not prove to be robust on the regional or global scale (Section 7.4.6). Although there is some evidence that ionization from cosmic rays may enhance aerosol nucleation in the free troposphere, there is *medium evidence and high agreement* that the cosmic ray–ionization mechanism is too weak to influence global concentrations of CCN or their change over the last century or during a solar cycle in any climatically significant way (Sections 7.4.6 and 8.4.1.5). The lack of trend in cosmic ray intensity over the 1960–2005 period (McCracken and Beer, 2007) provides another argument against the hypothesis of a major contribution of cosmic ray variations to the observed warming over that period given the existence of short time scales in the climate system response.

Thus, although there is *medium confidence* that solar variability has made contributions to past climate fluctuations, since the mid-20th century there has been little trend in solar forcing. There are at least two amplifying mechanisms that have been proposed and simulated in some models that could explain small observed regional and seasonal climate anomalies associated with the 11-year solar cycle, mostly in the Indo-Pacific region and northern mid to high latitudes.

Regarding possible future influences of the sun on the Earth's climate, there is *very low confidence* in our ability to predict future solar output, but there is *high confidence* that the effects from solar irradiance variations will be much smaller than the projected climate changes from increased RF due to GHGs (Sections 8.4.1.3 and 11.3.6.2.2).

Based on a range of detection and attribution analyses using multiple solar irradiance reconstructions and models, Hegerl et al. (2007b) concluded that it is *very likely* that GHGs caused more global warming than solar irradiance variations over the 1950–1999 period. Detection and attribution analyses applied to the CMIP5 simulations (Figure 10.4) indicate less than 0.1°C temperature change attributable to combined solar and volcanic forcing over the 1951–2010 period. Based on a regression of paleo temperatures onto the response to solar forcing simulated by an energy balance model, Scafetta and West (2007) find that up to 50% of the warming since 1900 may be solar-induced, but Benestad and Schmidt (2009) show this conclusion is not robust, being based on disregarding forcings other than solar in the preindustrial period, and assuming a high and precisely known value for climate sensitivity. Despite claims that more than half the warming since 1970 can be ascribed to solar variability (Loehle and Scaffetta, 2011) , a conclusion based on an incorrect assumption of no anthropogenic influence before 1950 and a 60-year solar cycle influence on global temperature (see also Mazzarella and Scafetta, 2012), several studies show that solar variations cannot explain global mean surface warming over the past 25 years, because solar irradiance has declined over this period (Lockwood and Fröhlich, 2007, 2008; Lockwood, 2008, 2012 ). Lean and Rind (2008) conclude that solar forcing explains only 10% of the warming over the past 100 years, while contributing a small cooling over the past 25 years. Thus while there is some evidence for solar influences on regional climate variability (Box 10.2) solar forcing has only had a small effect on GMST. Overall, we conclude that it is *extremely unlikely* that the contribution from solar forcing to the warming since 1950 was larger than that from GHGs.

A range of studies have used statistical methods to separate out the influence of known sources of internal variability, including ENSO and, in some cases, the AMO, from the response to external drivers, including volcanoes, solar variability and anthropogenic influence, in the recent GMST record: see, for example, Lockwood (2008), Lean and Rind (2009), Folland et al. (2013 ), Foster and Rahmstorf (2011) and Kaufmann et al. (2011). Representative results, as summarized in Imbers et al. (2013), are shown in Figure 10.6. These consistently attribute most of the warming over the past 50 years to anthropogenic influence, even allowing for potential confounding factors like the AMO. While results of such statistical approaches are sensitive to assumptions regarding the properties of both responses to external drivers and internal variability (Imbers et al., 2013), they provide a complementary approach to attribution studies based on global climate models.

Overall, given that the anthropogenic increase in GHGs *likely* caused 0.5°C to 1.3°C warming over 1951–2010, with other anthropogenic forcings probably contributing counteracting cooling, that the effects of natural forcings and natural internal variability are estimated to be small, and that well-constrained and robust estimates of net anthropogenic warming are substantially more than half the observed warming (Figure 10.4) we conclude that it is *extremely likely* that human activities caused more than half of the observed increase in GMST from 1951 to 2010.

### The early 20th century warming

The instrumental GMST record shows a pronounced warming during the first half of the 20th century (Figure 10.1a). Correction of residual biases in SST observations leads to a higher estimate of 1950s temperatures, but does not substantially change the warming between 1900 and 1940 (Morice et al., 2012). The AR4 concluded that 'the early 20th century warming is *very likely* in part due to external forcing' (Hegerl et al., 2007b), and that it is *likely* that anthropogenic forcing contributed to this warming. This assessment was based on studies including Shiogama et al. (2006) who find a contribution from solar and volcanic forcing to observed warming to 1949, and Min and Hense (2006), who find strong evidence for a forced (either natural or combined natural and anthropogenic) contribution to global warming from 1900 to 1949. Ring et al. (2012) estimate, based on time series analysis, that part of the early 20th century warming was due to GHG increases (see also Figure 10.6), but find a dominant contribution by internal variability. CMIP5 model simulations of the historical period show forced warming over the early 20th century (Figure 10.1a), consistent with earlier detection and attribution analyses highlighted in the AR4 and TAR. The early 20th century contributes to the detection of external forcings over the 20th century estimated by detection and attribution results (Figure 10.4; Gillett et al., 2013; Ribes and Terray, 2013) and to the detected change over the last millennium to 1950 (see Figure 10.19; Schurer et al., 2013).

The pattern of warming and residual differences between models and observations indicate a role for circulation changes as a contributor to early 20th cenury warming (Figure 10.2), and the contribution of internal variability to the early 20th century warming has been analysed in several publications since the AR4. Crook and Forster (2011) find that the observed 1918–1940 warming was significantly greater than that simulated by most of the CMIP3 models. A distinguishing feature of the early 20th century warming is its pattern (Brönnimann, 2009) which shows the most pronounced warming in the Arctic during the cold season, followed by North America during the warm season, the North Atlantic Ocean and the tropics. In contrast, there was no unusual warming in Australia among other regions (see Figure 10.2b). Such a pronounced pattern points to a role for circulation change as a contributing factor to the regional anomalies contributing to this warming. Some studies have suggested that the warming is a response to the AMO (Schlesinger and Ramankutty, 1994; Polyakov et al., 2005; Knight et al., 2006; Tung and Zhou, 2013), or a large but random expression of internal variability (Bengtsson et al., 2006; Wood and Overland, 2010). Knight et al. (2009) diagnose a shift from the negative to the positive phase of the AMO from 1910 to 1940, a mode of circulation that is estimated to contribute approximately 0.1°C, trough to peak, to GMST (Knight et al., 2005). Nonetheless, these studies do not challenge the AR4 assessment that external forcing *very likely* made a contribution to the warming over this period. In conclusion, the early 20th century warming is *very unlikely* to be due to internal variability alone. It remains difficult to quantify the contribution to this warming from internal variability, natural forcing and anthropogenic forcing, due to forcing and response uncertainties and incomplete observational coverage.

### Year-to-year and decade-to-decade variability of global mean surface temperature

Time series analyses, such as those shown in Figure 10.6, seek to partition the variability of GMST into components attributable to anthropogenic and natural forcings and modes of internal variability such as ENSO and the AMO. Although such time series analyses support

the major role of anthropogenic forcings, particularly due to increasing GHG concentrations, in contributing to the overall warming over the last 60 years, many factors, in addition to GHGs, including changes in tropospheric and stratospheric aerosols, stratospheric water vapour and solar output, as well as internal modes of variability, contribute to the year-to-year and decade-to-decade variability of GMST (Figure 10.6). Detailed discussion of the evolution of GMST of the past 15 years since 1998 is contained in Box 9.2.

#### 10.3.1.1.4 Attribution of regional surface temperature change

Anthropogenic influence on climate has been robustly detected on the global scale, but for many applications an estimate of the anthropogenic contribution to recent temperature trends over a particular region is more useful. However, detection and attribution of climate change at continental and smaller scales is more difficult than on the global scale for several reasons (Hegerl et al., 2007b; Stott et al., 2010).

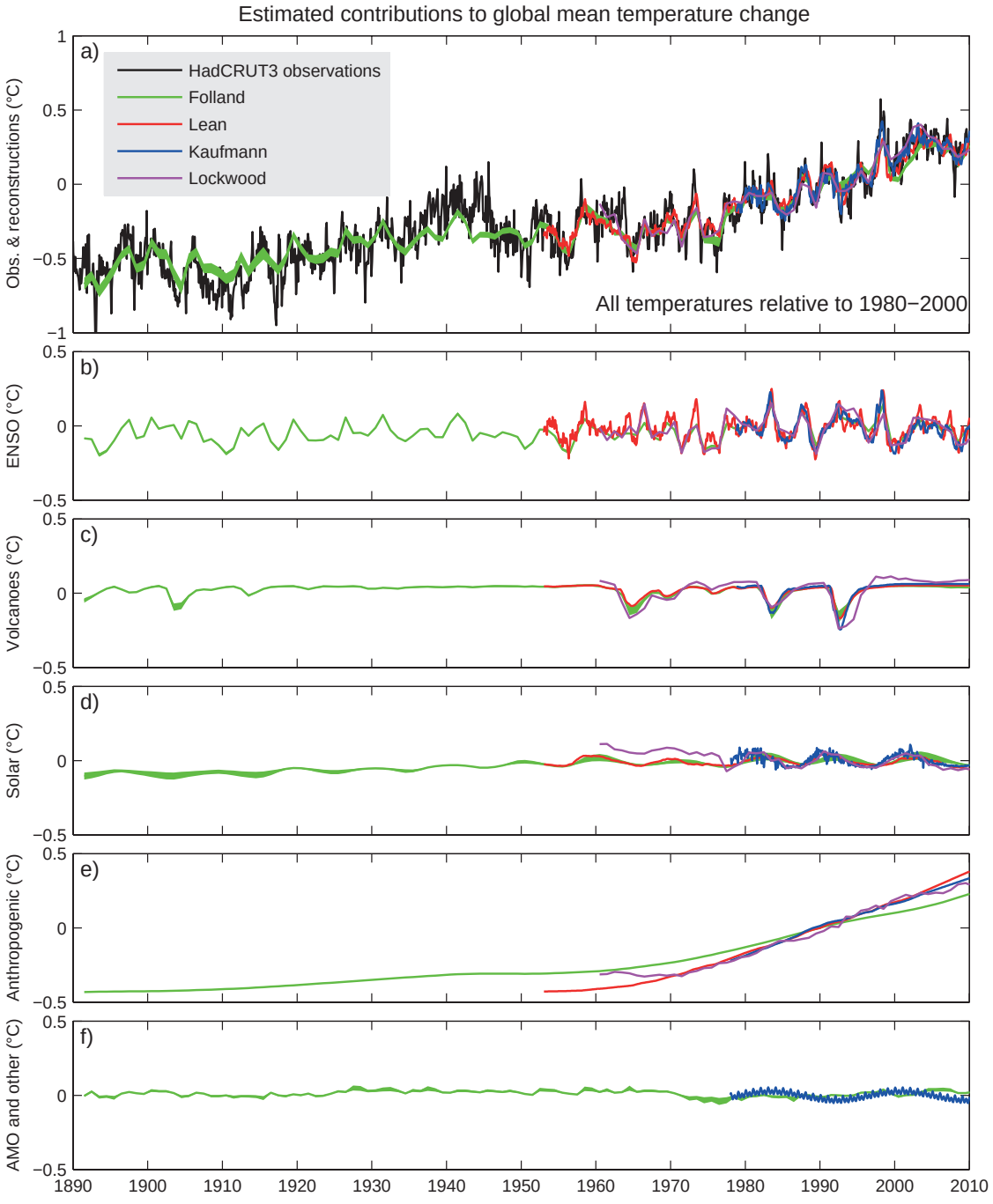


**Figure 10.6 |** (Top) The variations of the observed global mean surface temperature (GMST) anomaly from Hadley Centre/Climatic Research Unit gridded surface temperature data set version 3 (HadCRUT3, black line) and the best multivariate fits using the method of Lean (red line), Lockwood (pink line), Folland (green line) and Kaufmann (blue line). (Below) The contributions to the fit from (a) El Niño-Southern Oscillation (ENSO), (b) volcanoes, (c) solar forcing, (d) anthropogenic forcing and (e) other factors (Atlantic Multi-decadal Oscillation (AMO) for Folland and a 17.5-year cycle, semi-annual oscillation (SAO), and Arctic Oscillation (AO) from Lean). (From Lockwood (2008), Lean and Rind (2009), Folland et al. (2013 ) and Kaufmann et al. (2011), as summarized in Imbers et al. (2013).)

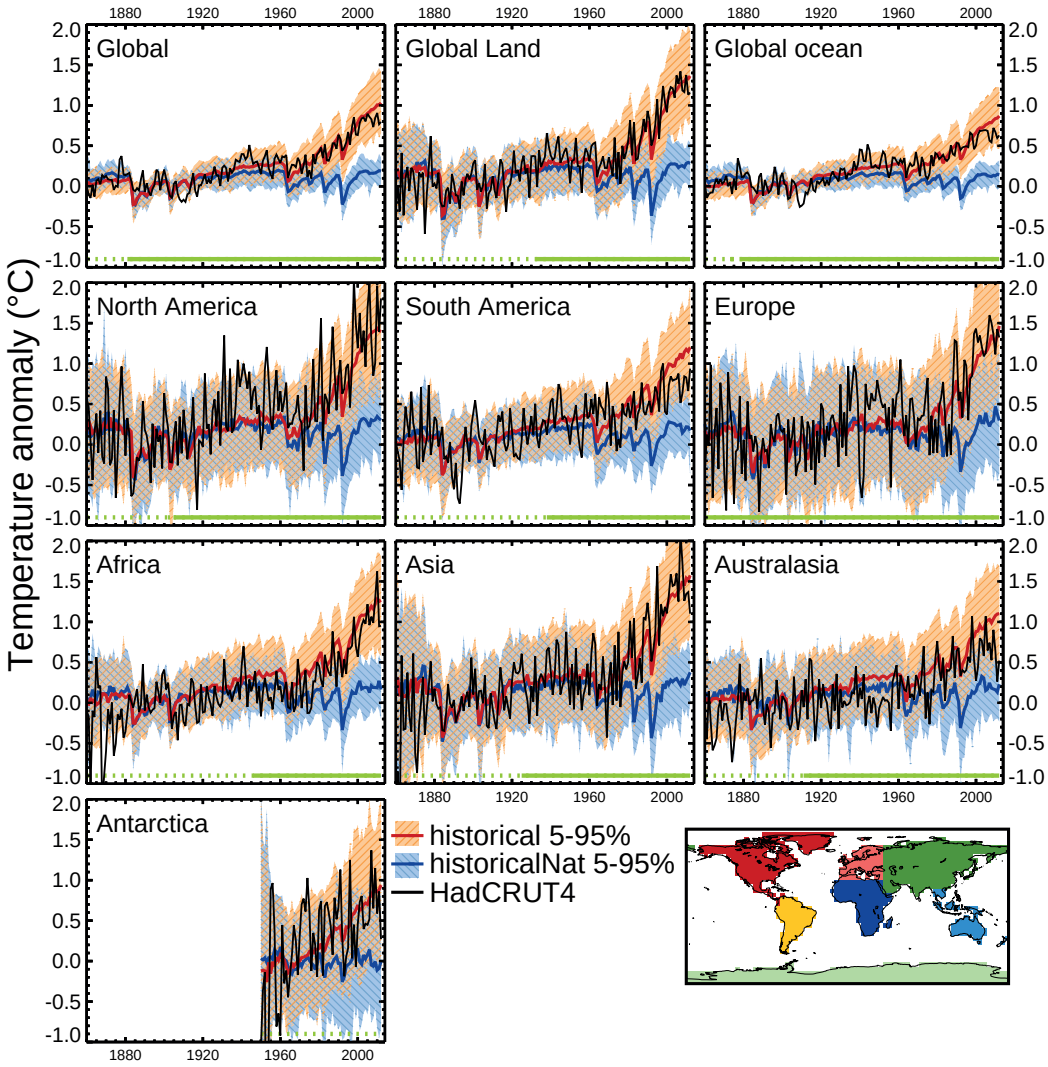


**Figure 10.7 |** Global, land, ocean and continental annual mean temperatures for CMIP3 and CMIP5 historical (red) and historicalNat (blue) simulations (multi-model means shown as thick lines, and 5 to 95% ranges shown as thin light lines) and for Hadley Centre/Climatic Research Unit gridded surface temperature data set 4 (HadCRUT4, black). Mean temperatures are shown for Antarctica and six continental regions formed by combining the sub-continental scale regions defined by Seneviratne et al. (2012). Temperatures are shown with respect to 1880–1919 for all regions apart from Antarctica where temperatures are shown with respect to 1950–2010. (Adapted from Jones et al., 2013.)

First, the relative contribution of internal variability compared to the forced response to observed changes tends to be larger on smaller scales, as spatial differences in internal variations are averaged out in large-scale means. Second, because the patterns of response to climate forcings tend to be large scale, there is less spatial information to help distinguish between the responses to different forcings when attention is restricted to a sub-global area. Third, forcings omitted in some global climate model simulations may be important on regional scales, such as land use change or BC aerosol. Lastly, simulated internal variability and responses to forcings may be less reliable on smaller scales than on the global scale. Knutson et al. (2013) find a tendency for CMIP5 models to overestimate decadal variability in the NH extratropics in individual grid cells and underestimate it elsewhere, although Karoly and Wu (2005) and Wu and Karoly (2007) find that variability is not generally underestimated in earlier generation models.

Based on several studies, Hegerl et al. (2007b) concluded that 'it is *likely* that there has been a substantial anthropogenic contribution to surface temperature increases in every continent except Antarctica since the middle of the 20th century'. Figure 10.7 shows comparisons of observed continental scale temperatures (Morice et al., 2012) with CMIP5 simulations including both anthropogenic and natural forcings (red lines) and including just natural forcings (blue lines). Observed temperatures are largely within the range of simulations with anthropogenic forcings for all regions and outside the range of simulations with only natural forcings for all regions except Antarctica (Jones et al., 2013 ). Averaging over all observed locations, Antarctica has warmed over the 1950–2008 period (Section 2.4.1.1; Gillett et al., 2008b; Jones et al., 2013 ), even though some individual locations have cooled, particularly in summer and autumn, and over the shorter 1960–1999 period (Thompson and Solomon, 2002; Turner et al., 2005). When temperature changes associated with changes in the Southern Annular Mode are removed by regression, both observations and model simulations indicate warming at all observed locations except the South Pole over the 1950–1999 period (Gillett et al., 2008b). An analysis of Antarctic land temperatures over the period 1950–1999

detected separate natural and anthropogenic responses of consistent magnitude in simulations and observations (Gillett et al., 2008b). Thus anthropogenic influence on climate has now been detected on all seven continents. However the evidence for human influence on Antarctic temperature is much weaker than for the other six continental regions. There is only one attribution study for this region, and there is greater observational uncertainty than the other regions, with very few data before 1950, and sparse coverage that is mainly limited to the coast and the Antarctic Peninsula. As a result of the observational uncertainties, there is *low confidence* in Antarctic region land surface air temperatures changes (Section 2.4.1.1) and we conclude for Antarctica there is *low confidence* that anthropogenic influence has contributed to the observed warming averaged over available stations.

Since the publication of the AR4 several other studies have applied attribution analyses to continental and sub-continental scale regions. Min and Hense (2007) applied a Bayesian decision analysis technique to continental-scale temperatures using the CMIP3 multi-model ensemble and concluded that forcing combinations including GHG increases provide the best explanation of 20th century observed changes in temperature on every inhabited continent except Europe, where the observational evidence is not decisive in their analysis. Jones et al. (2008) detected anthropogenic influence on summer temperatures over all NH continents and in many subcontinental NH land regions in an optimal detection analysis that considered the temperature responses to anthropogenic and natural forcings. Christidis et al. (2010) used a multi-model ensemble constrained by global-scale observed temperature changes to estimate the changes in probability of occurrence of warming or cooling trends over the 1950–1997 period over various sub-continental scale regions. They concluded that the probability of occurrence of warming trends had been at least doubled by anthropogenic forcing over all such regions except Central North America. The estimated distribution of warming trends over the Central North America region was approximately centred on the observed trend, so no inconsistency between simulated and observed trends was identified there. Knutson et al. (2013) demonstrated that observed temperature trends from the beginning of the observational record to 2010 averaged over Europe, Africa, Northern Asia, Southern Asia, Australia and South America are all inconsistent with the simulated response to natural forcings alone, and consistent with the simulated response to combined natural and anthropogenic forcings in the CMIP5 models. They reached a similar conclusion for the major ocean basins with the exception of the North Atlantic, where variability is high.

Several recent studies have applied attribution analyses to specific sub-continental regions. Anthropogenic influence has been found in winter minimum temperature over the western USA (Bonfils et al., 2008; Pierce et al., 2009), a conclusion that is found to be robust to weighting models according to various aspects of their climatology (Pierce et al., 2009); anthropogenic influence has been found in temperature trends over New Zealand (Dean and Stott, 2009) after circulation-related variability is removed as in Gillett et al. (2000); and anthropogenic influence has been found in temperature trends over France, using a first-order autoregressive model of internal variability (Ribes et al., 2010). Increases in anthropogenic GHGs were found to be the main driver of the 20th-century SST increases in both Atlantic and Pacific tropical cyclogenesis regions (Santer et al., 2006; Gillett et al., 2008a). Over both regions, the response to anthropogenic forcings is detected when the response to natural forcings is also included in the analysis (Gillett et al., 2008a). Knutson et al. (2013) detect an anthropogenic influence over Canada, but not over the continental USA, Alaska or Mexico.

Gillett et al. (2008b) detect anthropogenic influence on near-surface Arctic temperatures over land, with a consistent magnitude in simulations and observations. Wang et al. (2007) also find that observed Arctic warming is inconsistent with simulated internal variability. Both studies ascribe Arctic warmth in the 1930s and 1940s largely to internal variability. Shindell and Faluvegi (2009) infer a large contribution to both mid-century Arctic cooling and late century warming from aerosol forcing changes, with GHGs the dominant driver of long-term warming, though they infer aerosol forcing changes from temperature changes using an inverse approach which may lead to some changes associated with internal variability being attributed to aerosol forcing. We therefore conclude that despite the uncertainties introduced by limited observational coverage, high internal variability, modelling uncertainties (Crook et al., 2011) and poorly understood local forcings, such as the effect of BC on snow, there is sufficiently strong evidence to conclude that it is *likely* that there has been an anthropogenic contribution to the very substantial warming in Arctic land surface temperatures over the past 50 years.

Some attribution analyses have considered temperature trends at the climate model grid box scale. At these spatial scales robust attribution is difficult to obtain, since climate models often lack the processes needed to simulate regional details realistically, regionally important forcings may be missing in some models and observational uncertainties are very large for some regions of the world at grid box scale (Hegerl et al., 2007b; Stott et al., 2010). Nevertheless an attribution analysis has been carried out on Central England temperature, a record that extends back to 1659 and is sufficiently long to demonstrate that the representation of multi-decadal variability in the single grid box in the model used, Hadley Centre climate prediction model 3 (HadCM3) is adequate for detection (Karoly and Stott, 2006). The observed trend in Central England Temperature is inconsistent with either internal variability or the simulated response to natural forcings, but is consistent with the simulated response when anthropogenic forcings are included (Karoly and Stott, 2006).

Observed 20th century grid cell trends from Hadley Centre/Climatic Research Unit gridded surface temperature data set 2v (HadCRUT2v; Jones et al., 2001) are inconsistent with simulated internal variability at the 10% significance level in around 80% of grid cells even using HadCM2 which was found to overestimate variability in 5-year mean temperatures at most latitudes (Karoly and Wu, 2005). Sixty percent of grid cells were found to exhibit significant warming trends since 1951, a much larger number than expected by chance (Karoly and Wu, 2005; Wu and Karoly, 2007), and similar results apply when circulation-related variability is first regressed out (Wu and Karoly, 2007). However, as discussed in the AR4 (Hegerl et al., 2007b), when a global field significance test is applied, this becomes a global detection study; since not all grid cells exhibit significant warming trends the overall interpretation of the results in terms of attribution at individual locations remains problematic. Mahlstein et al. (2012) find significant changes in summer season temperatures in about 40% of low-latitude and about 20% of

extratropical land grid cells with sufficient observations, when testing against the null hypothesis of no change in the distribution of summer temperatures. Observed grid cell trends are compared with CMIP5 simulated trends in Figure 10.2i, which shows that in the great majority (89%) of grid cells with sufficient observational coverage, observed trends over the 1901–2010 period are inconsistent with a combination of simulated internal variability and the response to natural forcings (Jones et al., 2013). Knutson et al. (2013) find some deficiencies in the simulation of multi-decadal variability at the grid cell scale in CMIP5 models, but demonstrate that trends at more than 75% of individual grid cells with sufficient observational coverage in HadCRUT4 are inconsistent with the simulated response to natural forcings alone, and consistent or larger than the simulated response to combined anthropogenic and natural forcings in CMIP5 models.

In summary, it is *likely* that anthropogenic forcing has made a substantial contribution to the warming of each of the inhabited continents since 1950. For Antarctica large observational uncertainties result in *low confidence* that anthropogenic influence has contributed to the observed warming averaged over available stations. Anthropogenic influence has *likely* contributed to temperature change in many sub-continental regions. Detection and attribution of climate change at continental and smaller scales is more difficult than at the global scale due to the greater contribution of internal variability, the greater difficulty of distinguishing between different causal factors, and greater errors in climate models' representation of regional details. Nevertheless, statistically significant warming trends are observed at a majority of grid cells, and the observed warming is inconsistent with estimates of possible warming due to natural causes at the great majority of grid cells with sufficient observational coverage.

#### 10.3.1.2 Atmosphere

This section presents an assessment of the causes of global and regional temperature changes in the free atmosphere. In AR4, Hegerl et al. (2007b) concluded that 'the observed pattern of tropospheric warming and stratospheric cooling is *very likely* due to the influence of anthropogenic forcing, particularly greenhouse gases and stratospheric ozone depletion.' Since AR4, insight has been gained into regional aspects of free tropospheric trends and the causes of observed changes in stratospheric temperature.

Atmospheric temperature trends through the depth of the atmosphere offer the possibility of separating the effects of multiple climate forcings, as climate model simulations indicate that each external forcing produces a different characteristic vertical and zonal pattern of temperature response (Hansen et al., 2005b; Hegerl et al., 2007b; Penner et al., 2007; Yoshimori and Broccoli, 2008). GHG forcing is expected to warm the troposphere and cool the stratosphere. Stratospheric ozone depletion cools the stratosphere, with the cooling being most pronounced in the polar regions. Its effect on tropospheric temperatures is small, which is consistent with a small estimated RF of stratospheric ozone changes (SPARC CCMVal, 2010; McLandress et al., 2012). Tropospheric ozone increase, on the other hand, causes tropospheric warming. Reflective aerosols like sulphate cool the troposphere while absorbing aerosols like BC have a warming effect. Free atmosphere temperatures are also affected by natural forcings: solar irradiance increases cause a general warming of the atmosphere and volcanic aerosol ejected into the stratosphere causes tropospheric cooling and stratospheric warming (Hegerl et al., 2007b).

##### 10.3.1.2.1 Tropospheric temperature change

Chapter 2 concludes that it is *virtually certain* that globally the troposphere has warmed since the mid-twentieth century with only *medium* (NH extratropics) to *low confidence* (tropics and SH extratropics) in the rate and vertical structure of these changes. During the satellite era CMIP3 and CMIP5 models tend to warm faster than observations specifically in the tropics (McKitrick et al., 2010; Fu et al., 2011; Po-Chedley and Fu, 2012; Santer et al., 2013); however, because of the large uncertainties in observed tropical temperature trends (Section 2.4.4; Seidel et al. (2012); Figures 2.26 and Figure 2.27) there is only *low confidence* in this assessment (Section 9.4.1.4.2). Outside the tropics, and over the period of the radiosonde record beginning in 1961, the discrepancy between simulated and observed trends is smaller (Thorne et al., 2011; Lott et al., 2013; Santer et al., 2013). Specifically there is better agreement between observed trends and CMIP5 model trends for the NH extratropics (Lott et al., 2013). Factors other than observational uncertainties that contribute to inconsistencies between observed and simulated free troposphere warming include specific manifestation of natural variability in the observed coupled atmosphere–ocean system, forcing errors incorporated in the historical simulations and model response errors (Santer et al., 2013).

Utilizing a subset of CMIP5 models with single forcing experiments extending until 2010, Lott et al. (2013) detect influences of both human induced GHG increase and other anthropogenic forcings (e.g., ozone and aerosols) in the spatio-temporal changes in tropospheric temperatures from 1961 to 2010 estimated from radiosonde observations. Figure 10.8 illustrates that a subsample of CMIP5 models (see Supplementary Material for model selection) forced with both anthropogenic and natural climate drivers (red profiles) exhibit trends that are consistent with radiosonde records in the troposphere up to about 300 hPa, albeit with a tendency for this subset of models to warm more than the observations. This finding is seen in near-globally averaged data (where there is sufficient observational coverage to make a meaningful comparison: 60°S to 60°N) (right panel), as well as in latitudinal bands of the SH extratropics (Figure 10.8, first panel), tropics (Figure 10.8, second panel) and the NH extratropics (Figure 10.8, third panel). Figure 10.8 also illustrates that it is *very unlikely* that natural forcings alone could have caused the observed warming of tropospheric temperatures (blue profiles). The ensembles with both anthropogenic and natural forcings (red) and with GHG forcings only (green) are not clearly separated. This could be due to cancellation of the effects of increases in reflecting aerosols, which cool the troposphere, and absorbing aerosol (Penner et al., 2007) and tropospheric ozone, which both warm the troposphere. Above 300 hPa the three radiosonde data sets exhibit a larger spread as a result of larger uncertainties in the observational record (Thorne et al., 2011; Section 2.4.4). In this region of the upper troposphere simulated CMIP5 temperature trends tend to be more positive than observed trends (Figure 10.8). Further, an assessment of causes of observed trends in the upper troposphere is less confident than an assessment of overall atmospheric temperature changes because of observational uncertainties and potential remain-

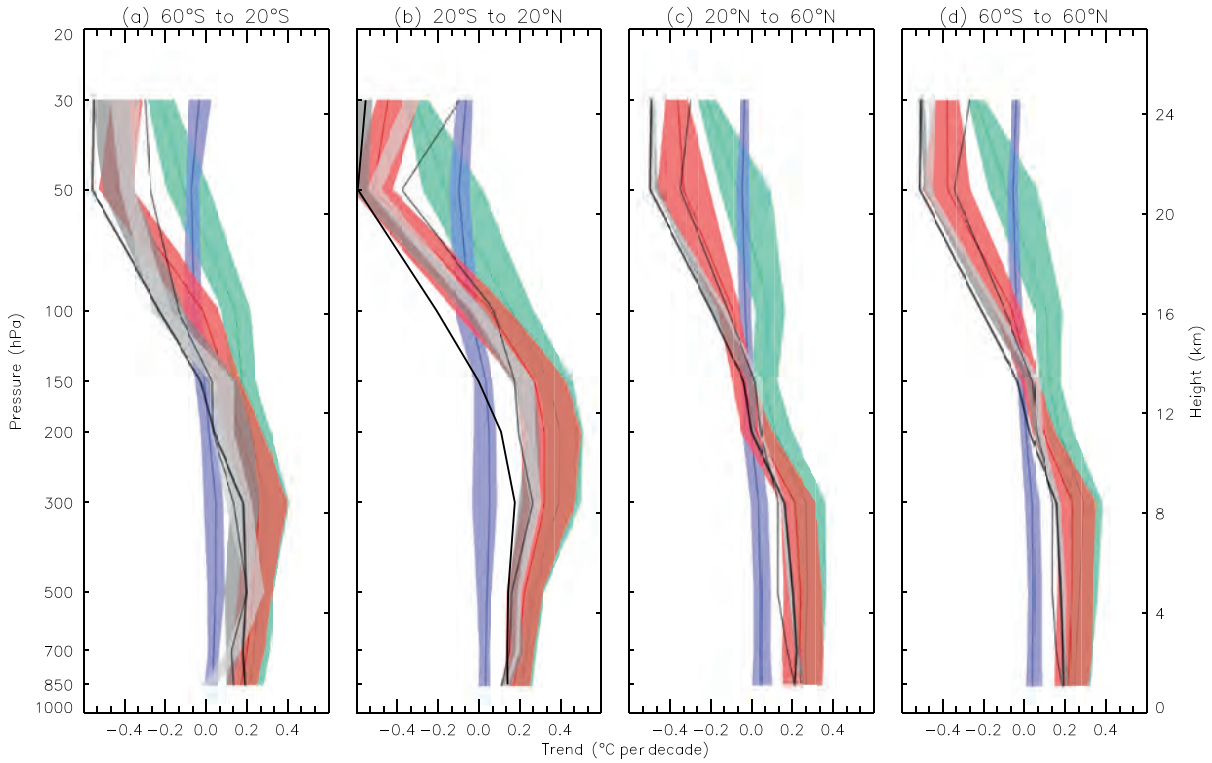


**Figure 10.8 |** Observed and simulated zonal mean temperatures trends from 1961 to 2010 for CMIP5 simulations containing both anthropogenic and natural forcings (red), natural forcings only (blue) and greenhouse gas forcing only (green) where the 5 to 95th percentile ranges of the ensembles are shown. Three radiosonde observations are shown (thick black line: Hadley Centre Atmospheric Temperature data set 2 (HadAT2), thin black line: RAdiosone OBservation COrrection using REanalyses 1.5 (RAOBCORE 1.5), dark grey band: Radiosonde Innovation Composite Homogenization (RICH)-obs 1.5 ensemble and light grey: RICH- $\tau$ 1.5 ensemble. (After Lott et al., 2013.)

ing systematic biases in observational data sets in this region (Thorne et al., 2011; Haimberger et al., 2012). An analysis of contributions of natural and anthropogenic forcings to more recent trends from 1979 to 2010 (Supplementary Material, Figure S.A.1) is less robust because of increased uncertainty in observed trends (consistent with Seidel et al. (2012)) as well as decreased capability to separate between individual forcings ensembles.

One approach to identify a climate change signal in a time series is the analysis of the ratio between the amplitude of the observed signal of change divided by the magnitude of internal variability, in other words the S/N ratio of the data record. The S/N ratio represents the result of a non-optimal fingerprint analysis (in contrast to optimal fingerprint analyses where model-simulated responses and observations are normalized by internal variability to improve the S/N ratio (see Section 10.2.3). For changes in the lower stratospheric temperature between 1979 and 2011, S/N ratios vary from 26 to 36, depending on the choice of observational data set. In the lower troposphere, the fingerprint strength in observations is smaller, but S/N ratios are still significant at the 1% level or better, and range from 3 to 8. There is no evidence that these ratios are spuriously inflated by model variability errors. After all global mean signals are removed, model fingerprints remain identifiable in 70% of the tests involving tropospheric temperature changes (Santer et al., 2013).

Hegerl et al. (2007a) concluded that increasing GHGs are the main cause for warming of the troposphere. This result is supported by a subsample of CMIP5 models that also suggest that the warming effect of well mixed GHGs is partly offset by the combined effects of reflecting aerosols and other forcings. Our understanding has been increased regarding the time scale of detectability of global scale troposphere temperature. Taken together with increased understanding of the uncertainties in observational records of tropospheric temperatures (including residual systematic biases; Section 2.4.4) the assessment remains as it was for AR4 that it is *likely* that anthropogenic forcing has led to a detectable warming of tropospheric temperatures since 1961.

#### 10.3.1.2.2 Stratospheric temperature change

Lower stratospheric temperatures have not evolved uniformly over the period since 1958 when the stratosphere has been observed with sufficient regularity and spatial coverage. A long-term global cooling trend is interrupted by three 2-year warming episodes following large volcanic eruptions (Section 2.4.4). During the satellite period the cooling evolved mainly in two steps occurring in the aftermath of the El Chichón eruption in 1982 and the Mt Pinatubo eruption of 1991, with each cooling transition being followed by a period of relatively steady temperatures (Randel et al., 2009; Seidel et al., 2011). Since the mid-1990s little net change has occurred in lower stratospheric temperatures (Section 2.4.4).

Since AR4, progress has been made in simulating the observed evolution of global mean lower stratospheric temperature. On the one hand, this has been achieved by using models with an improved

representation of stratospheric processes (chemistry–climate models and some CMIP5 models). It is found that in these models which have an upper boundary above the stratopause with an altitude of about 50 km (so-called high-top models) and improved stratospheric physics, variability of lower stratosphere climate in general is well simulated (Butchart et al., 2011; Gillett et al., 2011; Charlton-Perez et al., 2013) whereas in so-called low-top models (including models participating in CMIP3) it is generally underestimated (Cordero and Forster, 2006; Charlton-Perez et al., 2013). On the other hand, CMIP5 models all include changes in stratospheric ozone (Eyring et al., 2013) whereas only about half of the models participating in CMIP3 include stratospheric ozone changes (Section 9.4.1.4.5). A comparison of a low-top and high-top version of the HadGEM2 model shows detectable differences in modelled temperature changes, particularly in the lower tropical stratosphere, with the high-top version's simulation of temperature trends in the tropical troposphere in better agreement with radiosondes and reanalyses over 1981–2010 (Mitchell et al., 2013).

CMIP5 models forced with changes in WMGHGs and stratospheric ozone as well as with changes in solar irradiance and volcanic aerosol forcings simulate the evolution of observed global mean lower stratospheric temperatures over the satellite era reasonably well although they tend to underestimate the long-term cooling trend (Charlton-Perez et al., 2013; Santer et al., 2013). Compared with radiosonde data the cooling trend is also underestimated in a subset of CMIP5 simulations over the period 1961–2010 (Figure 10.8) and in CMIP3 models over the 1958–1999 period (Cordero and Forster, 2006). Potential causes for biases in lower stratosphere temperature trends are observational uncertainties (Section 2.4.4) and forcing errors related to prescribed stratospheric aerosol loadings and stratospheric ozone changes affecting the tropical lower stratosphere (Free and Lanzante, 2009; Solomon et al., 2012; Santer et al., 2013).

Since AR4, attribution studies have improved our knowledge of the role of anthropogenic and natural forcings in observed lower stratospheric temperature change. Gillett et al. (2011) use the suite of chemistry climate model simulations carried out as part of the Chemistry Climate Model Validation (CCMVal) activity phase 2 for an attribution study of observed changes in stratospheric zonal mean temperatures. Chemistry–climate models prescribe changes in ozone-depleting substances (ODS) and ozone changes are calculated interactively. Gillett et al. (2011) partition 1979–2005 Microwave Sounding Unit (MSU) lower stratospheric temperature trends into ODS-induced and GHG-induced changes and find that both ODSs and natural forcing contributed to the observed stratospheric cooling in the lower stratosphere with the impact of ODS dominating. The influence of GHGs on stratospheric temperature could not be detected independently of ODSs.

The step-like cooling of the lower stratosphere can only be explained by the combined effects of changes in both anthropogenic and natural factors (Figure 10.9; Eyring et al., 2006; Ramaswamy et al., 2006). Although the anthropogenic factors (ozone depletion and increases in WMGHGs) cause the overall cooling, the natural factors (solar irradiance variations and volcanic aerosols) modulate the evolution of the cooling (Figure 10.9; Ramaswamy et al., 2006; Dall'Amico et al., 2010) with temporal variability of global mean ozone contributing to the step-like temperature evolution (Thompson and Solomon, 2009).

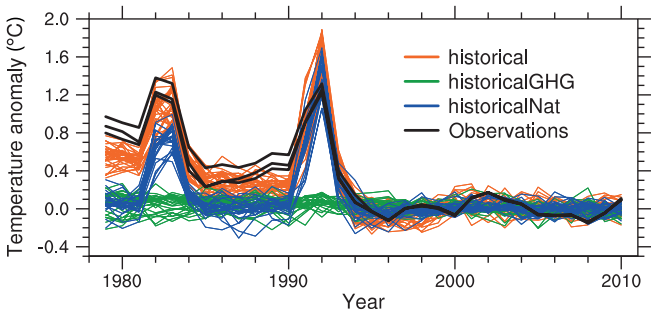


**Figure 10.9 |** Time series (1979–2010) of observed (black) and simulated global mean (82.5°S to 82.5°N) Microwave Sounding Unit (MSU) lower stratosphere temperature anomalies in a subset of CMIP5 simulations (simulations with both anthropogenic and natural forcings (red), simulations with well-mixed greenhouse gases (green), simulations with natural forcings (blue)). Anomalies are calculated relative to 1996–2010. (Adapted from Ramaswamy et al., 2006.)

Models disagree with observations for seasonally varying changes in the strength of the Brewer–Dobson circulation in the lower stratosphere (Ray et al., 2010) which has been linked to zonal and seasonal patterns of changes in lower stratospheric temperatures (Thompson and Solomon, 2009; Fu et al., 2010; Lin et al., 2010b; Forster et al., 2011; Free, 2011). One robust feature is the observed cooling in spring over the Antarctic, which is simulated in response to stratospheric ozone depletion in climate models (Young et al., 2012), although this has not been the subject of a formal detection and attribution study.

Since AR4, progress has been made in simulating the response of global mean lower stratosphere temperatures to natural and anthropogenic forcings by improving the representation of climate forcings and utilizing models that include more stratospheric processes. New detection and attribution studies of lower stratospheric temperature changes made since AR4 support an assessment that it is *very likely* that anthropogenic forcing, dominated by stratospheric ozone depletion due to ozone-depleting substances, has led to a detectable cooling of the lower stratosphere since 1979.

#### 10.3.1.2.3 Overall atmospheric temperature change

When temperature trends from the troposphere and stratosphere are analysed together, detection and attribution studies using CMIP5 models show robust detections of the effects of GHGs and other anthropogenic forcings on the distinctive fingerprint of tropospheric warming and stratospheric cooling seen since 1961 in radiosonde data (Lott et al., 2013; Mitchell et al., 2013). Combining the evidence from free atmosphere changes from both troposphere and stratosphere shows an increased confidence in the attribution of free atmosphere temperature changes compared to AR4 owing to improved understanding of stratospheric temperature changes. There is therefore stronger evidence than at the time of AR4 to support the conclusion that it is *very likely* that anthropogenic forcing, particularly GHGs and stratospheric ozone depletion, has led to a detectable observed pattern of tropospheric warming and lower stratospheric cooling since 1961.

Frequently Asked Questions

## FAQ 10.1 | Climate Is Always Changing. How Do We Determine the Causes of Observed Changes?

*The causes of observed long-term changes in climate (on time scales longer than a decade) are assessed by determining whether the expected 'fingerprints' of different causes of climate change are present in the historical record. These fingerprints are derived from computer model simulations of the different patterns of climate change caused by individual climate forcings. On multi-decade time scales, these forcings include processes such as greenhouse gas increases or changes in solar brightness. By comparing the simulated fingerprint patterns with observed climate changes, we can determine whether observed changes are best explained by those fingerprint patterns, or by natural variability, which occurs without any forcing.*

*The fingerprint of human-caused greenhouse gas increases is clearly apparent in the pattern of observed 20th century climate change. The observed change cannot be otherwise explained by the fingerprints of natural forcings or natural variability simulated by climate models. Attribution studies therefore support the conclusion that 'it is* extremely likely *that human activities have caused more than half of the observed increase in global mean surface temperatures from 1951 to 2010.'*



The Earth's climate is always changing, and that can occur for many reasons. To determine the principal causes of observed changes, we must first ascertain whether an observed change in climate is different from other fluctuations that occur without any forcing at all. Climate variability without forcing—called internal variability—is the consequence of processes within the climate system. Large-scale oceanic variability, such as El Niño-Southern Oscillation (ENSO) fluctuations in the Pacific Ocean, is the dominant source of internal climate variability on decadal to centennial time scales.

Climate change can also result from natural forcings external to the climate system, such as volcanic eruptions, or changes in the brightness of the sun. Forcings such as these are responsible for the huge changes in climate that are clearly documented in the geological record. Human-caused forcings include greenhouse gas emissions or atmospheric particulate pollution. Any of these forcings, natural or human caused, could affect internal variability as well as causing a change in average climate. Attribution studies attempt to determine the causes of a detected change in observed climate. Over the past century we know that global average temperature has increased, so if the observed change is forced then the principal forcing must be one that causes warming, not cooling.

Formal climate change attribution studies are carried out using controlled experiments with climate models. The model-simulated responses to specific climate forcings are often called the fingerprints of those forcings. A climate model must reliably simulate the fingerprint patterns associated with individual forcings, as well as the patterns of unforced internal variability, in order to yield a meaningful climate change attribution assessment. No model can perfectly reproduce all features of climate, but many detailed studies indicate that simulations using current models are indeed sufficiently reliable to carry out attribution assessments.

FAQ 10.1, Figure 1 illustrates part of a fingerprint assessment of global temperature change at the surface during the late 20th century. The observed change in the latter half of the 20th century, shown by the black time series in the left panels, is larger than expected from just internal variability. Simulations driven only by natural forcings (yellow and blue lines in the upper left panel) fail to reproduce late 20th century global warming at the surface with a spatial pattern of change (upper right) completely different from the observed pattern of change (middle right). Simulations including both natural and human-caused forcings provide a much better representation of the time rate of change (lower left) and spatial pattern (lower right) of observed surface temperature change.

Both panels on the left show that computer models reproduce the naturally forced surface cooling observed for a year or two after major volcanic eruptions, such as occurred in 1982 and 1991. Natural forcing simulations capture the short-lived temperature changes following eruptions, but only the natural + human caused forcing simulations simulate the longer-lived warming trend.

A more complete attribution assessment would examine temperature above the surface, and possibly other climate variables, in addition to the surface temperature results shown in FAQ 10.1, Figure 1. The fingerprint patterns associated with individual forcings become easier to distinguish when more variables are considered in the assessment.

*(continued on next page)*

*FAQ 10.1 (continued)*

Overall, FAQ 10.1, Figure 1 shows that the pattern of observed temperature change is significantly different than the pattern of response to natural forcings alone. The simulated response to all forcings, including human-caused forcings, provides a good match to the observed changes at the surface. We cannot correctly simulate recent observed climate change without including the response to human-caused forcings, including greenhouse gases, stratospheric ozone, and aerosols. Natural causes of change are still at work in the climate system, but recent trends in temperature are largely attributable to human-caused forcing.

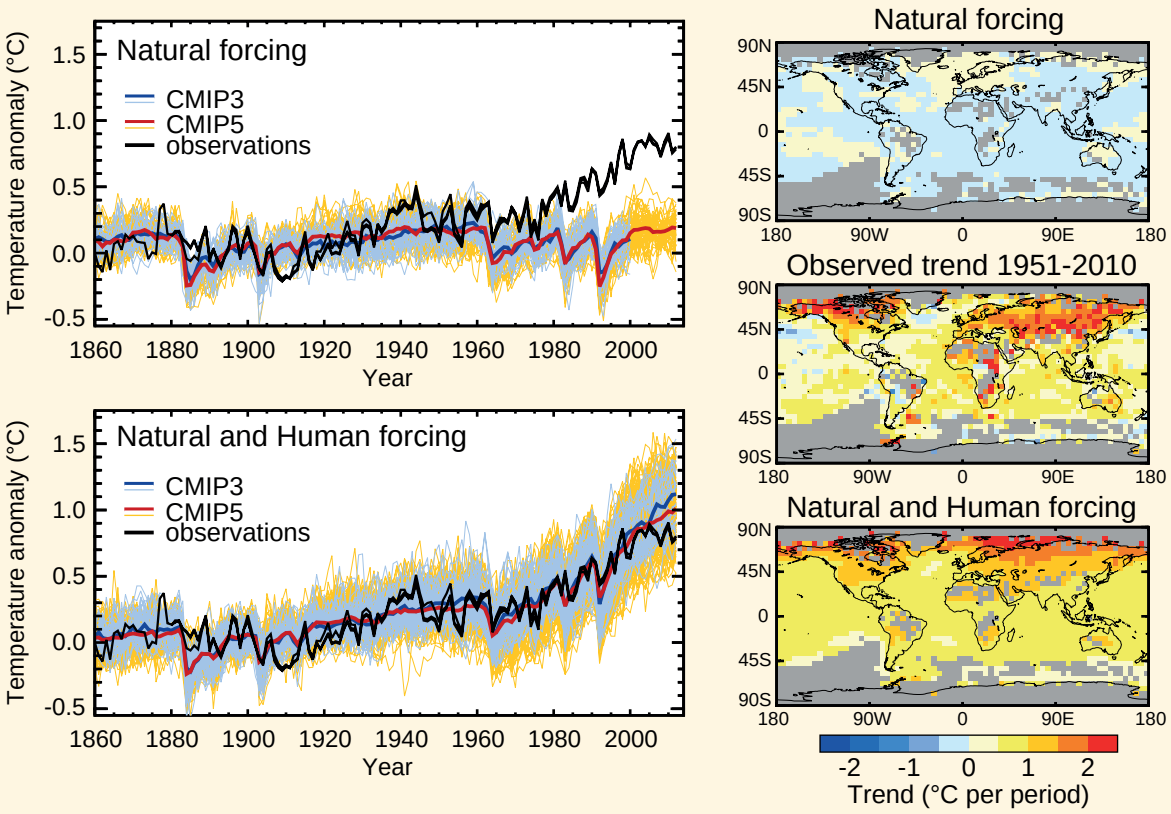


**FAQ 10.1, Figure 1 |** (Left) Time series of global and annual-averaged surface temperature change from 1860 to 2010. The top left panel shows results from two ensemble of climate models driven with just natural forcings, shown as thin blue and yellow lines; ensemble average temperature changes are thick blue and red lines. Three different observed estimates are shown as black lines. The lower left panel shows simulations by the same models, but driven with both natural forcing and human-induced changes in greenhouse gases and aerosols. (Right) Spatial patterns of local surface temperature trends from 1951 to 2010. The upper panel shows the pattern of trends from a large ensemble of Coupled Model Intercomparison Project Phase 5 (CMIP5) simulations driven with just natural forcings. The bottom panel shows trends from a corresponding ensemble of simulations driven with natural + human forcings. The middle panel shows the pattern of observed trends from the Hadley Centre/Climatic Research Unit gridded surface temperature data set 4 (HadCRUT4) during this period.

### 10.3.2 Water Cycle

Detection and attribution studies of anthropogenic change in hydrologic variables are challenged by the length and quality of observed data sets, and by the difficulty in simulating hydrologic variables in dynamical models. AR4 cautiously noted that the observed increase in atmospheric water vapour over oceans was consistent with warming of SSTs attributed to anthropogenic influence, and that observed changes in the latitudinal distribution of precipitation, and increased incidence of drought, were suggestive of a possible human influence. Many of the published studies cited in AR4, and some of the studies cited in this section, use less formal detection and attribution criteria than are often used for assessments of temperature change, owing to difficulties defining large-scale fingerprint patterns of hydrologic change in models and isolating those fingerprints in data. For example, correlations between observed hydrologic changes and the patterns of change in models forced by increasing GHGs can provide suggestive evidence towards attribution of change.

Since the publication of AR4, *in situ* hydrologic data sets have been reanalysed with more stringent quality control. Satellite-derived data records of worldwide water vapour and precipitation variations have

lengthened. Formal detection and attribution studies have been carried out with newer models that potentially offer better simulations of natural variability. Reviews of detection and attribution of trends in various components of the water cycle have been published by Stott et al. (2010) and Trenberth (2011b).

#### 10.3.2.1 Changes in Atmospheric Water Vapour

*In situ* surface humidity measurements have been reprocessed since AR4 to create new gridded analyses for climatic research, as discussed in Chapter 2. The HadCRUH Surface Humidity data set (Willett et al., 2008) indicates significant increases in surface specific humidity between 1973 and 2003 averaged over the globe, the tropics, and the NH, with consistently larger trends in the tropics and in the NH during summer, and negative or non significant trends in relative humidity. These results are consistent with the hypothesis that the distribution of relative humidity should remain roughly constant under climate change (see Section 2.5). Simulations of the response to historical anthropogenic and natural forcings robustly generate an increase in atmospheric humidity consistent with observations (Santer et al., 2007; Willett et al., 2007; Figure 9.9). A recent cessation of the upward trend in specific humidity is observed over multiple continental areas in HadCRUH and is also found in the European Centre for Medium range Weather Forecast (ECMWF) interim reanalysis of the global atmosphere and surface conditions (ERA-Interim; Simmons et al. 2010). This change in the specific humidity trend is temporally correlated with a levelling off of global ocean temperatures following the 1997–1998 El Niño event (Simmons et al., 2010).

The anthropogenic water vapour fingerprint simulated by an ensemble of 22 climate models has been identified in lower tropospheric moisture content estimates derived from Special Sensor Microwave/Imager (SSM/I) data covering the period 1988–2006 (Santer et al., 2007). Santer et al. (2009) find that detection of an anthropogenic response in column water vapour is insensitive to the set of models used. They rank models based on their ability to simulate the observed mean total column water vapour, and its annual cycle and variability associated with ENSO. They report no appreciable differences between the fingerprints or detection results derived from the best or worst performing models, and so conclude that attribution of water vapour changes to anthropogenic forcing is not sensitive to the choice of models used for the assessment.

In summary, an anthropogenic contribution to increases in specific humidity at and near the Earth's surface is found with *medium confidence*. Evidence of a recent levelling off of the long-term surface atmospheric moistening trend over land needs to be better understood and simulated as a prerequisite to increased confidence in attribution studies of water vapour changes. Length and quality of observational humidity data sets, especially above the surface, continue to limit detection and attribution studies of atmospheric water vapour.

#### 10.3.2.2 Changes in Precipitation

Analysis of CMIP5 model simulations yields clear global and regional scale changes associated with anthropogenic forcing (e.g., Scheff and Frierson, 2012a, 2012b), with patterns broadly similar to those identified from CMIP3 models (e.g., Polson et al., 2013). The AR4 concluded that 'the latitudinal pattern of change in land precipitation and observed increases in heavy precipitation over the 20th century appear to be consistent with the anticipated response to anthropogenic forcing'. Detection and attribution of regional precipitation changes generally focuses on continental areas using *in situ* data because observational coverage over oceans is limited to a few island stations (Arkin et al., 2010; Liu et al., 2012; Noake et al., 2012) , although model-data comparisons over continents also illustrate large observational uncertainties (Tapiador, 2010; Noake et al., 2012; Balan Sarojini et al., 2012; Polson et al., 2013). Available satellite data sets that could supplement oceanic studies are short and their long-term homogeneity is still unclear (Chapter 2); hence they have not yet been used for detection and attribution of changes. Continuing uncertainties in climate model simulations of precipitation make quantitative model/data comparisons difficult (e.g., Stephens et al., 2010), which also limits confidence in detection and attribution. Furthermore, sparse observational coverage of precipitation across much of the planet makes the fingerprint of precipitation change challenging to isolate in observational records (Balan Sarojini et al., 2012; Wan et al., 2013).

Considering just land regions with sufficient observations, the largest signal of differences between models with and without anthropogenic forcings is in the high latitudes of the NH, where increases in precipitation are a robust feature of climate model simulations (Scheff and Frierson, 2012a, 2012b). Such increases have been observed (Figure 10.10) in several different observational data sets (Min et al., 2008a; Noake et al., 2012; Polson et al., 2013), although high-latitude trends vary between data sets and with coverage (e.g., Polson et al., 2013).

Attribution of zonally averaged precipitation trends has been attempted using different observational products and ensembles of forced simulations from both the CMIP3 and CMIP5 archives, for annual-averaged (Zhang et al., 2007; Min et al., 2008a) and season-specific (Noake et al., 2012; Polson et al., 2013) results (Figure 10.11). Zhang et al. (2007) identify the fingerprint of anthropogenic changes in observed annual zonal mean precipitation averaged over the periods 1925–1999 and 1950–1999, and separate the anthropogenic fingerprint from the influence of natural forcing. The fingerprint of external forcing is also detected in seasonal means for boreal spring in all data sets assessed by Noake et al. (2012), and in all but one data set assessed by Polson et al. (2013) (Figure 10.11), and in boreal winter in all but one data set (Noake et al., 2012), over the period 1951–1999 and to 2005. The fingerprint features increasing high-latitude precipitation, and decreasing precipitation trends in parts of the tropics that are reasonably robustly observed in all four data sets considered albeit with large observational uncertainties north of 60°N (Figure 10.11). Detection of seasonal-average precipitation change is less convincing for June, July, August (JJA) and September, October, November (SON) and results vary with observation data set (Noake et al., 2012; Polson et al., 2013). Although Zhang et al. (2007) detect anthropogenic changes even if a separate fingerprint for natural forcings is considered, Polson et al. (2013) find that this result is sensitive to the data set used and that the fingerprints can be separated robustly only for the data set most closely constrained by station data. The analysis also finds that model simulated precipitation variability is smaller than observed variability in the tropics (Zhang et al., 2007;

Polson et al., 2013) which is addressed by increasing the estimate of variance from models (Figure 10.11).

Another detection and attribution study focussed on precipitation in the NH high latitudes and found an attributable human influence (Min et al., 2008a). Both Min et al. (2008a) and Zhang et al. (2007) find that the observed changes are significantly larger than the model simulated changes. However, Noake et al. (2012) and Polson et al. (2013) find that the difference between models and observations decreases if changes are expressed as a percentage of climatological precipitation and that the observed and simulated changes are largely consistent between CMIP5 models and observations given data uncertainty. Use of additional data sets illustrates remaining observational uncertainty in high latitudes of the NH (Figure 10.11). Regional-scale attribution of precipitation change is still problematic although regional climate models have yielded simulations consistent with observed wintertime changes for northern Europe (Bhend and von Storch, 2008; Tapiador, 2010).

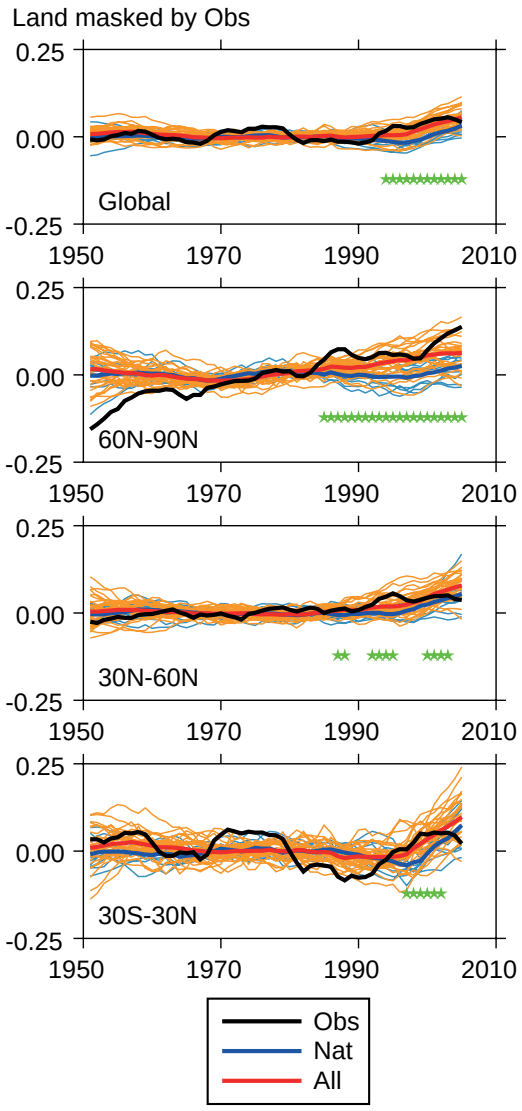


**Figure 10.10 |** Global and zonal average changes in annual mean precipitation (mm day$^{-1}$) over areas of land where there are observations, expressed relative to the baseline period of 1961–1990, simulated by CMIP5 models forced with both anthropogenic and natural forcings (red lines) and natural forcings only (blue lines) for the global mean and for three latitude bands. Multi-model means are shown in thick solid lines. Observations (gridded values derived from Global Historical Climatology Network station data, updated from Zhang et al. (2007) are shown as a black solid line. An 11-year smoothing is applied to both simulations and observations. Green stars show statistically significant changes at 5% level ($p$ value <0.05) between the ensemble of runs with both anthropogenic and natural forcings (red lines) and the ensemble of runs with just natural forcings (blue lines) using a two-sample two-tailed $t$-test for the last 30 years of the time series. (From Balan Sarojini et al., 2012.) Results for the Climate Research Unit (CRU) TS3.1 data set are shown in Figure 10.A.2.

Precipitation change over ocean has been attributed to human influence by Fyfe et al. (2012) for the high-latitude SH in austral summer, where zonally averaged precipitation has declined around 45°S and increased around 60°S since 1957, consistent with CMIP5 historical simulations, with the magnitude of the half-century trend outside the range of simulated natural variability. Confidence in this attribution result, despite limitations in precipitation observations, is enhanced by its consistency with trends in large-scale sea level pressure data (see Section 10.3.3).

In summary, there is *medium confidence* that human influence has contributed to large-scale changes in precipitation patterns over land. The expected anthropogenic fingerprints of change in zonal mean precipitation—reductions in low latitudes and increases in NH mid to high latitudes—have been detected in annual and some seasonal data. Observational uncertainties including limited global coverage and large natural variability, in addition to challenges in precipitation modeling, limit confidence in assessment of climatic changes in precipitation.

### 10.3.2.3 Changes in Surface Hydrologic Variables

This subsection assesses recent research on detection and attribution of long-term changes in continental surface hydrologic variables, including soil moisture, evapotranspiration and streamflow. Streamflows are often subject to large non-climatic human influence, such as diversions and land use changes, that must be accounted for in order to attribute detected hydrologic changes to climate change. Cryospheric aspects of surface hydrology are discussed in Section 10.5; extremes in surface hydrology (such as drought) and precipitation are covered in Section 10.6.1. The variables discussed here are subject to large modeling uncertainties (Chapter 9) and observational challenges (Chapter 2), which in combination place severe limits on climate change detection and attribution.

Direct observational records of soil moisture and surface fluxes tend to be sparse and/or short, thus limiting recent assessments of change in these variables (Jung et al., 2010). Assimilated land surface data sets and new satellite observations (Chapter 2) are promising tools, but assessment of past and future climate change of these variables (Hoekema and Sridhar, 2011) is still generally carried out on derived quantities such as the Palmer Drought Severity Index, as discussed more fully in Section 10.6.1. Recent observations (Jung et al., 2010) show regional trends towards drier soils. An optimal detection analysis of reconstructed evapotranspiration identifies the effects of anthropogenic forcing on evapotranspiration, with the Centre National de Recherches Météorologiques (CNRM)-CM5 model simulating changes consistent with those estimated to have occurred (Douville et al., 2013).

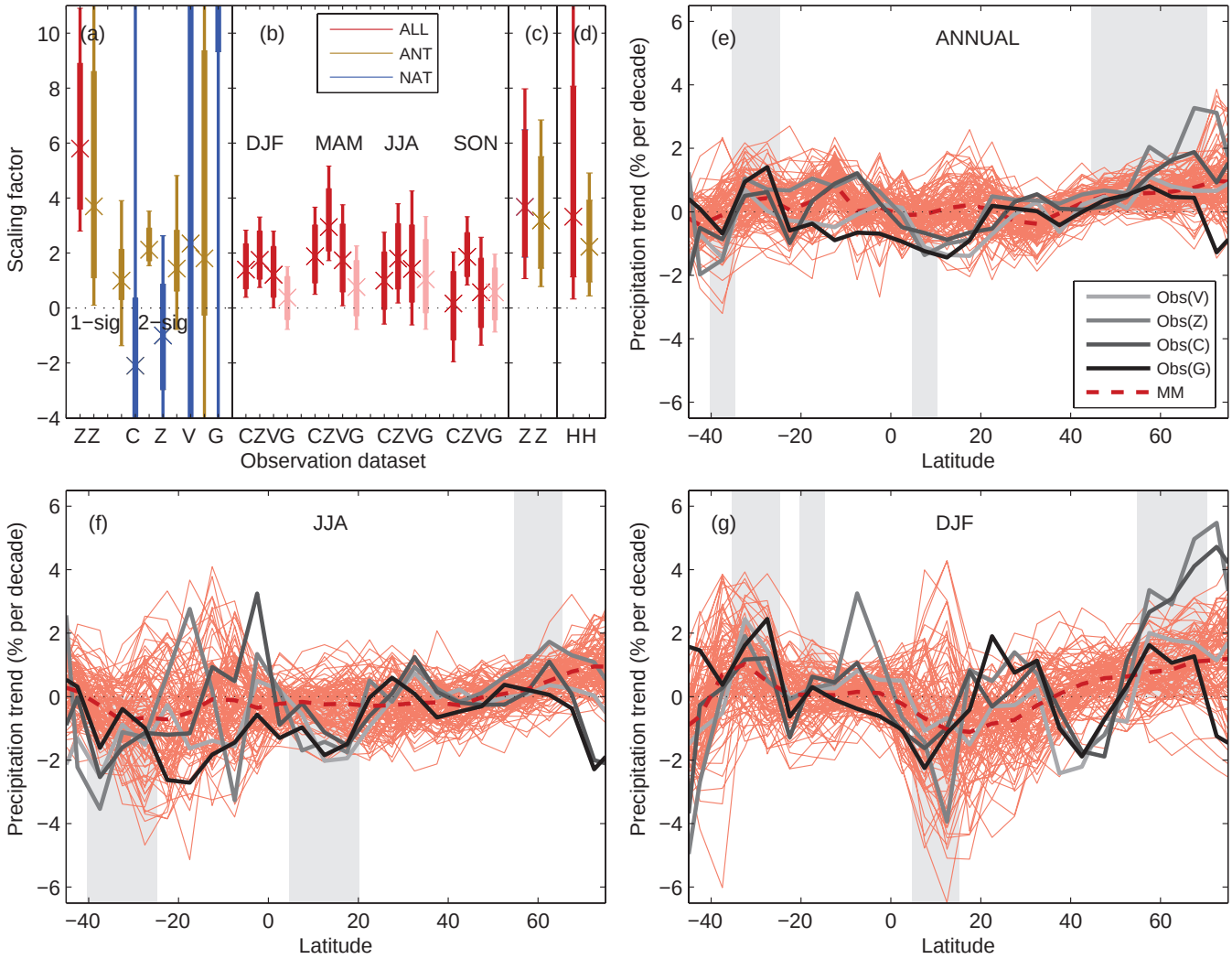


**Figure 10.11 |** Detection and attribution results for zonal land precipitation trends in the second half of the 20th century. (Top left) Scaling factors for precipitation changes. (Top right and bottom) Zonally averaged precipitation changes over continents from models and observations. (a) Crosses show the best-guess scaling factor derived from multi-model means. Thick bars show the 5 to 95% uncertainty range derived from model-simulated variability, and thin bars show the uncertainty range if doubling the multi-model variance. Red bars indicate scaling factors for the estimated response to all forcings, blue bars for natural-only forcing and brown bars for anthropogenic-only forcing. Labels on the *x*-axis identify results from four different observational data sets (Z is Zhang et al. (2007), C is Climate Research Unit (CRU), V is Variability Analyses of Surface Climate Observations (VASClimO), G is Global Precipitation Climatology Centre (GPCC), H is Hadley Centre gridded data set of temperature and precipitation extremes (HadEX)). (a) Detection and attribution results for annual averages, both single fingerprint ("1-sig"; 1950–1999) and two fingerprint results ("2-sig"; Z, C, G (1951–2005), V (1952–2000)). (b) Scaling factors resulting from single-fingerprint analyses for seasonally averaged precipitation (Z, C, G (1951–2005), V (1952–2000); the latter in pink as not designed for long-term homogeneity) for four different seasons. (c) Scaling factors for spatial pattern of Arctic precipitation trends (1951–1999). (d) Scaling factors for changes in large-scale intense precipitation (1951–1999). (e) Thick solid lines show observed zonally and annually averaged trends (% per decade) for four different observed data sets. Corresponding results from individual simulations from 33 different climate models are shown as thin solid lines, with the multimodel mean shown as a red dashed line. Model results are masked to match the spatial and temporal coverage of the GPCC data set (denoted G in the seasonal scaling factor panel). Grey shading indicates latitude bands within which >75% of simulations yield positive or negative trends. (f, g) Like (e) but showing zonally averaged precipitation changes for (f) June, July, August (JJA) and (g) December, January, February (DJF) seasons. Scaling factors (c) and (d) adapted from Min et al. (2008a) and Min et al. (2011), respectively; other results adapted from Zhang et al. (2007) and Polson et al. (2013).

Trends towards earlier timing of snowmelt-driven streamflows in western North America since 1950 have been demonstrated to be different from natural variability (Hidalgo et al., 2009). Similarly, internal variability associated with natural decade-scale fluctuations could not account for recent observed declines of northern Rocky Mountain streamflow (St Jacques et al., 2010). Statistical analyses of streamflows demonstrate regionally varying changes that are consistent with changes expected from increasing temperature, in Scandinavia (Wilson et al., 2010), Europe (Stahl et al., 2010) and the USA (Krakauer and Fung, 2008; Wang and Hejazi, 2011). Observed increases in Arctic river discharge, which could be a good integrator for monitoring changes in precipitation in high latitudes, are found to be explainable only if model simulations include anthropogenic forcings (Min et al., 2008a).

Barnett et al. (2008) analysed changes in the surface hydrology of the western USA, considering snow pack (measured as snow water equivalent), the seasonal timing of streamflow in major rivers, and average January to March daily minimum temperature over the region, the two hydrological variables they studied being closely related to temperature. Observed changes were compared with the output of a

regional hydrologic model forced by the Parallel Climate Model (PCM) and Model for Interdisciplinary Research On Climate (MIROC) climate models. They derived a fingerprint of anthropogenic changes from the two climate models and found that the observations, when projected onto the fingerprint of anthropogenic changes, show a positive signal strength consistent with the model simulations that falls outside the range expected from internal variability as estimated from 1600 years of downscaled climate model data. They conclude that there is a detectable and attributable anthropogenic signature on the hydrology of this region.

In summary, there is *medium confidence* that human influence on climate has affected stream flow and evapotranspiration in limited regions of middle and high latitudes of the NH. Detection and attribution studies have been applied only to limited regions and using a few models. Observational uncertainties are large and in the case of evapotranspiration depend on reconstructions using land surface models.

### 10.3.3 Atmospheric Circulation and Patterns of Variability

The atmospheric circulation is driven by various processes including the uneven heating of the Earth's surface by solar radiation, land–sea contrast and orography. The circulation transports heat from warm to cold regions and thereby acts to reduce temperature contrasts. Thus, changes in circulation and in patterns of variability are of critical importance for the climate system, influencing regional climate and regional climate variability. Any such changes are important for local climate change because they could act to reinforce or counteract the effects of external forcings on climate in a particular region. Observed changes in atmospheric circulation and patterns of variability are assessed in Section 2.7.5. Although new and improved data sets are now available, changes in patterns of variability remain difficult to detect because of large variability on interannual to decadal time scales (Section 2.7).

Since AR4, progress has been made in understanding the causes of changes in circulation-related climate phenomena and modes of variability such as the width of the tropical circulation, and the Southern Annular Mode (SAM). For other climate phenomena, such as ENSO, Indian Ocean Dipole (IOD), Pacific Decadal Oscillation (PDO), and monsoons, there are large observational and modelling uncertainties (see Section 9.5 and Chapter 14), and there is *low confidence* that changes in these phenomena, if observed, can be attributed to human-induced influence.

#### 10.3.3.1 Tropical Circulation

Various indicators of the width of the tropical belt based on independent data sets suggest that the tropical belt as a whole has widened since 1979; however, the magnitude of this change is very uncertain (Fu et al., 2006; Hudson et al., 2006; Hu and Fu, 2007; Seidel and Randel, 2007; Seidel et al., 2008; Lu et al., 2009; Fu and Lin, 2011; Hu et al., 2011; Davis and Rosenlof, 2012; Lucas et al., 2012; Wilcox et al., 2012; Nguyen et al., 2013) (Section 2.7.5). CMIP3 and CMIP5 simulations suggest that anthropogenic forcings have contributed to the observed widening of the tropical belt since 1979 (Johanson and Fu, 2009; Hu et al., 2013). On average the poleward expansion of the Hadley circulation and other indicators of the width of the tropical belt is greater than determined from CMIP3 and CMIP5 simulations (Seidel et al., 2008; Johanson and Fu, 2009; Hu et al., 2013; Figure 10.12). The causes as to why models underestimate the observed poleward expansion of the tropical belt are not fully understood. Potential factors are lack of understanding of the magnitude of natural variability as well as changes in observing systems that also affect reanalysis products (Thorne and Vose, 2010; Lucas et al., 2012; Box 2.3).

Climate model simulations suggest that Antarctic ozone depletion is a major factor in causing poleward expansion of the southern Hadley cell during austral summer over the last three to five decades with GHGs also playing a role (Son et al., 2008, 2009, 2010; McLandress et al., 2011; Polvani et al., 2011; Hu et al., 2013). In reanalysis data a detectable signal of ozone forcing is separable from other external forcing including GHGs when utilizing both CMIP5 and CMIP3 simulations combined (Min and Son, 2013). An analysis of CMIP3 simulations suggests that BC aerosols and tropospheric ozone were the main drivers of the observed poleward expansion of the northern Hadley cell in boreal summer (Allen et al., 2012). It is found that global greenhouse warming causes increase in static stability, such that the onset of baroclinicity is shifted poleward, leading to poleward expansion of the Hadley circulation (Frierson, 2006; Frierson et al., 2007; Hu and Fu, 2007; Lu et al., 2007, 2008). Tropical SST increase may also contribute to a widening of the Hadley circulation (Hu et al., 2011; Staten et al., 2012). Althoughe some Atmospheric General Circulation Model (AGCM) simulations forced by observed time-varying SSTs yield a widening by about 1° in latitude over 1979–2002 (Hu et al., 2011), other simulations suggest that SST changes have little effect on the tropical expansion when based on the tropopause metric of the tropical width (Lu et al., 2009). However, it is found that the tropopause metric is not

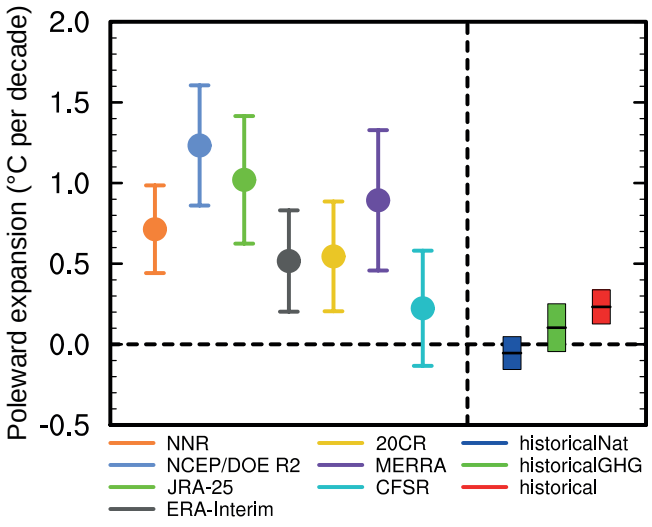


**Figure 10.12 |** December to February mean change of southern border of the Hadley circulation. Unit is degree in latitude per decade. Reanalysis data sets (see also Box 2.3) are marked with different colours. Trends are all calculated over the period of 1979–2005. The terms historicalNAT, historicalGHG, and historical denote CMIP5 simulations with natural forcing, with greenhouse gas forcing and with both anthropogenic and natural forcings, respectively. For each reanalysis data set, the error bars indicate the 95% confidence level of the standard *t*-test. For CMIP5 simulations, trends are first calculated for each model, and all ensemble members of simulations are used. Then, trends are averaged for multi-model ensembles. Trend uncertainty is estimated from multi-model ensembles, as twice the standard error. (Updated from Hu et al., 2013.)

very reliable because of the use of arbitrary thresholds (Birner, 2010; Davis and Rosenlof, 2012).

In summary, there are multiple lines of evidence that the Hadley cell and the tropical belt as a whole have widened since at least 1979; however, the magnitude of the widening is very uncertain. Based on modelling studies there is *medium confidence* that stratospheric ozone depletion has contributed to the observed poleward shift of the southern Hadley cell border during austral summer, with GHGs also playing a role. The contribution of internal climate variability to the observed poleward expansion of the Hadley circulation remains very uncertain.

### 10.3.3.2 Northern Annular Mode/North Atlantic Oscillation

The NAO, which exhibited a positive trend from the 1960s to the 1990s, has since exhibited lower values, with exceptionally low anomalies in the winters of 2009/2010 and 2010/2011 (Section 2.7.8). This means that the positive trend in the NAO discussed in the AR4 has considerably weakened when evaluated up to 2011. Similar results apply to the closely related Northern Annular Mode (NAM), with its upward trend over the past 60 years in the 20th Century Reanalysis (Compo et al., 2011) and in Hadley Centre Sea Level Pressure data set 2r (HadSLP2r; Allan and Ansell, 2006) not being significant compared to internal variability (Figure 10.13). An analysis of CMIP5 models shows that they simulate positive trends in NAM in the DJF season over this period, albeit not as large as those observed which are still within the range of natural internal variability (Figure 10.13).

Other work (Woollings, 2008) demonstrates that while the NAM is largely barotropic in structure, the simulated response to anthropogenic forcing has a strong baroclinic component, with an opposite geopotential height trends in the mid-troposphere compared to the surface in many models. Thus while the circulation response to anthropogenic forcing may project onto the NAM, it is not entirely captured by the NAM index.

Consistent with previous findings (Hegerl et al., 2007b), Gillett and Fyfe (2013) find that GHGs tend to drive a positive NAM response in the CMIP5 models. Recent modelling work also indicates that ozone changes drive a small positive NAM response in spring (Morgenstern et al., 2010; Gillett and Fyfe, 2013).

### 10.3.3.3 Southern Annular Mode

The Southern Annular Mode (SAM) index has remained mainly positive since the publication of the AR4, although it has not been as strongly positive as in the late 1990s. Nonetheless, an index of the SAM shows a significant positive trend in most seasons and data sets over the 1951–2011 period (Figure 10.13; Table 2.14). Recent modelling studies confirm earlier findings that the increase in GHG concentrations tends to lead to a strengthening and poleward shift of the SH eddy-driven polar jet (Karpechko et al., 2008; Son et al., 2008, 2010; Sigmond et al., 2011; Staten et al., 2012; Swart and Fyfe, 2012; Eyring et al., 2013; Gillett and Fyfe, 2013) which projects onto the positive phase of the SAM. Stratospheric ozone depletion also induces a strengthening and poleward shift of the polar jet in models, with the largest response in austral summer (Karpechko et al., 2008; Son et al., 2008, 2010; McLandress et al., 2011; Polvani et al., 2011; Sigmond et al., 2011; Gillett and Fyfe, 2013). Sigmond et al. (2011) find approximately equal contributions to simulated annual mean SAM trends from GHGs and stratospheric ozone depletion up to the present. Fogt et al. (2009) demonstrate that observed SAM trends over the period 1957–2005 are positive in all seasons, but only statistically significant in DJF and March, April, May (MAM), based on simulated internal variability. Roscoe and Haigh (2007) apply a regression-based approach and find that stratospheric ozone changes are the primary driver of observed trends in the SAM. Observed trends are also consistent with CMIP3 simulations including stratospheric ozone changes in all seasons, though in MAM observed trends are roughly twice as large as those simulated (Miller et al., 2006). Broadly consistent results are found when comparing observed trends and CMIP5 simulations (Figure 10.13), with a station-based SAM index showing a significant positive trend in MAM, JJA and DJF, compared

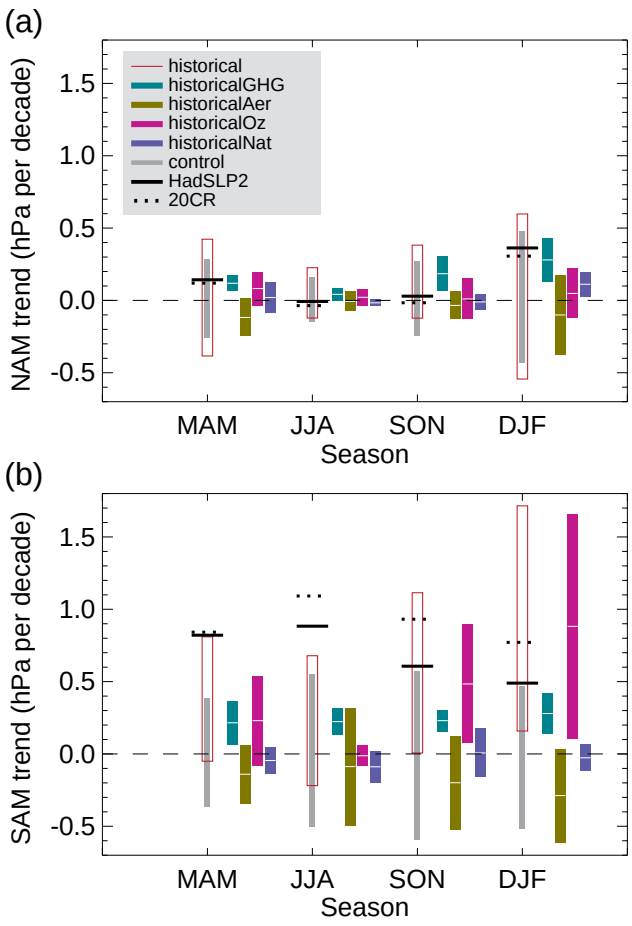


**Figure 10.13 |** Simulated and observed 1951–2011 trends in the Northern Annular Mode (NAM) index (a) and Southern Annular Mode (SAM) index (b) by season. The NAM is a Li and Wang (2003) index based on the difference between zonal mean seal level pressure (SLP) at 35°N and 65°N. and the, and the SAM index is a difference between zonal mean SLP at 40°S and 65°S (Gong and Wang, 1999). Both indices are defined without normalization, so that the magnitudes of simulated and observed trends can be compared. Black lines show observed trends from the HadSLP2r data set (Allan and Ansell, 2006) (solid), and the 20th Century Reanalysis (Compo et al., 2011) (dotted). Grey bars and red boxes show 5 to 95% ranges of trends in CMIP5 control and historical simulations respectively. Ensemble mean trends and their 5 to 95% uncertainties are shown for the response to greenhouse gases (light green), aerosols (dark green), ozone (magenta) and natural (blue) forcing changes, based on CMIP5 individual forcing simulations. (Adapted from Gillett and Fyfe, 2013.)

to simulated internal variability over the 1951–2010 period. Fogt et al. (2009) find that the largest forced response has likely occurred in DJF, the season in which stratospheric ozone depletion has been the dominant contributor to the observed trends.

Taking these findings together, it is *likely* that the positive trend in the SAM seen in austral summer since the mid-20th century is due in part to stratospheric ozone depletion. There is *medium confidence* that GHGs have also played a role.

#### 10.3.3.4 Change in Global Sea Level Pressure Patterns

A number of studies have applied formal detection and attribution studies to global fields of atmospheric SLP finding detection of human influence on global patterns of SLP (Gillett et al., 2003, 2005; Gillett and Stott, 2009). Analysing the contributions of different forcings to observed changes in SLP, Gillett and Stott (2009) find separately detectable influences of anthropogenic and natural forcings in zonal mean seasonal mean SLP, strengthening evidence for a human influence on SLP. Based on the robustness of the evidence from multiple models we conclude that it is *likely* that human influence has altered SLP patterns globally since 1951.

## 10.4 Changes in Ocean Properties

This section assesses the causes of oceanic changes in the main properties of interest for climate change: ocean heat content, ocean salinity and freshwater fluxes, sea level, oxygen and ocean acidification.

### 10.4.1 Ocean Temperature and Heat Content

The oceans are a key part of the Earth's energy balance (Boxes 3.1 and 13.1). Observational studies continue to demonstrate that the ocean heat content has increased in the upper layers of the ocean during the second half of the 20th century and early 21st century (Section 3.2; Bindoff et al., 2007), and that this increase is consistent with a net positive radiative imbalance in the climate system. It is of significance that this heat content increase is an order of magnitude larger than the increase in energy content of any other component of the Earth's ocean–atmosphere–cryosphere system and accounts for more than 90% of the Earth's energy increase between 1971 and 2010 (e.g., Boxes 3.1 and 13.1; Bindoff et al., 2007; Church et al., 2011; Hansen et al., 2011).

Despite the evidence for anthropogenic warming of the ocean, the level of confidence in the conclusions of the AR4 report—that the warming of the upper several hundred meters of the ocean during the second half of the 20th century was *likely* to be due to anthropogenic forcing—reflected the level of uncertainties at that time. The major uncertainty was an apparently large decadal variability (warming in the 1970s and cooling in the early 1980s) in the observational estimates that was not simulated by climate models (Hegerl et al., 2007b, see their Table 9.4). The large decadal variability in observations raised concerns about the capacity of climate models to simulate observed variability. There were also lingering concerns about the presence of non-climate–related biases in the observations of ocean heat content change (Gregory et al., 2004; AchutaRao et al., 2006). After the IPCC AR4 report in 2007, time-and depth-dependent systematic errors in bathythermograph temperatures were discovered (Gouretski and Koltermann, 2007; Section 3.2). Bathythermograph data account for a large fraction of the historical temperature observations and are therefore a source of bias in ocean heat content studies. Bias corrections were then developed and applied to observations. With the newer bias-corrected estimates (Domingues et al., 2008; Wijffels et al., 2008; Ishii and Kimoto, 2009; Levitus et al., 2009), it became obvious that the large decadal variability in earlier estimates of global upper-ocean heat content was an observational artefact (Section 3.2).

The interannual to decadal variability of ocean temperature simulated by the CMIP3 models agrees better with observations when the model data is sampled using the observational data mask (AchutaRao et al., 2007). In the upper 700 m, CMIP3 model simulations agreed more closely with observational estimates of global ocean heat content based on bias-corrected ocean temperature data, both in terms of the decadal variability and multi-decadal trend (Figure 10.14a) when forced with the most complete set of natural and anthropogenic forcings (Domingues et al., 2008). For the simulations with the most complete set of forcings, the multi-model ensemble mean trend was only 10% smaller than observed for 1961–1999. Model simulations that included only anthropogenic forcing (i.e., no solar or volcanic forcing) significantly overestimate the multi-decadal trend and underestimate decadal variability. This overestimate of the trend is partially caused by the ocean's response to volcanic eruptions, which results in rapid cooling followed by decadal or longer time variations during the recovery phase. Although it has been suggested (Gregory, 2010) that the cooling trend from successive volcanic events is an artefact because models were not spun up with volcanic forcing, this discrepancy is not expected to be as significant in the upper ocean as in the deeper layers where longer term adjustments take place (Gregory et al., 2012 ). Thus for the upper ocean, there is *high confidence* that the more frequent eruptions during the second half of the 20th century have caused a multi-decadal cooling that partially offsets the anthropogenic warming and contributes to the apparent decadal variability (Church et al., 2005; Delworth et al., 2005; Fyfe, 2006; Gleckler et al., 2006; Gregory et al., 2006; AchutaRao et al., 2007; Domingues et al., 2008; Palmer et al., 2009; Stenchikov et al., 2009).

Gleckler et al. (2012) examined the detection and attribution of upper-ocean warming in the context of uncertainties in the underlying observational data sets, models and methods. Using three bias-corrected observational estimates of upper-ocean temperature changes (Domingues et al., 2008; Ishii and Kimoto, 2009; Levitus et al., 2009) and models from the CMIP3 multi-model archive, they found that multi-decadal trends in the observations were best understood by including contributions from both natural and anthropogenic forcings. The anthropogenic fingerprint in observed upper-ocean warming, driven by global mean and basin-scale pattern changes, was also detected. The strength of this signal (estimated from successively longer trend periods of ocean heat content starting from 1970) crossed the 5% and 1% significance threshold in 1980 and progressively becomes more strongly detected for longer trend periods (Figure 10.14b), for all ocean heat content time series. This stronger detection for longer periods occurs because the noise (standard deviation of trends in the unforced chang-

es in pattern similarity from model control runs) tends to decrease for longer trend lengths. On decadal time scales, there is *limited evidence* that basin scale space-time variability structure of CMIP3 models is approximately 25% lower than the (poorly constrained) observations, this underestimate is far less than the factor of 2 needed to throw the anthropogenic fingerprint into question. This result is robust to a number of known observational, model, methodological and structural uncertainties.

An analysis of upper-ocean (0 to 700 m) temperature changes for 1955–2004, using bias-corrected observations and 20 global climate models from CMIP5 (Pierce et al., 2012) builds on previous detection and attribution studies of ocean temperature (Barnett et al., 2001, 2005; Pierce et al., 2006). This analysis found that observed temperature changes during the above period are inconsistent with the effects of natural climate variability. That is signal strengths are separated from zero at the 5% significance level, and the probability that the

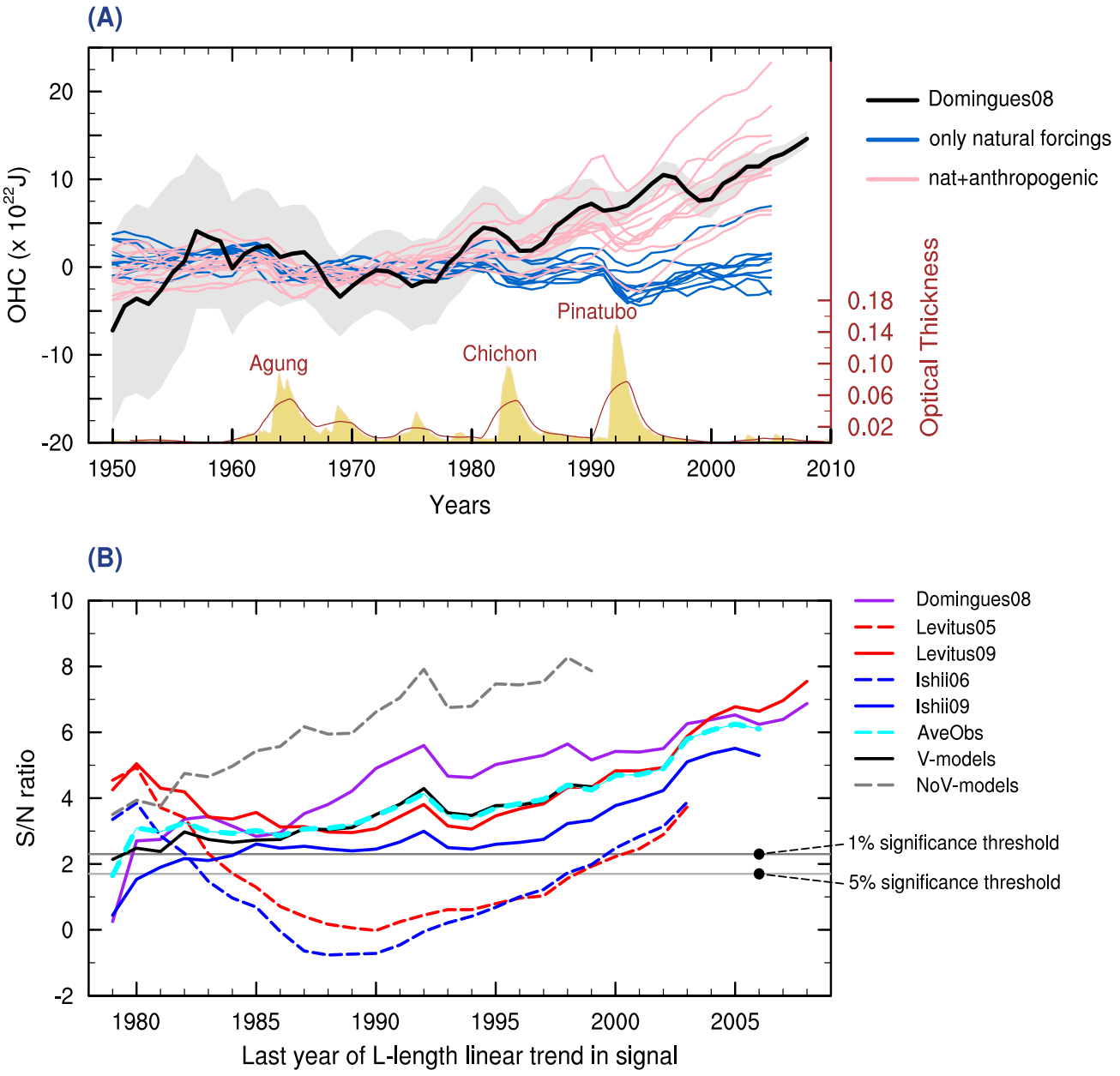


**Figure 10.14 |** (A) Comparison of observed global ocean heat content for the upper 700 m (updated from Domingues et al. 2008) with simulations from ten CMIP5 models that included only natural forcings ('HistoricalNat' runs shown in blue lines) and simulations that included natural and anthropogenic forcings ('Historical' runs in pink lines). Grey shading shows observational uncertainty. The global mean stratospheric optical depth (Sato et al., 1993) in beige at the bottom indicates the major volcanic eruptions and the brown curve is a 3-year running average of these values. (B) Signal-to-noise (S/N) ratio (plotted as a function of increasing trend length L) of basin-scale changes in volume averaged temperature of newer, expendable bathythermograph (XBT)-corrected data (solid red, purple and blue lines), older, uncorrected data (dashed red and blue lines); the average of the three corrected observational sets (AveObs; dashed cyan line); and simulations that include volcanic (V) or exclude volcanic eruptions (NoV) (black solid and grey dashed lines respectively). The start date for the calculation of signal trends is 1970 and the initial trend length is 10 years. The 1% and 5% significance thresholds are shown (as horizontal grey lines) and assume a Gaussian distribution of noise trends in the V-models control-run pseudo-principal components. The detection time is defined as the year at which S/N exceeds and remains above 1% or 5% significance threshold (Gleckler et al., 2012).

null hypothesis of observed changes being consistent with natural variability is less than 0.05 from variability either internal to the climate system alone, or externally forced by solar fluctuations and volcanic eruptions. However, the observed ocean changes are consistent with those expected from anthropogenically induced atmospheric changes from GHGs and aerosol concentrations.

Attribution to anthropogenic warming from recent detection and attribution studies (Gleckler et al., 2012; Pierce et al., 2012) have made use of new bias-corrected observations and have systematically explored methodological uncertainties, yielding more confidence in the results. With greater consistency and agreement across observational data sets and resolution of structural issues, the major uncertainties at the time of AR4 have now largely been resolved. The high levels of confidence and the increased understanding of the contributions from both natural and anthropogenic sources across the many studies mean that it is *very likely* that the increase in global ocean heat content observed in the upper 700 m since the 1970s has a substantial contribution from anthropogenic forcing.

Although there is *high confidence* in understanding the causes of global heat content increases, attribution of regional heat content changes are less certain. Earlier regional studies used a fixed depth data and only considered basin-scale averages (Barnett et al., 2005). At regional scales, however, changes in advection of ocean heat are important and need to be isolated from changes due to air–sea heat fluxes (Palmer et al., 2009; Grist et al., 2010). Their fixed isotherm (rather than fixed depth) approach to optimal detection analysis, in addition to being largely insensitive to observational biases, is designed to separate the ocean's response to air–sea flux changes from advective changes. Air–sea fluxes are the primary mechanism by which the oceans are expected to respond to externally forced anthropogenic and natural volcanic influences. The finer temporal resolution of the analysis allowed Palmer et al. (2009) to attribute distinct short-lived cooling episodes to major volcanic eruptions while, at multi-decadal time scales, a more spatially uniform near-surface (~ upper 200 m) warming pattern was detected across all ocean basins (except in high latitudes where the isotherm approach has limitations due to outcropping of isotherms at the ocean surface) and attributed to anthropogenic causes at the 5% significance level. Considering that individual ocean basins are affected by different observational and modelling uncertainties and that internal variability is larger at smaller scales, detection of significant anthropogenic forcing through space and time studies (Palmer et al., 2009; Pierce et al., 2012) provides more compelling evidence of human influence at regional scales of near-surface ocean warming observed during the second half of the 20th century.

### 10.4.2 Ocean Salinity and Freshwater Fluxes

There is increasing recognition of the importance of ocean salinity as an essential climate variable (Doherty et al., 2009), particularly for understanding the hydrological cycle. In the IPCC Fourth Assessment Report observed ocean salinity change indicated that there was a systematic pattern of increased salinity in the shallow subtropics and a tendency to freshening of waters that originate in the polar regions (Bindoff et al., 2007; Hegerl et al., 2007b) (Figure 10.15a, upper and lower panels). New atlases and revisions of the earlier work based on the increasing number of the Array for Real-time Geostrophic Oceanography (ARGO) profile data, and historical data have extended the observational salinity data sets allowing the examination of the long-term changes at the surface and in the interior of the ocean (Section 3.3) and supporting analyses of precipitation changes over land (see Sections 10.3.2.2 and 2.5.1).

Patterns of subsurface salinity changes largely follow the existing mean salinity pattern at the surface and within the ocean. For example, the inter-basin contrast between the Atlantic (salty) and Pacific Oceans (fresh) has intensified over the observed record (Boyer et al., 2005; Hosoda et al., 2009; Roemmich and Gilson, 2009; von Schuckmann et al., 2009; Durack and Wijffels, 2010). In the Southern Ocean, many studies show a coherent freshening of Antarctic Intermediate Water that is subducted at about 50°S (Johnson and Orsi, 1997; Wong et al., 1999; Bindoff and McDougall, 2000; Curry et al., 2003; Boyer et al., 2005; Roemmich and Gilson, 2009; Durack and Wijffels, 2010; Helm et al., 2010; Kobayashi et al., 2012). There is also a clear increase in salinity of the high-salinity subtropical waters (Durack and Wijffels, 2010; Helm et al., 2010).

The 50-year trends in surface salinity show that there is a strong positive correlation between the mean climate of the surface salinity and its temporal changes from 1950 to 2000 (see Figures 3.4 and 10.15b 'ocean obs' point). The correlation between the climate and the trends in surface salinity of 0.7 implies that fresh surface waters get fresher, and salty waters get saltier (Durack et al., 2012). Such patterns of surface salinity change are also found in Atmosphere–Ocean General Circulation Models (AOGCM) simulations both for the 20th century and projected future changes into the 21st century (Figure 10.15b). The pattern of temporal change in observations from CMIP3 simulations is particularly strong for those projections using Special Report on Emission Scenarios (SRES) with larger global warming changes (Figure 10.15b). For the period 1950–2000 the observed amplification of the surface salinity is 16 ± 10% per °C of warming and is twice the simulated surface salinity change in CMIP3 models. This difference between the surface salinity amplification is plausibly caused by the tendency of CMIP3 ocean models mixing surface salinity into deeper layers and consequently surface salinity increases at a slower rate than observed (Durack et al., 2012).

Although there are now many established observed long-term trends of salinity change at the ocean surface and within the interior ocean at regional and global scales (Section 3.3), there are relatively few studies that attribute these changes formally to anthropogenic forcing. Analysis at the regional scale of the observed recent surface salinity increases in the North Atlantic (20°N to 50°N) show a small signal that could be attributed to anthropogenic forcings but for this ocean is not significant compared with internal variability (Stott et al., 2008a; Terray et al., 2012; and Figure 10.15c). On a larger spatial scale, the surface salinity patterns in the band from 30°S to 50°N show anthropogenic contributions that are larger than the 5 to 95% uncertainty range (Terray et al., 2012). The strongest signals that can be attributed to anthropogenic forcing are in the tropics (TRO, 30°S to 30°N) and the western Pacific. These results also show the salinity contrast between the Pacific and Atlantic oceans is also enhanced with significant contributions from anthropogenic forcing.

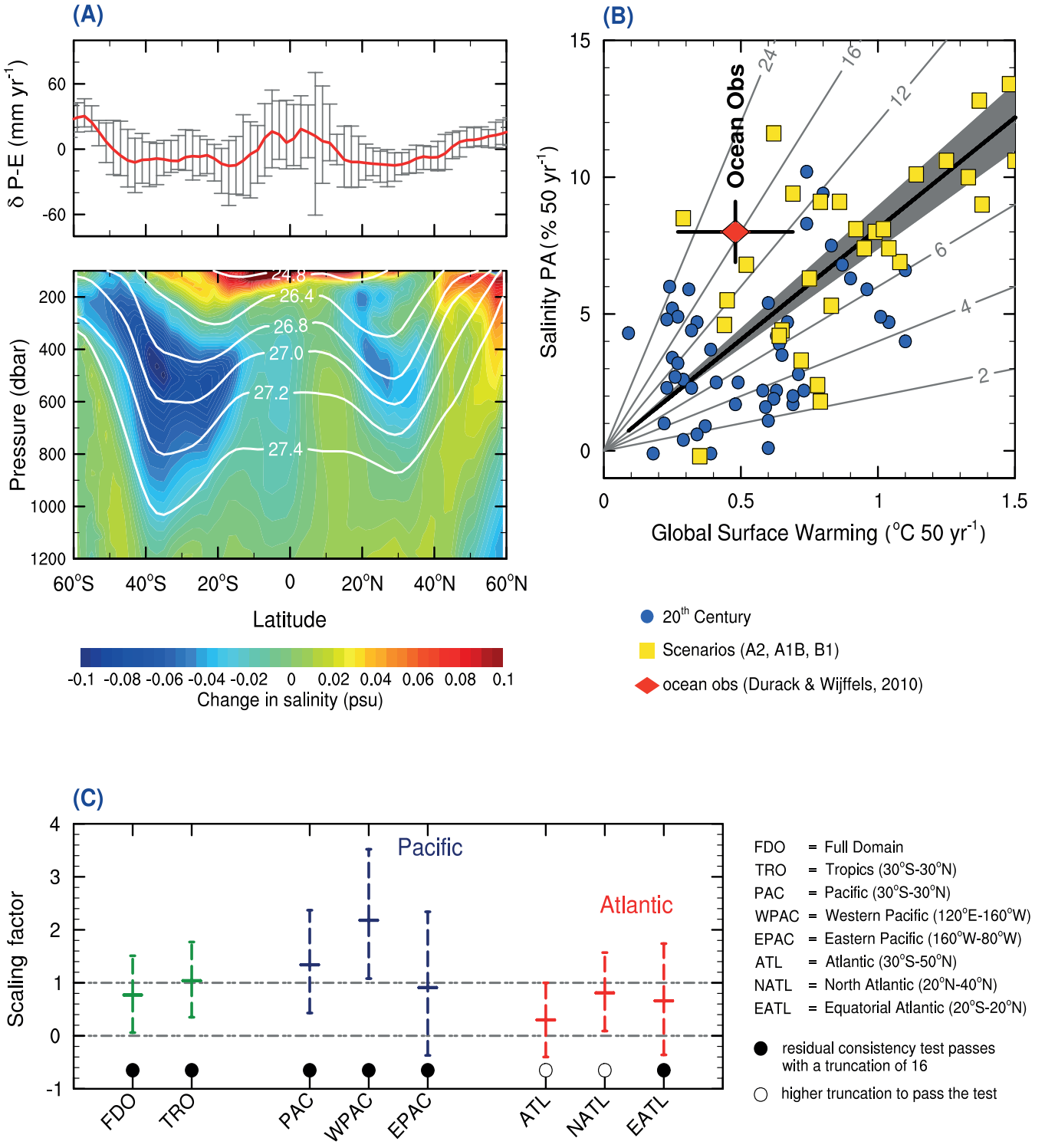


**Figure 10.15 |** Ocean salinity change and hydrologic cycle. (A) Ocean salinity change observed in the interior of the ocean (A, lower panel in practical salinity units or psu, and white lines are surfaces of constant density) and comparison with ten CMIP3 model projections of precipitation minus evaporation δ (P – E) in mm yr$^{-1}$ for the same period as the observed changes (1970 to 1990s) (A, top panel, red line is the mean of the simulations and error bars are the simulated range). (B) The amplification of the current surface salinity pattern over a 50-year period as a function of global temperature change. Ocean surface salinity pattern amplification has a 16% increase for the 1950–2000 period (red diamond, see text and Section 3.3). Also on this panel CMIP3 simulations from Special Report on Emission Scenarios (SRES) (yellow squares) and from 20th century simulations (blue circles). A total of 93 simulations have been used. (C) Regional detection and attribution in the equatorial Pacific and Atlantic Oceans for 1970 to 2002. Scaling factors for all forcings (anthropogenic) fingerprint are shown (see Box 10.1) with their 5 to 95% uncertainty range, estimated using the total least square approach. Full domain (FDO, 30°S to 50°N), Tropics (TRO, 30°S to 30°N), Pacific (PAC, 30°S to 30°N), west Pacific (WPAC, 120°E to 160°W), east Pacific (EPAC, 160°W to 80°W), Atlantic (ATL, 30°S to 50°N), subtropical north Atlantic (NATL, 20°N to 40°N) and equatorial Atlantic (EATL, 20°S to 20°N) factors are shown. Black filled dots indicate when the residual consistency test passes with a truncation of 16 whereas empty circles indicate a higher truncation was needed to pass the consistency test. Horizontal dashed lines indicate scaling factor of 0 or 1. (A, B and C are adapted from Helm et al. (2010), Durack et al. (2012) and Terray et al. (2012), respectively.)

On a global scale surface and subsurface salinity changes (1955–2004) over the upper 250 m of the water column cannot be explained by natural variability (probability is <0.05) (Pierce et al., 2012). However, the observed salinity changes match the model distribution of forced changes (GHG and tropospheric aerosols), with the observations typically falling between the 25th and 75th percentile of the model distribution at all depth levels for salinity (and temperature). Natural external variability taken from the simulations with just solar and volcanic variations in forcing do not match the observations at all, thus excluding the hypothesis that observed trends can be explained by just solar or volcanic variations.

The results from surface salinity trends and changes are consistent with the results from studies of precipitation over the tropical ocean from the shorter satellite record (Wentz et al., 2007; Allan et al., 2010). These surface salinity results are also consistent with our understanding of the thermodynamic response of the atmosphere to warming (Held and Soden, 2006; Stephens and Hu, 2010) and the amplification of the water cycle. The large number of studies showing patterns of change consistent with amplification of the water cycle, and the detection and attribution studies for the tropical oceans (Terray et al., 2012) and the global pattern of ocean salinity change (Pierce et al., 2012), when combined with our understanding of the physics of the water cycle and estimates of internal climate variability, give *high confidence* in our understanding of the drivers of surface and near surface salinity changes. It is *very likely* that these salinity changes have a discernable contribution from anthropogenic forcing since the 1960s.

### 10.4.3 Sea Level

At the time of the AR4, the historical sea level rise budget had not been closed (within uncertainties), and there were few studies quantifying the contribution of anthropogenic forcing to the observed sea level rise and glacier melting. Relying on expert assessment, the AR4 had concluded based on modelling and ocean heat content studies that ocean warming and glacier mass loss had *very likely* contributed to sea level rise during the latter half of the 20th century. The AR4 had reported that climate models that included anthropogenic and natural forcings simulated the observed thermal expansion since 1961 reasonably well, and that it is *very unlikely* that the warming during the past half century is due only to known natural causes (Hegerl et al., 2007b).

Since the AR4, corrections applied to instrumental errors in ocean temperature measurements have considerably improved estimates of upper-ocean heat content (see Sections 3.2 and 10.4.1), and therefore ocean thermal expansion. Closure of the global mean sea level rise budget as an evolving time series since the early1970s (Church et al., 2011) indicates that the two major contributions to the rate of global mean sea level rise have been thermal expansion and glacier melting with additional contributions from Greenland and Antarctic ice sheets. Observations since 1971 indicate with *high confidence* that thermal expansion and glaciers (excluding the glaciers in Antarctica) explain 75% of the observed rise (see Section 13.3.6). Ice sheet contributions remain the greatest source of uncertainty over this period and on longer time scales. Over the 20th century, the global mean sea level rise budget (Gregory et al., 2012 ) has been another important step in understanding the relative contributions of different drivers. The observed contribution from thermal expansion is well captured in climate model simulations with historical forcings as are contributions from glacier melt when simulated by glacier models driven by climate model simulations of historical climate (Church et al., 2013; Table 13.1). The model results indicate that most of the variation in the contributions of thermal expansion and glacier melt to global mean sea level is in response to natural and anthropogenic RFs (Domingues et al., 2008; Palmer et al., 2009; Church et al., 2013).

The strong physical relationship between thermosteric sea level and ocean heat content (through the equation of state for seawater) means that the anthropogenic ocean warming (Section 10.4.1) has contributed to global sea level rise over this period through thermal expansion. As Section 10.5.2 concludes, it is *likely* that the observed substantial mass loss of glaciers is due to human influence and that it is *likely* that anthropogenic forcing and internal variability are both contributors to recent observed changes on the Greenland ice sheet. The causes of recently observed Antarctic ice sheet contribution to sea level are less clear due to the short observational record and incomplete understanding of natural variability. Taking the causes of Greenland ice sheet melt and glacier mass loss together (see Section 10.5.2), it is concluded with *high confidence* that it is *likely* that anthropogenic forcing has contributed to sea level rise from melting glaciers and ice sheets. Combining the evidence from ocean warming and mass loss of glaciers we conclude that it is *very likely* that there is a substantial contribution from anthropogenic forcing to the global mean sea level rise since the 1970s.

On ocean basin scales, detection and attribution studies do show the emergence of detectable signals in the thermosteric component of sea level that can be largely attributed to human influence (Barnett et al., 2005; Pierce et al., 2012). Regional changes in sea level at the sub-ocean basin scales and finer exhibit more complex variations associated with natural (dynamical) modes of climate variability (Section 13.6). In some regions, sea level trends have been observed to differ significantly from global mean trends. These have been related to thermosteric changes in some areas and in others to changing wind fields and resulting changes in the ocean circulation (Han et al., 2010; Timmermann et al., 2010; Merrifield and Maltrud, 2011). The regional variability on decadal and longer time scales can be quite large (and is not well quantified in currently available observations) compared to secular changes in the winds that influence sea level. Detection of human influences on sea level at the regional scale (that is smaller than sub-ocean basin scales) is currently limited by the relatively small anthropogenic contributions compared to natural variability (Meyssignac et al., 2012) and the need for more sophisticated approaches than currently available.

### 10.4.4 Oxygen and Ocean Acidity

Oxygen is an important physical and biological tracer in the ocean (Section 3.8.3) and is projected to decline by 3 to 6% by 2100 in response to surface warming (see Section 6.4.5). Oxygen decreases are also observed in the atmosphere and linked to burning of fossil fuels (Section 6.1.3.2). Despite the relatively few observational studies of oxygen change in the oceans (Bindoff and McDougall, 2000; Ono et al., 2001; Keeling and Garcia, 2002; Emerson et al., 2004; Aoki et al., 2005;

Mecking et al., 2006; Nakanowatari et al., 2007; Brandt et al., 2010) they all show a pattern of change consistent with the known ocean circulation and surface ventilation. A recent global analysis of oxygen data from the 1960s to 1990s for change confirm these earlier results and extends the spatial coverage from local to global scales (Helm et al., 2011). The strongest decreases in oxygen occur in the mid-latitudes of both hemispheres, near regions where there is strong water renewal and exchange between the ocean interior and surface waters. The attribution study of oxygen decreases using two Earth System Models (ESMs) concluded that observed changes for the Atlantic Ocean are 'indistinguishable from natural internal variability'; however, the changes of the global zonal mean to external forcing (all forcings including GHGs) has a detectable influence at the 10% significance level (Andrews et al., 2013). The chief sources of uncertainty are the paucity of oxygen observations, particularly in time, the precise role of the biological pump and changes in ocean productivity in the models (see Sections 3.8.3 and 6.4.5), and model circulation biases particularly near the oxygen minimum zone in tropical waters (Brandt et al., 2010; Keeling et al., 2010; Stramma et al., 2010). These results of observed changes in oxygen and the attribution studies of oxygen changes (Andrews et al., 2013), along with the attribution of human influences on the physical factors that affect oxygen in the oceans such as surface temperatures changes (Section 10.3.2), increased ocean heat content (Section 10.4.1) and observed increased in ocean stratification (Section 3.2.2) provides evidence for human influence on oxygen. When these lines of evidence are taken together it is concluded that with *medium confidence* or *about as likely as not* that the observed oxygen decreases can be attributed in part to human influences.

The observed trends (since the 1980s) for ocean acidification and its cause from rising $CO_2$ concentrations is discussed in Section 3.8.2 (Box 3.2 and Table 10.1). There is *very high* confidence that anthropogenic $CO_2$ has resulted in the acidification of surface waters of between –0.0015 and –0.0024 pH units per year.

## 10.5 Cryosphere

This section considers changes in sea ice, ice sheets and ice shelves, glaciers, snow cover. The assessment of attribution of human influences on temperature over the Arctic and Antarctica is in Section 10.3.1.

### 10.5.1 Sea Ice

#### 10.5.1.1 Arctic and Antarctic Sea Ice

The Arctic cryosphere shows large observed changes over the last decade as noted in Chapter 4 and many of these shifts are indicators of major regional and global feedback processes (Kattsov et al., 2010). An assessment of sea ice models' capacity to simulate Arctic and Antarctic sea ice extent is given in Section 9.4.3. Of principal importance is 'Arctic Amplification' (see Box 5.1) where surface temperatures in the Arctic are increasing faster than elsewhere in the world.

The rate of decline of Arctic sea ice thickness and September sea ice extent has increased considerably in the first decade of the 21st century (Maslanik et al., 2007; Nghiem et al., 2007; Comiso and Nishio, 2008; Deser and Teng, 2008; Zhang et al., 2008; Alekseev et al., 2009; Comiso, 2012; Polyakov et al., 2012). Based on a sea ice reanalysis and verified by ice thickness estimates from satellite sensors, it is estimated that three quarters of summer Arctic sea ice volume has been lost since the 1980s (Schweiger et al., 2011; Maslowski et al., 2012; Laxon et al., 2013; Overland and Wang, 2013). There was also a rapid reduction in ice extent, to 37% less in September 2007 and to 49% less in September 2012 relative to the 1979–2000 climatology (Figure 4.11, Section 4.2.2). Unlike the loss record set in 2007 that was dominated by a major shift in climatological winds, sea ice loss in 2012 was more due to a general thinning of the sea ice (Lindsay et al., 2009; Wang et al., 2009a; Zhang et al., 2013). All recent years have ice extents that fall at least two standard deviations below the long-term sea ice trend.

The amount of old, thick multi-year sea ice in the Arctic has decreased by 50% from 2005 through 2012 (Giles et al., 2008; Kwok et al., 2009; Kwok and Untersteiner, 2011 and Figures 4.13 and 4.14). Sea ice has also become more mobile (Gascard et al., 2008). We now have seven years of data that show sea ice conditions are substantially different to that observed prior to 2006. The relatively large increase in the percentage of first year sea ice across the Arctic basin can be considered 'a new normal.'

Confidence in detection of change comes in part from the consistency of multiple lines of evidence. Since AR4, evidence has continued to accumulate from a range of observational studies that systematic changes are occurring in the Arctic. Persistent trends in many Arctic variables, including sea ice, the timing of spring snow melt, increased shrubbiness in tundra regions, changes in permafrost, increased area of forest fires, changes in ecosystems, as well as Arctic-wide increases in air temperatures, can no longer be associated solely with the dominant climate variability patterns such as the Arctic Oscillation, Pacific North American pattern or Atlantic Meridional Oscillation (AMO) (Quadrelli and Wallace, 2004; Vorosmarty et al., 2008; Overland, 2009; Brown and Robinson, 2011; Mahajan et al., 2011; Oza et al., 2011a; Wassmann et al., 2011; Nagato and Tanaka, 2012). Duarte et al. (2012) completed a meta-analysis showing evidence from multiple indicators of detectable climate change signals in the Arctic.

The increase in the magnitude of recent Arctic temperature and decrease in sea ice volume and extent are hypothesized to be due to coupled Arctic amplification mechanisms (Serreze and Francis, 2006; Miller et al., 2010). These feedbacks in the Arctic climate system suggest that the Arctic is sensitive to external forcing (Mahlstein and Knutti, 2012 ). Historically, changes were damped by the rapid formation of sea ice in autumn causing a negative feedback and a rapid seasonal cooling. But recently, the increased mobility and loss of multi-year sea ice, combined with enhanced heat storage in the sea ice-free regions of the Arctic Ocean form a connected set of processes with positive feedbacks causing an increase in Arctic temperatures and a decrease in sea ice extent (Manabe and Wetherald, 1975; Gascard et al., 2008; Serreze et al., 2009; Stroeve et al., 2012a, 2012b) . In addition to the well known *ice albedo* feedback where decreased sea ice cover decreases the amount of *insolation* reflected from the surface, there is a late summer/early autumn positive *ice insulation* feedback due to additional ocean heat storage in areas previously covered by sea ice

(Jackson et al., 2010). Arctic amplification may also have a contribution from poleward heat transport in the atmosphere and ocean (Langen and Alexeev, 2007; Graversen and Wang, 2009; Doscher et al., 2010; Yang et al., 2010).

It appears that recent Arctic changes are in response to a combination of global-scale warming, from warm anomalies from internal climate variability on different time scales, and are amplified from the multiple feedbacks described above. For example, when the 2007 sea ice minimum occurred, Arctic temperatures had been rising and sea ice extent had been decreasing over the previous two decades (Stroeve et al., 2008; Screen and Simmonds, 2010). Nevertheless, it took unusually persistent southerly winds along the dateline over the summer months to initiate the sea ice loss event in 2007 (Zhang et al., 2008; Wang et al., 2009b). Similar southerly wind patterns in previous years did not initiate major reductions in sea ice extent because the sea ice was too thick to respond (Overland et al., 2008). Increased oceanic heat transport through the Barents Sea in the first decade of the 21st century and the AMO on longer time scales may also have played a role in determining sea ice anomalies in the Atlantic Arctic (Dickson et al., 2000; Semenov, 2008; Zhang et al., 2008; Day et al., 2012) . Based on the evidence in the previous paragraphs there is *high confidence* that these Arctic amplification mechanisms are currently affecting regional Arctic climate. But it also suggests that the timing of future major sea ice loss events will be difficult to project. There is evidence therefore that internal variability of climate, long-term warming, and Arctic Amplification feedbacks have all contributed to recent decreases in Arctic sea ice (Kay et al., 2011b; Kinnard et al., 2011; Overland et al., 2011; Notz and Marotzke, 2012).

Turning to model-based attribution studies, Min et al. (2008b) compared the seasonal evolution of Arctic sea ice extent from observations with those simulated by multiple General Circulation Models (GCMs) for 1953–2006. Comparing changes in both the amplitude and shape of the annual cycle of the sea ice extent reduces the chance of spurious detection due to coincidental agreement between the response to anthropogenic forcing and other factors, such as slow internal variability. They found that human influence on the sea ice extent changes has been robustly detected since the early 1990s. The anthropogenic signal is also detectable for individual months from May to December, suggesting that human influence, strongest in late summer, now also extends into colder seasons. Kay et al. (2011b), Jahn et al. (2012) and Schweiger et al. (2011) used the Community Climate System Model 4 (CCSM4) to investigate the influence of anthropogenic forcing on late 20th century and early 21st century Arctic sea ice extent and volume trends. On all time scales examined (2 to 50+ years), the most extreme negative extent trends observed in the late 20th century cannot be explained by modeled internal variability alone. Comparing trends from the CCSM4 ensemble to observed trends suggests that internal variability could account for approximately half of the observed 1979–2005 September Arctic sea ice extent loss. Attribution of anthropogenic forcing is also shown by comparing September sea ice extent as projected by seven models from the set of CMIP5 models' hindcasts to control runs without anthropogenic forcing (Figure 10.16a; Wang and Overland, 2009). The mean of sea ice extents in seven models' ensemble members are below the level of their control runs by about 1995, similar to the result of Min et al. (2008b).

A question as recently as 6 years ago was whether the recent Arctic warming and sea ice loss was unique in the instrumental record and whether the observed trend would continue (Serreze et al., 2007). Arctic temperature anomalies in the 1930s were apparently as large as those in the 1990s and 2000s. There is still considerable discussion of the ultimate causes of the warm temperature anomalies that occurred in the Arctic in the 1920s and 1930s (Ahlmann, 1948; Veryard, 1963; Hegerl et al., 2007a, 2007b). The early 20th century warm period, while reflected in the hemispheric average air temperature record (Brohan et al., 2006), did not appear consistently in the mid-latitudes nor on the Pacific side of the Arctic (Johannessen et al., 2004; Wood and Overland, 2010). Polyakov et al. (2003) argued that the Arctic air temperature records reflected a natural cycle of about 50 to 80 years. However, many authors (Bengtsson et al., 2004; Grant et al., 2009; Wood and Overland, 2010; Brönnimann et al., 2012) instead link the 1930s temperatures to internal variability in the North Atlantic atmospheric and ocean circulation as a single episode that was sustained by ocean and sea ice processes in the Arctic and north Atlantic. The Arctic-wide increases of temperature in the last decade contrast with the episodic regional increases in the early 20th century, suggesting that it is unlikely that recent increases are due to the same primary climate process as the early 20th century.

In the case of the Arctic we have *high confidence* in observations since 1979, from models (see Section 9.4.3 and from simulations comparing with and without anthropogenic forcing), and from physical understanding of the dominant processes; taking these three factors together it is *very likely* that anthropogenic forcing has contributed to the observed decreases in Arctic sea ice since 1979.

Whereas sea ice extent in the Arctic has decreased, sea ice extent in the Antarctic has *very likely* increased (Section 4.2.3). Sea ice extent across the SH over the year as a whole increased by 1.3 to 1.67% per decade from 1979 to 2012, with the largest increase in the Ross Sea during the autumn, while sea ice extent decreased in the Amundsen-Bellingshausen Sea (Comiso and Nishio, 2008; Turner et al., 2009, 2013; Section 4.2.3; Oza et al., 2011b). The observed upward trend in Antarctic sea ice extent is found to be inconsistent with internal variability based on the residuals from a linear trend fitted to the observations, though this approach could underestimate multi-decadal variability (Section 4.2.3; Turner et al., 2013; Section 4.2.3; Zunz et al., 2013). The CMIP5 simulations on average simulate a decrease in Antarctic sea ice extent (Turner et al., 2013; Zunz et al., 2013; Figure 10.16b), though Turner et al. (2013) find that approximately 10% of CMIP5 simulations exhibit an increasing trend in Antarctic sea ice extent larger than observed over the 1979–2005 period. However, Antarctic sea ice extent variability appears on average to be too large in the CMIP5 models (Turner et al., 2013; Zunz et al., 2013). Overall, the shortness of the observed record and differences in simulated and observed variability preclude an assessment of whether or not the observed increase in Antarctic sea ice extent is inconsistent with internal variability. Based on Figure 10.16b and Meehl et al. (2007b), the trend of Antarctic sea ice loss in simulations due to changes in forcing is weak (relative to the Arctic) and the internal variability is high, and thus the time necessary for detection is longer than in the Arctic.

Several recent studies have investigated the possible causes of Antarctic sea ice trends. Early studies suggested that stratospheric ozone depletion may have driven increasing trends in Antarctic ice extent (Goosse et al., 2009; Turner et al., 2009; WMO (World Meteorological Organization), 2011), but recent studies demonstrate that simulated sea ice extent decreases in response to prescribed changes in stratospheric ozone (Sigmond and Fyfe, 2010; Bitz and Polvani, 2012). An alternative explanation for the lack of melting of Antarctic sea ice is that sub-surface ocean warming, and enhanced freshwater input possibly in part from ice shelf melting, have made the high-latitude Southern Ocean fresher (see Section 3.3) and more stratified, decreasing the upward heat flux and driving more sea ice formation (Zhang, 2007; Goosse et al., 2009; Bintanja et al., 2013). An idealized simulation of the response to freshwater input similar to that estimate due to ice shelf melting exhibited an increase in sea ice extent (Bintanja et al., 2013), but this result has yet to be reproduced with other models. Overall we conclude that there is *low confidence* in the scientific understanding of the observed increase in Antarctic sea ice extent since 1979, owing to

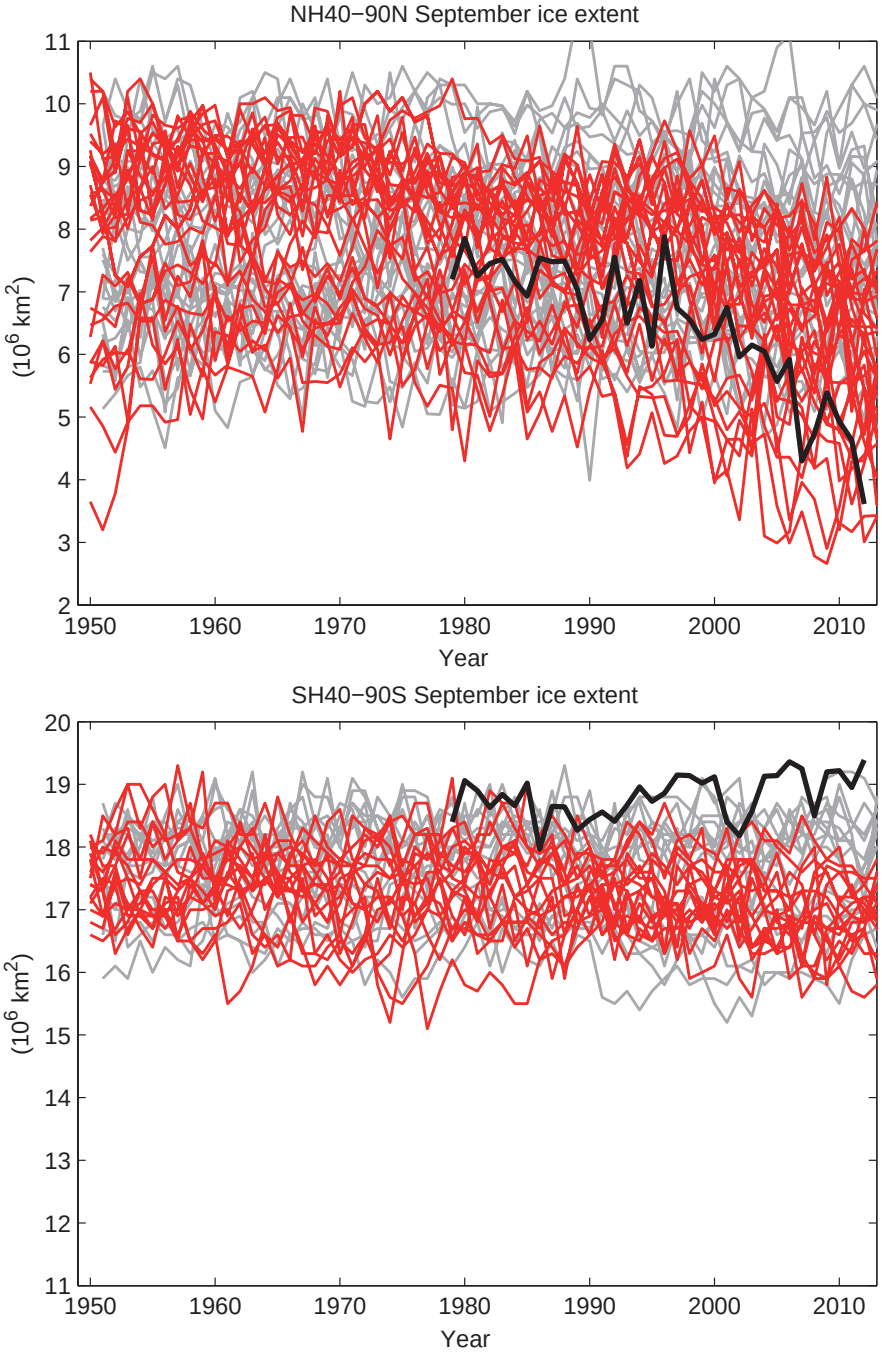


**Figure 10.16 |** September sea ice extent for Arctic (top) and Antarctic (bottom) adapted from (Wang and Overland, 2012). Only CMIP5 models that simulated seasonal mean and magnitude of seasonal cycle in reasonable agreement with observations are included in the plot. The grey lines are the runs from the pre-industrial control runs, and the red lines are from Historical simulations runs patched with RCP8.5 runs for the period of 2005–2012. The black line is based on data from National Snow and Ice Data Center (NSIDC). There are 24 ensemble members from 11 models for the Arctic and 21 members from 6 models for the Antarctic plot. See Supplementary Material for the precise models used in the top and bottom panel.

the larger differences between sea ice simulations from CMIP5 models and to the incomplete and competing scientific explanations for the causes of change and *low confidence* in estimates of internal variability (Section 9.4.3).

### 10.5.2 Ice Sheets, Ice Shelves and Glaciers

#### 10.5.2.1 Greenland and Antarctic Ice Sheets

The Greenland and Antarctic ice sheets are important to regional and global climate because (along with other cryospheric elements) they cause a polar amplification of surface temperatures, a source of fresh water to the ocean, and represent a source of potentially irreversible change to the state of the Earth system (Hansen and Lebedeff, 1987). These two ice sheets are important contributors to sea level rise representing two-thirds of the contributions from all ice covered regions (Jacob et al., 2012; Pritchard et al., 2012; see Sections 4.4 and 13.3.3). Observations of surface mass balance (increased ablation versus increased snowfall) are dealt with in Section 4.4.3 and ice sheet models are discussed in Sections 13.3 and 13.5.

Attribution of change is difficult as ice sheet and glacier changes are local and ice sheet processes are not generally well represented in climate models thus precluding formal single-step detection and attribution studies. However, Greenland observational records show large recent changes. Section 13.3 concludes that regional models for Greenland can reproduce trends in the surface mass balance loss quite well if they are forced with the observed meteorological record, but not with forcings from a Global Climate Model. Regional model simulations (Fettweis et al., 2013) show that Greenland surface melt increases nonlinearly with rising temperatures due to the positive feedback between surface albedo and melt.

There have been exceptional changes in Greenland since 2007 marked by record-setting high air temperatures, ice loss by melting and marine-terminating glacier area loss (Hanna et al., 2013; Section 4.4.4). Along Greenland's west coast temperatures in 2010 and 2011were the warmest since record keeping began in 1873 resulting in the highest observed melt rates in this region since 1958 (Fettweis et al., 2011). The annual rate of area loss in marine-terminating glaciers was 3.4 times that of the previous 8 years, when regular observations became available. In 2012, a new record for summertime ice mass loss was two standard deviations below the 2003–2012 mean, as estimated from the Gravity Recovery and Climate Experiment (GRACE) satellite (Tedesco et al., 2012). The trend of summer mass change during 2003–2012 is rather uniform over this period at $-29 \pm 11$ Gt yr$^{-1}$.

Record surface melts during 2007–2012 summers are linked to persistent atmospheric circulation that favored warm air advection over Greenland. These persistent events have changed in frequency since the beginning of the 2000s (L'Heureux et al., 2010; Fettweis et al., 2011). Hanna et al. (2013) show a weak relation of Greenland temperatures and ice sheet runoff with the AMO; they more strongly correlate with a Greenland atmospheric blocking index. Overland et al. (2012) and Francis and Vavrus (2012) suggest that the increased frequency of the Greenland blocking pattern is related to broader scale Arctic changes. Since 2007, internal variability is *likely* to have further enhanced the melt over Greenland. Mass loss and melt is also occurring in Greenland through the intrusion of warm water into the major glaciers such as Jacobshaven Glacier (Holland et al., 2008; Walker et al., 2009).

Hanna et al. (2008) attribute increased Greenland runoff and melt since 1990 to global warming; southern Greenland coastal and NH summer temperatures were uncorrelated between the 1960s and early 1990s but correlated significantly positively thereafter. This relationship was modulated by the NAO, whose summer index significantly negatively correlated with southern Greenland summer temperatures until the early 1990s but not thereafter. Regional modelling and observations tell a consistent story of the response of Greenland temperatures and ice sheet runoff to shifts in recent regional atmospheric circulation associated with larger scale flow patterns and global temperature increases. It is *likely* that anthropogenic forcing has contributed to surface melting of the Greenland ice sheet since 1993.

There is clear evidence that the West Antarctic ice sheet is contributing to sea level rise (Bromwich et al., 2013). Estimates of ice mass in Antarctic since 2000 show that the greatest losses are at the edges (see Section 4.4). An analysis of observations underneath a floating ice shelf off West Antarctica shows that ocean warming and more transport of heat by ocean circulation are largely responsible for increasing melt rates (Jacobs et al., 2011; Joughin and Alley, 2011; Mankoff et al., 2012; Pritchard et al., 2012).

Antarctica has regionally dependent decadal variability in surface temperature with variations in these trends depending on the strength of the SAM climate pattern. Recent warming in continental west Antarctica has been linked to SST changes in the tropical Pacific (Ding et al., 2011). As with Antarctic sea ice, changes in Antarctic ice sheets have complex causes (Section 4.4.3). The observational record of Antarctic mass loss is short and the internal variability of the ice sheet is poorly understood. Due to a low level of scientific understanding there is *low confidence* in attributing the causes of the observed loss of mass from the Antarctic ice sheet since 1993. Possible future instabilities in the west Antarctic ice sheet cannot be ruled out, but projection of future climate changes over West Antarctica remains subject to considerable uncertainty (Steig and Orsi, 2013).

#### 10.5.2.2 Glaciers

In the 20th century, there is robust evidence that large-scale internal climate variability governs interannual to decadal variability in glacier mass (Hodge et al., 1998; Nesje et al., 2000; Vuille et al., 2008; Huss et al., 2010; Marzeion and Nesje, 2012) and, along with glacier dynamics, impacts glacier length as well (Chinn et al., 2005). On time periods longer than years and decades, there is now evidence of recent ice loss (see Section 4.3.3) due to increased ambient temperatures and associated regional moisture changes. However, few studies evaluate the direct attribution of the current observed mass loss to anthropogenic forcing, owing to the difficulty associated with contrasting scales between glaciers and the large-scale atmospheric circulation (Mölg et al., 2012). Reichert et al. (2002) show for two sample sites at mid and high latitude that internal climate variability over multiple millennia as represented in a GCM would not result in such short glacier lengths as observed in the 20th century. For a sample site at low latitude using

multi-step attribution, Mölg et al. (2009) (and references therein) found a close relation between glacier mass loss and the externally forced atmosphere–ocean circulation in the Indian Ocean since the late 19th century. A second, larger group of studies makes use of century-scale glacier records (mostly glacier length but mass balance as well) to extract evidence for external drivers. These include local and regional changes in precipitation and air temperature, and related parameters (such as melt factors and solid/liquid precipitation ratio) estimated from the observed change in glaciers. In general these studies show that the glacier changes reveal unique departures since the 1970s, and that the inferred climatic drivers in the 20th century and particularly in most recent decades, exceed the variability of the earlier parts of the records (Oerlemans, 2005; Yamaguchi et al., 2008; Huss and Bauder, 2009; Huss et al., 2010; Leclercq and Oerlemans, 2011). These results underline the contrast to former centuries where observed glacier fluctuations can be explained by internal climate variability (Reichert et al., 2002; Roe and O'Neal, 2009; Nussbaumer and Zumbühl, 2012). Anthropogenic land cover change is an unresolved forcing, but a first assessment suggests that it does not confound the impacts of recent temperature and precipitation changes if the land cover changes are of local nature (Mölg et al., 2012). The robustness of the estimates of observed mass loss since the 1960s (Section 4.3, Figure 4.11), the confidence we have in estimates of natural variations and internal variability from long-term glacier records, and our understanding of glacier response to climatic drivers provides robust evidence and, therefore, *high confidence* that a substantial part of the mass loss of glaciers is *likely* due to human influence.

### 10.5.3 Snow Cover

Both satellite and *in situ* observations show significant reductions in the NH snow cover extent (SCE) over the past 90 years, with most reduction occurring in the 1980s (see Section 4.5). Formal detection and attribution studies have indicated anthropogenic influence on NH SCE (Rupp et al., 2013) and western USA snow water equivalent (SWE, Pierce et al., 2008). Pierce et al. (2008) detected anthropogenic influence in the ratio of 1 April SWE over October to March precipitation over the period 1950–1999. These reductions could not be explained by natural internal climate variability alone, nor by changes in solar and volcanic forcing. In their analysis of NH SCE using 13 CMIP5 simulations over the 1922–2005 period, Rupp et al. (2013) showed that some CMIP5 simulations with natural external and anthropogenic forcings could explain the observed decrease in spring SEC though the CMIP5 simulations with all forcing as a whole could only explain half of the magnitude of decrease, and that volcanic and solar variations (from four CMIP5 simulations) were inconsistent with observations. We conclude with *high confidence* in the observational and modelling evidence that the decrease in NH snow extent since the 1970s is *likely* to be caused by all external forcings and has an anthropogenic contribution (see Table 10.1).

## 10.6 Extremes

Because many of the impacts of climate changes may manifest themselves through weather and climate extremes, there is increasing interest in quantifying the role of human and other external influences on those extremes. SREX assessed causes of changes in different types of extremes including temperature and precipitation, phenomena that influence the occurrence of extremes (e.g., storms, tropical cyclones), and impacts on the natural physical environment such as drought (Seneviratne et al., 2012). This section assesses current understanding of causes of changes in weather and climate extremes, using AR4 as a starting point. Any changes or modifications to SREX assessment are highlighted.

### 10.6.1 Attribution of Changes in Frequency/ Occurrence and Intensity of Extremes

This sub-section assesses attribution of changes in the characteristics of extremes including frequency and intensity of extremes. Many of the extremes discussed in this sub-section are moderate extreme events that occur more than once in a year (see Box 2.4 for detailed discussion). Attribution of changes in the risk of specific extreme events, which are also very rare in general, is assessed in the next sub-section.

#### 10.6.1.1 Temperature Extremes

AR4 concluded that 'surface temperature extremes have *likely* been affected by anthropogenic forcing'. Many indicators of climate extremes and variability showed changes consistent with warming, including a widespread reduction in number of frost days in mid-latitude regions and evidence that in many regions warm extremes had become warmer and cold extremes had become less cold. We next assess new studies made since AR4.

Relatively warm seasonal mean temperatures (e.g., those that have a recurrence once in 10 years) have seen a rapid increase in frequency for many regions worldwide (Jones et al., 2008; Stott et al., 2011; Hansen et al., 2012) and an increase in the occurrence frequencies of unusually warm seasonal and annual mean temperatures has been attributed in part to human influence (Stott et al., 2011; Christidis et al., 2012a, 2012b).

A large amount of evidence supports changes in daily data based temperature extreme indices consistent with warming, despite different data sets or different methods for data processing having been used (Section 2.6). The effects of human influence on daily temperature extremes is suggested by both qualitative and quantitative comparisons between observed and CMIP3 based modelled values of warm days and warm nights (the number of days exceeding the 90th percentile of daily maximum and daily minimum temperatures referred to as TX90p and TN90p, see also Section 2.7) and cold days and cold nights (the number of days with daily maximum and daily minimum temperatures below the 10th percentile referred to as TX10p and TN10p; see also Section 2.7). Trends in temperature extreme indices computed for Australia (Alexander and Arblaster, 2009) and the USA (Meehl et al., 2007a) using observations and simulations of the 20th century with nine GCMs that include both anthropogenic and natural forcings are found to be consistent. Both observations and model simulations show a decrease in the number of frost days, and an increase in the growing season length, heatwave duration and TN90p in the second half of the 20th century. Two of the models (PCM and CCSM3) with simulations that include only anthropogenic or only natural forcings

indicate that the observed changes are simulated with anthropogenic forcings, but not with natural forcings (even though there are some differences in the details of the forcings). Morak et al. (2011) found that over many sub-continental regions, the number of warm nights (TN90p) shows detectable changes over the second half of the 20th century that are consistent with model simulated changes in response to historical external forcings. They also found detectable changes in indices of temperature extremes when the data were analysed over the globe as a whole. As much of the long-term change in TN90p can be predicted based on the interannual correlation of TN90p with mean temperature, Morak et al. (2013) conclude that the detectable changes are attributed in a multi-step approach (see Section 10.2.4) in part to GHG increases. Morak et al. (2013) have extended this analysis to TX10p, TN10p, TX90p as well as TN90p, using fingerprints from HadGEM1 and find detectable changes on global scales and in many regions (Figure 10.17).

Human influence has also been detected in two different measures of the intensity of extreme daily temperatures in a year. Zwiers et al. (2011) compared four extreme temperature variables including warmest daily maximum and minimum temperatures (annual maximum daily maximum and minimum temperatures, referred to as TXx, TNx) and coldest daily maximum and minimum temperatures (annual minimum daily maximum and minimum temperatures, referred to as TXn, TNn) from observations and from simulations with anthropogenic forcing or anthropogenic and natural external forcings from seven GCMs. They consider these extreme daily temperatures to follow generalized extreme value (GEV) distributions with location, shape and scale parameters. They fit GEV distributions to the observed extreme temperatures with location parameters as linear functions of signals obtained from the model simulation. They found that both anthropogenic influence and combined influence of anthropogenic and natural forcing can be detected in all four extreme temperature variables at the global scale over the land, and also regionally over many large land areas (Figure 10.17). In a complementary study, Christidis et al. (2011) used an optimal fingerprint method to compare observed and modelled time-varying location parameters of extreme temperature distributions. They detected the effects of anthropogenic forcing on warmest daily temperatures in a single fingerprint analysis, and were able to separate the effects of natural from anthropogenic forcings in a two fingerprint analysis.



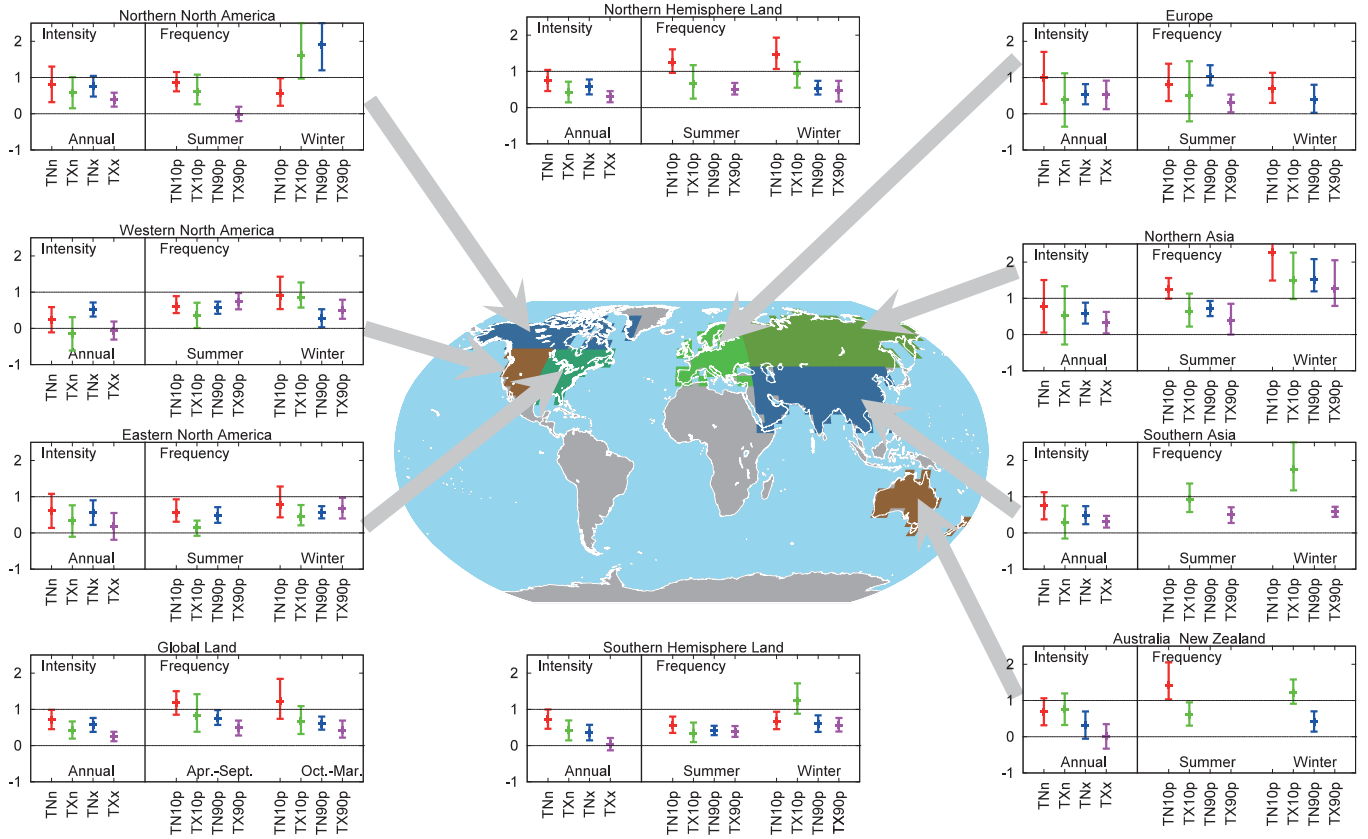


**Figure 10.17 |** Detection results for changes in intensity and frequency of extreme events. The left side of each panel shows scaling factors and their 90% confidence intervals for intensity of annual extreme temperatures in response to external forcings for the period 1951–2000. TNn and TXn represent coldest daily minimum and maximum temperatures, respectively, while TNx and TXx represent warmest daily minimum and maximum temperatures (updated from Zwiers et al., 2011). Fingerprints are based on simulations of climate models with both anthropogenic and natural forcings. Right-hand sides of each panel show scaling factors and their 90% confidence intervals for changes in the frequency of temperature extremes for winter (October to March for the Northern Hemisphere and April to September for the Southern Hemisphere), and summer half years. TN10p, TX10p are respectively the frequency of cold nights and days (daily minimum and daily maximum temperatures falling below their 10th percentiles for the base period 1961–1990). TN90p and TX90p are the frequency of warm nights and days (daily minimum and daily maximum temperatures above their respective 90th percentiles calculated for the 1961–1990 base period (Morak et al., 2013) with fingerprints based on simulations of Hadley Centre Global Environmental Model 1 (HadGEM1) with both anthropogenic and natural forcings. Detection is claimed at the 5% significance level if the 90% confidence interval of a scaling factor is entirely above the zero line. Grey represents regions with insufficient data.

Human influence on annual extremes of daily temperatures may be detected separately from natural forcing at the global scale (Christidis et al., 2011) and also at continental and sub-continental scales (Min et al., 2013). Over China, Wen et al. (2013) showed that anthropogenic influence may be separately detected from that of natural forcing in daily extreme temperatures (TNn, TNx, TXn and TXx), although the influence of natural forcing is not detected, and they also showed that the influence of GHGs in these indices may be separately detected from other anthropogenic forcings. Christidis et al. (2013) found that on a quasi-global scale, the cooling effect due to the decrease in tree cover and increase in grass cover since pre-industrial times as simulated by one ESM is detectable in the observed change of warm extremes. Urbanization may have also affected extreme temperatures in some regions; for example Zhou and Ren (2011) found that extreme temperature warms more in rural stations than in urban sites in China. The effect of land use change and urban heat Island is found to be small in GMST (Section 2.4.1.3). Consequently, this effect on extreme temperature is also expected to be small in the global average.

These new studies show that there is stronger evidence for anthropogenic forcing on changes in extreme temperatures than at the time of the SREX assessment. New evidence since SREX includes the separation of the influence of anthropogenic forcings from that of natural forcings on extreme daily temperatures at the global scale and to some extent at continental and sub-continental scales in some regions. These new results suggest more clearly the role of anthropogenic forcing on temperature extremes compared to results at the time of the SREX assessment. We assess that it is *very likely* that human influence has contributed to the observed changes in the frequency and intensity of daily temperature extremes on the global scale since the mid-20th century.



### 10.6.1.2 Precipitation Extremes

Observations have showed a general increase in heavy precipitation at the global scale. This appears to be consistent with the expected response to anthropogenic forcing as a result of an enhanced moisture content in the atmosphere but a direct cause-and-effect relationship between changes in external forcing and extreme precipitation had not been established at the time of the AR4. As a result, the AR4 concluded that increases in heavy precipitation were *more likely than not* consistent with anthropogenic influence during the latter half of the 20th century (Hegerl et al., 2007b).

Extreme precipitation is expected to increase with warming. A combination of evidence leads to this conclusion though by how much remains uncertain and may vary with time scale (Section 7.6.5). Observations and model projected future changes both indicate increase in extreme precipitation associated with warming. Analysis of observed annual maximum 1-day precipitation (RX1day) over global land areas with sufficient data smaples indicates a significant increase in extreme percipitation globally, with a median increase about 7% $°C^{-1}$ GMST increase (Westra et al., 2013). CMIP3 and CMIP5 simulations project an increase in the globally averaged 20-year return values of annual maximum 24-hour precipitation amounts of about 6 to 7% with each degree Celsius of global mean warming, with the bulk of models simulating values in the range of 4 to 10% $°C^{-1}$(Kharin et al., 2007; Kharin et al., 2013). Anthropogenic influence has been detected on various aspects of the global hydrological cycle (Stott et al., 2010), which is directly relevant to extreme precipitation changes. An anthropogenic influence on increasing atmospheric moisture content has been detected (see Section 10.3.2). A higher moisture content in the atmosphere would be expected to lead to stronger extreme precipitation as extreme precipitation typically scales with total column moisture if circulation does not change. An observational analysis shows that winter maximum daily precipitation in North America has statistically significant positive correlations with local atmospheric moisture (Wang and Zhang, 2008).

There is only a modest body of direct evidence that natural or anthropogenic forcing has affected global mean precipitation (see Section 10.3.2 and Figure 10.10), despite a robust expectation of increased precipitation (Balan Sarojini et al., 2012 ) and precipitation extremes (see Section 7.6.5). However, mean precipitation is expected to increase less than extreme precipitation because of energy constraints (e.g., Allen and Ingram, 2002). A perfect model analysis with an ensemble of GCM simulations shows that anthropogenic influence should be detectable in precipitation extremes in the second half of the 20th century at global and hemispheric scales, and at continental scale as well but less robustly (Min et al., 2008c), see also Hegerl et al. (2004). One study has also linked the observed intensification of precipitation extremes (including RX1day and annual maximum 5-day precipitation (RX5day)) over NH land areas to human influence using a limited set of climate models and observations (Min et al., 2011). However, the detection was less robust if using the fingerprint for combined anthropogenic and natural influences compared to that for anthropogenic influences only, possibly due to a number of factors including weak S/N ratio and uncertainties in observation and model simulations. Also, models still have difficulties in simulating extreme daily precipitation directly comparable with those observed at the station level, which has been addressed to some extent by Min et al. (2011) by independently transforming annual precipitation extremes in models and observations onto a dimensionless scale that may be more comparable between the two. Detection of anthropogenic influence on smaller spatial scales is more difficult due to the increased level of noise and uncertainties and confounding factors on local scales. Fowler and Wilby (2010) suggested that there may have only been a 50% likelihood of detecting anthropogenic influence on UK extreme precipitation in winter at that time, and a very small likelihood of detecting it in other seasons.

Given the evidence of anthropogenic influence on various aspects of the global hydrological cycle that implies that extreme precipitation would be expected to have increased and some limited direct evidence of anthropogenic influence on extreme precipitation, but given also the difficulties in simulating extreme precipitation by climate models and limited observational coverage, we assess, consistent with SREX (Seneviratne et al., 2012) that there is *medium confidence* that anthropogenic forcing has contributed to a global scale intensification of heavy precipitation over the second half of the 20th century in land regions where observational coverage is sufficient for assessment.

### 10.6.1.3 Drought

AR4 concluded that that an increased risk of drought was *more likely than not* due to anthropogenic forcing during the second half of the

20th century. This assessment was based on one detection study that identified an anthropogenic fingerprint in a global Palmer Drought Severity Index (PDSI) data set (Burke et al., 2006) and studies of some regions which indicated that droughts in those regions were linked to SST changes or to a circulation response to anthropogenic forcing. SREX (Seneviratne et al., 2012) assessed that there was *medium confidence* that anthropogenic influence has contributed to some changes in the drought patterns observed in the second half of the 20th century based on attributed impact of anthropogenic forcing on precipitation and temperature changes, and that there was *low confidence* in the assessment of changes in drought at the level of single regions.

Drought is a complex phenomenon that is affected by precipitation predominantly, as well as by other climate variables including temperature, wind speed and solar radiation (e.g., Seneviratne, 2012; Sheffield et al., 2012). It is also affected by non-atmospheric conditions such as antecedent soil moisture and land surface conditions. Trends in two important drought-related climate variables (precipitation and temperature) are consistent with the expected responses to anthropogenic forcing over the globe. However, there is large uncertainty in observed changes in drought (Section 2.6.2.3) and its attribution to causes globally. The evidence for changes in soil moisture indices and drought indices over the period since 1950 globally is conflicting (Hoerling et al., 2012; Sheffield et al., 2012; Dai, 2013), possibly due to the examination of different time periods, different forcing fields used to drive land surface models and uncertainties in land surface models (Pitman et al., 2009; Seneviratne et al., 2010; Sheffield et al., 2012). In a recent study, Sheffield et al. (2012) identify the representation of potential evaporation as solely dependent on temperature (using the Thornthwaite-based formulation) as a possible explanation for their finding that PDSI-based estimates might overestimate historical drought trends. This stands in partial contradiction to previous assessments suggesting that using a more sophisticated formulation (Penman-Monteith) for potential evaporation did not affect the results of respective PDSI trends (Dai, 2011; van der Schrier et al., 2011). Sheffield et al. (2012) argue that issues with the treatment of spurious trends in atmospheric forcing data sets and/or the choice of calibration periods explain these conflicting results. These conflicting results point out the challenges in quantitatively defining and detecting long-term changes in a multivariable phenomenon such as drought.

Recent long-term droughts in western North America cannot definitively be shown to lie outside the very large envelope of natural precipitation variability in this region (Cayan et al., 2010; Seager et al., 2010), particularly given new evidence of the history of high-magnitude natural drought and pluvial episodes suggested by palaeoclimatic reconstructions (see Chapter 5). Low-frequency tropical ocean temperature anomalies in all ocean basins appear to force circulation changes that promote regional drought (Hoerling and Kumar, 2003; Seager et al., 2005; Dai, 2011). Uniform increases in SST are not particularly effective in this regard (Schubert et al., 2009; Hoerling et al., 2012). Therefore, the reliable separation of natural variability and forced climate change will require simulations that accurately reproduce changes in large-scale SST gradients at all time scales.

In summary, assessment of new observational evidence, in conjunction with updated simulations of natural and forced climate variability, indicates that the AR4 conclusions regarding global increasing trends in droughts since the 1970s should be tempered. There is not enough evidence to support *medium* or *high confidence* of attribution of increasing trends to anthropogenic forcings as a result of observational uncertainties and variable results from region to region (Section 2.6.2.3). Combined with difficulties described above in distinguishing decadal scale variability in drought from long-term climate change we conclude consistent with SREX that there is *low confidence* in detection and attribution of changes in drought over global land areas since the mid-20th century.

#### 10.6.1.4 Extratropical Cyclones

AR4 concluded that an anthropogenic influence on extratropical cyclones was not formally detected, owing to large internal variability and problems due to changes in observing systems. Although there is evidence that there has been a poleward shift in the storm tracks (see Section 2.6.4), various causal factors have been cited including oceanic heating (Butler et al., 2010) and changes in large-scale circulation due to effects of external forcings (Section 10.3.3). Increases in mid-latitude SST gradients generally lead to stronger storm tracks that are shifted poleward and increases in subtropical SST gradients may lead to storm tracks shifting towards the equator (Brayshaw et al., 2008; Semmler et al., 2008; Kodama and Iwasaki, 2009; Graff and LaCasce, 2012). However, changes in storm-track intensity are much more complicated, as they are sensitive to the competing effects of changes in temperature gradients and static stability at different levels and are thus not linked to GMST in a simple way (Ulbrich et al., 2009; O'Gorman, 2010). Overall global average cyclone activity is expected to change little under moderate GHG forcing (O'Gorman and Schneider, 2008; Ulbrich et al., 2009; Bengtsson and Hodges, 2011), although in one study, human influence has been detected in geostrophic wind energy and ocean wave heights derived from sea level pressure data (Wang et al., 2009b).

#### 10.6.1.5 Tropical Cyclones

AR4 concluded that 'anthropogenic factors *more likely than not* have contributed to an increase in tropical cyclone intensity' (Hegerl et al., 2007b). Evidence that supports this assessment was the strong correlation between the Power Dissipation Index (PDI, an index of the destructiveness of tropical cyclones) and tropical Atlantic SSTs (Emanuel, 2005; Elsner, 2006) and the association between Atlantic warming and the increase in GMST (Mann and Emanuel, 2006; Trenberth and Shea, 2006). Observations suggest an increase globally in the intensities of the strongest tropical cyclones (Elsner et al., 2008) but it is difficult to attribute such changes to particular causes (Knutson et al., 2010). The US Climate Change Science Program (CCSP; Kunkel et al., 2008) discussed human contributions to recent hurricane activity based on a two-step attribution approach. They concluded merely that it is very likely (Knutson et al., 2010) that human-induced increase in GHGs has contributed to the increase in SSTs in the hurricane formation regions and that over the past 50 years there has been a strong statistical connection between tropical Atlantic SSTs and Atlantic hurricane activity as measured by the PDI. Knutson et al. (2010), assessed that '…it remains uncertain whether past changes in tropical cyclone activity have exceeded the variability expected from natural causes.' Senevi-

ratne et al. (2012) concurred with this finding. Section 14.6.1 gives a detailed account of past and future changes in tropical cyclones. This section assesses causes of observed changes.

Studies that directly attribute tropical cyclone activity changes to anthropogenic GHG emission are lacking. Among many factors that may affect tropical cyclone activity, tropical SSTs have increased and this increase has been attributed at least in part to anthropogenic forcing (Gillett et al., 2008a). However, there are diverse views on the connection between tropical cyclone activity and SST (see Section 14.6.1 for details). Strong correlation between the PDI and tropical Atlantic SSTs (Emanuel, 2005; Elsner, 2006) would suggest an anthropogenic influence on tropical cyclone activity. However, recent studies also suggest that regional potential intensity correlates with the difference between regional SSTs and spatially averaged SSTs in the tropics (Vecchi and Soden, 2007; Xie et al., 2010; Ramsay and Sobel, 2011) and projections are uncertain on whether the relative SST will increase over the 21st century under GHG forcing (Vecchi et al., 2008; Xie et al., 2010; Villarini and Vecchi, 2012, 2013) . Analyses of CMIP5 simulations suggest that while PDI over the North Atlantic is projected to increase towards late 21st century no detectable change in PDI should be present in the 20th century (Villarini and Vecchi, 2013) . On the other hand, Emanuel et al. (2013) point out that while GCM hindcasts indeed predict little change over the 20th century, downscaling driving by reanalysis data that incorporate historical observations are in much better accord with observations and do indicate a late 20th century increase.

Some recent studies suggest that the reduction in the aerosol forcing (both anthropogenic and natural) over the Atlantic since the 1970s may have contributed to the increase in tropical cyclone activity in the region (see Section 14.6.1 for details), and similarly that aerosols may have acted to reduce tropical cyclone activity in the Atlantic in earlier years when aerosol forcing was increasing (Villarini and Vecchi, 2013). However, there are different views on the relative contribution of aerosols and decadal natural variability of the climate system to the observed changes in Atlantic tropical cyclone activity among these studies. Some studies indicate that aerosol changes have been the main driver (Mann and Emanuel, 2006; Evan et al., 2009; Booth et al., 2012; Villarini and Vecchi, 2012, 2013). Other studies infer the influence of natural variability to be as large as or larger than that from aerosols (Zhang and Delworth, 2009; Villarini and Vecchi, 2012, 2013).

Globally, there is *low confidence* in any long-term increases in tropical cyclone activity (Section 2.6.3) and we assess that there is *low confidence* in attributing global changes to any particular cause. In the North Atlantic region there is *medium confidence* that a reduction in aerosol forcing over the North Atlantic has contributed at least in part to the observed increase in tropical cyclone activity since the 1970s. There remains substantial disagreement on the relative importance of internal variability, GHG forcing and aerosols for this observed trend. It remains uncertain whether past changes in tropical cyclone activity are outside the range of natural internal variability.

### 10.6.2 Attribution of Weather and Climate Events

Since many of the impacts of climate change are likely to manifest themselves through extreme weather, there is increasing interest in quantifying the role of human and other external influences on climate in specific weather events. This presents particular challenges for both science and the communication of results. It has so far been attempted for a relatively small number of specific events (e.g., Stott et al., 2004; Pall et al., 2011) although Peterson et al. (2012) attempt, for the first time, a coordinated assessment to place different high-impact weather events of the previous year in a climate perspective. In this assessment, selected studies are used to illustrate the essential principles of event attribution: see Stott et al. (2013) for a more exhaustive review.

Two distinct ways have emerged of framing the question of how an external climate driver like increased GHG levels may have contributed to an observed weather event. First, the 'attributable risk' approach considers the event as a whole, and asks how the external driver may have increased or decreased the probability of occurrence of an event of comparable magnitude. Second, the 'attributable magnitude' approach considers how different external factors contributed to the event or, more specifically, how the external driver may have increased the magnitude of an event of comparable occurrence probability. Hoerling et al. (2013) uses both methods to infer changes in magnitude and likelihood of the 2011 Texas heat wave.

Quantifying the absolute risk or probability of an extreme weather event in the absence of human influence on climate is particularly challenging. Many of the most extreme events occur because a self-reinforcing process that occurs only under extreme conditions amplifies an initial anomaly (e.g., Fischer et al., 2007). Hence the probability of occurrence of such events cannot, in general, be estimated simply by extrapolating from the distribution of less extreme events that are sampled in the historical record. Proxy records of pre-industrial climate generally do not resolve high-frequency weather, so inferring changes in probabilities requires a combination of hard-to-test distributional assumptions and extreme value theory. Quantifying absolute probabilities with climate models is also difficult because of known biases in their simulation of extreme events. Hence, with only a couple of exceptions (e.g., Hansen et al., 2012), studies have focussed on how risks have changed or how different factors have contributed to an observed event, rather than claiming that the absolute probability of occurrence of that event would have been extremely low in the absence of human influence on climate.

Even without considering absolute probabilities, there remain considerable uncertainties in quantifying changes in probabilities. The assessment of such changes will depend on the selected indicator, time period and spatial scale on which the event is analysed, and the way in which the event-attribution question is framed can substantially affect apparent conclusions . If an event occurs in the tail of the distribution, then a small shift in the distribution as a whole can result in a large increase in the probability of an event of a given magnitude: hence it is possible for the same event to be both 'mostly natural' in terms of attributable magnitude (if the shift in the distribution due to human influence is small compared to the anomaly in the natural variability that was the primary cause) and 'mostly anthropogenic' in terms of

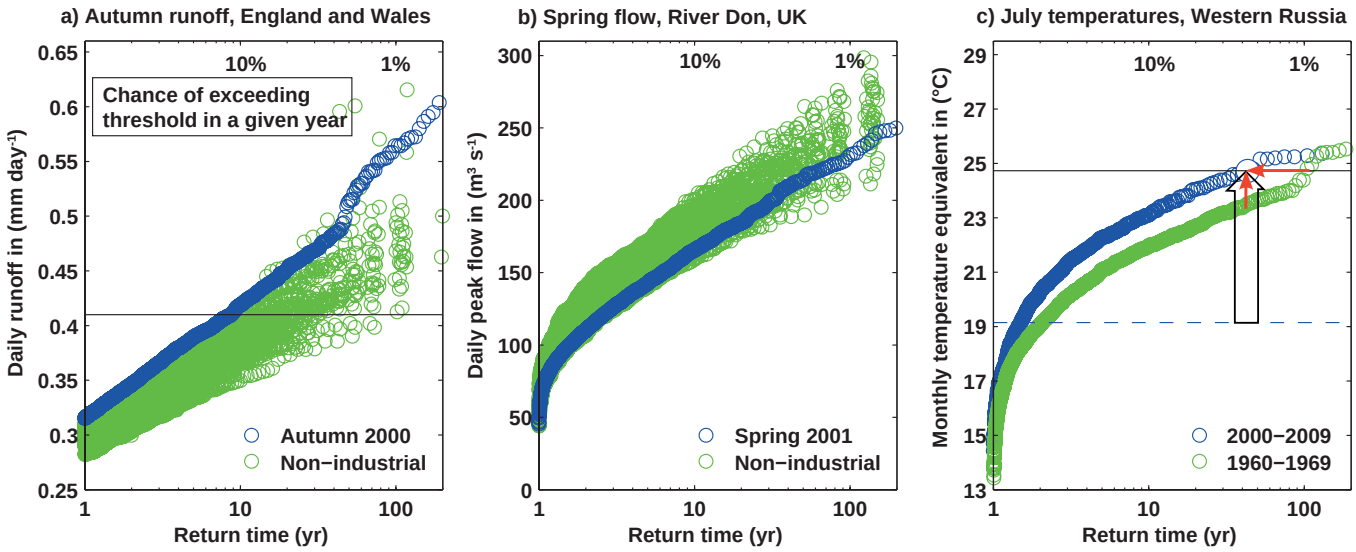


**Figure 10.18 |** Return times for precipitation-induced floods aggregated over England and Wales for (a) conditions corresponding to September to November 2000 with boundary conditions as observed (blue) and under a range of simulations of the conditions that would have obtained in the absence of anthropogenic greenhouse warming over the 20th century (green) with different AOGCMs used to define the greenhouse signal, black horizontal line corresponds to the threshold exceeded in autumn 2000 (from Pall et al., 2011); (b) corresponding to January to March 2001 with boundary conditions as observed (blue) and under a range of simulations of the condition that would have obtained in the absence of anthropogenic greenhouse warming over the 20th century (green) adapted from Kay et al. (2011a); (c) return periods of temperature-geopotential height conditions in the model simulations for the 1960s (green) and the 2000s (blue). The vertical black arrow shows the anomaly of the 2010 Russian heat wave (black horizontal line) compared to the July mean temperatures of the 1960s (dashed line). The vertical red arrow gives the increase in temperature for the event whereas the horizontal red arrow shows the change in the return period (from Otto et al., 2012).

attributable risk (if human influence has increased its probability of occurrence by more than a factor of 2). These issues are discussed further using the example of the 2010 Russian heat wave below.

The majority of studies have focussed on quantifying attributable risk. Formally, risk is a function of both hazard and vulnerability (IPCC, 2012), although most studies attempting to quantify risk in the context of extreme weather do not explicitly use this definition, which is discussed further in Chapter 19 of WGII, but use the term as a shorthand for the probability of the occurrence of an event of a given magnitude. Any assessment of change in risk depends on an assumption of 'all other things being equal', including natural drivers of climate change and vulnerability. Given this assumption, the change in hazard is proportional to the change in risk, so we will follow the published literature and continue to refer to Fraction Attributable Risk, defined as FAR = 1 – P0/P1, P0 being the probability of an event occurring in the absence of human influence on climate, and P1 the corresponding probability in a world in which human influence is included. FAR is thus the fraction of the risk that is attributable to human influence (or, potentially, any other external driver of climate change) and does not require knowledge of absolute values of P0 and P1, only their ratio.

For individual events with return times greater than the time scale over which the signal of human influence is emerging (30 to 50 years, meaning P0 and P1 less than 2 to 3% in any given year), it is impossible to observe a change in occurrence frequency directly because of the shortness of the observed record, so attribution is necessarily a multi-step procedure. Either a trend in occurrence frequency of more frequent events is attributed to human influence and a statistical model is then used to extrapolate to the implications for P0 and P1; or an attributable trend is identified in some other variable, such as surface temperature, and a physically based weather model is used to assess the implications for extreme weather risk. Neither approach is free of assumptions: no atmospheric model is perfect, but statistical extrapolation may also be misleading for reasons given above.

Pall et al. (2011) provide an example of multi-step assessment of attributable risk using a physically based model, applied to the floods that occurred in the UK in the autumn of 2000, the wettest autumn to have occurred in England and Wales since records began. To assess the contribution of the anthropogenic increase in GHGs to the risk of these floods, a several thousand member ensemble of atmospheric models with realistic atmospheric composition, SST and sea ice boundary conditions imposed was compared with a second ensemble with composition and surface temperatures and sea ice boundary conditions modified to simulate conditions that would have occurred had there been no anthropogenic increase in GHGs since 1900. Simulated daily precipitation from these two ensembles was fed into an empirical rainfall-runoff model and daily England and Wales runoff used as a proxy for flood risk. Results (Figure 10.18a) show that including the influence of anthropogenic greenhouse warming increases flood risk at the threshold relevant to autumn 2000 by around a factor of two in the majority of cases, but with a broad range of uncertainty: in 10% of cases the increase in risk is less than 20%.

Kay et al. (2011a), analysing the same ensembles but using a more sophisticated hydrological model found a reduction in the risk of snow melt–induced flooding in the spring season (Figure 10.18b) which, aggregated over the entire year, largely compensated for the increased risk of precipitation-induced flooding in autumn. This illustrates an

important general point: even if a particular flood event may have been made more likely by human influence on climate, there is no certainty that all kinds of flood events in that location, country or region have been made more likely.

Rahmstorf and Coumou (2011) provide an example of an empirical approach to the estimation of attributable risk applied to the 2010 Russian heat wave. They fit a nonlinear trend to central Russian temperatures and show that the warming that has occurred in this region since the 1960s has increased the risk of a heat wave of the magnitude observed in 2010 by around a factor of 5, corresponding to an FAR of 0.8. They do not address what has caused the trend since 1960, although they note that other studies have attributed most of the large-scale warming over this period to the anthropogenic increase in GHG concentrations.

Dole et al. (2011) take a different approach to the 2010 Russian heat wave, focussing on attributable magnitude, analysing contributions from various external factors, and conclude that this event was 'mainly natural in origin'. First, observations show no evidence of a trend in occurrence frequency of hot Julys in western Russia, and despite the warming that has occurred since the 1960s, mean July temperatures in that region actually display a (statistically insignificant) cooling trend over the century as a whole, in contrast to the case for central and southern European summer temperatures (Stott et al., 2004). Members of the CMIP3 multi-model ensemble likewise show no evidence of a trend towards warming summers in central Russia. Second, Dole et al. (2011) note that the 2010 Russian event was associated with a strong blocking atmospheric flow anomaly, and even the complete 2010 boundary conditions are insufficient to increase the probability of a prolonged blocking event in this region, in contrast again to the situation in Europe in 2003. This anomaly in the large-scale atmospheric flow led to low-pressure systems being redirected around the blocking over Russia causing severe flooding in Pakistan which could so far not be attributed to anthropogenic causes (van Oldenborgh et al., 2012), highlighting that a global perspective is necessary to unravel the different factors influencing individual extreme events (Trenberth and Fasullo, 2012).

Otto et al. (2012) argue that it is possible to reconcile the results of Rahmstorf and Coumou (2011) with those of Dole et al. (2011) by relating the attributable risk and attributable magnitude approaches to framing the event attribution question. This is illustrated in Figure 10.18c, which shows return times of July temperatures in western Russia in a large ensemble of atmospheric model simulations for the 1960s (in green) and 2000s (in blue). The threshold exceeded in 2010 is shown by the solid horizontal line which is almost 6°C above 1960s mean July temperatures, shown by the dashed line. The difference between the green and blue lines could be characterized as a 1.5°C increase in the magnitude of a 30-year event (the vertical red arrow, which is substantially smaller than the size of the anomaly itself, supporting the assertion that the event was 'mainly natural' in terms of attributable magnitude. Alternatively, it could be characterized as a threefold increase in the risk of the 2010 threshold being exceeded, supporting the assertion that risk of the event occurring was mainly attributable to the external trend, consistent with Rahmstorf and Coumou (2011). Rupp et al. (2012) and Hoerling et al. (2013) reach similar conclusions about the 2011 Texas heat wave, both noting the importance of La Niña conditions in the Pacific, with anthropogenic warming making a relatively small contribution to the magnitude of the event, but a more substantial contribution to the risk of temperatures exceeding a high threshold. This shows that the quantification of attributable risks and and changes in magnitude are affected by modelling error (e.g., Visser and Petersen, 2012) as they depend on the atmospheric model's ability to simulate the observed anomalies in the general circulation (Chapter 9).

Because much of the magnitude of these two heat waves is attributable to atmospheric flow anomalies, any evidence of a causal link between rising GHGs and the occurrence or persistence of flow anomalies such as blocking would have a very substantial impact on attribution claims. Pall et al. (2011) argue that, although flow anomalies played a substantial role in the autumn 2000 floods in the UK, thermodynamic mechanisms were primarily responsible for the change in risk between their ensembles. Regardless of whether the statistics of flow regimes themselves have changed, observed temperatures in recent years in Europe are distinctly warmer than would be expected for analogous atmospheric flow regimes in the past, affecting both warm and cold extremes (Yiou et al., 2007; Cattiaux et al., 2010).

In summary, increasing numbers of studies are finding that the probability of occurrence of events associated with extremely high temperatures has increased substantially due to the large-scale warming since the mid-20th century. Because most of this large-scale warming is *very likely* due to the increase in atmospheric GHG concentrations, it is possible to attribute, via a multi-step procedure, some of the increase in probability of these regional events to human influence on climate. Such an increase in probability is consistent with the implications of single-step attribution studies looking at the overall implications of increasing mean temperatures for the probabilities of exceeding temperature thresholds in some regions. We conclude that it is *likely* that human influence has substantially increased the probability of occurrence of heat waves in some locations. It is expected that attributable risks for extreme precipitation events are generally smaller and more uncertain, consistent with the findings in Kay et al. (2011a) and Pall et al. (2011). The science of event attribution is still confined to case studies, often using a single model, and typically focussing on high-impact events for which the issue of human influence has already arisen. While the increasing risk of heat waves measured as the occurrence of a previous temperature record being exceeded can simply be explained by natural variability superimposed by globally increasing temperature, conclusions for holistic events including general circulation patterns are specific to the events that have been considered so far and rely on the representation of relevant processes in the model.

Anthropogenic warming remains a relatively small contributor to the overall magnitude of any individual short-term event because its magnitude is small relative to natural random weather variability on short time scales (Dole et al., 2011; Hoerling et al., 2013). Because of this random variability, weather events continue to occur that have been made less likely by human influence on climate, such as extreme winter cold events (Massey et al., 2012), or whose probability of occurrence has not been significantly affected either way. Quantifying how different external factors contribute to current risks, and how risks are

changing, is possible with much higher confidence than quantifying absolute risk. Biases in climate models, uncertainty in the probability distribution of the most extreme events and the ambiguity of paleoclimatic records for short-term events mean that it is not yet possible to quantify the absolute probability of occurrence of any observed weather event in a hypothetical pristine climate. At present, therefore, the evidence does not support the claim that we are observing weather events that would, individually, have been *extremely unlikely* in the absence of human-induced climate change, although observed trends in the concurrence of large numbers of events (see Section 10.6.1) may be more easily attributable to external factors. The most important development since AR4 is an emerging consensus that the role of external drivers of climate change in specific extreme weather events, including events that might have occurred in a pre-industrial climate, can be quantified using a probabilistic approach.

## 10.7 Multi-century to Millennia Perspective

Evaluating the causes of climate change before the 20th century is important to test and improve our understanding of the role of internal and forced natural climate variability for the recent past. This section draws on assessment of temperature reconstructions of climate change over the past millennium and their uncertainty in Chapter 5 (Table 5.A.1; Sections 5.3.5 and 5.5.1 for regional records), and on comparisons of models and data over the pre-instrumental period in Chapters 5 and 9 (Sections 5.3.5, 5.5.1 and 9.5.3), and focuses on the evidence for the contribution by radiatively forced climate change to reconstructions and early instrumental records. In addition, the residual variability that is not explained by forcing from palaeoclimatic records provides a useful comparison to estimates of climate model internal variability. The model dependence of estimates of internal variability is an important uncertainty in detection and attribution results.

The inputs for detection and attribution studies for periods covered by indirect, or proxy, data are affected by more uncertainty than those from the instrumental period (see Chapter 5), owing to the sparse data coverage, particularly further back in time, and uncertainty in the link between proxy data and, for example, temperature. Records of past radiative influences on climate are also uncertain (Section 5.2; see Schmidt et al., 2011; Schmidt et al., 2012). For the preindustrial part of the last millennium changes in solar, volcanic, GHG forcing, and land use change, along with a small orbital forcing are potentially important external drivers of climate change. Estimates of solar forcing (Figure 5.1a; Box 10.2) are uncertain, particularly in their amplitude, as well as in modelling, for example, of the influence of solar forcing on atmospheric circulation involving stratospheric dynamics (see Box 10.2; Gray et al., 2010). Estimates of past volcanism are reasonably well established in their timing, but the magnitude of the RF of individual eruptions is uncertain (Figure 5.1a). It is possible that large eruptions had a more moderated climate effect than simulated by many climate models due to faster fallout associated with larger particle size (Timmreck et al., 2009), or increased amounts of injected water vapour (Joshi and Jones, 2009). Reconstructed changes in land cover and its effect on climate are also uncertain (Kaplan et al., 2009; Pongratz et al., 2009). Forcing of WMGHGs shows only very subtle variations over the last millennium up to 1750. This includes a small drop and partial recovery in the 17th century (Section 6.2.3, Figure 6.7), followed by increases in GHG concentrations with industrialization since the middle of the 18th century (middle of the 19th century for $N_2O$, Figure 6.11).

When interpreting reconstructions of past climate change with the help of climate models driven with estimates of past forcing, it helps that the uncertainties in reconstructions and forcing are independent from each other. Thus, uncertainties in forcing and reconstructions combined should lead to less, rather than more similarity between fingerprints of forced climate change and reconstructions, making it improbable that the response to external drivers is spuriously detected. However, this is the case only if all relevant forcings and their uncertainties are considered, reducing the risk of misattribution due to spurious correlations between external forcings, and if the data are homogeneous and statistical tests properly applied (e.g., Legras et al., 2010). Hence this section focuses on work that considers all relevant forcings simultaneously.

### 10.7.1 Causes of Change in Large-Scale Temperature over the Past Millennium

Despite the uncertainties in reconstructions of past NH mean temperatures, there are well-defined climatic episodes in the last millennium that can be robustly identified (Chapter 5, see also Figure 10.19). Chapter 5 concludes that in response to solar, volcanic and anthropogenic RFs, climate models simulate temperature changes in the NH which are generally consistent in magnitude and timing with reconstructions, within their broad uncertainty ranges (Section 5.3.5).

#### 10.7.1.1 Role of External Forcing in the Last Millennium

The AR4 concluded that 'A substantial fraction of the reconstructed NH inter-decadal temperature variability of the seven centuries prior to 1950 is *very likely* attributable to natural external forcing'. The literature since the AR4, and the availability of more simulations of the last millennium with more complete forcing (see Schmidt et al., 2012), including solar, volcanic and GHG influences, and generally also land use change and orbital forcing) and more sophisticated models, to a much larger extent coupled climate or coupled ESMs (Chapter 9), some of them with interactive carbon cycle, strengthens these conclusions.

Most reconstructions show correlations with external forcing that are similar to those found between pre-Paleoclimate Modelling Intercomparison Project Phase 3 (PMIP3) simulations of the last millennium and forcing, suggesting an influence by external forcing (Fernández-Donado et al., 2013). From a global scale average of new regional reconstructions, Past Global Changes 2k (PAGES 2k) Consortium (2013) find that periods with strong volcanic and solar forcing combined occurring over the last millennium show significantly cooler conditions than randomly selected periods from the last two millennia. Detection analyses based on PMIP3 and CMIP5 model simulations for the years from 850 to 1950 and also from 850 to 1850 find that the fingerprint of external forcing is detectable in all reconstructions of NH mean temperature considered (Schurer et al., 2013; see Figure 10.19), but only in about half the cases considered does detection also occur prior to 1400. The authors find a smaller response to forcing in reconstructions than simulated, but this discrepancy is consistent with

uncertainties in forcing or proxy response to it, particularly associated with volcanism. The discrepancy is reduced when using more strongly smoothed data or omitting major volcanic eruptions from the analysis. The level of agreement between fingerprints from multiple models in response to forcing and reconstructions decreases earlier in time, and the forced signal is detected only in about half the cases considered when analysing the period 851 to 1401. This may be partly due to weaker forcing and larger forcing uncertainty early in the millennium and partly due to increased uncertainty in reconstructions. Detection results indicate a contribution by external drivers to the warm conditions in the 11th to 12th century, but cannot explain the warmth around the 10th century in some of the reconstructions (Figure 10.19). This detection of a role of external forcing extends work reported in AR4 back into to the 9th century CE.

Detection and attribution studies support results from modelling studies that infer a strong role of external forcing in the cooling of NH temperatures during the Little Ice Age (LIA; see Chapter 5 and Glossary). Both model simulations (Jungclaus et al., 2010) and results from detection and attribution studies (Hegerl et al., 2007a; Schurer et al., 2013) suggest that a small drop in GHG concentrations may have contributed to the cool conditions during the 16th and 17th centuries. Note, however, that centennial variations of GHG during the late Holocene are very small relative to their increases since pre-industrial times (Section 6.2.3). The role of solar forcing is less clear except for decreased agreement if using very large solar forcing (e.g., Ammann et al., 2007; Feulner, 2011). Palastanga et al. (2011) demonstrate that neither a slowdown of the thermohaline circulation nor a persistently negative NAO alone can explain the reconstructed temperature pattern over Europe during the periods 1675–1715 and 1790–1820.



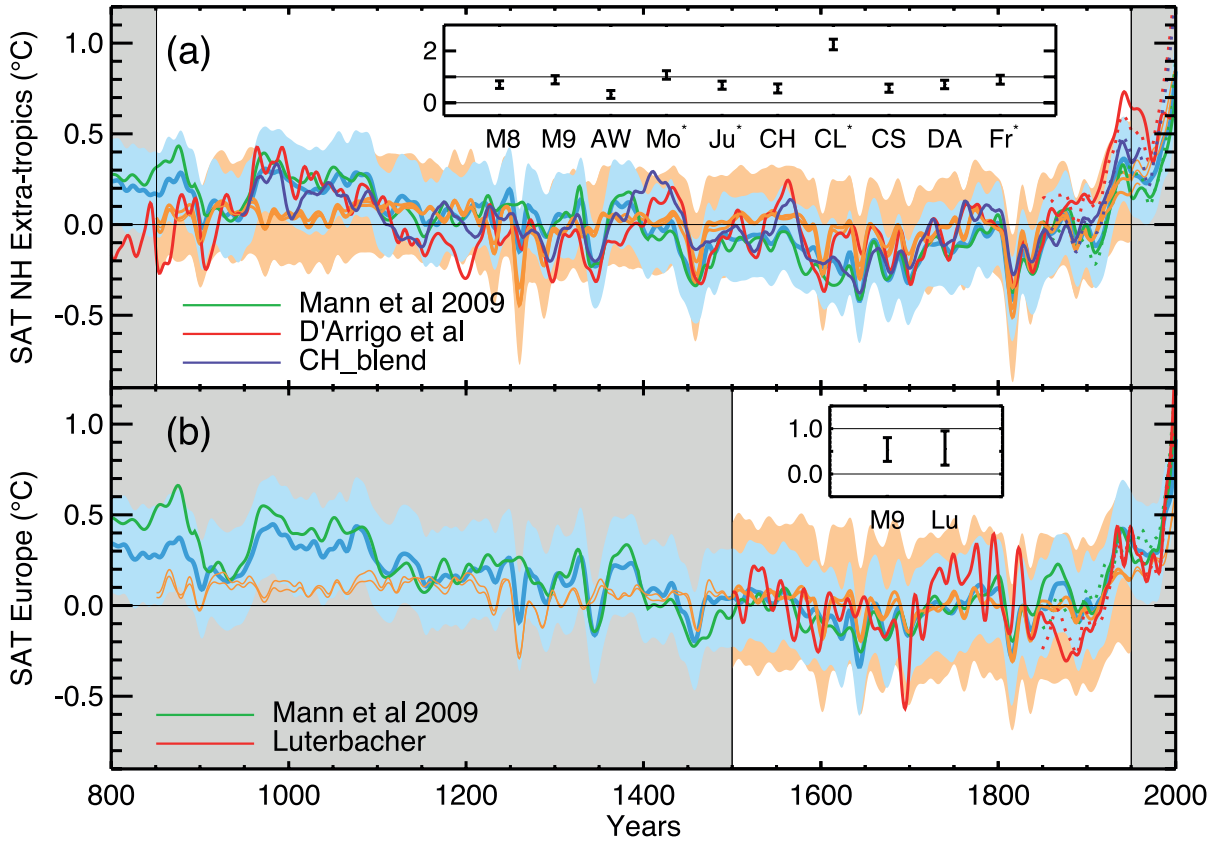


**Figure 10.19 |** The top panel compares the mean annual Northern Hemisphere (NH) surface air temperature from a multi-model ensemble to several NH temperature reconstructions. These reconstructions are: CH-blend from Hegerl et al. (2007a) in purple, which is a reconstruction of 30°N to 90°N land only (Mann et al., 2009), plotted for the region 30°N to 90°N land and sea (green) and D'Arrigo et al. (2006) in red, which is a reconstruction of 20°N to 90°N land only. The dotted coloured lines show the corresponding instrumental data. The multi-model mean for the reconstructed domain is scaled to fit each reconstruction in turn, using a total least squares (TLS) method. The best estimate of the detected forced signal is shown in orange (as an individual line for each reconstruction; lines overlap closely) with light orange shading indicating the range expected if accounting for internal variability. The best fit scaling values for each reconstruction are given in the insert as well as the detection results for six other reconstructions (M8; M9 (Mann et al., 2008, 2009); AW (Ammann and Wahl, 2007); Mo (Moberg et al., 2005); Ju (Juckes et al., 2007); CH (Hegerl et al., 2007a); CL (Christiansen and Ljungqvist, 2011) and inverse regressed onto the instrumental record CS; DA (D'Arrigo et al., 2006); Fr (Frank et al., 2007). An asterisk next to the reconstruction name indicates that the residuals (over the more robustly reconstructed period 1401–1950) are inconsistent with the internal variability generated by the combined control simulations of all climate models investigated (for details see Schurer et al., 2013). The ensemble average of a data-assimilation simulation (Goosse et al., 2012b) is plotted in blue, for the region 30°N to 90°N land and sea, with the error range shown in light blue shading. The bottom panel is similar to the top panel, but showing the European region, following Hegerl et al. (2011a) but using the simulations and method in Schurer et al. (2013). The detection analysis is performed for the period 1500–1950 for two reconstructions: Luterbacher et al. (2004)(representing the region 35°N to 70°N, 25°W to 40°E, "land only, labelled 'Lu' in the insert") shown in red, and Mann et al. (2009) (averaged over the region 25°N to 65°N, 0° to 60°E, land and sea, labelled 'M9' in the insert), shown in green. As in the top panel, best fit estimates are shown in dark orange with uncertainty range due to internal variability shown in light orange. The data assimilation from Goosse et al. (2012a), constrained by the Mann et al. (2009) reconstruction is shown in blue, with error range in light blue. All data are shown with respect to the mean of the period covered by the white part of the figure (850–1950 for the NH, 1500–1950 for European mean data).

Data assimilation studies support the conclusion that external forcing, together with internal climate variability, provides a consistent explanation of climate change over the last millennium. Goosse et al. (2010, 2012a, 2012b) select, from a very large ensemble with an EMIC, the individual simulations that are closest to the spatial reconstructions of temperature between 30°N and 60°N by Mann et al. (2009) accounting for reconstruction uncertainties. The method also varies the external forcing within uncertainties, determining a combined realization of the forced response and internal variability that best matches the data. Results (Figure 10.19) show that simulations reproduce the target reconstruction within the uncertainty range, increasing confidence in the consistency of the reconstruction and the forcing. The results suggest that long-term circulation anomalies may help to explain the hemispheric warmth early in the millennium, although results vary dependent on input parameters of the method.

#### 10.7.1.2 Role of Individual Forcings

Volcanic forcing shows a detectable influence on large-scale temperature (see AR4; Chapter 5), and volcanic forcing plays an important role in explaining past cool episodes, for example, in the late 17th and early 19th centuries (see Chapter 5 and 9; Hegerl et al., 2007b; Jungclaus et al., 2010; Miller et al., 2012) . Schurer et al. (2013) separately detect the response to GHG variations between 1400 and 1900 in most NH reconstructions considered, and that of solar and volcanic forcing combined in all reconstructions considered.

Even the multi-century perspective makes it difficult to distinguish century-scale variations in NH temperature due to solar forcing alone from the response to other forcings, due to the few degrees of freedom constraining this forcing (see Box 10.2). Hegerl et al. (2003, 2007a) found solar forcing detectable in some cases. Simulations with higher than best guess solar forcing may reproduce the warm period around 1000 more closely, but the peak warming occurs about a century earlier in reconstructions than in solar forcing and with it model simulations (Jungclaus et al., 2010; Figure 5.8; Fernández-Donado et al., 2013). Even if solar forcing were on the high end of estimates for the last millennium, it would not be able to explain the recent warming according both to model simulations (Ammann et al., 2007; Tett et al., 2007; Feulner, 2011) and detection and attribution approaches that scale the temporal fingerprint of solar forcing to best match the data (Hegerl et al., 2007a; Schurer et al., 2013; Figure 10.19). Some studies suggest that particularly for millennial and multi-millenial time scales orbital forcing may be important globally (Marcott et al., 2013) and for high-latitude trends (Kaufman et al., 2009) based on a comparison of the correspondence between long-term Arctic cooling in models and data though the last millennium up to about 1750 (see also PAGES 2k Consortium, 2013).

#### 10.7.1.3 Estimates of Internal Climate Variability

The interdecadal and longer-term variability in large-scale temperatures in climate model simulations with and without past external forcing is quite different (Tett et al., 2007; Jungclaus et al., 2010), consistent with the finding that a large fraction of temperature variance in the last millennium has been externally driven. The residual variability in past climate that is not explained by changes in RF provides an estimate of internal variability for NH mean temperature that is not directly derived from climate model simulation. This residual variability is somewhat larger than control simulation variability for some reconstructions if the comparison is extended to the full period since 850 CE (Schurer et al., 2013), However, when extracting 50- and 60-year trends from this residual variability, the distribution of these trends is similar to the multi-model control simulation ensemble used in Schurer et al. (2013). In all cases considered, the most recent 50-and 60-year trend from instrumental data is far outside the range of any 50-year trend in residuals from reconstructions of NH mean temperature of the past millennium.

### 10.7.2 Changes of Past Regional Temperature

Several reconstructions of European regional temperature variability are available (Section 5.5). While Bengtsson et al. (2006) emphasized the role of internal variability in pre-industrial European climate as reconstructed by Luterbacher et al. (2004), Hegerl et al. (2011a) find a detectable response to external forcing in summer temperatures in the period 1500–1900, for winter temperatures during 1500–1950 and 1500–2000; and throughout the record for spring. The fingerprint of the forced response shows coherent time evolution between models and reconstructed temperatures over the entire analysed period (compare to annual results in Figure 10.19, using a larger multi-model ensemble). This suggests that the cold European winter conditions in the late 17th and early 19th century and the warming in between were at least partly externally driven.

Data assimilation results focussing on the European sector suggests that the explanation of forced response combined with internal variability is self-consistent (Goosse et al., 2012a, Figure 10.19). The assimilated simulations reproduce the warmth of the MCA better than the forced only simulations do. The response to individual forcings is difficult to distinguish from each other in noisier regional reconstructions. An epoch analysis of years immediately following strong, largely tropical, volcanic eruptions shows that European summers show detectable fingerprints of volcanic response , while winters show a noisy response of warming in northern Europe and cooling in southern Europe (Hegerl et al., 2011a). Landrum et al. (2013) suggest similar volcanic responses for North America, with warming in the north of the continent and cooling in the south. There is also evidence for a decrease in SSTs following tropical volcanic forcing in tropical reconstructions over the past 450 years (D'Arrigo et al., 2009). There is also substantial literature suggesting solar influences on regional climate reconstructions, possibly due to circulation changes, for example, changes in Northern Annular Modes (e.g., Kobashi et al., 2013; see Box 10.2).

### 10.7.3 Summary: Lessons from the Past

Detection and attribution studies strengthen results from AR4 that external forcing contributed to past climate variability and change prior to the 20th century. Ocean–Atmosphere General Circulation Models (OAGCMs) simulate similar changes on hemispheric and annual scales as those by simpler models used earlier, and enable detection of regional and seasonal changes. Results suggest that volcanic forcing and GHG forcing in particular are important for explaining past changes in NH temperatures. Results from data assimilation runs confirm

that the combination of internal variability and external forcing provides a consistent explanation of the last millennium and suggest that changes in circulation may have further contributed to climate anomalies. The role of external forcing extends to regional records, for example, European seasonal temperatures. In summary, it is *very unlikely* that NH temperature variations from 1400 to 1850 can be explained by internal variability alone. There is *medium confidence* that external forcing contributed to NH temperature variability from 850 to 1400. There is *medium confidence* that external forcing (anthropogenic and natural forcings together) contributed to European temperatures of the last five centuries.

## 10.8 Implications for Climate System Properties and Projections

Detection and Attribution results can be used to constrain predictions of future climate change (see Chapters 11 and 12) and key climate system properties. These properties include: the Equilibrium Climate Sensitivity (ECS), which determines the long-term equilibrium warming response to stable atmospheric composition, but not accounting for vegetation or ice sheet changes (Section 12.5.3; see Box 12.2); the transient climate response (TCR), which is a measure of the magnitude of transient warming while the climate system, particularly the deep ocean, is not in equilibrium; and the transient climate response to cumulative $CO_2$ emissions (TCRE), which is a measure of the transient warming response to a given mass of $CO_2$ injected into the atmosphere, and combines information on both the carbon cycle and climate response. TCR is more tightly constrained by the observations of transient warming than ECS. The observational constraints on TCR, ECS and TCRE assessed here focus on information provided by recent observed climate change, complementing analysis of feedbacks and climate modelling information, which are assessed in Chapter 9. The assessment in this chapter also incorporates observational constraints based on palaeoclimatic information, building on Chapter 5, and contributes to the overall synthesis assessment in Chapter 12 (Box 12.2).

Because neither ECS nor TCR is directly observed, any inference about them requires some form of climate model, ranging in complexity from a simple zero-dimensional energy balance box model to OAGCMs (Hegerl and Zwiers, 2011). Constraints on estimates of long-term climate change and equilibrium climate change from recent warming hinge on the rate at which the ocean has taken up heat (Section 3.2), and by the extent to which recent warming has been reduced by cooling from aerosol forcing. Therefore, attempts to estimate climate sensitivity (transient or equilibrium) often also estimate the total aerosol forcing and the rate of ocean heat uptake, which are discussed in Section 10.8.3. The AR4 contained a detailed discussion on estimating quantities relevant for projections, and included an appendix with the relevant estimation methods. Here, we build on this assessment, repeating information and discussion only where necessary to provide context.

### 10.8.1 Transient Climate Response

The AR4 discussed for the first time estimates of the TCR. TCR was originally defined as the warming at the time of $CO_2$ doubling (i.e., after 70 years) in a 1% $yr^{-1}$ increasing $CO_2$ experiment (see Hegerl et al., 2007b), but like ECS, it can also be thought of as a generic property of the climate system that determines the global temperature response $\Delta T$ to any gradual increase in RF, $\Delta F$, taking place over an approximately 70-year time scale, normalized by the ratio of the forcing change to the forcing due to doubling $CO_2$, $F_{2\times CO2}$: TCR = $F_{2\times CO2}\ \Delta T/\Delta F$ (Frame et al., 2006; Gregory and Forster, 2008; Held et al., 2010; Otto et al., 2013). This generic definition of the TCR has also been called the 'Transient Climate Sensitivity' (Held et al., 2010). TCR is related to ECS and the global energy budget as follows: ECS = $F_{2\times CO2}/\alpha$, where $\alpha$ is the sensitivity parameter representing the net increase in energy flux to space per degree of warming given all feedbacks operating on these time scales. Hence, by conservation of energy, ECS = $F_{2\times CO2}\ \Delta T/(\Delta F - \Delta Q)$, where $\Delta Q$ is the change in the rate of increase of climate system heat content in response to the forcing $\Delta F$. On these time scales, deep ocean heat exchange affects the surface temperature response as if it were an enhanced radiative damping, introducing a slow, or 'recalcitrant', component of the response which would not be reversed for many decades even if it were possible to return RF to pre-industrial values (Held et al., 2010): hence the difficulty of placing an upper bound on ECS from observed surface warming alone (Forest et al., 2002; Frame et al., 2006). Because $\Delta Q$ is always positive at the end of a period of increasing forcing, before the climate system has re-equilibrated, TCR is always less than ECS, and since $\Delta Q$ is uncertain, TCR is generally better constrained by observations of recent climate change than ECS.

Because TCR focuses on the short- and medium-term response, constraining TCR with observations is a key step in narrowing estimates of future global temperature change in the relatively short term and under scenarios where forcing continues to increase or peaks and declines (Frame et al., 2006). After stabilization, the ECS eventually becomes the relevant climate system property. Based on observational constraints alone, the AR4 concluded that TCR is *very likely* to be larger than 1°C and *very unlikely* to be greater than 3.5°C (Hegerl et al., 2007b). This supported the overall assessment that the transient climate response is *very unlikely* greater than 3°C and *very likely* greater than 1°C (Meehl et al., 2007a). New estimates of the TCR are now available.

Scaling factors derived from detection and attribution studies (see Section 10.2) express how model responses to GHGs and aerosols need to be scaled to match the observations over the historical period. These scaled responses were used in AR4 to provide probabilistic projections of both TCR and future changes in global temperature in response to these forcings under various scenarios (Allen et al., 2000; Stott and Kettleborough, 2002; Stott et al., 2006, 2008b; Kettleborough et al., 2007; Meehl et al., 2007b; Stott and Forest, 2007). Allen et al. (2000), Frame et al. (2006) and Kettleborough et al. (2007) demonstrate a near linear relationship between 20th century warming, TCR and warming by the mid-21st century as parameters are varied in Energy Balance Models, justifying this approach. Forster et al. (2013 ) show how the ratio $\Delta T/\Delta F$ does depend on the forcing history, with very rapid increases in forcing giving lower values: hence any inference from past attributable warming to future warming or TCR depends on a model (which may be simple or complex, but ideally physically based) to relate these quantities. Such inferences also depend on forcing estimates and projections. Recent revisions to RF (see Chapter 8) suggest higher net anthropogenic forcing over the 20th century, and hence a smaller estimated

TCR. Stott et al. (2008b) demonstrated that optimal detection analysis of 20th century temperature changes (using HadCM3) are able to exclude the very high and low temperature responses to aerosol forcing. Consequently, projected 21st century warming may be more closely constrained than if the full range of aerosol forcings is used (Andreae et al., 2005). Stott and Forest (2007) demonstrate that projections obtained from such an approach are similar to those obtained by constraining EMIC parameters from observations. Stott et al. (2011), using HadGEM2-ES, and Gillett et al. (2012), using CanESM2, both show that the inclusion of observations between 2000 and 2010 in such an analysis reduces the uncertainties in projected warming in the 21st century, and tends to constrain the maximum projected warming to below that projected using data to 2000 only (Stott et al, 2006). Such an improvement is consistent with prior expectations of how additional data will narrow uncertainties (Stott and Kettleborough, 2002).

TCR estimates have been derived using a variety of methods (Figure 10.20a). Knutti and Tomassini (2008) compare EMIC simulations with 20th century surface and ocean temperatures to derive a probability density function for TCR skewed slightly towards lower values with a 5 to 95% range of 1.1°C to 2.3°C. Libardoni and Forest (2011) take a similar approach with a different EMIC and include atmospheric data and, under a variety of assumptions, obtain 5 to 95% ranges for TCR spanning 0.9°C to 2.4°C. Updating this study to include data to 2004 gives results that are essentially unchanged. Using a single model and observations from 1851 to 2010 Gillett et al. (2012) derive a 5 to 95% range of 1.3°C to 1.8°C and using a single model, but using multiple sets of observations and analysis periods ending in 2010 and beginning in 1910 or earlier, Stott et al. (2011) derive 5 to 95% ranges that were generally between 1°C and 3°C. Both Stott et al. (2011) and Gillett et al. (2012) find that the inclusion of data between 2000 and 2010 helps to constrain the upper bound of TCR. Gillett et al. (2012) find that the inclusion of data prior to 1900 also helps to constrain TCR, though Stott et al. (2011) do not. Gillett et al. (2013 ) account for a broader range of model and observational uncertainties, in particular addressing the efficacy of non-$CO_2$ gases, and find a range of 0.9°C to 2.3°C. Several of the estimates of TCR that were cited by Hegerl et al. (2007b) may have underestimated non-$CO_2$ efficacies relative to the more recent estimates in Forster et al. (2007). Because observationally constrained estimates of TCR are based on the ratio between past attributable warming and past forcing, this could account for a high bias in some of the inputs used for the AR4 TCR estimate.

Held et al. (2010) show that a two-box model originally proposed by Gregory (2000), distinguishing the 'fast' and 'recalcitrant' responses, fits both historical simulations and instantaneous doubled $CO_2$ simulations of the GFDL coupled model CM2.1. The fast response has a relaxation time of 3 to 5 years, and the historical simulation is almost completely described by this fast component of warming. Padilla et al. (2011) use this simple model to derive an observationally constrained estimate of the TCR of 1.3°C to 2.6°C. Schwartz (2012) uses this two-time scale formulation to obtain TCR estimates ranging from 0.9°C to 1.9°C, the lower values arising from higher estimates of forcing over the 20th century. Otto et al. (2013) update the analysis of Gregory et al. (2002) and Gregory and Forster (2008) using forcing estimates from Forster et al. (2013 ) to obtain a 5 to 95% range for TCR of 0.9°C to 2.0°C comparing the decade 2000–2009 with the period 1860–1879. They note, however, the danger of overinterpreting a single, possibly anomalous, decade, and report a larger TCR range of 0.7°C to 2.5°C replacing the 2000s with the 40 years 1970–2009.

Tung et al. (2008) examine the response to the 11-year solar cycle using discriminant analysis, and find a high range for TCR: >2.5°C to 3.6°C However, this estimate may be affected by different mechanisms by which solar forcing affects climate (see Box 10.2). The authors attempt to minimize possible aliasing with the response to other forcings in the 20th century and with internal climate variability, although some influence by them cannot be ruled out.

Rogelj et al. (2012) take a somewhat different approach, using a simple climate model to match the distribution of TCR to observational constraints and a consensus distribution of ECS (which will itself have been informed by recent climate change), following Meinshausen et al. (2009). Harris et al. (2013) estimate a distribution for TCR based on a large sample of emulated GCM equilibrium responses, constrained by multiannual mean observations of recent climate and adjusted to account for additional uncertainty associated with model structural deficiencies (Sexton et al., 2012). The equilibrium responses are scaled by global temperature changes associated with the sampled model variants, reweighting the projections based on the likelihood that they correctly replicate observed historical changes in surface temperature, to predict the TCR distribution. Both of these studies represent a combination of multiple lines of evidence, although still strongly informed by recent observed climate change, and hence are assessed here for completeness.

Based on this evidence, including the new 21st century observations that were not yet available to AR4, we conclude that, on the basis of constraints provided by recent observed climate change, TCR is *likely* to lie in the range 1°C to 2.5°C and *extremely unlikely* to be greater than 3°C. This range for TCR is smaller than given at the time of AR4, due to the stronger observational constraints and the wider range of studies now available. Our greater confidence in excluding high values of TCR arises primarily from higher and more confident estimates of past forcing: estimates of TCR are not strongly dependent on observations of ocean heat uptake.

### 10.8.2 Constraints on Long-Term Climate Change and the Equilibrium Climate Sensitivity

The equilibrium climate sensitivity (ECS) is defined as the warming in response to a sustained doubling of carbon dioxide in the atmosphere relative to pre-industrial levels (see AR4). The equilibrium to which the ECS refers to is generally assumed to be an equilibrium involving the ocean–atmosphere system, which does not include Earth system feedbacks such as long-term melting of ice sheets and ice caps, dust forcing or vegetation changes (see Chapter 5 and Section 12.5.3). The ECS cannot be directly deduced from transient warming attributable to GHGs, or from TCR, as the role of ocean heat uptake has to be taken into account (see Forest et al., 2000; Frame et al., 2005; Knutti and Hegerl, 2008). Estimating the ECS generally relies on the paradigm of a comparison of observed change with results from a physically based climate model, sometimes a very simple one, given uncertainty in the model, data, RF and due to internal variability.

For example, estimates can be based on the simple box model introduced in Section 10.8.1, ECS = $F_{2\times CO2}\ \Delta T/(\Delta F - \Delta Q)$. Simple energy balance calculations rely on a very limited representation of climate response time scales, and cannot account for nonlinearities in the climate system that may lead to changes in feedbacks for different forcings (see Chapter 9). Alternative approaches are estimates that use climate model ensembles with varying parameters that evaluate the ECS of individual models and then infer the probability density function (PDF) for the ECS from the model–data agreement or by using optimization methods (Tanaka et al., 2009).

As discussed in the AR4, the probabilistic estimates available in the literature for climate system parameters, such as ECS and TCR have all been based, implicitly or explicitly, on adopting a Bayesian approach and therefore, even if it is not explicitly stated, involve using some kind of prior information. The shape of the prior has been derived from expert judgement in some studies, observational or experimental evidence in others or from the distribution of the sample of models available. In all cases the constraint by data, for example, from transient warming, or observations related to feedbacks is fairly weak on the upper tail of ECS (e.g., Frame et al., 2005). Therefore, results are sensitive to the prior assumptions (Tomassini et al., 2007; Knutti and Hegerl, 2008; Sanso and Forest, 2009; Aldrin et al., 2012). When the prior distribution fails to taper off for high sensitivities, as is the case for uniform priors (Frame et al., 2005), this leads to long tails (Frame et al., 2005; Annan and Hargreaves, 2011; Lewis, 2013). Uniform priors have been criticized (e.g., Annan and Hargreaves, 2011; Pueyo, 2012; Lewis, 2013) since results assuming a uniform prior in ECS translates instead into a strongly structured prior on climate feedback parameter and vice versa (Frame et al., 2005; Pueyo, 2012). Objective Bayesian analyses attempt to avoid this paradox by using a prior distribution that is invariant to parameter transforms and rescaling, for example, a Jeffreys prior (Lewis, 2013). Estimated probability densities based on priors that are strongly non-uniform in the vicinity of the best fit to the data, as is typically the case for the Jeffreys prior in this instance, can peak at values very different from the location of the best fit, and hence need to be interpreted carefully. To what extent results are sensitive to priors can be evaluated by using different priors, and this has been done more consistently in studies than at the time of AR4 (see Figure 10.20b) and is assessed where available, illustrated in Figure 10.20. Results will also be sensitive to the extent to which uncertainties in forcing (Tanaka et al., 2009), models and observations and internal climate variability are taken into account, and can be acutely sensitive to relatively arbitrary choices of observation period, choice of truncation in estimated covariance matrices and so forth (Lewis, 2013), illustrating the importance of sensitivity studies. Analyses that make a more complete effort to estimate all uncertainties affecting the model–data comparison lead to more trustworthy results, but end up with larger uncertainties (Knutti and Hegerl, 2008).

The detection and attribution chapter in AR4 (Hegerl et al., 2007b) concluded that 'Estimates based on observational constraints indicate that it is *very likely* that the equilibrium climate sensitivity is larger than 1.5°C with a most likely value between 2°C and 3°C'. The following sections discuss evidence since AR4 from several lines of evidence, followed by an overall assessment of ECS based on observed climate changes, and a subset of available new estimates is shown in Figure 10.20b.

#### 10.8.2.1 Estimates from Recent Temperature Change

As estimates of ECS based on recent temperature change can only sample atmospheric feedbacks that occur with presently evolving climate change, they provide information on the 'effective climate sensitivity' (e.g., Forest et al., 2008). As discussed in AR4, analyses based on global scale data find that within data uncertainties, a strong aerosol forcing or a large ocean heat uptake might have masked a strong greenhouse warming (see, e.g., Forest et al., 2002; Frame et al., 2005; Stern, 2006; Roe and Baker, 2007; Hannart et al., 2009; Urban and Keller, 2009; Church et al., 2011). This is consistent with the finding that a set of models with a large range of ECS and aerosol forcing could be consistent with the observed warming (Kiehl, 2007). Consequently, such analyses find that constraints on aerosol forcing are essential to provide tighter constraints on future warming (Tanaka et al., 2009; Schwartz et al., 2010). Aldrin et al. (2012) analyse the observed record from 1850 to 2007 for hemispheric means of surface temperature, and upper 700 m ocean heat content since 1955. The authors use a simple climate model and a Markov Chain Monte Carlo Bayesian technique for analysis. The authors find a quite narrow range of ECS, which narrows further if using a uniform prior in 1/ECS rather than ECS (Figure 10.20). If observations are updated to 2010 and forcing estimates including further indirect aerosol effects are used (following Skeie et al., 2011), this yields a reduced upper tail (see Figure 10.20b, dash dotted). However, this estimate involves a rather simple model for internal variability, hence may underestimate uncertainties. Olson et al. (2012) use similar global scale constraints and surface temperature to 2006, and ocean data to 2003 and arrive at a wide range if using a uniform prior in ECS, and a quite well constrained range if using a prior derived from current mean climate and Last Glacial Maximum (LGM) constraints (see Figure 10.20b). Some of the differences between Olson et al. (2012) and Aldrin et al. (2012) may be due to structural differences in the model used (Aldrin et al. use a simple EBM while Olson use the UVIC EMIC), some due to different statistical methods and some due to use of global rather than hemispheric temperatures in the latter work. An approach based on regressing forcing histories used in 20th century simulations on observed surface temperatures (Schwartz, 2012) estimates ranges of ECS that encompass the AR4 ranges if accounting for data uncertainty (Figure 10.20). Otto et al. (2013) updated the Gregory et al. (2002) global energy balance analysis (see equation above), using temperature and ocean heat content data to 2009 and estimates of RF that are approximately consistent with estimates from Chapters 7 and 8, and ocean heat uptake estimates that are consistent with Chapter 3 and find that inclusion of recent deep ocean heat uptake and temperature data considerably narrow estimates of ECS compared to results using data to the less recent past.

Estimates of ECS and TCR that make use of both spatial and temporal information, or separate the GHG attributable warming using fingerprint methods, can yield tighter estimates (e.g., Frame et al., 2005; Forest et al., 2008; Libardoni and Forest, 2011). The resulting GHG attributable warming tends to be reasonably robust to uncertainties in aerosol forcing (Section 10.3.1.1.3). Forest et al. (2008) have updated their earlier study using a newer version of the MIT model and five different surface temperature data sets (Libardoni and Forest, 2011). Correction of statistical errors in estimation procedure pointed out by Lewis (see Lewis, 2013) changes their result only slightly (Libardoni

and Forest, 2013). The overarching 5 to 95% range of effective climate sensitivity widens to 1.2°C to 5.3°C when all five data sets are used, and constraints on effective ocean diffusivity become very weak (Forest et al., 2008). Uncertainties would likely further increase if estimates of forcing uncertainty, for example, due to natural forcings, are also included (Forest et al., 2006). Lewis (2013) reanalysed the data used in Forest et al. (2006) using an objective Bayesian method (see discussion at top of section). The author finds that use of a Jeffreys prior narrows the upper tail considerably, to 3.6°C for the 95th percentile. When revising the method, omitting upper air data, and adding 6 more years of data a much reduced 5 to 95% range of 1.2°C to 2.2°C results (see Figure 10.20), similar to estimates by Ring et al. (2012) using data to 2008. Lewis's upper limit extends to 3.0°C if accounting for forcing and surface temperature uncertainty (Lewis, 2013). Lewis (2013) also reports a range of 1.1°C to 2.9°C using his revised diagnostics and the Forest et al. (2006) statistical method, whereas adding 9 more years to the Libardoni and Forest (2013) corrected diagnostic (after Libardoni and Forest, 2011; Figure 10.20; using an expert prior in both cases), does not change results much (Figure 10.20b). The differences between results reported in Forest et al. (2008); Libardoni and Forest (2011); Lewis (2013); Libardoni and Forest (2013) are still not fully understood, but appear to be due to a combination of sensitivity of results to the choice of analysis period as well as differences in diagnostics and statistical approach.

In summary, analyses that use the most recent decade find a tightening of the range of ECS based on a combination of recent heat uptake and surface temperature data. Results consistently give low probability to ECS values under 1.0°C (Figure 10.20). The mode of the PDFs varies considerably with period considered as expected from the influence of internal variability on the single realization of observed climate change. Estimates including the most recent data tend to have reduced upper tails (Libardoni and Forest, 2011; Aldrin et al., 2012 and update; Ring et al., 2012 and update cf. Figure 10.20; Lewis, 2013; Otto et al., 2013), although further uncertainty in statistical assumptions and structural uncertainties in simple models used, as well as neglected uncertainties, for example, in forcings, increase assessed uncertainty.

#### 10.8.2.2 Estimates Based on Top of the Atmosphere Radiative Balance

With the satellite era, measurements are now long enough to allow direct estimates of variations in the energy budget of the planet, although the measurements are not sufficiently accurate to determine absolute top of the atmosphere (TOA) fluxes or trends (see Section 2.3 and Box 13.1). Using a simple energy balance relationship between net energy flow towards the Earth, net forcing and a climate feedback parameter and the satellite measurements Murphy et al. (2009) made direct estimates of the climate feedback parameter as the regression coefficient of radiative response against GMST. The feedback parameter in turn is inversely proportional to the ECS (see above, also Forster and Gregory, 2006). Such regression based estimates are, however, subject to uncertainties (see Section 7.2.5.7; see also, Gregory and Forster, 2008; Murphy and Forster, 2010). Lindzen and Choi (2009) used data from the radiative budget and simple energy balance models over the tropics to investigate feedbacks in climate models. Their result suggests that climate models overestimate the outgoing shortwave radiation compared to Earth Radiation Budget Experiment (ERBE) data, but this result was found unreliable owing to use of a limited sample of periods and of a domain limited to low latitudes (Murphy and Forster, 2010). Lindzen and Choi (2011) address some of these criticisms (Chung et al., 2010; Trenberth et al., 2010), but the results remains uncertain. For example, the lag-lead relationship between TOA balance and SST (Lindzen and Choi, 2011) is replicated by Atmospheric Model Intercomparison Project (AMIP) simulations where SST cannot respond (Dessler, 2011). Hence, as discussed in Section 7.2.5.7, the influence of internal temperature variations on short time scales seriously affects such estimates of feedbacks. In addition, the energy budget changes that are used to derive feedbacks are also affected by RF, which Lindzen and Choi (2009) do not account for. Murphy and Forster (2010) further question if estimates of the feedback parameter are suitable to estimate the ECS, as multiple time scales are involved in feedbacks that contribute to climate sensitivity (Knutti and Hegerl, 2008; Dessler, 2010). Lin et al. (2010a) use data over the 20th century combined with an estimate of present TOA imbalance based on modelling (Hansen et al., 2005a) to estimate the energy budget of the planet and give a best estimate of ECS of 3.1°C, but do not attempt to estimate a distribution that accounts fully for uncertainties. In conclusion, measurement and methodological uncertainties in estimates of the feedback parameter and the ECS from short-term variations in the satellite period preclude strong constraints on ECS. When accounting for these uncertainties, estimates of ECS based on the TOA radiation budget appear consistent with those from other lines of evidence within large uncertainties (e.g., Forster and Gregory, 2006; Figure 10.20b).

#### 10.8.2.3 Estimates Based on Response to Volcanic Forcing or Internal Variability

Some analyses used in AR4 were based on the well observed forcing and responses to major volcanic eruptions during the 20th century. The constraint is fairly weak because the peak response to short-term volcanic forcing depends nonlinearly on ECS (Wigley et al., 2005; Boer et al., 2007). Recently, Bender et al. (2010) re-evaluated the constraint and found a close relationship in 9 out of 10 AR4 models between the shortwave TOA imbalance, the simulated response to the eruption of Mt Pinatubo and the ECS. Applying the constraint from observations suggests a range of ECS of 1.7°C to 4.1°C. This range for ECS is subject to observational uncertainty and uncertainty due to internal climate variability, and is derived from a limited sample of models. Schwartz (2007) tried to relate the ECS to the strength of natural variability using the fluctuation dissipation theorem but studies suggest that the observations are too short to support a well constrained and reliable estimate and would yield an underestimate of sensitivity (Kirk-Davidoff, 2009); and that assuming single time scales is too simplistic for the climate system (Knutti and Hegerl, 2008) . Thus, credible estimates of ECS from the response to natural and internal variability do not disagree with other estimates, but at present cannot provide more reliable estimates of ECS.

#### 10.8.2.4 Paleoclimatic Evidence

Palaeoclimatic evidence is promising for estimating ECS (Edwards et al., 2007). This section reports on probabilistic estimates of ECS derived from paleoclimatic data by drawing on Chapter 5 information

on forcing and temperature changes. For periods of past climate, which were close to radiative balance or when climate was changing slowly, for example, the LGM, radiative imbalance and with it ocean heat uptake is less important than for the present (Sections 5.3.3.1 and 5.3.3.2). Treating the RF due to ice sheets, dust and $CO_2$ as forcings rather than feedbacks implies that the corresponding RF contributions are associated with considerable uncertainties (see Section 5.2.2.3). Koehler et al. (2010) used an estimate of LGM cooling along with its uncertainties together with estimates of LGM RF and its uncertainty to derive an overall estimate of climate sensitivity. This method accounts for the effect of changes in feedbacks for this very different climatic state using published estimates of changes in feedback factors (see Section 5.3.3.2; Hargreaves et al., 2007; Otto-Bliesner et al., 2009). The authors find a best estimate of 2.4°C and a 5 to 95% range of ECS from 1.4°C to 5.2°C, with sensitivities beyond 6°C difficult to reconcile with the data. In contrast, Chylek and Lohmann (2008b) estimate the ECS to be 1.3°C to 2.3°C based on data for the transition from the LGM to the Holocene. However, the true uncertainties are likely larger due to uncertainties in relating local proxies to large-scale temperature change observed over a limited time (Ganopolski and von Deimling, 2008; Hargreaves and Annan, 2009). The authors also use an aerosol RF estimate that may be high (see response by Chylek and Lohmann, 2008a; Ganopolski and von Deimling, 2008).

At the time of the AR4, several studies were assessed in which parameters in climate models had been perturbed systematically in order to estimate ECS, and further studies have been published since, some making use of expanded data for LGM climate change (see Section 5.3.3.2, Table 5.3). Sometimes substantial differences between estimates based on similar data reflect not only differences in assumptions on forcing and use of data, but also structural model uncertainties, for example, in how feedbacks change between different climatic states (e.g., Schneider von Deimling et al., 2006; Hargreaves et al., 2007; (see also Otto-Bliesner et al., 2009). Holden et al. (2010) analysed which versions of the EMIC Genie are consistent with LGM tropical SSTs and find a 90% range of 2.0°C to 5.0°C. Recently, new data synthesis products have become available for assessment with climate model simulations of the LGM which together with further data cover much more of the LGM ocean and land areas, although there are still substantial gaps and substantial data uncertainty (Section 5.3.3). An analysis of the recent SST and land temperature reconstructions for the LGM compared to simulations with an EMIC suggests a 90% range of 1.4°C to 2.8°C for ECS, with SST data providing a narrower range and lower values than land data only (see Figure 10.20; Schmittner et al., 2011). However, structural model uncertainty as well as data uncertainty may increase this range substantially (Fyke and Eby, 2012; Schmittner et al., 2012). Hargreaves et al. (2012) derived a relationship between ECS and LGM response for seven model simulations from PMIP2 simulations and found a linear relationship between tropical cooling and ECS (see Section 5.3.3.2) which has been used to derive an estimate of ECS (Figure 10.20); and has been updated using PMIP3 simulations (Section 5.3.3.2). However, uncertainties remain as the relationship is dependent on the ensemble of models used.

Estimates of ECS from other, more distant paleoclimate periods (e.g., Royer et al., 2007; Royer, 2008; Pagani et al., 2009; Lunt et al., 2010) are difficult to directly compare, as climatic conditions were very different from today and as climate sensitivity can be state dependent, as discussed above. Also, the response on very long time scales is determined by the Earth System Sensitivity, which includes very slow feedbacks by ice sheets and vegetation (see Section 12.5.3). Paleosens Members (2012) reanalysed the relationship between RF and temperature response from paleoclimatic studies, considering Earth system feedbacks as forcings in order to derive an estimate of ECS that is limited to atmospheric feecbacks (sometimes referred to as Charney sensitivity and directly comparable to ECS), and find that resulting estimates are reasonably consistent over the past 65 million years (see detailed discussion in Section 5.3.1). They estimate a 95% range of 1.1°C to 7.0°C, largely based on the past 800,000 years. However, uncertainties in paleoclimate estimates of ECS are likely to be larger than from the instrumental record, for example, due to changes in feedbacks between different climatic states. In conclusion, estimates of ECS have continued to emerge from palaeoclimatic periods that indicate that ECS is *very likely* less than 6°C and *very likely* greater than 1.0°C (see Section 5.3.3).

#### 10.8.2.5 Combining Evidence and Overall Assessment

Most studies find a lower 5% limit for ECS between 1°C and 2°C (Figure 10.20). The combined evidence thus indicates that the net feedbacks to RF are significantly positive. At present, there is no credible individual line of evidence that yields very high or very low climate sensitivity as best estimate. Some recent studies suggest a low climate sensitivity (Chylek et al., 2007; Schwartz et al., 2007; Lindzen and Choi, 2009). However, these are based on problematic assumptions, for example, about the climate's response time, the cause of climate fluctuations, or neglect uncertainty in forcing, observations and internal variability (as discussed in Foster et al., 2008; Knutti and Hegerl, 2008; Murphy and Forster, 2010). In some cases the estimates of the ECS have been refuted by testing the method of estimation with a climate model of known sensitivity (e.g., Kirk-Davidoff, 2009).

Several authors (Annan and Hargreaves, 2006; Hegerl et al., 2006; Annan and Hargreaves, 2010) had proposed combining estimates of climate sensitivity from different lines of evidence by the time of AR4; these and recent work is shown in the panel 'combined' in Figure 10.20. Aldrin et al. (2012) combined the Hegerl et al. (2006) estimate based on the last millennium with their estimate based on the 20th century; and Olson et al. (2012) combined weak constraints from climatology and the LGM in their prior, updated by data on temperature changes. This approach is robust only if the lines of evidence used are truly independent. The latter is hard to evaluate when using prior distributions based on expert knowledge (e.g., Libardoni and Forest, 2011). If lines of evidence are not independent, overly confident assessments of equilibrium climate sensitivity may result (Henriksson et al., 2010; Annan and Hargreaves, 2011).

In conclusion, estimates of the Equilibrium Climate Sensitivity (ECS) based on multiple and partly independent lines of evidence from observed climate change, including estimates using longer records of surface temperature change and new palaeoclimatic evidence, indicate that there is *high confidence* that ECS is *extremely unlikely* less than 1°C and *medium confidence* that the ECS is *likely* between 1.5°C and 4.5°C and *very unlikely* greater than 6°C. They complement the

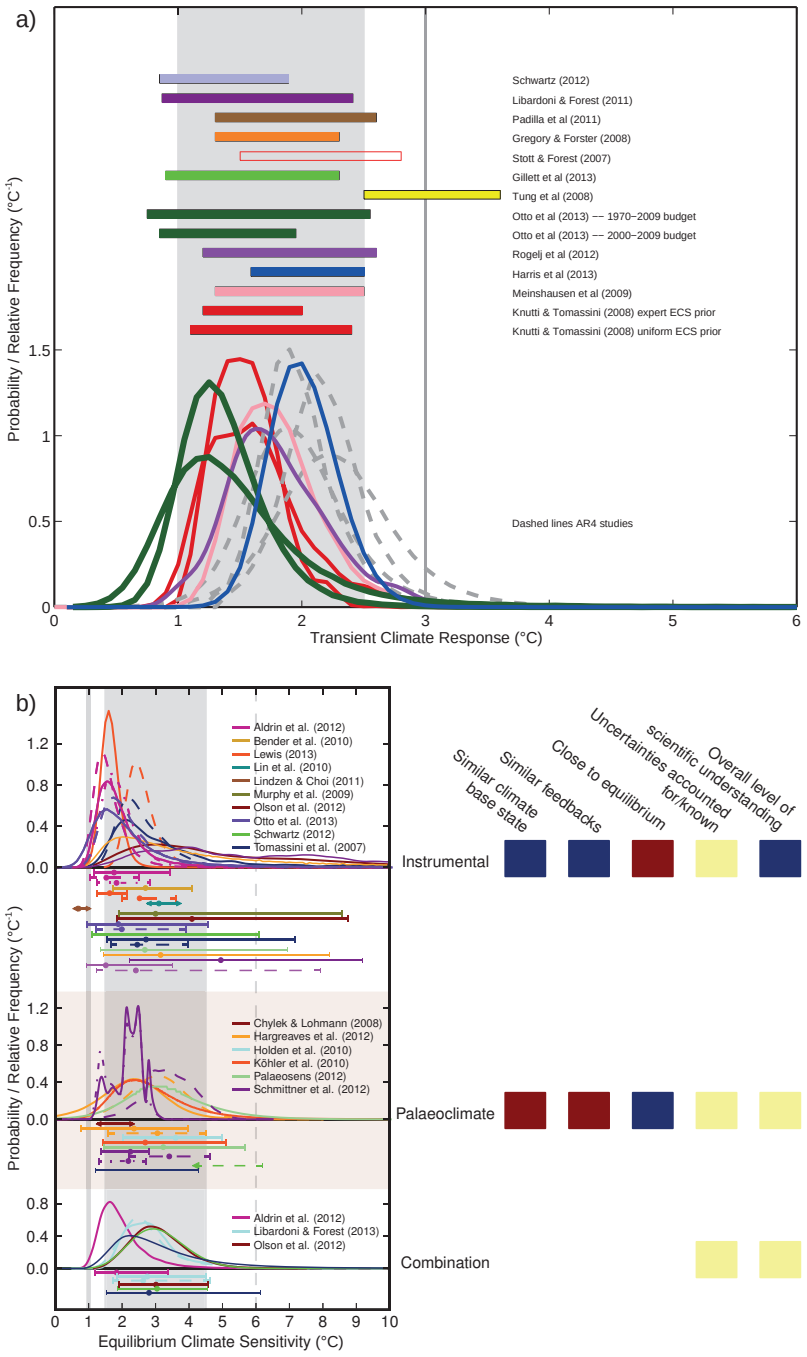


**Figure 10.20 |** (a) Examples of distributions of the transient climate response (TCR, top) and the equilibrium climate sensitivity (ECS, bottom) estimated from observational constraints. Probability density functions (PDFs), and ranges (5 to 95%) for the TCR estimated by different studies (see text). The grey shaded range marks the *very likely* range of 1°C to 2.5°C for TCR and the grey solid line represents the *extremely unlikely* <3°C upper bound as assessed in this section. Representative distributions from AR4 shown as dashed lines and open bar. (b) Estimates of ECS are compared to overall assessed *likely* range (solid grey), with solid line at 1°C and a dashed line at 6°C. The figure compares some selected old estimates used in AR4 (no labels, thin lines; for references see Supplementary Material) with new estimates available since AR4 (labelled, thicker lines). Distributions are shown where available, together with 5 to 95% ranges and median values (circles). Ranges that are assessed as being incomplete are marked by arrows; note that in contrast to the other estimates Schwartz (2012), shows a sampling range and Chylek and Lohmann a 95% range. Estimates are based on changes over the instrumental period (top row); and changes from palaeoclimatic data (2nd row). Studies that combine multiple lines of evidence are shown in the bottom panel. The boxes on the right-hand side indicate limitations and strengths of each line of evidence, for example, if a period has a similar climatic base state, if feedbacks are similar to those operating under $CO_2$ doubling, if the observed change is close to equilibrium, if, between all lines of evidence plotted, uncertainty is accounted for relatively completely, and summarizes the level of scientific understanding of this line of evidence overall. A blue box indicates an overall line of evidence that is well understood, has small uncertainty, or many studies and overall *high confidence*. Pale yellow indicates *medium*, and dark red *low*, *confidence* (i.e., poorly understood,very few studies, poor agreement, unknown limitations, after Knutti and Hegerl, 2008). Where available, results are shown using several different prior distributions; for example for Aldrin et al. (2012) solid shows the result using a uniform *prior* in ECS, which is shown as updated to 2010 in dash-dots; dashed: uniform *prior* in 1/ECS; and in bottom panel, result combining with Hegerl et al. (2006) *prior*, For Lewis (2013), dashed shows results using the Forest et al. (2006) diagnostic and an objective Bayesian *prior*, solid a revised diagnostic. For Otto et al. (2013), solid is an estimate using change to 1979–2009, dashed using the change to 2000–2009. Palaeoclimate: Hargreaves et al. (2012) is shown in solid, with dashed showing an update based on PMIP3 simulations (see Chapter 5); For Schmittner et al. (2011), solid is land-and-ocean, dashed land-only, and dash-dotted is ocean-only diagnostic.

evaluation in Chapter 9 and support the overall assessment in Chapter 12 that concludes between all lines of evidence with *high confidence* that ECS is *likely* in the range 1.5°C to 4.5°C. Earth system feedbacks can lead to different, probably larger, warming than indicated by ECS on very long time scales.

### 10.8.3 Consequences for Aerosol Forcing and Ocean Heat Uptake

Some estimates of ECS also yield estimates of aerosol forcing that are consistent with observational records, which we briefly mention here. Note that the estimate will reflect any forcings with a time or time–space pattern resembling aerosol forcing that is not explicitly included in the overall estimate (see discussion in Olson et al., 2012), for example, BC on snow; and should hence be interpreted as an estimate of aerosol plus neglected forcings. Estimates will also vary with the method applied and diagnostics used (e.g., analyses including spatial information will yield stronger results). Murphy et al. (2009) use correlations between surface temperature and outgoing shortwave and longwave flux over the satellite period to estimate how much of the total recent forcing has been reduced by aerosol total reflection, which they estimate as –1.1 ± 0.4 W $m^{-2}$ from 1970 to 2000 (1 standard deviation), while Libardoni and Forest (2011), see also Forest et al. (2008), based on the 20th century, find somewhat lower estimates, namely a 90% bound of –0.83 to –0.19 W $m^{-2}$ for the 1980s relative to preindustrial. Lewis (2013), using similar diagnostics but an objective Bayesian method, estimates a total aerosol forcing of about –0.6 to –0.1W $m^{-2}$ or –0.6 to 0.0 W $m^{-2}$ dependent on diagnostic used. The range of the aerosol forcing estimates that are based on the observed climate change are in-line with the expert judgement of the effective RF by aerosol radiation and aerosol cloud interactions combined (ERFaci+ari; Chapter 7) of –0.9 W $m^{-2}$ with a range from –1.9 to –0.1 W $m^{-2}$ that has been guided by climate models that include aerosol effects on mixed-phase and convective clouds in addition to liquid clouds, satellite studies and models that allow cloud-scale responses (see Section 7.5.2).

Several estimates of ECS also estimate a parameter that describe the efficiency with which the ocean takes up heat, e.g., effective global vertical ocean diffusivity (e.g., Tomassini et al., 2007; Forest et al., 2008; Olson et al., 2012; Lewis, 2013). Forest and Reynolds (2008) find that the effective global ocean diffusivity $K_v$ in many of the CMIP3 models lies above the median value based on observational constraints, resulting in a positive bias in their ocean heat uptake. Lewis (2013) similarly finds better agreement for small values of effective ocean diffusivity. However, such a finding was very sensitive to data sets used for surface temperature (Libardoni and Forest, 2011) and ocean data (Sokolov et al., 2010), is somewhat sensitive to the diagnostic applied (Lewis, 2013), and limited by difficulties observing heat uptake in the deep ocean (see, e.g., Chapters 3 and 13). Olson et al. (2012) and Tomassini et al. (2007) find that data over the historical period provide only a weak constraint on background ocean effective diffusivity. Comparison of the vertical profiles of temperature and of historical warming in models and observations suggests that the ocean heat uptake efficiency may be typically too large (Kuhlbrodt and Gregory, 2012; Section 13.4.1; see also Sections 9.4.2, 10.4.1, 10.4.3). If effective diffusivity were high in models this might lead to a tendency to bias ocean warming high relative to surface warming; but this uncertainty makes only a small contribution to uncertainty in TCR (Knutti and Tomassini, 2008; Kuhlbrodt and Gregory, 2012; see Section 13.4.1). Nonetheless, ocean thermal expansion and heat content change simulated in CMIP5 models show relatively good agreement with observations, although this might also be due to a compensation between ocean heat uptake efficiency and atmospheric feedbacks (Kuhlbrodt and Gregory, 2012). In summary, constraints on effective ocean diffusivity are presently not conclusive.

### 10.8.4 Earth System Properties

A number of papers have found the global warming response to $CO_2$ emissions to be determined primarily by total cumulative emissions of $CO_2$, irrespective of the timing of those emissions over a broad range of scenarios (Allen et al., 2009; Matthews et al., 2009; Zickfeld et al., 2009; Section 12.5.4.2), although Bowerman et al. (2011) find that, when scenarios with persistent 'emission floors' are included, the strongest predictor of peak warming is cumulative emissions to 2200. Moreover, the ratio of global warming to cumulative carbon emissions, known variously as the Absolute Global Temperature Change Potential (AGTP; defined for an infinitesimal pulse emission) (Shine et al., 2005), the Cumulative Warming Commitment (defined based on peak warming in response to a finite injection; CWC) (Allen et al., 2009) or the Carbon Climate Response (CCR) (Matthews et al., 2009), is approximately scenario-independent and constant in time.

The ratio of $CO_2$-induced warming realized by a given year to cumulative carbon emissions to that year is known as the Transient Climate Response to cumulative $CO_2$ Emissions (TCRE, see Chapter 12). TCRE depends on TCR and the Cumulative Airborne Fraction (CAF), which is the ratio of the increased mass of $CO_2$ in the atmosphere to cumulative $CO_2$ emissions (not including natural fluxes and those arising from Earth system feedbacks) over a long period, typically since pre-industrial times (Gregory et al., 2009): $\text{TCRE} = \text{TCR} \times \text{CAF}/C_0$, where $C_0$ is the mass of carbon (in the form of $CO_2$) in the pre-industrial atmosphere (590 PgC). Given estimates of CAF to the time of $CO_2$ doubling of 0.4 to 0.7 (Zickfeld et al., 2013), we therefore expect values of TCRE, if expressed in units of °C per 1000 PgC, to be similar to or slightly lower than, and more uncertain than, values of TCR (Gillett et al., 2013 ).

TCRE may be estimated from observations by dividing an estimate of warming to date attributable to $CO_2$ by historical cumulative carbon emissions, which gives a 5 to 95% range of 0.7°C to 2.0°C per 1000 PgC (Gillett et al., 2013 ), 1.0°C to 2.1°C per 1000 PgC (Matthews et al., 2009) or 1.4°C to 2.5°C per 1000 PgC (Allen et al., 2009), the higher range in the latter study reflecting a higher estimate of $CO_2$-attributable warming to 2000. The peak warming induced by a given total cumulative carbon emission (Peak Response to Cumulative Emissions (PRCE)) is less well constrained, since warming may continue even after a complete cessation of $CO_2$ emissions, particularly in high-response models or scenarios. Using a combination of observations and models to constrain temperature and carbon cycle parameters in a simple climate-carbon-cycle model, (Allen et al., 2009), obtain a PRCE 5 to 95% confidence interval of 1.3°C to 3.9°C per 1000 PgC. They also report that (Meinshausen et al., 2009) obtain a 5 to 95% range in PRCE of 1.1°C to 2.7°C per 1000 PgC using a Bayesian approach with a different simple model, with climate parameters constrained

by observed warming and carbon cycle parameters constrained by the C4MIP simulations (Friedlingstein et al., 2006).

The ratio of warming to cumulative emissions, the TCRE, is assessed to be *likely* between 0.8°C and 2.5°C per 1000 PgC based on observational constraints. This implies that, for warming due to $CO_2$ emissions alone to be *likely* less than 2°C at the time $CO_2$ emissions cease, total cumulative emissions from all anthropogenic sources over the entire industrial era would need to be limited to about 1000 PgC, or one trillion tonnes of carbon (see Section 12.5.4).

## 10.9 Synthesis

The evidence has grown since the Fourth Assessment Report that widespread changes observed in the climate system since the 1950s are attributable to anthropogenic influences. This evidence is documented in the preceding sections of this chapter, including for near surface temperatures (Section 10.3.1.1), free atmosphere temperatures (Section 10.3.1.2), atmospheric moisture content (Section 10.3.2.1), precipitation over land (Section 10.3.2.2), ocean heat content (Section 10.4.1), ocean salinity (Section 10.4.2), sea level (Section 10.4.3), Arctic sea ice (Section 10.5.1), climate extremes (Section 10.6) and evidence from the last millenium (Section 10.7). These results strengthen the conclusion that human influence on climate has played the dominant role in observed warming since the 1950s. However, the approach taken so far in this chapter has been to examine each aspect of the climate system—the atmosphere, oceans, cryosphere, extremes, and from paleoclimate archives—separately in each section and sub-section. In this section we look across the whole climate system to assess the extent that a consistent picture emerges across sub-systems and climate variables.

### 10.9.1 Multi-variable Approaches

Multi-variable studies provide one approach to gain a more comprehensive view across the climate system, although there have been relatively few applications of multi-variable detection and attribution studies in the literature. A combined analysis of near-surface temperature from weather stations and free atmosphere temperatures from radiosondes detected an anthropogenic influence on the joint changes in temperatures near the surface and aloft (Jones et al., 2003). In a Bayesian application of detection and attribution Schnur and Hasselmann (2005) combined surface temperature, diurnal temperature range and precipitation into a single analysis and showed strong net evidence for detection of anthropogenic forcings despite low likelihood ratios for diurnal temperature range and precipitation on their own. Barnett et al. (2008) applied a multi-variable approach in analysing changes in the hydrology of the Western United States (see also Section 10.3.2.3).

The potential for a multi-variable analysis to have greater power to discriminate between forced changes and internal variability has been demonstrated by Stott and Jones (2009) and Pierce et al. (2012). In the former case, they showed that a multi-variable fingerprint consisting of the responses of GMST and sub-tropical Atlantic salinity has a higher S/N ratio than the fingerprints of each variable separately. They found reduced detection times as a result of low correlations between the two variables in the control simulation although the detection result depends on the ability of the models to represent the co-variability of the variables concerned. Multi-variable attribution studies potentially provide a stronger test of climate models than single variable attribution studies although there can be sensitivity to weighting of different components of the multi-variable fingerprint. In an analysis of ocean variables, Pierce et al. (2012) found that the joint analysis of temperature and salinity changes yielded a stronger signal of climate change than 'either salinity or temperature alone'.

Further insights can be gained by considering a synthesis of evidence across the climate system. This is the subject of the next subsection.

### 10.9.2 Whole Climate System

To demonstrate how observed changes across the climate system can be understood in terms of natural and anthropogenic causes Figure 10.21 compares observed and modelled changes in the atmosphere, ocean and cryosphere. The instrumental records associated with each element of the climate system are generally independent (see FAQ 2.1), and consequently joint interpretations across observations from the main components of the climate system increases the confidence to higher levels than from any single study or component of the climate system. The ability of climate models to replicate observed changes (to within internal variability) across a wide suite of climate indicators also builds confidence in the capacity of the models to simulate the Earth's climate.

The coherence of observed changes for the variables shown in Figure 10.21 with climate model simulations that include anthropogenic and natural forcing is remarkable. Surface temperatures over land, SSTs and ocean heat content changes show emerging anthropogenic and natural signals with a clear separation between the observed changes and the alternative hypothesis of just natural variations (Figure 10.21, Global panels). These signals appear not just in the global means, but also at continental and ocean basin scales in these variables. Sea ice emerges strongly from the range expected from natural variability for the Arctic and Antarctica remains broadly within the range of natural variability consistent with expectations from model simulations including anthropogenic forcings.

Table 10.1 illustrates a larger suite of detection and attribution results across the climate system than summarized in Figure 10.21. These results include observations from both the instrumental record and paleo-reconstructions on a range of time scales ranging from daily extreme precipitation events to variability over millennium time scales.

From up in the stratosphere, down through the troposphere to the surface of the Earth and into the depths of the oceans there are detectable signals of change such that the assessed likelihood of a detectable, and often quantifiable, human contribution ranges from *likely* to *extremely likely* for many climate variables (Table 10.1). Indeed to successfully describe the observed warming trends in the atmosphere, ocean and at the surface over the past 50 years, contributions from both anthropogenic and natural forcings are required (e.g., results 1, 2, 3, 4, 5, 7, 9 in Table 10.1). This is consistent with anthropogenic forcings warming the surface of the Earth, troposphere and oceans superimposed with cooling events caused by the three large explosive volcanic eruptions since the 1960's. These two effects (anthropogenic warming and vol-

Frequently Asked Questions

## FAQ 10.2 | When Will Human Influences on Climate Become Obvious on Local Scales?

*Human-caused warming is already becoming locally obvious on land in some tropical regions, especially during the warm part of the year. Warming should become obvious in middle latitudes—during summer at first—within the next several decades. The trend is expected to emerge more slowly there, especially during winter, because natural climate variability increases with distance from the equator and during the cold season. Temperature trends already detected in many regions have been attributed to human influence. Temperature-sensitive climate variables, such as Arctic sea ice, also show detected trends attributable to human influence.*

Warming trends associated with global change are generally more evident in averages of global temperature than in time series of local temperature ('local' here refers generally to individual locations, or small regional averages). This is because most of the local variability of local climate is averaged away in the global mean. Multi-decadal warming trends detected in many regions are considered to be outside the range of trends one might expect from natural internal variability of the climate system, but such trends will only become obvious when the local mean climate emerges from the 'noise' of year-to-year variability. How quickly this happens depends on both the rate of the warming trend and the amount of local variability. Future warming trends cannot be predicted precisely, especially at local scales, so estimates of the future time of emergence of a warming trend cannot be made with precision.

In some tropical regions, the warming trend has already emerged from local variability (FAQ 10.2, Figure 1). This happens more quickly in the tropics because there is less temperature variability there than in other parts of the globe. Projected warming may not emerge in middle latitudes until the mid-21st century—even though warming trends there are larger—because local temperature variability is substantially greater there than in the tropics. On a seasonal basis, local temperature variability tends to be smaller in summer than in winter. Warming therefore tends to emerge first in the warm part of the year, even in regions where the warming trend is larger in winter, such as in central Eurasia in FAQ 10.2, Figure 1.

Variables other than land surface temperature, including some oceanic regions, also show rates of long-term change different from natural variability. For example, Arctic sea ice extent is declining very rapidly, and already shows a human influence. On the other hand, local precipitation trends are very hard to detect because at most locations the variability in precipitation is quite large. The probability of record-setting warm summer temperatures has increased throughout much of the Northern Hemisphere . High temperatures presently considered extreme are projected to become closer to the norm over the coming decades. The probabilities of other extreme events, including some cold spells, have lessened.

In the present climate, individual extreme weather events cannot be unambiguously ascribed to climate change, since such events could have happened in an unchanged climate. However the probability of occurrence of such events could have changed significantly at a particular location. Human-induced increases in greenhouse gases are estimated to have contributed substantially to the probability of some heatwaves. Similarly, climate model studies suggest that increased greenhouse gases have contributed to the observed intensification of heavy precipitation events found over parts of the Northern Hemisphere. However, the probability of many other extreme weather events may not have changed substantially. Therefore, it is incorrect to ascribe every new weather record to climate change.

The date of future emergence of projected warming trends also depends on local climate variability, which can temporarily increase or decrease temperatures. Furthermore, the projected local temperature curves shown in FAQ 10.2, Figure 1 are based on multiple climate model simulations forced by the same assumed future emissions scenario. A different rate of atmospheric greenhouse gas accumulation would cause a different warming trend, so the spread of model warming projections (the coloured shading in FAQ 10.2, Figure 1) would be wider if the figure included a spread of greenhouse gas emissions scenarios. The increase required for summer temperature change to emerge from 20th century local variability (regardless of the rate of change) is depicted on the central map in FAQ 10.2, Figure 1.

A full answer to the question of when human influence on local climate will become obvious depends on the strength of evidence one considers sufficient to render something 'obvious'. The most convincing scientific evidence for the effect of climate change on local scales comes from analysing the global picture, and from the wealth of evidence from across the climate system linking many observed changes to human influence. *(continued on next page)*

*FAQ 10.2 (continued)*

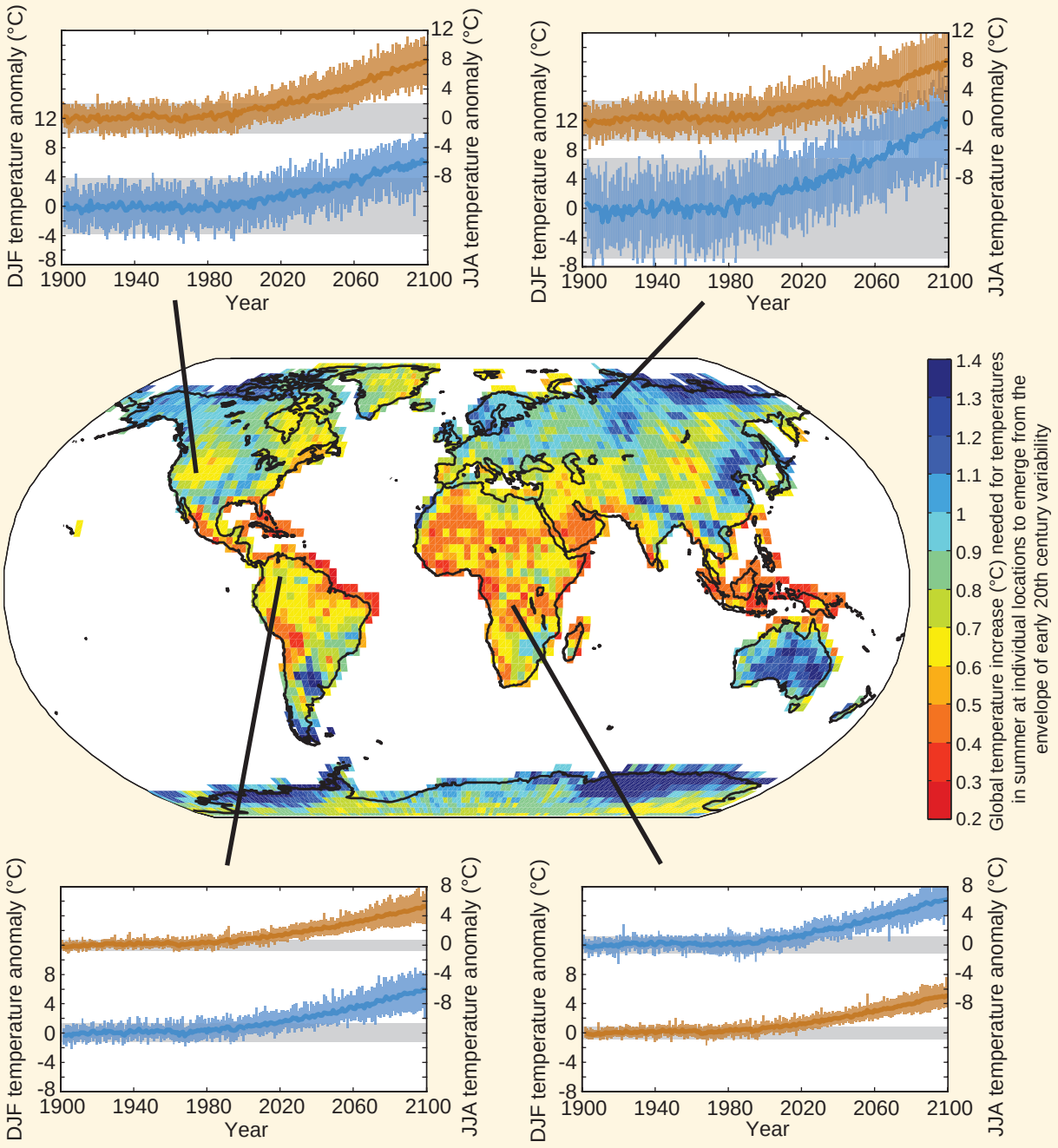


**FAQ 10.2, Figure 1 |** Time series of projected temperature change shown at four representative locations for summer (red curves, representing June, July and August at sites in the tropics and Northern Hemisphere or December, January and February in the Southern Hemisphere) and winter (blue curves). Each time series is surrounded by an envelope of projected changes (pink for the local warm season, blue for the local cold season) yielded by 24 different model simulations, emerging from a grey envelope of natural local variability simulated by the models using early 20th century conditions. The warming signal emerges first in the tropics during summer. The central map shows the global temperature increase (°C) needed for temperatures in summer at individual locations to emerge from the envelope of early 20th century variability. Note that warm colours denote the smallest needed temperature increase, hence earliest time of emergence. All calculations are based on Coupled Model Intercomparison Project Phase 5 (CMIP5) global climate model simulations forced by the Representative Concentration Pathway 8.5 (RCP8.5) emissions scenario. Envelopes of projected change and natural variability are defined as ±2 standard deviations. (Adapted and updated from Mahlstein et al., 2011.)

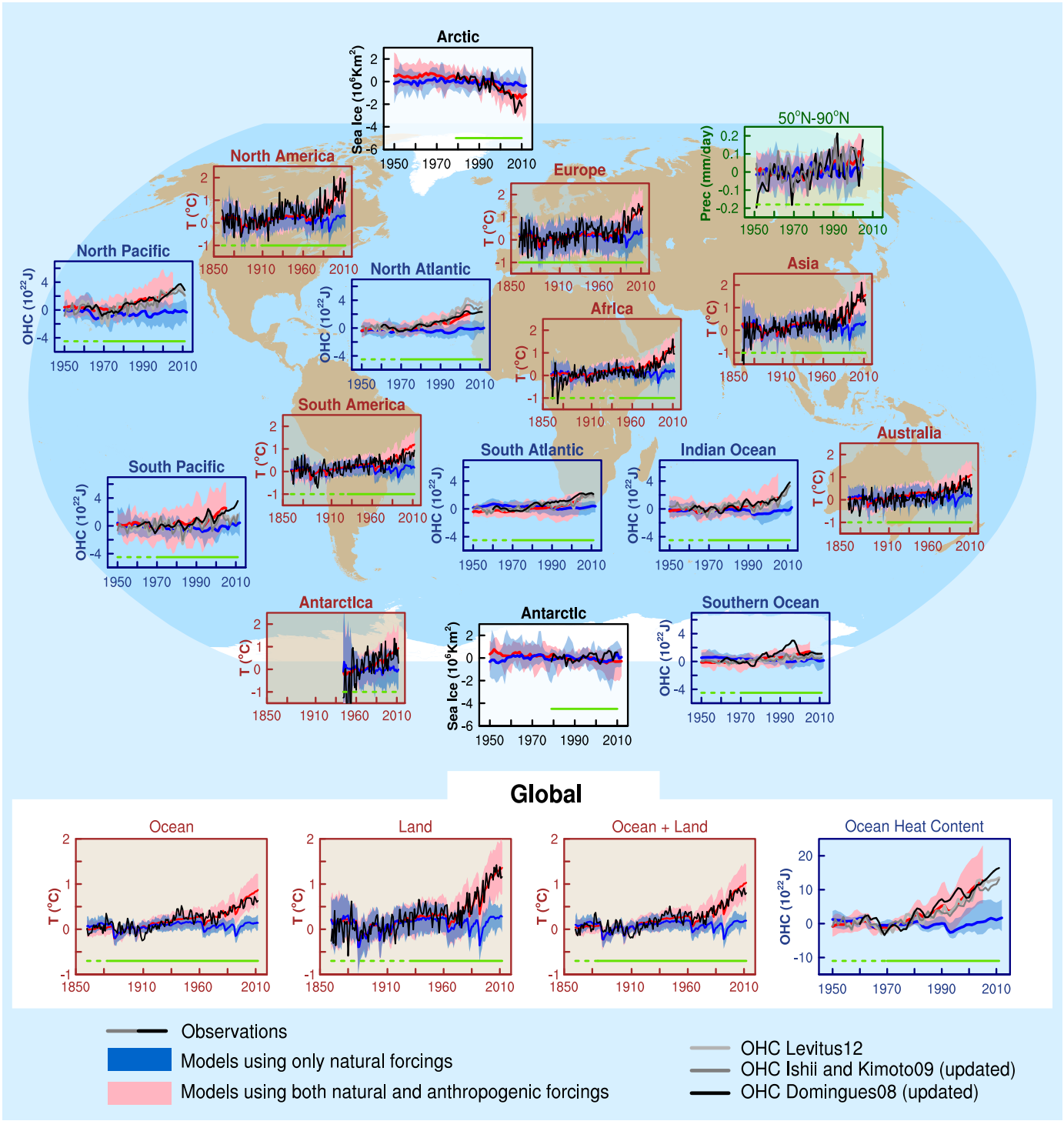


**Figure 10.21 |** Detection and attribution signals in some elements of the climate system, at regional scales (top panels) and global scales (bottom four panels). Brown panels are land surface temperature time series, green panels are precipitation time series, blue panels are ocean heat content time series and white panels are sea ice time series. Observations are shown on each panel in black or black and shades of grey. Blue shading is the model time series for natural forcing simulations and pink shading is the combined natural and anthropogenic forcings. The dark blue and dark red lines are the ensemble means from the model simulations. All panels show the 5 to 95% intervals of the natural forcing simulations, and the natural and anthropogenic forcing simulations. For surface temperature the results are from Jones et al. (2013 ) (and Figure 10.1). The observed surface temperature is from Hadley Centre/Climatic Research Unit gridded surface temperature data set 4 (HadCRUT4). Observed precipitation is from Zhang et al. (2007) (black line) and CRU TS 3.0 updated (grey line). Three observed records of ocean heat content (OHC) are shown. Sea ice anomalies (rather than absolute values) are plotted and based on models in Figure 10.16. The green horizontal lines indicate quality of the observations and estimates. For land and ocean surface temperatures panels and precipitation panels, solid green lines at bottom of panels indicate where data spatial coverage being examined is above 50% coverage and dashed green lines where coverage is below 50%. For example, data coverage of Antarctica never goes above 50% of the land area of the continent. For ocean heat content and sea ice panels the solid green line is where the coverage of data is good and higher in quality, and the dashed green line is where the data coverage is only adequate. More details of the sources of model simulations and observations are given in the Supplementary Material (10.SM.1).

canic eruptions) cause much of the observed response (see also Figures 10.5, 10.6, 10.9, 10.14a and 10.21). Both natural and anthropogenic forcings are required to understand fully the variability of the Earth system during the past 50 years.

Water in the free atmosphere is expected to increase, as a consequence of warming of the atmosphere (Section 10.6.1), and atmospheric circulation controls the global distribution of precipitation and evaporation. Simulations show that GHGs increase moisture in the atmosphere and change its transport in such a way as to produce patterns of precipitation and evaporation that are quite distinct from the observed patterns of warming. Our assessment shows that anthropogenic forcings have contributed to observed increases in moisture content in the atmosphere (result 16, *medium confidence*, Table 10.1), to global scale changes in precipitation patterns over land (result 14, *medium confidence*), to a global scale intensification of heavy precipitation in land regions where there observational coverage is sufficient to make an assessment (result 15, *medium confidence*), and to changes in surface and sub-surface ocean salinity (result 11, *very likely*). Combining evidence from both atmosphere and ocean that systematic changes in precipitation over land and ocean salinity can be attributed to human influence supports an assessment that it is *likely* that human influence has affected the global water cycle since 1960.

Warming of the atmosphere and the oceans affects the cryosphere, and in the case of snow and sea ice warming leads to positive feedbacks that amplify the warming response in the atmosphere and oceans. Retreat of mountain glaciers has been observed with an anthropogenic influence detected (result 17, *likely*, Table 10.1), Greenland ice sheet has melted at the edges and accumulating snow at the higher elevations is consistent with GHG warming supporting an assessment for an anthropogenic influence on the negative surface mass balance of Greenland's ice sheet (result 18, *likely*, Table 10.1). Our level of scientific understanding is too low to provide a quantifiable explanation of the observed mass loss of the Antarctic ice sheet (*low confidence*, result 19, Table 10.1). Sea ice in the Arctic is decreasing rapidly and the changes now exceed internal variability and with an anthropogenic contribution detected (result 20, *very likely*, Table 10.1). Antarctic sea ice extent has grown overall over the last 30 years but there is low scientific understanding of the spatial variability and changes in Antarctic sea ice extent (result 21, Table 10.1). There is evidence for an anthropogenic component to observed reductions in NH snow cover since the 1970s (*likely*, result 22, Table 10.1).

Anthropogenic forcing has also affected temperature on continental scales, with human influences having made a substantial contribution to warming in each of the inhabited continents (results 28, *likely*, Table 10.1), and having contributed to the very substantial Arctic warming over the past 50 years (result 29, *likely*, Table 10.1) while because of large observational uncertainties there is *low confidence* in attribution of warming averaged over available stations over Antarctica (result 30, Table 10.1). There is also evidence that anthropogenic forcings have contributed to temperature change in many sub-continental regions (result 32, *likely*, Table 10.1) and that anthropogenic forcings have contributed to the observed changes in the frequency and intensity of daily temperature extremes on the global scale since the mid-20th century (result 8, *very likely*, Table 10.1). Furthermore there is evidence that human influence has substantially increased the probability of occurrence of heat waves in some locations (result 33, *likely*, Table 10.1).

An analysis of these results (from Table 10.1) shows that there is *high confidence* in attributing many aspects of changes in the climate system to human influence including from atmospheric measurements of temperature. Synthesizing the results in Table 10.1 shows that the combined evidence from across the climate system increases the level of confidence in the attribution of observed climate change to human influence and reduces the uncertainties associated with assessments based on a single variable. From this combined evidence, it is *virtually certain* that human influence has warmed the global climate system.

## Acknowledgements

We acknowledge the major contributions of the following scientists who took a substantial part in the production of key figures: Beena Balan Sarojini, Oliver Browne, Jara Imbers Quintana, Gareth Jones, Fraser Lott, Irina Mahlstein, Alexander Otto, Debbie Polson, Andrew Schurer, Lijun Tao, and Muyin Wang. We also acknowledge the contributions of Viviane Vasconcellos de Menezes for her work on the production of figures and for her meticulous management of the bibliography database used for this chapter.

**Table 10.1 |** Synthesis of detection and attribution results across the climate system from this chapter. Note that we follow the guidance note for lead authors of the IPCC AR5 on consistent treatment of uncertainties (Mastrandrea et al., 2011). Where the confidence is *medium* or less there is no assessment given of the quantified likelihood measure, and the table cell is marked not applicable (N/A).

| Result | (1) Statement about variable or property: time, season | (2) Confidence (*Very high*, *High*, *medium* or *low*, *very low*) | (3) Quantified measure of uncertainty where the probability of the outcome can be quantified (Likelihood given generally only if high or very high confidence) | (4) Data sources Observational evidence (Chapters 2 to 5); Models (Chapter 9) | (5) Type, amount, quality, consistency of evidence from attribution studies and degree of agreement of studies. | (6) Factors contributing to the assessments including physical understanding, observational and modelling uncertainty, and caveats. |
|---|---|---|---|---|---|---|
| ***Global Scale Atmospheric Temperature Changes*** | | | | | | |
| **1** | More than half of the observed increase in global mean surface temperatures from 1951 to 2010 is due to the observed anthropogenic increase in greenhouse gas (GHG) concentrations. | *High* | *Very likely* | Four global surface temperature series (HadCRUT3, HadCRUT4, MLOST, GISTEMP). CMIP3 and CMIP5 models. | · Many formal attribution studies, including optimal fingerprint time-space studies and time series based studies.<br>· Robust evidence. Attribution of more than half of warming since 1950 to GHGs seen in multiple independent analyses using different observational data sets and climate models.<br>· High agreement. Studies agree in robust detection of GHG contribution to observed warming that is larger than any other factor including internal variability. | The observed warming is well understood in terms of contributions of anthropogenic forcings such as greenhouse gases (GHGs) and tropospheric aerosols and natural forcings from volcanic eruptions. Solar forcing is the only other forcing that could explain long-term warming but pattern of warming is not consistent with observed pattern of change in time, vertical change and estimated to be small. AMO could be confounding influence but studies that find significant role for AMO show this does not project strongly onto 60-year trends. (Section 10.3.1.1, Figures 10.4 and 10.5) |
| **2** | More than half of the observed increase in global mean surface temperatures from 1951 to 2010 is due to human influence on climate. | *High* | *Extremely likely* | Mutliple CMIP5 models and multiple methodologies. | · Formal attribution studies including different optimal detection methodologies and time series based studies.<br>· Robust evidence of well-constrained estimates of net anthropogenic warming estimated in optimal detection studies.<br>· High agreement. Both optimal detection and time series studies agree in robust detection of anthropogenic influence that is substantially more than half of the observed warming. | The observed warming is well understood in terms of contributions of anthropogenic and natural forcings. Solar forcing and AMO could be confounding influence but are estimated to be smaller than the net effects of human influence. (Section 10.3.1.1, Figures 10.4, 10.5, 10.6) |
| **3** | Early 20th century warming is due in part to external forcing. | *High* | *Very likely* | Instrumental global surface temperature series and reconstructions of the last millenium. CMIP3 and CMIP5 models. | · Formal detection and attribution studies looking at early century warming and studies for the last few hundred years.<br>· High agreement across a number of studies in detecting external forcings when including early 20th century period although they vary in contributions from different forcings. | Modelling studies show contribution from external forcings to early century warming. Residual differences between models and observations indicate role for circulation changes as contributor. (Section 10.3.1.1, Figures 10.1, 10.2, 10.6) |
| **4** | Warming since 1950 cannot be explained without external forcing. | *High* | *Virtually certain* | Estimates of internal variability from CMIP3 and CMIP5 models, observation based time series and space pattern analyses, and estimating residuals of the non-forced component from paleo data. | · Many, including optimal fingerprint time-space studies, observation based time series and space pattern analyses and paleo data studies.<br>· Robust evidence and high agreement.<br>· Detection of anthropogenic fingerprint robustly seen in independent analyses using different observational data sets, climate models, and methodological approaches. | Based on all evidence above combined. Observed warming since 1950 is very large compared to climate model estimates of internal variability, which are assessed to be adequate at global scale. The Northern Hemisphere (NH) mean warming since 1950 is far outside the range of any similar length trend in residuals from reconstructions of NH mean temperature of the past millennium. The spatial pattern of observed warming differs from those associated with internal variability. (Sections 9.5.3.1, 10.3.1.1, 10.7.1) |

*(continued on next page)*

*Table 10.1 (continued)*

| Result | (1) Statement about variable or property: time, season | (2) Confidence (*Very high*, *High*, *medium* or *low*, *very low*) | (3) Quantified measure of uncertainty where the probability of the outcome can be quantified (Likelihood given generally only if high or very high confidence) | (4) Data sources Observational evidence (Chapters 2 to 5); Models (Chapter 9) | (5) Type, amount, quality, consistency of evidence from attribution studies and degree of agreement of studies. | (6) Factors contributing to the assessments including physical understanding, observational and modelling uncertainty, and caveats. |
|---|---|---|---|---|---|---|
| **5** | Anthropogenic forcing has led to a detectable warming of troposphere temperatures since 1961. | *High* | *Likely* | Multiple radiosonde data sets from 1958 and satellite data sets from 1979 to present. CMIP3 and CMIP5 models. | · Formal attribution studies with CMIP3 models (assessed in AR4) and CMIP5 models.<br>· Robust detection and attribution of anthropogenic influence on tropospheric warming with large signal-to-noise (S/N) ratios estimated.<br>· Studies agree in detecting an anthropogenic influence on tropospheric warming trends. | Observational uncertainties in radiosondes are now much better documented than at time of AR4. It is virtually certain that the troposphere has warmed since the mid-20th century but there is only *medium confidence* in the rate and vertical structure of those changes in the NH extratropical troposphere and *low confidence* elsewhere. Most, though not all, CMIP3 and CMIP5 models overestimate the observed warming trend in the tropical troposphere during the satellite period although observational uncertainties are large and outside the tropics and over the period of the radiosonde record beginning in 1961 there is better agreement between simulated and observed trends. (Sections 2.4.4, 9.4.1.4.2, 10.3.1.2, Figure 10.8) |
| **6** | Anthropogenic forcing dominated by the depletion of the ozone layer due to ozone depleting substances, has led to a detectable cooling of lower stratosphere temperatures since 1979. | *High* | *Very Likely* | Radiosonde data from 1958 and satellite data from 1979 to present. CCMVal, CMIP3 and CMIP5 simulations. | · A formal optimal detection attribution study using stratosphere resolving chemistry climate models and a detection study analysing the S/N ratio of the data record together with many separate modelling studies and observational studies.<br>· Physical reasoning and model studies show very consistent understanding of observed evolution of stratospheric temperatures, consistent with formal detection and attribution results.<br>· Studies agree in showing very strong cooling in stratosphere that can be explained only by anthropogenic forcings dominated by ozone depleting substances. | New generation of stratosphere resolving models appear to have adequate representation of lower stratospheric variability. Structure of stratospheric temperature trends and variations is reasonably well represented by models. CMIP5 models all include changes in stratospheric ozone while only about half of the models participating in CMIP3 include stratospheric ozone changes. (Sections 9.4.1.4.5, 10.3.1.2.2, Figures10.8 and 10.9) |
| **7** | Anthropogenic forcing, particularly GHGs and stratospheric ozone depletion has led to a detectable observed pattern of tropospheric warming and lower stratospheric cooling since 1961. | *High* | *Very likely* | Radiosonde data from 1958 and satellite data from 1979 to present. | · Attribution studies using CMIP3 and CMIP5 models.<br>· Physical reasoning and modelling supports robust expectation of fingerprint of anthropogenic influence of tropospheric warming and lower stratospheric cooling which is robustly detected in multiple observational records.<br>· Fingerprint of anthropogenic influence is detected in different measures of free atmosphere temperature changes including tropospheric warming, and a very clear identification of stratospheric cooling in models that include anthropogenic forcings. | Fingerprint of changes expected from physical understanding and as simulated by models is detected in observations. Understanding of stratospheric changes has improved since AR4. Understanding of observational uncertainty has improved although uncertainties remain particularly in the tropical upper troposphere. (Sections 2.4.4, 10.3.1.2.3, Figures 10.8, 10.9) |

*(continued on next page)*

*Table 10.1 (continued)*

| Result | (1) Statement about variable or property: time, season | (2) Confidence (*Very high*, *High*, *medium* or *low*, *very low*) | (3) Quantified measure of uncertainty where the probability of the outcome can be quantified (Likelihood given generally only if high or very high confidence) | (4) Data sources Observational evidence (Chapters 2 to 5); Models (Chapter 9) | (5) Type, amount, quality, consistency of evidence from attribution studies and degree of agreement of studies. | (6) Factors contributing to the assessments including physical understanding, observational and modelling uncertainty, and caveats. |
|---|---|---|---|---|---|---|
| **8** | Anthropogenic forcing has contributed to the observed changes in the frequency and intensity of daily temperatures extremes on the global scale since the mid-20th century. | *High* | *Very Likely* | Indices for frequency and intensity of extreme temperatures including annual maximum and annual minimum daily temperatures, over land areas of the World except parts of Africa, South America and Antarctica. CMIP3 and CMIP5 simulations, 1950–2005. | · Several studies including fingerprint time–space studies.<br>· Detection of anthropogenic influence robustly seen in independent analysis using different statistical methods and different indices. | Expected from physical principles that changes in mean temperature should bring changes in extremes, confirmed by detection and attribution studies. New evidence since AR4 for detection of human influence on extremely warm daytime maximum temperatures and new evidence that influence of anthropogenic forcing can be separately detected from natural forcing. More limited observational data and greater observational uncertainties than for mean temperatures. (Section 10.6.1.1, Figure 10.17) |
| *Oceans* | | | | | | |
| **9** | Anthropogenic forcings have made a substantial contribution to upper ocean warming (above 700 m) observed since the 1970s.<br><br>This anthropogenic ocean warming has contributed to global sea level rise over this period through thermal expansion. | *High* | *Very likely* | Several observational data sets since the 1970s. CMIP3 and CMIP5 models. | · Several new attribution studies detect role of anthropogenic forcing on observed increase in ocean's global heat content with volcanic forcing also contributing to observed variability.<br>· The evidence is very robust, and tested against known structural deficiencies in the observations, and in the models.<br>· High levels of agreement across attribution studies and observation and model comparison studies. The strong physical relationship between thermosteric sea level and ocean heat content means that the anthropogenic ocean warming has contributed to global sea level rise over this period through thermal expansion. | New understanding of the structural errors in the temperature data sets has led to their correction which means that the unexplained multi-decadal scale variability reported in AR4 has largely been resolved as being spurious. The observations and climate simulations have similar trends (including anthropogenic and volcanic forcings) and similar decadal variability. The detection is well above S/N levels required at 1 and 5% significance levels. The new results show the conclusions to be very robust to structural uncertainties in observational data sets and transient climate simulations. (Sections 3.2.5, 10.4.1, 10.4.3, 13.3.6, Figure 10.14) |
| **10** | Anthropogenic forcing has contributed to sea level rise through melting glaciers and Greenland ice sheet. | *High* | Likely | Observational evidence of melting glaciers (Section 4.3) and ice sheets (Section 4.4). Global mean sea level budget closure to within uncertainties. (Section13.3.6) | · Several new mass balance studies quantifying glacier and ice sheet melt rates (Section 10.5.2) and their contributions to sea level rise. (Section 13.3) | Strong observational evidence of contribution from melting glaciers and *high confidence* in attribution of glacier melt to human influence. Increasing rates of ice sheet contributions albeit from short observational record (especially of Antarctic mass loss). Current climate models do not represent glacier and ice sheet processes. Natural variability of glaciers and ice sheets not fully understood. (Sections 10.4.3, 10.5.2) |

*(continued on next page)*

*Table 10.1 (continued)*

| Result | (1) Statement about variable or property: time, season | (2) Confidence (*Very high*, *High*, *medium* or *low*, *very low*) | (3) Quantified measure of uncertainty where the probability of the outcome can be quantified (Likelihood given generally only if high or very high confidence) | (4) Data sources Observational evidence (Chapters 2 to 5); Models (Chapter 9) | (5) Type, amount, quality, consistency of evidence from attribution studies and degree of agreement of studies. | (6) Factors contributing to the assessments including physical understanding, observational and modelling uncertainty, and caveats. |
|---|---|---|---|---|---|---|
| **11** | The observed ocean surface and sub-surface salinity changes since the 1960s are due, in part, to anthropogenic forcing. | *High* | *Very likely* | Oceans chapter (Section 3.3) and attribution studies in Section 10.4.2. | · Robust observational evidence for amplification of climatological patterns of surface salinity.<br>· CMIP3 simulations show patterns of salinity change consistent with observations, but there are only a few formal attributions studies that include a full characterization of internal variability.<br>· Physical understanding of expected patterns of change in salinity due to changes in water cycle support results from detection and attriution studies. | More than 40 studies of regional, global surface and subsurface salinity observations show patterns of change consistent with acceleration of hydrological water cycle. Climate models that include anthropgenic forcings show the same consistent pattern of surface salinity change. (Sections 3.3.5, 10.4.2, Figure 10.15) |
| **12** | Observed increase in surface ocean acidification since 1980s is a resulted of rising atmospheric $CO_2$ | *Very high* | *Very likely* | Evidence from Section 3.8.2 and Box 3.2, Figure 3.18. | · Based on ocean chemistry, expert judgement, and many analyses of time series and other indirect measurements<br>· Robust evidence from time series measurements. Measurements have a high degree of certainty (see Table 3.2) and instrumental records show increase in ocean acidity.<br>· High agreement of the observed trends. | *Very high confidence*, based on the number of studies, the updates to earlier results in AR4, and the very well established physical understanding of gas exchange between atmosphere and surface ocean, and the sources of excess carbon dioxide in the atmosphere. Alternative processes and hypotheses can be excluded. (Section 3.8.2, Box 3.2, Section 10.4.4) |
| **13** | Observed pattern of decrease in oxygen content is, in part, attributable to anthropogenic forcing."<br>To correctly read: Observed pattern of decrease in oxygen content from the 1960s to the 1990s is, in part, attributable to anthropogenic forcing. | *Medium* | *About as likely as not* | Evidence from Section 3.8.3 and attribution studies in Section 10.4.4. | · Qualitative expert judgement based on comparison of observed and expected changes in response to increasing $CO_2$.<br>· Medium evidence. One specific global ocean study, many studies of hydrographic sections and repeat station data, high agreement across observational studies.<br>· Medium agreement. One attribution study, and only limited regional and large-scale modelling and observation comparisons. | Physical understanding of ocean circulation and ventilation, and from the global carbon cycle, and from simulations of ocean oxygen concentrations from coupled bio-geochemical models with OAGCMs. Main uncertainty is observed decadal variability which is not well understood in global and regional inventories of dissolved oxygen in the oceans. (Section 10.4.4) |
| ***Water Cycle*** | | | | | | |
| **14** | Global scale precipitation patterns over land have changed due to anthropogenic forcings including increases in NH mid to high latitudes. | *Medium* | N/A | Multiple observational data sets based on rain gauges over land, with coverage dominated by the NH. CMIP3 and CMIP5 models. | · Several land precipitation studies examining annual and seasonal precipitation.<br>· Evidence for consistency between observed and modelled changes in global precipitation patterns over land regions with sufficient observations.<br>· Medium degree of agreement of studies. Expected anthropogenic fingerprints of changes in zonal mean precipitation found in annual and some seasonal data with some sensitivity of attribution results to observational data set used. | Increases of precipitation at high latitudes of the NH are a robust feature of climate model simulations and are expected from process understanding. Global-land average long-term changes small at present time, whereas decadal variability over some land areas is large. Observations are very uncertain and poor coverage of precipitation expected to make fingerprint of changes much more indistinct. (Sections 2.5.1, 10.3.2.2, Figures 10.10 and 10.11) |

*(continued on next page)*

*Table 10.1 (continued)*

| Result | (1) Statement about variable or property: time, season | (2) Confidence (*Very high*, *High*, *medium* or *low*, *very low*) | (3) Quantified measure of uncertainty where the probability of the outcome can be quantified (Likelihood given generally only if high or very high confidence) | (4) Data sources Observational evidence (Chapters 2 to 5); Models (Chapter 9) | (5) Type, amount, quality, consistency of evidence from attribution studies and degree of agreement of studies. | (6) Factors contributing to the assessments including physical understanding, observational and modelling uncertainty, and caveats. |
|---|---|---|---|---|---|---|
| **15** | In land regions where observational coverage is sufficient for assessment, anthropogenic forcing has contributed to global-scale intensification of heavy precipitation over the second half of the 20th century. | *Medium* | N/A | Wettest 1-day and 5-day precipitation in a year obtained from rain guage observations, CMIP3 simulations. | · Only one detection and attribution study restricted to NH land where observations were available.<br>· Study found stronger detectability for models with natural forcings but not able to differentiate anthropogenic from natural forcings.<br>· Although only one formal detection and attribution study, observations of a general increase in heavy precipitation at the global scale agree with physical expectations. | Evidence for anthropogenic influence on various aspects of the hydrological cycle that implies extreme precipitation would be expected to increase. There are large observational uncertainties and poor global coverage which makes assessment difficult. (Section 10.6.1.2, Figure 10.11) |
| **16** | Anthropogenic contribution to atmospheric specific humidity since 1973. | *Medium* | N/A | Observations of atmospheric moisture content over ocean from satellite; observations of surface humidity from weather stations and radiosondes over land. | · Detection and attribution studies of both surface humidity from weather stations over land and atmospheric moisture content over oceans from satellites.<br>· Detection of anthropogenic influence on atmospheric moisture content over oceans robust to choice of models.<br>· Studies looking at different variables agree in detecting specific humidity changes. | Recent reductions in relative humidity over land and levelling off of specific humidity not fully understood. Length and quality of observational data sets limit detection and attribution and assimilated analyses not judged sufficiently reliable for detection and attribution. (Section 10.3.2.1) |
| ***Hemispheric Scale Changes; Basin Scale Changes*** | | | | | | |
| ***Cryosphere*** | | | | | | |
| **17** | A substantial part of glaciers mass loss since the 1960's is due to human influence. | *High* | *Likely* | Robust agreement from long-term glacier records. (Section 4.3.3) | · Several new recent studies since last assessment.<br>· High agreement across a limited number of studies. | Well established records of glacier length, and better methods of estimating glacier volumes and mass loss. Better characterization of internal variability, and better understanding of the response to natural variability, and local land cover change. (Sections 4.3.3, 10.5.2) |
| **18** | Anthropogenic forcing has contributed to surface melting of the Greenland ice sheet since 1993. | *High* | *Likely* | Robust agreement across *in situ* and satellite derived estimates of surface mass balance (Section 4.4). Nested or downscaled model simulations show pattern of change consistent with warming. | · Several new studies since last assessment.<br>· Robust evidence from different sources.<br>· High agreement across a limited number of studies. | Documented evidence of surface mass loss. Uncertainty caused by poor characterization of the internal variability of the surface mass balance (strong dependence on atmospheric variability) that is not well represented in CMIP5 models. (Section 4.4.2, 10.5.2.1) |
| **19** | Antarctic ice sheet mass balance loss has a contribution from anthropogenic forcing. | *Low* | N/A | Observational evidence for Antarctic mass sheet loss is well established across a broad range of studies. (Section 4.4) | · No formal studies exist. Processes for mass loss for Antarctica are not well understood. Regional warming and changed wind patterns (increased westerlies, increase in the Southern Annular Mode (SAM)) could contribute to enhanced melt of Antarctica. High agreement in observational studies. | *Low confidence* assessment based on low scientific understanding. (Sections 4.4.2, 13.4, 10.5.2) |
| **20** | Anthropogenic forcing has contributed to the Arctic sea ice loss since 1979. | *High* | *Very likely* | Robust agreement across all observations. (Section 4.2) | · Multiple detection and attribution studies, large number of model simulations and data comparisons for instrumental record.<br>· Robust set of studies of simulations of sea ice and observed sea ice extent.<br>· High agreement between studies of sea ice simulations and observed sea ice extent. | *High confidence* based on documented observations of ice extent loss, and also good evidence for a significant reduction in sea ice volume. The physics of Arctic sea ice is well understood and consistent with the observed warming in the region, and from simulations of Arctic sea ice extent with anthropogenic forcing. (Sections 9.4.3, 10.5.1) |

*(continued on next page)*

*Table 10.1 (continued)*

| Result | (1) Statement about variable or property: time, season | (2) Confidence (*Very high*, *High*, *medium* or *low*, *very low*) | (3) Quantified measure of uncertainty where the probability of the outcome can be quantified (Likelihood given generally only if high or very high confidence) | (4) Data sources Observational evidence (Chapters 2 to 5); Models (Chapter 9) | (5) Type, amount, quality, consistency of evidence from attribution studies and degree of agreement of studies. | (6) Factors contributing to the assessments including physical understanding, observational and modelling uncertainty, and caveats. |
|---|---|---|---|---|---|---|
| **21** | Incomplete scientific explanations of the observed increase in Antarctic sea ice extent precludes attribution at this time. | N/A | N/A | The increase in sea ice extent in observations is robust, based on satellite measurements and ship-based measurements. (Section 4.5.2) | · No formal attribution studies.<br>· Estimates of internal variability from CMIP5 simulations exceed observed sea ice variability.<br>· Modelling studies have a low level of agreement for observed increase, and there are competing scientific explanations. | *Low confidence* based on low scientific understanding of the spatial variability and changes in the Antarctic sea ice. (Sections 4.5.2, 10.5.1, 9.4.3) |
| **22** | There is an anthropogenic component to observed reductions in NH snow cover since 1970 | *High* | *Likely* | Observations show decrease in NH snow cover. | · Two snow cover attribution studies.<br>· Decrease in snow cover in the observations are consistent among many studies. (Section 4.5.2, 4.5.3)<br>· Reductions in observed snow cover inconsistent with internal variability and can be explained only by climate models that include anthropogenic forcings. | Expert judgement and attribution studies support the human influence on reduction in snow cover extent. (Sections 4.5.2, 4.5.3, 10.5.3) |
| ***Atmospheric Circulation and Patterns of Variability*** | | | | | | |
| **23** | Human influence has altered sea level pressure patterns globally since 1951. | *High* | *Likely* | An observational gridded data set and reanalyses. Multiple climate models. | · A number of studies find detectable anthropogenic influence on sea level pressure patterns.<br>· Detection of anthropogenic influence is found to be robust to currently sampled modelling and observational uncertainty. | Detectable anthropogenic influence on changes in sea level pressure patterns is found in several attribution studies that sample observational and modelling uncertainty. Observational uncertainties not fully sampled as results based largely on variants of one gridded data set although analyses based on reanalyses also support the finding of a detectable anthropogenic influence. (Section 10.3.3.4) |
| **24** | The positive trend in the SAM seen in austral summer since 1951 is due in part to stratospheric ozone depletion. | *High* | *Likely* | Measurements since 1957. Clear signal of SAM trend in December, January and February (DJF) is robust to observational uncertainty. | · Many studies comparing consistency of observed and modelled trends, and consistency of observed trend with simulated internal variability.<br>· Observed trends are consistent with CMIP3 and CMIP5 simulations that include stratospheric ozone depletion.<br>· Several studies show that the observed increase in the DJF SAM is inconsistent with simulated internal variability. High agreement of modelling studies that ozone depletion drives an increase in the DJF SAM index. There is *medium confidence* that GHGs have also played a role. | Consistent result of modelling studies is that the main aspect of the anthropogenically forced response on the DJF SAM is the impact of ozone depletion. The observational record is relatively short, observational uncertainties remain, and the DJF SAM trend since 1951 is only marginally inconsistent with internal variability in some data sets. (Section 10.3.3.3, Figure 10.13) |
| **25** | Stratospheric ozone depletion has contributed to the observed poleward shift of the Southern Hadley cell during austral summer. | *Medium* | N/A | Multiple observational lines of evidence for widening but large spread in the magnitude. Reanalysis suggest a southward shift of southern Hadley cell border during DJF which is also seen in CMIP3 and CMIP5 models. | · Consistent evidence for effects of stratospheric ozone depletion.<br>· Evidence from modelling studies is robust that stratospheric ozone drives a poleward shift of the southern Hadley Cell border during austral summer. The magnitude of the shift is very uncertain and appears to be underestimated by models. There is *medium confidence* that GHGs have also played a role. | The observed magnitude of the tropical belt widening is uncertain. The contribution of internal climate variability to the observed poleward expansion of the Hadley circulation remains very uncertain. (Section 10.3.3.1, Figure 10.12) |

*(continued on next page)*

*Table 10.1 (continued)*

| Result | (1) Statement about variable or property: time, season | (2) Confidence (*Very high*, *High*, *medium* or *low*, *very low*) | (3) Quantified measure of uncertainty where the probability of the outcome can be quantified (Likelihood given generally only if high or very high confidence) | (4) Data sources Observational evidence (Chapters 2 to 5); Models (Chapter 9) | (5) Type, amount, quality, consistency of evidence from attribution studies and degree of agreement of studies. | (6) Factors contributing to the assessments including physical understanding, observational and modelling uncertainty, and caveats. |
|---|---|---|---|---|---|---|
| **26** | Attribution of changes in tropical cyclone activity to human influence. | *Low* | N/A | Incomplete and short observational records in most basins. | · Formal attribution studies on SSTs in tropics. However, mechanisms linking anthropogenically induced SST increases to changes in tropical cyclone activity poorly understood.<br>· Attribution assessments depend on multi-step attribution linking anthropogenic influence to large-scale drivers and thence to tropical cyclone activity.<br>· Low agreement between studies, medium evidence. | Insufficient observational evidence of multi-decadal scale variability. Physical understanding lacking. There remains substantial disagreement on the relative importance of internal variability, GHG forcing, and aerosols. (Sections 10.6.1.5, 14.6.1) |
| ***Millennium Time Scale*** | | | | | | |
| **27** | External forcing contributed to NH temperature variability from 1400 to 1850, and from 850 to 1400. | *High* for period from 1400 to 1850; *medium* for period from 850 to 1400. | *Very likely* for period from 1400 to 1850. | See Chapter 5 for reconstructions; simulations from PMIP3 and CMIP5 models, with more robust detection results for 1400 onwards. | · A small number of detection and attribution studies and further evidence from climate modelling studies; comparison of models with reconstructions and results from data assimilation.<br>· Robust agreement from a number of studies using a range of reconstructions and models (EBMs to ESMs) that models are able to reproduce key features of last seven centuries.<br>· Detection results and simulations indicate a contribution by external drivers to the warm conditions in the 11th to 12th century, but cannot explain the warmth around the 10th century in some reconstructions. | Large uncertainty in reconstructions particularly for the first half of the millennium but good agreement between reconstructed and simulated large scale features from 1400. Detection of forced influence robust for a large range of reconstructions. Difficult to separate role of individual forcings. Results prior to 1400 much more uncertain, partly due to larger data and forcing uncertainty. (Sections 10.7.1, 10.7.2, 10.7.3) |
| ***Continental to Regional Scale Changes*** | | | | | | |
| **28** | Anthropogenic forcing has made a substantial contribution to warming to each of the inhabited continents. | *High* | *Likely* | Robust observational evidence except for Africa due to poor sampling. Detection and attribution studies with CMIP3 and CMIP5 models. | · New studies since AR4 detect anthropogenic warming on continental and sub-continental scales.<br>· Robust detection of human influence on continental scales agrees with global attribution of widespread warming over land to human influence.<br>· Studies agree in detecting human influence on continental scales. | Anthropogenic pattern of warming widespread across all inhabited continents. Lower S/N ratios at continental scales than global scales. Separation of response to forcings more difficult at these scales. Models have greater errors in representation of regional details. (Section 10.3.1.1,4, Box 11.2) |
| **29** | Anthropogenic contribution to very substantial Arctic warming over the past 50 years. | *High* | *Likely* | Adequate observational coverage since 1950s. Detection and attribution analysis with CMIP3 models. | · Multiple models show amplification of Arctic temperatures from anthropogenic forcing.<br>· Large positive Arctic-wide temperature anomalies in observations over last decade and models are consistent only when they include external forcing. | Large temperature signal relative to mid-latitudes but also larger internal variability and poorer observational coverage than at lower latitudes. Known multiple processes including albedo shifts and added heat storage contribute to faster warming than at lower latitudes. (Sections 10.3.1.1.4. 10.5.1.1) |

*(continued on next page)*

*Table 10.1 (continued)*

| Result | (1) Statement about variable or property: time, season | (2) Confidence (*Very high*, *High*, *medium* or *low*, *very low*) | (3) Quantified measure of uncertainty where the probability of the outcome can be quantified (Likelihood given generally only if high or very high confidence) | (4) Data sources Observational evidence (Chapters 2 to 5); Models (Chapter 9) | (5) Type, amount, quality, consistency of evidence from attribution studies and degree of agreement of studies. | (6) Factors contributing to the assessments including physical understanding, observational and modelling uncertainty, and caveats. |
|---|---|---|---|---|---|---|
| **30** | Human contribution to observed warming averaged over available stations over Antarctica. | *Low* | N/A | Poor observational coverage of Antarctica with most observations around the coast. Detection and attribution studies with CMIP3 and CMIP5 models. | · One optimal detection study, and some modelling studies.<br>· Clear detection in one optimal detection study. | Possible contribution to changes from SAM increase. Residual when SAM induced changes are removed shows warming consistent with expectation due to anthropogenic forcing. High observational uncertainty and sparse data coverage (individual stations only mostly around the coast). (Sections 10.3.1.1.4, 2.4.1.1) |
| **31** | Contribution by forcing to reconstructed European temperature variability over last five centuries. | *Medium* | N/A | European seasonal temperatures from 1500 onwards. | · One detection and attribution study and several modelling studies.<br>· Clear detection of external forcings in one study; robust volcanic signal seen in several studies (see also Chapter 5). | Robust volcanic response detected in Epoch analyses in several studies. Models reproduce low-frequency evolution when include external forcings. Uncertainty in overall level of variability, uncertainty in reconstruction particularly prior to late 17th century. (Sections 10.7.2, 5.5.1) |
| **32** | Anthropogenic forcing has contributed to temperature change in many sub-continental regions of the world. | *High* | *Likely* | Good observational coverage for many regions (e.g., Europe) and poor for others (e.g., Africa, Arctic). Detection and attribution studies with CMIP3 and CMIP5 models. | · A number of detection and attribution studies have analysed temperatures on scales from Giorgi regions to climate model grid box scale.<br>· Many studies agree in showing that an anthropogenic signal is apparent in many sub-continental scale regions. In some sub-continental-scale regions circulation changes may have played a bigger role. | Larger role of internal variability at smaller scales relative to signal of climate change. In some regions observational coverage is poor. Local forcings and feedbacks as well as circulation changes are important in many regions and may not be well simulated in all regions. (Section 10.3.1.1.4, Box 11.2) |
| **33** | Human influence has substantially increased the probability of occurrence of heat waves in some locations. | *High* | *Likely* | Good observational coverage for some regions and poor for others (thus biasing studies to regions where observational coverage is good). Coupled modeling studies examining the effects of anthropogonic warming and the probability of occurrence of very warm seasonal temperatures and targeted experiments with models forced with prescribed sea surface temperatures. | · Multi-step attribution studies of some events including the Europe 2003, Western Russia 2010, and Texas 2011 heatwaves have shown an anthropogenic contribution to their occurrence probability, backed up by studies looking at the overall implications of increasing mean temperatures for the probability of exceeding seasonal mean temperature thresholds in some regions.<br>· To infer the probability of a heatwave, extrapolation has to be made from the scales on which most attribution studies have been carried out to the spatial and temporal scales of heatwaves.<br>· Studies agree in finding robust evidence for anthropogenic influence on increase in probability of occurrence of extreme seasonal mean temperatures in many regions. | In some instances, circulation changes could be more important than thermodynamic changes. This could be a possible confounding influence since much of the magnitude (as opposed to the probability of occurrence) of many heat waves is attributable to atmospheric flow anomalies. (Sections 10.6.1, 10.6.2) |

## References


AchutaRao, K. M., B. D. Santer, P. J. Gleckler, K. E. Taylor, D. W. Pierce, T. P. Barnett, and T. M. L. Wigley, 2006: Variability of ocean heat uptake: Reconciling observations and models. *J. Geophys. Res. Oceans*, **111**, C05019.

AchutaRao, K. M., et al., 2007: Simulated and observed variability in ocean temperature and heat content. *Proc. Natl. Acad. Sci. U.S.A.*, **104**, 10768–10773.

Ahlmann, H. W., 1948: The present climatic fluctuation. *Geogr.J.*, **112**, 165–195.

Aldrin, M., M. Holden, P. Guttorp, R. B. Skeie, G. Myhre, and T. K. Berntsen, 2012: Bayesian estimation of climate sensitivity based on a simple climate model fitted to observations of hemispheric temperatures and global ocean heat content. *Environmetrics*, **23**, 253–271.

Alekseev, G. V., A. I. Danilov, V. M. Kattsov, S. I. Kuz'mina, and N. E. Ivanov, 2009: Changes in the climate and sea ice of the Northern Hemisphere in the 20th and 21st centuries from data of observations and modeling. *Izvestiya Atmospheric and Oceanic Physics*, **45**, 675–686.

Alexander, L. V., and J. M. Arblaster, 2009: Assessing trends in observed and modelled climate extremes over Australia in relation to future projections. *Int. J. Climatol.*, **29**, 417–435.

Allan, R., and T. Ansell, 2006: A new globally complete monthly historical gridded mean sea level pressure dataset (HadSLP2): 1850–2004. *J. Clim.*, **19**, 5816–5842.

Allan, R. P., B. J. Soden, V. O. John, W. Ingram, and P. Good, 2010: Current changes in tropical precipitation. *Environ. Res. Lett.*, **5**, 025205.

Allen, M., 2011: In defense of the traditional null hypothesis: Remarks on the Trenberth and Curry WIREs opinion articles. *WIREs Clim. Change*, **2**, 931–934.

Allen, M. R., and S. F. B. Tett, 1999: Checking for model consistency in optimal fingerprinting. *Clim. Dyn.*, **15**, 419–434.

Allen, M. R., and W. J. Ingram, 2002: Constraints on future changes in climate and the hydrologic cycle. *Nature*, **419**, 224–232.

Allen, M. R., and P. A. Stott, 2003: Estimating signal amplitudes in optimal fingerprinting. Part I: Theory. *Clim. Dyn.*, **21**, 477–491.

Allen, M. R., P. A. Stott, J. F. B. Mitchell, R. Schnur, and T. L. Delworth, 2000: Quantifying the uncertainty in forecasts of anthropogenic climate change. *Nature*, **407**, 617–620.

Allen, M. R., D. J. Frame, C. Huntingford, C. D. Jones, J. A. Lowe, M. Meinshausen, and N. Meinshausen, 2009: Warming caused by cumulative carbon emissions towards the trillionth tonne. *Nature*, **458**, 1163–1166.

Allen, M. R., et al., 2006: Quantifying anthropogenic influence on recent near-surface temperature change. *Surv. Geophys.*, **27**, 491–544.

Allen, R. J., S. C. Sherwood, J. R. Norris, and C. S. Zender, 2012: Recent Northern Hemisphere tropical expansion primarily driven by black carbon and tropospheric ozone. *Nature*, **485**, 350–354.

Ammann, C. M., and E. R. Wahl, 2007: The importance of the geophysical context in statistical evaluations of climate reconstruction procedures. *Clim. Change*, **85**, 71–88.

Ammann, C. M., F. Joos, D. S. Schimel, B. L. Otto-Bliesner, and R. A. Tomas, 2007: Solar influence on climate during the past millennium: Results from transient simulations with the NCAR Climate System Model. *Proc. Natl. Acad. Sci. U.S.A.*, **104**, 3713–3718.

Andreae, M. O., C. D. Jones, and P. M. Cox, 2005: Strong present-day aerosol cooling implies a hot future. *Nature*, **435**, 1187–1190.

Andrews, O. D., N. L. Bindoff, P. R. Halloran, T. Ilyina, and C. Le Quéré, 2013: Detecting an external influence on recent changes in oceanic oxygen using an optimal fingerprinting method. *Biogeosciences*, **10**, 1799–1813.

Annan, J. D., and J. C. Hargreaves, 2006: Using multiple observationally-based constraints to estimate climate sensitivity. *Geophys. Res. Lett.*, **33**, L06704.

Annan, J. D., and J. C. Hargreaves, 2010: Reliability of the CMIP3 ensemble. *Geophys. Res. Lett.*, **37**, L02703.

Annan, J. D., and J. C. Hargreaves, 2011: On the generation and interpretation of probabilistic estimates of climate sensitivity. *Clim. Change*, **104**, 423–436.

Aoki, S., N. L. Bindoff, and J. A. Church, 2005: Interdecadal water mass changes in the Southern Ocean between 30 degrees E and 160 degrees E. *Geophys. Res. Lett.*, **32**, L07607.

Arkin, P. A., T. M. Smith, M. R. P. Sapiano, and J. Janowiak, 2010: The observed sensitivity of the global hydrological cycle to changes in surface temperature. *Environ. Res. Lett.*, **5**, 035201.

Bal, S., S. Schimanke, T. Spangehl, and U. Cubasch, 2011: On the robustness of the solar cycle signal in the Pacific region. *Geophys. Res. Lett.*, **38**, L14809.

Balachandran, N. K., D. Rind, P. Lonergan, and D. T. Shindell, 1999: Effects of solar cycle variability on the lower stratosphere and the troposphere. *J. Geophys. Res. Atmos.*, **104**, 27321–27339.

Balan Sarojini, B., P. Stott, E. Black, and D. Polson, 2012 Fingerprints of changes in annual and seasonal precipitation from CMIP5 models over land and ocean. *Geophys. Res. Lett.*, **39**, L23706.

Barnett, T. P., D. W. Pierce, and R. Schnur, 2001: Detection of anthropogenic climate change in the world's oceans. *Science*, **292**, 270–274.

Barnett, T. P., D. W. Pierce, K. Achutarao, P. Gleckler, B. Santer, J. Gregory, and W. Washington, 2005: Penetration of human-induced warming into the world's oceans. *Science*, **309**, 284–287.

Barnett, T. P., et al., 2008: Human-induced changes in the hydrology of the western United States. *Science*, **319**, 1080–1083.

Barriopedro, D., R. Garcia-Herrera, and R. Huth, 2008: Solar modulation of Northern Hemisphere blocking. *J. Geophys. Res. Atmos.*, **113**, D14118.

Beenstock, M., Y. Reingewertz, and N. Paldor, 2012: Polynomial cointegration tests of anthropogenic impact on global warming. *Earth Syst. Dyn. Discuss.*, **3**, 561–596.

Bender, F. A. M., A. M. L. Ekman, and H. Rodhe, 2010: Response to the eruption of Mount Pinatubo in relation to climate sensitivity in the CMIP3 models. *Clim. Dyn.*, **35**, 875–886.

Benestad, R. E., and G. A. Schmidt, 2009: Solar trends and global warming. *J. Geophys. Res. Atmos.*, **114**, D14101.

Bengtsson, L., and K. I. Hodges, 2011: On the evaluation of temperature trends in the tropical troposphere. *Clim. Dyn.*, **36** 419–430.

Bengtsson, L., V. A. Semenov, and O. M. Johannessen, 2004: The early twentieth-century warming in the Arctic—A possible mechanism. *J. Clim.*, **17**, 4045–4057.

Bengtsson, L., K. I. Hodges, E. Roeckner, and R. Brokopf, 2006: On the natural variability of the pre-industrial European climate. *Clim. Dyn.*, **27**, 743–760.

Berliner, L. M., A. L. Richard, and J. S. Dennis, 2000: Bayesian climate change assessment. *J. Clim.*, **13**, 3805–3820.

Bhend, J., and H. von Storch, 2008: Consistency of observed winter precipitation trends in northern Europe with regional climate change projections. *Clim. Dyn.*, **31**, 17–28.

Bindoff, N. L., and T. J. McDougall, 2000: Decadal changes along an Indian ocean section at 32 degrees S and their interpretation. *J. Phys. Oceanogr.,* **30**, 1207–1222.

Bindoff, N. L., et al., 2007: Observations: Oceanic climate change and sea level. In: *Climate Change 2007: The Physical Science Basis. Contribution of Working Group I to the Fourth Assessment Report of the Intergovernmental Panel on Climate Change* [Solomon, S., D. Qin, M. Manning, Z. Chen, M. Marquis, K. B. Averyt, M. Tignor and H. L. Miller (eds.)] Cambridge University Press, Cambridge, United Kingdom and New York, NY, USA, pp. 385–432.

Bintanja, R., G. J. van Oldenborgh, S. S. Drijfhout, B. Wouters, and C. A. Katsman, 2013: Important role for ocean warming and increased ice-shelf melt in Antarctic sea-ice expansion. *Nature Geosci.*, **6**, 376–379.

Birner, T., 2010: Recent widening of the tropical belt from global tropopause statistics: Sensitivities. *J. Geophys. Res. Atmos.*, **115**, D23109.

Bitz, C. M., and L. M. Polvani, 2012: Antarctic climate response to stratospheric ozone depletion in a fine resolution ocean climate model. *Geophys. Res. Lett.*, **39**, L20705.

Boer, G. J., 2011: The ratio of land to ocean temperature change under global warming *Clim. Dyn.*, **37**, 2253–2270.

Boer, G. J., M. Stowasser, and K. Hamilton, 2007: Inferring climate sensitivity from volcanic events. *Clim. Dyn.*, **28**, 481–502.

Bonfils, C., P. B. Duffy, B. D. Santer, T. M. L. Wigley, D. B. Lobell, T. J. Phillips, and C. Doutriaux, 2008: Identification of external influences on temperatures in California. *Clim. Change*, **87**, S43–S55.

Booth, B. B. B., N. J. Dunstone, P. R. Halloran, T. Andrews, and N. Bellouin, 2012: Aerosols implicated as a prime driver of twentieth-century North Atlantic climate variability. *Nature*, **484**, 228–232.

Bowerman, N. H. A., D. J. Frame, C. Huntingford, J. A. Lowe, and M. R. Allen, 2011: Cumulative carbon emissions, emissions floors and short-term rates of warming: Implications for policy. *Philos. Trans. R. Soc. A,* **369**, 45–66.

Boyer, T. P., S. Levitus, J. I. Antonov, R. A. Locarnini, and H. E. Garcia, 2005: Linear trends in salinity for the World Ocean, 1955–1998. *Geophys. Res. Lett.*, **32**, L01604.

Brandt, P., et al., 2010: Changes in the ventilation of the oxygen minimum zone of the tropical North Atlantic. *J. Phys. Oceanogr.*, **40**, 1784–1801.

Brayshaw, D. J., B. Hoskins, and M. Blackburn, 2008: The storm-track response to idealized SST perturbations in an aquaplanet GCM. *J. Atmos. Sci.*, **65**, 2842–2860.

Brohan, P., J. J. Kennedy, I. Harris, S. F. B. Tett, and P. D. Jones, 2006: Uncertainty estimates in regional and global observed temperature changes: A new data set from 1850. *J. Geophys. Res. Atmos.*, **111**, D12106.

Bromwich, D. H., J. P. Nicolas, A. J. Monaghan, M. A. Lazzara, L. M. Keller, G. A. Weidner, and A. B. Wilson, 2013: Central West Antarctica among the most rapidly warming regions on Earth. *Nature Geosci.*, **6**, 139–145.

Brönnimann, S., 2009: Early twentieth-century warming. *Nature Geosci.*, **2**, 735–736.

Brönnimann, S., et al., 2012: A multi-data set comparison of the vertical structure of temperature variability and change over the Arctic during the past 100 year. *Clim. Dyn.*, **39** 1577–1598.

Brown, R. D., and D. A. Robinson, 2011: Northern Hemisphere spring snow cover variability and change over 1922–2010 including an assessment of uncertainty. *Cryosphere*, **5**, 219–229.

Burke, E. J., S. J. Brown, and N. Christidis, 2006: Modeling the recent evolution of global drought and projections for the twenty-first century with the Hadley Centre climate model. *J. Hydrometeorol.*, **7** 1113–1125.

Butchart, N., et al., 2011: Multimodel climate and variability of the stratosphere. *J. Geophys. Res. Atmos.*, **116**, D05102.

Butler, A. H., D. W. Thompson, and R. Heikes, 2010: The steady-state atmospheric circulation response to climate change–like thermal forcings in a simple general circulation model. *J. Clim.*, **23**, 3474–3496.

Cai, M., and K.-K. Tung, 2012: Robustness of dynamical feedbacks from radiative forcing: 2% solar versus 2XCO2 experiments in an idealized GCM. *J. Atmos. Sci.*, **69**, 2256–2271.

Cattiaux, J., R. Vautard, C. Cassou, P. Yiou, V. Masson-Delmotte, and F. Codron, 2010: Winter 2010 in Europe: A cold extreme in a warming climate. *Geophys. Res. Lett.*, **37**, L20704.

Cayan, D. R., T. Das, D. W. Pierce, T. P. Barnett, M. Tyree, and A. Gershunov, 2010: Future dryness in the southwest US and the hydrology of the early 21st century drought. *Proc. Natl. Acad. Sci. U.S.A.*, **107**, 21271–21276.

Charlton-Perez, A. J., et al., 2013: On the lack of stratospheric dynamical variability in low-top versions of the CMIP5 models. *J. Geophys. Res. Atmos.*, **118**, 2494–2505.

Chinn, T., S. Winkler, M. J. Salinger, and N. Haakensen, 2005: Recent glacier advances in Norway and New Zealand: A comparison of their glaciological and meteorological causes. *Geograf. Annal. A,* **87**, 141–157.

Christiansen, B., and F. C. Ljungqvist, 2011: Reconstruction of the extratropical NH mean temperature over the last millennium with a method that preserves low-frequency variability. *J. Clim.*, **24**, 6013–6034.

Christidis, N., P. A. Stott, and S. J. Brown, 2011: The role of human activity in the recent warming of extremely warm daytime temperatures. *J. Clim.*, **24**, 1922–1930.

Christidis, N., P. A. Stott, G. C. Hegerl, and R. A. Betts, 2013: The role of land use change in the recent warming of daily extreme temperatures. *Geophys. Res. Lett.*, **40**, 589–594.

Christidis, N., P. A. Stott, F. W. Zwiers, H. Shiogama, and T. Nozawa, 2010: Probabilistic estimates of recent changes in temperature: A multi-scale attribution analysis. *Clim. Dyn.*, **34**, 1139–1156.

Christidis, N., P. A. Stott, F. W. Zwiers, H. Shiogama, and T. Nozawa, 2012a: The contribution of anthropogenic forcings to regional changes in temperature during the last decade. *Clim. Dyn.*, **39**, 1259–1274.

Christidis, N., P. A. Stott, G. S. Jones, H. Shiogama, T. Nozawa, and J. Luterbacher, 2012b: Human activity and anomalously warm seasons in Europe. *Int. J. Climatol.*, **32**, 225–239.

Chung, E. S., B. J. Soden, and B. J. Sohn, 2010: Revisiting the determination of climate sensitivity from relationships between surface temperature and radiative fluxes. *Geophys. Res. Lett.*, **37**, L10703.

Church, J., N. White, and J. Arblaster, 2005: Significant decadal-scale impact of volcanic eruptions on sea level and ocean heat content. *Nature*, **438**, 74–77.

Church, J. A., D. Monselesan, J. M. Gregory, and B. Marzeion, 2013: Evaluating the ability of process based models to project sealevel change. *Environ. Res. Lett.*, **8**, 014051.

Church, J. A., et al., 2011: Revisiting the Earth's sea-level and energy budgets from 1961 to 2008. *Geophys. Res. Lett.*, **38**, L18601.

Chylek, P., and U. Lohmann, 2008a: Reply to comment by Andrey Ganopolski and Thomas Schneider von Deimling on "Aerosol radiative forcing and climate sensitivity deduced from the Last Glacial Maximum to Holocene transition". *Geophys. Res. Lett.*, **35**, L23704.

Chylek, P., and U. Lohmann, 2008b: Aerosol radiative forcing and climate sensitivity deduced from the last glacial maximum to Holocene transition. *Geophys. Res. Lett.*, **35**, L04804.

Chylek, P., U. Lohmann, M. Dubey, M. Mishchenko, R. Kahn, and A. Ohmura, 2007: Limits on climate sensitivity derived from recent satellite and surface observations. *J. Geophys. Res. Atmos.*, **112**, D24S04.

Comiso, J. C., 2012: Large decadal decline in Arctic multiyear ice cover. *J. Clim.*, **25**, 1176–1193.

Comiso, J. C., and F. Nishio, 2008: Trends in the sea ice cover using enhanced and compatible AMSR-E, SSM/I, and SMMR data. *J. Geophys. Res. Oceans*, **113**, C02S07.

Compo, G. P., et al., 2011: The twentieth century reanalysis project. *Q. J. R. Meteorol. Soc.*, **137**, 1–28.

Cordero, E. C., and P. M. D. Forster, 2006: Stratospheric variability and trends in models used for the IPCC AR4. *Atmos. Chem. Phys.*, **6**, 5369–5380.

Crook, J. A., and P. M. Forster, 2011: A balance between radiative forcing and climate feedback in the modeled 20th century temperature response. *J. Geophys. Res. Atmos.*, **116**, D17108.

Crook, J. A., P. M. Forster, and N. Stuber, 2011: Spatial patterns of modeled climate feedback and contributions to temperature response and polar amplification. *J. Clim.*, **24**, 3575–3592.

Curry, J. A., and P. J. Webster, 2011: Climate science and the uncertainty monster. *Bull. Am. Meteorol. Soc.*, **92**, 1667–1682.

Curry, R., B. Dickson, and I. Yashayaev, 2003: A change in the freshwater balance of the Atlantic Ocean over the past four decades. *Nature*, **426**, 826–829

D'Arrigo, R., R. Wilson, and G. Jacoby, 2006: On the long-term context for late twentieth century warming. *J. Geophys. Res. Atmos.*, **111** D03103.

D'Arrigo, R., R. Wilson, and A. Tudhope, 2009: The impact of volcanic forcing on tropical temperatures during the past four centuries. *Nature Geosci.*, **2**, 51–56.

Dai, A., 2011: Drought under global warming: A review. *WIREs Clim. Change*, **2**, 45–65.

Dai, A., 2013: Increasing drought under global warming in observations and models. *Nature Clim. Change*, **3**, 52–58.

Dall'Amico, M., L. J. Gray, K. H. Rosenlof, A. A. Scaife, K. P. Shine, and P. A. Stott, 2010: Stratospheric temperature trends: Impact of ozone variability and the QBO. *Clim. Dyn.*, **34**, 381–398.

Davis, S. M., and K. H. Rosenlof, 2012: A multidiagnostic intercomparison of tropical-width time series using reanalyses and satellite observations. *J. Clim.*, **25**, 1061–1078.

Day, J. J., J. C. Hargreaves, J. D. Annan, and A. Abe-Ouchi, 2012: Sources of multi-decadal variability in Arctic sea ice extent. *Environ. Res. Lett.*, **7**, 034011.

Dean, S. M., and P. A. Stott, 2009: The effect of local circulation variability on the detection and attribution of New Zealand temperature trends. *J. Clim.*, **22**, 6217–6229.

DelSole, T., M. K. Tippett, and J. Shukla, 2011: A significant component of unforced multidecadal variability in the recent acceleration of global warming. *J. Clim.*, **24**, 909–926.

Delworth, T., V. Ramaswamy, and G. Stenchikov, 2005: The impact of aerosols on simulated ocean temperature and heat content in the 20th century. *Geophys. Res. Lett.*, **32**, L24709.

Delworth, T. L., and M. E. Mann, 2000: Observed and simulated multidecadal variability in the Northern Hemisphere. *Clim. Dyn.*, **16**, 661–676.

Deser, C., and H. Teng, 2008: Evolution of Arctic sea ice concentration trends and the role of atmospheric circulation forcing, 1979–2007. *Geophys. Res. Lett.*, **35**, L02504.

Dessler, A. E., 2010: A determination of the cloud feedback from climate variations over the past decade. *Science*, **330**, 1523–1527.

Dessler, A. E., 2011: Cloud variations and the Earth's energy budget. *Geophys. Res. Lett.*, **38**, L19701.

Dickson, R. R., et al., 2000: The Arctic Ocean response to the North Atlantic oscillation. *J. Clim.*, **13**, 2671–2696.

Ding, Q. H., E. J. Steig, D. S. Battisti, and M. Kuttel, 2011: Winter warming in West Antarctica caused by central tropical Pacific warming. *Nature Geosci.*, **4**, 398–403.

Doherty, S. J., et al., 2009: Lessons learned from IPCC AR4 scientific developments needed to understand, predict, and respond to climate change. *Bull. Am. Meteorol. Soc.*, **90**, 497–513.

Dole, R., et al., 2011: Was there a basis for anticipating the 2010 Russian heat wave? *Geophys. Res. Lett.*, **38**, L06702.

Domingues, C., J. Church, N. White, P. Gleckler, S. Wijffels, P. Barker, and J. Dunn, 2008: Improved estimates of upper-ocean warming and multi-decadal sea-level rise. *Nature*, **453**, 1090–1093.

Doscher, R., K. Wyser, H. E. M. Meier, M. W. Qian, and R. Redler, 2010: Quantifying Arctic contributions to climate predictability in a regional coupled ocean-ice-atmosphere model. *Clim. Dyn.*, **34**, 1157–1176.

Douglass, D. H., E. G. Blackman, and R. S. Knox, 2004: Corrigendum to: Temperature response of Earth to the annual solar irradiance cycle [Phys. Lett. A 323 (2004) 315]. *Phys. Lett. A*, **325**, 175–176.

Douville, H., A. Ribes, B. Decharme, R. Alkama, and J. Sheffield, 2013: Anthropogenic influence on multidecadal changes in reconstructed global evapotranspiration. *Nature Clim. Change*, **3**, 59–62.

Driscoll, S., A. Bozzo, L. J. Gray, A. Robock, and G. Stenchikov, 2012: Coupled Model Intercomparison Project 5 (CMIP5) simulations of climate following volcanic eruptions. *J. Geophys. Res.*, **117**, D17105.

Drost, F., and D. Karoly, 2012 Evaluating global climate responses to different forcings using simple indices. *Geophys. Res. Lett.*, **39**, L16701.

Drost, F., D. Karoly, and K. Braganza, 2012: Communicating global climate change using simple indices: An update *Clim. Dyn.*, **39**, 989–999.

Duarte, C. M., T. M. Lenton, P. Wadhams, and P. Wassmann, 2012: Abrupt climate change in the Arctic. *Nature Clim. Change*, **2**, 60–62.

Durack, P., S. Wijffels, and R. Matear, 2012: Ocean salinities reveal strong global water cycle intensification during 1950 to 2000. *Science*, **336**, 455–458.

Durack, P. J., and S. E. Wijffels, 2010: Fifty-year trends in global ocean salinities and their relationship to broad-scale warming. *J. Clim.*, **23**, 4342–4362.

Edwards, T. L., M. Crucifix, and S. P. Harrison, 2007: Using the past to constrain the future: How the palaeorecord can improve estimates of global warming. *Prog. Phys. Geogr.*, **31**, 481–500.

Elsner, J. B., 2006: Evidence in support of the climate change—Atlantic hurricane hypothesis. *Geophys. Res. Lett.*, **33**, L16705.

Elsner, J. B., J. P. Kossin, and T. H. Jagger, 2008: The increasing intensity of the strongest tropical cyclones. *Nature*, **455**, 92–95.

Emanuel, K., 2005: Increasing destructiveness of tropical cyclones over the past 30 years. *Nature*, **436**, 686–688.

Emanuel, K., S. Solomon, D. Folini, S. Davis, and C. Cagnazzo, 2013: Influence of tropical tropopause layer cooling on Atlantic hurricane activity. *J. Clim.*, **26**, 2288–2301.

Emerson, S., Y. W. Watanabe, T. Ono, and S. Mecking, 2004: Temporal trends in apparent oxygen utilization in the upper pycnocline of the North Pacific: 1980–2000. *J. Oceanogr.*, **60**, 139–147.

Engle, R. F., and C. W. J. Granger, 1987: Co-integration and error correction: Representation, estimation, and testing. *Econometrica*, **55**, 251–276.

Esper, J., et al., 2012: Orbital forcing of tree-ring data. *Nature Clim. Change*, **2**, 862–866.

Evan, A. T., G. R. Foltz, D. X. Zhang, and D. J. Vimont, 2011: Influence of African dust on ocean-atmosphere variability in the tropical Atlantic. *Nature Geosci.*, **4**, 762–765.

Evan, A. T., D. J. Vimont, A. K. Heidinger, J. P. Kossin, and R. Bennartz, 2009: The role of aerosols in the evolution of tropical North Atlantic Ocean temperature anomalies. *Science*, **324**, 778–781.

Eyring, V., et al., 2013: Long-term changes in tropospheric and stratospheric ozone and associated climate impacts in CMIP5 simulations. *J. Geophys. Res. Atmos.*, doi:10.1002/jgrd.50316.

Eyring, V., et al., 2006: Assessment of temperature, trace species, and ozone in chemistry-climate model simulations of the recent past. *J. Geophys. Res. Atmos.*, **111**, D22308.

Fernández-Donado, L., et al., 2013: Large-scale temperature response to external forcing in simulations and reconstructions of the last millennium. *Clim. Past*, **9**, 393–421.

Fettweis, X., G. Mabille, M. Erpicum, S. Nicolay, and M. Van den Broeke, 2011: The 1958–2009 Greenland ice sheet surface melt and the mid-tropospheric atmospheric circulation. *Clim. Dyn.*, **36**, 139–159.

Fettweis, X., B. Franco, M. Tedesco, J. H. van Angelen, J. T. M. Lenaerts, M. R. van den Broeke, and H. Gallée, 2013: Estimating the Greenland ice sheet surface mass balance contribution to future sea level rise using the regional atmospheric climate model MAR. *Cryosphere*, **7**, 469–489.

Feulner, G., 2011: Are the most recent estimates for Maunder Minimum solar irradiance in agreement with temperature reconstructions? *Geophys. Res. Lett.*, **38**, L16706.

Fischer, E. M., S. I. Seneviratne, P. L. Vidale, D. Luthi, and C. Schar, 2007: Soil moisture –atmosphere interactions during the 2003 European summer heat wave. *J. Clim.*, **20**, 5081–5099.

Fogt, R. L., J. Perlwitz, A. J. Monaghan, D. H. Bromwich, J. M. Jones, and G. J. Marshall, 2009: Historical SAM variability. Part II: Twentieth-century variability and trends from reconstructions, observations, and the IPCC AR4 models. *J. Clim.*, **22**, 5346–5365.

Folland, C. K., et al., 2013 High predictive skill of global surface temperature a year ahead. *Geophys. Res. Lett.*, **40**, 761–767.

Forest, C. E., and R. W. Reynolds, 2008: Climate change—Hot questions of temperature bias. *Nature*, **453**, 601–602.

Forest, C. E., P. H. Stone, and A. P. Sokolov, 2006: Estimated PDFs of climate system properties including natural and anthropogenic forcings. *Geophys. Res. Lett.*, **33**, L01705.

Forest, C. E., P. H. Stone, and A. P. Sokolov, 2008: Constraining climate model parameters from observed 20th century changes. *Tellus A*, **60**, 911–920.

Forest, C. E., M. R. Allen, P. H. Stone, and A. P. Sokolov, 2000: Constraining uncertainties in climate models using climate change detection techniques. *Geophys. Res. Lett.*, **27**, 569–572.

Forest, C. E., P. H. Stone, A. P. Sokolov, M. R. Allen, and M. D. Webster, 2002: Quantifying uncertainties in climate system properties with the use of recent climate observations. *Science*, **295**, 113–117.

Forster, P., et al., 2007: Changes in atmospheric constituents and in radiative forcing. In: *Climate Change 2007: The Physical Science Basis. Contribution of Working Group I to the Fourth Assessment Report of the Intergovernmental Panel on Climate Change* [Solomon, S., D. Qin, M. Manning, Z. Chen, M. Marquis, K. B. Averyt, M. Tignor and H. L. Miller (eds.)] Cambridge University Press, Cambridge, United Kingdom and New York, NY, USA, pp. 129–234.

Forster, P. M., T. Andrews, P. Good, J. M. Gregory, L. S. Jackson, and M. Zelinka, 2013 Evaluating adjusted forcing and model spread for historical and future scenarios in the CMIP5 generation of climate models. *J. Geophys. Res. Atmos.*, **118**, 1139–1150.

Forster, P. M., et al., 2011: Stratospheric changes and climate. In: *Scientific Assessment of Ozone Depletion: 2010*. Global Ozone Research and Monitoring Project-Report No. 52 [P. M. Forster and D. W. J. Thompson (eds.)]. World Meteorological Organization, Geneva, Switzerland, 516 pp.

Forster, P. M. D., and J. M. Gregory, 2006: The climate sensitivity and its components diagnosed from Earth Radiation Budget data. *J. Clim.*, **19**, 39–52.

Foster, G., and S. Rahmstorf, 2011: Global temperature evolution 1979–2010. *Environ. Res. Lett.*, **6**, 044022.

Foster, G., J. D. Annan, G. A. Schmidt, and M. E. Mann, 2008: Comment on "Heat capacity, time constant, and sensitivity of Earth's climate system" by S. E. Schwartz. *J. Geophys. Res. Atmos.*, **113**, D15102.

Fowler, H. J., and R. L. Wilby, 2010: Detecting changes in seasonal precipitation extremes using regional climate model projections: Implications for managing fluvial flood risk. *Water Resour. Res.*, **46**, W03525.

Frame, D. J., D. A. Stone, P. A. Stott, and M. R. Allen, 2006: Alternatives to stabilization scenarios. *Geophys. Res. Lett.*, **33**, L14707.

Frame, D. J., B. B. B. Booth, J. A. Kettleborough, D. A. Stainforth, J. M. Gregory, M. Collins, and M. R. Allen, 2005: Constraining climate forecasts: The role of prior assumptions. *Geophys. Res. Lett.*, **32**, L09702.

Francis, J. A., and S. J. Vavrus 2012: Evidence linking Arctic amplification to extreme weather in mid-latitudes. *Geophys. Res. Lett.*, **39**, L06801.

Frank, D., J. Esper, and E. R. Cook, 2007: Adjustment for proxy number and coherence in a large-scale temperature reconstruction. *Geophys. Res. Lett.*, **34**, L16709.

Frank, D. C., J. Esper, C. C. Raible, U. Buntgen, V. Trouet, B. Stocker, and F. Joos, 2010: Ensemble reconstruction constraints on the global carbon cycle sensitivity to climate. *Nature*, **463**, 527–530.

Franzke, C., 2010: Long-range dependence and climate noise characteristics of Antarctic temperature data. *J. Clim.*, **23**, 6074–6081.

Free, M., 2011: The seasonal structure of temperature trends in the tropical lower stratosphere. *J. Clim.*, **24**, 859–866.

Free, M., and J. Lanzante, 2009: Effect of volcanic eruptions on the vertical temperature profile in radiosonde data and climate models. *J. Clim.*, **22**, 2925–2939.

Friedlingstein, P., et al., 2006: Climate–carbon cycle feedback analysis: Results from the C4MIP model intercomparison. *J. Clim.*, **19**, 3337–3353.

Frierson, D. M. W., 2006: Robust increases in midlatitude static stability in simulations of global warming. *Geophys. Res. Lett.*, **33**, L24816.

Frierson, D. M. W., J. Lu, and G. Chen, 2007: Width of the Hadley cell in simple and comprehensive general circulation models. *Geophys. Res. Lett.*, **34**, L18804.

Fu, Q., and P. Lin, 2011: Poleward shift of subtropical jets inferred from satellite-observed lower stratospheric temperatures. *J. Clim.*, **24**, 5597–5603.

Fu, Q., S. Solomon, and P. Lin, 2010: On the seasonal dependence of tropical lower-stratospheric temperature trends. *Atmos. Chem. Phys.*, **10**, 2643–2653.

Fu, Q., S. Manabe, and C. M. Johanson, 2011: On the warming in the tropical upper troposphere: Models versus observations. *Geophys. Res. Lett.*, **38**, L15704.

Fu, Q., C. M. Johanson, J. M. Wallace, and T. Reichler, 2006: Enhanced mid-latitude tropospheric warming in satellite measurements. *Science*, **312**, 1179–1179.

Fyfe, J. C., 2006: Southern Ocean warming due to human influence. *Geophys. Res. Lett.*, **33**, L19701.

Fyfe, J. C., N. P. Gillett, and D. W. J. Thompson, 2010: Comparing variability and trends in observed and modelled global-mean surface temperature. *Geophys. Res. Lett.*, **37**, L16802.

Fyfe, J. C., N. P. Gillett, and G. J. Marshal, 2012: Human influence on extratropical Southern Hemisphere summer precipitation. *Geophys. Res. Lett.*, **39**, L23711.

Fyke, J., and M. Eby, 2012: Comment on "Climate sensitivity estimated from temperature reconstructions of the Last Glacial Maximum". *Science*, **337**, 1294.

Ganopolski, A., and T. S. von Deimling, 2008: Comment on "Aerosol radiative forcing and climate sensitivity deduced from the Last Glacial Maximum to Holocene transition" by Petr Chylek and Ulrike Lohmann. *Geophys. Res. Lett.*, **35**, L23703.

Gascard, J. C., et al., 2008: Exploring Arctic transpolar drift during dramatic sea ice retreat. *Eos Trans. Am. Geophys. Union*, **89**, 21–22.

Gay-Garcia, C., F. Estrada, and A. Sanchez, 2009: Global and hemispheric temperature revisited. *Clim. Change*, **94**, 333–349

Giles, K. A., S. W. Laxon, and A. L. Ridout, 2008: Circumpolar thinning of Arctic sea ice following the 2007 record ice extent minimum. *Geophys. Res. Lett.*, **35**, L22502.

Gillett, N. P., and P. A. Stott, 2009: Attribution of anthropogenic influence on seasonal sea level pressure. *Geophys. Res. Lett.*, **36**, L23709.

Gillett, N. A., and J. C. Fyfe, 2013: Annular Mode change in the CMIP5 simulations. *Geophys. Res. Lett.*, **40**, 1189–1193.

Gillett, N. P., R. J. Allan, and T. J. Ansell, 2005: Detection of external influence on sea level pressure with a multi-model ensemble. *Geophys. Res. Lett.*, **32**, L19714.

Gillett, N. P., P. A. Stott, and B. D. Santer, 2008a: Attribution of cyclogenesis region sea surface temperature change to anthropogenic influence. *Geophys. Res. Lett.*, **35**, L09707.

Gillett, N. P., G. C. Hegerl, M. R. Allen, and P. A. Stott, 2000: Implications of changes in the Northern Hemisphere circulation for the detection of anthropogenic climate change. *Geophys. Res. Lett.*, **27**, 993–996.

Gillett, N. P., F. W. Zwiers, A. J. Weaver, and P. A. Stott, 2003: Detection of human influence on sea-level pressure. *Nature*, **422**, 292–294.

Gillett, N. P., M. F. Wehner, S. F. B. Tett, and A. J. Weaver, 2004: Testing the linearity of the response to combined greenhouse and sulfate aerosol forcing. *Geophys. Res. Lett.*, **31**, L14201.

Gillett, N. P., V. K. Arora, G. M. Flato, J. F. Scinocca, and K. von Salzen, 2012: Improved constraints on 21st-century warming derived using 160 years of temperature observations. *Geophys. Res. Lett.*, **39**, L01704.

Gillett, N. P., V. K. Arora, D. Matthews, P. A. Stott, and M. R. Allen, 2013 Constraining the ratio of global warming to cumulative $CO_2$ emissions using CMIP5 simulations. *J. Clim.*, doi:10.1175/JCLI-D-12–00476.1.

Gillett, N. P., et al., 2008b: Attribution of polar warming to human influence. *Nature Geosci.*, **1**, 750–754.

Gillett, N. P., et al., 2011: Attribution of observed changes in stratospheric ozone and temperature. *Atmos. Chem. Phys.*, **11** 599–609.

Gleckler, P. J., T. M. L. Wigley, B. D. Santer, J. M. Gregory, K. AchutaRao, and K. E. Taylor, 2006: Volcanoes and climate: Krakatoa's signature persists in the ocean. *Nature*, **439**, 675–675.

Gleckler, P. J., et al., 2012: Human-induced global ocean warming on multidecadal timescales. *Nature Clim. Change*, **2**, 524–529.

Gong, D., and S. Wang, 1999: Definition of Antarctic oscillation index. *Geophys. Res. Lett.*, **26**, 459–462.

Goosse, H., W. Lefebvre, A. de Montety, E. Crespin, and A. H. Orsi, 2009: Consistent past half-century trends in the atmosphere, the sea ice and the ocean at high southern latitudes. *Clim. Dyn.*, **33**, 999–1016.

Goosse, H., J. Guiot, M. E. Mann, S. Dubinkina, and Y. Sallaz-Damaz, 2012a: The medieval climate anomaly in Europe: Comparison of the summer and annual mean signals in two reconstructions and in simulations with data assimilation. *Global Planet. Change*, **84–85**, 35–47.

Goosse, H., E. Crespin, A. de Montety, M. E. Mann, H. Renssen, and A. Timmermann, 2010: Reconstructing surface temperature changes over the past 600 years using climate model simulations with data assimilation. *J. Geophys. Res. Atmos.*, **115**, D09108.

Goosse, H., et al., 2012b: The role of forcing and internal dynamics in explaining the ''Medieval Climate Anomaly'. *Clim. Dyn.*, **39**, 2847–2866.

Gouretski, V., and K. Koltermann, 2007: How much is the ocean really warming? *Geophys. Res. Lett.*, **34**, L01610.

Graff, L. S., and J. H. LaCasce, 2012: Changes in the extratropical storm tracks in response to changes in SST in an GCM. *J. Clim.*, **25**, 1854–1870.

Grant, A. N., S. Bronnimann, T. Ewen, T. Griesser, and A. Stickler, 2009: The early twentieth century warm period in the European Arctic. *Meteorol. Z.*, **18** 425–432.

Graversen, R. G., and M. H. Wang, 2009: Polar amplification in a coupled climate model with locked albedo. *Clim. Dyn.*, **33**, 629–643.

Gray, L. J., et al., 2010: Solar influences on climate. *Rev. Geophys.*, **48** RG4001.

Gregory, J. M., 2000: Vertical heat transports in the ocean and their effect an time-dependent climate change. *Clim. Dyn.*, **16**, 501–515.

Gregory, J. M., 2010: Long-term effect of volcanic forcing on ocean heat content. *Geophys. Res. Lett.*, **37**, L22701.

Gregory, J. M., and P. M. Forster, 2008: Transient climate response estimated from radiative forcing and observed temperature change. *J. Geophys. Res. Atmos.*, **113**, D23105.

Gregory, J. M., J. A. Lowe, and S. F. B. Tett, 2006: Simulated global-mean sea level changes over the last half-millennium. *J. Clim.*, **19**, 4576–4591.

Gregory, J. M., C. D. Jones, P. Cadule, and P. Friedlingstein, 2009: Quantifying carbon cycle feedbacks. *J. Clim.*, **22**, 5232–5250.

Gregory, J. M., R. J. Stouffer, S. C. B. Raper, P. A. Stott, and N. A. Rayner, 2002: An observationally based estimate of the climate sensitivity. *J. Clim.*, **15**, 3117–3121.

Gregory, J. M., H. T. Banks, P. A. Stott, J. A. Lowe, and M. D. Palmer, 2004: Simulated and observed decadal variability in ocean heat content. *Geophys. Res. Lett.*, **31**, L15312.

Gregory, J. M., et al., 2012 Twentieth-century global-mean sea-level rise: Is the whole greater than the sum of the parts? *J. Clim.*, doi:10.1175/JCLI-D-12-00319.1.

Grist, J., et al., 2010: The roles of surface heat flux and ocean heat transport convergence in determining Atlantic Ocean temperature variability. *Ocean Dyn.*, **60**, 771–790.

Haam, E., and K. K. Tung, 2012: Statistics of solar cycle-La Niña connection: Correlation of two autocorrelated time series. *J. Atmos. Sci.*, **69** 2934–2939.

Haigh, J., M. Blackburn, and R. Day, 2005: The response of tropospheric circulation to perturbations in lower-stratospheric temperature. *J. Clim.*, **18**, 3672–3685.

Haigh, J. D., 1996: The impact of solar variability on climate. *Science*, **272** 981–984.

Haimberger, L., C. Tavolato, and S. Sperka, 2012: Homogenization of the global radiosonde temperature dataset through combined comparison with reanalysis background series and neighboring stations. *J. Clim.*, **25**, 8108–8131.

Han, W., et al., 2010: Patterns of Indian Ocean sea-level change in a warming climate. *Nature Geosci.*, **3**, 546–550.

Hanna, E., J. M. Jones, J. Cappelen, S. H. Mernild, L. Wood, K. Steffen, and P. Huybrechts, 2013: The influence of North Atlantic atmospheric and oceanic forcing effects on 1900–2010 Greenland summer climate and ice melt/runoff. *Int. J. Climatol.*, **33**, 862–880.

Hanna, E., et al., 2008: Increased runoff from melt from the Greenland ice sheet: A response to global warming. *J. Clim.*, **21**, 331–341.

Hannart, A., J. L. Dufresne, and P. Naveau, 2009: Why climate sensitivity may not be so unpredictable. *Geophys. Res. Lett.*, **36**, L16707.

Hansen, J., and S. Lebedeff, 1987: Global trends of measured surface air-temperature. *J. Geophys. Res. Atmos.*, **92**, 13345–13372.

Hansen, J., M. Sato, and R. Ruedy, 2012: Perception of climate change. *Proc. Natl. Acad. Sci. U.S.A.*, **109**, 14726–14727.

Hansen, J., M. Sato, P. Kharecha, and K. von Schuckmann, 2011: Earth's energy imbalance and implications. *Atmos. Chem. Phys.*, **11**, 13421–13449.

Hansen, J., et al., 2005a: Earth's energy imbalance: Confirmation and implications. *Science*, **308**, 1431–1435.

Hansen, J., et al., 2005b: Efficacy of climate forcings. *J. Geophys. Res. Atmos.*, **110**, D18104.

Hargreaves, J. C., and J. D. Annan, 2009: Comment on 'Aerosol radiative forcing and climate sensitivity deduced from the Last Glacial Maximum to Holocene transition', by P. Chylek and U. Lohmann, Geophys. Res. Lett., doi:10.1029/2007GL032759., 2008. Clim. Past, 5, 143–145.

Hargreaves, J. C., A. Abe-Ouchi, and J. D. Annan, 2007: Linking glacial and future climates through an ensemble of GCM simulations. *Clim. Past*, **3**, 77–87.

Hargreaves, J. C., J. D. Annan, M. Yoshimori, and A. Abe-Ouchi, 2012: Can the Last Glacial Maximum constrain climate sensitivity? *Geophys. Res. Lett.*, **39**, L24702.

Harris, G. R., D. M. H. Sexton, B. B. B. Booth, M. Collins, and J. M. Murphy, 2013: Probabilistic projections of transient climate change. *Clim. Dyn.*, doi:10.1007/s00382-012-1647-y.

Hasselmann, K., 1997: Multi-pattern fingerprint method for detection and attribution of climate change. *Clim. Dyn.*, **13**, 601–611.

Hegerl, G., and F. Zwiers, 2011: Use of models in detection and attribution of climate change. *WIREs Clim. Change*, **2**, 570–591.

Hegerl, G., J. Luterbacher, F. Gonzalez-Rouco, S. F. B. Tett, T. Crowley, and E. Xoplaki, 2011a: Influence of human and natural forcing on European seasonal temperatures. *Nature Geosci.*, **4**, 99–103.

Hegerl, G. C., F. W. Zwiers, and C. Tebaldi, 2011b: Patterns of change: Whose fingerprint is seen in global warming? *Environ. Res. Lett.*, **6**, 044025.

Hegerl, G. C., F. W. Zwiers, P. A. Stott, and V. V. Kharin, 2004: Detectability of anthropogenic changes in annual temperature and precipitation extremes. *J. Clim.*, **17**, 3683–3700.

Hegerl, G. C., T. J. Crowley, W. T. Hyde, and D. J. Frame, 2006: Climate sensitivity constrained by temperature reconstructions over the past seven centuries. *Nature*, **440**, 1029–1032.

Hegerl, G. C., P. Stott, S. Solomon, and F. W. Zwiers, 2011c: Comment on "Climate science and the uncertainty monster by J.A. Curry and P.J. Webster". *Bull. Am. Meteorol. Soc.*, **92**, 1683–1685.

Hegerl, G. C., T. J. Crowley, S. K. Baum, K. Y. Kim, and W. T. Hyde, 2003: Detection of volcanic, solar and greenhouse gas signals in paleo-reconstructions of Northern Hemispheric temperature. *Geophys. Res. Lett.*, **30**, 1242.

Hegerl, G. C., T. J. Crowley, M. Allen, W. T. Hyde, H. N. Pollack, J. Smerdon, and E. Zorita, 2007a: Detection of human influence on a new, validated 1500-year temperature reconstruction. *J. Clim.*, **20**, 650–666.

Hegerl, G. C., et al., 2010: Good practice guidance paper on detection and attribution related to anthropogenic climate change. In: *Meeting Report of the Intergovernmental Panel on Climate Change Expert Meeting on Detection and Attribution of Anthropogenic Climate Change* [T. F. Stocker, et al. (eds.)]. IPCC Working Group I Technical Support Unit, University of Bern, Bern, Switzerland, 8 pp.

Hegerl, G. C., et al., 2007b: Understanding and attributing climate change. In: *Climate Change 2007: The Physical Science Basis. Contribution of Working Group I to the Fourth Assessment Report of the Intergovernmental Panel on Climate Change* [Solomon, S., D. Qin, M. Manning, Z. Chen, M. Marquis, K. B. Averyt, M. Tignor and H. L. Miller (eds.)] Cambridge University Press, Cambridge, United Kingdom and New York, NY, USA, pp. 663–745.

Held, I. M., and B. J. Soden, 2006: Robust responses of the hydrological cycle to global warming. *J. Clim.*, **19**, 5686–5699.

Held, I. M., M. Winton, K. Takahashi, T. Delworth, F. R. Zeng, and G. K. Vallis, 2010: Probing the fast and slow components of global warming by returning abruptly to preindustrial forcing. *J. Clim.*, **23**, 2418–2427.

Helm, K. P., N. L. Bindoff, and J. A. Church, 2010: Changes in the global hydrological-cycle inferred from ocean salinity. *Geophys. Res. Lett.*, **37**, L18701.

Helm, K. P., N. L. Bindoff, and J. A. Church, 2011: Observed decreases in oxygen content of the global ocean. *Geophys. Res. Lett.*, **38**, L23602.

Henriksson, S. V., E. Arjas, M. Laine, J. Tamminen, and A. Laaksonen, 2010: Comment on 'Using multiple observationally-based constraints to estimate climate sensitivity' by J. D. Annan and J. C. Hargreaves, *Geophys. Res. Lett.*, doi:10.1029/2005GL025259, 2006. *Clim. Past*, **6**, 411–414.

Hidalgo, H. G., et al., 2009: Detection and attribution of streamflow timing changes to climate change in the Western United States. *J. Clim.*, **22**, 3838–3855.

Hodge, S. M., D. C. Trabant, R. M. Krimmel, T. A. Heinrichs, R. S. March, and E. G. Josberger, 1998: Climate variations and changes in mass of three glaciers in western North America. *J. Clim.*, **11**, 2161–2179.

Hoekema, D. J., and V. Sridhar, 2011: Relating climatic attributes and water resources allocation: A study using surface water supply and soil moisture indices in the Snake River basin, Idaho. *Water Resour. Res.*, **47**, W07536.

Hoerling, M., and A. Kumar, 2003: The perfect ocean for drought. *Science*, **299**, 691–694.

Hoerling, M., et al., 2013: Anatomy of an extreme event. *J. Clim.*, **26**, 2811–2832.

Hoerling, M. P., J. K. Eischeid, X.-W. Quan, H. F. Diaz, R. S. Webb, R. M. Dole, and D. R. Easterling, 2012: Is a transition to semipermanent drought conditions imminent in the U.S. great plains? *J. Clim.*, **25**, 8380–8386.

Holden, P. B., N. R. Edwards, K. I. C. Oliver, T. M. Lenton, and R. D. Wilkinson, 2010: A probabilistic calibration of climate sensitivity and terrestrial carbon change in GENIE-1. *Clim. Dyn.*, **35**, 785–806.

Holland, D. M., R. H. Thomas, B. De Young, M. H. Ribergaard, and B. Lyberth, 2008: Acceleration of Jakobshavn Isbrae triggered by warm subsurface ocean waters. *Nature Geosci.*, **1**, 659–664.

Hood, L. L., and R. E. Soukharev, 2012: The lower-stratospheric response to 11-yr solar forcing: Coupling to the troposphere-ocean response. *J. Atmos. Sci.*, **69**, 1841–1864.

Hosoda, S., T. Suga, N. Shikama, and K. Mizuno, 2009: Global surface layer salinity change detected by Argo and its implication for hydrological cycle intensification. *J. Oceanogr.*, **65**, 579–586.

Hu, Y., and Q. Fu, 2007: Observed poleward expansion of the Hadley circulation since 1979. *Atmos. Chem. Phys.*, **7**, 5229–5236.

Hu, Y. Y., C. Zhou, and J. P. Liu, 2011: Observational evidence for poleward expansion of the Hadley circulation. *Adv. Atmos. Sci.*, **28**, 33–44.

Hu, Y. Y., L. J. Tao, and J. P. Liu, 2013: Poleward expansion of the Hadley circulation in CMIP5 simulations. *Adv. Atmos. Sci.*, **30**, 790–795.

Huber, M., and R. Knutti, 2011: Anthropogenic and natural warming inferred from changes in Earth's energy balance. *Nature Geosci.*, **5**, 31–36.

Hudson, R. D., M. F. Andrade, M. B. Follette, and A. D. Frolov, 2006: The total ozone field separated into meteorological regimes—Part II: Northern Hemisphere mid-latitude total ozone trends. *Atmos. Chem. Phys.*, **6**, 5183–5191.

Huntingford, C., P. A. Stott, M. R. Allen, and F. H. Lambert, 2006: Incorporating model uncertainty into attribution of observed temperature change. *Geophys. Res. Lett.*, **33**, L05710.

Huss, M., and A. Bauder, 2009: 20th-century climate change inferred from four long-term point observations of seasonal mass balance. *Ann. Glaciol.*, **50**, 207–214.

Huss, M., R. Hock, A. Bauder, and M. Funk, 2010: 100-year mass changes in the Swiss Alps linked to the Atlantic Multidecadal Oscillation. *Geophys. Res. Lett.*, **37**, L10501.

Huybers, P., 2010: Compensation between model feedbacks and curtailment of climate sensitivity. *J. Clim.*, **23**, 3009–3018.

Imbers, J., A. Lopez, C. Huntingford, and M. R. Allen, 2013: Testing the robustness of the anthropogenic climate change detection statements using different empirical models. *J. Geophys. Res. Atmos.*, doi:10.1002/jgrd.50296.

Ineson, S., A. A. Scaife, J. R. Knight, J. C. Manners, N. M. Dunstone, L. J. Gray, and J. D. Haigh, 2011: Solar forcing of winter climate variability in the Northern Hemisphere. *Nature Geosci.*, **4**, 753–757.

Ingram, W. J., 2007: Detection and attribution of climate change, and understanding solar influence on climate. In: *Solar Variability and Planetary Climates* [Y. Calisesi, R.-M. Bonnet , L. Gray , J. Langen, and M. Lockwood (eds.)]. Springer Science+Business Media, New York, NY, USA, and Heidelberg, Germany, pp. 199–211.

IPCC, 2012: Managing the risks of extreme events and disasters to advance climate change adaptation. *A Special Report of Working Groups I and II of the Intergovernmental Panel on Climate Change* [C. B. Field et al. (eds.)]. *Cambridge University Press, Cambridge, UK, and New York, NY, USA,* 582.

Ishii, M., and M. Kimoto, 2009: Reevaluation of historical ocean heat content variations with time-varying XBT and MBT depth bias corrections. *J. Oceanogr.*, **65**, 287–299.

Jackson, J. M., E. C. Carmack, F. A. McLaughlin, S. E. Allen, and R. G. Ingram, 2010: Identification, characterization, and change of the near-surface temperature maximum in the Canada Basin, 1993–2008. *J. Geophys. Res.J. Geophys. Res. Oceans*, **115**, C05021.

Jacob, T., J. Wahr, W. T. Pfeffer, and S. Swenson, 2012: Recent contributions of glaciers and ice caps to sea level rise. *Nature*, **482** 514–518.

Jacobs, S. S., A. Jenkins, C. F. Giulivi, and P. Dutrieux, 2011: Stronger ocean circulation and increased melting under Pine Island Glacier ice shelf. *Nature Geosci.*, **4**, 519–523.

Jahn, A., et al., 2012: Late-twentieth-century simulation of Arctic sea-ice and ocean properties in the CCSM4. *J. Clim.*, **25**, 1431–1452.
Johannessen, O. M., et al., 2004: Arctic climate change: Observed and modelled temperature and sea-ice variability *Tellus A*, **56**, 559–560.
Johanson, C. M., and Q. Fu, 2009: Hadley cell widening: Model simulations versus observations. *J. Clim.*, **22**, 2713–2725.
Johnson, G. C., and A. H. Orsi, 1997: Southwest Pacific Ocean water-mass changes between 1968/69 and 1990/91. *J. Clim.*, **10**, 306–316.
Jones, G. S., and P. A. Stott, 2011: Sensitivity of the attribution of near surface temperature warming to the choice of observational dataset. *Geophys. Res. Lett.*, **38**, L21702.
Jones, G. S., S. F. B. Tett, and P. A. Stott, 2003: Causes of atmospheric temperature change 1960–2000: A combined attribution analysis. *Geophys. Res. Lett.*, **30**, 1228.
Jones, G. S., P. A. Stott, and N. Christidis, 2008: Human contribution to rapidly increasing frequency of very warm Northern Hemisphere summers. *J. Geophys. Res. Atmos.*, **113**, D02109.
Jones, G. S., N. Christidis, and P. A. Stott, 2011: Detecting the influence of fossil fuel and bio-fuel black carbon aerosols on near surface temperature changes. *Atmos. Chem. Phys.*, **11** 799–816.
Jones, G. S., M. Lockwood, and P. A. Stott, 2012: What influence will future solar activity changes over the 21st century have on projected global near surface temperature changes ? *J. Geophys. Res. Atmos.*, **117**, D05103.
Jones, G. S., P. A. Stott, and N. Christidis, 2013 Attribution of observed historical near surface temperature variations to anthropogenic and natural causes using CMIP5 simulations. *J. Geophys. Res. Atmos.*, doi:10.1002/jgrd.50239.
Jones, P. D., et al., 2001: Adjusting for sampling density in grid box land and ocean surface temperature time series. *J. Geophys. Res. Atmos.*, **106**, 3371–3380.
Joshi, M. M., and G. S. Jones, 2009: The climatic effects of the direct injection of water vapour into the stratosphere by large volcanic eruptions. *Atmos. Chem. Phys.*, **9**, 6109–6118.
Joughin, I., and R. B. Alley, 2011: Stability of the West Antarctic ice sheet in a warming world. *Nature Geosci.*, **4**, 506–513.
Juckes, M. N., et al., 2007: Millennial temperature reconstruction intercomparison and evaluation. *Clim. Past*, **3**, 591–609.
Jung, M., et al., 2010: Recent decline in the global land evapotranspiration trend due to limited moisture supply. *Nature*, **467**, 951–954.
Jungclaus, J. H., et al., 2010: Climate and carbon-cycle variability over the last millennium. *Clim. Past*, **6**, 723–737.
Kaplan, J. O., K. M. Krumhardt, and N. Zimmermann, 2009: The prehistoric and preindustrial deforestation of Europe. *Quat. Sci. Rev.*, **28**, 3016–3034.
Karoly, D. J., and Q. G. Wu, 2005: Detection of regional surface temperature trends. *J. Clim.*, **18**, 4337–4343.
Karoly, D. J., and P. A. Stott, 2006: Anthropogenic warming of central England temperature. *Atmos. Sci. Lett.*, **7** 81–85.
Karpechko, A. Y., N. P. Gillett, G. J. Marshall, and A. A. Scaife, 2008: Stratospheric influence on circulation changes in the Southern Hemisphere troposphere in coupled climate models. *Geophys. Res. Lett.*, **35**, L20806.
Kattsov, V. M., et al., 2010: Arctic sea-ice change: A grand challenge of climate science. *J. Glaciol.*, **56**, 1115–1121.
Kaufman, D. S., et al., 2009: Recent warming reverses long-term arctic cooling. *Science*, **325**, 1236–1239.
Kaufmann, R. K., and D. I. Stern, 1997: Evidence for human influence on climate from hemispheric temperature relations. *Nature*, **388**, 39–44.
Kaufmann, R. K., and D. I. Stern, 2002: Cointegration analysis of hemispheric temperature relations. *J. Geophys. Res. Atmos.*, **107**, 4012.
Kaufmann, R. K., H. Kauppi, and J. H. Stock, 2006: Emission, concentrations, & temperature: A time series analysis. *Clim. Change*, **77**, 249–278.
Kaufmann, R. K., H. Kauppi, M. L. Mann, and J. H. Stock, 2011: Reconciling anthropogenic climate change with observed temperature 1998–2008. *Proc. Natl. Acad. Sci. U.S.A.*, **108**, 11790–11793.
Kaufmann, R. K., H. Kauppi, M. L. Mann, and J. H. Stock, 2013: Does temperature contain a stochastic trend: Linking statistical results to physical mechanisms. *Clim. Change*, doi:10.1007/s10584–012–0683–2.
Kay, A. L., S. M. Crooks, P. Pall, and D. A. Stone, 2011a: Attribution of Autumn/Winter 2000 flood risk in England to anthropogenic climate change: A catchment-based study. *J. Hydrol.*, **406**, 97–112.
Kay, J. E., M. M. Holland, and A. Jahn, 2011b: Inter-annual to multi-decadal Arctic sea ice extent trends in a warming world. *Geophys. Res. Lett.*, **38**, L15708.
Keeling, R. F., and H. E. Garcia, 2002: The change in oceanic $O_2$ inventory associated with recent global warming. *Proc. Natl. Acad. Sci. U.S.A.*, **99**, 7848–7853.
Keeling, R. F., A. Kortzinger, and N. Gruber, 2010: Ocean deoxygenation in a warming world. *Annu. Rev. Mar. Sci.*, **2**, 199–229.
Kettleborough, J. A., B. B. B. Booth, P. A. Stott, and M. R. Allen, 2007: Estimates of uncertainty in predictions of global mean surface temperature. *J. Clim.*, **20**, 843–855.
Kharin, V. V., F. W. Zwiers, X. Zhang, and G. C. Hegerl, 2007: Changes in temperature and precipitation extremes in the IPCC ensemble of global coupled model simulations. *J. Clim.*, **20**, 1419–1444.
Kharin, V. V., F. W. Zwiers, X. Zhang, and M. Wehner, 2013: Changes in temperature and precipitation extremes in the CMIP5 ensemble. *Clim. Change*, doi:10.1007/s10584-013-0705-8.
Kiehl, J. T., 2007: Twentieth century climate model response and climate sensitivity. *Geophys. Res. Lett.*, **34**, L22710.
Kinnard, C., C. M. Zdanowicz, D. A. Fisher, E. Isaksson, A. Vernal, and L. G. Thompson, 2011: Reconstructed changes in Arctic sea ice cover over the past 1450 years. *Nature*, **479**, 509–513.
Kirk-Davidoff, D. B., 2009: On the diagnosis of climate sensitivity using observations of fluctuations. *Atmos. Chem. Phys.*, **9**, 813–822.
Knight, J., et al., 2009: Do global temperature trends over the last decade falsify climate predictions? In: State of the Climate in 2008. *Bull. Am. Meteorol. Soc.*, **90**, S22–S23.
Knight, J. R., C. K. Folland, and A. A. Scaife, 2006: Climate impacts of the Atlantic Multidecadal Oscillation. *Geophys. Res. Lett.*, **33**, L17706.
Knight, J. R., R. J. Allan, C. K. Folland, M. Vellinga, and M. E. Mann, 2005: A signature of persistent natural thermohaline circulation cycles in observed climate. *Geophys. Res. Lett.*, **32**, L20708.
Knutson, T. R., F. Zeng, and A. T. Wittenberg, 2013: Multi-model assessment of regional surface temperature trends. *J. Clim.*, doi:10.1175/JCLI-D-12-00567.1.
Knutson, T. R., et al., 2010: Tropical cyclones and climate change. *Nature Geosci.*, **3**, 157–163.
Knutti, R., 2008: Why are climate models reproducing the observed global surface warming so well? *Geophys. Res. Lett.*, **35**, L18704.
Knutti, R., and G. C. Hegerl, 2008: The equilibrium sensitivity of the Earth's temperature to radiation changes. *Nature Geosci.*, **1**, 735–743.
Knutti, R., and L. Tomassini, 2008: Constraints on the transient climate response from observed global temperature and ocean heat uptake. *Geophys. Res. Lett.*, **35**, L09701.
Knutti, R., S. Krähenmann, D. J. Frame, and M. R. Allen, 2008: Comment on "Heat capacity, time constant, and sensitivity of Earth's climate system" by S. E. Schwartz. *J. Geophys. Res. Atmos.*, **113**, D15103.
Kobashi, T., D. T. Shindell, K. Kodera, J. E. Box, T. Nakaegawa, and K. Kawamura, 2013: On the origin of multidecadal to centennial Greenland temperature anomalies over the past 800 yr. *Clim. Past*, **9**, 583–596.
Kobayashi, T., K. Mizuno, and T. Suga, 2012: Long-term variations of surface and intermediate waters in the southern Indian Ocean along 32°S. *J. Oceanogr.*, **68**, 243–265.
Kodama, C., and T. Iwasaki, 2009: Influence of the SST rise on baroclinic instability wave activity under an aquaplanet condition. *J. Atmos. Sci.*, **66**, 2272–2287.
Kodera, K., 2004: Solar influence on the Indian Ocean monsoon through dynamical processes. *Geophys. Res. Lett.*, **31**, L24209.
Kodera, K., 2006: The role of dynamics in solar forcing. *Space Sci. Rev.*, **23** 319–330.
Kodera, K., and Y. Kuroda, 2002: Dynamical response to the solar cycle. *J. Geophys. Res. Atmos.*, **107**, 4749.
Kodera, K., K. Coughlin, and O. Arakawa, 2007: Possible modulation of the connection between the Pacific and Indian Ocean variability by the solar cycle. *Geophys. Res. Lett.*, **34**, L03710.
Koehler, P., R. Bintanja, H. Fischer, F. Joos, R. Knutti, G. Lohmann, and V. Masson-Delmotte, 2010: What caused Earth's temperature variations during the last 800,000 years? Data-based evidence on radiative forcing and constraints on climate sensitivity. *Quat. Sci. Rev.*, **29**, 129–145.
Korhonen, H., K. S. Carslaw, P. M. Forster, S. Mikkonen, N. D. Gordon, and H. Kokkola, 2010: Aerosol climate feedback due to decadal increases in Southern Hemisphere wind speeds. *Geophys. Res. Lett.*, **37**, L02805.
Krakauer, N. Y., and I. Fung, 2008: Mapping and attribution of change in streamflow in the coterminous United States. *Hydrol. Earth Syst. Sci.*, **12**, 1111–1120.

Kuhlbrodt, T., and J. M. Gregory, 2012: Ocean heat uptake and its consequences for the magnitude of sea level rise and climate change. *Geophys. Res. Lett.*, **39**, L18608.

Kunkel, K. E., et al., 2008: Observed changes in weather and climate extremes. In: *Weather and Climate Extremes in a Changing Climate. Regions of Focus: North America, Hawaii, Caribbean, and U.S. Pacific Islands* [G. A. M. T. R. Karl, C. D. Miller, S. J. Hassol, A. M. Waple, and W. L. Murray (eds.)]. A Report by the U.S. Climate Change Science Program and the Subcommittee on Global Change Research, Washington, DC, pp. 35–80.

Kwok, R., and N. Untersteiner, 2011: The thinning of Arctic sea ice. *Physics Today*, **64**, 36–41.

Kwok, R., G. F. Cunningham, M. Wensnahan, I. Rigor, H. J. Zwally, and D. Yi, 2009: Thinning and volume loss of the Arctic Ocean sea ice cover: 2003–2008. *J. Geophys. Res.J. Geophys. Res. Oceans*, **114**, C07005.

L'Heureux, M., A. H. Butler, B. Jha, A. Kumar, and W. Q. Wang, 2010: Unusual extremes in the negative phase of the Arctic Oscillation during 2009. *Geophys. Res. Lett.*, **37**, L10704.

Lamarque, J.-F., et al., 2010: Historical (1850–2000) gridded anthropogenic and biomass burning emissions of reactive gases and aerosols: Methodology and application. *Atmos. Chem. Phys.*, **10**, 7017–7039.

Landrum, L., B. L. Otto-Bliesner, E. R. Wahl, A. Conley, P. J. Lawrence, N. Rosenbloom, and H. Teng, 2013: Last millennium climate and its variability in CCSM4. *J. Clim.*, **26**, 1085–1111.

Langen, P. L., and V. A. Alexeev, 2007: Polar amplification as a preferred response in an idealized aquaplanet GCM. *Clim. Dyn.*, **29**, 305–317.

Latif, M., et al., 2004: Reconstructing, monitoring, and predicting multidecadal-scale changes in the North Atlantic thermohaline circulation with sea surface temperature. *J. Clim.*, **17**, 1605–1614.

Laxon, S. W., et al., 2013: CryoSat-2 estimates of Arctic sea ice thickness and volume. *Geophys. Res. Lett.*, **40**, 732–737.

Lean, J. L., 2006: Comment on "Estimated solar contribution to the global surface warming using the ACRIM TSI satellite composite" by N. Scafetta and B. J. West. *Geophys. Res. Lett.*, **33**, L15701.

Lean, J. L., and D. H. Rind, 2008: How natural and anthropogenic influences alter global and regional surface temperatures: 1889 to 2006. *Geophys. Res. Lett.*, **35**, L18701.

Lean, J. L., and D. H. Rind, 2009: How will Earth's surface temperature change in future decades? *Geophys. Res. Lett.*, **36**, L15708.

Leclercq, P. W., and J. Oerlemans, 2011: Global and hemispheric temperature reconstruction from glacier length fluctuations. *Clim. Dyn.*, **38**, 1065–1079.

Ledoit, O., and M. Wolf, 2004: A well-conditioned estimator for large-dimensional covariance matrices. *J. Multivar. Anal.*, **88**, 365–411.

Legras, B., O. Mestre, E. Bard, and P. Yiou, 2010: A critical look at solar-climate relationships from long temperature series. *Clim. Past*, **6**, 745–758.

Leibensperger, E. M., et al., 2012: Climatic effects of 1950–2050 changes in US anthropogenic aerosols—Part 1: Aerosol trends and radiative forcing. *Atmos. Chem. Phys.*, **12**, 3333–3348.

Levitus, S., J. I. Antonov, T. P. Boyer, R. A. Locarnini, H. E. Garcia, and A. V. Mishonov, 2009: Global ocean heat content 1955–2008 in light of recently revealed instrumentation problems. *Geophys. Res. Lett.*, **36**, L07608.

Lewis, N., 2013: An objective Bayesian, improved approach for applying optimal fingerprint techniques to estimate climate sensitivity. *J. Clim.*, doi:10.1175/JCLI-D-12-00473.1.

Li, J. P., and J. L. X. L. Wang, 2003: A modified zonal index and its physical sense. *Geophys. Res. Lett.*, **30**, 1632.

Libardoni, A. G., and C. E. Forest, 2011: Sensitivity of distributions of climate system properties to the surface temperature dataset. *Geophys. Res. Lett.*, **38**, L22705.

Libardoni, A. G., and C. E. Forest, 2013: Correction to "Sensitivity of distributions of climate system properties to the surface temperature dataset". *Geophys. Res. Lett.*, doi:10.1002/grl.50480.

Lin, B., et al., 2010a: Estimations of climate sensitivity based on top-of-atmosphere radiation imbalance. *Atmos. Chem. Phys.*, **10**, 1923–1930.

Lin, P., Q. A. Fu, S. Solomon, and J. M. Wallace, 2010b: Temperature trend patterns in Southern Hemisphere high latitudes: Novel indicators of stratospheric change *J. Clim.*, **22**, 6325–6341.

Lindsay, R. W., J. Zhang, A. Schweiger, M. Steele, and H. Stern, 2009: Arctic sea ice retreat in 2007 follows thinning trend. *J. Clim.*, **22**, 165–176.

Lindzen, R. S., and Y. S. Choi, 2009: On the determination of climate feedbacks from ERBE data. *Geophys. Res. Lett.*, **36**, L16705.

Lindzen, R. S., and Y. S. Choi, 2011: On the observational determination of climate sensitivity and its implications. *Asia-Pacific J. Atmos. Sci.*, **47**, 377–390.

Liu, C., R. P. Allan, and G. J. Huffman, 2012: Co-variation of temperature and precipitation in CMIP5 models and satellite observations. *Geophys. Res. Lett.*, **39**, L13803.

Lockwood, M., 2008: Recent changes in solar outputs and the global mean surface temperature. III. Analysis of contributions to global mean air surface temperature rise. *Proc. R. Soc. London A*, **464**, 1387–1404.

Lockwood, M., 2012: Solar influence on global and regional climates. *Surv. Geophys.*, **33**, 503–534.

Lockwood, M., and C. Fröhlich, 2007: Recent oppositely directed trends in solar climate forcings and the global mean surface air temperature *Proc. R. Soc. London A*, **463**, 2447–2460.

Lockwood, M., and C. Fröhlich, 2008: Recent oppositely directed trends in solar climate forcings and the global mean surface air temperature: II. Different reconstructions of the total solar irradiance variation and dependence on response time scale. *Proc. R. Soc. London A*, **464**, 1367–1385.

Lockwood, M., R. G. Harrison, T. Woollings, and S. K. Solanki, 2010: Are cold winters in Europe associated with low solar activity? *Environ. Res. Lett.*, **5**, 024001.

Loehle, C., and N. Scaffetta, 2011: Climate change attribution using empirical decomposition of climatic data. *Open Atmos. Sci. J.*, **5**, 74–86.

Lott, F. C., et al., 2013: Models versus radiosondes in the free atmosphere: A new detection and attribution analysis of temperature. *J. Geophys. Res. Atmos.*, **118**, 2609–2619.

Lu, J., G. A. Vecchi, and T. Reichler, 2007: Expansion of the Hadley cell under global warming. *Geophys. Res. Lett.*, **34**, L06805.

Lu, J., G. Chen, and D. M. W. Frierson, 2008: Response of the zonal mean atmospheric circulation to El Nino versus global warming. *J. Clim.*, **21**, 5835–5851.

Lu, J., C. Deser, and T. Reichler, 2009: Cause of the widening of the tropical belt since 1958. *Geophys. Res. Lett.*, **36**, L03803.

Lucas, C., H. Nguyen, and B. Timbal, 2012: An observational analysis of Southern Hemisphere tropical expansion. *J. Geophys. Res. Atmos.*, **117**, D17112.

Lunt, D. J., A. M. Haywood, G. A. Schmidt, U. Salzmann, P. J. Valdes, and H. J. Dowsett, 2010: Earth system sensitivity inferred from Pliocene modelling and data. *Nature Geosci.*, **3**, 60–64.

Luterbacher, J., D. Dietrich, E. Xoplaki, M. Grosjean, and H. Wanner, 2004: European seasonal and annual temperature variability, trend, and extremes since 1500. *Science*, **303**, 1499–1503.

Mahajan, S., R. Zhang, and T. L. Delworth, 2011: Impact of the Atlantic Meridional Overturning Circulation (AMOC) on Arctic surface air temperature and sea ice variability. *J. Clim.*, **24**, 6573–6581.

Mahlstein, I., and R. Knutti, 2012 September Arctic sea ice predicted to disappear for 2oC global warming above present. *J. Geophys. Res. Atmos.*, **117**, D06104.

Mahlstein, I., G. Hegerl, and S. Solomon, 2012: Emerging local warming signals in observational data. *Geophys. Res. Lett.*, **39**, L21711.

Mahlstein, I., R. Knutti, S. Solomon, and R. W. Portmann, 2011: Early onset of significant local warming in low latitude countries. *Environ. Res. Lett.*, **6**, 034009.

Manabe, S., and R. T. Wetherald, 1975: The effects of doubling the $CO_2$ concentration on the climate of a General Circulation Model. *J. Atmos. Sci.*, **32**, 3–15.

Mankoff, K. D., S. S. Jacobs, S. M. Tulaczyk, and S. E. Stammerjohn, 2012: The role of Pine Island Glacier ice shelf basal channels in deep water upwelling, polynyas and ocean circulation in Pine Island Bay, Antarctica. *Ann. Glaciol.*, **53**, 123–128.

Mann, M. E., 2011: On long range temperature dependence in global surface temperature series. *Clim. Change*, **107**, 267–276.

Mann, M. E., and K. A. Emanuel, 2006: Atlantic hurricane trends linked to climate change. *Eos Trans. Am. Geophys. Union*, **87**, 233–238.

Mann, M. E., Z. H. Zhang, M. K. Hughes, R. S. Bradley, S. K. Miller, S. Rutherford, and F. B. Ni, 2008: Proxy-based reconstructions of hemispheric and global surface temperature variations over the past two millennia. *Proc. Natl. Acad. Sci. U.S.A.*, **105**, 13252–13257.

Mann, M. E., et al., 2009: Global signatures and dynamical origins of the Little Ice age and medieval climate anomaly. *Science*, **326**, 1256–1260.

Marcott, S. A., J. D. Shakun, P. U. Clark, and A. C. Mix, 2013: A reconstruction of regional and global temperature for the past 11,300 years. *Science*, **339**, 1198–1201

Marzeion, B., and A. Nesje, 2012: Spatial patterns of North Atlantic Oscillation influence on mass balance variability of European glaciers. *Cryosphere*, **6**, 661–673.

Maslanik, J. A., C. Fowler, J. Stroeve, S. Drobot, J. Zwally, D. Yi, and W. Emery, 2007: A younger, thinner Arctic ice cover: Increased potential for rapid, extensive sea-ice loss. *Geophys. Res. Lett.*, **34**, L24501.

Maslowski, W., J. C. Kinney, M. Higgins, and A. Roberts, 2012: The future of Arctic sea ice. *Annu. Rev. Earth Planet. Sci.*, **40**, 625–654.

Massey, N., T. Anna, R. C., F. E. L. Otto, S. Wilson, R. G. Jones, and M. R. Allen, 2012: Have the odds of warm November temperatures and of cold December temperatures in central england changed? *Bull. Am. Meteorol. Soc.*, **93**, 1057–1059.

Mastrandrea, M. D., et al., 2011: Guidance note for lead authors of the IPCC Fifth Assessment Report on consistent treatment of uncertainties. Intergovernmental Panel on Climate Change (IPCC), Geneva, Switzerland.

Matthes, K., Y. Kuroda, K. Kodera, and U. Langematz, 2006: Transfer of the solar signal from the stratosphere to the troposphere: Northern winter. *J. Geophys. Res. Atmos.*, **111** D06108.

Matthews, H. D., N. P. Gillett, P. A. Stott, and K. Zickfeld, 2009: The proportionality of global warming to cumulative carbon emissions. *Nature*, **459**, 829–U3.

Mazzarella, A., and N. Scafetta, 2012: Evidences for a quasi 60-year North Atlantic Oscillation since 1700 and its meaning for global climate change. *Theor. Appl. Climatol.*, **107**, 599–609.

McCracken, K. G., and J. Beer, 2007: Long-term changes in the cosmic ray intensity at Earth, 1428–2005. *J. Geophys. Res. Space Physics*, **112**, A10101.

McKitrick, R., and L. Tole, 2012: Evaluating explanatory models of the spatial pattern of surface climate trends using model selection and Bayesian averaging methods. *Clim. Dyn.*, **39**, 2867–2882.

McKitrick, R., S. McIntyre, and C. Herman, 2010: Panel and multivariate methods for tests of trend equivalence in climate data series. *Atmos. Sci. Lett.*, **11**, 270–277.

McLandress, C., J. Perlwitz, and T. G. Shepherd, 2012: Comment on "Tropospheric temperature response to stratospheric ozone recovery in the 21st century" by Hu et al. , 2011. *Atmos. Chem. Phys.*, **12**, 2533–2540.

McLandress, C., T. G. Shepherd, J. F. Scinocca, D. A. Plummer, M. Sigmond, A. I. Jonsson, and M. C. Reader, 2011: Separating the dynamical effects of climate change and ozone depletion. Part II: Southern Hemisphere troposphere. *J. Clim.*, **24**, 1850–1868.

Mecking, S., M. J. Warner, and J. L. Bullister, 2006: Temporal changes in pCFC-12 ages and AOU along two hydrographic sections in the eastern subtropical North Pacific. *Deep-Sea Res. Pt. I*, **53**, 169–187.

Meehl, G. A., and J. M. Arblaster, 2009: A lagged warm event-like response to peaks in solar forcing in the Pacific region. *J. Clim.*, **22**, 3647–3660.

Meehl, G. A., J. M. Arblaster, and C. Tebaldi, 2007a: Contributions of natural and anthropogenic forcing to changes in temperature extremes over the U.S. *Geophys. Res. Lett.*, **34**, L19709.

Meehl, G. A., J. M. Arblaster, G. Branstator, and H. van Loon, 2008: A coupled air-sea response mechanism to solar forcing in the Pacific region. *J. Clim.*, **21** 2883–2897.

Meehl, G. A., W. M. Washington, T. M. L. Wigley, J. M. Arblaster, and A. Dai, 2003: Solar and greenhouse gas forcing and climate response in the 20th century. *J. Clim.*, **16** 426–444.

Meehl, G. A., J. M. Arblaster, K. Matthes, F. Sassi, and H. van Loon, 2009: Amplifying the Pacific climate system response to a small 11-747year solar cycle forcing. *Science*, **325** 1114–1118.

Meehl, G. A., et al., 2007b: Global climate projections. In: *Climate Change 2007: The Physical Science Basis. Contribution of Working Group I to the Fourth Assessment Report of the Intergovernmental Panel on Climate Change* [Solomon, S., D. Qin, M. Manning, Z. Chen, M. Marquis, K. B. Averyt, M. Tignor and H. L. Miller (eds.)] Cambridge University Press, Cambridge, United Kingdom and New York, NY, USA, pp. 747–846.

Meinshausen, M., et al., 2009: Greenhouse-gas emission targets for limiting global warming to 2 °C. *Nature*, **458**, 1158–1162.

Merrifield, M., and M. Maltrud, 2011: Regional sea level trends due to a Pacific trade wind intensification. *Geophys. Res. Lett.*, **38**, L21605.

Meyssignac, B., D. Salas y Melia, M. Becker, W. Llovel, and A. Cazenave, 2012: Tropical Pacific spatial trend patterns in observed sea level: Internal variability and/or anthropogenic signature? *Clim. Past*, **8**, 787–802.

Miller, G. H., R. B. Alley, J. Brigham-Grette, J. J. Fitzpatrick, L. Polyak, M. C. Serreze, and J. W. C. White, 2010: Arctic amplification: Can the past constrain the future? *Quat. Sci. Rev.*, **29**, 1779–1790.

Miller, G. H., et al., 2012: Abrupt onset of the Little Ice Age triggered by volcanism and sustained by sea-ice/ocean feedbacks. *Geophys. Res. Lett.*, **39**, L02708.

Miller, R. L., G. A. Schmidt, and D. T. Shindell, 2006: Forced annular variations in the 20th century intergovernmental panel on climate change fourth assessment report models. *J. Geophys. Res. Atmos.*, **111**, D18101.

Mills, T. C., 2009: How robust is the long-run relationship between temperature and radiative forcing? *Clim. Change*, **94**, 351–361.

Min, S.-K., and A. Hense, 2006: A Bayesian assessment of climate change using multimodel ensembles. Part I: Global mean surface temperature. *J. Clim.*, **19**, 3237–3256.

Min, S.-K., and A. Hense, 2007: A Bayesian assessment of climate change using multimodel ensembles. Part II: Regional and seasonal mean surface temperatures. *J. Clim.*, **20**, 2769–2790.

Min, S.-K., and S.-W. Son, 2013: Multi-model attribution of the Southern Hemisphere Hadley cell widening: Major role of ozone depletion. *J. Geophys. Res. Atmos.*, **118**, 3007–3015.

Min, S.-K., X. B. Zhang, and F. Zwiers, 2008a: Human-induced arctic moistening. *Science*, **320**, 518–520.

Min, S.-K., X. B. Zhang, F. W. Zwiers, and T. Agnew, 2008b: Human influence on Arctic sea ice detectable from early 1990s onwards. *Geophys. Res. Lett.*, **35**, L21701.

Min, S.-K., X. Zhang, F. W. Zwiers, and G. C. Hegerl, 2011: Human contribution to more intense precipitation extremes. *Nature*, **470**, 378–381.

Min, S.-K., X. Zhang, F. W. Zwiers, P. Friederichs, and A. Hense, 2008c: Signal detectability in extreme precipitation changes assessed from twentieth century climate simulations. *Clim. Dyn.*, **32**, 95–111.

Min, S.-K., X. Zhang, F. Zwiers, H. Shiogama, Y.-S. Tung, and M. Wehner, 2013: Multi-model detection and attribution of extreme temperature changes. *J. Clim.*, doi:10.1175/JCLI-D-12-00551.w.

Misios, S., and H. Schmidt, 2012: Mechanisms involved in the amplification of the 11-yr solar cycle signal in the Tropical Pacific ocean. *J. Clim.*, **25**, 5102–5118.

Mitchell, D. M., P. A. Stott, L. J. Gray, F. C. Lott, N. Butchart, S. C. Hardiman, and S. M. Osprey, 2013: The impact of stratospheric resolution on the detectability of climate change signals in the free atmosphere. *Geophys. Res. Lett.*, **40**, 937–942.

Miyazaki, C., and T. Yasunari, 2008: Dominant interannual and decadal variability of winter surface air temperature over Asia and the surrounding oceans. *J. Clim.*, **21**, 1371–1386.

Moberg, A., D. M. Sonechkin, K. Holmgren, N. M. Datsenko, and W. Karlen, 2005: Highly variable Northern Hemisphere temperatures reconstructed from low- and high-resolution proxy data. *Nature*, **433**, 613–617.

Mölg, T., N. J. Cullen, D. R. Hardy, M. Winkler, and G. Kaser, 2009: Quantifying climate change in the tropical midtroposphere over East Africa from glacier shrinkage on Kilimanjaro. *J. Clim.*, **22**, 4162–4181.

Mölg, T., M. Großhauser, A. Hemp, M. Hofer, and B. Marzeion, 2012: Limited forcing of glacier loss through land-cover change on Kilimanjaro. *Nature Clim. Change*, **2**, 254–258.

Morak, S., G. C. Hegerl, and J. Kenyon, 2011: Detectable regional changes in the number of warm nights. *Geophys. Res. Lett.*, **38**, L17703.

Morak, S., G. C. Hegerl, and N. Christidis, 2013: Detectable changes in the frequency of temperature extremes. *J. Clim.*, **26**, 1561–1574.

Morgenstern, O., et al., 2010: Anthropogenic forcing of the Northern Annular Mode in CCMVal-2 models. *J. Geophys. Res. Atmos.*, **115**, D00M03.

Morice, C. P., J. J. Kennedy, N. A. Rayner, and P. D. Jones, 2012: Quantifying uncertainties in global and regional temperature change using an ensemble of observational estimates: The HadCRUT4 data set. *J. Geophys. Res. Atmos.*, **117**, D08101.

Murphy, D. M., and P. M. Forster, 2010: On the accuracy of deriving climate feedback parameters from correlations between surface temperature and outgoing radiation. *J. Clim.*, **23** 4983–4988.

Murphy, D. M., S. Solomon, R. W. Portmann, K. H. Rosenlof, P. M. Forster, and T. Wong, 2009: An observationally based energy balance for the Earth since 1950. *J. Geophys. Res. Atmos.*, **114**, D17107.

Nagato, Y., and H. L. Tanaka, 2012: Global warming trend without the contribution from decadal variability of the Arctic oscillation. *Polar Sci.*, **6**, 15–22.

Nakanowatari, T., K. I. Ohshima, and M. Wakatsuchi, 2007: Warming and oxygen decrease of intermediate water in the northwestern North Pacific, originating from the Sea of Okhotsk, 1955–2004. *Geophys. Res. Lett.*, **34**, L04602.

National Research Council, 2012: *The Effects of Solar Variability on Earth's Climate: A Workshop Report.* The National Academies Press, Washington, DC, 70 pp.

Nesje, A., O. Lie, and S. O. Dahl, 2000: Is the North Atlantic Oscillation reflected in Scandinavian glacier mass balance records? *J. Quat. Sci.*, **15**, 587–601.

Nghiem, S. V., I. G. Rigor, D. K. Perovich, P. Clemente-Colon, J. W. Weatherly, and G. Neumann, 2007: Rapid reduction of Arctic perennial sea ice. *Geophys. Res. Lett.*, **34**, L19504.

Nguyen, H., B. Timbal, A. Evans, C. Lucas, and I. Smith, 2013: The Hadley circulation in reanalyses: Climatology, variability and change. *J. Clim.*, **26**, 3357–3376.

Noake, K., D. Polson, G. Hegerl, and X. Zhang, 2012: Changes in seasonal land precipitation during the latter 20th Century. *Geophys. Res. Lett.*, **39**, L03706.

North, G. R., and M. J. Stevens, 1998: Detecting climate signals in the surface temperature record. *J. Clim.*, **11**, 563–577.

Notz, D., and J. Marotzke, 2012: Observations reveal external driver for Arctic sea-ice retreat. *Geophys. Res. Lett.*, **39**, L08502.

Nussbaumer, S. U., and H. J. Zumbühl, 2012: The Little Ice Age history of the Glacier des Bossons (Mont Blanc massif, France): A new high-resolution glacier length curve based on historical documents. *Clim. Change*, **111**, 301–334.

O'Gorman, P. A., and T. Schneider, 2008: Energy of midlatitude transient eddies in idealized simulations of changed climates. *J. Clim.*, **21**, 5797–5806.

O'Gorman, P. A., 2010: Understanding the varied response of the extratropical storm tracks to climate change. *Proc. Natl. Acad. Sci. U.S.A.*, **107**, 19176–19180.

Oerlemans, J., 2005: Extracting a climate signal from 169 glacier records. *Science*, **308**, 675–677.

Olson, R., R. Sriver, M. Goes, N. M. Urban, H. D. Matthews, M. Haran, and K. Keller, 2012: A climate sensitivity estimate using Bayesian fusion of instrumental observations and an Earth System model. *J. Geophys. Res. Atmos.*, **117**, D04103.

Ono, T., T. Midorikawa, Y. W. Watanabe, K. Tadokoro, and T. Saino, 2001: Temporal increases of phosphate and apparent oxygen utilization in the subsurface waters of western subarctic Pacific from 1968 to 1998. *Geophys. Res. Lett.*, **28**, 3285–3288.

Otto-Bliesner, B. L., et al., 2009: A comparison of PMIP2 model simulations and the MARGO proxy reconstruction for tropical sea surface temperatures at last glacial maximum. *Clim. Dyn.*, **32**, 799–815.

Otto, A., et al., 2013: Energy budget constraints on climate response. *Nature Geosci.*, **6**, 415–416.

Otto, F. E. L., N. Massey, G. J. van Oldenborgh, R. G. Jones, and M. R. Allen, 2012: Reconciling two approaches to attribution of the 2010 Russian heat wave. *Geophys. Res. Lett.*, **39**, L04702.

Overland, J. E., 2009: The case for global warming in the Arctic. In: *Influence of Climate Change on the Changing Arctic and Sub-Arctic Conditions. NATO Science for Peace and Security Series C: Environmental Security* [J. C. J. Nihoul and A. G. Kostianoy (eds.)]. Springer Science+Business Media, Dordrecht, Netherlands, pp. 13–23.

Overland, J. E., and M. Wang, 2013: When will the summer arctic be nearly sea ice free? *Geophys. Res. Lett.*, doi:10.1002/grl.50316.

Overland, J. E., M. Wang, and S. Salo, 2008: The recent Arctic warm period. *Tellus A*, **60**, 589–597.

Overland, J. E., K. R. Wood, and M. Wang, 2011: Warm Arctic-cold continents: Climate impacts of the newley open Arctic sea. *Polar Res.*, **30**, 15787.

Overland, J. E., J. A. Francis, E. Hanna, and W. M., 2012: The recent shift in early summer Arctic atmospheric circulation. *Geophys. Res. Lett.*, **39**, L19804.

Oza, S. R., R. K. K. Singh, N. K. Vyas, and A. Sarkar, 2011a: Spatio-Temporal analysis of melting onset dates of sea–ice in the Arctic. *Indian J. Geo-Mar. Sci.*, **40**, 497–501.

Oza, S. R., R. K. K. Singh, A. Srivastava, M. K. Dash, I. M. L. Das, and N. K. Vyas, 2011b: Inter-annual variations observed in spring and summer antarctic sea ice extent in recent decade. *Mausam*, **62**, 633–640.

Padilla, L. E., G. K. Vallis, and C. W. Rowley, 2011: Probabilistic estimates of transient climate sensitivity subject to uncertainty in forcing and natural variability. *J. Clim.*, **24**, 5521–5537.

Pagani, M., K. Caldeira, R. Berner, and D. J. Beerling, 2009: The role of terrestrial plants in limiting atmospheric $CO_2$ decline over the past 24 million years. *Nature*, **460**, 85–88.

PAGES 2k Consortium, 2013: Continental-scale temperature variability during the past two millennia. *Nature Geosci.*, **6**, 339–346.

Palastanga, V., G. van der Schrier, S. L. Weber, T. Kleinen, K. R. Briffa, and T. J. Osborn, 2011: Atmosphere and ocean dynamics: Contributors to the Little Ice Age and Medieval Climate Anomaly. *Clim. Dyn.*, **36**, 973–987.

Paleosens Members, 2012: Making sense of palaeoclimate sensitivity. *Nature*, **491**, 683–691.

Pall, P., et al., 2011: Anthropogenic greenhouse gas contribution to UK autumn flood risk. *Nature*, **470**, 382–385.

Palmer, M. D., S. A. Good, K. Haines, N. A. Rayner, and P. A. Stott, 2009: A new perspective on warming of the global oceans. *Geophys. Res. Lett.*, **36**, L20709.

Penner, J. E., M. Wang, A. Kumar, L. Rotstayn, and B. Santer, 2007: Effect of black carbon on mid-troposphere and surface temperature trends. In: *Human-Induced Climate Change: An Interdisciplinary Assessment* [M. Schlesinger, et al. (ed.)], Cambridge University Press, Cambridge, United Kingdom, and New York, NY, USA, pp. 18–33.

Peterson, T. C., P. A. Stott, and S. Herring, 2012: Explaining extreme events of 2011 from a climate perspective. *Bull. Am. Meteorol. Soc.*, **93**, 1041–1067.

Pierce, D. W., T. P. Barnett, B. D. Santer, and P. J. Gleckler, 2009: Selecting global climate models for regional climate change studies. *Proc. Natl. Acad. Sci. U.S.A.*, **106**, 8441–8446.

Pierce, D. W., P. J. Gleckler, T. P. Barnett, B. D. Santer, and P. J. Durack, 2012: The fingerprint of human-induced changes in the ocean's salinity and temperature fields. *Geophys. Res. Lett.*, **39**, L21704.

Pierce, D. W., T. P. Barnett, K. AchutaRao, P. Gleckler, J. Gregory, and W. Washington, 2006: Anthropogenic warming of the oceans: Observations and model results. *J. Clim.*, **19**, 1873–1900.

Pierce, D. W., et al., 2008: Attribution of declining Western U.S. snowpack to human effects. *J. Clim.*, **21**, 6425–6444.

Pitman, A. J., et al., 2009: Uncertainties in climate responses to past land cover change: First results from the LUCID intercomparison study. *Geophys. Res. Lett.*, **36**, L14814.

Po-Chedley, S., and Q. Fu, 2012: Discrepancies in tropical upper tropospheric warming between atmospheric circulation models and satellites. *Environ. Res. Lett.*, **7**, 044018.

Polson, D., G. C. Hegerl, X. Zhang, and T. J. Osborn, 2013: Causes of robust seasonal land precipitation changes. *J. Clim.*, doi:10.1175/JCLI-D-12-00474.1.

Polvani, L. M., D. W. Waugh, G. J. P. Correa, and S. W. Son, 2011: Stratospheric ozone depletion: The main driver of twentieth-century atmospheric circulation changes in the southern hemisphere. *J. Clim.*, **24**, 795–812.

Polyakov, I. V., J. E. Walsh, and R. Kwok, 2012: Recent changes of Arctic multiyear sea ice coverage and the likely causes. *Bull. Am. Meteorol. Soc.*, **93**, 145–151.

Polyakov, I. V., U. S. Bhatt, H. L. Simmons, D. Walsh, J. E. Walsh, and X. Zhang, 2005: Multidecadal variability of North Atlantic temperature and salinity during the twentieth century. *J. Clim.*, **18**, 4562–4581.

Polyakov, I. V., et al., 2003: Variability and trends of air temperature and pressure in the maritime Arctic, 1875–2000. *J. Clim.*, **16**, 2067–2077.

Pongratz, J., C. H. Reick, T. Raddatz, and M. Claussen, 2009: Effects of anthropogenic land cover change on the carbon cycle of the last millennium. *Global Biogeochem. Cycles*, **23**, GB4001.

Pritchard, H. D., S. R. M. Ligtenberg, H. A. Fricker, D. G. Vaughan, M. R. van den Broeke, and L. Padman, 2012: Antarctic ice sheet loss driven by basal melting of ice shelves. *Nature*, **484**, 502–505.

Pueyo, S., 2012: Solution to the paradox of climate sensitivity. *Clim. Change*, **113**, 163–179

Quadrelli, R., and J. M. Wallace, 2004: A simplified linear framework for interpreting patterns of Northern Hemisphere wintertime climate variability. *J. Clim.*, **17**, 3728–3744.

Rahmstorf, S., and D. Coumou, 2011: Increase of extreme events in a warming world. *Proc. Natl. Acad. Sci. U.S.A.*, **108**, 17905–17909.

Ramaswamy, V., M. D. Schwarzkopf, W. J. Randel, B. D. Santer, B. J. Soden, and G. L. Stenchikov, 2006: Anthropogenic and natural influences in the evolution of lower stratospheric cooling. *Science*, **311**, 1138–1141.

Ramsay, H. A., and A. H. Sobel, 2011: The effects of relative and absolute sea surface temperature on tropical cyclone potential intensity using a single column model. *J. Clim.*, **24**, 183–193.

Randel, W. J., et al., 2009: An update of observed stratospheric temperature trends. *J. Geophys. Res. Atmos.*, **114**, D02107.

Ray, E. A., et al., 2010: Evidence for changes in stratospheric transport and mixing over the past three decades based on multiple data sets and tropical leaky pipe analysis. *J. Geophys. Res. Atmos.*, **115**, D21304.

Rea, W., M. Reale, and J. Brown, 2011: Long memory in temperature reconstructions. *Clim. Change*, **107**, 247–265.

Reichert, B. K., L. Bengtsson, and J. Oerlemans, 2002: Recent glacier retreat exceeds internal variability. *J. Clim.*, **15**, 3069–3081.

Ribes, A., and L. Terray, 2013: Application of regularised optimal fingerprint analysis for attribution. Part II: Application to global near-surface temperature *Clim. Dyn.*, doi:10.1007/s00382-013-1736-6.

Ribes, A., J. M. Azais, and S. Planton, 2009: Adaptation of the optimal fingerprint method for climate change detection using a well-conditioned covariance matrix estimate. *Clim. Dyn.*, **33**, 707–722.

Ribes, A., J. M. Azais, and S. Planton, 2010: A method for regional climate change detection using smooth temporal patterns. *Clim. Dyn.*, **35**, 391–406.

Ribes, A., S. Planton, and L. Terray, 2013: Application of regularised optimal fingerprint for attribution. Part I: Method, properties and idealised analysis. *Clim. Dyn.*, doi:10.1007/s00382-013-1735-7.

Rind, D., J. Lean, J. Lerner, P. Lonergan, and A. Leboisitier, 2008: Exploring the stratospheric/troposheric response to solar forcing. *J. Geophys. Res. Atmos.*, **113** D24103.

Ring, M. J., D. Lindner, E. F. Cross, and M. E. Schlesinger, 2012: Causes of the global warming observed since the 19th century. atmospheric and climate sciences *Atmos. Clim. Sci.*, **2**, 401–415.

Roe, G. H., and M. B. Baker, 2007: Why is climate sensitivity so unpredictable? *Science*, **318**, 629–632.

Roe, G. H., and M. A. O'Neal, 2009: The response of glaciers to intrinsic climate variability: Observations and models of late-Holocene variations in the Pacific Northwest. *J. Glaciol.*, **55**, 839–854.

Roemmich, D., and J. Gilson, 2009: The 2004–2008 mean and annual cycle of temperature, salinity, and steric height in the global ocean from the Argo Program. *Prog. Oceanogr.*, **82**, 81–100.

Rogelj, J., M. Meinshausen, and R. Knutti, 2012: Global warming under old and new scenarios using IPCC climate sensitivity range estimates. *Nature Clim. Change*, **2**, 248–253.

Rohde, R., et al., 2013: A new estimate of the average Earth surface land temperature spanning 1753 to 2011. *Geoinf. Geostat. Overview*, **1**, 1.

Roscoe, H. K., and J. D. Haigh, 2007: Influences of ozone depletion, the solar cycle and the QBO on the Southern Annular Mode. *Q. J. R. Meteorol. Soc.*, **133**, 1855–1864.

Roy, I., and J. D. Haigh, 2010: Solar cycle signals in sea level pressure and sea surface temperature. *Atmos. Chem. Phys.*, **10** 3147–3153.

Roy, I., and J. D. Haigh, 2012: Solar cycle signals in the Pacific and the issue of timings. *J. Atmos. Sci.*, **69** 1446–1451.

Royer, D. L., 2008: Linkages between $CO_2$, climate, and evolution in deep time. *Proc. Natl. Acad. Sci. U.S.A.*, **105**, 407–408.

Royer, D. L., R. A. Berner, and J. Park, 2007: Climate sensitivity constrained by $CO_2$ concentrations over the past 420 million years. *Nature*, **446**, 530–532.

Rupp, D. E., P. W. Mote, N. L. Bindoff, P. A. Stott, and D. A. Robinson, 2013: Detection and attribution of observed changes in Northern Hemisphere spring snow cover. *J. Clim.*, doi:10.1175/JCLI-D-12-00563.1.

Rupp, D. E., P. W. Mote, N. Massey, J. R. Cameron, R. Jones, and M. R. Allen, 2012: Did human influence on climate make the 2011 Texas drought more probable? *Bull. Am. Meteorol. Soc.*, **93**, 1052–1054.

Sanso, B., and C. Forest, 2009: Statistical calibration of climate system properties. *J. R. Stat. Soc. C*, **58**, 485–503.

Santer, B. D., W. Bruggemann, U. Cubasch, K. Hasselmann, H. Hock, E. Maierreimer, and U. Mikolajewicz, 1994: Signal-to-noise analysis of time-dependent greenhouse warming experiments: 1. Pattern-analysis. *Clim. Dyn.*, **9**, 267–285.

Santer, B. D., et al., 2009: Incorporating model quality information in climate change detection and attribution studies. *Proc. Natl. Acad. Sci. U.S.A.*, **106** 14778–14783.

Santer, B. D., et al., 2007: Identification of human-induced changes in atmospheric moisture content. *Proc. Natl. Acad. Sci. U.S.A.*, **104**, 15248–15253.

Santer, B. D., et al., 2006: Forced and unforced ocean temperature changes in Atlantic and Pacific tropical cyclogenesis regions. *Proc. Natl. Acad. Sci. U.S.A.*, **103**, 13905–13910.

Santer, B. D., et al., 2013: Identifying human influences on atmospheric temperature. *Proc. Natl. Acad. Sci. U.S.A.*, **110**, 26–33.

Sato, M., J. E. Hansen, M. P. McCormick, and J. B. Pollack, 1993: Stratospheric aerosol optical depth, 1850–1990. *J. Geophys. Res. Atmos.*, **98**, 22987–22994.

Scafetta, N., and B. J. West, 2007: Phenomenological reconstructions of the solar signature in the Northern Hemisphere surface temperature records since 1600. *J. Geophys. Res. Atmos.*, **112**, D24S03.

Scheff, J., and D. M. W. Frierson, 2012a: Robust future precipitation declines in CMIP5 largely reflect the poleward explansion of the model subtropical dry zones. *Geophys. Res. Lett.*, **39**, L18704.

Scheff, J., and D. M. W. Frierson, 2012b: Twenty-first-century multimodel subtropical precipitation declines are mostly midlatitude shifts. *J. Clim.*, **25**, 4330–434.

Schlesinger, M. E., and N. Ramankutty, 1994: An oscillation in the global climate system of period 65–70 years. *Nature*, **367**, 723–726.

Schmidt, G., et al., 2012: Climate forcing reconstructions for use in PMIP simulations of the last millennium (v1.1). *Geosci. Model Dev.*, **5**, 185–191.

Schmidt, G. A., et al., 2011: Climate forcing reconstructions for use in PMIP simulations of the last millennium (v1.0). *Geosci. Model Dev.*, **4**, 33–45.

Schmittner, A., et al., 2011: Climate sensitivity estimated from temperature reconstructions of the last glacial maximum. *Science*, **334**, 1385–1388.

Schmittner, A., et al., 2012: Response to comment on "Climate sensitivity estimated from temperature reconstructions of the Last Glacial Maximum". *Science*, **337** 1294

Schneider, T., and I. M. Held, 2001: Discriminants of twentieth-century changes in earth surface temperatures. *J. Clim.*, **14** 249–254.

Schneider von Deimling, T., H. Held, A. Ganopolski, and S. Rahmstorf, 2006: Climate sensitivity estimated from ensemble simulations of glacial climate. *Clim. Dyn.*, **27**, 149–163.

Schnur, R., and K. I. Hasselmann, 2005: Optimal filtering for Bayesian detection and attribution of climate change. *Clim. Dyn.*, **24**, 45–55.

Schubert, S., et al., 2009: A US CLIVAR project to assess and compare the responses of global climate models to drought-related sst forcing patterns: Overview and results. *J. Clim.*, **22**, 5251–5272.

Schurer, A., G. Hegerl, M. E. Mann, S. F. B. Tett, and S. J. Phipps, 2013: Separating forced from chaotic climate variability over the past millennium. *J. Clim.*, doi:10.1175/JCLI-D-12-00826.1.

Schwartz, S. E., 2007: Heat capacity, time constant, and sensitivity of Earth's climate system. *J. Geophys. Res. Atmos.*, **112**, D24S05.

Schwartz, S. E., 2012: Determination of Earth's transient and equilibrium climate sensitivities from observations over the twentieth century: Strong dependence on assumed forcing. *Surv. Geophys.*, **33** 745–777.

Schwartz, S. E., R. J. Charlson, and H. Rodhe, 2007: Quantifying climate change—too rosy a picture? *Nature Rep. Clim. Change*, doi:10.1038/climate.2007.22, 23–24.

Schwartz, S. E., R. J. Charlson, R. A. Kahn, J. A. Ogren, and H. Rodhe, 2010: Why hasn't Earth warmed as much as expected? *J. Clim.*, **23**, 2453–2464.

Schweiger, A., R. Lindsay, J. Zhang, M. Steele, H. Stern, and R. Kwok, 2011: Uncertainty in modeled Arctic sea ice volume. *J. Geophys. Res.J. Geophys. Res. Oceans*, **116**, C00D06.

Screen, J. A., and I. Simmonds, 2010: Increasing fall-winter energy loss from the Arctic Ocean and its role in Arctic temperature amplification. *Geophys. Res. Lett.*, **37**, L16707.

Seager, R., N. Naik, and G. A. Vecchi, 2010: Thermodynamic and dynamic mechanisms for large-scale changes in the hydrological cycle in response to global warming. *J. Clim.*, **23**, 4651–4668.

Seager, R., Y. Kushnir, C. Herweijer, N. Naik, and J. Velez, 2005: Modeling of tropical forcing of persistent droughts and pluvials over western North America: 1856–2000. *J. Clim.*, **18**, 4065–4088.

Sedlacek, K., and R. Knutti, 2012: Evidence for external forcing on 20th-century climate from combined ocean atmosphere warming patterns. *Geophys. Res. Lett.*, **39**, L20708.

Seidel, D. J., and W. J. Randel, 2007: Recent widening of the tropical belt: Evidence from tropopause observations. *J. Geophys. Res. Atmos.*, **112**, D20113.

Seidel, D. J., Q. Fu, W. J. Randel, and T. J. Reichler, 2008: Widening of the tropical belt in a changing climate. *Nature Geosci.*, **1**, 21–24.

Seidel, D. J., N. P. Gillett, J. R. Lanzante, K. P. Shine, and P. W. Thorne, 2011: Stratospheric temperature trends: Our evolving understanding. *WIREs Clim. Change*, **2**, 592–616.

Seidel, D. J., Y. Zhang, A. Beljaars, J.-C. Golaz, A. R. Jacobson, and B. Medeiros, 2012: Climatology of the planetary boundary layer over the continental United States and Europe. *J. Geophys. Res. Atmos.*, **117**, D17106.

Semenov, V. A., 2008: Influence of oceanic inflow to the Barents Sea on climate variability in the Arctic region. *Doklady Earth Sci.*, **418**, 91–94.

Semmler, T., S. Varghese, R. McGrath, P. Nolan, S. L. Wang, P., and C. O'Dowd, 2008: Regional climate model simulations of NorthAtlantic cyclones: Frequency and intensity changes. *Clim. Res*, **36**, 1–16.

Seneviratne, S. I., 2012: Historical drought trends revisited. *Nature*, **491**, 338–339.

Seneviratne, S. I., et al., 2010: Investigating soil moisture-climate interactions in a changing climate: A review. *Earth Sci. Rev.*, **99**, 125–161.

Seneviratne, S. I., et al., 2012: Changes in climate extremes and their impacts on the natural physical environment. In: *Managing the Risks of Extreme Events and Disasters to Advance Climate Change Adaptation.* A Special Report of Working Groups I and II of the Intergovernmental Panel on Climate Change (IPCC) [C. B. Field et al. (eds.)]. Cambridge University Press, Cambridge, United Kingdom, and New York, NY, USA, pp. 109–230.

Serreze, M. C., and J. A. Francis, 2006: The arctic amplification debate. *Clim. Change*, **76**, 241–264.

Serreze, M. C., M. M. Holland, and J. Stroeve, 2007: Perspectives on the Arctic's shrinking sea-ice cover. *Science*, **315**, 1533–1536.

Serreze, M. C., A. P. Barrett, J. C. Stroeve, D. N. Kindig, and M. M. Holland, 2009: The emergence of surface-based Arctic amplification. *Cryosphere*, **3**, 9.

Sexton, D. M. H., J. M. Murphy, M. Collins, and M. J. Webb, 2012: Multivariate probabilistic projections using imperfect climate models part I: Outline of methodology. *Clim. Dyn.*, **38**, 2513–2542.

Sheffield, J., E. F. Wood, and M. Roderick, 2012: Little change in global drought over the past 60 years *Nature*, **491**, 435–438.

Shindell, D., and G. Faluvegi, 2009: Climate response to regional radiative forcing during the twentieth century. *Nature Geosci.*, **2**, 294–300.

Shindell, D., D. Rind, N. Balachandran, J. Lean, and J. Lonergan, 1999: Solar cycle variability, ozone, and climate. *Science*, **284**, 305–308.

Shindell, D. T., G. A. Schmidt, R. L. Miller, and D. Rind, 2001: Northern Hemisphere winter climate response to greenhouse gas, ozone, solar, and volcanic forcing. *J. Geophys. Res. Atmos.*, **106**, 7193–7210.

Shine, K. P., J. S. Fuglestvedt, K. Hailemariam, and N. Stuber, 2005: Alternatives to the global warming potential for comparing climate impacts of emissions of greenhouse gases. *Clim. Change*, **68**, 281–302.

Shiogama, H., T. Nagashima, T. Yokohata, S. A. Crooks, and T. Nozawa, 2006: Influence of volcanic activity and changes in solar irradiance on surface air temperatures in the early twentieth century. *Geophys. Res. Lett.*, **33**, L09702.

Shiogama, H., D. A. Stone, T. Nagashima, T. Nozawa, and S. Emori, 2012: On the linear additivity of climate forcing-response relationships at global and continental scales. *Int. J. Climatol.*, doi:10.1002/joc.3607.

Sigmond, M., and J. C. Fyfe, 2010: Has the ozone hole contributed to increased Antarctic sea ice extent? *Geophys. Rese. Lett.*, **37**, L18502.

Sigmond, M., M. C. Reader, J. C. Fyfe, and N. P. Gillett, 2011: Drivers of past and future Southern Ocean change: Stratospheric ozone versus greenhouse gas impacts. *Geophys. Res. Lett.*, **38**, L12601.

Simmons, A. J., K. M. Willett, P. D. Jones, P. W. Thorne, and D. P. Dee, 2010: Low-frequency variations in surface atmospheric humidity, temperature, and precipitation: Inferences from reanalyses and monthly gridded observational data sets. *J. Geophys. Res. Atmos.*, **115**, D01110

Skeie, R. B., T. K. Berntsen, G. Myhre, K. Tanaka, M. M. Kvalevåg, and C. R. Hoyle, 2011: Anthropogenic radiative forcing time series from pre-industrial times until 2010. *Atmos. Chem. Phys.*, **11**, 11827–11857.

Smirnov, D. A., and I. I. Mokhov, 2009: From Granger causality to long-term causality: Application to climatic data. *Phys. Rev. E*, **80**, 016208.

Sokolov, A., C. Forest, and P. Stone, 2010: Sensitivity of climate change projections to uncertainties in the estimates of observed changes in deep-ocean heat content. *Clim. Dyn.*, **34**, 735–745.

Solomon, S., P. J. Young, and B. Hassler, 2012: Uncertainties in the evolution of stratospheric ozone and implications for recent temperature changes in the tropical lower stratosphere. *Geophys. Res. Lett.*, **39**, L17706.

Solomon, S., et al., 2007: Technical Summary. In: *Climate Change 2007: The Physical Science Basis. Contribution of Working Group I to the Fourth Assessment Report of the Intergovernmental Panel on Climate Change* [Solomon, S., D. Qin, M. Manning, Z. Chen, M. Marquis, K. B. Averyt, M. Tignor and H. L. Miller (eds.)] Cambridge University Press, Cambridge, United Kingdom and New York, NY, USA, pp. 19–92.

Son, S. W., N. F. Tandon, L. M. Polvani, and D. W. Waugh, 2009: Ozone hole and Southern Hemisphere climate change. *Geophys. Res. Lett.*, **36**, L15705.

Son, S. W., et al., 2008: The impact of stratospheric ozone recovery on the Southern Hemisphere westerly jet. *Science*, **320**, 1486–1489.

Son, S. W., et al., 2010: Impact of stratospheric ozone on Southern Hemisphere circulation change: A multimodel assessment. *J. Geophys. Res. Atmos.*, **115**, D00M07.

SPARC CCMVal, 2010: *SPARC Report on the Evaluation of Chemistry-Climate Models.* SPARC Report No. 5, WCRP-132, WMO/TD-No. 1526, [V. Eyring, T. G. Shepherd and D. W. Waugh (eds.)]. Stratospheric Processes And their Role in Climate. Available at: http://www.atmosp.physics.utoronto.ca/SPARC.

St Jacques, J. M., D. J. Sauchyn, and Y. Zhao, 2010: Northern Rocky Mountain streamflow records: Global warming trends, human impacts or natural variability? *Geophys. Res. Lett.*, **37**, L06407.

Stahl, K., et al., 2010: Streamflow trends in Europe: Evidence from a dataset of near-natural catchments. *Hydrol. Earth Syst. Sci.*, **14**, 2367–2382.

Staten, P. W., J. J. Rutz, T. Reichler, and J. Lu, 2012: Breaking down the tropospheric circulation response by forcing. *Clim. Dyn.*, **39** 2361–2375.

Steig, E. J., and A. J. Orsi, 2013: The heat is on in Antarctica. *Nature Geosci.*, **6** 87–88.

Stenchikov, G., T. L. Delworth, V. Ramaswamy, R. J. Stouffer, A. Wittenberg, and F. Zeng, 2009: Volcanic signals in oceans. *J. Geophys. Res. Atmos.*, **114**, D16104.

Stephens, G. L., and Y. X. Hu, 2010: Are climate-related changes to the character of global-mean precipitation predictable? *Environ. Res. Lett.*, **5**, 025209.

Stephens, G. L., et al., 2010: Dreary state of precipitation in global models. *J. Geophys. Res. Atmos.*, **115**, D24211.

Stern, D. I., 2006: An atmosphere-ocean time series model of global climate change. *Comput. Stat. Data Anal.*, **51**, 1330–1346.

Stone, D. A., and M. R. Allen, 2005: Attribution of global surface warming without dynamical models. *Geophys. Res. Lett.*, **32**, L18711.

Stott, P. A., and J. Kettleborough, 2002: Origins and estimates of uncertainty in predictions of twenty-first century temperature rise *Nature*, **416**, 723–726.

Stott, P. A., and C. E. Forest, 2007: Ensemble climate predictions using climate models and observational constraints. *Philos. Trans. R. Soc. A*, **365**, 2029–2052.

Stott, P. A., and G. S. Jones, 2009: Variability of high latitude amplification of anthropogenic warming. *Geophys. Res. Lett.*, **36**, L10701.

Stott, P. A., and G. S. Jones, 2012: Observed 21st century temperatures further constrain decadal predictions of future warming. *Atmos. Sci. Lett.*, **13**, 151–156.

Stott, P. A., D. A. Stone, and M. R. Allen, 2004: Human contribution to the European heatwave of 2003. *Nature*, **432**, 610–614.

Stott, P. A., R. T. Sutton, and D. M. Smith, 2008a: Detection and attribution of Atlantic salinity changes. *Geophys. Res. Lett.*, **35**, L21702.

Stott, P. A., C. Huntingford, C. D. Jones, and J. A. Kettleborough, 2008b: Observed climate change constrains the likelihood of extreme future global warming. *Tellus B*, **60**, 76–81.

Stott, P. A., G. S. Jones, N. Christidis, F. W. Zwiers, G. Hegerl, and H. Shiogama, 2011: Single-step attribution of increasing frequencies of very warm regional temperatures to human influence. *Atmos. Sci. Lett.*, **12**, 220–227.

Stott, P. A., J. F. B. Mitchell, M. R. Allen, T. L. Delworth, J. M. Gregory, G. A. Meehl, and B. D. Santer, 2006: Observational constraints on past attributable warming and predictions of future global warming. *J. Clim.*, **19**, 3055–3069.

Stott, P. A., N. P. Gillett, G. C. Hegerl, D. J. Karoly, D. A. Stone, X. Zhang, and F. Zwiers, 2010: Detection and attribution of climate change: A regional perspective. *WIREs Clim. Change*, **1**, 192–211.

Stott, P. A., et al., 2013: Attribution of weather and climate-related events. In: *Climate Science for Serving Society: Research, Modelling and Prediction Priorities* [G. R. Asrar and J. W. Hurrell (eds.)]. Springer Science+Business Media, Dordrecht, Netherlands, 477 pp.

Stramma, L., S. Schmidtko, L. Levin, and G. Johnson, 2010: Ocean oxygen minima expansions and their biological impacts. *Deep-Sea Res. Pt. I*, **57**, 587–595.

Stroeve, J., et al., 2008: Arctic Sea ice extent plumments in 2007. *Eos Trans. Am. Geophys. Union*, **89**, 13–14.

Stroeve, J. C., M. C. Serreze, M. M. Holland, J. E. Kay, W. Meier, and A. P. Barrett, 2012a: The Arctic's rapidly shrinking sea ice cover: A research synthesis. *Clim. Change*, **110** 1005–1027.

Stroeve, J. C., V. Kattsov, A. Barrett, M. Serreze, T. Pavlova, M. Holland, and W. N. Meier, 2012b: Trends in Arctic sea ice extent from CMIP5, CMIP3 and observations. *Geophys. Res. Lett.*, **39**, L16502.

Swanson, K. L., G. Sugihara, and A. A. Tsonis, 2009: Long-term natural variability and 20th century climate change. *Proc. Natl. Acad. Sci. U.S.A.*, **106**, 16120–16123.

Swart, N. C., and J. C. Fyfe, 2012: Observed and simulated changes in the Southern Hemisphere surface westerly wind-stress. *Geophys. Res. Lett.*, **39**, L16711.

Tanaka, K., T. Raddatz, B. C. O'Neill, and C. H. Reick, 2009: Insufficient forcing uncertainty underestimates the risk of high climate sensitivity. *Geophys. Res. Lett.*, **36** L16709.

Tapiador, F. J., 2010: A joint estimate of the precipitation climate signal in Europe using eight regional models and five observational datasets. *J. Clim.*, **23**, 1719–1738.

Taylor, K. E., R. J. Stouffer, and G. A. Meehl, 2012: An overview of CMIP5 and the experiment design. *Bull. Am. Meteorol. Soc.*, **93**, 485–498.

Tedesco, M., J. E. Box, J. Cappellen, T. Mote, R. S. W. van der Wal, and J. Wahr, 2012: Greenland ice sheet. In State of the Climate in 2011. *Bull. Am. Meteorol. Soc.*, **93**, S150–S153.

Terray, L., 2012: Evidence for multiple drivers of North Atlantic multi-decadal climate variability. *Geophys. Res. Lett.*, **39**, L19712.

Terray, L., L. Corre, S. Cravatte, T. Delcroix, G. Reverdin, and A. Ribes, 2012: Near-Surface salinity as nature's rain gauge to detect human influence on the tropical water cycle. *J. Clim.*, **25**, 958–977.

Tett, S. F. B., et al., 2007: The impact of natural and anthropogenic forcings on climate and hydrology since 1550. *Clim. Dyn.*, **28**, 3–34.

Thompson, D. W. J., and S. Solomon, 2002: Interpretation of recent Southern Hemisphere climate change. *Science*, **296**, 895–899.

Thompson, D. W. J., and S. Solomon, 2009: Understanding recent stratospheric climate change. *J. Clim.*, **22**, 1934–1943.

Thompson, D. W. J., J. M. Wallace, P. D. Jones, and J. J. Kennedy, 2009: Identifying signatures of natural climate variability in time series of global-mean surface temperature: Methodology and insights. *J. Clim.*, **22**, 6120–6141.

Thorne, P. W., and R. S. Vose, 2010: Reanalyses suitable for characterizing long-term trends *Bull. Am. Meteorol. Soc.*, **91**, 353–361.

Thorne, P. W., et al., 2011: A quantification of uncertainties in historical tropical tropospheric temperature trends from radiosondes. *J. Geophys. Res. Atmos.*, **116**, D12116.

Timmermann, A., S. McGregor, and F. F. Jin, 2010: Wind effects on past and future regional sea level trends in the southern Indo-Pacific. *J. Clim.*, **23**, 4429–4437.

Timmreck, C., S. J. Lorenz, T. J. Crowley, S. Kinne, T. J. Raddatz, M. A. Thomas, and J. H. Jungclaus, 2009: Limited temperature response to the very large AD 1258 volcanic eruption. *Geophys. Res. Lett.*, **36**, L21708.

Ting, M. F., Y. Kushnir, R. Seager, and C. H. Li, 2009: Forced and internal twentieth-century sst trends in the North Atlantic. *J. Clim.*, **22** 1469–1481.

Tomassini, L., P. Reichert, R. Knutti, T. F. Stocker, and M. E. Borsuk, 2007: Robust bayesian uncertainty analysis of climate system properties using Markov chain Monte Carlo methods. *J. Clim.*, **20**, 1239–1254.

Trenberth, K., 2011a: Attribution of climate variations and trends to human influences and natural variability. *WIREs Clim. Change*, **2**, 925–930.

Trenberth, K., 2011b: Changes in precipitation with climate change. *Clim. Research*, **47**, 123–138.

Trenberth, K. E., and D. J. Shea, 2006: Atlantic hurricanes and natural variability in 2005. *Geophys. Res. Lett.*, **33**, L12704.

Trenberth, K. E., and J. T. Fasullo, 2012: Climate extremes and climate change: The Russian heat wave and other climate extremes of 2010. *J. Geophys. Res. Atmos.*, **117**, D17103.

Trenberth, K. E., J. T. Fasullo, C. O'Dell, and T. Wong, 2010: Relationships between tropical sea surface temperature and top-of-atmosphere radiation. *Geophys. Res. Lett.*, **37**, L03702.

Tung, K.-K., and J. Zhou, 2010: The Pacific's response to surface heating in 130 yr of SST: La Niña-like or El Niño-like? *J. Atmos. Sci.*, **67**, 2649–2657.

Tung, K.-K., and J. Zhou, 2013: Using data to attribute episodes of warming and cooling in instrumental records. *Proc. Natl. Acad. Sci. U.S.A.*, **110** 2058–2063.

Tung, K. K., J. S. Zhou, and C. D. Camp, 2008: Constraining model transient climate response using independent observations of solar-cycle forcing and response. *Geophys. Res. Lett.*, **35** L17707.

Turner, J., T. J. Bracegirdle, T. Phillips, G. J. Marshall, and J. S. Hosking, 2013: An initial assessment of Antarctic sea ice extent in the CMIP5 models. *J. Clim.*, **26**, 1473–1484.

Turner, J., et al., 2005: Antarctic change during the last 50 years. *Int. J. Climatol.*, **25**, 1147–1148.

Turner, J., et al., 2009: Non-annular atmospheric circulation change induced by stratospheric ozone depletion and its role in the recent increase of Antarctic sea ice extent. *Geophys. Res. Lett.*, **36**, L08502.

Ulbrich, U., G. C. Leckebusch, and J. G. Pinto, 2009: Extra-tropical cyclones in the present and future climate: A review. *Theor. Appl. Climatol.*, **96**, 117–131.

Urban, N. M., and K. Keller, 2009: Complementary observational constraints on climate sensitivity. *Geophys. Res. Lett.*, **36**, L04708.

van der Schrier, G., P. D. Jones, and K. R. Briff, 2011: The sensitivity of the PDSI to the Thornthwaite and Penman-Monteith parameterizations for potential evapotranspiration. *J. Geophys. Res. Atmos.*, **116**, D03106.

van Loon, H., and G. A. Meehl, 2008: The response in the Pacific to the sun's decadal peaks and contrasts to cold events in the Southern Oscillation. *J. Atmos. Sol. Terres. Phys.*, **70** 1046–1055.

van Loon, H., and G. A. Meehl, 2012: The Indian summer monsoon during peaks in the 11 year sunspot cycle. *Geophys. Res. Lett.*, **39** L13701.

van Loon, H., G. A. Meehl, and D. J. Shea, 2007: Coupled air-sea response to solar forcing in the Pacific region during northern winter. *J. Geophys. Res. Atmos.*, **112**, D02108.

van Oldenborgh, G. J., A. van Urk, and M. Allen, 2012: The absence of a role of climate change in the 2011 Thailand floods. *Bull. Am. Meteorol. Soc.*, **93**, 1047–1049.

van Oldenborgh, G. J., F. J. Doblas Reyes, S. S. Drijfhout, and E. Hawkins, 2013: Reliability of regional climate model trends. *Environ. Res. Lett.*, **8**, 014055.

Vecchi, G. A., and B. J. Soden, 2007: Global warming and the weakening of the tropical circulation. *J. Clim.*, **20**, 4316–4340.

Vecchi, G. A., K. L. Swanson, and B. J. Soden, 2008: Whither hurricane activity. *Science*, **322**, 687–689

Veryard, H. G., 1963: A review of studies on climate fluctuations during the period of the meteorological. *Changes of Climate: Proceedings of the Rome Symposium Organised by UNESCO and WMO*, pp. 3–15.

Villarini, G., and G. A. Vecchi, 2012: Twenty-first-century projections of North Atlantic tropical storms from CMIP5 models. *Nature Clim. Change*, **2**, 604–607.

Villarini, G., and G. A. Vecchi, 2013: Projected increases in North Atlantic tropical cyclone intensity from CMIP5 models. *J. Clim.*, **26**, 3231–3240.

Visser, H., and A. C. Petersen, 2012: Inference on weather extremes and weather related disasters: A review of statistical methods. *Clim. Past*, **8** 265–286.

von Schuckmann, K., F. Gaillard, and P. Y. Le Traon, 2009: Global hydrographic variability patterns during 2003–2008. *J. Geophys. Res.J. Geophys. Res. Oceans*, **114**, C09007.

Vorosmarty, C., L. Hinzman, and J. Pundsack, 2008: Introduction to special section on changes in the arctic freshwater system: Identification, attribution, and impacts at local and global scales. *J. Geophys. Res. Biogeosci.*, **113**, G01S91.

Vuille, M., G. Kaser, and I. Juen, 2008: Glacier mass balance variability in the Cordillera Blanca, Peru and its relationship with climate and the large-scale circulation. *Global Planet. Change*, **62**, 14–28.

Walker, R. T., T. K. Dupont, D. M. Holland, B. R. Parizek, and R. B. Alley, 2009: Initial effects of oceanic warming on a coupled ocean-ice shelf-ice stream system. *Earth Planet. Sci. Lett.*, **287**, 483–487.

Wan, H., X. Zhang, F. W. Zwiers, and H. Shiogama, 2013: Effect of data coverage on the estimation of mean and variability of precipitation at global and regional scales. *J. Geophys. Res. Atmos.*, **118**, 534–546.

Wang, D. B., and M. Hejazi, 2011: Quantifying the relative contribution of the climate and direct human impacts on mean annual streamflow in the contiguous United States. *Water Resour. Res.*, **47**, W00J12.

Wang, J., and X. Zhang, 2008: Downscaling and projection of winter extreme daily precipitation over North America. *J. Clim.*, **21**, 923–937.

Wang, J., et al., 2009a: Is the Dipole Anomaly a major driver to record lows in Arctic summer sea ice extent? *Geophys. Res. Lett.*, **36**, L05706.

Wang, M., and J. E. Overland, 2012: A sea ice free summer Arctic within 30 years: An update from CMIP5 models. *Geophys. Res. Lett.*, **39**, L18501.

Wang, M. Y., and J. E. Overland, 2009: A sea ice free summer Arctic within 30 years? *Geophys. Res. Lett.*, **36**, L07502.

Wang, M. Y., J. E. Overland, V. Kattsov, J. E. Walsh, X. D. Zhang, and T. Pavlova, 2007: Intrinsic versus forced variation in coupled climate model simulations over the Arctic during the twentieth century. *J. Clim.*, **20** 1093–1107.

Wang, X. L., V. R. Swail, F. W. Zwiers, X. Zhang, and Y. Feng, 2009b: Detection of external influence on trends of atmospheric storminess and northern oceans wave heights. *Clim. Dyn.*, **32**, 189–203.

Wassmann, P., C. M. Duarte, S. Agusti, and M. K. Sejr, 2011: Footprints of climate change in the Arctic marine ecosystem. *Global Change Biol.*, **17**, 1235–1249.

Wen, Q. H., X. Zhang, Y. Xu, and B. Wang, 2013: Detecting human influence on extreme temperatures in China. *Geophys. Res. Lett.*, **40**, 1171–1176.

Wentz, F. J., L. Ricciardulli, K. Hilburn, and C. Mears, 2007: How much more rain will global warming bring? *Science*, **317** 233–235.

Westra, S., L. V. Alexander, and F. W. Zwiers, 2013: Global increasing trends in annual maximum daily precipitation. *J. Clim.*, doi:10.1175/JCLI-D-12-00502.1.

White, W. B., and Z. Y. Liu, 2008: Non-linear alignment of El Nino to the 11-yr solar cycle. *Geophys. Res. Lett.*, **35**, L19607.
Wigley, T. M. L., and B. D. Santer, 2013: A probabilistic quantification of the anthropogenic component of twentieth century global warming. *Clim. Dyn.*, **40**, 1087–1102.
Wigley, T. M. L., C. M. Ammann, B. D. Santer, and K. E. Taylor, 2005: Comment on "Climate forcing by the volcanic eruption of Mount Pinatubo" by David H. Douglass and Robert S. Knox. *Geophys. Res. Lett.*, **32**, L20709.
Wijffels, S., et al., 2008: Changing expendable bathythermograph fall rates and their impact on estimates of thermosteric sea level rise. *J. Clim.*, **21**, 5657–5672.
Wilcox, L. J., B. J. Hoskins, and K. P. Shine, 2012: A global blended tropopause based on ERA data. Part II: Trends and tropical broadening. *Q. J. R. Meteorol. Soc.*, **138**, 576–584.
Willett, K. M., N. P. Gillett, P. D. Jones, and P. W. Thorne, 2007: Attribution of observed surface humidity changes to human influence. *Nature*, **449**, 710–712
Willett, K. M., P. D. Jones, N. P. Gillett, and P. W. Thorne, 2008: Recent changes in surface humidity: Development of the HadCRUH dataset. *J. Clim.*, **21**, 5364–5383.
Wilson, D., H. Hisdal, and D. Lawrence, 2010: Has streamflow changed in the Nordic countries? Recent trends and comparisons to hydrological projections. *J. Hydrol.*, **394**, 334–346.
WMO (World Meteorological Organization), 2011: *Scientific Assessment of Ozone Depletion: 2010*. Global Ozone Research and Monitoring Project–Report No. 52, World Meterological Organization, Geneva, Switzerland, 516 pp.
Wong, A. P. S., N. L. Bindoff, and J. A. Church, 1999: Large-scale freshening of intermediate waters in the Pacific and Indian oceans. *Nature*, **400**, 440–443.
Wood, K. R., and J. E. Overland, 2010: Early 20th century Arctic warming in retrospect. *Int. J. Climatol.*, **30**, 1269–1279.
Woollings, T., 2008: Vertical structure of anthropogenic zonal-mean atmospheric circulation change. *Geophys. Res. Lett.*, **35**, L19702.
Woollings, T., M. Lockwood, G. Masato, C. Bell, and L. J. Gray, 2010: Enhanced signatures of solar variability in Eurasian winter climate. *Geophys. Res. Lett.*, **37** L20805.
Wu, Q. G., and D. J. Karoly, 2007: Implications of changes in the atmospheric circulation on the detection of regional surface air temperature trends. *Geophys. Res. Lett.*, **34**, L08703.
Wu, Z. H., N. E. Huang, J. M. Wallace, B. V. Smoliak, and X. Y. Chen, 2011: On the time-varying trend in global-mean surface temperature. *Clim. Dyn.*, **37** 759–773.
Xie, S.-P., C. Deser, G. A. Vecchi, J. Ma, H. Teng, and A. T. Wittenberg, 2010: Global warming pattern formation: Sea surface temperature and rainfall. *J. Clim.*, **23**, 966–986.
Yamaguchi, S., R. Naruse, and T. Shiraiwa, 2008: Climate reconstruction since the Little Ice Age by modelling Koryto glacier, Kamchatka Peninsula, Russia. *J. Glaciol.*, **54**, 125–130.
Yang, X., J. C. Fyfe, and G. M. Flato, 2010: The role of poleward energy transport in Arctic temperature. *Geophys. Res. Lett.*, **37**, L14803.
Yiou, P., R. Vautard, P. Naveau, and C. Cassou, 2007: Inconsistency between atmospheric dynamics and temperatures during the exceptional 2006/2007 fall/winter and recent warming in Europe. *Geophys. Res. Lett.*, **34**, L21808.
Yoshimori, M., and A. J. Broccoli, 2008: Equilibrium response of an atmosphere-mixed layer ocean model to different radiative forcing agents: Global and zonal mean response. *J. Clim.*, **21**, 4399–4423.
Young, P. J., et al., 2012: Agreement in late twentieth century Southern Hemisphere stratospheric temperature trends in observations and CCMVal-2, CMIP3 and CMIP5 models. *J. Geophys. Res. Atmos.*, **118** 605–613.
Zhang, J., R. Lindsay, A. Schweiger, and M. Steele, 2013: The impact of an intense summer cyclone on 2012 Arctic sea ice retreat. *Geophys. Res. Lett.*, **40**, 720–726.
Zhang, J. L., 2007: Increasing Antarctic sea ice under warming atmospheric and oceanic conditions. *J. Clim.*, **20**, 2515–2529.
Zhang, R., and T. L. Delworth, 2009: A new method for attributing climate variations over the Atlantic Hurricane Basin's main development region. *Geophys. Res. Lett.*, **36**, L06701.
Zhang, R., et al., 2012: Have aerosols caused the observed Atlantic Multidecadal Variability? *J. Atmos. Sci.*, **70**, 1135–1144.
Zhang, X. B., et al., 2007: Detection of human influence on twentieth-century precipitation trends. *Nature*, **448**, 461–465.
Zhang, X. D., A. Sorteberg, J. Zhang, R. Gerdes, and J. C. Comiso, 2008: Recent radical shifts of atmospheric circulations and rapid changes in Arctic climate system. *Geophys. Res. Lett.*, **35**, L22701.
Zhou, J., and K.-K. Tung, 2013a: Deducing multidecadal anthropogenic global warming trends using multiple regression analysis. *J. Atmos. Sci.*, **70**, 3–8.
Zhou, J., and K.-K. Tung, 2013b: Observed tropospheric temperature response to 11-yr solar cycle and what it reveals about mechanisms. *J. Atmos. Sci.*, **70**, 9–14.
Zhou, Y., and G. Ren, 2011: Change in extreme temperature event frequency over mainland China, 1961–2008. *Climate Research*, **50**, 125–139.
Zickfeld, K., M. Eby, H. D. Matthews, and A. J. Weaver, 2009: Setting cumulative emissions targets to reduce the risk of dangerous climate change. *Proc. Natl. Acad. Sci. U.S.A.*, **106**, 16129–16134.
Zickfeld, K., et al., 2013: Long-term climate change commitment and reversibility: An EMIC intercomparison. *J. Clim.*, doi:10.1175/JCLI-D-12–00584.1.
Zorita, E., T. F. Stocker, and H. von Storch, 2008: How unusual is the recent series of warm years? *Geophys. Res. Lett.*, **35**, L24706.
Zunz, V., H. Goosse, and F. Massonnet, 2013: How does internal variability influence the ability of CMIP5 models to reproduce the recent trend in Southern Ocean sea ice extent? *Cryosphere*, **7**, 451–468.
Zwiers, F. W., X. Zhang, and Y. Feng, 2011: Anthropogenic influence on long return period daily temperature extremes at regional scales. *J. Clim.*, **24**, 881–892.